IMPROVE

Interagency Monitoring of Protected Visual Environments

Spatial and Seasonal Patterns and Temporal Variability of Haze and its Constituents in the United States

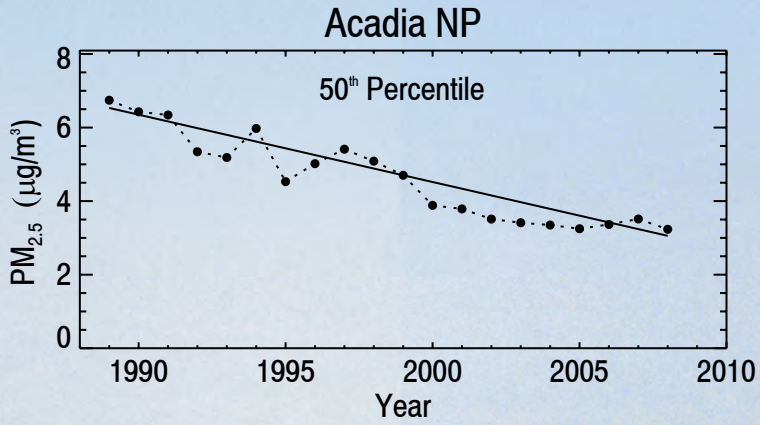

Report V

June 2011

ISSN 0737-5352-87

CIRA
Cooperative Institute for Research in the Atmosphere

Colorado State University

In celebration of the IMPROVE network's 25th anniversary, we dedicate this report to all of the hard working operators, technicians, and scientists who have contributed to the success of the IMPROVE network over the years.

Description of the cover:
The front cover displays a split screen of two images from Acadia National Park that represent visibility levels corresponding to the 50th percentile, $PM_{2.5}$ fine mass aerosol concentrations in 1989 (left) compared to those in 2008 (right). A noticeable improvement in visibility levels occurred due to the decrease in aerosol concentrations over the 20-year span. We used the WinHaze 2.9.9 computer software program (Air Resource Specialists, 2011), a powerful tool for visualizing the impact of aerosol trends on visibility conditions.

Spatial and Seasonal Patterns and Temporal Variability of Haze and its Constituents in the United States
Report V

ISSN 0737-5352-87

Principal Author:
Jenny L. Hand[1]

[1]Cooperative Institute for Research in the Atmosphere
Colorado State University
Fort Collins, CO 80523-1375

Contributors:

Scott A. Copeland[1]
Derek E. Day[1]
Ann M. Dillner[2]
Hege Indresand[2]
William C. Malm[1]
Chuck E. McDade[2]
Charles T. (Tom) Moore, Jr.[3]
Marc L. Pitchford[4]
Bret A. Schichtel[5]
John G. Watson[6]

[2]Crocker Nuclear Laboratory
University of California
Davis, CA 95616-8569

[3]Western Governors' Association – Western Regional Air Partnership
CSU/CIRA
Fort Collins, CO 80523-1375

[4]National Oceanic and Atmospheric Administration
Desert Research Institute
Las Vegas, NV 89119-7363

[5]National Park Service
CSU/CIRA
Fort Collins, CO 80523-1375

[6]Desert Research Institute
Reno, NV 89512

Disclaimer
The assumptions, findings, conclusions, judgments, and views presented herein are those of the authors and should not be interpreted as necessarily representing the National Park Service or National Oceanic and Atmospheric Administration policies.

TABLE OF CONTENTS

Appendices available at
http://vista.cira.colostate.edu/improve/Publications/improve_reports.htm or on cd by request.

LIST OF FIGURES

LIST OF TABLES

IMPROVE REPORT V

OVERVIEW AND SUMMARY

S.1 INTRODUCTION

This report describes aerosol speciation data collected by the Interagency Monitoring of Protected Visual Environments (IMPROVE) network. The IMPROVE program is a cooperative measurement effort between the U. S. Environmental Protection Agency (EPA), federal land management agencies, and state agencies. The network is designed to

1. establish current visibility and aerosol conditions in 156 mandatory Class I areas (CIAs);
2. identify chemical species and emission sources responsible for existing anthropogenic visibility impairment;
3. document long-term trends for assessing progress towards the national visibility goal;
4. and, with the enactment of the Regional Haze Rule, provide regional haze monitoring representing all visibility-protected federal CIAs where practical.

This report is the fifth in a series of IMPROVE reports that describes the monitoring methods and changes to instrumentation over time, as well as reports on measured aerosol concentrations and aerosol-derived visibility estimates. This report does not include data summaries of IMPROVE's direct atmospheric optical monitoring using nephelometers and transmissometers and scene monitoring using still and video camera systems. The IMPROVE and FED[1] web sites include descriptions of the aerosol, optical, and scene monitoring activities and provide access to the resulting data.

Air quality measurements in the IMPROVE network began in 1988. Due to resource and funding limitations in the early network, measurements in all 156 mandatory Class I areas were not possible. Instead, 36 sites were selected to represent aerosol concentrations and visibility over the United States. The first IMPROVE report was published in 1993 and described data that were collected at the initial 36 sites from March 1988 through February 1991 (Sisler et al., 1993). Beginning with the initial report, and in the reports that followed, spatial patterns and seasonal trends in speciated aerosol concentrations and reconstructed light extinction coefficients were presented. In addition, in the first report, focus was placed on aerosol measurement quality, aerosol acidity, and transmissometer measurements. In 1996 the second IMPROVE report was published and described data from March 1992 through February 1995 from 43 sites in the network (Sisler et al., 1996). In addition to spatial and seasonal trends, the second report included an exploration of aerosol light extinction efficiencies and long-term trends in fine mass and sulfur, using stacked filter unit measurements. In 2000, the third IMPROVE report was produced that included descriptions of data from 49 sites during the period from March 1996 through February 1999 (Malm et al., 2000). In addition to spatial and seasonal trends, this report included a discussion of the contributions of aerosol species to periods of high and low mass concentrations. Temporal (long-term and diurnal) trends in visibility and aerosol concentration were also reported. The fourth report was published in 2006 and covered data from 2000 through 2004 (Debell et al., 2006). The number of sites increased to 159 due to the expansion of the

[1] The VIEWS website, where data were previously available, has recently transitioned to the Federal Environmental Database (FED) website (http://views.cira.colostate.edu/fed/).

network to meet the goals of the Regional Haze Rule. In addition to data from the IMPROVE sites, data from 84 sites from the EPA's Speciated Trends Network (STN) were included to expand the spatial and seasonal aerosol and reconstructed light extinction coefficient trends to include urban areas and to investigate the differences in urban and rural aerosol concentrations. The 2006 report also included an initial investigation into the comparability of IMPROVE and STN data. Focus was also placed on IMPROVE quality assurance procedures.

At the timing of this report, the IMPROVE network consisted of 212 sites (170 current and 42 discontinued sites). This report, the fifth in the series, describes analyses for the 2005–2008 time period for 168 IMPROVE sites and 176 sites from the EPA's Chemical Speciation Network (CSN, formally STN). As in the previous reports, the fifth report includes the spatial and seasonal trends in aerosol mass and reconstructed light extinction coefficients for major aerosol species, including sea salt for the first time. The additional analyses in this report include an examination of urban and rural aerosol differences ("urban excess") and their spatial patterns using IMPROVE and CSN data. A deeper exploration of the seasonality in speciated aerosol mass concentrations and reconstructed light extinction coefficients is also presented. With the long temporal record of IMPROVE data, "long-term" (1989–2008) and "short-term" (2000–2008) trends in speciated aerosol concentrations for seasonal and statistical parameters were explored. Descriptions of regional haze metrics, including comparisons of visibility between the Regional Haze Rule baseline period (2000–2004) and period 1 (2005–2009) are presented. An assessment of biases in fine mass measurements is also included. The following summary provides highlights of the material contained in the fifth (2011) IMPROVE report; the reader is encouraged to refer to the full report for more detail.

S.2 AEROSOL DATA

The version II IMPROVE sampler, deployed in 2000, consists of four independent modules (A, B, C, and D) that collect 24-hour samples every third day. Each module incorporates a separate inlet, filter pack, and pump assembly. Modules A, B, and C are equipped with a 2.5 µm cyclone that allows for sampling of particles with aerodynamic diameters less than 2.5 µm, while module D is fitted with a PM_{10} inlet to collect particles with aerodynamic diameters less than 10 µm. Each module contains a filter substrate specific to the analysis planned. Module A is equipped with at Teflon® filter that is analyzed for $PM_{2.5}$ gravimetric fine mass, elemental concentration, and light absorption. Module B is fitted with a Nylasorb (nylon) filter and analyzed for the anions sulfate, nitrate, nitrite, and chloride using ion chromatography. Module C utilizes a quartz fiber filter that are analyzed by thermal optical reflectance (TOR) for organic and light absorbing carbon (OC and LAC, respectively) (Chow et al., 1993). We use the term "light absorbing carbon" instead of "elemental carbon" or "EC" in this report to reflect the recent literature regarding light absorption by carbonaceous aerosols (Bond and Bergstrom, 2006). Finally, module D is fitted with a PM_{10} inlet and utilizes a Teflon filter. PM_{10} aerosol mass concentrations are determined gravimetrically. Details regarding aerosol sampling and analyses can be found in Chapter 1. IMPROVE data are available for download from http://views.cira.colostate.edu/fed/. Current and discontinued IMPROVE sites are listed by region in Table 1.1 in Chapter 1. A map of IMPROVE sites (grouped by region) is shown in Figure S.2.1. See Chapter 1 for more detail regarding how the regions were specified.

CSN data were also used extensively in this report. CSN operates approximately 50 long-term-trend sites, with another ~150 sites operated by state, local, and tribal agencies, primarily in urban/suburban settings. All CSN samplers utilize a $PM_{2.5}$ inlet and three channels containing Teflon, nylon, and quartz filters. Like the IMPROVE network, CSN samplers operate on a 24-hour schedule from midnight to midnight every third day. $PM_{2.5}$ gravimetric mass and elemental compositions are analyzed from the Teflon filter, ions from the nylon filter, and carbon from the quartz filter. The carbon analysis was historically performed with thermal optical transmittance (TOT) using a NIOSH-type protocol. The recognition that IMPROVE samplers and TOR analysis produce different OC and LAC concentrations than CSN samplers and TOT analysis has motivated the CSN transition to TOR analysis for consistency with the IMPROVE network. In addition to the transition from TOT to TOR, in April 2005 EPA decided to replace the carbon channel sampling and analysis methods with a URG 3000N sampler that is similar to the IMPROVE version II module C sampler. The conversion began in May 2007 with 56 sites, followed by another 63 sites in April 2009 and 78 additional sites in October 2009. Additional detail regarding IMPROVE and CSN sampling and analysis methods for each species is provided in Chapter 2 and includes a discussion of aerosol species mass calculations. A discussion of the adjustments developed for this report and applied to CSN carbon data collected prior to the transition to the new analyses and monitors is also included. Adjustments to CSN carbon data were required for IMPROVE and CSN data to be combined. A map of 321 CSN sites is provided in Figure S.2.2 with the general regions depicted. A subset of these sites (176) was used in this report, based on completeness criteria outlined in Chapter 2. A description of the how the regions were defined is in Chapter 1.4.

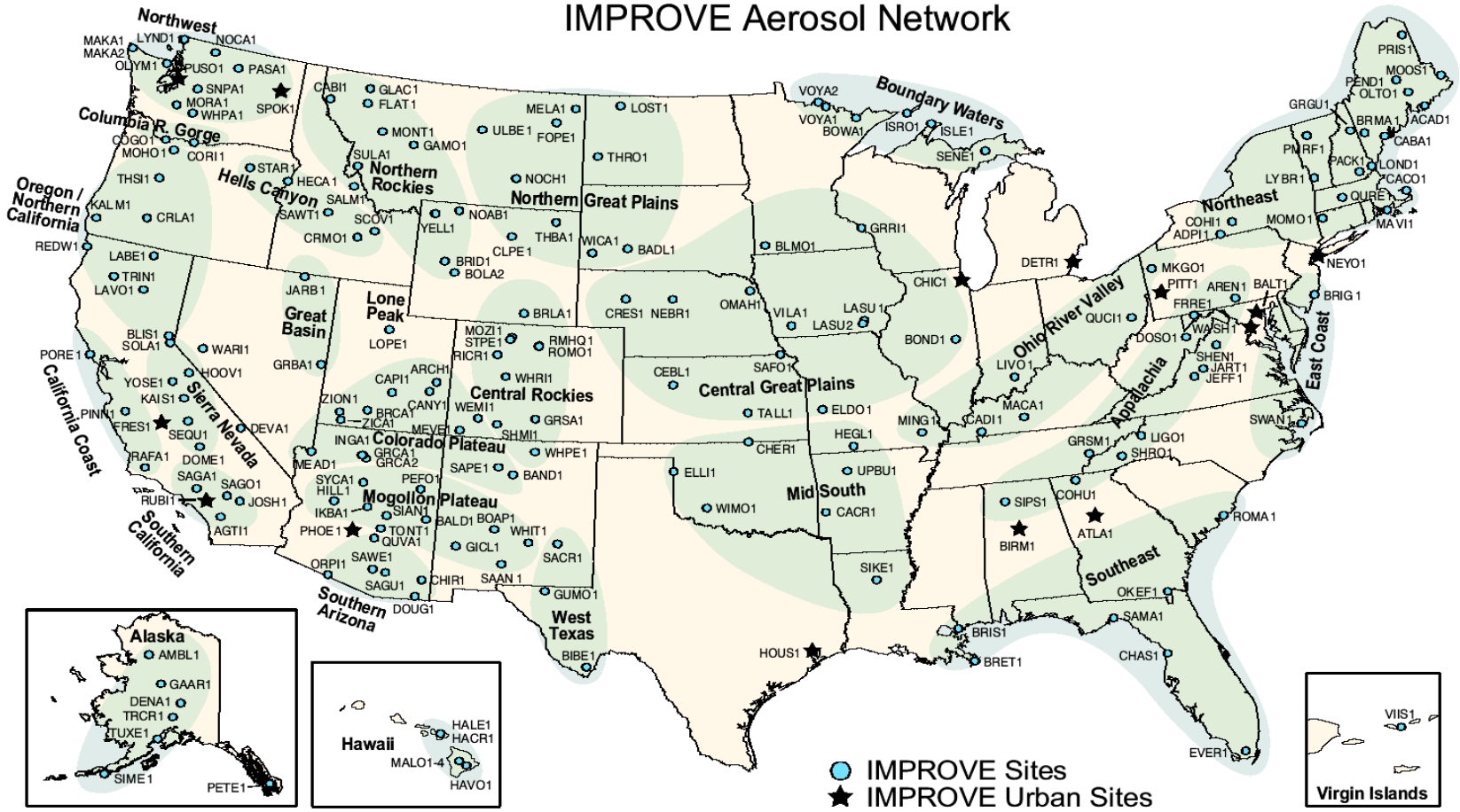

Figure S.2.1. Locations of IMPROVE and IMPROVE protocol sites for all discontinued and current sites. The IMPROVE regions used for grouping the sites are indicated by shading and bold text. Urban sites included in the IMPROVE network for quality assurance purposes are identified by stars.

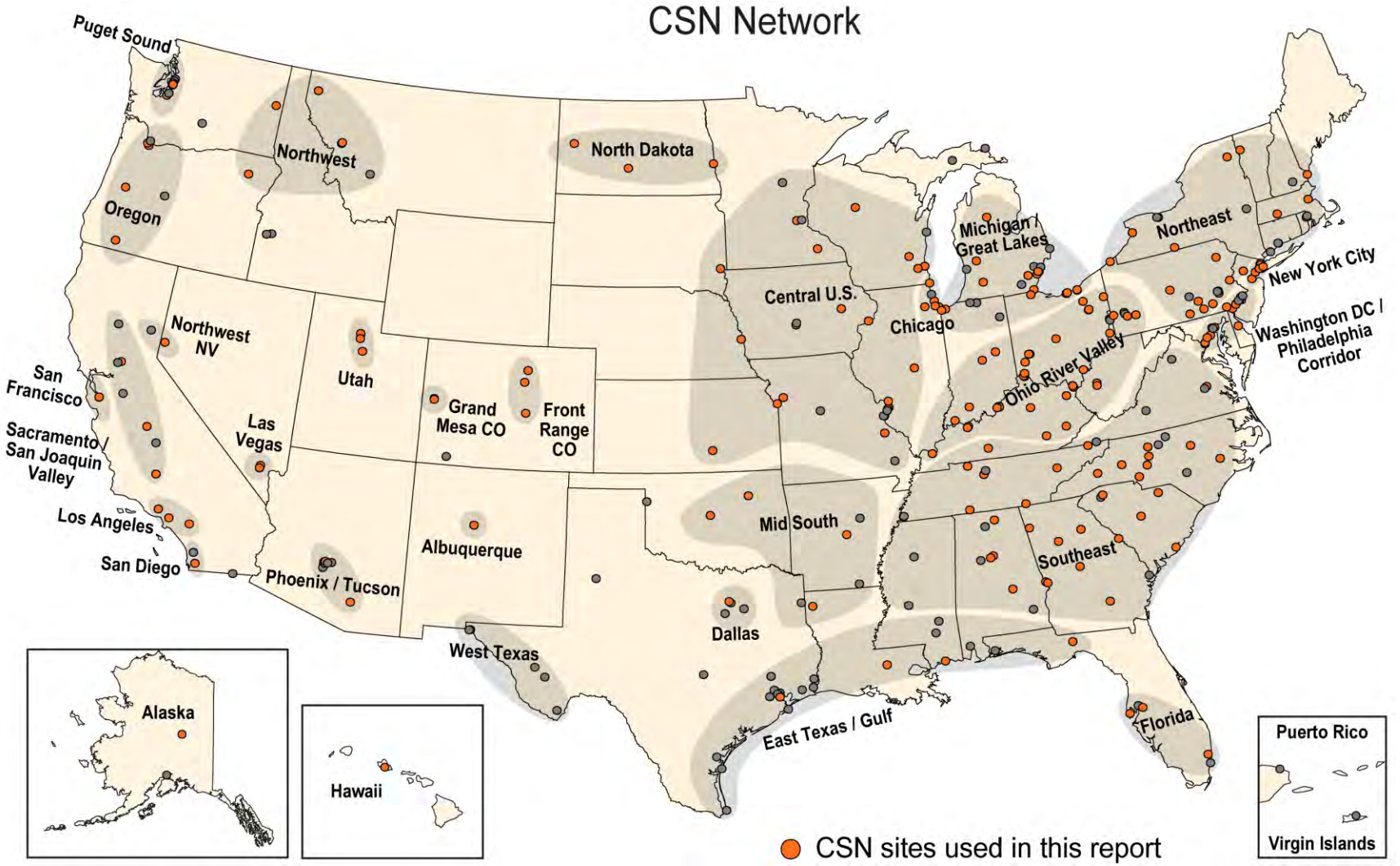

Figure S.2.2. Current and discontinued Chemical Speciation Network (CSN) sites (grey and orange) operated by the Environmental Protection Agency. Regions are shown as shaded areas and bold text. The sites included in the analyses in this report are shown as orange circles.

The IMPROVE and CSN networks operate collocated samplers in several urban sites. Collocated sites with data that met the completeness criteria outlined in Chapter 2 were compared to identify relative biases between IMPROVE and CSN speciated aerosol concentrations. Daily data from Baltimore, Maryland; Birmingham, Alabama; Fresno, California; New York City (Bronx), New York; Phoenix, Arizona; Puget Sound (Seattle), Washington; and Washington, D.C. for 2005–2008 were used. Ammonium sulfate (AS), ammonium nitrate (AN), organic carbon (OC), light absorbing carbon (LAC), soil, sea salt, $PM_{2.5}$ gravimetric fine mass (FM), and reconstructed fine mass (RCFM) were compared. A summary of results is provided in Table S.2.2. Errors were fairly low for most species (<20%), with the exception of soil (37.0%) and sea salt (78.3%), which also had high biases. IMPROVE sea salt concentrations were computed as 1.8 times chloride ion concentrations, whereas CSN sea salt concentrations were computed as 1.8 times chlorine concentrations. However, biases for other species were generally low, ranging from 5.7% for LAC to 18.4% for FM. The errors and relative biases between unadjusted CSN carbon and IMPROVE carbon data were 95.9% and 111.2 % for OC, respectively, and 26.7% and -17.3% for unadjusted LAC, respectively. The close agreement in adjusted OC and LAC data suggests that the adjustments applied to those data were appropriate and effective (see Chapter 2). It should also be noted that while IMPROVE applies artifact corrections to ion data, CSN does not; some of the discrepancy between ion data from the two networks could be due this difference.

The large errors and biases for soil and sea salt indicate that IMPROVE had much higher concentrations compared to CSN concentrations. Recall that these data are from collocated sites so the biases reflected differences in sampling or analytical techniques. The biases in soil and sea salt are sufficiently large that combined data analyses should be treated as semiquantitative. CSN concentrations were somewhat higher than IMPROVE concentrations for most other species (positive biases correspond to higher CSN concentrations), but data from the two networks were fairly highly correlated. The general agreement for most species indicates that it was appropriate to combine data.

Table S.2.2. Comparisons between collocated IMPROVE and CSN sites for all data from 2005 through 2008. Species include organic carbon (OC), light absorbing carbon (LAC), ammonium sulfate (AS), ammonium nitrate (AN), soil, sea salt, $PM_{2.5}$ gravimetric fine mass (FM), and $PM_{2.5}$ reconstructed fine mass (RCFM). "OC_{unadj}" and "LAC_{unadj}" refer to comparisons between unadjusted CSN carbon data and IMPROVE carbon data; "OC_{adj}" and "LAC_{adj}" refer tocomparisons between adjusted CSN carbon and IMPROVE carbon data.

Statistic	OC_{unadj}	LAC_{unadj}	OC_{adj}	LAC_{adj}	AS[3]	AN[4]	Soil	Sea salt[5]	FM	RCFM
Average IMPROVE ($\mu g\ m^{-3}$)	2.8	1.3	2.7	1.2	3.9	2.3	1.4	0.3	12.6	13.5
Average CSN ($\mu g\ m^{-3}$)	5.2	1.0	3.0	1.2	4.1	2.6	0.9	0.11	14.3	13.5
Bias[1] (%)	111.2	-17.3	8.3	5.7	7.0	17.2	-31.0	-62.8	18.4	0.04
Error[2] (%)	95.9	26.7	16.0	20.2	7.5	13.9	37.0	78.3	14.1	8.5
r	0.92	0.87	0.93	0.88	0.98	0.99	0.85	0.84	0.9	0.95
IMP/CSN	0.54	1.3	0.93	1.0	0.96	0.92	1.6	3.2	0.9	1.0
Number of data points (N)	2087	2077	2675	2665	2687	2689	2646	1904	2636	2535

[1] $\text{Error} = \text{median}\left(\left|\frac{\overline{X}_i - \overline{Y}_i}{\overline{Y}_i}\right|\right)$

[2] $\text{Bias} = \frac{1}{N}\sum_i^N \frac{\overline{X}_i - \overline{Y}_i}{\overline{Y}_i}$; $\overline{X}_i$ and $\overline{Y}_i$ are the daily data for CSN and IMPROVE concentrations, respectively. The number of data points is given by N.

[3] AS = 1.375[sulfate ion]

[4] AN = 1.29[nitrate ion]

[5] Sea salt = 1.8[chloride ion] for IMPROVE and 1.8[chlorine] for CSN.

S.3 SPATIAL PATTERNS IN RURAL AND URBAN SPECIATED AEROSOL CONCENTRATIONS: IMPLICATIONS FOR URBAN EXCESS

Urban excess is defined as the difference in aerosol mass concentrations at an urban site compared to the regional background concentration. Urban excess studies provide estimates of the relative magnitude of local versus regional contributions to aerosol concentrations and subsequently increase our understanding of aerosol sources and lifetimes in the atmosphere. Different aerosol species correspond to a range in urban excess values, depending on their sources and lifetimes.

Data from 344 IMPROVE and CSN sites were combined to explore the spatial variability in major aerosol species, as well as their impacts on urban excess. Urban excess was investigated for 2005–2008 annual mean ammonium sulfate (AS), ammonium nitrate (AN), particulate organic matter (POM=1.8OC), light absorbing carbon (LAC), and $PM_{2.5}$ gravimetric fine mass (FM). Sea salt and fine soil were not included because of the relative biases derived for those species from analyses of data from collocated IMPROVE and CSN sites (see Table S.2.2), nor was coarse mass as CSN does not monitor for it. Although urban excess estimates were computed for annual mean concentrations, estimates undoubtedly varied temporally, as the seasonal aerosol concentrations for urban and rural sources were very distinct (see section S.4 and Chapter 4 in the main report). Urban excess estimates, defined as the ratio of urban to rural

concentrations, for AS, AN, POM, and LAC are summarized here; further discussions regarding the spatial variability and urban excess in mass concentrations, including the absolute differences in concentration, in these and other species can be found in Chapter 4 and Chapter 7, respectively.

Isopleth maps of annual mean mass concentrations were created for each species for combined IMPROVE and CSN data. Isopleth maps created using a Kriging algorithm should be viewed and interpreted with caution. The isopleths are intended to help visualize the data and identify large spatial patterns only. Similar maps were created for urban excess estimates.

Regional background concentrations at urban locations were determined from interpolated rural IMPROVE data at the grid cell corresponding to a CSN urban site. Urban sites were limited to locations with at least one IMPROVE site within 150 km, resulting in 114 CSN sites used in the urban excess analysis. Urban CSN data (not interpolated data) were used. No elevation corrections (standard pressure and temperature) were applied to the urban and rural data, with the assumption that if the sites were within 150 km, the corrections based on elevation differences would be negligible (it is unlikely that a site at sea level would be 150 km from a site at an elevation of 3 km). A more important elevation issue is the possibility that urban and rural sites with a significant elevation difference were actually sampling different air masses as some IMPROVE monitors could be above the boundary layer (e.g., Rocky Mountain National Park and Denver, Colorado).

S.3.1 Ammonium Sulfate

The spatial distribution of AS with the rural and urban sites combined (see Figure S.3.1a) was very similar to the pattern of the rural sites alone (see Chapter 2), suggesting that regional impacts of high AS concentrations influenced both urban and rural sites similarly. Notice the difference in site density between the IMPROVE and CSN networks in Figure S.3.1.a, with many more CSN sites in the eastern United States; these sites provide additional detail to the spatial patterns of AS in that section of the country. The combination of high sulfur dioxide emissions and high relative humidity produced the highest concentrations (4–8 $\mu g\ m^{-3}$) of AS in the eastern United States that centered on the Ohio River valley and Appalachia regions. AS concentrations decreased sharply towards the western United States. In fact, concentrations in the western United States were typically less than 2 $\mu g\ m^{-3}$.

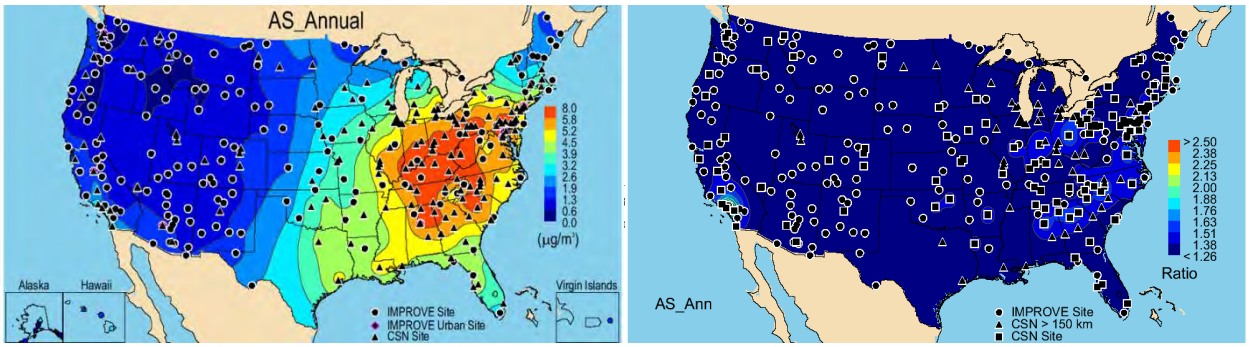

Figure S.3.1. (a) IMPROVE and CSN $PM_{2.5}$ ammonium sulfate (AS) 2005–2008 annual mean mass concentrations (μg m^{-3}). (b) Interpolated ratios of urban (CSN) to rural (IMPROVE) annual mean AS concentrations for 2005–2008. IMPROVE sites are shown as circles; CSN sites used in the analysis are shown as squares. CSN sites with no IMPROVE site within 150 km are shown as triangles. These sites were not used in the analysis.

The ratio of urban to rural AS concentrations is shown in Figure S.3.1b. CSN site locations with an IMPROVE monitor within 150 km are depicted with square symbols; sites not meeting this criteria are shown as triangles. In addition to the southern California area, higher ratios occurred for a swath of area southeast of the Appalachia Mountains and the Ohio River valley. The lowest ratios occurred in the central, western, northwestern, and northeastern United States. Similar concentrations of AS for rural and urban sites suggested strong regional impacts, not surprising given the regional nature of its sources; however, some urban excess in AS occurred. The mean (one standard deviation) ratio for all 114 urban sites was 1.4 ± 0.3. Some of the excess could be explained by the small relative bias between AS data from the CSN and IMPROVE networks (Table S.2.2).

S.3.2 Ammonium Nitrate

Not surprisingly, locations where ammonia and nitric acid concentrations were the highest corresponded to the regions where AN concentrations were the largest (Figure S.3.2a). Higher sources of precursors to AN in agricultural regions in the Midwest resulted in the highest AN concentrations for rural sites in the United States. Generally, urban concentrations of AN were considerably higher than rural concentrations. Urban concentrations were also higher in the Midwest and were considerably higher than rural concentrations in the same region.

The impacts of urban sources of AN to surrounding rural regions were apparent by examining the ratio of urban to rural AN concentrations as shown in Figure S.3.2b. Several western cities corresponded to relatively high ratios with sharp spatial gradients. Significant urban excess was expected in the Midwest based on the differences in the rural and urban concentrations in that region. However, none of the urban sites in that area were associated with rural sites within 150 km; therefore low urban excess in that area was due to lack of data. The mean ratio (one standard deviation) was 2.5±1.3, considerably higher than the mean ratio for AS. Relative biases in AN data from the IMPROVE and CSN networks contributed slightly.

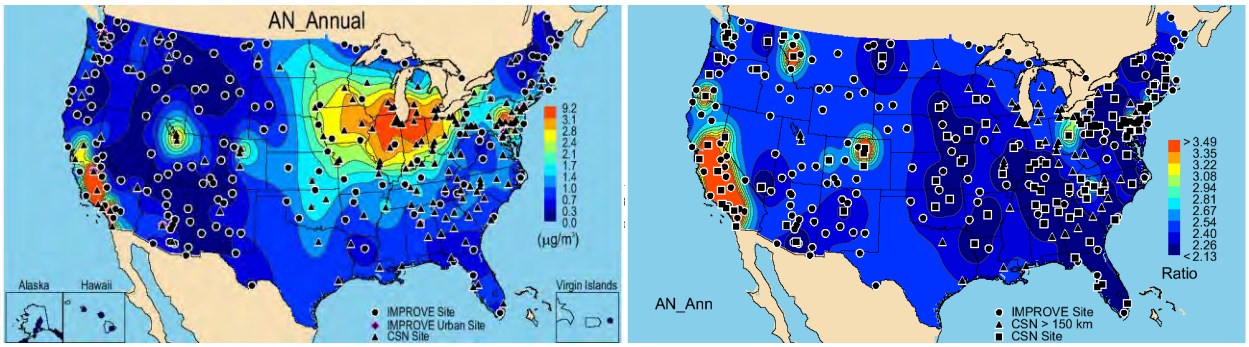

Figure S.3.2. (a) IMPROVE and CSN $PM_{2.5}$ ammonium nitrate (AN) 2005–2008 annual mean mass concentrations (μg m^{-3}). (b) Interpolated ratios of urban (CSN) to rural (IMPROVE) annual mean AN concentrations for 2005–2008. IMPROVE sites are shown as circles; CSN sites used in the analysis are shown as squares. CSN sites with no IMPROVE site within 150 km are shown as triangles. These sites were not used in the analysis.

S.3.3 Particulate Organic Matter

The highest rural annual mean POM concentrations corresponded to a large area in the southeastern United States (Figure S.3.3a), most likely associated with biogenic emissions and perhaps biomass smoke emissions (Tanner et al., 2004; Bench et al., 2007). The western United States was associated with more localized regions of higher POM concentrations; rural concentrations in Idaho and Montana were near 3 μg m^{-3}, most likely from biomass burning emissions. Higher POM concentrations and more localized impacts of urban POM sources were apparent in the western United States, with sharper gradients compared to the eastern United States.

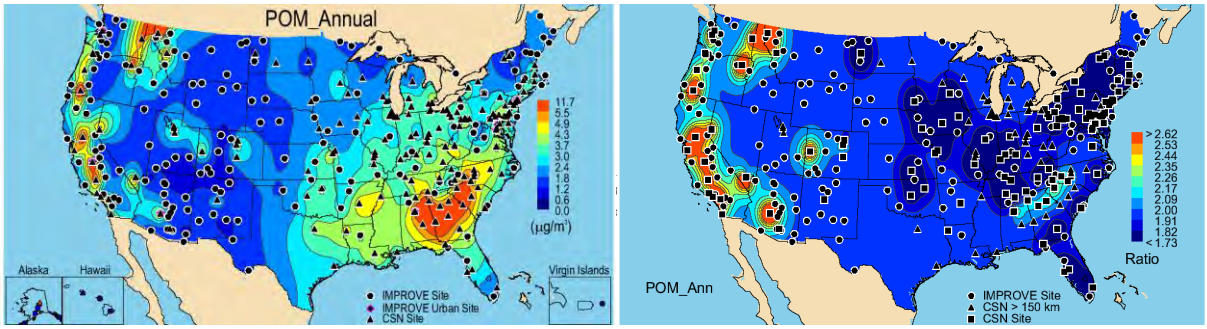

Figure S.3.3. (a) IMPROVE and CSN $PM_{2.5}$ particulate organic matter (POM) 2005–2008 annual mean mass concentrations (μg m^{-3}). (b) Interpolated ratios of urban (CSN) to rural (IMPROVE) annual mean POM concentrations for 2005–2008. IMPROVE sites are shown as circles; CSN sites used in the analysis are shown as squares. CSN sites with no IMPROVE site within 150 km are shown as triangles. These sites were not used in the analysis.

Urban excess estimates for POM did not account for different types of organic aerosols known to exist in urban versus rural settings. Urban organic aerosols from local sources are less aged and correspond to lower molecular weight per carbon weight ratios compared to rural aerosols (e.g., Turpin and Lim, 2001). The difference in the organic carbon multiplier for urban versus rural aerosols was not accounted for in this analysis (a value of 1.8 was applied to both), although Malm et al. (2011) suggested that the urban organic multiplier was 5–15% lower than

that for rural sites after investigating biases in fine mass data from the IMPROVE and CSN networks.

The pattern of localized influences seen in Figure S.3.3a is displayed more clearly as the urban to rural POM concentration ratio in Figure S.3.3b. Several western cities were associated with higher ratios (urban concentrations over 2.5 times higher than rural concentrations). Ratios of ~2.3 corresponded to a swath of area to the southeast of the Appalachia Mountains the eastern United States. This area was associated with the highest urban concentrations and the fewest number of IMPROVE sites. Urban concentrations were 1.9 ± 0.9 times higher than rural concentrations on average, although relative biases between data from the two networks contributed slightly to this excess. The mean POM ratio was higher than the mean AS ratio, but lower than the AN ratio, suggesting that POM was more regional in extent in some areas of the country (e.g., southeastern United States) but also was influenced by local urban sources.

S.3.4 Light Absorbing Carbon

The IMPROVE rural annual mean LAC concentrations in the western United States typically were less than ~0.3 μg m^{-3}. The rural concentrations in the eastern United States were higher (0.4–0.5 μg m^{-3}) and tended to be located in the southern United States and Ohio River valley areas, as well as parts of Pennsylvania (Figure S.3.4a). Major hotspots of LAC concentrations were associated with urban sites. Urban LAC concentrations generally were localized around individual site locations in the western United States and were more regional in extent in the eastern United States, although not to the degree of POM. The largest urban LAC concentrations were near 2.5 μg m^{-3}.

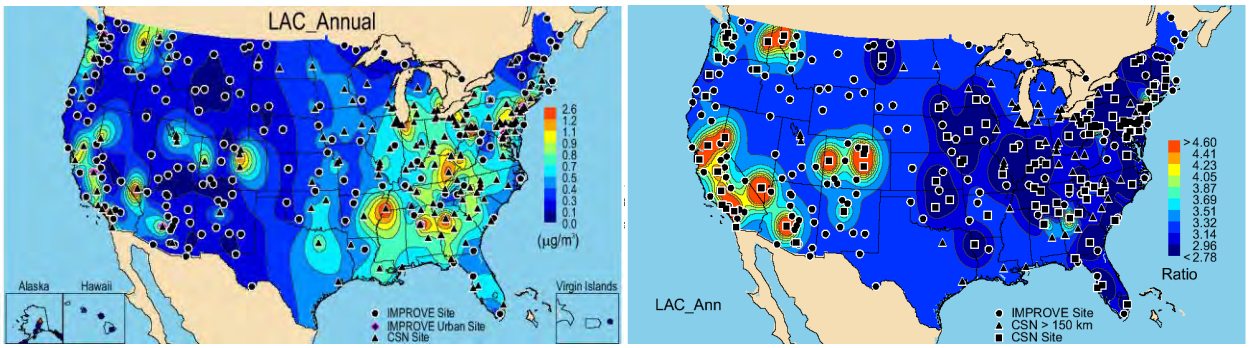

Figure S.3.4. (a) IMPROVE and CSN $PM_{2.5}$ light absorbing carbon (LAC) 2005–2008 annual mean mass concentrations (μg m^{-3}). (b) Interpolated ratios of urban (CSN) to rural (IMPROVE) annual mean LAC concentrations for 2005–2008. IMPROVE sites are shown as circles; CSN sites used in the analysis are shown as squares. CSN sites with no IMPROVE site within 150 km are shown as triangles. These sites were not used in the analysis.

The ratio of urban to rural LAC concentrations demonstrated the localized impact from primary emissions of LAC on surrounding rural regions. Fewer sites in the eastern United States were associated with higher ratios compared to western sites (Figure S.3.4b). Although areas associated with high ratios were similar for POM and LAC, LAC ratios were much larger, suggesting urban LAC sources were significantly larger than rural sources. In addition, LAC urban excess estimates were less regional in extent than POM, indicating local source contributions of LAC rather than more regional sources like biomass combustion from controlled

or wild fires. The mean ratio was 3.3 ± 1.9 and was much larger than the mean ratio for AS, AN, or POM.

Analyses of interpolated IMPROVE and CSN aerosol concentrations provided spatial patterns of urban excess for the United States. For certain species, such as POM, LAC, and AN, annual mean urban concentrations were considerably higher than rural concentrations. As a summary, the urban excess mean ratios for AS, AN, POM, and LAC were 1.4 ± 0.3, 2.5 ± 1.3, 1.9 ± 0.9, and 3.3 ± 1.9, respectively. Although not shown here, the mean FM ratio was 2.0 ± 0.6. Urban excess values include the relative biases between data from the two networks. Urban excess estimates varied widely as a function of location. While the isopleths of urban excess were semiquantitative, they indicated the spatial extent of urban impacts on surrounding rural and remote areas as a function of species. For example, while LAC corresponded to the highest mean urban to rural concentration ratio, its spatial extent was generally the lowest and associated with sharp spatial gradients, suggesting local sources. In contrast, the spatial patterns in urban excess associated with species such as AS, POM, and FM were more regional in extent, especially in the eastern United States, although impacts from local sources were also apparent.

S.4 SEASONAL DISTRIBUTIONS IN AEROSOL MASS CONCENTRATIONS

The seasonality of speciated aerosol mass concentrations can be significant depending on species and region and is a function of the source emissions, meteorological parameters, and local and long-range transport. Examining aerosol concentrations on a regional basis, rather than a site-specific basis, can lead to insights regarding air quality issues on regional scales.

IMPROVE and CSN data from 2005 through 2008 were regionally and monthly averaged according to previously defined regions (see Section S.2 and Chapter 1.2 and 1.4) and plotted as stacked bar charts on maps of the United States. The CSN and IMPROVE regions coincide a closely as possible, but do depend on available sites in a given area. Some regions consist of only one site (e.g., IMPROVE urban sites). The monthly mean concentrations of ammonium sulfate (AS), ammonium nitrate (AN), particulate organic matter (POM), light absorbing carbon (LAC), soil, sea salt, and gravimetric fine mass (FM) and coarse mass (CM) were computed. Stacked bar charts provide a detailed view of the changes in monthly mean aerosol concentrations during the year at different regions in the United States. In addition, analyses were performed that complement the stacked bar charts by summarizing the detailed information in the bar charts in such a way that quickly and easily convey the temporal changes in the data. Seasonality was defined in terms of the ratio of the maximum to minimum monthly concentration for a given region. Seasonal periods included winter (December, January, and February), spring (March, April, and May), summer (June, July, and August), and fall (September, October, and November). Maps of seasonality were created in which each region was associated with a set of triangles. The color of the upward-pointing triangle refers to the season with the maximum monthly mean concentration. The color of the downward-pointing triangle refers to the season with the minimum monthly mean concentration. The size of the triangle corresponds to the ratio of maximum to minimum monthly concentration such that large triangles represent larger degrees of seasonality. The location of the triangle on the map represents the region and may not be placed directly over a specific site location. Highlights in seasonality of mass concentrations for IMPROVE and CSN concentrations are included here; additional detail, including regional

stacked bar charts, are provided in Chapter 4. Similar results for reconstructed light extinction coefficients are reported in Chapter 5.

S.4.1 Ammonium Sulfate

AS was associated with a high degree of seasonality, with the majority of IMPROVE regions corresponding to ratios of maximum to minimum monthly mean mass concentrations greater than 2 (Figure S.4.1a). The maximum AS mass concentrations were predominantly observed in summer at many IMPROVE regions, with the exception of spring maxima in the northwestern United States. The minimum season for almost all regions occurred in winter. AS concentrations at CSN regions were somewhat less seasonal than rural regions (Figure S.4.1b). Most CSN regions corresponded to summer maxima and winter and fall minima.

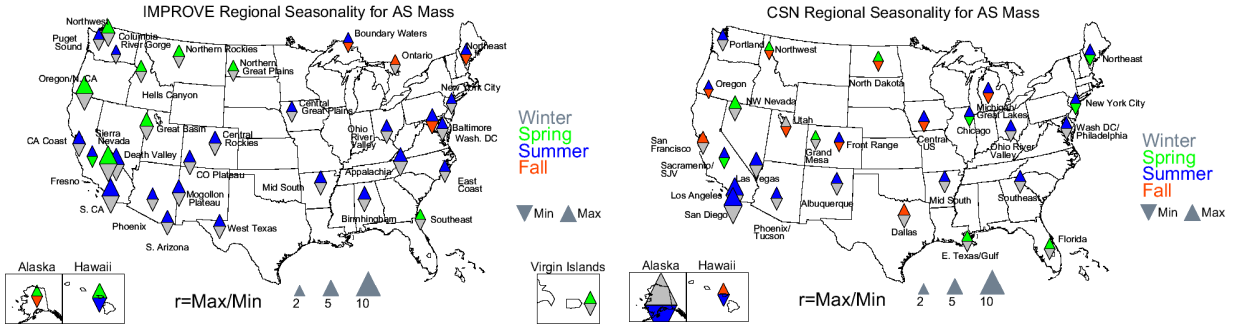

Figure S.4.1. (a) Seasonal variability for 2005–2008 monthly mean IMPROVE ammonium sulfate (AS) mass concentrations. (b) The same as (a), but for the CSN. The color of the upward-pointing triangle refers to the season with the maximum monthly mean concentration, and the downward-pointing triangle refers to the season with the minimum monthly mean concentration. The size of the triangles refers to the magnitude of the ratio of maximum to minimum monthly mean mass concentration.

S.4.2 Ammonium Nitrate

IMPROVE rural AN concentrations were typically higher in winter due to more favorable conditions of nitrate particle formation in that season. The winter maxima at most regions were very obvious from the depiction of seasonality in Figure S.4.2a. Most of the IMPROVE regions were associated with a high degree of seasonality in monthly mean AN concentrations. CSN regions demonstrated a strong seasonality, with only one region having a maximum to minimum ratio less than or equal to 2 (Florida, 2.0) (Figure S.4.2b). The maximum monthly mean AN concentration occurred in winter for the majority of CSN regions. More urban regions corresponded to winter maxima compared to the IMPROVE regions and were subject to a higher degree of seasonality. Western regions had higher seasonality than eastern regions. Many regions had minimum concentrations in the fall.

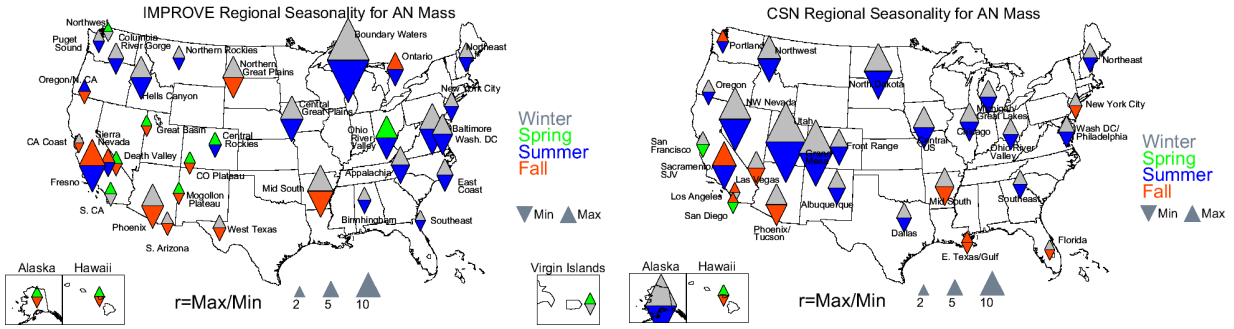

Figure S.4.2. (a) Seasonal variability for 2005–2008 monthly mean IMPROVE ammonium nitrate (AN) mass concentrations. (b) The same as (a), but for the CSN. The color of the upward-pointing triangle refers to the season with the maximum monthly mean concentration, and the downward-pointing triangle refers to the season with the minimum monthly mean concentration. The size of the triangles refers to the magnitude of the ratio of maximum to minimum monthly mean mass concentration.

S.4.3 Particulate Organic Matter

Most of the IMPROVE regions demonstrated a high level of seasonality in monthly mean POM concentrations (Figure S.4.3a). The western United States corresponded to much higher seasonality in IMPROVE POM concentrations compared to the eastern United States, probably because of the impacts from biomass burning in summer. Most western regions had summer maxima and winter minima, with the exception of the IMPROVE urban sites of Fresno, Phoenix, and Puget Sound, all of which had winter maxima. A few regions had spring minima. In the eastern United States, the maxima predominantly occurred in summer, but minima occurred during all seasons. Maximum and minimum can both occur in the same season (i.e., Baltimore). The seasonality of POM monthly mean concentrations was much different for urban CSN regions compared to rural IMPROVE regions. Lower seasonality was observed in general, and the winter minima/summer maxima that occurred in most western IMPROVE regions (and Alaska) were replaced with nearly the opposite: winter maxima and spring and summer minima (Figure S.4.3b). In the eastern United States, the seasonality varied per region, with several regions having summer maxima and winter and spring minima. Several regions along the eastern coast corresponded to similar summer maxima/spring minima and degree of seasonality as the rural regions.

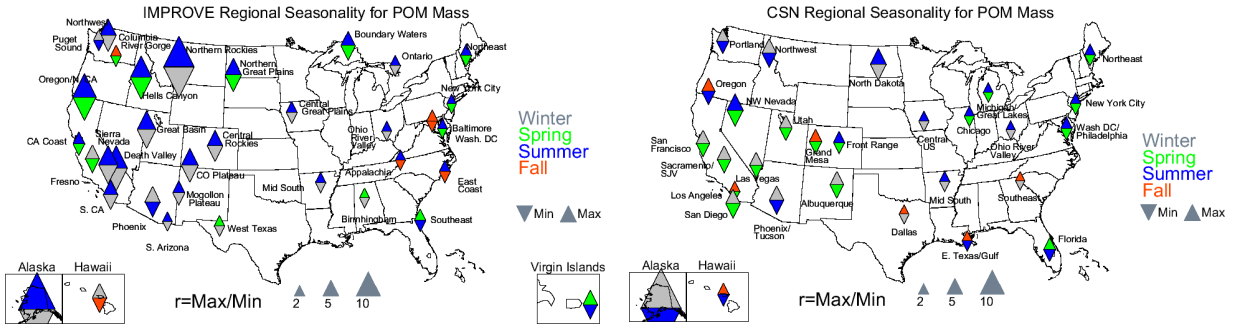

Figure S.4.3. (a) Seasonal variability for 2005–2008 monthly mean IMPROVE particulate organic matter (POM) mass concentrations. (b) The same as (a), but for the CSN. The color of the upward-pointing triangle refers to the season with the maximum monthly mean concentration, and the downward-pointing triangle refers to the season with the minimum monthly mean concentration. The size of the triangles refers to the magnitude of the ratio of maximum to minimum monthly mean mass concentration.

S.4.4 Light Absorbing Carbon

IMPROVE LAC monthly mean concentrations corresponded to some degree of seasonality, although less than POM concentrations. Western regions corresponded to a higher degree of seasonality compared to the eastern United States (Figure S.4.4a). Many western regions corresponded to summer maxima and winter minima. Similar to POM concentrations, some of the urban IMPROVE regions had the opposite seasonality (winter maxima/summer minima). Several eastern regions corresponded to fall maxima. CSN LAC concentrations demonstrated a degree of seasonality similar to urban POM concentrations, but with different seasons corresponding to maximum and minimum, especially in the eastern United States (Figure S.4.4.b). Several western regions corresponded to winter maxima and spring minima and higher seasonality compared to eastern regions. In contrast, several eastern regions had fall maxima and summer minima.

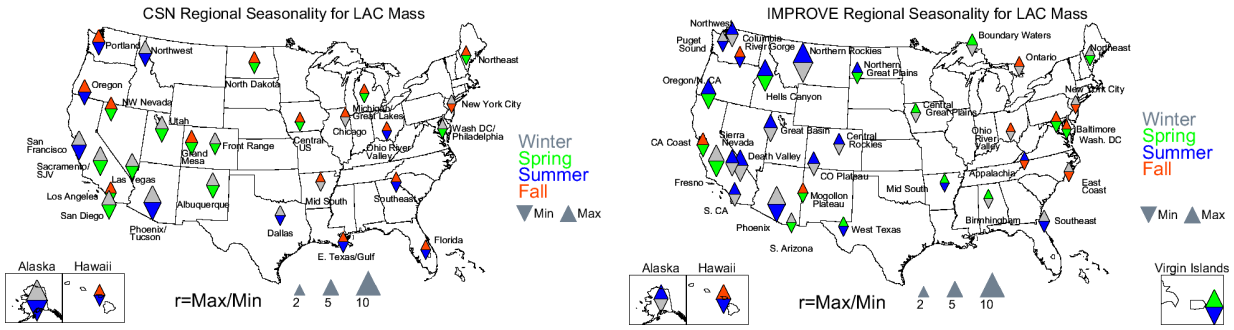

Figure S.4.4. (a) Seasonal variability for 2005–2008 monthly mean IMPROVE light absorbing carbon (LAC) mass concentrations. (b) The same as (a), but for the CSN. The color of the upward-pointing triangle refers to the season with the maximum monthly mean concentration, and the downward-pointing triangle refers to the season with the minimum monthly mean concentration. The size of the triangles refers to the magnitude of the ratio of maximum to minimum monthly mean mass concentration.

S.4.5 $PM_{2.5}$ Soil Mass

IMPROVE monthly mean soil concentrations were highly seasonal, with only four regions having maximum to minimum ratios less than 2 (all urban regions), consistent with the often episodic impacts of soil emissions. Maxima occurred primarily in the spring in the western and southwestern United States and in summer in the northwestern and eastern United States for most regions, and minima often occurred in winter. CSN urban regions experienced a much lower degree of seasonality compared to IMPROVE rural regions (Figure S.4.5b), especially in the western United States. While the seasons corresponding to maxima and minima were similar, the range in concentration between minimum and maximum months was much lower.

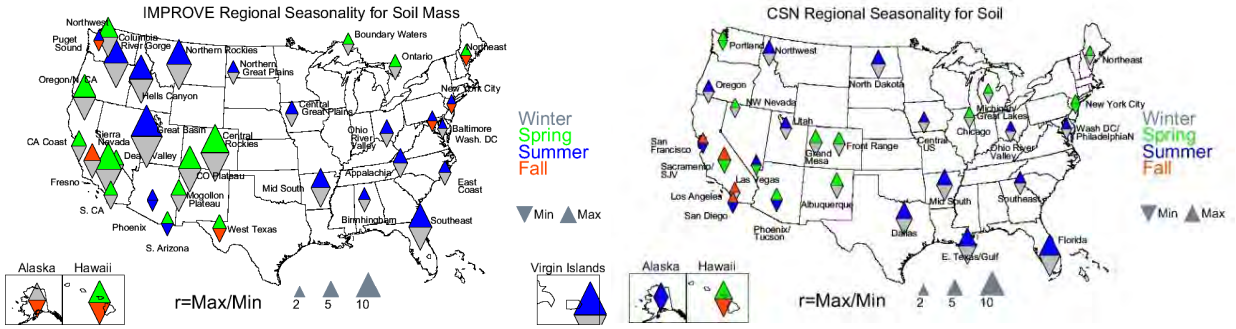

Figure S.4.5. (a) Seasonal variability for 2005–2008 monthly mean IMPROVE fine soil mass concentrations. (b) The same as (a), but for the CSN. The color of the upward-pointing triangle refers to the season with the maximum monthly mean concentration, and the downward-pointing triangle refers to the season with the minimum monthly mean concentration. The size of the triangles refers to the magnitude of the ratio of maximum to minimum monthly mean mass concentration.

S.4.6 $PM_{2.5}$ Gravimetric Fine Mass

Most of the IMPROVE regions corresponded to summer maxima and winter minima in FM monthly mean concentrations, with the exception of several regions along the eastern coast that had summer maxima and fall minima (Figure S.4.6a). Summer maxima in the western United States were most likely associated with the seasonal dominance of POM concentrations in the northwestern and southwestern United States (Figure S.4.3a). Eastern regional maxima were most likely associated with summer peaks in AS concentrations (see Figure S.4.1a). In general, FM concentrations were less seasonal compared to concentrations in individual species. Higher seasonality occurred in the western compared to the eastern United States. In contrast to the IMPROVE network, many CSN regions corresponded to winter maxima and spring minima in CSN monthly mean FM concentrations (Figure S.4.6b). The regional seasonal patterns of CSN FM concentrations were very different than the IMPROVE regional seasonal patterns. Many regions in the western United States corresponded to winter maxima and spring minima, most likely due to the prevalence of peaks in AN and POM concentrations in winter (see Figure S.4.2b). Eastern regions corresponded to summer maxima and winter and fall minima and probably were associated with summer peaks in AS concentrations, since it dominated FM in summer in this area. In general, the urban regions demonstrated a lower degree of seasonality in FM concentrations compared to rural regions.

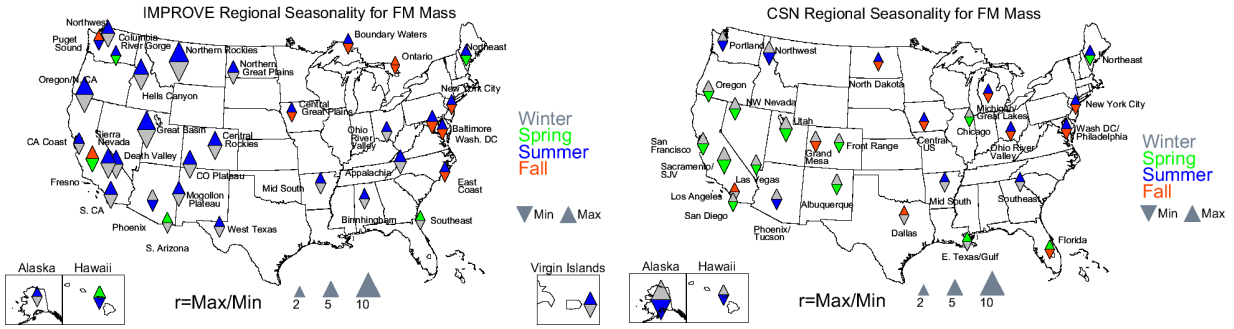

Figure S.4.6. (a) Seasonal variability for 2005–2008 monthly mean IMPROVE $PM_{2.5}$ gravimetric fine mass (FM) concentrations. (b) The same as (a), but for the CSN. The color of the upward-pointing triangle refers to the season with the maximum monthly mean concentration, and the downward-pointing triangle refers to the season with the minimum monthly mean concentration. The size of the triangles refers to the magnitude of the ratio of maximum to minimum monthly mean mass concentration.

S.4.7 Discussion

The differences observed in the seasonal and spatial patterns in species concentrations for the rural regions of the IMPROVE network and the urban locations in the CSN network are indicative of the spatial extent of aerosol sources, atmospheric processes, regional transport, and sinks. For example, AS seasonal patterns and concentrations were similar for corresponding IMPROVE rural and CSN urban regional groups, with summer maxima in the eastern half of the country. This pattern reflected the higher emissions of sulfur dioxide in this region and favorable conditions for aerosol formation in summer. Seasonal patterns in AN were consistent between CSN and IMPROVE regions. Winter maxima were observed for urban locations and in the central United States, demonstrating the regional impacts of agricultural sources in that area and favorable aerosol formation conditions during that season. CSN urban AN concentrations were considerably higher than rural IMPROVE concentrations. Maximum contributions of AN to fine mass occurred in winter for both rural and urban regions.

The strong summer maxima in POM concentrations at western rural regions contrasted with the summer/fall/winter maxima observed at CSN urban regions, suggesting that wildfire activity is a major contributor to POM concentrations in rural areas, especially in the western and northwestern United States in summer. Biogenic secondary organic aerosol also could have contributed significantly to high summer POM concentrations as well (Bench et al., 2007). Winter urban maxima at some urban regions were probably due in part to meteorological conditions but also to local sources. LAC concentrations followed patterns similar to POM concentrations, although summer maxima rural concentrations were not as dominant as POM concentrations. CSN LAC concentrations corresponding to fall/winter urban maxima were probably associated with local sources like residential heating and transportation. Both CSN POM and LAC concentrations were considerably higher than those measured in rural IMPROVE regions.

Soil concentrations were influenced by both local and long-range transport. Major regions of higher dust concentrations were evident in the urban and rural regions, especially in the southwestern United States in spring/summer and Southeast/Gulf regions in summer. Both networks had many “hot spots” of high soil that were similar in some seasons and not others,

suggesting fairly localized fugitive dust sources (Kavouras et al., 2007; 2009). The maximum contributions of soil to fine mass occurred in spring for many rural and urban regions, perhaps associated with agricultural sources. While the seasons corresponding to maxima and minima for coarse mass and fine soil concentrations agreed in some regions (e.g., the northwestern United States), for most regions these seasons did not coincide. One would expect that if soil was the main contributor to CM, their seasonality would be similar. However, based on work by Malm et al. (2007), who investigated the speciation of CM at select IMPROVE sites for a year, the speciation of CM varied significantly depending region and month. The only regions with consistent seasonal maxima and minima between soil and CM were the Columbia River Gorge, Hells Canyon, Northern Rocky Mountains, Great Basin, Death Valley, and Colorado Plateau regions. It is possible and probably quite likely that the seasonality of CM was impacted by the variability of species other than soil.

Gravimetric fine mass concentrations were noticeably higher in urban regions than rural regions. The highest concentrations of fine mass for the CSN network occurred in California, in the Sacramento/San Joaquin Valley region during December, where AN and POM composed the majority of the fine mass. Similarly, the urban IMPROVE site of Fresno had the highest fine mass concentrations in November, again dominated by AN and POM. The highest IMPROVE nonurban fine mass concentration corresponded to the Appalachia region in the eastern United States in August, where AS dominated the fine mass composition in summer.

S.5 SPATIAL AND SEASONAL PATTERNS IN RELATIVE RECONSTRUCTED AEROSOL LIGHT EXTINCTION COEFFICIENTS

Reconstructed aerosol light extinction coefficients (b_{ext}) were computed from speciated aerosol mass concentrations, multiplied by the species' extinction efficiency and the humidification factor (f(RH)), and summed over all species. The extinction algorithm used to compute b_{ext} in this report was somewhat different than the algorithm applied in previous reports, based on recommendations from a review of the algorithm (Hand and Malm, 2006). The original algorithm included contributions from $PM_{2.5}$ species such as ammonium sulfate (AS), ammonium nitrate (AN), particulate organic matter (POM), light absorbing carbon (LAC), and soil, and coarse mass (CM), and a constant term for Rayleigh scattering contributions (10 Mm^{-1}). The modified original algorithm used in this report included contributions from the above species, in addition to sea salt, site-specific Rayleigh scattering, and a change in the multiplier used to convert organic carbon to POM from 1.4 to 1.8. A similar f(RH) factor was applied to AS and AN, while an f(RH) for sea salt was computed specifically (see Chapter 3). The algorithm used in this report adopted some of the features of the revised algorithm used by the Regional Haze Rule (Pitchford et al., 2007) but applies constant mass extinction efficiency values for each aerosol component as used by the original IMPROVE algorithm. Mean light extinction coefficients computed this way should not differ significantly from those that would be obtained using the revised IMPROVE algorithm. The modified original algorithm is presented in equation S.5.1:

$$b_{ext} = 3f(RH)[\text{ ammonium sulfate}] + 3f(RH)[\text{ammonium nitrate}] + 4[\text{particulate organic matter}] + 10[\text{light absorbing carbon}] + 1[\text{soil}] + 1.7f(RH)_{ss}[\text{sea salt}] + 0.6[\text{coarse mass}] + \text{site-specific Rayleigh scattering} \quad \text{S.5.1}$$

The units of b_{ext} and Rayleigh scattering are in inverse megameters (Mm^{-1}). Mass concentrations of aerosol species are in $\mu g\ m^{-3}$, and mass scattering and absorption efficiencies have units of $m^2\ g^{-1}$. Values of 3 $m^2\ g^{-1}$ were used for both ammonium sulfate and ammonium nitrate, 4 $m^2\ g^{-1}$ for particulate organic matter, 10 $m^2\ g^{-1}$ for light absorbing carbon, 1 $m^2\ g^{-1}$ for soil, 1.7 $m^2\ g^{-1}$ for sea salt, and 0.6 $m^2\ g^{-1}$ for coarse mass. These values correspond to a wavelength of 550 nm.

Visual range and extinction measurements are nonlinear with respect to human perception of visual scene changes caused by haze. The haziness index expressed in deciview units (dv) was developed such that a 1 dv change would be a small but likely perceptible change in uniform haze conditions, regardless of the baseline visibility level (Pitchford and Malm, 1994). Haziness index values increase with increased light extinction coefficients, with a value of 0 dv corresponding to an extinction coefficient of 10 Mm^{-1}(i.e., pristine conditions). Deciview values were calculated from reconstructed total light extinction coefficients (including contributions from $PM_{2.5}$ species, coarse mass, and site-specific Rayleigh scattering instead of a constant 10 Mm^{-1}). The spatial variability in dv and b_{ext} are analogous to the spatial variability in aerosol mass concentrations; however, because of relative humidity effects on b_{ext}, the relative contributions from individual species to total b_{ext} may be different than their contributions to reconstructed fine mass.

Monthly mean (2005–2008) reconstructed b_{ext} values were computed for the major aerosol species listed earlier. These monthly mean b_{ext} values were averaged to regional means based on the IMPROVE and CSN regions discussed in section S.1 and Chapter 1. Highlights of the spatial and seasonal patterns in dv, and the seasonal and regional patterns in the monthly mean relative contribution of individual $PM_{2.5}$ species to b_{ext} are presented for AS, AN, POM, LAC, soil, and sea salt. The relative contribution of individual species to b_{ext} can vary significantly depending on the season or region and is important for understanding the causes of haze. In addition, the contribution of a given species to total b_{ext} can be quite different than its contribution to RCFM due to hygroscopic effects and relative optical efficiencies. Seasonal stacked bar charts for relative b_{ext} are grouped onto maps corresponding to four areas of the country: the northwestern, southwestern, and eastern United States, and OCONUS (Outside the Contiguous United States, e.g., Hawaii, Alaska, and Virgin Islands). Further details regarding the seasonality in absolute reconstructed b_{ext} can be found in Chapter 5, including results for CSN regions.

S.5.1 Deciview

The annual mean dv is presented in the spatial map in Figure S.5.1a. The highest dv occurred in the eastern United States and along the Ohio River valley. The values ranged from 4.65 to 22.19. The major contributor to dv in the eastern United States was AS. Higher dv values in the western United States corresponded to contributions from AN and POM. Soil contributed to dv in the southwestern United States. Further discussions of the relative contributions of individual species to visibility degradation will be provided in sections S.5.2–S.5.4.

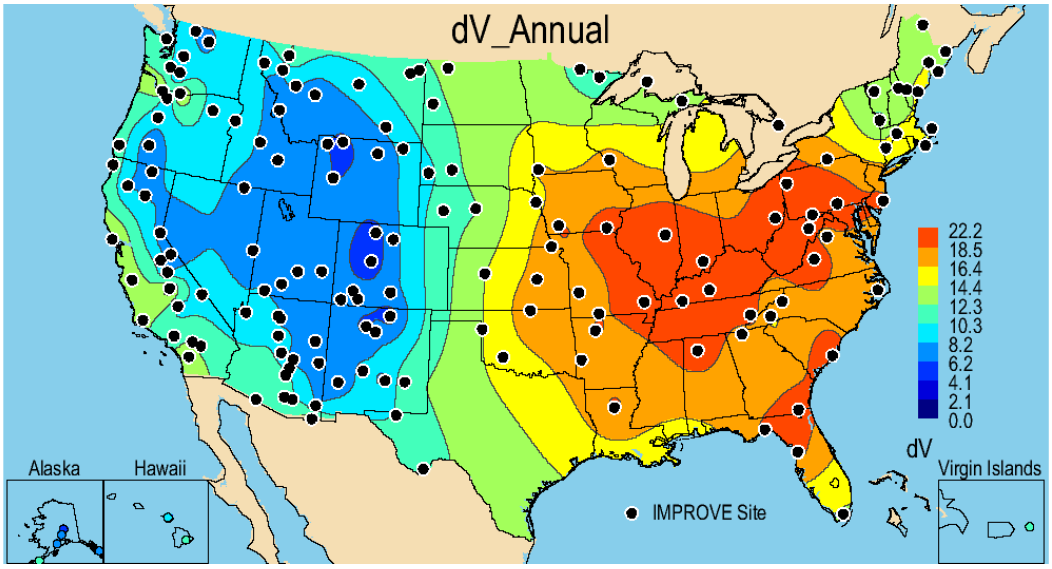

Figure S.5.1a. Annual mean $PM_{2.5}$ deciview (dv) for 2005–2008 for rural IMPROVE sites. Wavelength corresponds to 550 nm.

The seasonality in dv is shown in Figure S.5.1b. Maximum dv occurred in summer for most of the IMPROVE regions, probably associated with POM in the western and AS in the eastern United States. The high AS mass concentrations in summer in the eastern United States, along with increased relative humidity, lead to decreased visibility on regional scales during summer months. Winter maxima also occurred, as did spring. Fall maxima occurred only at the Puget Sound region. Winter and fall minima were common for most regions.

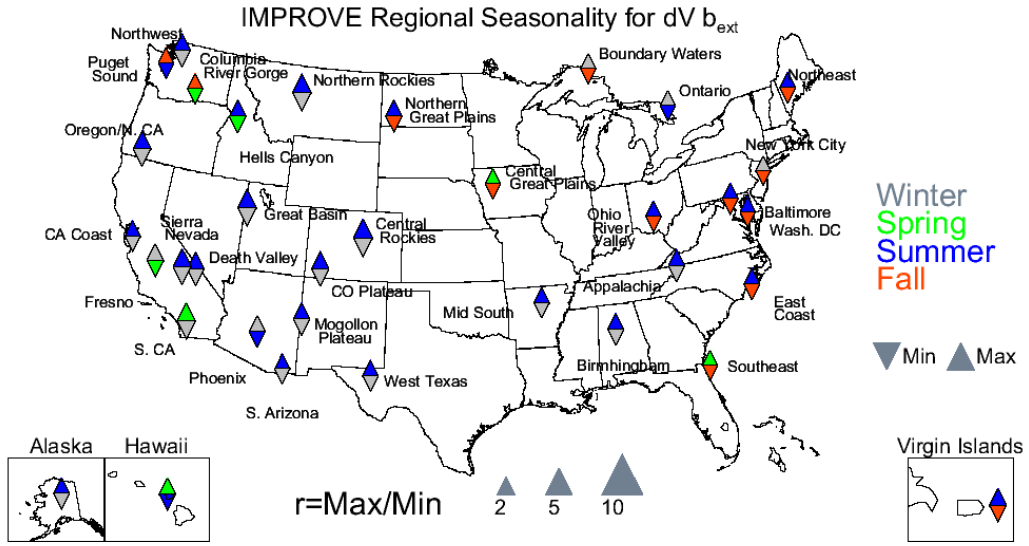

Figure S.5.1b. Seasonal variability for 2005–2008 monthly mean IMPROVE deciview (dv) light extinction coefficient (b_{ext}). The color of the upward-pointing triangle refers to the season with the maximum monthly mean concentration, and the downward-pointing triangle refers to the season with the minimum monthly mean concentration. The size of the triangles refers to the magnitude of the ratio of maximum to minimum monthly mean mass concentration.

S.5.2 Ammonium Sulfate Light Extinction Coefficients

Reconstructed light extinction coefficients from AS, b_{ext_AS}, were computed using a dry extinction efficiency of 3 m^2 g^{-1} and a humidification factor (f(RH)) to account for growth of the hygroscopic aerosol under elevated relative humidity conditions (see equation S.5.1). The b_{ext_AS} may closely resemble AS mass concentrations, but differences will arise due to hygroscopic effects. The largest relative b_{ext} contribution from AS to b_{ext} occurred at the Hawaii region in March (84.6%), most likely due to volcanic emissions, and contributions were 60% or greater year-round (Figure S.5.2.1). AS dominated b_{ext} in the eastern United States, with percent contributions ranging from 40% up to ~80% during summer (Figure S.5.2.2). The percent contribution of AS to b_{ext} was lower in the southwestern United States, roughly 20–40% at most regions (Figure S.5.2.3) but was slightly higher than the AS mass fractions in the same regions. A similar pattern was observed at the regions in the northwestern United States, where b_{ext_AS} fractions were higher than AS mass fractions. Percent contributions of AS to b_{ext} ranged from 15 to 50% and decreased during summer months at every region except the Columbia River Gorge region (Figure S.5.2.4). The seasonal b_{ext_AS} was similar to AS mass concentrations, with strong summer maxima and winter minima, However, most IMPROVE regions did not experience highly seasonal contributions of AS to b_{ext}, suggesting that AS was a consistent contributor to b_{ext} year-round.

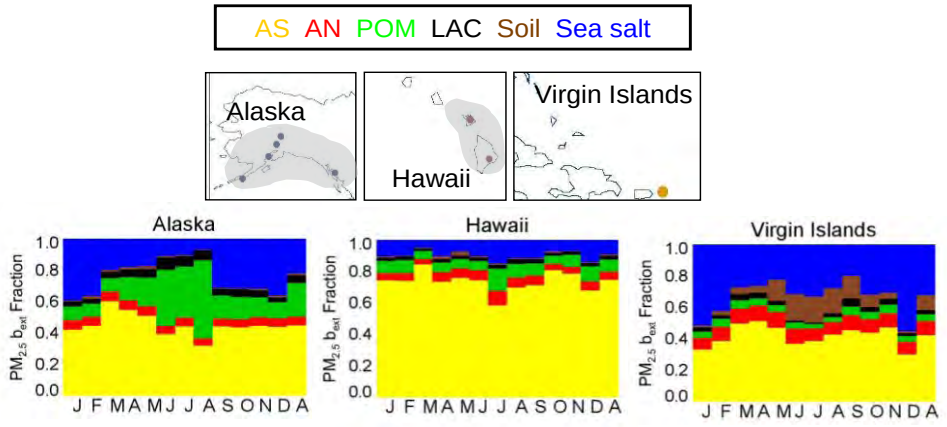

Figure S.5.2.1. IMPROVE regional monthly mean (2005–2008) $PM_{2.5}$ light extinction coefficient (b_{ext}) fractions for Hawaii, Alaska, and the Virgin Islands. The letters on the x-axis correspond to the month and "A" corresponds to "annual" mean. Ammonium sulfate (AS) is in yellow, ammonium nitrate (AN) in red, particulate organic matter (POM) in green, light absorbing carbon (LAC) in black, soil in brown, and sea salt in blue. The shaded area corresponds to the regions that comprise the sites, shown as dots.

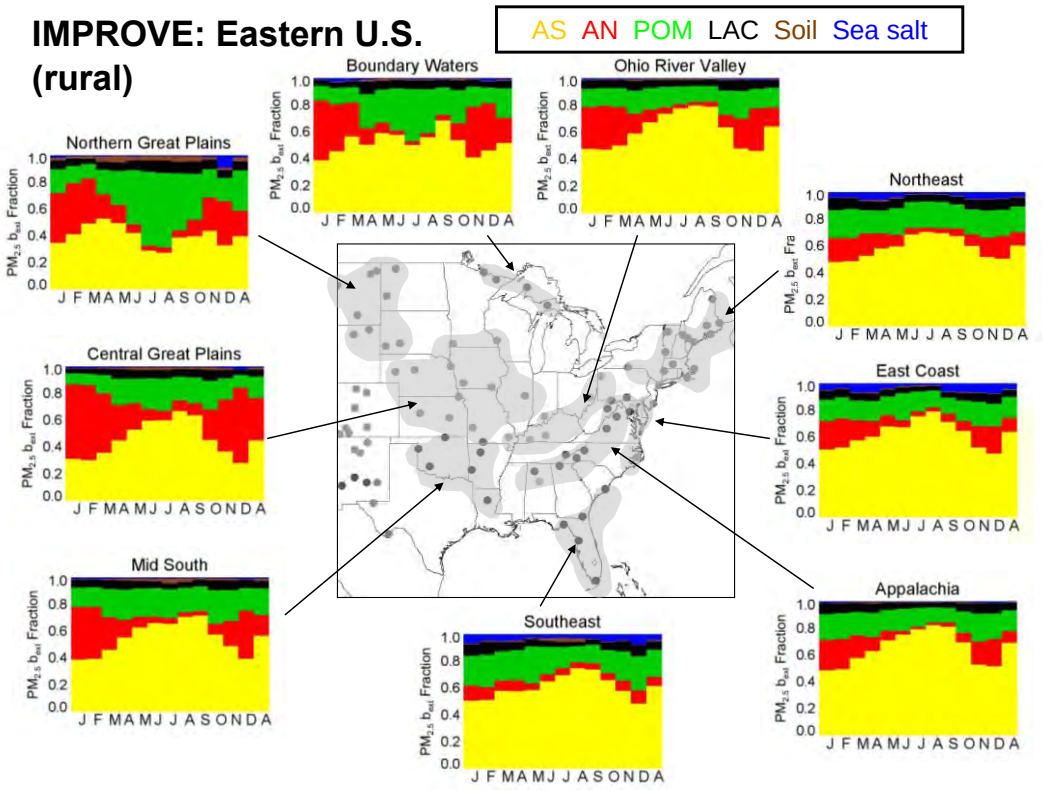

Figure S.5.2.2. IMPROVE regional monthly mean (2005–2008) $PM_{2.5}$ light extinction coefficient (b_{ext}) fractions for the eastern United States. The letters on the x-axis correspond to the month and "A" corresponds to "annual" mean. Ammonium sulfate (AS) is in yellow, ammonium nitrate (AN) in red, particulate organic matter (POM) in green, light absorbing carbon (LAC) in black, soil in brown, and sea salt in blue. The shaded area corresponds to the regions that comprise the sites, shown as dots.

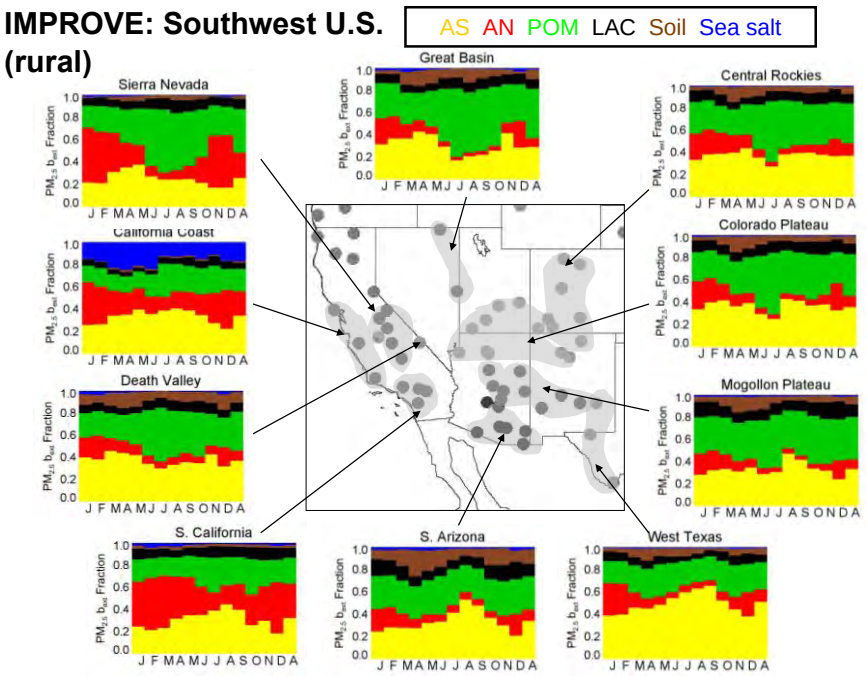

Figure S.5.2.3. IMPROVE regional monthly mean (2005–2008) $PM_{2.5}$ light extinction coefficient (b_{ext}) fractions for the southwestern United States. The letters on the x-axis correspond to the month and "A" corresponds to "annual" mean. Ammonium sulfate (AS) is in yellow, ammonium nitrate (AN) in red, particulate organic matter (POM) in green, light absorbing carbon (LAC) in black, soil in brown, and sea salt in blue. The shaded area corresponds to the regions that comprise the sites, shown as dots.

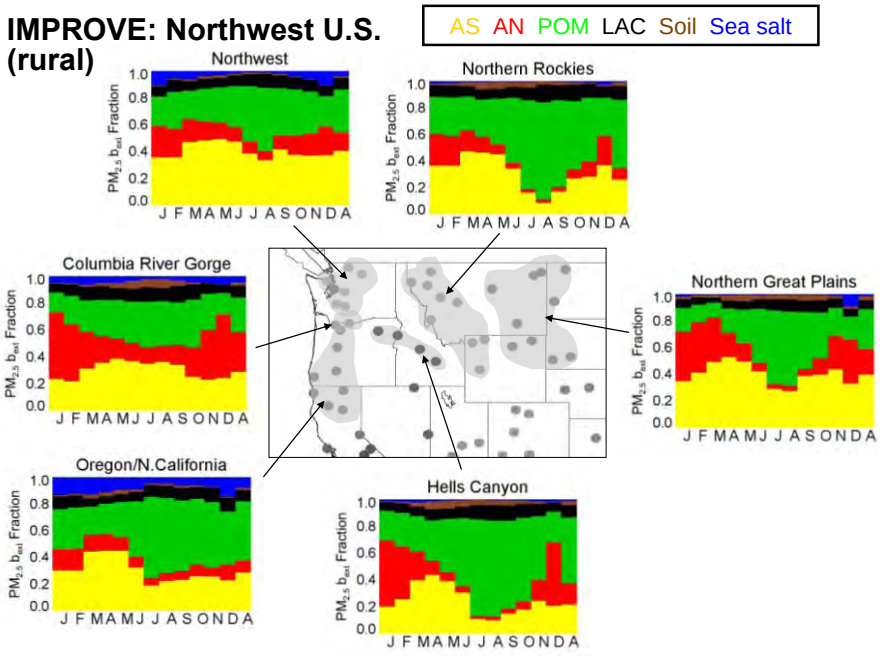

Figure S.5.2.4. IMPROVE regional monthly mean (2005–2008) $PM_{2.5}$ light extinction coefficient (b_{ext}) fractions for the northwestern United States. The letters on the x-axis correspond to the month and "A" corresponds to "annual" mean. Ammonium sulfate (AS) is in yellow, ammonium nitrate (AN) in red, particulate organic matter (POM) in green, light absorbing carbon (LAC) in black, soil in brown, and sea salt in blue. The shaded area corresponds to the regions that comprise the sites, shown as dots.

S.5.3 Ammonium Nitrate Light Extinction Coefficients

The extinction efficiency and f(RH) values used to compute the contributions of AN to b_{ext} (b_{ext_AN}) were the same as those used to compute b_{ext_AS}. In a similar manner, while general spatial and seasonal patterns of b_{ext_AN} mostly follow AN mass concentrations, differences may occur due to hygroscopic effects. The AN contributions to b_{ext} were generally the lowest in the eastern United States (Figure S.5.2.2). Values reached 40% or more in winter at regions in the central United States. In fact, AN dominated the IMPROVE b_{ext} in the Central Great Plains region in December (56.2%) (Figure S.5.2.2). Contributions of AN to b_{ext} were even higher than its contributions to reconstructed fine mass (RCFM) at these regions, in part due to its hygroscopic properties and higher extinction efficiencies relative to other species (e.g., soil). Percent contributions of AN to b_{ext} of 40% were common at rural IMPROVE regions in the northwestern United States (Figure S.5.2.4). The relative contribution of AN to b_{ext} was somewhat lower in the southwestern United States (Figure S.5.2.3). Values near 20% were more common for regions in this area, although higher contributions in the winter still occurred. These regions also experienced higher contributions of AN to b_{ext} compared to RCFM but not to the same degree as other regions in the United States. Compared to other regions, the AN contributions to b_{ext} in the OCONUS regions were relatively low (<10%) (Figure S.5.2.1). Most IMPROVE regions showed a high degree of seasonality for the contribution of AN to b_{ext}, and most regions corresponded to winter maxima and summer minima.

S.5.4 Particulate Organic Matter Light Extinction Coefficients

POM light extinction coefficients (b_{ext_POM}) were scaled to POM mass because, unlike AS and AN, POM was considered nonhygroscopic. On a similar dry mass basis, b_{ext_POM} would be higher than that for b_{ext_AS} or b_{ext_AN}, because its extinction efficiency was higher (4 m^2 g^{-1} versus 3 $m^2 g^{-1}$). While the patterns of b_{ext_POM} were the same as those of POM mass concentrations, its relative contribution to reconstructed b_{ext} was not because of the hygroscopic and optical properties of other species contributing to b_{ext}. In the eastern United States, the b_{ext_POM} fraction was generally lower than the POM mass fraction at several regions, due to the increased importance of hygroscopic AS on b_{ext}. The percent contribution of POM to b_{ext} was fairly constant year-round at most regions in the eastern United States (Figure S.5.2.2). Contributions of POM to b_{ext} were significant at regions in the northwestern United States (Figure S.5.2.4); however, the relative b_{ext_POM} values were generally lower than POM mass fraction for these regions. POM contributions to b_{ext} were typically 20–30% at most regions in the southwestern United States (Figure S.5.2.3). The Alaska region was the only OCONUS region that had considerable contributions of POM to b_{ext} (Figure S.5.2.1). These contributions peaked in summer and dropped off fairly rapidly in fall, probably related to biomass burning emissions. Relative contributions of POM to b_{ext} were fairly low (~10% or less) in the Hawaii and Virgin Islands regions. The relative b_{ext_POM} had a much lower degree of seasonality compared to absolute b_{ext_POM}, especially in the western United States. Summer maxima were still the most common.

S.5.5 Light Absorbing Carbon Light Extinction Coefficients

Light extinction coefficients due to LAC (b_{ext_LAC}) were computed by scaling the LAC mass by its extinction efficiency (10 m^2 g^{-1}), which is higher than the other species due to its

ability to both scatter and absorb visible light. This higher extinction efficiency increased LAC's relative contribution to b_{ext} compared to its contributions to RCFM, especially at most regions in the eastern United States. Contributions were less than 10% at most regions and higher in fall and winter (Figure S.5.2.2). Somewhat higher LAC contributions to b_{ext} occurred for regions in the southwestern United States (Figure S.5.2.3). Relative b_{ext_LAC} contributions of 10% or more were common at most regions in the northwestern United States and fairly steady year-round (Figure S.5.2.4). Of the OCONUS regions, the Alaska region had the highest b_{ext_LAC} contributions (Figure S.5.2.1). The Hawaii and Virgin Islands regions had the lowest b_{ext_LAC} contributions of any regions in the United States; in fact, the smallest contribution in the United States occurred at the Virgin Islands region in July (0.97%). The relative b_{ext_LAC} had a much lower degree of seasonality compared to absolute b_{ext_LAC}, especially in the western United States. Summer minima were common in the eastern United States and at some regions in the southwestern United States.

S.5.6 $PM_{2.5}$ Soil Mass Light Extinction Coefficients

The soil extinction efficiency used to compute light extinction coefficients from soil (b_{ext_soil}) was 1 m^2g^{-1}. Soil is nonhygroscopic, therefore b_{ext_soil} values were the same as the soil mass concentrations, as were its seasonal and regional patterns. Relative contributions of soil to b_{ext} in the eastern United States were negligible at most rural regions, reaching only a few percent (Figure S.5.2.2). In contrast, soil contributions to RCFM reached 10–20% at these same regions, depending on time of year. Compared to the eastern United States, soil contributions to b_{ext} were higher in the southwestern United States and reached up to 15–20%, especially during spring months (Figure S.5.2.3). However, at these same regions soil contributed up to 50% to RCFM. Contributions of only a few percent were common at regions in the northwestern United States Figure S.5.2.4). Soil contributions to b_{ext} reached ~20% at the Virgin Islands region during summer (Figure S.5.2.1); however its contribution to RCFM was near 60% during the same months. Relative b_{ext_soil} values were low at other OCONUS regions. Strong seasonality in relative b_{ext_soil} for IMPROVE regions was observed. Contributions to b_{ext} from soil were typically highest in the spring. Most regional minima occurred during winter for relative b_{ext_soil}.

S.6 TRENDS IN IMPROVE SPECIATED AEROSOL MASS CONCENTRATIONS

As stated in the IMPROVE objectives, one of the main purposes of the network is to document long-term trends for assessing progress towards the national visibility goals. Twenty years of data were available to evaluate trends in this report for many sites within the IMPROVE network. Trend analyses were performed for "long-term" (1989–2008) and "short-term" (2000–2008) time periods for eight parameters: annual mean, 10^{th}, 50^{th}, and 90^{th} percentiles, and four seasons (winter, spring, summer, and fall). A Theil regression was performed with the concentration data as the dependent variable and the year as the independent variable (Theil, 1950). A trend was considered statistically significant at 5% ($p \leq 0.05$), meaning that there was a 95% chance that the slope was not due to random chance. Trends that were significant at 15% ($0.05 < p \leq 0.15$) are also reported. Further details regarding the linear regression calculations are provided in Chapter 6. "Trend" is defined as percent change per year (% yr^{-1}) and was computed by dividing the slope derived from the Theil regression by the median mass concentration value over the time period of the trend at a given site, multiplied by 100%. Reporting trend instead of

slope reflects the relative change in concentration at a given site. However, trends can be quite large (>100%) when median concentrations are very low (e.g., 10th percentile).

Long-term trends for sulfate ion, total carbon (TC = organic carbon + light absorbing carbon), fine soil, fine mass (FM), coarse mass (CM), and PM_{10} concentrations were computed. In addition to the species listed above, short-term trends were computed for nitrate ion. Highlights from the trend analyses are presented here; details can be found in Chapter 6.

Trend results for each species and site are presented on maps of the United States. Sites with positive trends with significance levels of 95% and greater ($p \leq 0.05$) correspond to solid red, upward-pointing triangles. Positive trends with significance levels of 85–95% ($0.05 < p \leq 0.15$) correspond to red, unfilled, upward-pointing triangles. A similar methodology was applied to sites with decreasing trends but in blue. Sites with insignificant trends correspond to black-filled triangles. The size of the triangle corresponds to the magnitude of the trend, with the same scale maintained for all species and parameters for comparison purposes. Sites with no significant trends are shown as black triangles.

S.6.1 Sulfate Ion Trends

Decreasing trends in sulfate ion concentrations were typical for most IMPROVE sites, regardless of the percentile, season, or time period. Both the 10th percentile and winter season corresponded to sites with large negative significant trends as shown in the map of average winter long-term sulfate ion trends in Figure S.6.1.1. Recall that the lowest concentrations in regional mean ammonium sulfate (derived from sulfate ion concentrations) from 2005 through 2008 occurred during winter in the southwestern United States (see Figure S.4.1a). The long-term trends suggested that the lowest sulfate ion concentration days, most likely occurring in winter, have been decreasing for several years at many sites.

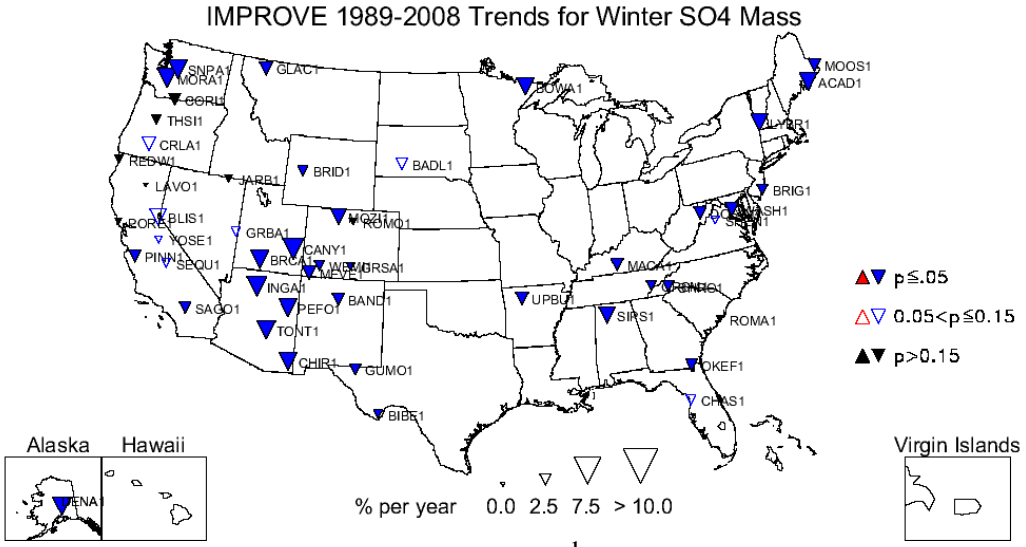

Figure S.6.1.1. Long-term (1989–2008) trends (% yr^{-1}) in average winter sulfate ion mass concentrations. Sites with statistically significant trends ($p \leq 0.05$) are designated by filled red (increasing) and blue (decreasing) triangles. Insignificant trends ($p > 0.15$) are designated by filled black triangles.

In comparison, the 90th percentile, spring and summer season trends in sulfate ion concentrations were less negative (not shown). In fact, positive long-term trends occurred at Big Bend, Texas (BIBE1), for the 90th percentile and spring season and also at Lassen Volcanic NP, California (LAVO1), during summer. These sites were the only IMPROVE locations that corresponded to positive sulfate ion trends for any long-term trend parameter investigated.

A larger number of sites had significant positive short-term sulfate ion trends compared to the long-term trends. In fact, some sites with decreasing long-term trends had positive short-term trends. For example, sulfate ion concentrations at the Denali, Alaska, site (DENA1) started increasing in later years. Upward-trending sulfate ion concentrations occurred during the most recent 10 years at DENA1, which was the period evaluated for the short-term trend analyses.

The least negative overall short-term sulfate ion trends occurred for the 50th percentile and spring season. Short-term sulfate ion trends during spring were very interesting, as shown in Figure S.6.1.2. Many sites in the western United States corresponded to positive trends in the spring, the only season to exhibit such patterns. Recall that the maximum monthly mean ammonium sulfate concentrations also occurred in spring for many regions in the western United States (see Section S.4.1).

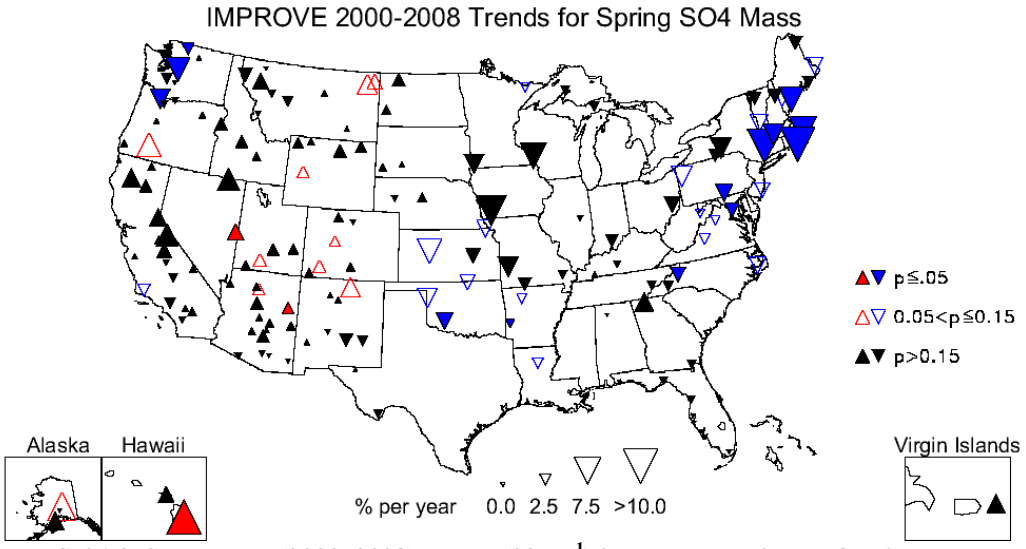

Figure S.6.1.2. Short-term (2000–2008) trends (% yr^{-1}) in average spring sulfate ion mass concentrations. Sites with statistically significant trends (p≤0.05) are designated by filled red (increasing) and blue (decreasing) triangles. Insignificant trends (p>0.15) are designated by filled black triangles.

S.6.2 Nitrate Ion Trends

During the late 1990s, IMPROVE nitrate ion concentrations at many sites fell below historical values during winter months. Investigations into a period from 1996 to 2000 revealed lower than usual concentrations during winter months, and the cause remains unknown (McDade, 2007). Concentrations returned to normal levels after 2000, after which the data were deemed valid. Given these uncertainties in earlier nitrate ion concentrations, only short-term trends for nitrate ion concentrations were computed.

The 10th percentile nitrate ion trends at most sites were relatively large compared to the sulfate ion trends and highly significant ($p<0.05$) at most sites around the United States (see Figure S.6.2.1). No sites were associated with positive 10th percentile, short-term nitrate ion trends. Large decreasing trends occurred for sites all around the United States during fall months, and no positive trends occurred at any site for fall or summer seasons.

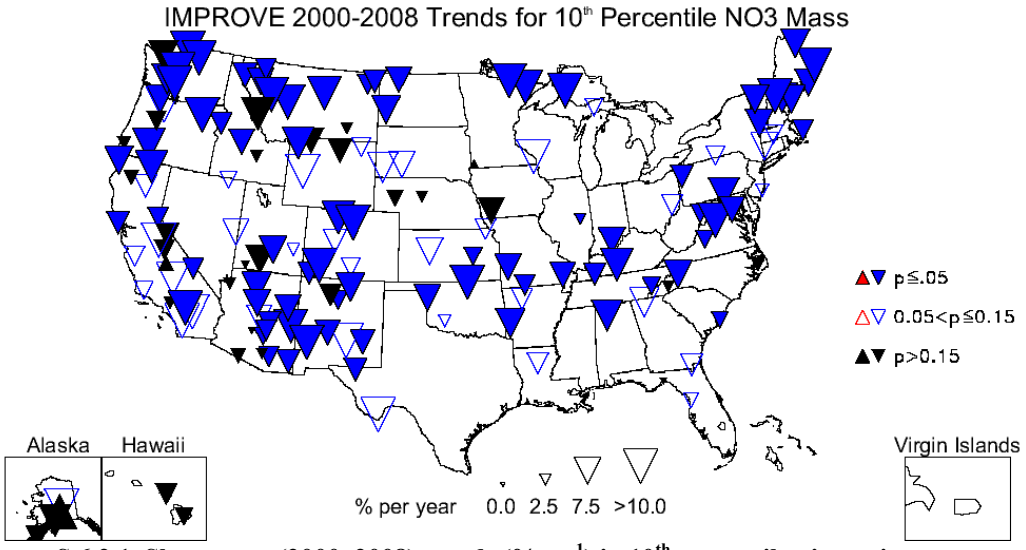

Figure S.6.2.1. Short-term (2000–2008) trends (% yr^{-1}) in 10th percentile nitrate ion mass concentrations. Sites with statistically significant trends ($p\leq0.05$) are designated by filled red (increasing) and blue (decreasing) triangles. Insignificant trends ($p>0.15$) are designated by filled black triangles.

A map for the 50th percentile trends is shown in Figure S.6.2.2. As was the case with the trends for the 10th percentile and fall season, the magnitude of 50th percentile nitrate ion trends was fairly consistent for most sites across the United States, although several sites in the Mountain West corresponded to less significant ($p\leq0.15$) negative trends. Positive trends occurred at several sites, including the Virgin Islands (VIIS1) and Denali, Alaska (DENA1), where the maximum monthly mean ammonium nitrate concentrations also occurred during spring months.

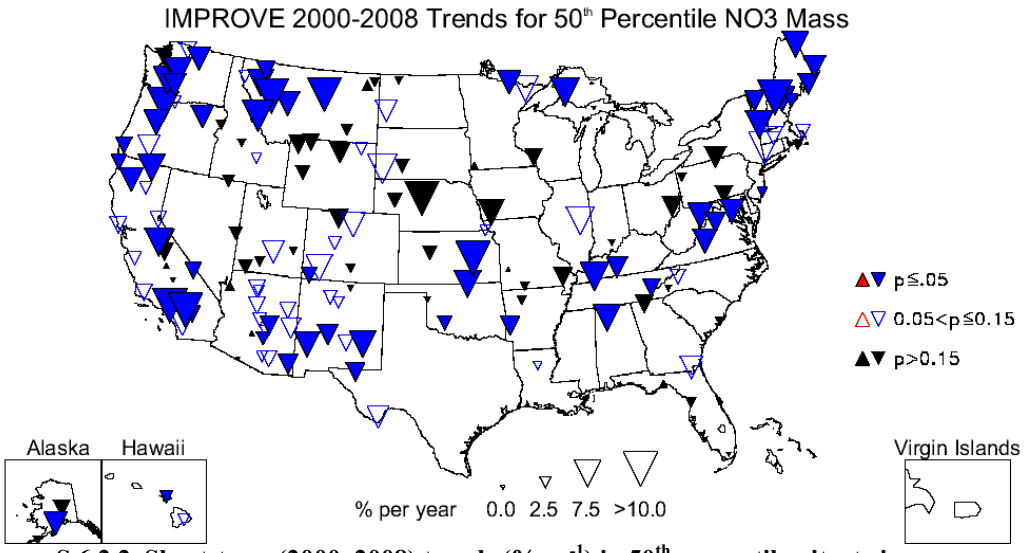

Figure S.6.2.2. Short-term (2000–2008) trends (% yr^{-1}) in 50th percentile nitrate ion mass concentrations. Sites with statistically significant trends (p≤0.05) are designated by filled red (increasing) and blue (decreasing) triangles. Insignificant trends (p>0.15) are designated by filled black triangles.

S.6.3 Total Carbon Trends

Trends in TC, rather than on OC and LAC, were computed because changes in analytical methods due to hardware upgrades on January 1, 2005, resulted in potential changes in the split between OC and LAC that introduced uncertainty to trend analyses (Chow et al., 2007; White, 2007). Higher LAC/TC ratios were reported after the change in analytical methods, but no changes in total carbon were detected.

The largest negative long-term TC trends corresponded to the 10th percentile and winter season (see map of 10th percentile TC trends in Figure S.6.3.1). Sites with larger negative trends were located along the western coast. No positive trends were associated with any site for 10th percentile concentrations. The winter season was also associated with large decreasing trends and corresponded to sites in the western United States. It is possible that the low TC concentrations associated with the 10th percentile occurred mainly in winter; in the western United States both OC and LAC were associated with minimum monthly mean concentrations (2005–2008) during winter months for many regions (see Figure S.4.3.a and Figure S.4.4.b, respectively). Concentrations on these already low concentration days in winter appeared to be decreasing.

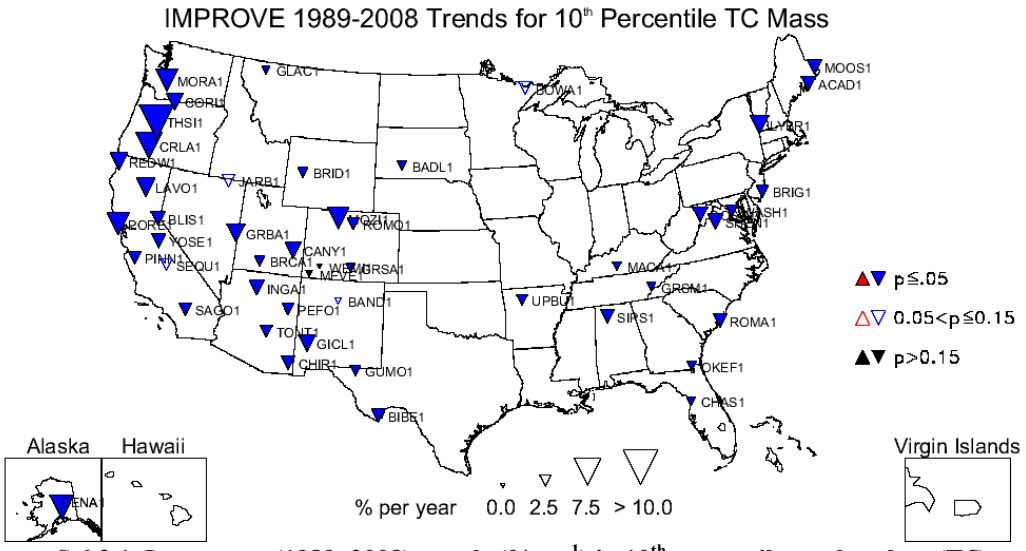

Figure S.6.3.1. Long-term (1989–2008) trends (% yr^{-1}) in 10th percentile total carbon (TC = organic carbon + light absorbing carbon) mass concentrations. Sites with statistically significant trends (p≤0.05) are designated by filled red (increasing) and blue (decreasing) triangles. Insignificant trends (p>0.15) are designated by filled black triangles.

Long-term, summer TC trends were associated with the largest number of significant positive trends of all parameters. Magnitudes of summer trends were fairly consistent (and low) around the United States. Recall that most regions in the western United States corresponded to summer maxima in both OC and LAC concentrations (Figures S.4.3.b and S.4.4.b, respectively). Unlike the strongly decreasing TC 10th percentile concentrations that likely occurred during winter days, the highest concentrations that were likely associated with summer months were decreasing to a much lower degree and at some sites actually increasing.

Short-term TC trends were much larger for many sites around the United States compared to long-term trends. There were no sites associated with positive short-term TC trends for any of the percentiles. Spring, summer, and fall, short-term, TC trends were associated with positive trends, with summer having the highest number.

S.6.4 Gravimetric $PM_{2.5}$ Fine Mass Trends

Given the previous discussions, one might attempt to deduce trends in $PM_{2.5}$ fine mass (FM), as it is largely composed of the species presented in previous sections. However, inferring FM trends based on the trends of other species is complicated because of the difference in the behavior and seasonality of a given species in relation to another. Due to sampling artifacts like those discussed in Chapter 8, FM does not equal the simple sum of all species. Finally, the significance level of trends at a given site may differ for individual species and for FM, complicating comparisons of trends at a specific location.

The magnitudes of 10th percentile, long-term FM trends were fairly similar across the United States, although sites in the southeastern United States had less negative trends, similar to the sulfate ion and TC 10th percentile trends (Figure S.6.4.1). No sites were associated with positive 10th percentile trends. Winter long-term FM trends were larger in magnitude (more

negative) at most sites compared to 10th percentile trends, and no sites corresponded to positive winter trends. FM monthly mean concentrations (2005–2008) were at a minimum during winter months for many regions in the United States (Figure S.4.6b). The negative winter trends suggested that the days with the lowest FM concentrations were getting cleaner.

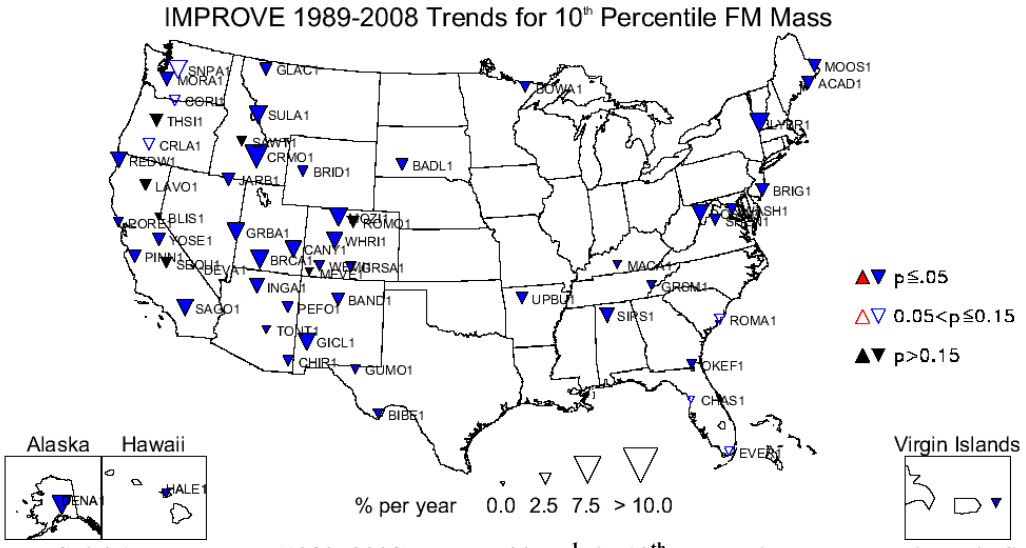

Figure S.6.4.1. Long-term (1989–2008) trends (% yr^{-1}) in 10th percentile $PM_{2.5}$ gravimetric fine mass (FM) concentrations. Sites with statistically significant trends (p≤0.05) are designated by filled red (increasing) and blue (decreasing) triangles. Insignificant trends (p>0.15) are designated by filled black triangles.

Positive long-term FM trends were associated with the 90th percentile and spring, summer, and fall seasons. Long-term FM trends in the summer in the eastern United States were decreasing at most sites. Many sites in the western United States were associated with either low, negative long-term FM trends or trends that were statistically insignificant. Most of the regions in the United States were associated with maximum FM monthly mean concentrations in the summer months (see Figure S.4.6.1b). Trend results suggested that these summer FM concentrations appeared to be decreasing less over time compared to other seasons.

All of the short-term FM trend parameters included some sites with positive trends. Several sites had positive 50th percentile, short-term trends, and eleven sites were associated with positive trends in fall, more than any other season. Most of these sites were located in the western United States and in Alaska and Hawaii. No sites in the eastern United States were associated with positive fall trends. The only species to be associated with positive short-term fall trends in the western United States were the sulfate ion (in Alaska, Hawaii and Arizona), soil (several sites in the western United States.), and total carbon at a couple of western sites; therefore the fall positive trends in FM in the western United States could be driven by different species, depending on the site.

Additional discussions of IMPROVE trends, including results for soil, CM, and PM_{10} can be found in Chapter 6. No trends were computed for CSN data because trends are sensitive to changes in CSN sampling methodology (e.g., sampler and analytical methodology vary from site to site and over time) and the network's shorter duration (established in 2000 with additional sites coming online over a period of several years).

The trend results presented in this section were intended as a summary of the temporal changes in the mass concentrations of major aerosol species over short and long time periods. Results suggested that, for most species, concentrations were decreasing at IMPROVE sites around the United States, and these decreasing trends were largest for the lowest concentrations and during winter seasons. Because normalized trends were presented, it is not surprising that the 10^{th} percentile trends were typically the largest in magnitude because they were normalized with the lowest concentrations. This general result may not hold for individual sites or for given species (e.g., soil) but overall this consistent pattern emerged. A similar pattern was reported in *Air Quality in National Parks 2009 Annual Performance and Progress Report* (NPS, 2010), which demonstrated larger decreasing trends in deciview on the clearest days compared to the haziest days.

S.7 REGIONAL HAZE RULE METRICS

The EPA established the Regional Haze Rule in 1999 (RHR, U.S. EPA, 1999), a major effort to improve air quality in national parks and wilderness areas. The RHR calls for state and federal agencies to collaborate to improve visibility in 156 visibility-protected federal Class I areas (CIA) (see Figure 1.1 in Chapter 1). The RHR specifies a default method to track progress towards the national visibility goal of no anthropogenic visibility impairment. The RHR focuses on reducing pollution on the 20% worst visibility days each year while allowing no degradation of the 20% best visibility days. Haziness is defined by the deciview metric and is calculated using the "original" IMPROVE algorithm (RHR1) or the "revised" IMPROVE algorithm (RHR2) (Pitchford et al., 2007). Since nearly all states and regional planning organizations used the RHR2 algorithm for state implementation plan development, modeling, and source apportionment, the RHR2 algorithm was applied in the analyses presented in Chapter 9. The RHR2 algorithm differs from that applied in the rest of the report in that it applies size mode-dependent mass extinction efficiencies.

Central to the RHR is the concept of the uniform rate of progress (URP). The URP is the yearly rate of change required to achieve natural dv conditions by 2064 in a linear fashion beginning in 2004. The URP provides a reference to evaluate progress made in the context of the change required to reach natural conditions in 60 years. It should be noted that the nature of emissions control programs makes it likely that actual progress will be somewhat erratic and that failure to achieve the URP at any point in the process should be considered in the context of changes to emissions inventories.

Descriptions and evaluations of RHR metrics are provided in Chapter 9 and Appendix G and H. These evaluations focus on comparisons of the 20% worst and best visibility days for the baseline (2000–2004) and period 1 (2005–2009) time periods. Summaries of the changes from baseline to period 1 compared to the URP are presented on maps to evaluate regional progress toward natural conditions. Detailed timelines and yearly data are also presented for case studies in Chapter 9 and for all complete IMPROVE regional haze tracking sites, organized by state, in Appendix H. The analysis provided in Chapter 9 is intended as an evaluation of the progress towards meeting RHR goals and should not necessarily be interpreted in the context of regulatory requirements.

REFERENCES

Bench, G., S. Fallon, B. Schichtel, W. Malm, and C. McDade (2007), Relative contributions of fossil and contemporary carbon sources to PM2.5 aerosols at nine Interagency Monitoring of Protected Visual Environments (IMPROVE) network sites, *J. Geophys. Res., 112,* D10205, doi:10.1029/2006JD007708.

Bond, T. C., and R. W. Bergstrom (2006), Light absorption by carbonaceous particles: An investigative review, *Aerosol Sci. Techno., 40,* 27-67.

Chow, J. C., J. G. Watson, L. C. Pritchett, W. R. Pierson, C. A. Frazier, and R. G. Purcell (1993), The DRI thermal/optical reflectance carbon analysis system: Description, evaluation and applications in U.S. air quality studies, *Atmos. Env., 27A(8)*, 1185-1201.

Chow, J. C., J. G. Watson, L.-W. A. Chen, M. C. O. Chang, N. F. Robinson, D. Trimble, and S. Kohl (2007), The IMPROVE_A temperature protocol for thermal/optical carbon analysis: Maintaining consistency with a long-term database, *J. Air & Waste Manage. Assoc., 57,* 1014-1023.

Debell, L. J., K. Gebhart, J. L. Hand, W. C. Malm, M. L. Pitchford, B. A. Schichtel, and W. H. White (2006), IMPROVE (Interagency Monitoring of Protected Visual Environments): Spatial and seasonal patterns and temporal variability of haze and its constituents in the United States: Report IV, CIRA Report ISSN: 0737-5352-74, Colo. State Univ., Fort Collins, http://vista.cira.colostate.edu/improve/Publications/Reports/2006/2006.htm.

Hand, J. L., and W. C. Malm (2006), Review of the IMPROVE equation for estimating ambient light extinction coefficients, CIRA Report, ISSN: 0737-5352-71, Colo. State Univ., Fort Collins.

Kavouras, I. G., V. Etyemezian, J. Xu, D. W. Dubois, M. Green, and M. Pitchford (2007), Assessment of the local windblown component of dust in the western United States, *J. Geophys. Res., 112,* D08211, doi:10.1029/2006JD007832.

Kavouras, I. G., V. Etyemezian, D. W. Dubois, J. Xu, and M. Pitchford (2009), Source reconciliation of atmospheric dust causing visibility impairment in Class I areas of the western United States, *J. Geophys. Res., 114,* D02308, doi:10.1029/2008JD009923.

Malm, W. C., J. F. Sisler, M. L. Pitchford, M. Scruggs, R. Ames, S. Copeland, K. A. Gebhart, and D. E. Day (2000), IMPROVE (Interagency Monitoring of Protected Visual Environments): Spatial and seasonal patterns and temporal variability of haze and its constituents in the United States: Report III, CIRA Report ISSN: 0737-5352-47, Colo. State Univ., Fort Collins, http://vista.cira.colostate.edu/improve/Publications/Reports/2000/2000.htm.

Malm, W. C., M. L. Pitchford, C. McDade, and L. L. Ashbaugh (2007), Coarse particle speciation at selected locations in the rural continental United States, *Atmos. Environ., 41,* 2225-2239.

Malm, W. C., B. A. Schichtel, and M. L. Pitchford (2011), Uncertainties in $PM_{2.5}$ gravimetric and speciation measurements and what we can learn from them, *J. Air Waste Manage,* In press.

McDade, C. E. (2007), Diminshed wintertime nitrate concentrations in the late 1990s, Doc. # da0002, http://vista.cira.colostate.edu/improve/Data/QA_QC/Advisory/da0002/da0002_WinterNO3.pdf).

NPS (2010), Air quality in National Parks, 2009 Annual Performance and Progress Report, Natural Resource Report NPS/NRPC/ARD/NRR-2010/266., http://www.nature.nps.gov/air/Pubs/pdf/gpra/AQ_Trends_In_Parks_2009_Final_Web.pdf

Pitchford, M., W. Malm, B. Schichtel, N. Kumar, D. Lowenthal and J. Hand (2007), Revised algorithm for estimating light extinction from IMPROVE particle speciation data, *J. Air & Waste Manage. Assoc., 57,* 1326-1336.

Pitchford, M. L. and W. C. Malm (1994), Development and applications of a standard visual index, *Atmos. Environ, 28,* 5, 1049-1054.

Sisler, J. F., D. Huffman, and D. A. Latimer (1993), Spatial and temporal patterns and the chemical composition of the haze in the United States: An analysis of data from the IMPROVE network, 1988–1991, CIRA Report ISSN: 0737-5352-26, Colo. State Univ., Fort Collins, http://vista.cira.colostate.edu/improve/Publications/Reports/1993/1993.htm.

Sisler, J. F., W. C. Malm and K. G. Gebhart (1996), Spatial and seasonal patterns and long term variability of the composition of haze in the United States: An analysis of data from the IMPROVE network, CIRA Report ISSN: 0737-5352-32, Colo. State Univ., Fort Collins, http://vista.cira.colostate.edu/improve/Publications/Reports/1996/1996.htm.

Tanner, R. L., W. J. Parkhurst, M. L. Valente, and W. D. Phillips (2004), Regional composition of $PM_{2.5}$ aerosols measured at urban, rural, and "background" sites in the Tennessee valley, *Atmos. Environ., 38,* 3143-3153.

Theil, H. (1950), A rank-invariant method of linear and polynomial regression analysis, *Proc. Kon. Ned. Akad. V. Wetensch. A., 53,* 386-392, 521-525, 1397-1412.

Turpin, B. J., and H.-J. Lim (2001), Species contributions to $PM_{2.5}$ mass concentrations: Revisiting common assumptions for estimating organic mass, *Aerosol Sci. Technol., 35,* 602-610.

U.S. EPA (1999), Regional Haze Regulations; Final Rule, 40 CFR 51, Federal Register, 64, 35714-35774.

White, W. H. (2007), Shift in EC/OC split with 1 January 2005 TOR hardware upgrade, Doc. # da0016, http://vista.cira.colostate.edu/improve/Data/QA_QC/Advisory/da0016/da0016_TOR2005.pdf.

Chapter 1. Interagency Monitoring of Protected Visual Environments (IMPROVE) Network: Configuration and Measurements

1.1 INTRODUCTION

The Regional Haze Rule (RHR, U.S. EPA, 1999a) requires monitoring in locations representative of the 156 visibility-protected federal Class I areas (CIA, see Figure 1.1) in order to track progress toward the goal of returning visibility to natural conditions. Air quality monitoring under the RHR began in 2000. The haziness index in deciview units (Pitchford and Malm, 1994), calculated from speciated particle composition concentrations, was selected to track haze levels for the RHR. Computing the haziness index from particle speciation data entails sampling and analysis of major aerosol species, using methods employed by the IMPROVE network since 1987 (Joseph et al., 1987; Malm et al., 1994; Sisler, 1996). These methods are consistent with the aerosol monitoring portion of the 1999 Visibility Monitoring Guidance document issued by the U.S. Environmental Protection Agency (EPA) (U.S. EPA, 1999b).

The IMPROVE program is a cooperative measurement effort designed to

1. establish current visibility and aerosol conditions in mandatory CIAs;
2. identify chemical species and emission sources responsible for existing anthropogenic and natural visibility impairment;
3. document long-term trends for assessing progress towards the national visibility goal;
4. and, with the enactment of the RHR, provide regional haze monitoring representing all visibility-protected federal CIAs where practical.

The program is managed by the IMPROVE steering committee, which consists of representatives from the EPA; the four federal land managers (FLMs): the National Park Service, U.S. Forest Service, U.S. Fish and Wildlife Service, and Bureau of Land Management; the National Oceanic and Atmospheric Administration; four organizations representing state air quality organizations: the State and Territorial Air Pollution Program Administrators/Association of Local Air Pollution Control Officials (STAPA/ALAPCO), Western Regional Air Partnership (WRAP), Northeast States for Coordinated Air Use Management (NESCAUM), and Mid-Atlantic Regional Air Management Association (MARAMA); and an associate member, the State of Arizona Department of Environmental Quality.

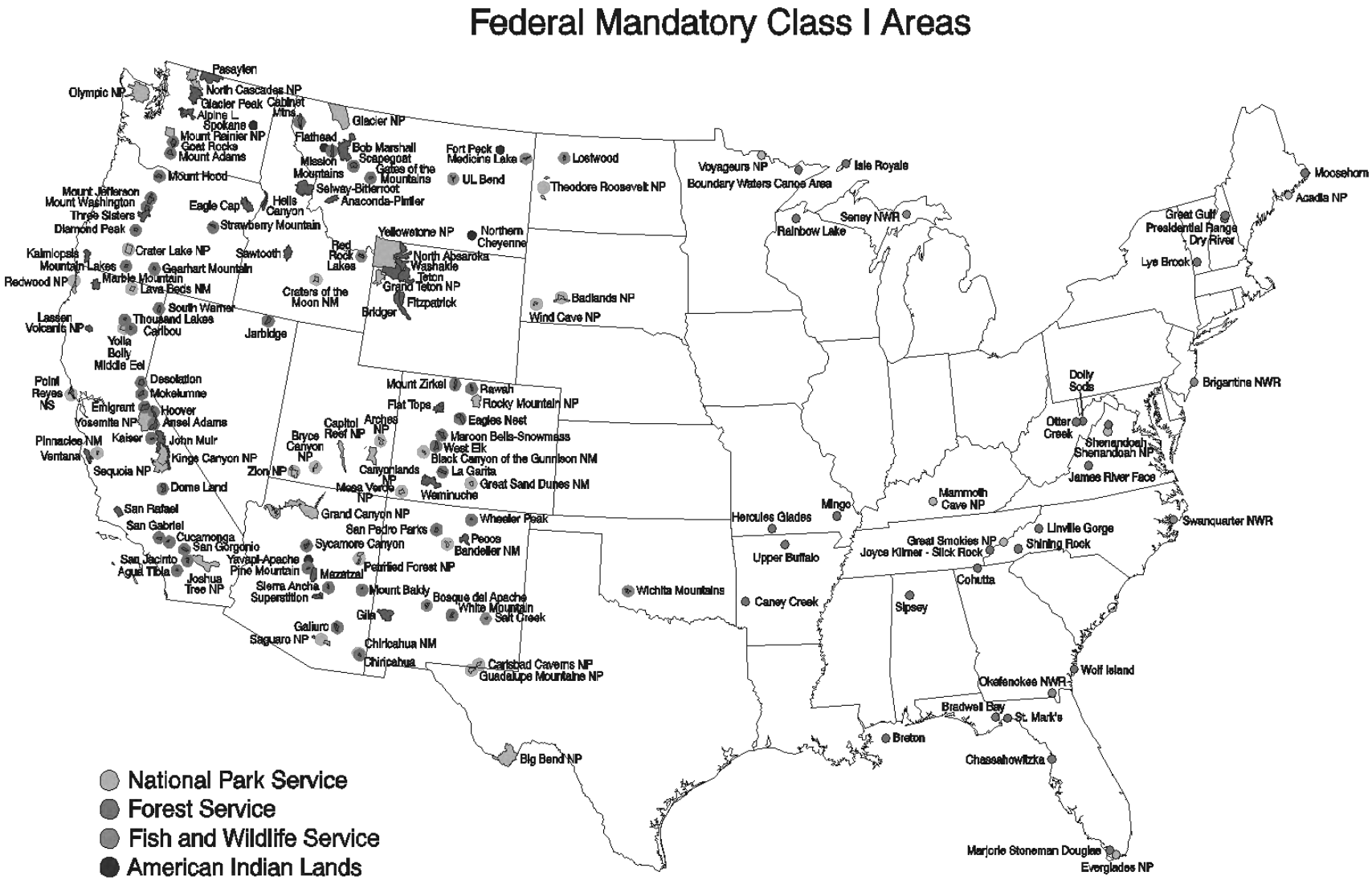

Figure 1.1. Class I areas of the contiguous United States. The shade coding identifies the managing agency of each Class I area.

1.2 OVERVIEW OF THE IMPROVE MONITORING NETWORK

1.2.1 Site Location

The IMPROVE network initially consisted of 30 monitoring sites in CIAs: twenty of these sites began operation in 1987, followed by the others in the early 1990s. An additional ~40 sites, most in remote areas, that used the same instrumentation, monitoring, and analysis protocols (called IMPROVE protocol sites) began operation prior to 2000 and were separately sponsored by individual federal or state organizations, though they were operated identically to other sites in the IMPROVE network. Adjustments to the number of monitoring sites in the network or the suite of measurements collected at an individual site occurred on several occasions, due in some cases to scientific considerations and in others to resource and funding limitations. Many of the sites also included optical monitoring with a nephelometer, a transmissometer, and/or color photography to document scenic appearance. The optical monitoring sites are detailed below in section 1.2.3.

In 1998 the EPA increased its support of IMPROVE to expand the network in Class I areas to provide the monitoring required under the RHR. Details regarding the selection process of additional sites was provided in the third IMPROVE report (Malm et al., 2000). The selection process was completed by the end of 1999 and installations began shortly thereafter. Currently the network consists of 212 sites (170 operating and 42 discontinued), including representative sites for the CIAs, and additional sites to fill in the spatial gaps where CIAs are sparse or absent. A list of sampling sites is provided in Table 1.1, including the site name, site code, state, latitude, longitude, elevation, and dates of operation. The sites are grouped by region, an empirical categorization that organizes sites with similar aerosol species and concentrations by location. Class I areas and their representative sites are listed in Table 1.2. A map of the site locations is provided in Figure 1.2, including IMPROVE and IMPROVE protocol sites. The sites are depicted by their site code and shaded based on their region, as defined in Table 1.1. There are 41 IMPROVE regions, 28 of which are rural and an additional thirteen that correspond to a single urban site per region (listed individually under “Urban Quality Assurance Sites” in Table 1.1). Of the rural sites, four regions include only one site (Death Valley, Lone Peak, Virgin Islands, and Ontario).

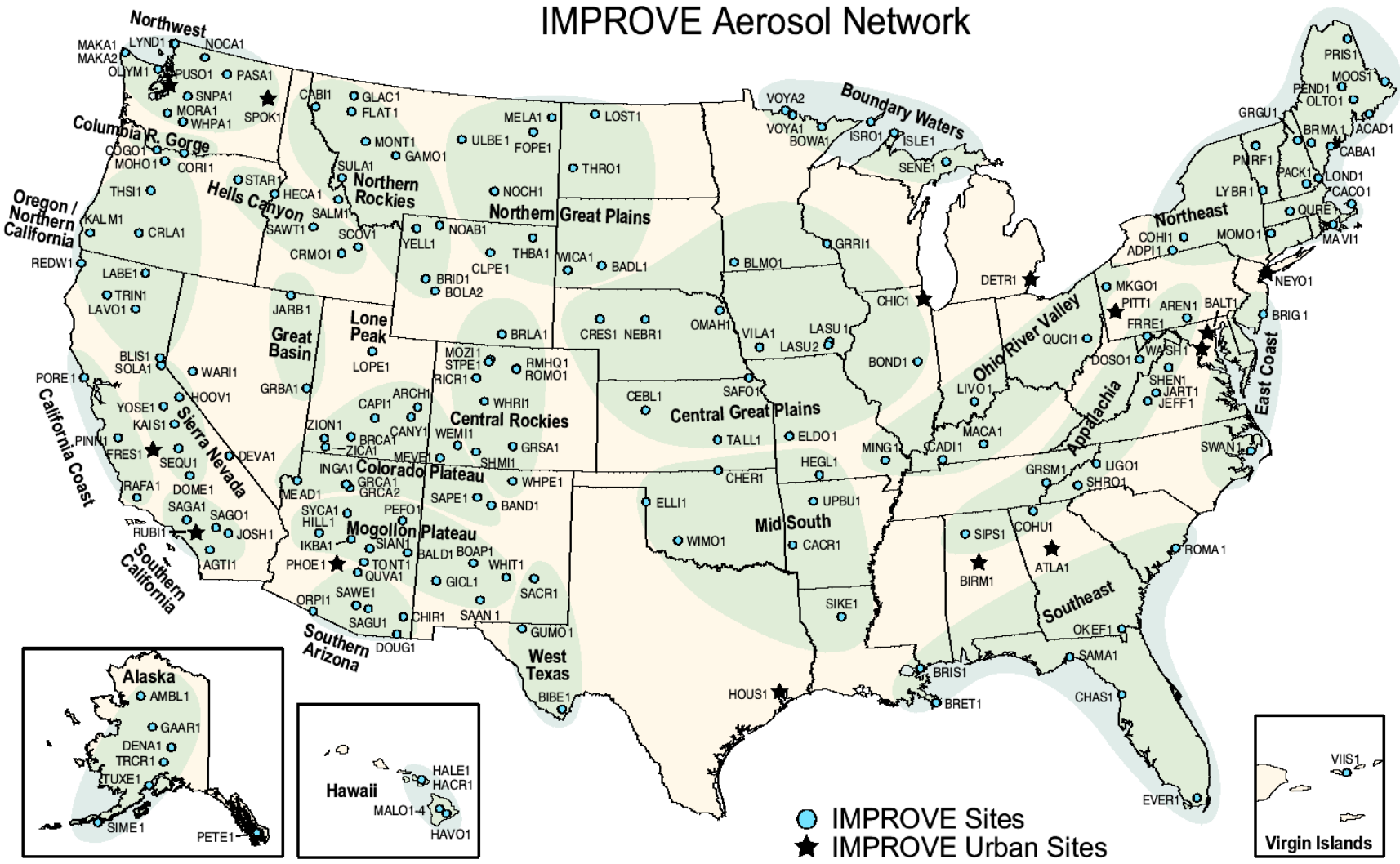

Figure 1.2. Locations of IMPROVE and IMPROVE protocol sites are shown for all discontinued and current sites as of December 2010. The IMPROVE regions used for grouping the sites are indicated by shading and bold text. Urban sites included in the IMPROVE network for quality assurance purposes are identified by stars.

Table 1.1. Currently operating and discontinued IMPROVE particulate monitoring sites. The sites are grouped by region, as displayed in Figure 1.2.

Site Name	Site Code	State	Latitude	Longitude	Elevation (m)	Dates of Operation
Alaska						
Ambler	AMBL1	AK	67.099	-157.872	67	07/2004-08/2005
Denali NP	DENA1	AK	63.723	-148.968	675	03/1988-present
Gates of the Arctic	GAAR1	AK	66.931	-151.492	205	10/2008-present
Petersburg	PETE1	AK	56.611	-132.812	12	07/2004-09/2009
Simeonof	SIME1	AK	55.325	-160.506	57	09/2001-present
Trapper Creek	TRCR1	AK	62.315	-150.316	155	09/2001-present
Tuxedni	TUXE1	AK	59.992	-152.666	15	12/2001-present
Alberta						
Barrier Lake	BALA1	AB	51.029	-115.034	1391	01/2011-present
Appalachia						
Arendtsville	AREN1	PA	39.923	-77.308	267	04/2001-12/2010
Cohutta	COHU1	GA	34.785	-84.626	735	05/2000-present
Dolly Sods WA	DOSO1	WV	39.105	-79.426	1182	09/1991-present
Frostburg	FRRE1	MD	39.706	-79.012	767	04/2004-present
Great Smoky Mountains NP	GRSM1	TN	35.633	-83.942	811	03/1988-present
James River Face Wilderness	JARI1	VA	37.627	-79.513	290	06/2000-present
Jefferson NF	JEFF1	VA	37.617	-79.483	219	09/1994-05/2000
Linville Gorge	LIGO1	NC	35.972	-81.933	969	03/2000-present
Shenandoah NP	SHEN1	VA	38.523	-78.435	1079	03/1988-present
Shining Rock WA	SHRO1	NC	35.394	-82.774	1617	07/1994-present
Sipsy Wilderness	SIPS1	AL	34.343	-87.339	286	03/1992-present
Boundary Waters						
Boundary Waters Canoe Area	BOWA1	MN	47.947	-91.496	527	08/1991-present
Isle Royale NP	ISLE1	MI	47.46	-88.149	182	11/1999-present
Isle Royale NP	ISRO1	MI	47.917	-89.15	213	06/1988-07/1991
Seney	SENE1	MI	46.289	-85.95	215	11/1999-present
Voyageurs NP #1	VOYA1	MN	48.413	-92.83	426	03/1988-09/1996
Voyageurs NP #2	VOYA2	MN	48.413	-92.829	429	11/1999-present
California Coast						
Pinnacles NM	PINN1	CA	36.483	-121.157	302	03/1988-present
Point Reyes National Seashore	PORE1	CA	38.122	-122.909	97	03/1988-present
San Rafael	RAFA1	CA	34.734	-120.007	957	02/2000-present
Central Great Plains						
Blue Mounds	BLMO1	MN	43.716	-96.191	473	07/2002-present
Bondville	BOND1	IL	40.052	-88.373	263	03/2001-present
Cedar Bluff	CEBL1	KS	38.77	-99.763	666	06/2002-present
Crescent Lake	CRES1	NE	41.763	-102.434	1207	07/2002-present

Site Name	Site Code	State	Latitude	Longitude	Elevation (m)	Dates of Operation
El Dorado Springs	ELDO1	MO	37.701	-94.035	298	06/2002-present
Great River Bluffs	GRRI1	MN	43.937	-91.405	370	07/2002-present
Lake Sugema	LASU1	IA	40.688	-91.988	223	06/2002-11/2004
Lake Sugema	LASU2	IA	40.693	-92.006	229	12/2004-present
Nebraska NF	NEBR1	NE	41.889	-100.339	883	07/2002-present
Omaha	OMAH1	NE	42.149	-96.432	430	08/2003-08/2008
Sac and Fox	SAFO1	KS	39.979	-95.568	293	06/2002-present
Tallgrass	TALL1	KS	38.434	-96.56	390	09/2002-present
Viking Lake	VILA1	IA	40.969	-95.045	371	06/2002-present
Central Rocky Mountains						
Brooklyn Lake	BRLA1	WY	41.365	-106.240	3196	09/1993-12/2003
Great Sand Dunes NM	GRSA1	CO	37.725	-105.519	2498	05/1988-present
Mount Zirkel WA	MOZI1	CO	40.538	-106.677	3243	07/1994-present
Ripple Creek	RICR1	CO	40.085	-107.312	2934	02/2009-present
Rocky Mountain NP HQ	RMHQ1	CO	40.362	-105.564	2408	03/1988-02/1991
Rocky Mountain NP	ROMO1	CO	40.278	-105.546	2760	09/1990-present
Storm Peak	STPE1	CO	40.445	-106.74	3220	12/1993-07/1994
Shamrock Mine	SHMI1	CO	37.303	-107.484	2351	7/2004-present
Wheeler Peak	WHPE1	NM	36.585	-105.452	3366	08/2000-present
White River NF	WHRI1	CO	39.154	-106.821	3414	07/1993-present
Colorado Plateau						
Arches NP	ARCH1	UT	38.783	-109.583	1722	03/1988-05/1992
Bandelier NM	BAND1	NM	35.78	-106.266	1988	03/1988-present
Bryce Canyon NP	BRCA1	UT	37.618	-112.174	2481	03/1988-present
Canyonlands NP	CANY1	UT	38.459	-109.821	1798	03/1988-present
Capitol Reef NP	CAPI1	UT	38.302	-111.293	1897	03/2000-present
Hopi Point #1	GRCA1	AZ	36.066	-112.154	2164	03/1988-08/1998
Hance Camp at Grand Canyon NP	GRCA2	AZ	35.973	-111.984	2267	09/1997-present
Indian Gardens	INGA1	AZ	36.078	-112.129	1166	10/1989-present
Meadview	MEAD1	AZ	36.019	-114.068	902	09/1991-09/1992 02/2003-present
Mesa Verde NP	MEVE1	CO	37.198	-108.491	2172	03/1988-present
San Pedro Parks	SAPE1	NM	36.014	-106.845	2935	08/2000-present
Weminuche WA	WEMI1	CO	37.659	-107.8	2750	03/1988-present
Zion Canyon	ZICA1	UT	37.198	-113.151	1215	12/2002-present
Zion	ZION1	UT	37.459	-113.224	1545	03/2000-08/2004
Columbia River Gorge						

Site Name	Site Code	State	Latitude	Longitude	Elevation (m)	Dates of Operation
Columbia Gorge #1	COGO1	WA	45.569	-122.21	230	09/1996-present
Columbia River Gorge	CORI1	WA	45.664	-121.001	179	06/1993-present
Death Valley						
Death Valley NP	DEVA1	CA	36.509	-116.848	130	10/1993-present
East Coast						
Brigantine NWR	BRIG1	NJ	39.465	-74.449	5	09/1991-present
Swanquarter	SWAN1	NC	35.451	-76.207	-4	06/2000-present
Great Basin						
Great Basin NP	GRBA1	NV	39.005	-114.216	2066	05/1992-present
Jarbidge WA	JARB1	NV	41.893	-115.426	1869	03/1988-present
Hawaii						
Haleakala Crater NP	HACR1	HI	20.759	-156.248	2158	01/2007-present
Haleakala NP	HALE1	HI	20.809	-156.282	1153	02/1991-present
Hawaii Volcanoes NP	HAVO1	HI	19.431	-155.258	1259	03/1988-present
Mauna Loa Observatory #1	MALO1	HI	19.536	-155.577	3439	03/1995-present
Mauna Loa Observatory #2	MALO2	HI	19.536	-155.577	3439	03/1995-present
Mauna Loa Observatory #3	MALO3	HI	19.539	-155.578	3400	04/1996-05/1996
Mauna Loa Observatory #4	MALO4	HI	19.539	-155.578	3400	04/1996-05/1996
Hells Canyon						
Craters of the Moon NM	CRMO1	ID	43.461	-113.555	1818	05/1992-present
Hells Canyon	HECA1	OR	44.97	-116.844	655	08/2000-present
Sawtooth NF	SAWT1	ID	44.17	-114.927	1990	01/1994-present
Scoville	SCOV1	ID	43.65	-113.033	1500	05/1992-05/1997
Starkey	STAR1	OR	45.225	-118.513	1259	03/2000-present
Lone Peak						
Lone Peak WA	LOPE1	UT	40.445	-111.708	1768	12/1993-08/2001
Mid South						
Caney Creek	CACR1	AR	34.454	-94.143	683	06/2000-present
Cherokee Nation	CHER1	OK	36.956	-97.031	342	09/2002-present
Ellis	ELLI1	OK	36.085	-99.935	697	06/2002-present
Hercules-Glades	HEGL1	MO	36.614	-92.922	404	03/2001-present
Sikes	SIKE1	LA	32.057	-92.435	45	03/2001-12/2010
Upper Buffalo WA	UPBU1	AR	35.826	-93.203	723	12/1991-present
Wichita Mountains	WIMO1	OK	34.732	-98.713	509	03/2001-present
Mogollon Plateau						
Mount Baldy	BALD1	AZ	34.058	-109.441	2509	02/2000-present

Site Name	Site Code	State	Latitude	Longitude	Elevation (m)	Dates of Operation
Bosque del Apache	BOAP1	NM	33.87	-106.852	1390	04/2000-present
Gila WA	GICL1	NM	33.22	-108.235	1776	04/1994-present
Hillside	HILL1	AZ	34.429	-112.963	1511	04/2001-06/2005
Ike's Backbone	IKBA1	AZ	34.34	-111.683	1298	04/2000-present
Petrified Forest NP	PEFO1	AZ	35.078	-109.769	1766	03/1988-present
San Andres	SAAN1	NM	32.687	-106.484	1326	10/1997-08/2000
Sierra Ancha	SIAN1	AZ	34.091	-110.942	1600	02/2000-present
Sycamore Canyon	SYCA1	AZ	35.141	-111.969	2046	09/1991-present
Tonto NM	TONT1	AZ	33.655	-111.107	775	04/1988-present
White Mountain	WHIT1	NM	33.469	-105.535	2064	01/2002-present
Northeast						
Acadia NP	ACAD1	ME	44.377	-68.261	157	03/1988-present
Addison Pinnacle	ADPI1	NY	42.091	-77.21	512	04/2001-06/2010
Bridgton	BRMA1	ME	44.107	-70.729	234	03/2001-present
Casco Bay	CABA1	ME	43.833	-70.064	27	03/2001-present
Cape Cod	CACO1	MA	41.976	-70.024	49	04/2001-present
Connecticut Hill	COHI1	NY	42.401	-76.653	519	04/2001-07/2006
Great Gulf WA	GRGU1	NH	44.308	-71.218	454	06/1995-present
Londonderry	LOND1	NH	42.862	-71.380	124	12/2010-present
Lye Brook WA	LYBR1	VT	43.148	-73.127	1015	09/1991-present
Martha's Vineyard	MAVI1	MA	41.331	-70.785	3	01/2003-present
Mohawk Mt.	MOMO1	CT	41.821	-73.297	522	09/2001-present
Moosehorn NWR	MOOS1	ME	45.126	-67.266	78	12/1994-present
Old Town	OLTO1	ME	44.933	-68.646	51	07/2001-06/2006
Pack Monadnock Summit	PACK1	NH	42.862	-71.879	695	10/2007-present
Penobscot	PENO1	ME	44.948	-68.648	45	1/2006-present
Proctor Maple Research Facility	PMRF1	VT	44.528	-72.869	401	12/1993-present
Presque Isle	PRIS1	ME	46.696	-68.033	166	03/2001-present
Quabbin Summit	QURE1	MA	42.298	-72.335	318	03/2001-present
Northern Great Plains						
Badlands NP	BADL1	SD	43.743	-101.941	736	03/1988-present
Cloud Peak	CLPE1	WY	44.334	-106.957	2471	06/2002-present
Fort Peck	FOPE1	MT	48.308	-105.102	638	06/2002-present
Lostwood	LOST1	ND	48.642	-102.402	696	12/1999-present
Medicine Lake	MELA1	MT	48.487	-104.476	606	12/1999-present
Northern Cheyenne	NOCH1	MT	45.65	-106.557	1283	06/2002-present
Thunder Basin	THBA1	WY	44.663	-105.287	1195	06/2002-present

Site Name	Site Code	State	Latitude	Longitude	Elevation (m)	Dates of Operation
Theodore Roosevelt	THRO1	ND	46.895	-103.378	853	12/1999-present
UL Bend	ULBE1	MT	47.582	-108.72	891	01/2000-present
Wind Cave	WICA1	SD	43.558	-103.484	1296	12/1999-present
Northern Rocky Mountains						
Boulder Lake	BOLA1	WY	42.846	-109.640	2296	10/2009-present
Bridger WA	BRID1	WY	42.975	-109.758	2627	03/1988-present
Cabinet Mountains	CABI1	MT	47.955	-115.671	1441	07/2000-present
Flathead	FLAT1	MT	47.773	-114.269	1580	06/2002-present
Gates of the Mountains	GAMO1	MT	46.826	-111.711	2387	07/2000-present
Glacier NP	GLAC1	MT	48.511	-113.997	975	03/1988-present
Monture	MONT1	MT	47.122	-113.154	1282	03/2000-present
North Absaroka	NOAB1	WY	44.745	-109.382	2483	01/2000-present
Salmon NF	SALM1	ID	45.159	-114.026	2788	12/1993-08/2000
Sula Peak	SULA1	MT	45.86	-114	1896	08/1994-present
Yellowstone NP 1	YELL1	WY	44.565	-110.4	2442	03/1988-07/1996
Yellowstone NP 2	YELL2	WY	44.565	-110.4	2425	07/1996-present
Northwest						
Lynden	LYND1	WA	48.953	-122.559	28	10/1996-08/1997
Makah Indian Reservation	MAKA1	WA	48.372	-124.595	9	9/2006-10/2010
Makah Indian Reservation	MAKA2	WA	48.298	-124.625	480	10/2010-present
Mount Rainier NP	MORA1	WA	46.758	-122.124	439	03/1988-present
North Cascades	NOCA1	WA	48.732	-121.065	569	03/2000-present
Olympic	OLYM1	WA	48.007	-122.973	600	07/2001-present
Pasayten	PASA1	WA	48.388	-119.927	1627	11/2000-present
Snoqualmie Pass	SNPA1	WA	47.422	-121.426	1049	07/1993-present
Spokane Res.	SPOK1	WA	47.904	-117.861	552	07/2001-06/2005
White Pass	WHPA1	WA	46.624	-121.388	1827	02/2000-present
Not Assigned						
Walker River Paiute Tribe	WARI1	NV	38.952	-118.815	1250	06/2003-11/2005
Ohio River Valley						
Cadiz	CADI1	KY	36.784	-87.85	192	03/2001-12/2010
Livonia	LIVO1	IN	38.535	-86.26	282	03/2001-12/2010
Mammoth Cave NP	MACA1	KY	37.132	-86.148	235	09/1991-present
Mingo	MING1	MO	36.972	-90.143	111	05/2000-present
M.K. Goddard	MKGO1	PA	41.427	-80.145	380	04/2001-12/2010
Quaker City	QUCI1	OH	39.943	-81.338	366	05/2001-present
Ontario						
Egbert	EGBE1		44.231	-79.783	251	5/2005-present
Oregon and Northern California						
Bliss SP (TRPA)	BLIS1	CA	38.976	-120.103	2131	11/1990-present

Site Name	Site Code	State	Latitude	Longitude	Elevation (m)	Dates of Operation
Crater Lake NP	CRLA1	OR	42.896	-122.136	1996	03/1988-present
Kalmiopsis	KALM1	OR	42.552	-124.059	80	03/2000-present
Lava Beds NM	LABE1	CA	41.712	-121.507	1460	03/2000-present
Lassen Volcanic NP	LAVO1	CA	40.54	-121.577	1733	03/1988-present
Mount Hood	MOHO1	OR	45.289	-121.784	1531	03/2000-present
Redwood NP	REDW1	CA	41.561	-124.084	244	03/1988-present
Three Sisters WA	THSI1	OR	44.291	-122.043	885	07/1993-present
Trinity	TRIN1	CA	40.786	-122.805	1014	07/2000-present
Phoenix						
Phoenix	PHOE1	AZ	33.504	-112.096	342	04/2001-present
Puget Sound						
Puget Sound	PUSO1	WA	47.57	-122.312	98	03/1996-present
Sierra Nevada						
Dome Lands WA	DOLA1	CA	35.699	-118.202	914	08/1994-10/1998
Dome Lands WA	DOME1	CA	35.728	-118.138	927	02/2000-present
Hoover	HOOV1	CA	38.088	-119.177	2561	07/2001-present
Kaiser	KAIS1	CA	37.221	-119.155	2598	01/2000-present
Sequoia NP	SEQU1	CA	36.489	-118.829	519	03/1992-present
South Lake Tahoe	SOLA1	CA	38.933	-119.967	1900	03/1989-06/1997
Yosemite NP	YOSE1	CA	37.713	-119.706	1603	03/1988-present
Southeast						
Breton	BRET1	LA	29.119	-89.207	11	06/2000-09/2005
Breton Island	BRIS1	LA	30.109	-89.762	-7	01/2008-present
Chassahowitzka NWR	CHAS1	FL	28.748	-82.555	4	04/1993-present
Everglades NP	EVER1	FL	25.391	-80.681	1	09/1988-present
Okefenokee NWR	OKEF1	GA	30.741	-82.128	48	09/1991-present
Cape Romain NWR	ROMA1	SC	32.941	-79.657	5	09/1994-present
St. Marks	SAMA1	FL	30.093	-84.161	8	06/2000-present
Southern Arizona						
Chiricahua NM	CHIR1	AZ	32.009	-109.389	1555	03/1988-present
Douglas	DOUG1	AZ	31.349	-109.54	1230	06/2004-present
Organ Pipe	ORPI1	AZ	31.951	-112.802	504	01/2003-present
Queen Valley	QUVA1	AZ	33.294	-111.286	661	04/2001-present
Saguaro NM	SAGU1	AZ	32.175	-110.737	941	06/1988-present
Saguaro West	SAWE1	AZ	32.249	-111.218	714	04/2001-present
Southern California						
Agua Tibia	AGTI1	CA	33.464	-116.971	508	11/2000-present
Joshua Tree NP	JOSH1	CA	34.069	-116.389	1235	02/2000-present
Joshua Tree NP	JOTR1	CA	34.069	-116.389	1228	09/1991-07/1992
San Gabriel	SAGA1	CA	34.297	-118.028	1791	12/2000-present
San Gorgonio WA	SAGO1	CA	34.194	-116.913	1726	03/1988-present
Urban Quality Assurance Sites						
Atlanta	ATLA1	GA	33.688	-84.29	243	04/2004-present

Site Name	Site Code	State	Latitude	Longitude	Elevation (m)	Dates of Operation
Baltimore	BALT1	MD	39.255	-76.709	78	06/2004-02/2007
Birmingham	BIRM1	AL	33.553	-86.815	176	04/2004-present
Chicago	CHIC1	IL	41.751	-87.713	195	11/2003-09/2005
Detroit	DETR1	MI	42.229	-83.209	180	11/2003-present
Fresno	FRES1	CA	36.782	-119.773	100	09/2004-present
Houston	HOUS1	TX	29.67	-95.129	7	05/2004-09/2005
New York City	NEYO1	NY	40.816	-73.902	45	08/2004-04/2010
Pittsburgh	PITT1	PA	40.465	-79.961	268	04/2004-present
Rubidoux	RUBI1	CA	34	-117.416	248	09/2004-09/2005
Virgin Islands						
Virgin Islands NP	VIIS1	VI	18.336	-64.796	51	10/1990-present
Washington D.C.						
Washington D.C.	WASH1	DC	38.876	-77.034	15	03/1988-present
West Texas						
Big Bend NP	BIBE1	TX	29.303	-103.178	1067	03/1988-present
Guadalupe Mountains NP	GUMO1	TX	31.833	-104.809	1672	03/1988-present
Salt Creek	SACR1	NM	33.46	-104.404	1072	04/2000-present

NF = National Forest
NM = National Monument
NP = National Park
NWR = National Wildlife Refuge
WA = Wilderness Area

Table 1.2. Class I areas and the representative monitoring site.

Class I Area Name	Site Name	Site Code
Acadia	Acadia NP	ACAD1
Agua Tibia	Agua Tibia	AGTI1
Alpine Lakes	Snoqualmie Pass	SNPA1
Anaconda-Pintler	Sula Peak	SULA1
Ansel Adams	Kaiser	KAIS1
Arches	Canyonlands NP	CANY1
Badlands	Badlands NP	BADL1
Bandelier	Bandelier NM	BAND1
Big Bend	Big Bend NP	BIBE1
Black Canyon of the Gunnison	Weminuche WA	WEMI1
Bob Marshall	Monture	MONT1
Bosque del Apache	Bosque del Apache	BOAP1
Boundary Waters Canoe Area	Boundary Waters Canoe Area	BOWA1
Breton	Breton	BRIS1
Bridger	Bridger WA	BRID1
Brigantine	Brigantine NWR	BRIG1
Bryce Canyon	Bryce Canyon NP	BRCA1
Cabinet Mountains	Cabinet Mountains	CABI1
Caney Creek	Caney Creek	CACR1
Canyonlands	Canyonlands NP	CANY1
Cape Romain	Cape Romain NWR	ROMA1
Capitol Reef	Capitol Reef NP	CAPI1
Caribou	Lassen Volcanic NP	LAVO1
Carlsbad Caverns	Guadalupe Mountains NP	GUMO1

Class I Area Name	Site Name	Site Code
Chassahowitzka	Chassahowitzka NWR	CHAS1
Chiricahua NM	Chiricahua NM	CHIR1
Chiricahua W	Chiricahua NM	CHIR1
Cohutta	Cohutta	COHU1
Crater Lake	Crater Lake NP	CRLA1
Craters of the Moon	Craters of the Moon NM	CRMO1
Cucamonga	San Gabriel	SAGA1
Denali	Denali NP	DENA1
Desolation	Bliss SP (TRPA)	BLIS1
Diamond Peak	Crater Lake NP	CRLA1
Dolly Sods	Dolly Sods WA	DOSO1
Dome Land	Dome Lands WA	DOME1
Eagle Cap	Starkey	STAR1
Eagles Nest	White River NF	WHRI1
Emigrant	Yosemite NP	YOSE1
Everglades	Everglades NP	EVER1
Fitzpatrick	Bridger WA	BRID1
Flat Tops	White River NF	WHRI1
Galiuro	Chiricahua NM	CHIR1
Gates of the Mountains	Gates of the Mountains	GAMO1
Gearhart Mountain	Crater Lake NP	CRLA1
Gila	Gila WA	GICL1
Glacier	Glacier NP	GLAC1
Glacier Peak	North Cascades	NOCA1
Goat Rocks	White Pass	WHPA1
Grand Canyon	Hance Camp at Grand Canyon NP	GRCA2
Grand Teton	Yellowstone NP 2	YELL2
Great Gulf	Great Gulf WA	GRGU1
Great Sand Dunes	Great Sand Dunes NM	GRSA1
Great Smoky Mountains	Great Smoky Mountains NP	GRSM1
Guadalupe Mountains	Guadalupe Mountains NP	GUMO1
Haleakala	Haleakala NP	HALE1
Hawaii Volcanoes	Hawaii Volcanoes NP	HAVO1
Hells Canyon	Hells Canyon	HECA1
Hercules-Glade	Hercules-Glades	HEGL1
Hoover	Hoover	HOOV1
Isle Royale	Isle Royale NP	ISLE1
James River Face	James River Face WA	JARI1
Jarbidge	Jarbidge WA	JARB1
John Muir	Kaiser	KAIS1
Joshua Tree	Joshua Tree NP	JOSH1
Joyce Kilmer-Slickrock	Great Smoky Mountains NP	GRSM1
Kaiser	Kaiser	KAIS1
Kalmiopsis	Kalmiopsis	KALM1
Kings Canyon	Sequoia NP	SEQU1
La Garita	Weminuche WA	WEMI1
Lassen Volcanic	Lassen Volcanic NP	LAVO1
Lava Beds	Lava Beds NM	LABE1
Linville Gorge	Linville Gorge	LIGO1
Lostwood	Lostwood	LOST1
Lye Brook	Lye Brook WA	LYBR1
Mammoth Cave	Mammoth Cave NP	MACA1

Class I Area Name	Site Name	Site Code
Marble Mountain	Trinity	TRIN1
Maroon Bells-Snowmass	White River NF	WHRI1
Mazatzal	Ike's Backbone	IKBA1
Medicine Lake	Medicine Lake	MELA1
Mesa Verde	Mesa Verde NP	MEVE1
Mingo	Mingo	MING1
Mission Mountains	Monture	MONT1
Mokelumne	Bliss SP (TRPA)	BLIS1
Moosehorn	Moosehorn NWR	MOOS1
Mount Adams	White Pass	WHPA1
Mount Baldy	Mount Baldy	BALD1
Mount Hood	Mount Hood	MOHO1
Mount Jefferson	Three Sisters WA	THSI1
Mount Rainier	Mount Rainier NP	MORA1
Mount Washington	Three Sisters WA	THSI1
Mount Zirkel	Mount Zirkel WA	MOZI1
Mountain Lakes	Crater Lake NP	CRLA1
North Absaroka	North Absaroka	NOAB1
North Cascades	North Cascades	NOCA1
Okefenokee	Okefenokee NWR	OKEF1
Olympic	Olympic	OLYM1
Otter Creek	Dolly Sods WA	DOSO1
Pasayten	Pasayten	PASA1
Pecos	Wheeler Peak	WHPE1
Petrified Forest	Petrified Forest NP	PEFO1
Pine Mountain	Ike's Backbone	IKBA1
Pinnacles	Pinnacles NM	PINN1
Point Reyes	Point Reyes National Seashore	PORE1
Presidential Range-Dry River	Great Gulf WA	GRGU1
Rawah	Mount Zirkel WA	MOZI1
Red Rock Lakes	Yellowstone NP 2	YELL2
Redwood	Redwood NP	REDW1
Rocky Mountain	Rocky Mountain NP	ROMO1
Roosevelt Campobello	Moosehorn NWR	MOOS1
Saguaro	Saguaro NM	SAGU1
Saint Marks	St. Marks	SAMA1
Salt Creek	Salt Creek	SACR1
San Gabriel	San Gabriel	SAGA1
San Gorgonio	San Gorgonio WA	SAGO1
San Jacinto	San Gorgonio WA	SAGO1
San Pedro Parks	San Pedro Parks	SAPE1
San Rafael	San Rafael	RAFA1
Sawtooth	Sawtooth NF	SAWT1
Scapegoat	Monture	MONT1
Selway-Bitterroot	Sula Peak	SULA1
Seney	Seney	SENE1
Sequoia	Sequoia NP	SEQU1
Shenandoah	Shenandoah NP	SHEN1
Shining Rock	Shining Rock WA	SHRO1
Sierra Ancha	Sierra Ancha	SIAN1
Simeonof	Simeonof	SIME1
Sipsey	Sipsy WA	SIPS1

Class I Area Name	Site Name	Site Code
South Warner	Lava Beds NM	LABE1
Strawberry Mountain	Starkey	STAR1
Superstition	Tonto NM	TONT1
Swanquarter	Swanquarter	SWAN1
Sycamore Canyon	Sycamore Canyon	SYCA1
Teton	Yellowstone NP 2	YELL2
Theodore Roosevelt	Theodore Roosevelt	THRO1
Thousand Lakes	Lassen Volcanic NP	LAVO1
Three Sisters	Three Sisters WA	THSI1
Tuxedni	Tuxedni	TUXE1
UL Bend	UL Bend	ULBE1
Upper Buffalo	Upper Buffalo WA	UPBU1
Ventana	Pinnacles NM	PINN1
Virgin Islands	Virgin Islands NP	VIIS1
Voyageurs	Voyageurs NP #2	VOYA2
Washakie	North Absaroka	NOAB1
Weminuche	Weminuche WA	WEMI1
West Elk	White River NF	WHRI1
Wheeler Peak	Wheeler Peak	WHPE1
White Mountain	White Mountain	WHIT1
Wichita Mountains	Wichita Mountains	WIMO1
Wind Cave	Wind Cave	WICA1
Wolf Island	Okefenokee NWR	OKEF1
Yellowstone	Yellowstone NP 2	YELL2
Yolla Bolly-Middle Eel	Trinity	TRIN1
Yosemite	Yosemite NP	YOSE1
Zion	Zion	ZION1

NF = National Forest
NM = National Monument
NP = National Park
NWR = National Wildlife Refuge
WA = Wilderness Area

1.2.2 Aerosol Sampling and Analysis

The current configuration of the IMPROVE monitor collects 24-hour samples every third day. As previous reports have detailed, the samplers have undergone modifications over time (Malm et al., 2000; Debell et al., 2006). The version II sampler began operating in November 1999 through early 2000 and is in use currently at all IMPROVE sites. The version II sampler was implemented to allow for protocol changes that occurred in 2000 with the expansion of the IMPROVE network and the need for consistency with the EPA's fine mass and fine speciation monitoring network. Specifically, the need for consistency with the EPA's sampling schedule. Other sampling configuration changes for IMPROVE occurred to ensure more consistency regarding data collection protocols (e.g., inlet height, filter collection time after sampling). Other differences between the networks were not addressed, such as shipping temperatures and the suite of analytes. Details regarding the version I sampler can be found in previous reports (e.g., Malm et al., 2000).

The IMPROVE samplers (versions I and II) consist of four independent modules (A, B, C, and D; see Figure 1.3). Each module incorporates a separate inlet, filter pack, and pump

assembly. Modules A, B, and C are equipped with a 2.5 μm cyclone that allows for sampling of particles with aerodynamic diameters less than 2.5 μm, while module D is fitted with a PM_{10} inlet to collect particles with aerodynamic diameters less than 10 μm. Each module contains a filter substrate specific to the analysis planned (Figure 1.3).

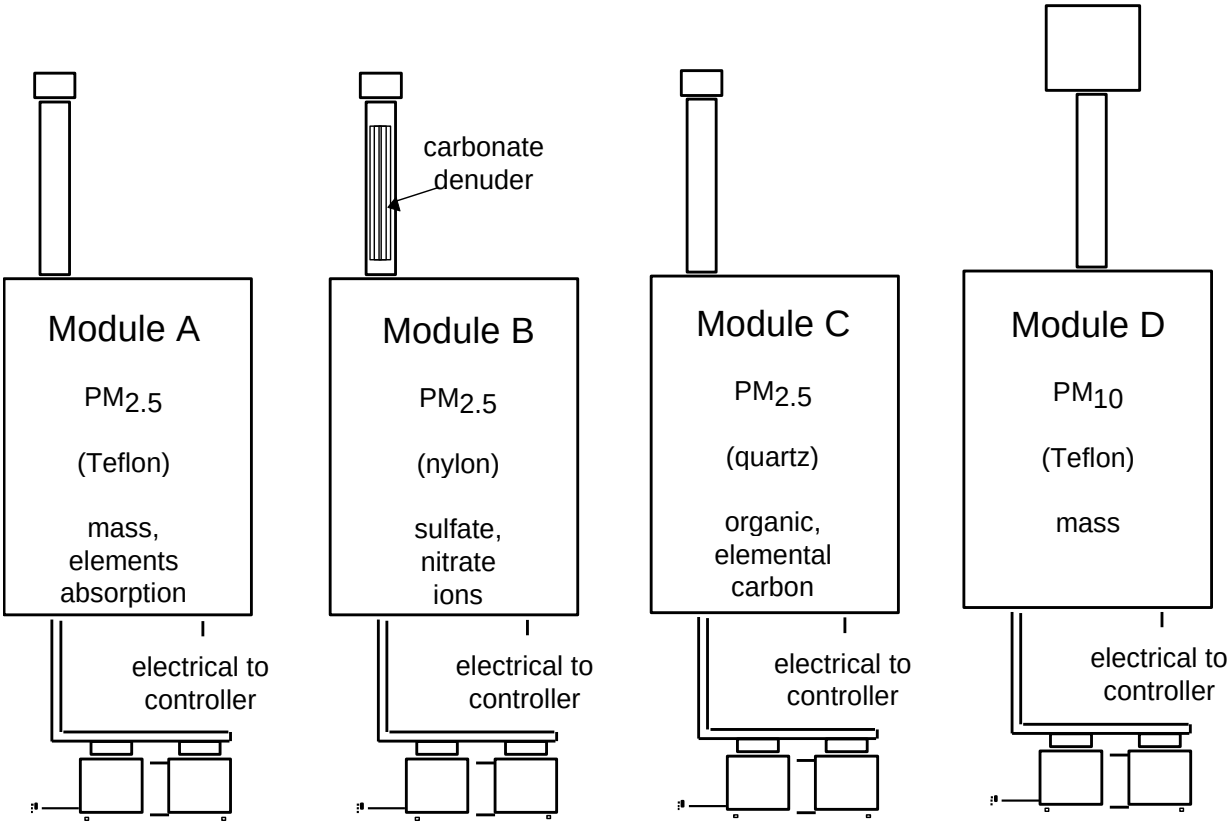

Figure 1.3. Schematic view of the IMPROVE sampler showing the four modules with separate inlets and pumps. The substrates with analyses performed for each module are also shown.

The version II sampler is controlled with a microprocessor programmed to maintain a given sampling schedule. Flow rate, sample temperature, and other performance-related information are recorded every 15 minutes throughout the sample period on a memory card reader/writer. The microprocessor also permits programming changes to be distributed to the controller on chips that are installed during annual maintenance visits, allowing for programming changes to be implemented consistently, without requiring programming in the field.

To accommodate the every-third-day sampling schedule, the version II sampler has a four-filter manifold for each module. The manifold with the solenoids sits directly above the filter cassettes and is raised or lowered as a unit to unload and load the filters. The four filter cassettes are held in a cartridge (shown in Figure 1.4) that is designed to allow only one orientation in the sampler. Fully prepared date- and site-labeled filter cartridges, along with memory cards, are sent from the analysis laboratory to the field and are returned in special mailing containers to prevent confusion concerning the order of sampling among the filters. If filter change service is performed on a sample day, the operator moves the cassette containing that day's filter to the open position in the newly loaded cartridge. The few minutes that it takes

to perform this sample change is recorded by the microprocessor on the memory card so that the correct air volume is used to calculate concentrations.

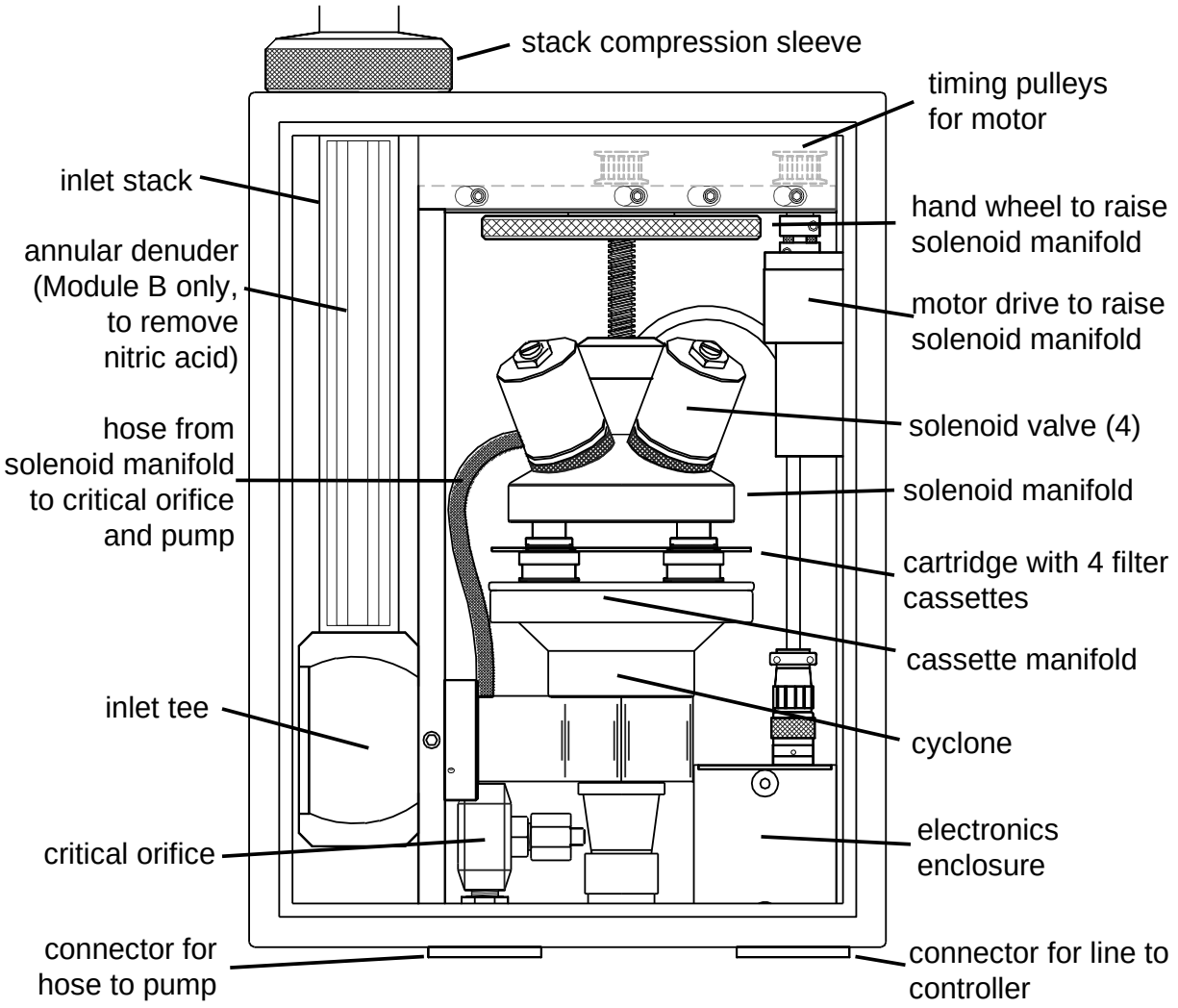

Figure 1.4. Schematic of the version II IMPROVE sampler $PM_{2.5}$ module.

The design of the version II IMPROVE sampler simplifies the addition of a fifth module to accommodate replicate sampling and analysis for mass and composition. This quality assurance module is operated for each sampling period and collects a replicate sample for one of the four modules (A, B, C, or D) so that, over time, relative precision information can be developed for each parameter. Starting in 2003, collocated modules were installed at 25 sites across the network, providing ~4% replication for each of the four modules (Table 1.3).

Table 1.3. Sites with a fifth collocated module.

Site Name	Site	A	B	C	D	Start Date	End Date
Mesa Verde NP	MEVE1	X				8/13/2003	
Olympic NP	OLYM1	X				11/8/2003	
Proctor Maple Research Facility	PMRF1	X				9/3/2003	
Sac and Fox	SAFO1	X				11/20/2003	
St. Marks	SAMA1	X				11/18/2004	

Site Name	Site	A	B	C	D	Start Date	End Date
Trapper Creek	TRCR1	X				6/22/2004	
Big Bend NP	BIBE1		X			8/30/2003	
Blue Mounds	BLMO1		X			9/16/2004	
Frostburg	FRRE1		X			4/15/2004	
Gates of the Mountains	GAMO1		X			9/23/2003	
Lassen Volcanic NP	LAVO1		X			4/18/2003	
Mammoth Cave NP	MACA1		X			5/12/2003	
Everglades NP	EVER1			X		7/11/2003	
Hercules-Glades	HEGL1			X		8/24/2004	
Hoover	HOOV1			X		8/13/2003	
Medicine Lake	MELA1			X		9/25/2003	
Saguaro West	SAWE1			X		3/25/2004	
Seney	SENE1			X		8/10/2003	
Houston	HOUS1				X	4/30/2004	9/1/2005
Jarbidge WA	JARB1				X	6/30/2004	
Joshua Tree NP	JOSH1				X	8/7/2003	
Quabbin Summit	QURE1				X	9/4/2003	
Swanquarter	SWAN1				X	11/9/2004	
Wind Cave	WICA1				X	9/17/2004	
Breton	BRIS1				X	1/28/2008	

NP = National Park
WA = Wilderness Area

The laboratory at University of California, Davis (UC Davis)[1] prepares the sample cartridges for the IMPROVE sites. Every 3 weeks, UC Davis sends a mailing container with the necessary sampling supplies to each site. The containers are typically received 10 days before the first sample-change day of the next 3-week cycle. Often there will be two containers at a site, one in current use and the second ready for the next period or ready to be shipped back to UC Davis. The site operators are expected to send the container with the exposed filters back to UC Davis within a day or two following the completion of each 3-week cycle. All shipments, to and from the field, are sent by second-day express delivery. Thus, a sample container typically spends a little over a month between shipment from and delivery to UC Davis, with the filters installed in the sampler during one week of that period.

As these filters arrive at UC Davis from the field sites, they are placed in Petri dishes and accumulate until a shipping tray has been filled, usually 400 filters. Nylon filters are sent to RTI (Research Triangle Institute)[2] for ion analysis and quartz filters are sent to DRI (Desert Research Institute)[3] for carbon analysis. Full trays of each type are sent to RTI and DRI approximately once a week by overnight express.

Module A is equipped with at Teflon® filter that is analyzed for $PM_{2.5}$ gravimetric fine mass, elemental analysis, and light absorption. Samples are pre- and post-weighed to gravimetrically determine $PM_{2.5}$ fine mass using electro-microbalance, after equilibrating at 30–40% relative humidity and 20–30° C. This procedure for determining gravimetric fine mass is associated with both positive and negative artifacts. Negative artifacts include loss of

[1] UC Davis is the NPS contractor during the time period of this report.
[2] RTI is the NPS contractor for the ion analyses during the time period of this report.
[3] DRI is the NPS contractor for the carbon analyses during the time period of this report.

semivolatile species such as ammonium nitrate (AN) and some organic species from the Teflon filter during sampling. Positive artifacts include particle-bound water associated with hygroscopic aerosol species such as sulfates, nitrates, sea salt, and perhaps some organic species. Reactions with atmospheric gases may also contribute to positive artifacts. Storage conditions and shipping conditions may also contribute to artifacts.

Elemental analysis is performed on the module A Teflon filters for elements with atomic number greater than 11 (Na) and less than 82 (Pb) by X-ray florescence (XRF). The techniques used for elemental analysis for the IMPROVE network have included proton elastic scattering analysis (PESA), proton induced X-ray emission (PIXE), and XRF. Elemental hydrogen is quantified using PESA. PIXE was used for quantifying nearly all elements with atomic number greater than 11 and less than 82. Beginning in 1992, however, analysis of heavier elements with atomic weights from 26 (Fe) to 82 (Pb) switched to XRF with a molybdenum (Mo) anode source. PIXE was discontinued in late 2001 and analysis of the lighter elements with Z from 11 (Na) to 25 (Mn) was changed from PIXE to XRF using a copper (Cu) anode source. Also, in late 2001, the analysis of Fe was changed from Mo anode XRF to Cu anode XRF. In both cases the change from PIXE to XRF provided lower minimum detection limits (MDL) for most elements of interest, as well as better sample preservation for reanalysis. The exceptions were Na, Mg, Al, and to a lesser extent Si, where the change to Cu XRF resulted in significantly increased MDL and uncertainty. The details on the transitions from PIXE to XRF are provided in section 1.3 below.

The light absorption coefficient (f_{abs}, Mm^{-1}) is determined from the channel A Teflon filter using a hybrid integrating plate/sphere system (HIPS) that involves the direct measurement of the absorption of a laser beam (wavelength of 633 nm) over the area of the sample. Prior to March 1, 1994, a laser integrating plate method (LIPM) was used.

Module B is fitted with a sodium carbonate denuder tube in the inlet to remove gaseous nitric acid in the air sample, followed by a Nylasorb (nylon) filter as the collection substrate. The material collected on the nylon filter is extracted ultrasonically in an aqueous solution that is subsequently analyzed for the anions sulfate, nitrate, nitrite, and chloride using ion chromatography. The negative artifact associated with the loss of nitrate on Teflon filters is not as critical for nylon filters, as they have been shown to be more effective at capturing and retaining nitrate from semivolatile AN than Teflon filters (Yu et al., 2005).

Field blanks for the B module are collected to determine positive artifacts that are used to correct concentrations of all the reported anions. A field blank nylon filter is placed in an unused port in the filter cassette where it is exposed to all aspects of the filter handling process, with the exception of sample air drawn being through it (McDade et al., 2004). Each site receives a nylon filter field blank every 2–3 months, on average, resulting in approximately 70 field blanks collected each month (McDade et al., 2004). A single artifact correction is applied for each species for every site in the network for the time period being processed. The artifact correction is calculated as the median of the filter blank values and subtracted from concentrations before they are reported. Monthly artifact corrections are computed currently, although prior to June 2002 seasonal quarters artifacts were applied. Sulfate ion artifacts are typically less than 10% of the ambient concentrations, and nitrate artifacts range between 10% and 20% for the filters used prior to 2004 (McDade et al., 2004). The filters introduced in 2004 were significantly cleaner,

with typical median blank values of 0.00 (below the MDL) for sulfate and nitrate and 0.01 $\mu g\ m^{-3}$ for chloride, approximately 100 times smaller than the chloride blank values observed prior to 2004.

Module C utilizes quartz fiber filters that are analyzed by thermal optical reflectance (TOR) for particulate organic and light absorbing carbon (OC and LAC, respectively) (Chow et al., 1993) and to estimate the organic carbon artifact from organic gases collected on the secondary filter. We use the term "light absorbing carbon" instead of elemental carbon (EC) to reflect the transition to this term in the scientific literature because of the operational definition, and sometimes morphology, associated with EC (Bond and Bergstrom, 2006; Malm et al., 1994). Light absorbing carbon particles may evolve in high temperature environments but not be graphitic (e.g., Hand et al., 2005). Replacing EC with LAC avoids potential confusion regarding the type of carbon particles responsible for light absorption.

Organic carbon concentrations reported by IMPROVE are corrected for an approximate positive artifact (Dillner et al., 2009). After-filters have been collected at six sites since 2001 (Chiricahua, Arizona, CHIR1; Grand Canyon, Arizona, GRCA2; Yosemite, California, YOSE1; Okefenokee, Georgia, OKEF1; Shenandoah, Virginia, SHEN1; and Mount Rainier, Washington, MORA1), and a monthly median artifact is used in a seasonal correction across the entire IMPROVE network (Watson et al., 2009; Chow et al., 2010). This correction assumes that the positive artifact is similar throughout the United States and also assumes that organic vapors are adsorbed uniformly throughout the front and back filters. These assumptions may not always be appropriate (Watson et al., 2009). Typical artifacts for OC can correspond to half of the reported ambient concentration (McDade et al., 2004). Negative artifacts due to the volatilization of particulate organics are not accounted for because they are thought to be small (Turpin et al., 2000), although some studies suggest they could be important. Changes in analytical methods due to hardware upgrades on January 1, 2005, resulted in changes in the split between OC and LAC (Chow et al., 2007; White, 2007)). Higher LAC/total carbon ratios were reported after the change in analytical methods, but no changes in total carbon were detected (see Section 1.3.1.1).

Finally, module D is fitted with a PM_{10} inlet and utilizes a Teflon filter. PM_{10} aerosol mass concentrations are determined gravimetrically.

All IMPROVE data are available for download from http://views.cira.colostate.edu/fed/.

1.2.3 Optical Sampling and Analysis

Routine optical monitoring includes light extinction and scattering coefficients as measured by transmissometer and nephelometer, respectively. Optical monitoring is conducted at a subset of IMPROVE monitoring sites. The number of sites has decreased significantly due to budgetary constraints.

The Optec LPV-2 transmissometer (Optec, Inc., Lowell, Michigan) has been used in the IMPROVE network since 1986. The Optec LPV-2 operates at a wavelength of 550 nm over path lengths up to 15 km. Its use in remote locations such as national parks is discussed by Molenar et al. (1989), while its use in urban settings is presented by Dietrich et al. (1989). Data processing

algorithms that incorporate corrections for interferences are thoroughly discussed by Molenar and Malm (1992).

Molenar et al. (1989) discuss the inherent uncertainties associated with the measurement. The accuracy of the transmission measurement, as determined by field and laboratory calibrations, is better than 1%. However, the accuracy of the derived extinction coefficient is dependent on the accuracy of the transmission measurement in field conditions. The transmission calculation is determined from an absolute (as opposed to relative) measurement of irradiance of a light source of known intensity that is located some known distance from the receiver. The measurement is made using optics exposed to the ambient atmosphere but is assumed to be free of dust or other films. The uncertainties associated with these parameters contribute to the overall uncertainty of the measurement. The estimated uncertainty is about 4 Mm^{-1} for a typical 5-km path length. A list of operating and discontinued transmissometers is provided in Table 1.4, including the locations of the receiver and transmitter. Only two transmissometers are currently operating (Bridger, Wyoming, BRID1, and San Gorgonio, California, SAGO1).

Table 1.4. Transmissometer receiver and transmitter locations.

Location	Site Name	Receiver Lon (deg)	Lat (deg)	Elevation (m)	Bearing (deg)	Transmitter Lon (deg)	Lat (deg)	Elevation (m)	Mean Elevation	Elevation Angle (deg)	Distance	Start Date	End Date	Sponsor
ACAD1	Acadia NP	-68.26	44.37	122	134	-68.23	44.35	466	300	5	4	11/12/1987	6/9/1993	NPS
BADL1	Badlands NP	-101.9	43.79	772	239	-101.95	43.77	805	805	-0.01	4.151	1/13/1988	9/30/2006	NPS
BAND1	Bandelier NM	-106.26	35.78	2028	315	-106.3	35.81	2143	2077	1.65	4.058	10/5/1988	9/30/2006	NPS
BIBE2	Big Bend NP	-103.21	29.39	1037								1/27/2000	10/1/2005	NPS
BIBE1	Big Bend NP	103.21	29.35	1082								12/1/1988	8/28/2003	NPS
BRID1	Bridger WA	-109.79	42.93	2396	11	-109.77	42.97	2568	2479	2.01	5.083	7/20/1988		USFS
CANY1	Canyonlands NP	-109.82	38.46	1809	73	-109.75	38.48	1774	1790	-0.29	6.426	12/20/1986	9/30/2006	NPS
CHIR3	Chiricahua NM	-109.36	32.01	1698								7/1/2001	12/16/2003	NPS
CHIR2	Chiricahua NM	-109.39	32.01	1573	97	-112.54	32.01	1682	1625	2.07	3.18	1/23/1999	7/1/2001	NPS
CHIR1	Chiricahua NM	-109.39	32.01	1567	84	-109.32	32.01	2235	1901	6.26	6.123	2/17/1989	1/1/1999	NPS
CRLA1	Crater Lake NP	-122.05	42.96	2050								9/1/1988	9/10/1991	NPS
GLAC1	Glacier NP	-113.94	48.56	968	232	-113.99	48.53	975	972	0.08	5.276	2/2/1988	9/30/2006	NPS
GRBA1	Great Basin NP	-114.21	38.99	2139	315	-114.24	39.02	2365	2248	3.44	3.913	8/20/1992	9/30/2006	NPS
GRCA1	Grand Canyon NP	-111.99	36.0	2256	81	-111.93	36.01	2170	2213	-0.85		12/18/1986	10/1/2007	NPS
	Grandview (on the rim)													
GRCW1	Grand Canyon NP	-112.12	36.07	2177	205	-112.09	36.11	755	1450	-15.78	5.11	12/13/1989	10/1/2007	NPS
	Yavapai (in canyon)													
GUMO1	Guadalupe Mountains NP	-104.81	31.83	1664	249	-104.86	31.82	1317	1467	-3.53	4.858	11/17/1988	9/30/2006	NPS
MEVE2	Mesa Verde NP	-108.49	37.22	2245								7/19/1991	7/28/1993	NPS
MEVE1	Mesa Verde NP	-108.49	37.20	2205								9/15/1988	7/23/1990	NPS
PEFO1	Petrified Forest NP	-109.77	35.08	1755	173	-109.75	34.94	1690	1731	-0.3	15.44	4/17/1987	7/6/1987	NPS
PEFO2	Petrified Forest NP	-109.8	34.9	1698	48	-109.75	34.95	1700	1695	0.1	5.938	7/1/1987	11/30/2004	NPS

Location	Site Name	Receiver Lon (deg)	Lat (deg)	Elevation (m)	Bearing (deg)	Transmitter Lon (deg)	Lat (deg)	Elevation (m)	Mean Elevation	Elevation Angle (deg)	Distance	Start Date	End Date	Sponsor
PINN1	Pinnacles NM	-121.15	36.47	448	317	-121.18	36.5	428	438	-0.25	4.799	3/23/1988	7/25/1993	NPS
ROMO1	Rocky Mountain NP	-105.58	40.36	2536	305	-105.63	40.39	2932	2734	4.31	5.274	11/25/1987	7/8/1997	NPS
ROMO2	Rocky Mountain NP	-105.58	40.37	2413	302	-105.63	40.39	2932	2717	5.01	4.921	10/3/1998	9/30/2006	NPS
SAGO1	San Gorgonio WA	-116.91	34.19	1679	211	-116.94	34.16	1731	1721	0.29	4.099	4/27/1988	5/31/2006	USFS
SAGO1	San Gorgonio WA	-116.91	34.19									3/8/2007		USFS
SHEN2	Shenandoah NP	-78.42	38.51	1054	310	-78.44	38.52	1061	1717	-0.49	1.412	9/15/1991	10/30/2003	NPS
SHEN1	Shenandoah NP	-78.43	38.51	1061								12/8/1988	3/22/1991	NPS
TONT1	Tonto NM	-111.03	33.62	733	115	-111.11	33.65	786	760	0.42	7.203	4/12/1989	9/17/1991	NPS
YELL1	Yellowstone NP	-110.69	44.97	1836	125	-110.65	44.95	1951	1894	1.54	4.285	7/18/1989	7/28/1993	NPS
YOSE1	Yosemite NP	-119.7	37.71	1608	242	-119.73	37.7	1370	1489	-5.04	2.711	8/18/1988	9/30/2006	NPS

NM = National Monument
NP = National Park
WA = Wilderness Area

The Optec NGN-2 open air nephelometer measures total ambient light scattering coefficients for all particles sizes at an effective wavelength of 550 nm (Molenar, 1989). The instrument's open-air design has minimal heating and allows a larger distribution of particle sizes to pass through it. It is also designed with solid-state electronics that are very stable over a wide temperature and humidity range. It still has an inherent limitation of an abbreviated acceptance angle in that it only samples light scattered between 5° and 175°, and the cut point of the instrument has not been characterized. Calibration of the instrument and data validation and processing algorithms are discussed in detail in Molenar and Malm (1992). Unlike transmissometers, where an uncertainty in transmittance leads to an additive error in extinction coefficients, uncertainties in nephelometer calibration lead to multiplicative errors in measured scattering coefficients. Typical uncertainties for the Optec NGN-2 are on the order of 5–10% (Molenar and Malm, 1992).

During high humidity and precipitation events, the nephelometer can report erroneously high scattering coefficient values. This is due to water condensing on the walls of the nephelometer and spray from rain drops impacting the screen on the nephelometer inlet. This water collects in the light trap and reflects light directly into the scattered-light detector, causing extremely high readings. In order to minimize this problem, the door of the nephelometer closes during heavy precipitation events, and a wick was added to the light trap to facilitate the removal of any collected water. A list with nephelometer sites is provided in Table 1.5. Sixteen nephelometers are currently in operation.

Table 1.5. IMPROVE nephelometer network site locations.

Site	Code	State	Latitude	Longitude	Elevation	Start Date	End Date
Acadia NP	ACAD1	ME	44.37	-68.26	122	6/10/1993	12/1/1997
Acadia NP	ACAD2	ME	44.38	-68.26	158	12/1/1997	
Big Bend NP	BIBE1	TX	29.30	-103.18	1052	2/1/1998	
Desolation WA	BLIS1	CA	38.98	-120.11	2109	8/12/1996	6/1/2006
Boundary Waters Canoe Area WA	BOWA1	MN	47.95	-91.50	515	5/4/1993	9/30/1997
Cedar Bluff State Park	CEBL1	KS	38.70	-99.76	669	9/1/2004	8/31/2007
Chiricahua National Monument	CHIR1	AZ	32.01	-109.39	1570	12/1/2003	9/30/2007
Chiricahua National Monument	CHIR1	AZ	32.01	-109.39	1570	10/1/2007	5/11/2010
Tucson	CHPA1	AZ	32.30	-110.98	704	6/1/2003	10/1/2010
Columbia River Gorge National Scenic Area	COGO2	WA	45.57	-122.21	240	6/1/2001	3/9/2005
Cohutta WA	COHU1	GA	34.79	-84.63	743	2/1/2004	3/31/2007
Columbia River Gorge National Scenic Area	CORI1	WA	45.66	-121.00	198	8/25/1993	5/1/2000
Columbia River Gorge National Scenic Area	CORI1	WA	45.66	-121.00	198	6/1/2001	3/9/2005
Tucson	CRAY1	AZ	32.20	-110.88	809	2/1/2001	10/1/2010
Dolly Sods WA	DOSO1	WV	39.11	-79.43	1158	5/9/1993	9/30/1997
Dolly Sods WA	DOSO1	WV	39.11	-79.43	1158	11/1/2003	11/30/2006
Phoenix	DYRT1	AZ	33.64	-112.34	364	7/1/2003	
Edwin B. Forsythe NWR	EBFO1	NJ	39.47	-74.45	5	4/14/1993	4/1/1994
Phoenix	ESTR1	AZ	33.39	-112.39	290	2/1/2003	
Gila WA	GICL1	NM	33.22	-108.23	1783	4/1/1994	10/1/2003
Glacier NP	GLAC2	MT	48.51	-114.00	939	11/7/2007	

Site	Code	State	Latitude	Longitude	Elevation	Start Date	End Date
Great Basin NP	GRBA2	NV	39.01	-114.22	2052	1/23/2008	
Mount Baldy WA	GRER1	AZ	34.06	-109.44	2513	5/1/2001	5/11/2010
Great Gulf WA	GRGU1	NH	44.31	-71.22	439	6/7/1995	3/31/2005
Great Smoky Mountains NP	GRSM1	TN	35.63	-83.94	793	4/28/1993	
Green River Basin	GRVS1	WY	41.84	-109.61	1951	7/1/1996	10/17/2000
Grand Canyon NP	HANC1	AZ	35.97	-111.98	2235	12/18/1997	
Pine Mountain WA	HUMB1	AZ	33.98	-111.80	1586	3/1/1997	11/1/2003
Mazatzal WA	IKBA1	AZ	34.34	-111.68	1280	6/1/2001	5/11/2010
Grand Canyon NP	INGA1	AZ	36.08	-112.13	1164	6/1/2004	
Jarbidge WA	JARB1	NV	41.89	-115.43	1889	4/9/1993	9/30/1997
James River Face WA	JARI1	VA	37.63	-79.51	299	12/5/2000	10/1/2003
Lone Peak WA	LOPE1	UT	40.45	-111.70	1740	11/16/1993	9/1/2001
South Lake Tahoe	LTBV1	CA	38.95	-119.96	1902	2/1/1996	5/1/2004
South Lake Tahoe	LTBV2	CA	38.93	-119.96	1904	12/1/2005	6/30/2006
Lye Brook WA	LYBR1	VT	43.15	-73.12	1010	8/5/1993	3/31/1994
Lye Brook WA	LYBR1	VT	43.15	-73.12	1010	5/30/1996	12/31/2000
Lye Brook WA	LYBR1	VT	43.15	-73.12	1010	1/1/2001	10/1/2003
Mammoth Cave NP	MACA1	KY	37.22	-86.07	219	3/11/1993	7/1/1997
Mammoth Cave NP	MACA2	KY	37.13	-86.15	243	7/23/1997	
Mayville	MAYV1	WI	43.44	-88.53	306	11/1/2000	12/31/2006
Mazatzal WA	MAZA1	AZ	33.91	-111.41	2164	4/1/1997	8/30/2000
Sierra Ancha WA	MCFD1	AZ	33.91	-110.97	2175	10/30/1997	2/1/2000
Milwaukee	MILW1	WI	43.00	-87.89	193	6/1/2004	6/30/2006
Mount Rainier NP	MORA1	WA	46.76	-122.12	423	2/13/1993	
Mount Zirkel WA	MOZI1	CO	40.46	-106.74	3215	11/1/1993	8/1/1994
Mount Zirkel WA	MOZI2	CO	40.54	-106.68	3242	11/5/1993	7/31/2009
Galiuro WA	MUSR1	AZ	32.33	-110.23	1402	7/8/1997	6/30/2005
National Capitol - Central	NACA1	DC	38.88	-77.03	20	4/24/2003	
Nebraska National Forest	NEBR1	NE	41.89	-100.34	888	8/10/2005	8/31/2007
Okefenokee NWR	OKEF1	GA	30.74	-82.12	15	2/12/1993	6/24/1997
Organ Pipe Cactus National Monument	ORPI1	AZ	31.95	-112.80	514	6/1/2003	5/11/2010
Petrified Forest NP	PEFO3	AZ	34.82	-109.89	1709	11/18/2003	9/30/2007
Petrified Forest NP	PEFO3	AZ	34.82	-109.89	1709	10/1/2007	5/11/2010
Phoenix	PHON1	AZ	33.50	-112.10	366	4/1/1997	9/30/2009
Quaker City	QUAK1	OH	39.94	-81.34	372	3/26/2002	1/14/2004
Superstition WA	QUVA1	AZ	33.29	-111.29	668	6/1/2003	5/11/2010
Cape Romain NWR	ROMA1	SC	32.94	-79.66	2	1/1/2004	
Rocky Mountain NP	ROMO3	CO	40.28	-105.55	2735	12/31/2007	
Chiricahua WA	RUCA1	AZ	31.78	-109.30	1637	11/17/1997	5/1/2001
Seney NWR	SENY1	MI	46.29	-85.95	227	1/7/2002	7/1/2006
Shenandoah NP	SHEN1	VA	38.52	-78.43	1073	9/19/1996	
Shining Rock WA	SHRO1	NC	35.38	-82.77	1612	6/8/1994	8/1/1999
Sierra Ancha WA	SIAN1	AZ	34.09	-110.94	1595	8/1/2000	5/11/2010
Alpine Lakes WA	SNPA1	WA	47.42	-121.43	1152	8/26/1993	5/1/2001
Sycamore Canyon WA	SYCA1	AZ	35.14	-111.97	2040	7/1/1998	5/11/2010
Three Sisters WA	THSI1	OR	44.29	-122.04	881	7/23/1993	5/1/2001
Tucson	TUCN1	AZ	32.24	-110.96	745	4/1/1997	4/8/2009
Saguaro NP	TUMO1	AZ	32.28	-111.17	754	12/1/1996	11/1/2001
Saguaro NP	TUMO2	AZ	32.25	-111.22	718	11/1/2001	5/11/2010
Upper Buffalo WA	UPBU1	AR	35.83	-93.20	701	2/26/1993	9/30/1997
Upper Buffalo WA	UPBU1	AR	35.83	-93.20	701	9/1/2004	10/1/2009
Phoenix	VEIX1	AZ	33.46	-112.00	345	6/1/2003	

Site	Code	State	Latitude	Longitude	Elevation	Start Date	End Date
Virgin Islands NP	VIIS1	VI	18.34	-64.80	64	4/23/1998	9/30/2005
Wichita Mountains NWR	WIMO1	OK	34.73	-98.71	517	9/1/2004	8/31/2007

NP = National Park
NWR = National Wildlife Refuge
SP = State Park
WA = Wilderness Area

1.3 PROTOCOL AND EQUIPMENT CHANGES

While consistency through time is critical to a monitoring program interested in trends, changes in sampling, analysis, and data-handling protocols and equipment are inevitable in any long-term monitoring program. Significant changes in sampling, analysis, and data processing have occurred in the history of the IMPROVE network. Most of the changes were implemented to improve the quality or usefulness of the IMPROVE dataset or to increase the overall effectiveness of the network within available resources. Assessments were conducted prior to many of the changes to assess and, where possible, identify approaches that would minimize the effects of changes on the dataset. In addition, IMPROVE routinely conducts data consistency assessments, specifically designed to identify and attempt to explain data discontinuities and trends that are not thought to be associated with changes in atmospheric conditions. The results of these assessments are used to inform decisions concerning the operation of IMPROVE and to alert data users via data advisories posted on the IMPROVE website.

This section encompasses changes that have occurred since the last IMPROVE report was published in 2006 (Debell, 2006), covering samples collected from January 2005 to the present. Some of the key changes, including the reasoning behind the decision and the ramifications for the IMPROVE dataset, are described below and listed in Table 1.7. The final subsection describes some inadvertent changes or interferences that were discovered in the course of data analysis and quality control review. Many of the summaries in this section are referenced to data advisories on the IMPROVE website that provide additional information, including data plots and useful graphics.

1.3.1 Analytical Changes

1.3.1.1 Introduction of a New Model Carbon Analyzer

Organic carbon (OC) and light absorbing carbon (LAC) on quartz filters have been quantified by the Desert Research Institute (DRI) since the beginning of the IMPROVE network, using laboratory analyzers developed at the Oregon Graduate Center (OGC). These instruments use a thermal/optical reflectance (TOR) protocol to determine OC and LAC.

By the late 1990s it was evident that the DRI/OGC analyzers were deteriorating. Some components were no longer manufactured and the data acquisition system was antiquated. The Model 2001 (Atmoslytic Inc., Calabasas, CA) analyzer was developed and made commercially available as a replacement. The Model 2001 has a number of enhancements, including better characterization of sample temperature and sample atmosphere, automatic sample positioning, more rapid temperature response, improved seals and flow control, greater heating capacity, advanced electronics, modern data acquisition, the potential for an automated sample changer,

and the ability to simultaneously measure reflectance and transmittance. Concurrent with the hardware modifications was the application of a new TOR protocol, named IMPROVE_A, designed to reflect the more accurate and less variable temperature and instrument-atmospheric conditions provided by the new instruments.

The Model 2001 analyzer was applied for routine analysis of IMPROVE samples collected on or after January 1, 2005. Extensive testing prior to deployment had suggested that observable differences in the data record would be minimal (Chow et al., 2005). However, subsequent examination of data from the first two years of analysis (2005 and 2006) revealed unforeseen differences between data from the old and new instruments (White, 2007a). The differences vary as a function of site, but the new data generally identify a higher proportion of total carbon as LAC and a lower proportion as OC than were observed in the final years of the old instruments. The LAC/OC distinction is operationally defined, and the differences are not fully understood.

1.3.1.2 Transition from He Flush to Vacuum Chamber Cu-Anode XRF

Light-element concentrations in samples collected after December 1, 2001, have been determined by X-ray fluorescence (XRF) analysis using a Cu-anode tube as the source. Until 2005, analyses were conducted at ambient pressure in a He-flushed atmosphere. That system was replaced on January 1, 2005 (sample date), with a new system that operates under vacuum.

In 2001 proton-induced X-ray emission (PIXE) switched to He-flushed XRF and resulted in substantially decreased sensitivity for sodium, the lightest of the elements reported. Sensitivities improved for 2005 and later samples after the conversion of the XRF system to vacuum operation but are still below those from PIXE (White, 2007b).

A second vacuum XRF system, with the same design, was then developed and tested for equivalence with the first (White, 2007c). Samples collected in October 2005 were the first to be reported from the second system. Data from samples collected after October 1, 2005, are reported with an added indicator of the Cu-anode XRF system used in analysis: the first (1) or the second (2). (All light-element data from January through September 2005 samples are from the first system.)

The two Cu-anode systems are designed to be equivalent and are calibrated against the same reference foils. The two systems report concentrations for the single-element calibration foils that agree within prescribed tolerances. However, the two systems do exhibit some detectable differences for actual samples.

1.3.1.3 Introduction of New Calibration Foils for Mo-Anode XRF

A molybdenum-anode XRF instrument is used to analyze the heavier elements (Ni, Cu, Zn, As, Se, Br, Rb, Sr, Zr, and Pb). During the analysis of September 2005 samples, new calibration foils with lighter deposits were acquired and used in the Mo-anode XRF system (Flocchini, 2007). The new calibration foils resulted in changes to the calibration factors for the elements Ni, As, Se, Br, Rb, and Pb that could be observed in their effects on reported ambient concentrations.

The new foils represent an attempt to utilize reference foils that more closely match ambient samples in loading. These foils were used in preparing a calibration table that provides the reference points for converting the X-rays collected during analysis to elemental concentrations on filter samples collected in the atmosphere. The uncertainties quoted by the manufacturer for these new foils were ±10% compared to ±5% for the older, more heavily loaded foils. After a number of ambient samples had been analyzed, it became apparent that these new foils resulted in ambient concentrations that were inconsistent with those observed in prior years.

Changes in the percent change in the calibration factors with the old standards compared to the new standards ranged from 0% (no change) for Sr and Zr to -76% change for As. The percentages represent the differences between the last calibration performed with the old foils and the first calibration performed with the new foils. The calibration factors are multiplicative factors in the estimations of the reported concentrations that can introduce systematic biases between the previous and current data. The resulting shifts in concentration must be accounted for in any analysis of trends.

1.3.1.4 Processing XRF Calibration Data

XRF sulfur data reported for sample dates in 2004 and most of 2003 were based on a nonstandard value for the sulfur calibration foil: the value 12.0 $\mu g\ cm^{-2}$ was substituted for the value 13.8 $\mu g\ cm^{-2}$ quoted by the supplier (White, 2006a). The adjusted value was used as early as February 2003 and may have been used still earlier. The rationale for using an adjusted value was not documented and may have been to improve agreement with ion-chromatographic sulfate measurements.

Sulfur data for sample dates beginning in January 2005 are based on the quoted value of the foil, which yields higher reported values by the factor 13.8/12.0 = 1.15, or 15%. This reporting change, not the simultaneous switch from a helium-flushed system to one operating in vacuum, accounts for the bulk of the increase in reported sulfur relative to reported $SO_4^=$ between December 2004 and January 2005. The magnitude of the reporting change is small relative to the range of sulfur concentrations reported across the network. However its systematic impact is likely to be evident in interannual comparisons and should be accounted for in their interpretation.

The procedure for analyzing XRF system calibration data was modified beginning with samples collected in January 2007. In prior years the calibration for any element had been based upon the quoted concentration of the calibration standard foil for that element, as reported by Micromatter, the manufacturer of the standard foils. Beginning with the January 2007 data, a standard was analyzed for each element and then a smooth curve was drawn through the resulting instrument responses. The curve fit value for each element was then used as the basis for calibration. This new curve fitting approach was initiated in an attempt to dampen the concentration uncertainty associated with any single standard foil. The result is a shift in the typical concentrations reported for some elements.

1.3.1.5 New XRF Quality Assurance Reports & Clarification of Data Acceptance Criteria

Beginning with samples collected in January 2005, quarterly reports have been prepared to summarize the findings of quality control checks on the XRF data (http://vista.cira.colostate.edu/improve/Data/QA_QC/QAQC_UCD.htm). January 2005 also marked the initial use of the vacuum chamber Cu-anode XRF system, which replaced the helium flush system.

The quarterly reports present detection rates for each element, as well as results from calibrations and calibration checks, X-ray energy calibrations, field blank analyses, reanalysis of selected filters, and comparison of the Cu and Mo anode systems for elements measured on both. The reports also document the system settings that were used for that quarter's analytical session.

The initiation of quarterly reports in 2005 also marked the formalization of acceptance criteria for XRF data. The performance of the systems is monitored approximately weekly by monitoring the ratios of the system response at each calibration check to the response observed at the last calibration. If the ratios lie within the acceptance limits 0.9–1.1 for all quantitative elements, then the system is considered stable and the existing calibration factors continue to be used. Deviations beyond 10% trigger an investigation of the problem and possible system recalibration. After a recalibration, all samples analyzed since the last successful calibration verification are reanalyzed with the new calibration factors.

1.3.2 Sampling Equipment Changes

1.3.2.1 Filter Masks Removed

Until recently, masks were used at many sites to reduce the nominal collection area of module A filters from 3.53 cm^2 to 2.20 cm^2. Masking improved XRF sensitivities at low concentrations, but caused occasional clogs at high concentrations. By the beginning of 2008, all filters had been unmasked.

A relative bias between masked and unmasked elemental measurements can be seen by comparing the sulfur/sulfate ratios measured under both conditions, as sulfate ion concentrations have been measured by the same protocol at all sites since 2001 (White, 2008). Unmasked sites have generally reported about 5% more sulfur than masked sites at a given measured sulfate concentration, and the sulfur reported from masked sites has typically risen by about 5% when they have converted to unmasked operation. It is not known whether these differences reflect under-reporting from masked samples, over-reporting from unmasked samples, or contributions from both.

IMPROVE's hybrid integrating plate/sphere (HIPS) is designed to measure the absorption thickness of a Teflon filter sample. Absorption thickness can be thought of as the absorption cross-section ($m^2\ g^{-1}$) of the absorbing material times the material's areal mass loading ($g\ m^{-2}$) on the filter. Well-recognized artifacts of the method cause measured absorption to increase less than proportionately with the mass loading. Because masking generates higher areal loadings at the same atmospheric concentrations, some bias toward lower absorption

readings for masked samples can be expected to result from this loading dependence (White, 2010).

1.3.2.2 Quartz Backup Filters Added at Six Sites

For many years the IMPROVE network has collected quartz backup filters behind the primary quartz filters at six sites. IMPROVE has used the monthly median carbon data from these six sites to adjust for a presumed positive artifact for all sites in the network. Experts from IMPROVE and other similar networks met at a carbon particulate matter monitoring workshop in January 2008 to consider improvements to this approach for estimating sampling artifacts. Their focus was on improving spatial coverage, understanding urban/rural differences, and better understanding the observed relationship between front filter and backup filter organic carbon concentrations The following recommendations were phased into the IMPROVE network between mid-2008 and mid-2009:

- Continue quartz backup filters at the six original sites: Chiricahua, Arizona (CHIR1), Grand Canyon (GRCA2), Mount Rainier, Washington (MORA1), Okefenokee, Georgia (OKEF1), Shenandoah, Virginia (SHEN1), and Yosemite (YOSE1). Inaugurate backup filters at six additional sites: Blue Mounds, Minnesota (BLMO1), Hercules-Glades, Missouri (HEGL1) (both collocated samplers), Lye Brook, Vermont (LYBR1), Phoenix (PHOE1) (both collocated samplers), Washington, D.C. (WASH1), and Yellowstone (YELL1).
- Collect quartz field blanks only at the sites listed above and discontinue them elsewhere in the network. Collect a set of field blanks with every filter cartridge (every week, beginning on Tuesday). To conserve funding, only two-thirds of the field blank sets will be analyzed, only those for weeks beginning or ending with a Tuesday sampling day. Both the front and back field blanks will be analyzed. The field blanks from the intervening week will be archived but will not be analyzed.
- Only backup filters collected during the weeks of field blank analysis will be analyzed, i.e., two-thirds of the secondary filters. The backup filters from the intervening week will be archived but will not be analyzed. All sampled front filters will be analyzed, from all weeks.

1.3.2.3 New Cassette Design for the IMPROVE Sampler

The IMPROVE group at UC Davis has developed a new filter cassette design that will be implemented in the IMPROVE network during 2011. In the new design the metal screen that supports the filter is detached, unlike the older screens which were permanently attached to the plastic cassette body. This new design results in more consistently uniform sample deposits on the filters, thereby improving the reliability of measurements such as the XRF analysis that is used to determine elemental concentrations.

The new cassette design is shown in Figure 1.5. The metal screen can be removed by the technicians for cleaning and then re-installed along with a clean filter for the next sampling event. Once the cassette is reassembled with the cassette cap in place, the filter fits snugly against the screen, just as it did with the old design. For comparison, Figure 1.6 shows the old cassette design, with the screen permanently attached. Because the cassettes are serviced and

reassembled in the UC Davis laboratory, the change to the new cassette screens is transparent to the site operators. The assembled cartridges that are shipped to the sites in blue shipping boxes look the same before and after the change to the new screens.

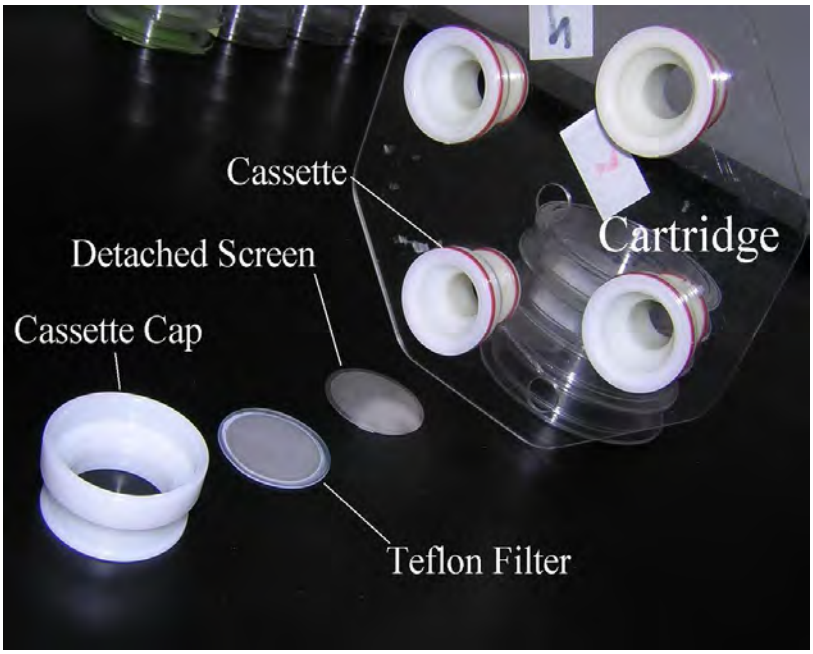

Figure 1.5. Detached screen cassette.

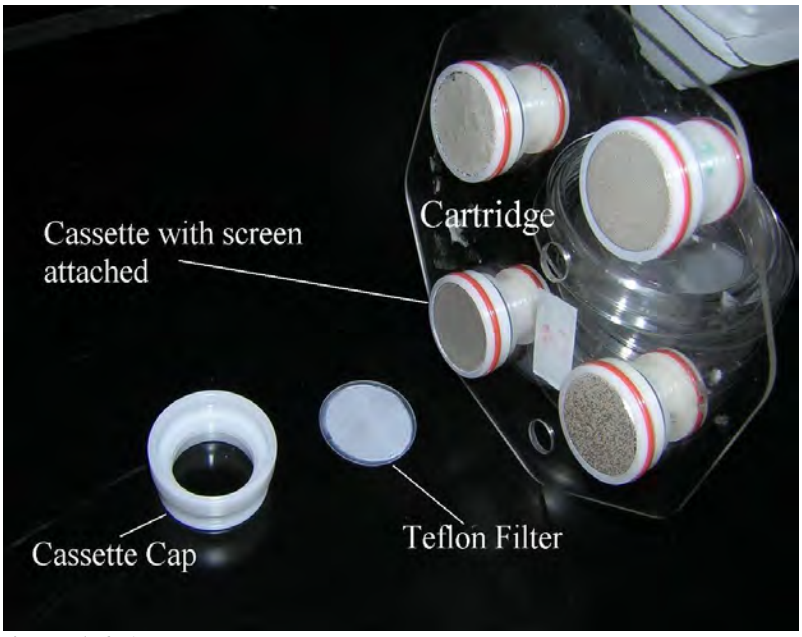

Figure 1.6. Attached screen cassette.

The switch to the new design was motivated initially by some changes in the cassette manufacturing process. The IMPROVE network was in need of additional cassettes to replace damaged pieces and to accommodate new sites. Due to some engineering changes in the manufacturer's shop it was no longer possible to manufacture cassettes in precisely the same configuration as the existing cassettes. Attempts were made to produce a modified attached

screen cassette that would be comparable to those already in use in the network. However, field tests of attached screen prototypes using the manufacturer's modified approach were unable to demonstrate satisfactory measurement agreement with the existing design.

Reengineering of the cassette design was needed to achieve comparability between the old and new units, so the UC Davis group decided to take advantage of the opportunity to come up with a superior design. Their literature review found that essentially all samplers used in other aerosol networks employ a detached screen design. Furthermore, initial prototype tests indicated that a detached screen design would improve sample uniformity. A redesign and testing program led to the final detached screen cassette design to be deployed in the network.

Prototype units of the new detached screen design were prepared and tested extensively at UC Davis to ensure comparability with the existing attached screen design. UC Davis has an outdoor IMPROVE sampler test facility where up to sixteen sampler modules can be operated concurrently. Tests were run using paired sets of attached and detached screen cassettes, all sampling the ambient UC Davis air at the same time. The flow rate through each sampler module was carefully set and calibrated so that flow rate differences among the modules would be insignificant, thereby ensuring that the flow rate-dependent cyclone particle size cutpoint would be the same for each module.

Teflon filter samples were collected at UC Davis and then were weighed and subjected to XRF analysis to determine elemental concentrations and to laser absorption measurements to quantify aerosol light absorption. These tests demonstrated that samples collected using the old attached screen cassettes and the new detached screen cassettes were comparable. The differences observed between the sets were very small and were well within the statistical uncertainty of the routine IMPROVE measurements.

Because multiple samples from each cassette type were acquired during each test, it was also possible to determine the measurement precision within each type. These results indicated that the precision of the mass and elemental measurements using the new detached screen design is typically tighter, a welcome improvement over the existing design.

The improved precision is likely the result of improved sample uniformity. Figures 1.7 and Figure 1.8 show typical sample deposit patterns using attached and detached screens, respectively. The deposit on the attached screen filter exhibits non-uniformity around the edge of the filter. The edge areas with no deposit are a result of the process used to press the screen into the plastic cassette body, whereby plastic clogs some of the screen holes around the perimeter. The deposit on the detached screen filter exhibits no edge effects, since intact holes extend all the way to the edge of the filter.

Figure 1.7. Filter sample collected using attached screen cassette.

Figure 1.8. Filter sample collected using detached screen cassette.

New screens are being purchased for all cassettes, but the existing plastic cassette bodies can be used with the detached screen design. Equipment in the UC Davis machine shop is used to punch the attached screen out of each unit and then smooth any rough edges that remain on the plastic body. Once that quick procedure is completed the detached screen fits precisely into each cassette body. Some new cassette bodies, identical to the existing ones, have also been purchased to increase the inventory of available cassettes.

Only the 25 millimeter cassettes are being converted to the detached screen design. The 37 millimeter B-module cassettes will remain unchanged and will retain the attached screen design. The 37 millimeter nylon filters are extracted in solution which is then used for ion analysis, so the uniformity of the sample deposit does not influence the analysis.

The 25 millimeter cassettes used in the A, C, and D modules are all being converted to the detached screen design in order to achieve consistency throughout the measurement set. However, the benefits of improved sample uniformity are expected only for the A-module Teflon® filter. XRF, laser absorption, and proton beam hydrogen measurements apply an incident beam that covers only the central portion of the filter, so uniformity is crucial in extrapolating the results to the entire filter. The D-module PM_{10} Teflon filters are weighed only, so sample uniformity does not impact the analysis.

The C-module employs a quartz filter, with physical characteristics that differ from Teflon. Teflon is a plastic and Teflon filters are pulled down firmly to the surface of the screen when the vacuum pump is on. Hence, sample material is deposited only in the immediate area of the screen holes, so the characteristics of the screen can influence the sample deposit. The "imprint" of the screen holes can be seen clearly when Teflon filter deposits are viewed under a microscope. Quartz filters, on the other hand, are made of multiple layers of randomly oriented media and have a porous or fibrous texture that distributes the sample uniformly across the entire filter surface, independent of the geometry of the backing screen.

1.3.3 Data Processing Changes

1.3.3.1 Change in the Definition of Flow Rate Native Flags

Recent work performed to characterize the IMPROVE cyclone suggested that the equations relating cut point to flow rate developed at UC Davis are invalid (J. Turner, 2006, personal communication). Therefore, the native validation flags based on flow rate have been revised and applied to samples collected in January 2005 and onward (McDade, 2007).

The IMPROVE cyclone is based on the AIHL cyclone specifications. The recent characterization work was consistent with the original AIHL characterization performed by John and Reischl (1980), and it was therefore decided to use the original John and Reischl (1980) equation for the IMPROVE cyclones used in the A, B, and C sampler modules (J. Turner, 2006, personal communication). The John and Reischl (1980) equation is much less sensitive to flow rate than the UC Davis equation used in the past, and the cut point is 2.4 μm rather than 2.5 μm at the IMPROVE nominal flow rate of 22.8 LPM.

UC Davis applies one of four "native" (i.e., initial) flags to data to indicate unusual flow rates: CL (clogged), CG (clogging), RF (extremely high or low flow rate), and LF (moderately high or low flow rate). The CL flag is based on the accuracy of the flow rate equation and is therefore not affected by this new cyclone information. The criteria for CG and RF flow rate flags are now stricter in terms of cut point because the cut point equation is less sensitive to flow rate. These criteria apply only to modules A, B, and C. The numerical flow rate criterion for the LF flag has been altered because the prior criterion is not centered on 2.5 μm as a result of the shift in the equation. The native flags LF and RF translate to a V5 status flag in the IMPROVE

VIEWS database, native flag CG translates to a V6 status flag, and native flag CL translates to an M3 status flag. Table 1.6 provides the validation flags and how they have been applied.

Table 1.6. Updated flow rate-related validation flag definitions and application criteria.

Validation Flag	Definition	Concentration Reported?	Old Criteria: applied to Jan 2000 through Dec 2004 samples	Updated criteria: applied to samples collected in Jan 2005 and onward
CL	Clogged filter	No	Flow rate less than 15 LPM for more than 1 hour	Same criterion: based on the flow rate calculation inaccuracy not cut point
CG	Clogging filter	Yes	Flow rate less than 18 LPM for more than 1 hour	Same criterion: corresponds to a cut point of 3 μm
LF	Low/high flow rate	Yes	Average flow rate results in cut point outside 2 to 3 μm (corresponds to flow rates of 21.3 LPM and 24.3 LPM).	Average flow rate results in cut point outside 2.25 to 2.75 μm : corresponds to flow rates of 19.7 and 24.1 LPM
RF	Really high flow rate	Yes	Average flow rate greater than 27 LPM	Same criterion: corresponds to a cut point of 2 μm

1.3.4 Changes or Interferences Noted Through Data Analysis

1.3.4.1 Sulfur Interference in the Determination of Silicon

The primary XRF peak for sulfur has a shoulder that overlaps the primary XRF peak for silicon. Due to this peak interference, accurate determination of Si is difficult when S concentrations greatly exceed Si concentrations (White, 2006b). Reported concentrations then depart from expectations based on Fe and other crustal elements.

The degree of interference by S is sensitive to details of system performance that can change from month to month. Furthermore, reported uncertainties and detection limits for Si do not adequately account for the interference by S. Data analysts are encouraged to distrust reported Si concentrations when [S] >> [Si] and to disregard reported uncertainties and MDLs for Si.

1.3.4.2 Shifts in the $S/SO_4^=$ Ratio

Most fine-particle sulfur is present as sulfate. Measured concentrations are therefore expected to exhibit a sulfur-to-sulfate mass ratio of approximately 1 to 3. Reported concentrations often depart from this ratio by more than their reported uncertainties (White, 2007d). Empirical evidence points to XRF measurement bias as the source of most of the observed variation. As one example, sulfur/sulfate ratios throughout the network exhibited a decreasing trend during 2003–2004 that was offset by two abrupt increases, each coming at the start of a new sample month. The XRF analyses, unlike the ion-chromatographic analyses, are quality assured in calendar-month batches, and both of the observed jumps coincided with recalibrations of the Cu-anode system used to determine sulfur. The fact that abrupt changes in the sulfur/sulfate ratio were associated with recalibrations of the XRF system suggests that the gradual changes observed at other times may be due to drift in that system's calibration.

A further 15% shift at the start of 2005 was explained as the result of a change in the value used for the sulfur calibration foil from a legacy adjustment to the manufacturer's quote. Since that time further shifts have occurred, including a drop of about 10% in sulfur/sulfate ratios at the start of 2007 (White, 2009). Calibrations in 2005–2006 were based on the quoted value of a foil for each element. Calibrations in 2007–2008 were based on a curve fit to several different elemental foils, and this fit effectively assigned a value to the sulfur foil different from the manufacturer's quote.

The XRF change from helium flushing to vacuum operation at the start of 2005 yielded a somewhat tighter relationship between sulfur and sulfate concentrations. A second vacuum system, designed to be equivalent and calibrated against the same reference foils, was introduced in October 2005 to speed processing. The two systems report concentrations for the single-element foils that agree within prescribed tolerances but exhibit some detectable differences in actual samples. All IMPROVE samples for a given month are analyzed with the same system, and similar intersystem differences for sulfur may contribute some month-to-month variability to the sulfur/sulfate ratio.

Table 1.7. Major networkwide changes in sampling, analysis, and data reporting affecting samples collected January 2005 and later.

Change Date	Change Description
1/1/2005	Changed carbon analysis instrument from DRI/OGC to Model 2001 Thermal/Optical Carbon Analyzer. Changed analysis protocol from IMPROVE to IMPROVE_A
1/1/2005	Changed Cu-anode XRF from helium flush to vacuum chamber system
1/1/2005	Began reporting XRF-determined sulfur based on the quoted value of the calibration foil, replacing empirical value that had been used in 2003 and 2004
1/1/2005	Introduced quarterly XRF QA reports.
1/1/2005	Flow rate native flags revised to reflect new cyclone cut point characterization
9/1/2005	Introduced new calibration foils for Mo-anode XRF system, with lighter deposits
10/1/2005	Introduced a second Cu-anode XRF vacuum chamber system
1/1/2007	Introduced XRF curve fit calibration procedure
12/23/2007	Last sampling date using masked Teflon filters at any site
8/7/2008-6/4/2009	Quartz backup filters added at six sites

1.4. CHEMICAL SPECIATION NETWORK

The objectives of the EPA's Chemical Speciation Network (CSN) are to track progress of emission reduction strategies through the characterization of trends, validation of air quality modeling and source apportionment activities, support of regulatory efforts such as the Regional Haze Rule, and support of health effects and exposure studies. CSN operates approximately 50 long-term trend sites, with another ~150 sites operated by state, local, and tribal agencies, primarily in urban/suburban settings.

The EPA's $PM_{2.5}$ speciation program was established in 1997 as a complement to the $PM_{2.5}$ Federal Reference Method (FRM) mass network. The pilot phase of the program included thirteen sites that operated from February through July 2000. The Speciated Trends Network (now referred to as the CSN) was deployed in the fall of 2000 (U.S. EPA, 2004). Historically, CSN utilized several types of samplers, including the Thermo Andersen RAAS, Met One SASS,

and the URG MASS. The specific sampler employed at a given site was chosen by the state, local, or tribal agency; however, the Met One is the predominant sampler used. All samplers utilize a $PM_{2.5}$ inlet and three channels containing Teflon, nylon, and quartz filters. A magnesium oxide denuder is used ahead of the nylon filter. Samplers operate on a 24-h schedule from midnight to midnight every third day. Supplemental sites may differ in sampler type, analysis laboratory, and sampling schedule (1-in-6 versus 1-in-3 day periods). Filters from most Trend sites are analyzed at the RTI International Laboratory in Research Triangle Park, North Carolina. $PM_{2.5}$ gravimetric mass and elemental compositions are analyzed from the Teflon filter, ions from the nylon filter, and carbon from the quartz filter. The carbon analysis was historically performed using thermal optical transmittance (TOT) using a NIOSH-type protocol. The recognition that IMPROVE samplers and TOR analysis produce different OC and LAC concentrations than CSN samplers and TOT analysis has motivated the CSN transition to TOR analysis for consistency with the IMPROVE network. In addition to the transition from TOT to TOR, in April 2005 the EPA decided to replace the carbon channel sampling and analysis methods with a new, modified IMPROVE version II module C sampler (URG 3000N). The conversion began in May 2007 with 56 sites, followed by another 63 sites in April 2009 and 78 additional sites in October 2009 (U.S. EPA, 2009). Additional detail regarding IMPROVE and CSN sampling and analysis methods for each species is provided in Chapter 2 and includes discussion of aerosol species mass calculations. A discussion of the adjustments applied to CSN carbon data collected prior to the transition to the new analyses and monitors is also included. Adjustments to CSN carbon data were required for IMPROVE and CSN data to be combined. A map of 321 current and discontinued CSN sites is provided in Figure 1.9, with the general regions depicted. We empirically defined 31 regions for the CSN sites based on seasonal distribution of aerosol concentrations and site location. For comparison purposes we grouped sites in regions similar to those defined for the IMPROVE network. Of the 31 regions, eight had only 1 site per region. A list of the 176 sites that met the completeness criteria outlined in Chapter 2 is provided in Table 1.8, including site location, region, and setting (urban, suburban, or rural). The “complete” sites are shown as orange circles on Figure 1.9. CSN data can be downloaded from http://views.cira.colostate.edu/fed/ or http://www.epa.gov/ttn/airs/airsaqs/.

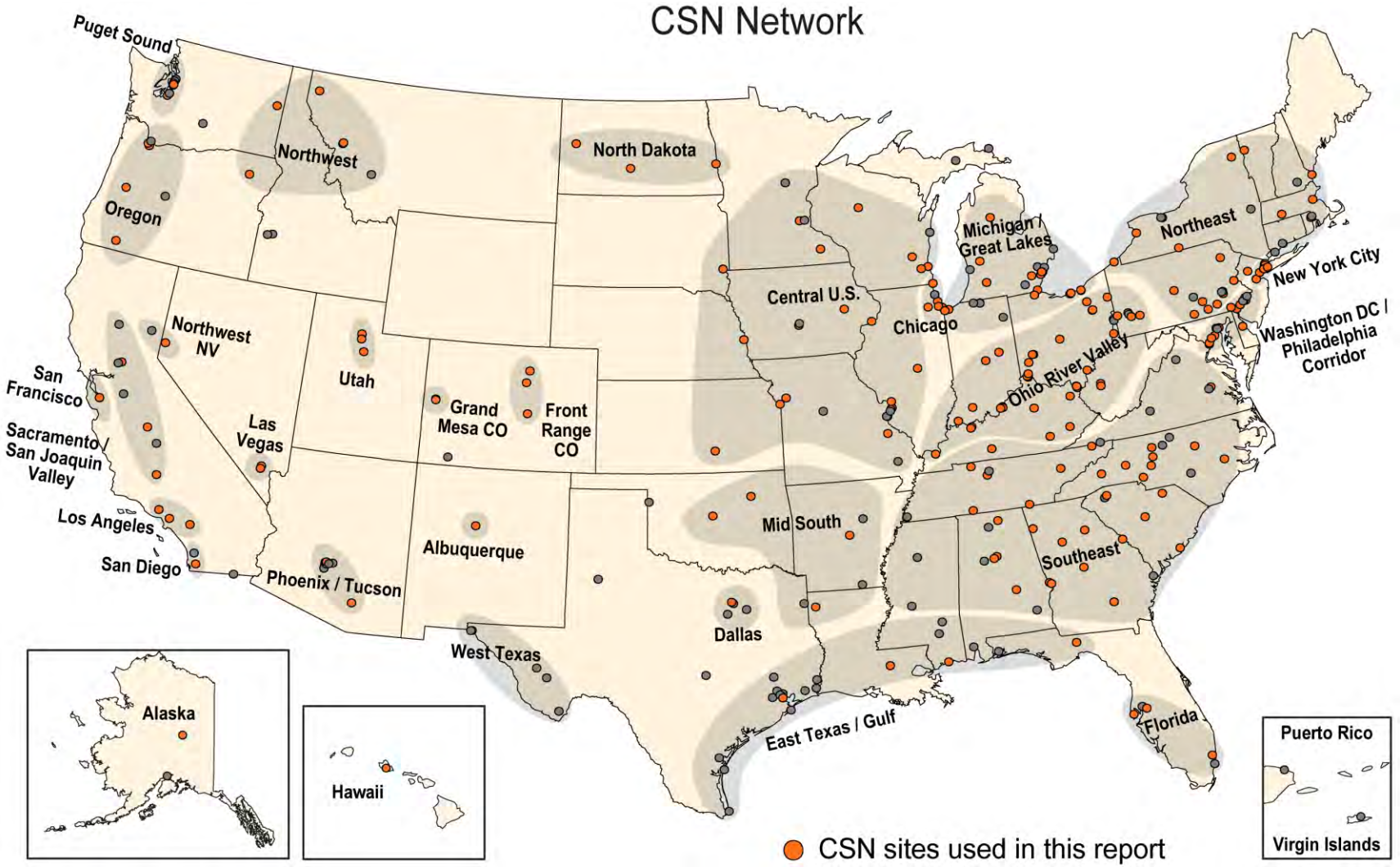

Figure 1.9. Current and discontinued Chemical Speciation Network (CSN) sites (grey and orange) operated by the Environmental Protection Agency. Regions are shown as shaded areas and bold text. The sites included in the analyses in this report are shown as orange circles.

Table 1.8. Chemical Speciation Network (CSN) site location, setting and region.

Site	City	State	Region	Latitude (deg)	Longitude (deg)	Elevation (m)	Setting
10730023	Birmingham	AL	Southeast	33.553	-86.815	177	urban
10732003	Birmingham	AL	Southeast	33.500	-86.924	180	suburban
10890014	Hunstville	AL	Southeast	34.688	-86.586	180	urban
11011002	Montgomery	AL	Southeast	32.407	-86.256	64	suburban
11130001	Phenix City/Columbus	AL	Southeast	32.476	-84.999	91	urban
20900010	Fairbanks	AK	Alaska	64.841	-147.720	132	urban
40139997	Phoenix	AZ	Phoenix/Tucson	33.504	-112.095	355	urban
40191028	Tucson	AZ	Phoenix/Tucson	32.295	-110.982	710	urban
51190007	Little Rock	AR	Mid South	34.756	-92.276	77	urban
60190008	Fresno	CA	Sacramento/San Joaquin Valley	36.781	-119.772	91	suburban
60290014	Bakersfield	CA	Sacramento/San Joaquin Valley	35.356	-119.040	118	urban
60371103	Los Angeles	CA	Los Angeles	34.067	-118.227	126	urban
60658001	Rubidoux	CA	Los Angeles	34.000	-117.416	250	suburban
60670006	Sacramento	CA	Sacramento/San Joaquin Valley	38.614	-121.367	19	suburban
60730003	El Cajon	CA	San Diego	32.791	-116.942	169	suburban
60850005	San Jose	CA	San Francisco	37.349	-121.895	21	urban
61112002	Simi Valley	CA	Los Angeles	34.278	-118.685	308	suburban
80010006	Commerce City	CO	Front Range CO	39.826	-104.937	1558	suburban
80410011	Colorado Springs	CO	Front Range CO	38.831	-104.828	1828	urban
80770017	Grand Junction	CO	Grand Mesa CO	39.064	-108.561	1524	urban
81230008	Platteville	CO	Front Range CO	40.209	-104.823	1464	rural
90090027	New Haven	CT	Northeast	41.301	-72.903	5	urban
100010003	Dover	DE	Washington D.C. /Philadelphia Corridor	39.155	-75.518	6	suburban
100032004	Wilmington	DE	Washington D.C. /Philadelphia Corridor	39.739	-75.558	31	urban
110010043	Washington D.C.	DC	Washington D.C. /Philadelphia Corridor	38.919	-77.013	31	urban
120111002	Davie	FL	Florida	26.083	-80.238	3	suburban
120573002	Valrico	FL	Florida	27.966	-82.230	28	rural
120730012	Tallahassee	FL	East Texas/Gulf	30.440	-84.348	16	suburban
121030026	Pinellas Park	FL	Florida	27.850	-82.715	2	suburban
130210007	Macon	GA	Southeast	32.777	-83.641	103	suburban
130590001	Athens	GA	Southeast	33.946	-83.372	214	suburban
130690002	Douglas	GA	Southeast	31.513	-82.750	64	rural
130890002	Panthersville	GA	Southeast	33.688	-84.290	244	suburban
131150005	Rome	GA	Southeast	34.263	-85.305	213	suburban
132150011	Columbus	GA	Southeast	32.431	-84.932	78	suburban
132450091	Augusta	GA	Southeast	33.434	-82.022	57	suburban
150032004	Pearl City	HI	Hawaii	21.397	-157.972	24	urban
170310057	Chicago	IL	Chicago	41.915	-87.723	185	suburban
170310076	Chicago	IL	Chicago	41.751	-87.714	188	suburban
170314201	Northbrook	IL	Chicago	42.140	-87.799	194	suburban
170434002	Naperville	IL	Chicago	41.771	-88.153	213	urban

Site	City	State	Region	Latitude (deg)	Longitude (deg)	Elevation (m)	Setting
171150013	Decatur	IL	Central U.S.	39.867	-88.926	206	suburban
171192009	Alton	IL	Central U.S.	38.903	-90.143	154	suburban
180372001	Jasper	IN	Ohio River Valley	38.391	-86.929	139	urban
180390003	Elkhart	IN	Michigan/Great Lakes	41.668	-85.969	229	urban
180650003	Middleton	IN	Ohio River Valley	40.012	-85.524	309	rural
180890022	Gary	IN	Michigan/Great Lakes	41.607	-87.305	179	urban
180892004	Hammond	IN	Michigan/Great Lakes	41.585	-87.474	182	urban
180970078	Indianapolis	IN	Ohio River Valley	39.811	-86.115	240	suburban
181630012	Evansville	IN	Ohio River Valley	38.022	-87.569	124	urban
191130037	Cedar Rapids	IA	Central U.S.	42.008	-91.679	254	urban
191530030	Des Moines	IA	Central U.S.	41.603	-93.643	282	urban
191630015	Davenport	IA	Central U.S.	41.530	-90.588	212	urban
201730010	Wichita	KS	Central U.S.	37.701	-97.314	405	urban
202090021	Kansas City	KS	Central U.S.	39.118	-94.636	269	urban
210190017	Ashland	KY	Ohio River Valley	38.459	-82.641	189	suburban
210670012	Lexington	KY	Ohio River Valley	38.065	-84.500	296	suburban
211110043	Louisville	KY	Ohio River Valley	38.233	-85.825	140	suburban
211170007	Covington	KY	Ohio River Valley	39.073	-84.525	220	suburban
211930003	Hazard	KY	Ohio River Valley	37.283	-83.220	414	suburban
220150008	Shreveport	LA	Mid South	32.534	-93.750	47	urban
220330009	Baton Rouge	LA	East Texas/Gulf	30.461	-91.177	16	urban
240053001	Essex	MD	Washington D.C. /Philadelphia Corridor	39.311	-76.474	10	suburban
240330030	Beltsville	MD	Washington D.C. /Philadelphia Corridor	39.055	-76.878	47	suburban
250130008	Westover AFB	MA	Northeast	42.195	-72.556	60	suburban
250250042	Boston	MA	Northeast	42.329	-71.083	5	urban
260770008	Kalamazoo	MI	Michigan/Great Lakes	42.278	-85.542	238	urban
260810020	Grand Rapids	MI	Michigan/Great Lakes	42.984	-85.671	190	urban
261130001	Houghton Lake	MI	Michigan/Great Lakes	44.311	-84.892	347	rural
261150005	Erie	MI	Michigan/Great Lakes	41.764	-83.472	175	rural
261610008	Ypsilanti	MI	Michigan/Great Lakes	42.241	-83.600	225	urban
261630001	Allen Park	MI	Michigan/Great Lakes	42.229	-83.208	182	suburban
261630033	Detroit	MI	Michigan/Great Lakes	42.307	-83.149	179	suburban
270530963	Minneapolis	MN	Central U.S.	44.955	-93.258	265	urban
271095008	Rochester	MN	Central U.S.	43.997	-92.450	318	suburban
280470008	Gulfport	MS	East Texas/Gulf	30.390	-89.050	6	rural
290470005	Liberty	MO	Central U.S.	39.303	-94.376	273	rural
290990012	Arnold	MO	Central U.S.	38.438	-90.361	150	suburban
291860005	Bonne Terre	MO	Central U.S.	37.897	-90.422	250	rural

Site	City	State	Region	Latitude (deg)	Longitude (deg)	Elevation (m)	Setting
295100085	St. Louis	MO	Central U.S.	38.656	-90.198	144	urban
300530018	Libby	MT	Northwest	48.384	-115.548	819	urban
300630031	Missoula	MT	Northwest	46.875	-113.995	1020	urban
310550019	Omaha	NE	Central U.S.	41.247	-95.976	347	suburban
320030020	Las Vegas	NV	Las Vegas	36.245	-115.092	583	urban
320030561	Las Vegas	NV	Las Vegas	36.164	-115.114	562	urban
320310016	Reno	NV	Northwest Nevada	39.525	-119.808	1403	urban
330150014	Portsmouth	NH	Northeast	43.075	-70.748	1	urban
340070003	Camden	NJ	Northeast	39.923	-75.098	2	suburban
340230006	New Brunswick	NJ	Northeast	40.473	-74.423	24	rural
340273001	Chester	NJ	Northeast	40.788	-74.676	256	rural
340390004	Elizabeth	NJ	Northeast	40.641	-74.208	3	suburban
350010023	Albuquerque	NM	Albuquerque	35.134	-106.586	1578	urban
360050110	Bronx	NY	New York City	40.816	-73.902	14	urban
360290005	Buffalo	NY	Northeast	42.877	-78.810	186	urban
360310003	Wilmington	NY	Northeast	44.393	-73.859	584	rural
360551007	Rochester	NY	Northeast	43.146	-77.548	146	urban
360610134	New York City	NY	New York City	40.714	-73.996	5	urban
360810124	Queens	NY	New York City	40.736	-73.823	13	suburban
361010003	Addison	NY	Northeast	42.091	-77.210	490	rural
370210034	Asheville	NC	Southeast	35.610	-82.351	706	suburban
370350004	Hickory	NC	Southeast	35.729	-81.366	341	suburban
370570002	Lexington	NC	Southeast	35.814	-80.263	237	urban
370670022	Winston-Salem	NC	Southeast	36.111	-80.227	279	urban
371070004	Kinston	NC	Southeast	35.232	-77.569	12	suburban
371190041	Charlotte	NC	Southeast	35.240	-80.786	223	urban
371590021	Rockwell	NC	Southeast	35.552	-80.395	224	rural
371830014	Raleigh	NC	Southeast	35.856	-78.574	92	suburban
380150003	Bismarck	ND	North Dakota	46.825	-100.768	548	suburban
380171004	Fargo	ND	North Dakota	46.934	-96.855	273	suburban
380530002	Watford City	ND	North Dakota	47.581	-103.300	629	rural
390171004	Middletown	OH	Ohio River Valley	39.530	-84.393	227	suburban
390350038	Cleveland	OH	Ohio River Valley	41.477	-81.682	186	urban
390350060	Cleveland	OH	Michigan/Great Lakes	41.494	-81.679	197	urban
390490081	Columbus	OH	Ohio River Valley	40.088	-82.960	263	suburban
390610040	Cincinatti	OH	Ohio River Valley	39.129	-84.504	213	urban
390870010	Ironton	OH	Ohio River Valley	38.520	-82.666	183	suburban
390933002	Sheffield	OH	Michigan/Great Lakes	41.463	-82.114	182	suburban
390950026	Toledo	OH	Michigan/Great Lakes	41.621	-83.641	191	suburban
390990014	Youngstown	OH	Ohio River Valley	41.096	-80.658	281	urban
391130031	Dayton	OH	Ohio River Valley	39.759	-84.144	250	suburban
391130032	Dayton	OH	Ohio River Valley	39.760	-84.188	242	urban
391510017	Canton	OH	Ohio River Valley	40.787	-81.394	334	urban
391530023	Akron	OH	Ohio River Valley	41.088	-81.542	313	urban
401091037	Edmond	OK	Mid South	35.614	-97.475	344	suburban
401431127	Tulsa	OK	Mid South	36.205	-95.977	193	urban
410290133	Medford	OR	Oregon	42.314	-122.879	433	urban
410390060	Eugene	OR	Oregon	44.026	-123.084	183	urban
410510080	Portland	OR	Oregon	45.497	-122.602	86	suburban

Site	City	State	Region	Latitude (deg)	Longitude (deg)	Elevation (m)	Setting
410510246	Portland	OR	Oregon	45.561	-122.679	61	urban
410610119	La Grande	OR	Northwest	45.339	-117.905	916	urban
420010001	Arendtsville	PA	Northeast	39.920	-77.310	241	rural
420030008	Pittsburgh	PA	Ohio River Valley	40.466	-79.961	312	suburban
420030064	Liberty	PA	Ohio River Valley	40.324	-79.868	279	suburban
420270100	State College	PA	Northeast	40.811	-77.877	354	rural
420290100	Toughkenamon	PA	Washington D.C. /Philadelphia Corridor	39.834	-75.769	91	rural
420430401	Harrisburg	PA	Northeast	40.245	-76.845	125	rural
420450002	Chester	PA	Washington D.C. /Philadelphia Corridor	39.836	-75.373	1	urban
420490003	Erie	PA	Northeast	42.142	-80.039	202	suburban
420692006	Scranton	PA	Northeast	41.443	-75.623	265	suburban
420710007	Lancaster	PA	Northeast	40.047	-76.283	99	suburban
420950025	Freemansburg	PA	Northeast	40.628	-75.341	93	suburban
421010004	Philadelphia	PA	Washington D.C. /Philadelphia Corridor	40.009	-75.098	25	urban
421010055	Philadelphia	PA	Washington D.C. /Philadelphia Corridor	39.923	-75.187	12	urban
421255001	Burgettstown	PA	Ohio River Valley	40.445	-80.421	344	rural
421290008	Greensburg	PA	Ohio River Valley	40.305	-79.506	378	suburban
421330008	York	PA	Northeast	39.965	-76.699	125	suburban
440070022	Providence	RI	Northeast	41.808	-71.415	17	urban
450190049	Charleston	SC	Southeast	32.791	-79.959	0	urban
450250001	Chesterfield	SC	Southeast	34.615	-80.199	122	rural
450450009	Taylors	SC	Southeast	34.901	-82.313	300	suburban
450790019	Columbia	SC	Southeast	33.993	-81.024	62	urban
460990006	Sioux Falls	SD	Central U.S.	43.544	-96.726	439	urban
470370023	Nashville	TN	Southeast	36.176	-86.739	153	urban
470654002	Chattanooga	TN	Southeast	35.051	-85.293	258	urban
470931020	Knoxville	TN	Southeast	36.019	-83.874	309	suburban
470990002	Loretto	TN	Southeast	35.116	-87.470	230	rural
471251009	Clarksville	TN	Southeast	36.514	-87.328	139	suburban
471570024	Memphis	TN	Southeast	35.151	-90.041	74	suburban
471631007	Kingsport	TN	Southeast	36.541	-82.522	394	suburban
481130069	Dallas	TX	Dallas	32.820	-96.860	132	urban
482011039	Deer Park	TX	East Texas/Gulf	29.670	-95.129	9	suburban
490110004	Bountiful	UT	Utah	40.903	-111.885	1307	suburban
490353006	Salt Lake City	UT	Utah	40.736	-111.872	1309	suburban
490494001	Lindon	UT	Utah	40.341	-111.714	1456	suburban
500070012	Burlington	VT	Northeast	44.480	-73.214	42	urban
510870014	Richmond	VA	Southeast	37.558	-77.400	34	suburban
530330080	Seattle	WA	Puget Sound	47.570	-122.309	58	urban
530530029	Tacoma	WA	Puget Sound	47.186	-122.452	97	suburban
530630016	Spokane	WA	Northwest	47.661	-117.357	596	suburban
540390011	Charleston	WV	Ohio River Valley	38.449	-81.684	264	rural
540391005	Charleston	WV	Ohio River Valley	38.368	-81.694	206	suburban
540511002	Moundsville	WV	Ohio River Valley	39.916	-80.734	245	suburban

Site	City	State	Region	Latitude (deg)	Longitude (deg)	Elevation (m)	Setting
550270007	Mayville	WI	Central U.S.	43.435	-88.528	348	rural
550790026	Milwaukee	WI	Central U.S.	43.061	-87.913	216	urban
551198001	Perkinstown	WI	Central U.S.	45.204	-90.600	449	rural
551330027	Waukesha	WI	Central U.S.	43.020	-88.215	263	urban

The IMPROVE and CSN networks operate collocated samplers in several urban/suburban sites. Collocated sites with data that met the completeness criteria outlined in Chapter 2 were compared to identify relative biases between IMPROVE and CSN speciated aerosol concentrations. We used daily data from Baltimore, Birmingham, Fresno, New York City, Phoenix, Puget Sound, and Washington, D.C., for 2005–2008. We compared ammonium sulfate (AS), ammonium nitrate (AN), organic carbon (OC), light absorbing carbon (LAC), soil, sea salt, $PM_{2.5}$ gravimetric fine mass (FM), and reconstructed fine mass (RCFM). Descriptions of how species mass was calculated are listed in Table 2.1 in Chapter 2.

Scatter plots of comparisons between IMPROVE and CSN species mass concentrations for all sites and years are presented in Figure 1.10. A summary of results is provided in Table 1.9. Errors were fairly low for most species (<20%), with the exception of soil (37.0%) and sea salt (78.3%), which also had high relative biases. IMPROVE sea salt concentrations were computed as 1.8 times chloride ion concentrations, whereas CSN sea salt concentrations were computed as 1.8 times chlorine concentrations. However, biases for other species were generally low, ranging from 5.7% for LAC to 18.4% for FM. The errors and relative biases between unadjusted CSN carbon and IMPROVE carbon data were 95.9% and 111.2 % for OC, respectively, and 26.7% and -17.3% for unadjusted LAC, respectively. The close agreement in OC and LAC suggests that the adjustments applied to those data were appropriate and effective (see Chapter 2). It should also be noted that while IMPROVE applies artifact corrections to ion data, CSN does not; some of the discrepancy between ion data from the two networks could be due to this difference.

It is worth discussing the relative biases associated with RCFM and FM. Relative biases in RCFM were low (0.04%) due to close agreement in the concentration of other major species, especially the adjusted CSN carbon concentrations. However, CSN FM concentrations were higher than IMPROVE FM concentrations on average, with a relative bias of 18.4%. As discussed in Chapter 2 and Chapter 8, OC concentrations measured by CSN samplers are roughly 20% higher than those obtained with IMPROVE samplers, most likely due to differences in filter face velocities and associated sampling artifacts between the two networks. The IMPROVE sampler has a much higher filter face velocity compared to the samplers used by CSN (Malm et al., 2011; Rattigan et al., 2011). Negative artifacts associated with the sampling systems also likely affect FM measurements on Teflon filters, and contribute to the relative bias in FM concentrations between the two networks. In this report, CSN carbon data have been adjusted for sampling artifacts to agree with IMPROVE carbon data, but FM data have not. Comparisons of FM and RCFM for CSN data are affected by this discrepancy, which may be an issue now that CSN has completed the transition to the URG 3000N sampling system for its carbon monitoring, but maintains its FM measurement using samplers with much lower filter face velocities. Examples of the effects of this discrepancy are presented in Chapter 2.2.9 with the comparison of FM and RCFM for the CSN and IMPROVE network.

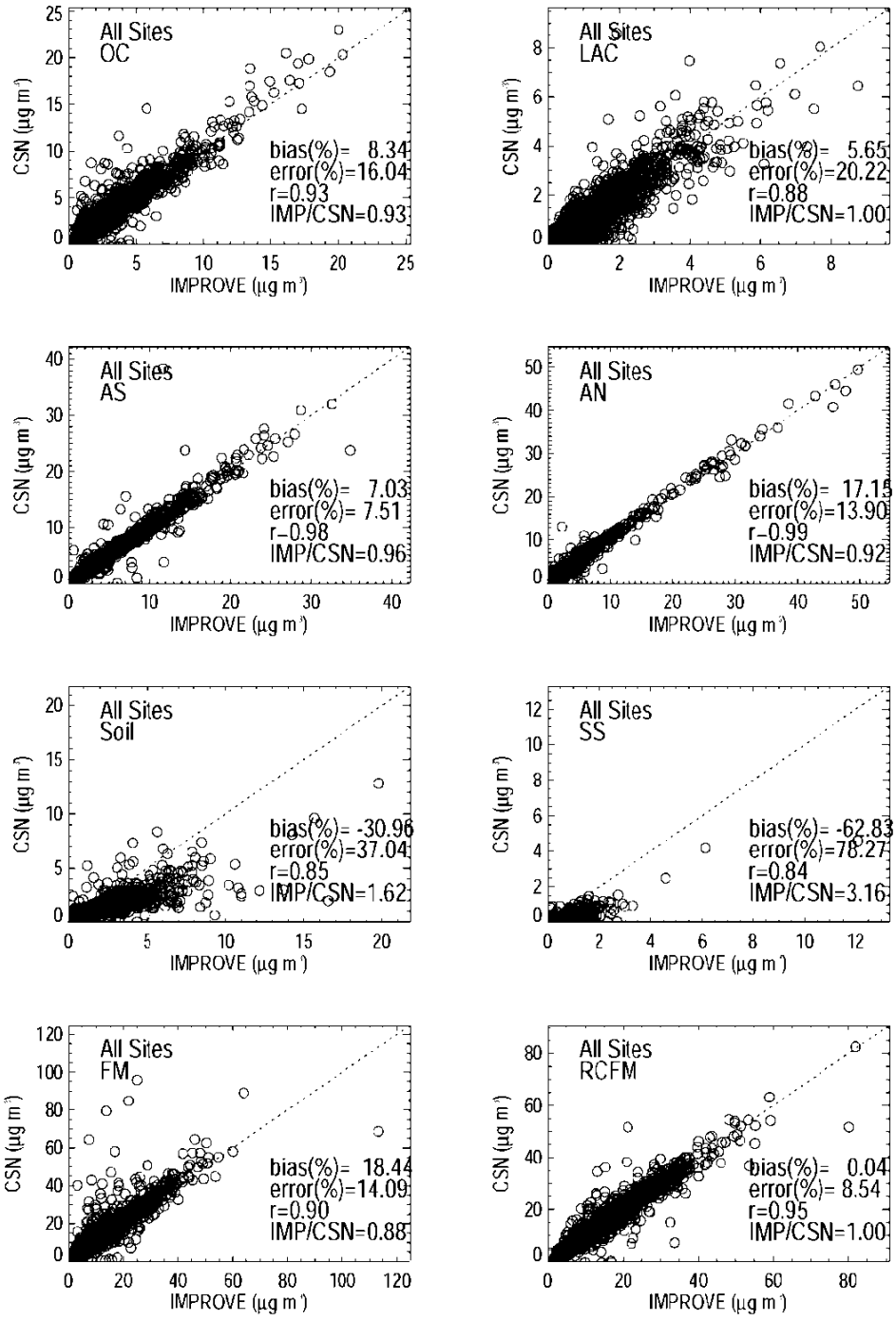

Figure 1.10. Comparisons of 2005–2008 aerosol mass concentration data (µg m^{-3}) for seven collocated IMPROVE and CSN sites (see text) for adjusted organic carbon (OC), adjusted light absorbing carbon (LAC), ammonium sulfate (AS), ammonium nitrate (AN), soil, sea salt (SS), $PM_{2.5}$ gravimetric fine mass (FM), and $PM_{2.5}$ reconstructed fine mass (RCFM).

The large errors and relative biases for soil and sea salt indicate that IMPROVE had much higher soil and sea salt mass concentrations compared to CSN. Recall that these data are from collocated sites, so the relative biases stem from differences in sampling or analytical techniques. As discussed in Chapter 2, sea salt is computed as 1.8 times chloride ion concentrations for IMPROVE and 1.8 times chlorine concentrations from the CSN (the CSN does not report chloride ion concentrations). Relative biases in sea salt reflect differences in these measurements and analyses. The relative biases in soil and sea salt mass concentrations are sufficiently large that combined data analyses should be treated as semiquantitative. CSN concentrations were somewhat higher than IMPROVE concentrations for most species (positive relative biases correspond to higher CSN concentrations), but data from the two networks were fairly highly correlated. The general agreement for most species indicates that the data can be combined.

Comparisons between IMPROVE and CSN data are separated by site and year and presented in Appendix A. Similar comparisons of elemental species used to construct soil and sea salt mass concentrations (Al, Si, Ca, Fe, Ti, and Cl^-, see Chapter 2) are also presented in Appendix A, as are comparisons between unadjusted and adjusted carbon data.

Table 1.9. Comparisons between collocated IMPROVE and CSN sites for all data from 2005 through 2008. Species include organic carbon (OC), light absorbing carbon (LAC), ammonium sulfate (AS), ammonium nitrate (AN), soil, sea salt, $PM_{2.5}$ gravimetric fine mass (FM), and $PM_{2.5}$ reconstructed fine mass (RCFM). "OC_{unadj}" and "LAC_{unadj}" refer to comparisons between unadjusted CSN carbon data and IMPROVE carbon data; "OC_{adj}" and "LAC_{adj}" refer tocomparisons between adjusted CSN carbon and IMPROVE carbon data.

Statistic	OC_{unadj}	LAC_{unadj}	OC_{adj}	LAC_{adj}	AS[3]	AN[4]	Soil	Sea salt[5]	FM	RCFM
Average IMPROVE ($\mu g\ m^{-3}$)	2.8	1.3	2.7	1.2	3.9	2.3	1.4	0.3	12.6	13.5
Average CSN ($\mu g\ m^{-3}$)	5.2	1.0	3.0	1.2	4.1	2.6	0.9	0.11	14.3	13.5
Bias[1] (%)	111.2	-17.3	8.3	5.7	7.0	17.2	-31.0	-62.8	18.4	0.04
Error[2] (%)	95.9	26.7	16.0	20.2	7.5	13.9	37.0	78.3	14.1	8.5
r	0.92	0.87	0.93	0.88	0.98	0.99	0.85	0.84	0.9	0.95
IMP/CSN	0.54	1.3	0.93	1.0	0.96	0.92	1.6	3.2	0.9	1.0
Number of data points (N)	2087	2077	2675	2665	2687	2689	2646	1904	2636	2535

[1] $\text{Error} = \text{median}\left(\left|\frac{\overline{X}_i - \overline{Y}_i}{\overline{Y}_i}\right|\right)$

[2] $\text{Bias} = \frac{1}{N}\sum_i^N \frac{\overline{X}_i - \overline{Y}_i}{\overline{Y}_i}$; $\overline{X}_i$ and $\overline{Y}_i$ are the daily data for CSN and IMPROVE concentrations, respectively. The number of data points is given by N.

[3] AS = 1.375[sulfate ion]

[4] AN = 1.29[nitrate ion]

[5] Sea salt = 1.8[chloride ion] for IMPROVE and 1.8[chlorine] for CSN.

REFERENCES

Bond, T. C., and R. W. Bergstrom (2006), Light absorption by carbonaceous particles: An investigative review, *Aerosol Sci. Techno., 40,* 27-67.

Chow, J. C., J. G Watson, L. C. Pritchett, W. R. Pierson, C A. Frazier, and R G. Purcell (1993), The DRI thermal/optical reflectance carbon analysis system: description, evaluation, and applications in U.S. air quality studies, *Atmos. Environ*., *27(A)*(8), 1185-1201.

Chow, J. C., J. G. Watson, L.-W. Antony Chen, M.-C. Oliver Chang, G. Paredes-Miranda (2005), Comparison of the DRI/OGC and Model 2001 Thermal/Optical Carbon Analyzers, http://vista.cira.colostate.edu/improve/Publications/GrayLit/013_CarbonAnalyzer/IMPROVECarbonAnalyzerAssessment.pdf.

Chow, J. C., J. G. Watson, L.-W.A. Chen, J. Rice, and N. H. Frank (2010), Quantification of $PM_{2.5}$ organic carbon sampling artifacts in U.S. networks, *Atmos. Chem. Phys., 10,* 5223-5339.

Debell, L. J., K. Gebhart, J. L. Hand, W. C. Malm, M. L. Pitchford, B. A. Schichtel, and W. H. White (2006), IMPROVE (Interagency Monitoring of Protected Visual Environments): Spatial and seasonal patterns and temporal variability of haze and its constituents in the United States: Report IV, CIRA Report ISSN: 0737-5352-74, Colo. State Univ., Fort Collins.

Dietrich, D.L., J. D. Molenar, and J. F. Faust (1989), Transmissometer extinction measurements in an urban environment, In *Visibility and Fine Particles*, C.V. Mathai, Ed., AWMA, Pittsburgh, pages 374-383.

Dillner, A. M., C. H. Phuah, and J. R. Turner (2009), Effects of post-sampling conditions on ambient carbon aerosol filter measurements, *Atmos. Environ., 43,* 5937-5943.

Flocchini, R. (2007), Shifts in Mo-anode XRF element calibration factors, Doc. # da0014, http://vista.cira.colostate.edu/improve/Data/QA_QC/Advisory/da0014/da0014_Mo_drop.pdf.

Hand, J. L., W. C. Malm, A. Laskin, D. Day, T. Lee, C. Wang, C. Carrico, J. Carrillo, J. P. Cowin, J. Collett, Jr., and M. J. Iedema (2005), Optical, physical, and chemical properties of tar balls observed during the Yosemite Aerosol Characterization Study, *J. Geophys. Res., 110,* D21210, doi:10.1029/2004JD005728.

John, W., and G. Reischl (1980), A cyclone for size-selective sampling of air, *J. Air Poll. Contr. Assoc., 30,* 872-876.

Joseph, D. B., J. Metsa, W. C. Malm, and M. L. Pitchford (1987), Plans for IMPROVE: a federal program to monitor visibility in class I areas, In: *Visibility Protection: Research and Policy Aspects*, P.S. Bhardwaja (Ed.), APCA, Pittsburgh PA.

Malm, W. C., J. F. Sisler, D. Huffman, R. A. Eldred, and T. A. Cahill (1994), Spatial and seasonal trends in particle concentration and optical extinction in the United States, *J. Geo. Res*., *99*(D1), 1347-1370.

Malm, W. C., J. F. Sisler, M. L. Pitchford, M. Scruggs, R. Ames, S. Copeland, K. A. Gebhart, and D. E. Day (2000), IMPROVE (Interagency Monitoring of Protected Visual Environments): Spatial and seasonal patterns and temporal variability of haze and its constituents in the United States: Report III, CIRA Report ISSN: 0737-5352-47, Colo. State Univ., Fort Collins, http://vista.cira.colostate.edu/improve/Publications/Reports/2000/2000.htm.

McDade, C. E., R. A. Eldred, and L. L. Ashbaugh (2004), Artifact corrections in IMPROVE, internal report.

McDade, C. E. (2007), Change in definition of flowrate native flags, Doc. # da0015, http://vista.cira.colostate.edu/improve/Data/QA_QC/Advisory/da0015/da0015_NewFlowFlags.pdf.

Molenar, J. F, D. L. Dietrich, and R. M. Tree (1989), Application of a long-range transmissometer to measure the ambient atmospheric extinction coefficient in remote pristine environments, In *Visibility and Fine Particles*, C.V. Mathai, Ed., AWMA, Pittsburgh, 374-383.

Molenar, J. F., and W. C. Malm (1992), Ambient optical monitoring techniques, presented at the Conference on Visibility and Fine Particles, Vienna, Austria, September.

Pitchford, M. L., and W. C. Malm (1994), Development and applications of a standard visual index, *Atmos. Environ., 28(5),* 1049-1054.

Rattigan, O. V., H. D. Felton, M.-S. Bae, J. J. Schwab, K. L. Demerjian (2011), Comparison of long-term $PM_{2.5}$ carbon measurements at an urban and rural location in New York, *Atmos. Environ., 45,* 3228-3236.

Sisler, J. F. (1996), Spatial and seasonal patterns and long term variability of the composition of the haze in the United States: An analysis of data from the IMPROVE network, Cooperative Institute for Research in the Atmosphere, Colorado State University, ISSN 0737-5352-32.

Turner, J. R. (2006), personal communication.

U.S. EPA (1999a), Regional Haze Regulations; Final Rule, 40 CFR 51, Federal Register, 64, 35714-35774.

U.S. EPA (1999b), Visibility Monitoring Guidance, Office of Air Quality Planning and Standards, Research Triangle Park, NC 27711, EPA-454/R-99-003.

U.S. EPA (2004), PM2.5 Speciation Network Newsletter, Volume 1, Issue 1, (http://www.epa.gov/ttn/amtic/files/ambient/pm25/spec/spnews1.pdf)

U.S. EPA (2009), PM2.5 Speciation Network Newsletter, Issue 6, Summer 2009, (http://www.epa.gov/ttn/amtic/files/ambient/pm25/spec/spnews6.pdf).

Watson, J. G., J. C. Chow, L.-W.A. Chen, N. H. Frank (2009), Methods to assess carbonaceous aerosol sampling artifacts for IMPROVE and other long-term networks, *J. Air Waste Manage. Assoc., 59,* 898-911.

White, W. (2006a), Changed reporting of XRF sulfur, Doc. # da0009, http://vista.cira.colostate.edu/improve/Data/QA_QC/Advisory/da0009/da0009_S_reporting.pdf.

White, W. (2006b), S interference in XRF determination of Si, Doc. # da0011, http://vista.cira.colostate.edu/improve/Data/QA_QC/Advisory/da0011/da0011_S_Si.pdf.

White, W. (2007a), Shift in EC/OC split with 1 January 2005 TOR harware upgrade, Doc. # da0016, http://vista.cira.colostate.edu/improve/Data/QA_QC/Advisory/da0016/da0016_TOR2005.pdf.

White, W. (2007b), Changes in sodium data quality, Doc. # da0017, http://vista.cira.colostate.edu/improve/Data/QA_QC/Advisory/da0017/da0017_Na.pdf.

White, W. (2007c), Introduction of a second copper-anode XRF system, Doc. # da0013, http://vista.cira.colostate.edu/improve/Data/QA_QC/Advisory/da0013/da0013_TwoVacs.pdf.

White, W. (2007d), Varying bias in XRF sulfur relative to IC sulfate, Doc. # da0012, http://vista.cira.colostate.edu/improve/Data/QA_QC/Advisory/da0012/da0012_SSO4.pdf.

White, W. (2008), Bias between masked and unmasked elemental measurements, Doc. # da0019, http://vista.cira.colostate.edu/improve/Data/QA_QC/Advisory/da0019/da0019_masks.pdf.

White, W. (2009), Inconstant bias in XRF sulfur- Advisory Update to da0012, Doc. # da0023, http://vista.cira.colostate.edu/improve/Data/QA_QC/Advisory/da0023/da0023_DA_SSO4_update.pdf.

White, W. (2010), Bias between masked and unmasked light absorption measurements, Doc. # da0028, http://vista.cira.colostate.edu/improve/Data/QA_QC/Advisory/da0028/da0028_DA_mask_Fabs.pdf.

Yu, X-Y., T. Lee, B. Ayres, S. M. Kreidenweis, J. L. Collett, Jr., and W. C. Malm (2005), Particulate nitrate measurement using nylon filters, *J. Air Waste Manage. Assoc., 55*, 1100-1110.

Chapter 2. Spatial Patterns of Speciated $PM_{2.5}$ Aerosol Mass Concentrations

Characterizing the composition of major aerosol species is essential for estimating their contribution to $PM_{2.5}$ total mass concentration and visibility degradation. Analyzing the spatial variability of major aerosol species is important for understanding their sources and local and regional impacts. Data from the IMPROVE network are particularly useful for this type of analysis, given their spatial distribution and long temporal record. In addition to the mostly remote/rural sites operated by IMPROVE, the Chemical Speciation Network (CSN), operated by the Environmental Protection Agency (EPA), collects $PM_{2.5}$ speciated aerosol data at approximately 200 urban/suburban monitoring sites. Data from the IMPROVE and CSN networks are useful independently, but by combining data from the two networks, a more complete spatial analysis of key aerosol species can be explored as a function of geographical region by specifically exploring the differences in urban and rural aerosol signatures. In this section we examine the 2005–2008 annual mean mass concentrations of ammonium sulfate (AS), ammonium nitrate (AN), particulate organic matter (POM), light absorbing carbon (LAC), mineral soil aerosols, sea salt, and $PM_{2.5}$ gravimetric fine mass (FM) (we use $PM_{2.5}$ gravimetric mass and fine mass interchangeably in this report), as well as their contribution to $PM_{2.5}$ reconstructed fine mass (RCFM), PM_{10} (particles with aerodynamic diameters less than 10 μm from the EPA's PM_{10} network), and coarse mass (CM) (the difference between PM_{10} and $PM_{2.5}$ at IMPROVE sites only).

The CSN (a subset of which is formerly known as the Speciated Trends Network, or STN) was initiated in early 2000 with the purpose of identifying sources, developing implementation plans, and supporting ongoing health-effects research. Currently, it operates approximately 200 sites in mostly urban and suburban locations. The CSN has operated many different samplers, depending on the site, including the Andersen Reference Ambient Air Sampler (RAAS), MetOne SASS, URG, R&P2300, and R&P2025. The flow rates and face velocities of these samplers can differ significantly from the IMPROVE sampler, which could lead to differences in concentrations, especially for carbon. CSN now mostly operates the MetOne and the URG3000N. For most species, CSN and IMPROVE measurements and analyses are similar (see section 1.4 for a comparison of data from collocated sites). Both networks maintain a one-in-three-day sampling frequency (some CSN sites are one-in-six day). CSN cold-ships their samples while IMPROVE does not . As discussed in section 1.4, samples for gravimetric and elemental analyses are collected with Teflon filters. Gravimetric mass is determined using electro-microbalance techniques, and energy dispersive X-ray fluorescence is used for trace elements. Samples for ion chromatography analysis are collected using nylon substrates, and samples for carbon analyses are collected on quartz fiber substrates. The major difference between the analyses performed by IMPROVE and the CSN had been the determination of organic carbon (OC) and LAC[1]. IMPROVE uses thermal optical reflectance (TOR) and the CSN uses thermal optical transmission (TOT), both of which are known to produce similar total carbon concentrations but different splits between OC and LAC (Chow et

[1] The CSN network changed the sampler and analysis method for carbonaceous $PM_{2.5}$ monitoring beginning in the spring of 2007 to be more compatible with the methods used by IMPROVE. For more information see http://www.epa.gov/ttn/amtic/specurg3000.html

al., 2004). In addition, the CSN applies the NIOSH-like (National Institute for Occupational Safety and Health) analysis protocol that differs from the IMPROVE protocol for determining the split between OC and LAC. Furthermore, the handling of carbon sampling artifacts is different between the networks. Positive artifacts are associated with adsorption of organic gases onto the filter, and negative artifacts occur due to volatilization of particulate organics (Turpin et al., 2000). While blank corrections for the positive artifact are routinely applied to IMPROVE carbon data, they are not applied routinely as part of the CSN protocol; however they can be found elsewhere (www.epa.gov/airexplorer). More discussion of the carbon data comparisons can be found in section 2.1.3, including a discussion of new artifact corrections for CSN data used for this report.

Data from a 4-year time period (2005–2008) are examined in this chapter. To ensure that the data are representative of the entire time period, certain completeness criteria first were applied. Fifty percent completeness of the data (two years of valid monthly mean data) for a given site was required to be included in the analysis. Half of the total observations in a given month had to be valid for a monthly mean. In addition, 66% of each 3-month season was required for an annual mean (a total of 8 months, but represented across each season, were required for an annual mean). Seasons correspond to winter (December, January, February), spring (March, April, May), summer (June, July, August) and fall (September, October, November). These criteria were applied for each species separately. Values below the minimum detection limit (MDL) were handled according to how they were reported by each network, i.e., we made no additional corrections for values below MDLs. For IMPROVE, ion and carbon data were reported below their MDLs. XRF data were reported as zero if they were below MDLs. Data from the CSN were handled similarly. Average reconstructed mass calculations were performed by summing the averages; for example, an average concentration of each species was computed and summed to obtain an average RCFM. Valid data for all of the species were required to compute monthly mean RCFM, with the exception of sea salt. This approach was used to avoid small sample sizes and provide a more accurate representation of average conditions. Applying the completeness criteria resulted in 168 IMPROVE sites and 176 CSN sites used in the analyses.

Maps of monthly mean and annual mean concentrations were created for each species from sites that met the completeness criteria. A Kriging algorithm was used to interpolate concentrations between site locations in order to create concentration isopleths.Maps based on interpolation schemes should be viewed and interpreted with caution. The maps are intended to help visualize the data and identify large spatial patterns only. The density of site locations obviously affects the interpolated fields, and neither the IMPROVE nor CSN networks have uniformly distributed site locations around the United States. Given this caveat, there is still interesting and useful information that can be gained from these maps, especially by examining the differences that occur when maps based only on the rural/remote IMPROVE network are compared to those created when integrating the urban/suburban CSN data with IMPROVE data. The following sections include discussions of spatial patterns for annual mean concentrations of AS, AN, POM, LAC, soil, sea salt, FM, the difference between FM and RCFM, coarse mass (IMPROVE only), and PM_{10} mass. The top number in the scale shown on each contour map corresponds to the maximum concentrations for all sites, although the contour levels themselves were created with the highest level corresponding to the 95^{th} percentile in mass concentration. Maps of species percent contribution to RCFM are also included. Tables listing 2005–2008

annual mean concentrations as a function of site for the IMPROVE network and the CSN are provided in Appendix B.1. Annual mean $PM_{2.5}$ mass fractions are listed according to site for the IMPROVE network and the CSN in Appendix B.2.

2.1 AEROSOL SPECIES COMPOSITION

In order to reconstruct $PM_{2.5}$ mass concentrations, assumptions about the molecular form of assumed species must be made. Table 2.1 presents the assumptions used in this report and those applied in previous report. More detail regarding each species will be presented in the following sections. Similar assumptions were made for IMPROVE and CSN unless otherwise noted in Table 2.1.

Table 2.1. Form of molecular species assumed in this report.

$PM_{2.5}$ Aerosol Species	**Previous Report**	**This Report**	**Assumptions**
Ammonium Sulfate (AS = $(NH_4)_2SO_4$)	4.125[S]	1.375[SO_4^{-2}]	Sulfate [SO_4^{-2}] is assumed to be fully neutralized. Previous assumptions used sulfur (S).
Ammonium Nitrate (AN = NH_4NO_3)	Same	1.29[NO_3^-]	Nitrate [NO_3^-] is assumed to be ammonium nitrate.
Particulate Organic Matter (POM)	1.8[OC]	1.8[OC]	Derived from organic carbon (OC) assuming average organic molecule is 55% carbon. Previous assumptions used a 1.4 factor.
Light Absorbing Carbon (LAC)	Same	LAC	Also referred to as EC in previous reports.
CSN POM	NA	1.8[OC]	Mathematically adjusted to compare with IMPROVE POM.
CSN LAC	NA	LAC	Mathematically adjusted to compare with IMPROVE LAC.
Sea Salt	Not considered.	1.8[Cl^-]	Sea salt is 55% chloride ion by weight. Previously not considered.
CSN Sea Salt	NA	1.8[Cl]	Sea salt is derived using chlorine concentrations from XRF.
Soil	Same	2.2[Al] + 2.49[Si] + 1.63[Ca] + 2.42[Fe] + 1.94[Ti]	Soil potassium = 0.6[Fe]. Fe and Fe_2O_3 are equally abundant. A factor of 1.16 is used to account for other compounds such as MgO, Na_2O, H_2O and CO_3.
Gravimetric $PM_{2.5}$ Mass (FM)	Same	$PM_{2.5}$	A $PM_{2.5}$ cut point on the fine mass sample.
Coarse Mass (CM)	Same	PM_{10} - $PM_{2.5}$	PM_{10} cut point on the mass sample.
IMPROVE PM_{10}	Same	PM_{10}	PM_{10} cut point.
EPA PM_{10}	NA	PM_{10}	PM_{10} cut point.
Reconstructed Fine Mass (RCFM)	[AS]+[AN]+[POM]+[LAC]+[Soil]	AS + AN + POM + LAC + Soil + Sea Salt	Represents $PM_{2.5}$ fine aerosol mass, including sea salt.
Mass Difference (dM)	NA	FM - RCFM	

2.1.1 $PM_{2.5}$ Ammonium Sulfate Mass Concentrations

The majority of sulfate in the atmosphere is produced through chemical reactions of sulfur dioxide (SO_2). Anthropogenic SO_2 is emitted through industrial activities such as coal and diesel fuel combustion. Regions that host electric utilities and industrial boilers (such as the eastern United States) are sources of SO_2 emissions that, combined with the elevated relative humidity or other aqueous pathways, create the most efficient conditions for sulfate production. The degree of acidity of sulfate (from acidic sulfuric acid to fully neutralized AS) depends on the availability of ammonia to neutralize the sulfuric acid formed from SO_2. Sulfate acidity can vary spatially and temporally (e.g., Gebhart et al., 1994; Liu et al., 1996; Day et al., 1997; Lowenthal et al., 2000; Lefer and Talbot, 2001; Quinn et al., 2002a; Chu et al., 2004; Hogrefe et al., 2004; Schwab et al., 2004; Tanner et al., 2004; Zhang et al., 2005), but without additional measurements of ammonium ion concentration, the degree of neutralization is unknown. We therefore assumed sulfate is in the form of fully neutralized AS (see Table 2.1), an upper bound of mass associated with dry sulfate.

2.1.2 $PM_{2.5}$ Ammonium Nitrate Mass Concentrations

Ammonium nitrate (AN) forms from the reversible reaction of gas-phase ammonia and nitric acid. Sources of oxidized nitrogen include combustion of fossil fuels from point sources such as coal-fired powered plants, on-road mobile sources and non-road mobile sources. Other high-temperature processes such as biomass burning also contribute oxidized nitrogen, as do biogenic sources such as soil emissions (Vitousek et al, 1997). Sources of ammonia include agricultural activities including animal husbandry, as well as mobile sources and natural emissions. The equilibrium reactions producing particle phase AN are sensitive to small changes in temperature and relative humidity that can shift the equilibrium between the particle and gas phase. Lower temperatures and higher relative humidity favor particulate AN, while higher temperatures and lower relative humidity favor the gas phase. Nitrate (as AN) is often assumed to be in the fine mode, and this is probably a reasonable assumption in regions with high ammonia and nitric acid concentrations and low sulfate concentrations. However, Lee et al. (2008) showed that in many locations nitrate is associated with the coarse mode from reactions of gas-phase nitric acid with sea salt or calcium carbonate. In these situations the nitrate measured in the fine mode is actually the tail of coarse-mode nitrate. Using data reported by Lee et al. (2008), Hand and Malm (2006) found that when fine mode nitrate concentrations were greater than 0.5 $\mu g\ m^{-3}$, AN contributed over 70% of the observed total nitrate in the fine mode at certain locations. For the purposes of reconstructing fine mass and light extinction coefficients, and because the necessary measurements to determine the form of nitrate are not regularly available, we assumed nitrate is in the form of AN.

2.1.3 $PM_{2.5}$ Particulate Organic Matter and Light Absorbing Carbon Mass Concentrations

The sources of POM in the atmosphere are both primary emissions and secondary formation. Primary emissions include particle mass emitted directly from combustion of fossil fuels or biomass. Secondary organic aerosols form in the atmosphere from the oxidation of gas-phase precursors from both anthropogenic and biogenic sources. Accurate estimates of POM are required in order to compute $PM_{2.5}$ mass closure and to estimate optical properties such as light scattering coefficients. Estimating the contributions of organic carbon (OC) aerosol to mass or

scattering requires an estimate of the total mass associated with OC. The OC multiplier (R_{oc}) used to estimate particulate organic material is an estimate of the average molecular weight per carbon weight for OC aerosol and takes into account contributions from other elements associated with the organic matter, such as N, O, and H. It is spatially and temporally variable. Typical values range from 1.2 to 2.6 (Turpin and Lim, 2001; El-Zanan et al., 2005). It is impossible to determine which and how many elements are associated with POM without knowing the chemical formula of the organic compound, and it is common for ~20–40% of organic aerosol mass to remain unidentified (Turpin and Lim, 2001). Because the organic compounds that compose POM are largely unknown, the approach for taking into account other elements in POM mass has been to apply an average multiplier. As Turpin and Lim (2001) review, the often-used value of 1.4 dates back to samples collected in Pasadena in the early 1970s and 1980s (Grosjean and Friedlander, 1975; White and Roberts, 1977; Van Vaeck and Van Cauwenberghe, 1978; Countess et al., 1980; Japar et al., 1984). Turpin and Lim (2001) have reviewed several estimates of R_{oc} in terms of the types of compounds known to compose POM, and to summarize their findings, they recommend a factor of 1.6 ± 0.2 for urban organic aerosols, a factor of 2.1 ± 0.2 for nonurban organic aerosols, and values ranging from 2.2 to 2.6 for samples with impacts from biomass burning. As part of the IMPROVE equation assessment that occurred in 2006, the value of 1.4 was deemed too low based on a summary of current literature. Instead, a value of 1.8 was recommended based on available data (Malm and Hand, 2007) and is applied here. Further examination of the multiplier is presented in Chapter 8 (Malm et al., 2011).

LAC, also referred to as black carbon, elemental carbon, graphitic carbon or soot, is produced directly through emission from incomplete combustion of fossil fuels or biomass (fires). LAC is the most abundant light-absorbing particle in the atmosphere in the visible spectrum. A comprehensive review of light absorption by LAC was provided by Bond and Bergstrom (2006). We use the term “light absorbing carbon” instead of elemental carbon (EC) to reflect the transition to this term in the scientific literature because of the operational definition, and sometimes morphology, associated with EC (Bond and Bergstrom, 2006; Malm et al., 1994). Light absorbing carbon particles may evolve in high temperature environments but not be graphitic (e.g., Hand et al., 2005). Replacing EC with LAC avoids potential confusion regarding the type of carbon particles responsible for light absorption.

Prior to 2007 the IMPROVE and CSN networks employed different samplers, analytical methods, and data processing routines for measuring total particulate carbon and the organic and LAC fractions. One of the major differences between the networks is the treatment for sampling artifacts. Positive artifacts occur when organic gases are trapped by the quartz filters used for sampling and can induce a bias of ~50% of OC mass. Negative artifacts occur when particulate species are volatilized from the filter, resulting in losses of -80% (Turpin, 2000). One significant difference between the CSN and IMPROVE is that IMPROVE reports carbon concentrations that have been corrected for positive artifacts while the CSN does not make adjustments to the data reported to the EPA air quality system (AQS, http://www.epa.gov/ttn/airs/aqsdatamart/). Differences in the face velocities of the various samplers operated by IMPROVE and the CSN lead to discrepancies in concentrations due to negative and positive artifacts. In addition, the CSN applies the NIOSH-like protocol and TOT analysis (Chow et al., 2004), while IMPROVE applies its own sampling protocol and TOR to determine carbon fractions. Differences of up to 30% in LAC concentrations have been reported due to the TOR versus TOT method (TOR

larger, Chow et al., 2004). These differences in sampling and analysis lead to discrepancies between carbon concentrations reported by the two networks.

To combine the carbon data between the IMPROVE and CSN networks, we applied corrections to the CSN carbon data, based on comparisons of data from collocated CSN and IMPROVE samplers, to account for all of the differences described above. We used data from twelve urban monitoring sites with collocated samplers for the time period of 2005–2006. CSN total carbon concentrations (TC) were systematically higher than IMPROVE TC, with the magnitude of the biases dependent on the CSN sampler type but independent of monitoring site. A linear regression of TC from the two networks resulted in a positive intercept in the CSN data that indicated an additive bias that was most likely associated with a positive OC artifact. The sampler dependence appeared to be related to the sampler operating conditions (e.g., flow rate and face velocity) because the closest agreement occurred for the CSN sampler that was most similar to the IMPROVE sampler. A sampler-dependent multiplicative bias was also evident, with the bias increasing with increasing face velocity. The multiplicative bias was interpreted as a negative organic artifact associated with the loss of semivolatile OC species due to the pressure drop across the filter. In contrast to TC, IMPROVE LAC concentrations were systematically higher than CSN LAC, consistent with the known differences in TOR versus TOT methods (Chow et al., 2004). The biases were multiplicative, suggesting analytical biases. No additive bias was observed, consistent with minimal LAC measured on back up filters (Eldred, 2002). These comparisons were used to derive monthly correction factors that were applied to the CSN data. A detailed description of the derivation of data corrections and the resulting concentration comparisons can be found in Chapter 8 and Malm et al. (2011). Equations 2.1 and 2.2 were used to adjust the CSN OC and LAC data:

$$LAC_{adj}=1.3(LAC_{CSN}) \quad 2.1$$

$$OC_{adj}=\frac{OC_{CSN}-0.3LAC_{CSN}-A}{M} \quad 2.2$$

LAC_{adj} and OC_{adj} refer to the adjusted CSN LAC and OC data, respectively, and were used in the analyses presented in this report. The adjustements were applied as a function of month and sampler. The top row of Table 2.1.3 lists the multiplicative negative artifact (M) as a function of CSN sampler. The columns of Table 2.1.3 list the additive positive organic artifact (A) as a function of month and sampler.

Table 2.1.3. The negative multiplicative artifact (M) and the monthly positive additive organic artifact (A_{month}) used to adjust the CSN carbon concentrations for comparisons with IMPROVE. The units for the positive artifacts are μg m^{-3} and M is unitless. Adjustments are listed as a function of sampler (columns).

	MetOne	Anderson	URG	R&P-2300	R&P-2025
M	1.2	1.2	1.1	1.1	1.1
A_{Jan}	1.1	0.92	0.24	1.2	0.24
A_{Feb}	1.3	1.1	0.27	1.4	0.27
A_{Mar}	1.2	1.0	0.26	1.4	0.26
A_{Apr}	1.4	1.2	0.29	1.5	0.29
A_{May}	1.6	1.3	0.33	1.7	0.33
A_{Jun}	1.7	1.4	0.35	1.8	0.35
A_{Jul}	1.8	1.5	0.38	2.0	0.38
A_{Aug}	1.9	1.6	0.41	2.1	0.41

	MetOne	Anderson	URG	R&P-2300	R&P-2025
A_{Sep}	1.5	1.2	0.31	1.6	0.31
A_{Oct}	1.2	0.90	0.23	1.2	0.23
A_{Nov}	1.0	0.85	0.22	1.1	0.22
A_{Dec}	1.1	0.89	0.23	1.2	0.23

Scatter plots of original and corrected data are presented in the detailed discussion in Chapter 8 and Malm et al. (2011) and in Appendix A. In the spring of 2007 the CSN began converting its carbon samplers to URG model 3000N samplers and applying TOR analysis using the IMPROVE protocol for carbon measurements in an effort to converge toward an IMPROVE-like measurement. These data were used for the sites where they were available. The only adjustments made to the IMPROVE-like CSN data were a positive artifact correction to OC concentrations. Although this artifact is most likely seasonal, a constant correction of 0.3 μg m^{-3} was applied based on carbon artifact investigations for IMPROVE quartz filters (Eldred, 2002).

2.1.4 $PM_{2.5}$ Soil Mass Concentration

Sources of soil dust in the atmosphere include entrainment from deserts, paved and unpaved roads, agricultural activity, construction, and fire (Seinfeld and Pandis, 1998). Deposition of dust usually corresponds to large particles that settle near their source regions, although there are many exceptions. Several studies have shown that contributions of Asian dust to U.S. fine soil concentrations can be significant episodically, affecting aerosol concentrations and mineralogy across the United States, typically in the spring (e.g., Husar et al., 2001; Prospero et al., 2002; VanCuren and Cahill, 2002; Jaffe et al., 2003; VanCuren, 2003). Transport of North African dust to the United States occurs regularly in summer, affecting aerosol concentrations in the Virgin Islands, the eastern and southeastern United States (Perry et al., 1997), and even as far west as Big Bend, Texas (Hand et al., 2002). Soil concentrations in desert regions of the Southwest are expected to be higher due to the impacts of local sources as well as transboundary transport from the Chihuahuan desert in Mexico, especially in winter and spring (Rivera Rivera et al., 2009).

Fine soil as characterized by $PM_{2.5}$ samplers most likely corresponds to the fine tail of the coarse mode. Variability in soil concentrations could be due to changes in the magnitudes of mass concentrations for a given size mode or to shifting size distribution that results in more or less mass available in the fine mode size range. Due to the spatial and temporal variability in dust sources, it is very difficult to characterize an appropriate aerosol soil composition for each measurement site. Soil mass concentrations are therefore estimated by a general method that sums the oxides of elements that are typically associated with soil (Al_2O_3, SiO_2, CaO, K_2O, FeO, Fe_2O_3, TiO_2), with a correction for other compounds such as MgO, Na_2O, H_2O and carbonates (Malm et al., 1994). Elemental concentrations are multiplied by factors that represent the mass concentrations of the oxide forms. Several corrections are also made. Molar concentrations of iron are assumed to be equally abundant in the forms of FeO and Fe_2O_3. Potassium has a nonsoil contribution from biomass smoke, so the soil potassium is estimated by using Fe as a surrogate, or *[K] = 0.6[Fe]*. The formula for computing soil concentration is given in Table 2.1 and has been divided by 0.86 to take into account missing compounds.

Comparisons of IMPROVE and CSN data performed for this report (see section 1.4) and those performed previously (Debell et al., 2006) suggested that relative biases of up to 30% or

more in soil concentrations between collocated IMPROVE and CSN samplers existed, with higher IMPROVE concentrations. In addition, analyses of IMPROVE data suggested that $PM_{2.5}$ soil mass concentrations may be underestimated by as much as 20% and have some regional dependence (Malm and Hand, 2007). Given these uncertainties, the combination of IMPROVE and CSN soil concentrations should be interpreted as semiquantitative.

2.1.5 $PM_{2.5}$ Sea Salt Mass Concentration

Sea salt can be a significant fraction of the RCFM at many coastal locations, (e.g., the Virgin Islands), as well as contribute significantly to light scattering (e.g., Quinn et al., 2001, 2002b, 2004). Sea salt concentrations are typically computed from sea salt markers like the sodium ion, chloride ion, or combination of ions (Quinn et al., 2001). Difficulties in computing sea salt from data from the IMPROVE network arise because positive ions are not analyzed; therefore sodium ion data (the strongest indicator of sea salt) are not available. Elemental sodium data are available from XRF analyses; however, sensitivity issues regarding poor detection of Na result in large uncertainties corresponding to Na from XRF (White, 2008). Issues also arise when using the chloride ion or chlorine to estimate sea salt because the reaction of gaseous nitric acid with sea salt produces sodium nitrate particles and the release of gaseous HCl. The depletion of chloride during this reaction results in an underestimation of sea salt when using chloride to compute it. However, given these limitations, it was proposed that calculations for reconstructing mass include sea salt by multiplying the chloride ion (Cl^-) by 1.8 (sea salt is 55% Cl by weight as defined by the composition of sea water by Seinfeld and Pandis, 1998). Because the chloride ion is not analyzed by the CSN, sea salt is computed using the 1.8 factor multiplied by chlorine as measured by XRF. Comparisons of sea salt concentrations between collocated CSN and IMPROVE sites (see section 1.4) suggested that IMPROVE concentrations were up to three times higher on average compared to CSN, with a relative bias of 63%. Given these disparities in concentrations, the integration of CSN and IMPROVE sea salt data should be interpreted with caution.

2.1.6 $PM_{2.5}$ Gravimetric Fine Mass and Reconstructed Fine Mass

Gravimetric fine mass concentrations (FM) are determined gravimetrically by pre- and post-weighting of Teflon filters. The filters are equilibrated to 20–23 degrees C and 30–40% relative humidity. Teflon filters have known sampling artifacts. For example, nitrate loss and volatilization of some organic species contribute to negative artifacts (Hering and Cass, 1999; Ashbaugh and Eldred, 2004; Frank, 2006), while positive artifacts correspond to retention of water associated with acidic species (Frank, 2006).

Reconstructed fine mass is the sum of AS, AN, POM, LAC, soil, and sea salt. RCFM should equal FM if the assumptions regarding molecular forms of species are appropriate and if there are minimal biases associated with the measurements.

2.1.7 $PM_{2.5}$ Mass Difference

Differences in FM and RCFM (dM = FM - RCFM) were computed to investigate the degree to which the algorithm for computing RCFM was capturing the FM concentrations. Some of the differences were related to the sampling artifacts associated with FM discussed earlier,

such as loss of volatile species or retained water on the filter. In addition, incorrect molecular forms of assumed species could have contributed. More acidic forms of sulfate, nitrate species other than AN, different OC multipliers, or soil formulas could have contributed to differences between FM and RCFM. A detailed investigation into biases associated with FM measurements is presented in Chapter 8 and Malm et al. (2011).

2.1.8 PM_{10} and Coarse Mass Concentrations

Coarse mass (CM) is the difference between gravimetric PM_{10} and $PM_{2.5}$ mass concentrations (PM_{10} - $PM_{2.5}$) measured gravimetrically and is not routinely analyzed for speciation. To investigate the speciation of CM, a coarse particle speciation network was initiated at nine IMPROVE sites in 2003. Sites were selected to be representative of the continental United States and were operated according to IMPROVE protocol analytic procedures for a period of one year, with additional A, B, and C modules operating with PM_{10} inlets. Malm et al. (2007) reported that soil (as defined by the IMPROVE soil equation) was the largest contributor to CM at most sites and ranged from 34% at Mount Rainier National Park to 76% at Grand Canyon National Park. With the exception of Mount Rainier, annual average soil contributions to CM were higher in the western United States. POM was the next highest contributor, ranging from 9% at Grand Canyon National Park to 59% at Mount Rainier National Park. Nitrate was next highest contributor (4–12%), probably associated with sea salt on the coast and dust in the inner and western areas of the country (Lee et al., 2008). Sulfate was a minor contributor to CM, with its fractional contribution less than a few percent. The optical, physical, chemical, and hygroscopic properties of coarse-mode aerosols can vary significantly, depending on the composition and size distribution of CM, and could have important implications to total scattering, because in some remote areas contributions to total scattering from the coarse-mode scattering could be comparable to fine-mode contributions. For example, there were several periods in Big Bend, Texas when up to 80% of total scattering was attributable to the coarse mode (Hand, 2001; Hand et al., 2002).

PM_{10} concentrations are not measured routinely as part of the CSN protocol, so no CM estimation could be made for urban sites. However, the EPA maintains a large network of PM_{10} samplers at over 700 sites around the United States. Several of these sites are collocated with CSN sites. Instead of introducing errors by interpolating PM_{10} concentrations to CSN sites with no collocated PM_{10} sampler, we compared PM_{10} concentrations, instead of CM concentrations, for IMPROVE and EPA monitors to investigate the rural and urban differences in PM_{10}.

2.2 SPATIAL PATTERNS IN ANNUAL MEAN MASS CONCENTRATIONS

2.2.1 $PM_{2.5}$ Ammonium Sulfate Mass

The rural 2005–2008 IMPROVE annual mean AS concentrations ranged from 0.36 μg m^{-3} in Petersburg, Alaska (PETE1), to 6.11 μg m^{-3} in Livonia, Indiana (LIVO1). The combination of high SO_2 emissions and high relative humidity produced the highest concentrations (4–6 μg m^{-3}) of AS in the eastern United States that centered on the Ohio River valley and Appalachia regions (see Figure 2.2.1a). The concentrations of AS decreased sharply in the surrounding regions of the country. In fact, concentrations in the western United States were typically less than 2 μg m^{-3}, with the lowest concentrations in the Northwest and in

Montana and Idaho. The low concentrations of AS that corresponded to most of the IMPROVE sites was a consequence of site location; around 62% of IMPROVE sites are located in the western half of the country (west of -100º), where SO_2 emissions are lower.

The regional impact of AS concentrations was evidenced by the similar concentrations of AS at the urban CSN sites. A maximum CSN concentration of 8.01 μg m^{-3} occurred in southwestern Pennsylvania (Liberty, #420030064), similar to the maximum concentration observed in the IMPROVE network. Most of the CSN sites had AS concentrations greater than 2 μg m^{-3}, due to the fact that the majority of CSN sites are located in the East (80% of CSN sites are east of -100º). The lowest concentration (0.75 μg m^{-3}) occurred at La Grande (#410610119) in eastern Oregon. The spatial distribution of AS with the rural and urban sites combined (see Figure 2.2.1b) was very similar to the pattern of the rural sites alone, suggesting that regional impacts of high AS concentrations in the East influenced both urban and rural sites similarly. The addition of urban sites in the Ohio River valley provided some additional structure in the isopleths in Figure 2.2.1b but did not alter the overall pattern considerably.

RCFM was primarily composed of AS in the eastern United States (see Figure 2.2.1c). IMPROVE AS mass fractions above 50% occurred for 19 sites in the eastern and northeastern United States, and the spatial pattern of AS mass fraction was similar to that of AS mass concentrations with some exceptions. For example, the Northeast had high mass fractions even though the AS concentrations were fairly low (especially compared to the mid-South and Southeast), suggesting that these regions had fairly low concentrations of AS but that the RCFM is still dominated by AS. These differences were also observed in the West. Higher mass fractions extend into west Texas due to the Big Bend NP site (BIBE1), where the influence of AS to RCFM has been well documented (Lee et al., 2004; Barna et al., 2006; Gebhart et al., 2006; Schichtel et al., 2006). The fraction of AS in the central United States approached 40% and declined to the west, with the lowest fractions (10–15%) in the Northwest. The highest IMPROVE AS fraction actually occurred in Hawaii Volcanoes NP (HAVO1, 79.2%), most likely due to the high levels of emissions of SO_2 during eruptions in March of 2008 that signaled a new phase of activity at the Halema`uma`u Crater (http://www.nps.gov/havo/planyourvisit/halemaumau_newgasvent.htm). The lowest fraction occurred in northern California site of Trinity (9.7%, TRIN1).

The spatial pattern of AS mass fraction for rural plus urban sites was similar to the rural sites alone (Figure 2.2.1d), especially in the East. The highest urban mass fraction was less than the maximum rural mass fraction and occurred in Charleston, West Virginia (60.0%, #540390011); the lowest mass fraction (5.6%) occurred in northwestern Montana (Libby, #300530018). The AS mass fraction in many urban centers was lower than the surrounding urban area (e.g., Salt Lake City, Denver, and the Eastern Seaboard). As will be shown in the next sections, these gradients were mostly likely due to the higher contributions of ammonium nitrate (AN) and carbonaceous aerosols in urban versus rural sites. The inclusion of urban sites in the interpolation scheme often adjusted the spatial patterns to account for the additional information. For example, in Texas and the Gulf states, regions along the coast had higher mass fractions compared to the rural map due to the addition of sites in this region. This change in spatial patterns emphasizes the caution that must be applied when examining these types of maps. The similarity in the urban and rural AS concentrations and fractions of RCFM demonstrates the

regional impact of the sources and atmospheric processes that lead to elevated levels of AS in the atmosphere.

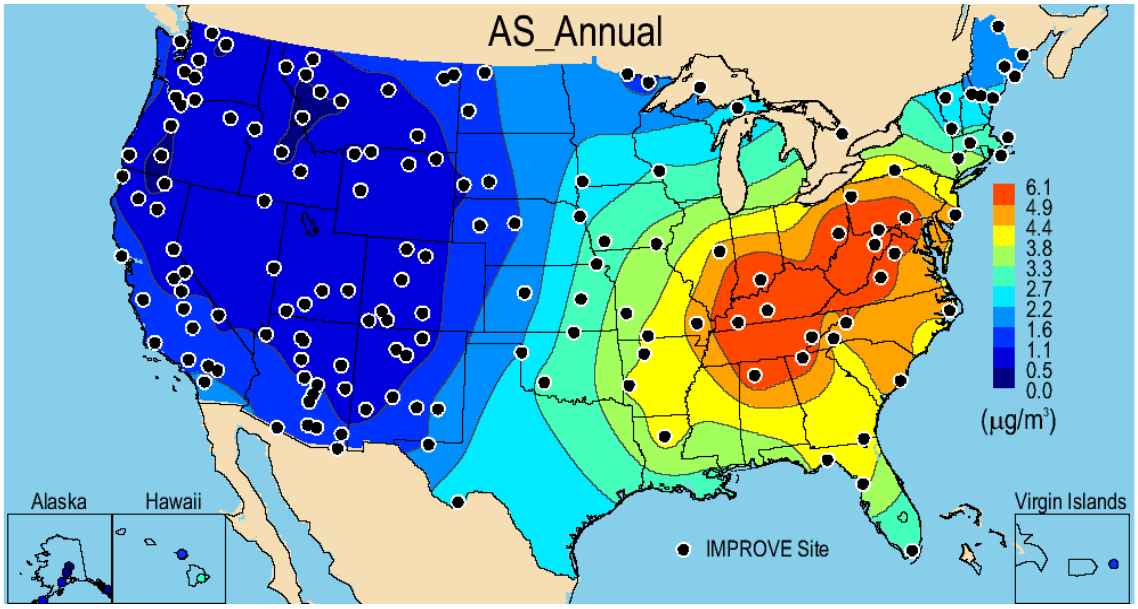

Figure 2.2.1a. IMPROVE (rural) 2005–2008 $PM_{2.5}$ ammonium sulfate (AS) annual mean mass concentrations (µg m^{-3}).

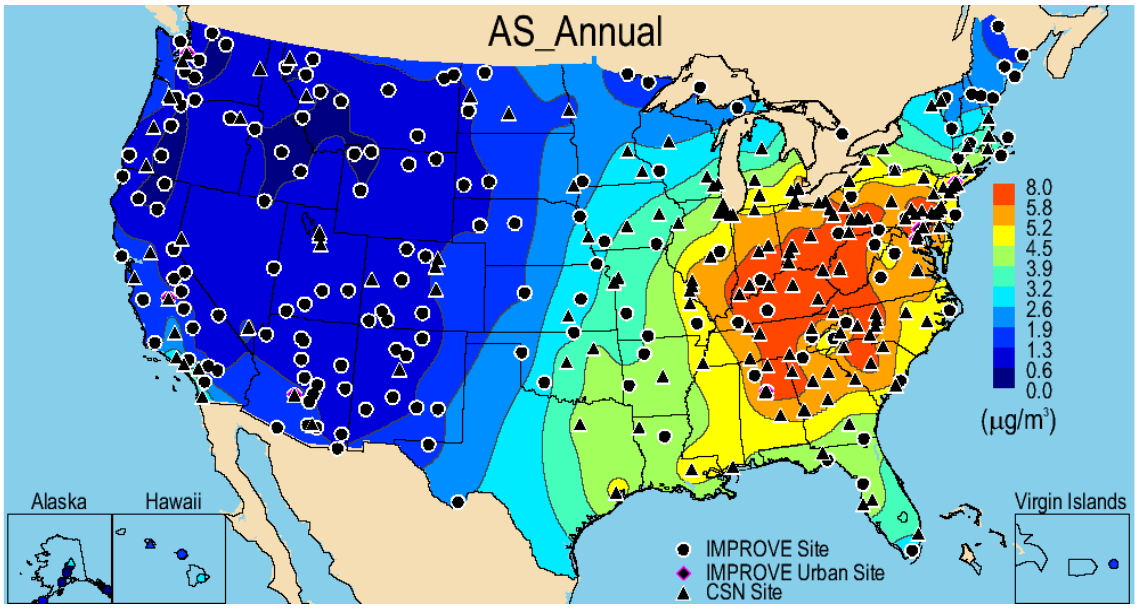

Figure 2.2.1b. IMPROVE and CSN 2005–2008 $PM_{2.5}$ ammonium sulfate (AS) annual mean mass concentrations (µg m^{-3}).

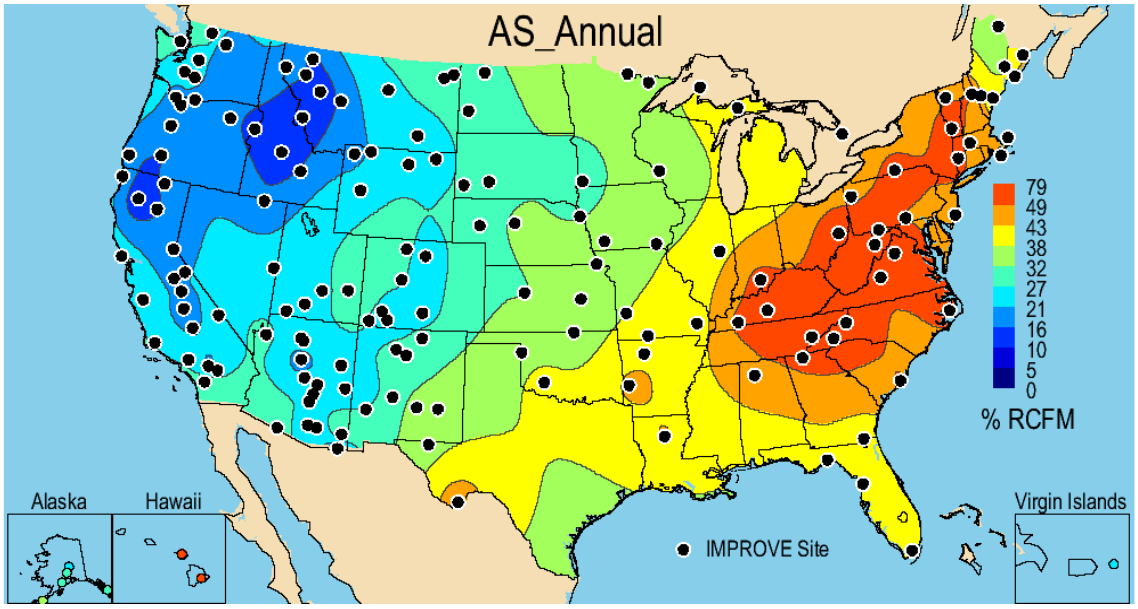

Figure 2.2.1c. IMPROVE (rural) 2005–2008 annual mean percent (%) contributions of ammonium sulfate (AS) to $PM_{2.5}$ reconstructed fine mass (RCFM).

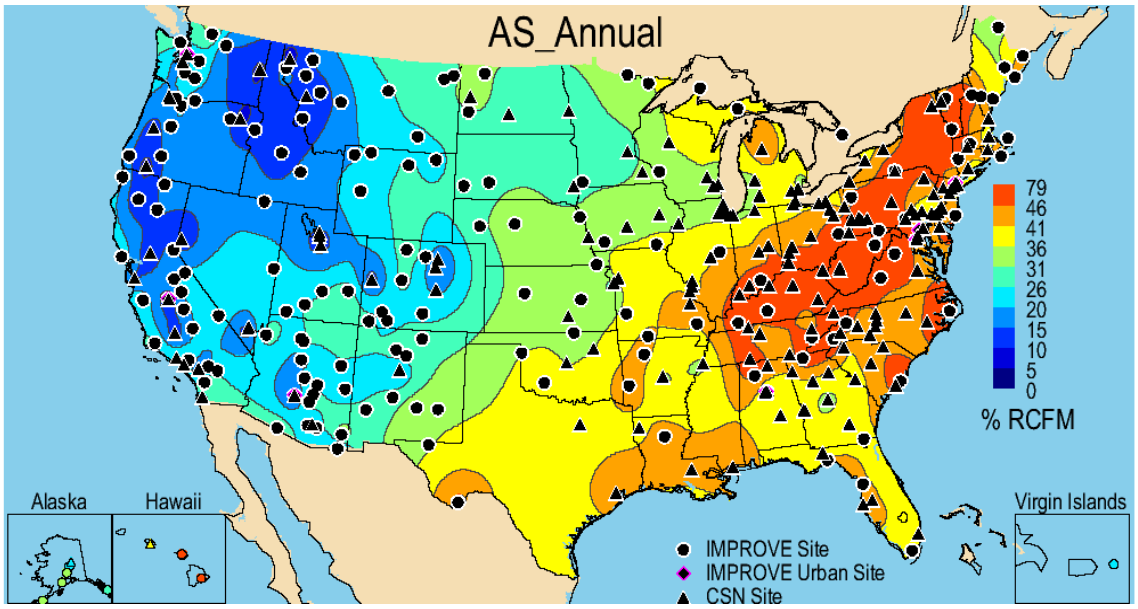

Figure 2.2.1d. IMPROVE and CSN 2005–2008 annual mean percent (%) contributions of ammonium sulfate (AS) to $PM_{2.5}$ reconstructed fine mass (RCFM).

2.2.2 $PM_{2.5}$ Ammonium Nitrate Mass

The AN "bulge" in the central/midwestern United States has been reported previously by Pitchford et al. (2009). Not surprisingly, locations where ammonia and nitric acid emissions were the highest correspond to the regions where AN concentrations were the largest (see Figure 2.2.2a). The maximum IMPROVE 2005–2008 rural concentration of 2.79 μg m^{-3} occurred at Bondville, Illinois (BOND1), a site located in the agricultural Midwest. The lowest rural concentration occurred in Petersburg, Alaska (0.04 μg m^{-3}, PETE1). Seven sites in the central United States had annual AN concentrations greater than 2 μg m^{-3}. Urban IMPROVE sites also

corresponded to higher AN concentrations. The annual AN concentration at the Fresno site (FRES1) was almost 2.5 times higher than even those in the central United States (6.47 μg m^{-3}). Surrounding rural sites, such as Sequoia NP (SEQU1) seemed to be influenced by urban AN, with an annual mean AN concentration of 2.11 μg m^{-3}. All of the other IMPROVE urban sites corresponded to concentrations between 1 and 2 μg m^{-3}, including Phoenix (PHOE1), New York City (NEYO1), Birmingham (BIRM1), Puget Sound (PUSO1), and Washington, D.C. (WASH1). Concentrations were much lower outside of the central United States and urban IMPROVE areas; the majority of the sites around the country had concentrations less than 0.5 μg m^{-3}.

The inclusion of CSN sites provided more structure to the AN spatial pattern and showed the impact of urban AN concentrations on surrounding areas (Figure 2.2.2b). The central "bulge" extended to include sites surrounding Lake Michigan. AN concentrations at sites in Michigan, Illinois, Wisconsin, and Indiana were typically 3–4 μg m^{-3}. Urban sites in the Northeast also had higher AN concentrations compared to the rural sites. In California, particularly Rubidoux (#060658001), annual concentrations reached 9.16 μg m^{-3}, and several other California sites had concentrations above 6 μg m^{-3}. The lowest CSN AN concentration occurred at Pearl City, Hawaii (0.26 μg m^{-3}, #150032004). Generally, urban concentrations of AN were considerably higher than rural concentrations.

Sites with high concentrations of AN were also in regions where a considerable fraction of the RCFM was composed of AN. The central U.S. and California sites were an example, with an AN RCFM fraction of 25% (Figure 2.2.2c). The rural IMPROVE site at Blue Mounds, Minnesota (BLMO1) had the highest annual contribution of AN to RCFM (31.6%), compared to the lowest at Sawtooth, Idaho (2.0 %, SAWT1). In general, however, most rural IMPROVE sites were not highly influenced by AN contributions to RCFM. The maximum fraction of AN at an urban IMPROVE site occurred at Fresno (35.6%, FRES1), compared to the lowest at Birmingham (5.8%, BIRM1) (Figure 2.2.2d). With the addition of the urban CSN sites, the influence of the contribution of AN to RCFM extended farther west from the central United States, where sites in Colorado and Utah ranged from 25 to 30% AN, and sites in California ranged up to 42.7% (Rubidoux, California, #060658001). The lowest urban CSN fraction occurred in the southern Georgia city of Douglas (#130690002, 4.3%).

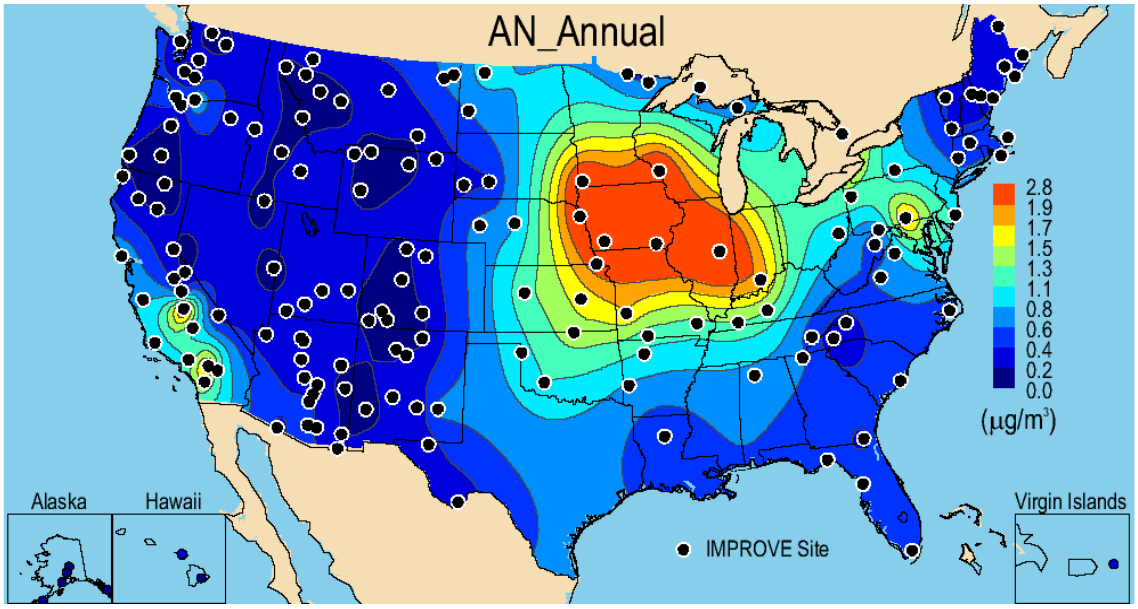

Figure 2.2.2a. IMPROVE (rural) 2005–2008 $PM_{2.5}$ ammonium nitrate (AN) annual mean mass concentrations (µg m^{-3}).

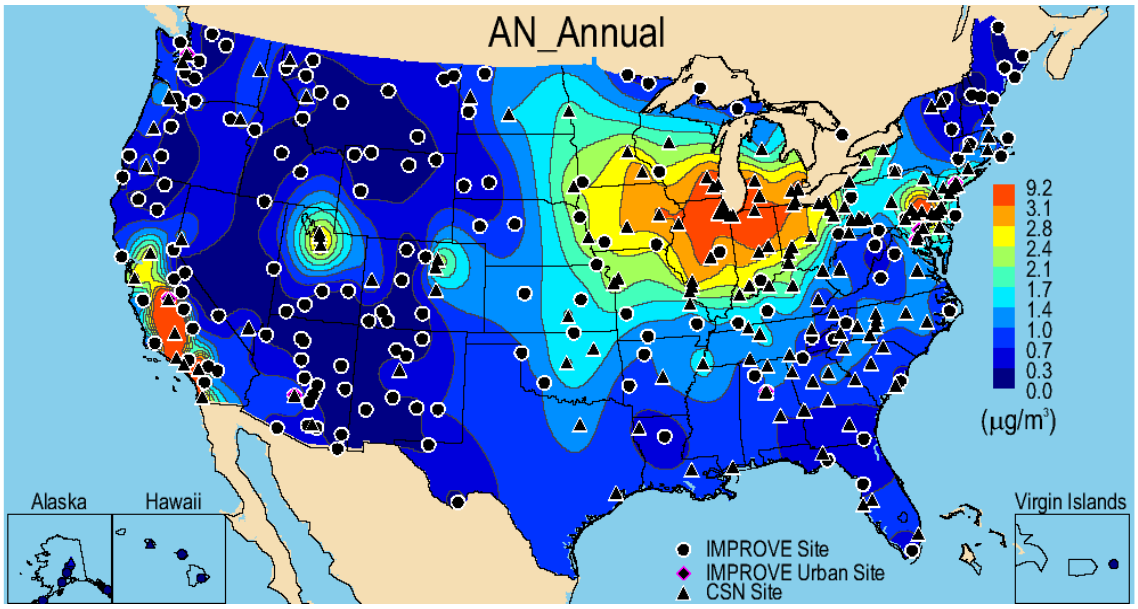

Figure 2.2.2b. IMPROVE and CSN 2005–2008 $PM_{2.5}$ ammonium nitrate (AN) annual mean mass concentrations (µg m^{-3}).

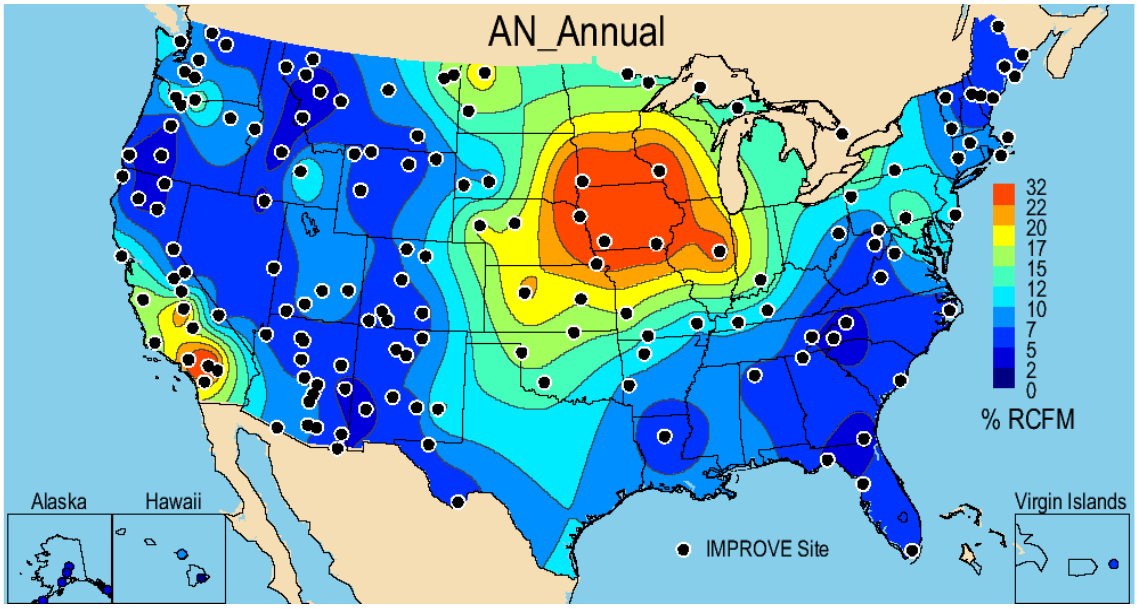

Figure 2.2.2c. IMPROVE (rural) 2005–2008 annual mean percent (%) contributions of ammonium nitrate (AN) to $PM_{2.5}$ reconstructed fine mass (RCFM).

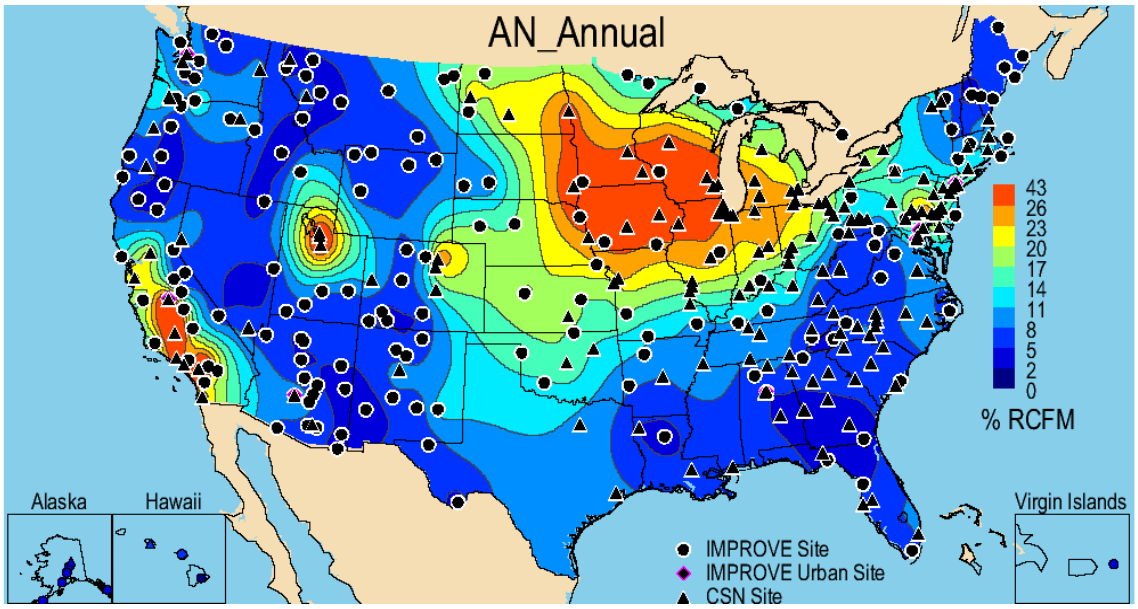

Figure 2.2.2d. IMPROVE and CSN 2005–2008 annual mean percent (%) contributions of ammonium nitrate (AN) to $PM_{2.5}$ reconstructed fine mass (RCFM).

2.2.3 $PM_{2.5}$ Particulate Organic Matter Mass

The eastern part of the United States had the highest 2005–2008 annual mean rural IMPROVE POM concentrations, with several sites in the Southeast having concentrations over 3.2 μg m^{-3} and most sites in the Northeast over 2 μg m^{-3} (Figure 2.2.3a). Elevated levels of POM in the East were most likely due to primary emissions of biomass combustion (especially in the Southeast) and secondary emissions from biogenic sources (Bench et al., 2007). The lowest concentrations occurred in the West. Concentrations in western Colorado, portions of Wyoming and New Mexico, and the Four Corners region were less than 1 μg m^{-3}. The lowest annual POM

concentration of 0.14 μg m^{-3} occurred at Haleakala Crater, Hawaii (HACR1). Portions of the Northwest and California were associated with higher concentrations. Concentrations in Idaho and Montana were near 3 μg m^{-3}, most likely from biomass burning emissions. The higher concentrations in California were associated with Trinity (TRIN1, 4.56 μg m^{-3}) and Sequoia NP (SEQU1, 3.75 μg m^{-3}). High POM concentrations were associated with urban IMPROVE sites, especially in Fresno (6.90 μg m^{-3}, FRES1) and Phoenix (4.51 μg m^{-3}, PHOE1). The urban IMPROVE site with the lowest concentration was Puget Sound (3.59 μg m^{-3}, PUSO1).

The incorporation of CSN sites in the POM spatial map resulted in higher concentrations in more focused regions, especially in the Southeast (Figure 2.2.3b). Portions of Alabama, Georgia, South Carolina, and North Carolina had POM concentrations greater than 5.5 μg m^{-3}. Urban regions along the West Coast and in the Southwest had similar patterns at the rural-only isopleths but with higher concentrations. The highest CSN concentration corresponded to a site in northwestern Montana (11.68 μg m^{-3}, Libby, #300530018), probably due to wintertime residential wood combustion as POM peaked in winter at this site (Ward et al., 2006). The maximum CSN urban POM concentration was 2.5 times higher than the maximum rural IMPROVE concentration. As in the IMPROVE network, the lowest CSN concentration occurred in Pearl City, Hawaii (0.34 μg m^{-3}, #150032004).

The areas with the highest IMPROVE POM mass fractions did not correspond to the areas with the highest POM mass concentrations, as they did for AS and AN (compare Figures 2.2.3a and 2.2.3c, for example). Many rural IMPROVE sites in the West had mass fractions higher than 54%, with the highest mass fraction of 75.1% in the rural site at Trinity, California (TRIN1) (see Figure 2.2.3c), and 79.7% at the CSN site of Libby, Montana (#300530018) (Figure 2.2.3d). Generally, in the rest of the United States the contribution of POM to RCFM was less; in fact, POM contributed less than 50% of RCFM at 86% of all IMPROVE sites and 93% of all CSN sites. In the central and eastern United States the POM contribution to RCFM was near 25–30% for both IMPROVE and CSN. However, POM was a significant contributor to RCFM at several urban CSN sites in Georgia, Alabama, and South Carolina, with contributions to RCFM greater than 40%.

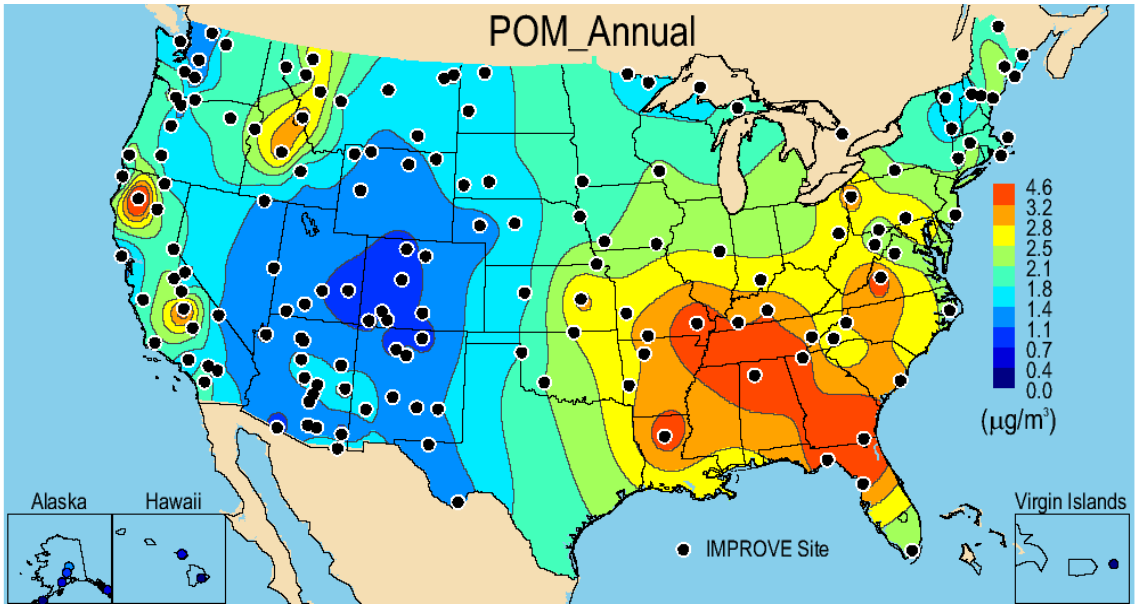

Figure 2.2.3a. IMPROVE (rural) 2005–2008 $PM_{2.5}$ particulate organic matter (POM) annual mean mass concentrations (µg m^{-3}).

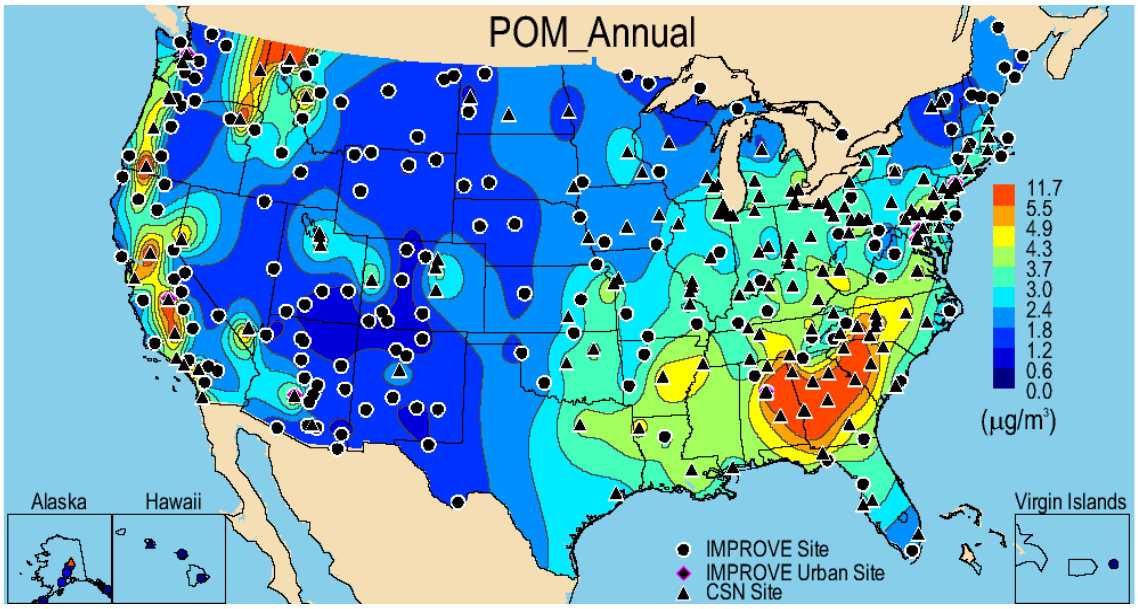

Figure 2.2.3b. IMPROVE and CSN 2005–2008 $PM_{2.5}$ particulate organic matter (POM) annual mean mass concentrations (µg m^{-3}).

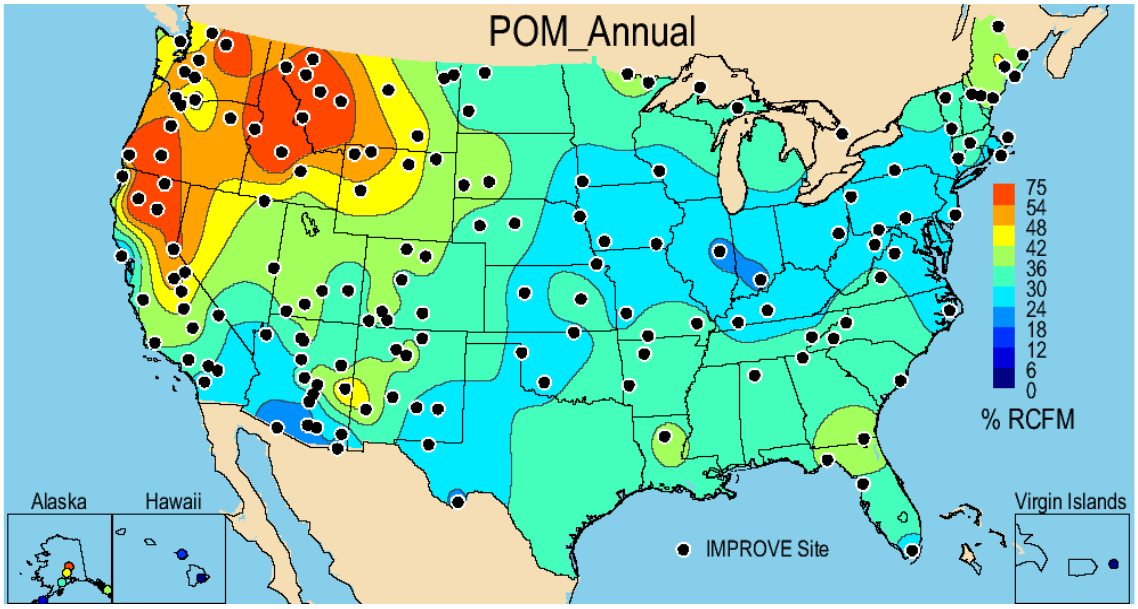

Figure 2.2.3c. IMPROVE (rural) 2005–2008 annual mean percent (%) contributions of particulate organic matter (POM) to $PM_{2.5}$ reconstructed fine mass (RCFM).

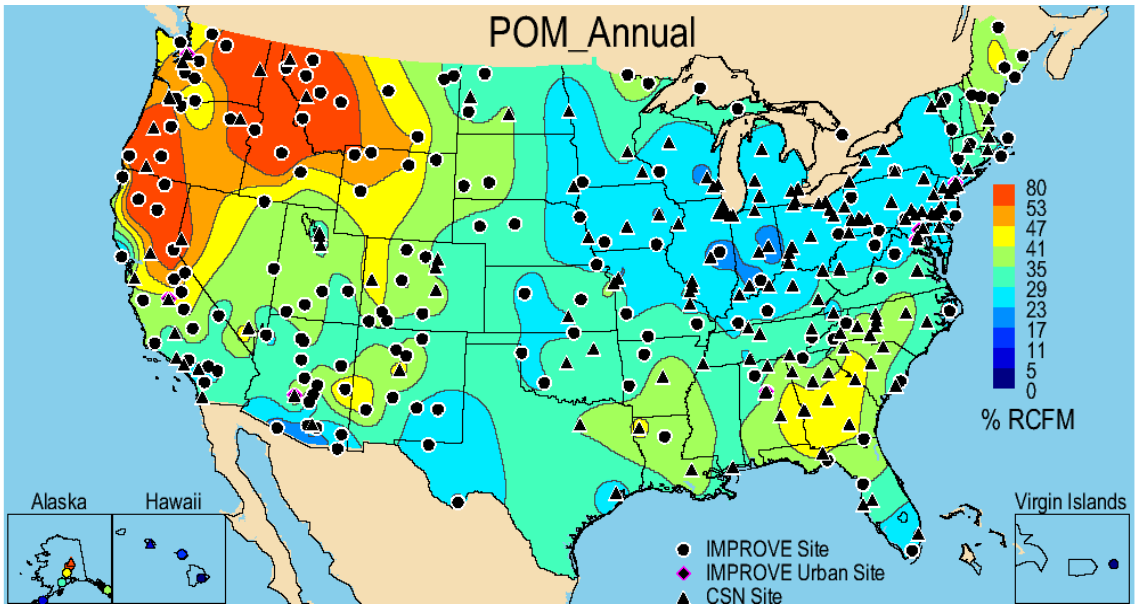

Figure 2.2.3d. IMPROVE and CSN 2005–2008 annual mean percent (%) contributions of particulate organic matter (POM) to $PM_{2.5}$ reconstructed fine mass (RCFM).

2.2.4 $PM_{2.5}$ Light Absorbing Carbon Mass

The IMPROVE rural 2005–2008 annual mean concentration ranged from 0.02 μg m^{-3} in Haleakala Crater, Hawaii (HACR1), to 0.59 μg m^{-3} in James River Face Wilderness, Virginia (JARI1). The concentrations in the West were less than 0.3 μg m^{-3}. The concentrations in the East were higher (0.4–0.5 μg m^{-3}) and tended to be located in the mid-South and Ohio River valley areas, as well as parts of Pennsylvania (Figure 2.2.4a). Major hotspots of LAC in the IMPROVE network were associated with urban sites, with the highest at Birmingham (BIRM1, 1.66 μg m^{-3}). Sites at Fresno (FRES1), Phoenix (PHOE1), Washington, D.C. (WASH1),

Baltimore (BALT1), and New York City (NEYO1) were also associated with higher concentrations (> 1 μg m^{-3}), while the lowest urban IMPROVE concentration occurred at Puget Sound (PUSO1, 0.85 μg m^{-3}).

Urban CSN concentrations were generally higher than IMPROVE (maximum of 2.58 μg m^{-3} in Liberty, Pennsylvania, #420030064, and 2.13 μg m^{-3} in Elizabeth, New Jersey, # 340390004). The spatial pattern of LAC differed from the spatial pattern of POM, suggesting different sources. For example, in the West the rural POM map showed larger regions of higher POM concentrations compared to the more localized LAC concentrations (compare Figure 2.2.3a to 2.2.4b). In addition, the urban excess noticed in the comparison of rural and urban LAC concentration maps was indicative of local urban emissions (e.g., mobile sources) of LAC rather than regional sources like biomass combustion from controlled or wild fires. The steep spatial gradient in the hotspots of LAC in the combined urban and rural map indicated that the spatial extent of the excess was small and concentrations diluted quickly before they had regional impacts (2.2.4b).

LAC is a minor contributor to RCFM at most rural sites around the United States (LAC contributed less than 5% of RCFM for 85% of rural IMPROVE sites, see Figure 2.2.4c). However, in urban regions and some northwestern sites it was as high as 7%, such as at Glacier NP in Montana (GLAC1) and Mount Rainier NP in Washington (MORA1). In the CSN urban network, LAC contributed as much as 15% (Las Vegas, #320030020) to RCFM and contributed less than 5% to RCFM for only 13% of the sites. Urban regions definitely had higher contributions from LAC in general (Figure 2.2.4d), similar to higher mass concentrations, and this influence appeared to be fairly localized.

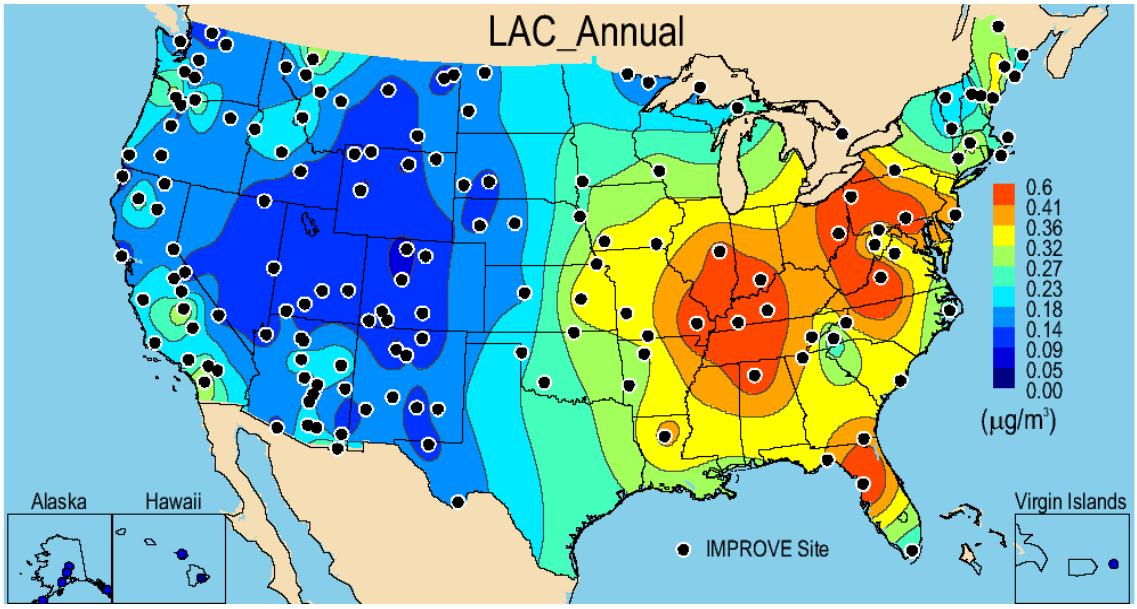

Figure 2.2.4a. IMPROVE (rural) 2005–2008 $PM_{2.5}$ light absorbing carbon (LAC) annual mean mass concentrations (μg m^{-3}).

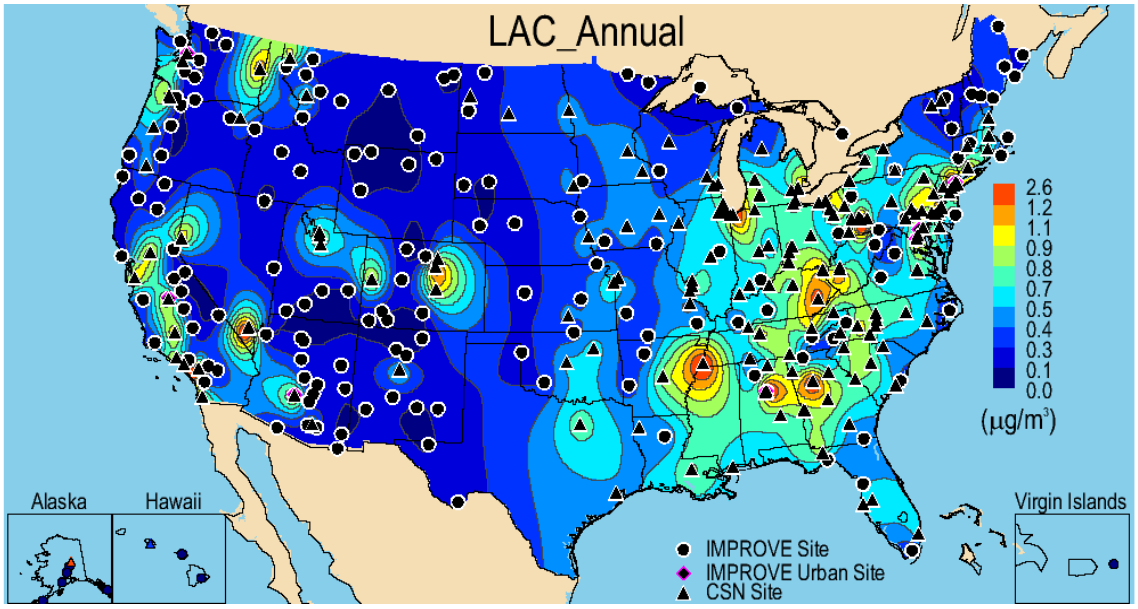

Figure 2.2.4b. IMPROVE and CSN 2005–2008 $PM_{2.5}$ light absorbing carbon (LAC) annual mean mass concentrations (μg m^{-3}).

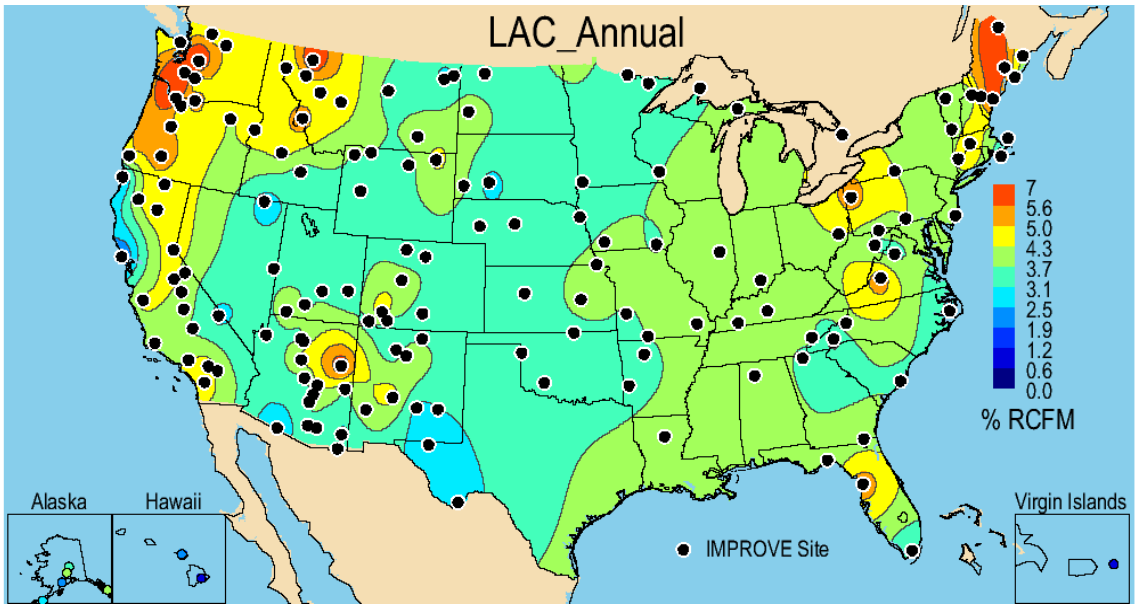

Figure 2.2.4c. IMPROVE (rural) 2005–2008 annual mean percent (%) contributions of light absorbing carbon (LAC) to $PM_{2.5}$ reconstructed fine mass (RCFM).

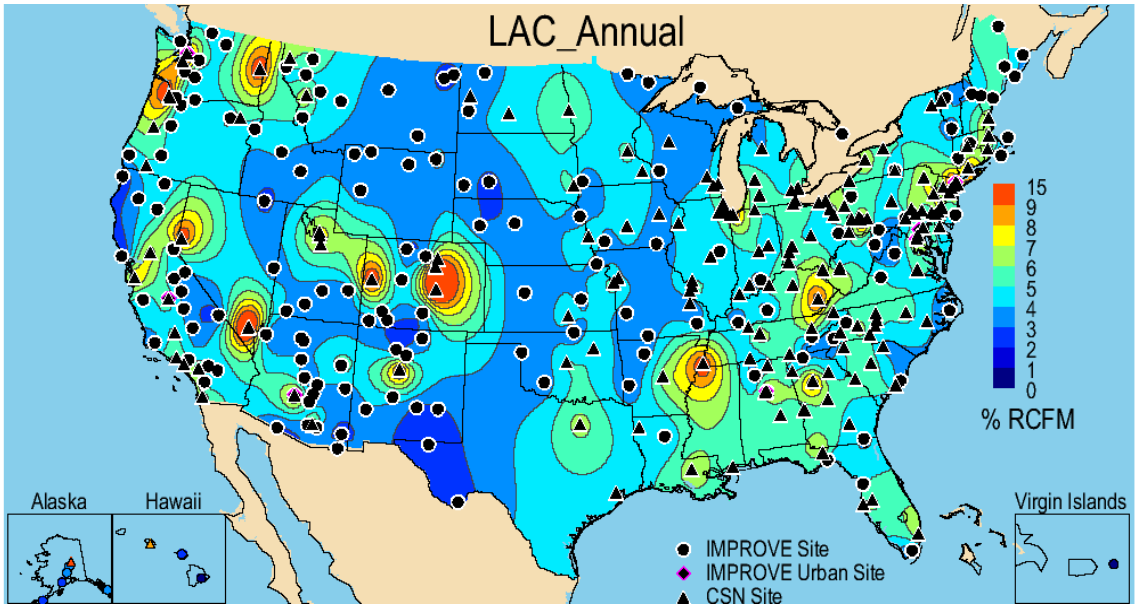

Figure 2.2.4d. IMPROVE and CSN 2005–2008 annual mean percent (%) contributions of light absorbing carbon (LAC) to $PM_{2.5}$ reconstructed fine mass (RCFM).

2.2.5 $PM_{2.5}$ Soil Mass

The patterns observed in the 2005–2008 annual mean rural IMPROVE soil concentrations were reflective of the expected transport pathways described earlier, with the exception of the Asian dust influence. The highest annual mean concentrations were in the Southwest, with the highest at Douglas, Arizona (4.41 μg m^{-3}, DOUG1). Additional sites in Arizona ranged from 1.5 to 4.4 μg m^{-3}. Sites around the Colorado Plateau and Nevada (Jarbidge, JARB1) as well as sites in southern New Mexico and west Texas had higher concentrations (> 1 μg m^{-3}, see Figure 2.2.5a). In the central United States, the highest annual mean concentration occurred at the Cherokee Nation, Oklahoma, site (1.4 μg m^{-3}, CHER1), and the urban IMPROVE site of Birmingham had the highest concentration in the South (2.0 μg m^{-3}, BIRM1). With other species the spatial patterns divided along the east/west orientation; in the case of soil the division was north/south. The concentrations at northern sites tended to be lower (~0.5 μg m^{-3}), with no "hot spots" of high soil concentration as observed in the southern regions. The minimum rural IMPROVE soil concentration occurred at Petersburg, Alaska (0.11 μg m^{-3}, PETE1). Soil is a unique case for IMPROVE, where the rural maximum concentration was higher than the urban IMPROVE maximum (3.21 μg m^{-3}, Phoenix, PHOE1). In general, adding the CSN urban sites to the spatial map did not dramatically alter the spatial pattern but did add a few urban locations where soil was more prevalent (see Figure 2.2.5b). For example, the CSN sites at Denver, Spokane, Detroit, and Rubidoux, California, corresponded to higher soil concentrations. CSN sites in the Southwest, especially Las Vegas, were also higher. The CSN Birmingham site (#10732003), which corresponded to the highest concentration for CSN (2.01 μg m^{-3}), agreed very closely with the concentration from the nearby urban IMPROVE site (BIRM1,1.99 μg m^{-3}). However, the mean soil concentration at the second CSN Birmingham site (#10730023), collocated with the urban IMPROVE sampler, was much lower (1.35 μg m-3), reflecting the relative bias reported in Table 1.9. The mean soil concentration at the collocated IMPROVE and CSN site in Birmingham was 1.35 μg m^{-3}, which was more typical of the level of agreement between IMPROVE and CSN soil concentrations reported in Table 1.9. The lowest concentration

in the CSN network was measured in northeastern New York (0.12 µg m^{-3}, Wilmington, #360310003).

Soil contributed a substantial fraction of RCFM only in the West and Southwest (Figure 2.2.5c), where contributions were typically above 25%. The highest fraction occurred at Douglas, Arizona (51.0%, DOUG1), coincident with the highest concentration. The site at Phoenix (PHOE1) corresponded to the highest fractional contribution at an urban IMPROVE site (27.3%), and Baltimore was the lowest (4.5%, BALT1). The lowest nonurban IMPROVE fractional contribution occurred at Point Reyes, California (3.2%, PORE1). Soil contributed less than 25% to the RCFM for 85% of the IMPROVE sites, along the western coast and the eastern half of the United States. The soil fraction of RCFM was less than 25% for all of the CSN urban sites (Figure 2.2.5d). The maximum fraction occurred in Las Vegas (21.8%, #320030020) and the lowest at Biglerville in south-central Pennsylvania (2.2%, #420010001).

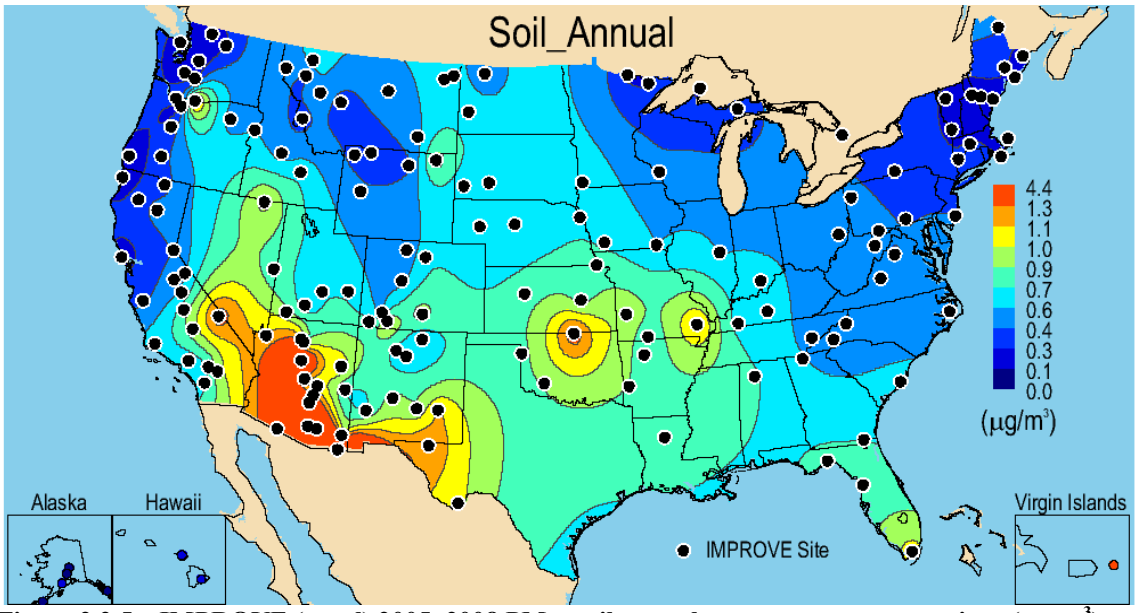

Figure 2.2.5a. IMPROVE (rural) 2005–2008 $PM_{2.5}$ soil annual mean mass concentrations (µg m^{-3}).

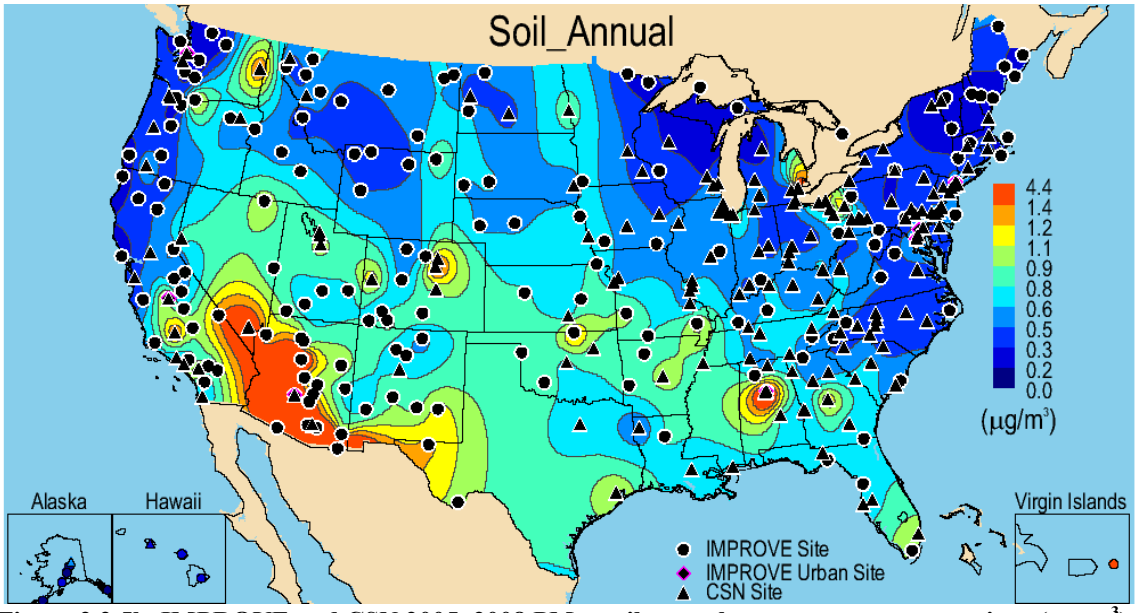

Figure 2.2.5b. IMPROVE and CSN 2005–2008 $PM_{2.5}$ soil annual mean mass concentrations (μg m^{-3}).

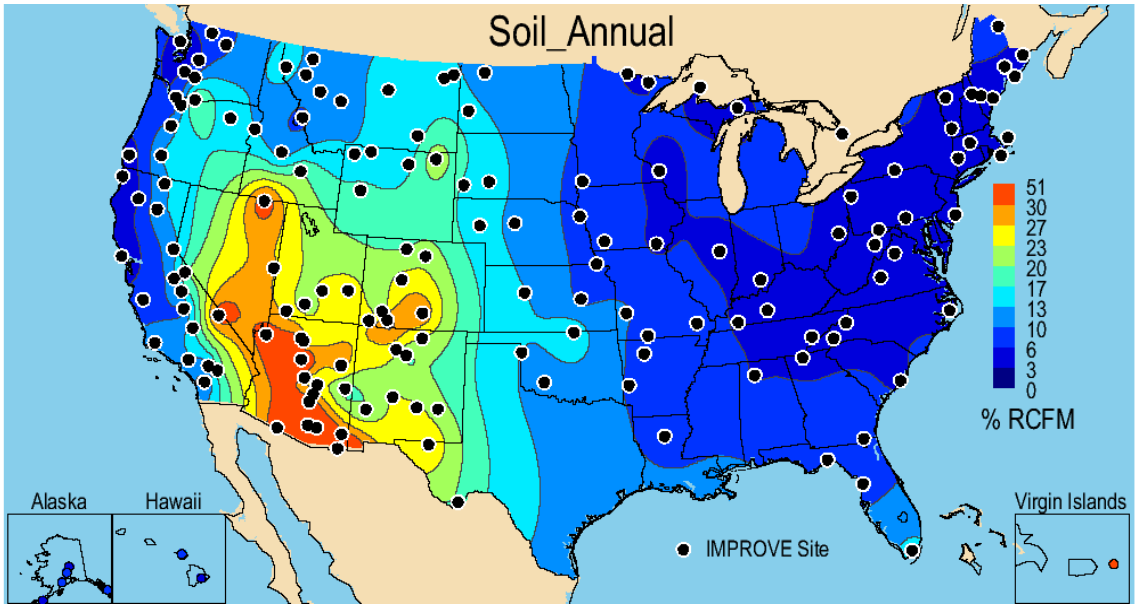

Figure 2.2.5c. IMPROVE (rural) 2005–2008 annual mean percent (%) contributions of soil to $PM_{2.5}$ reconstructed fine mass (RCFM).

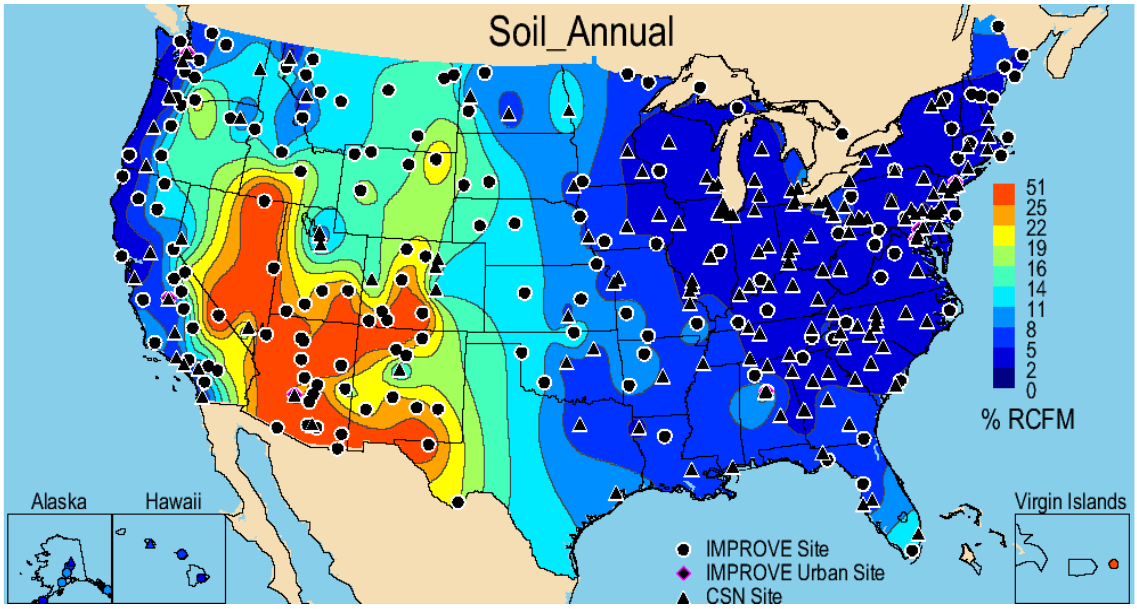

Figure 2.2.5d. IMPROVE and CSN 2005–2008 annual mean percent (%) contributions of soil to $PM_{2.5}$ reconstructed fine mass (RCFM).

2.2.6 $PM_{2.5}$ Sea Salt Mass

The IMPROVE sites with the highest 2005–2008 annual mean sea salt concentrations were, not surprisingly, at the east and west coasts (Figure 2.2.6a). Concentrations at rural IMPROVE sites ranged from 0.004 μg m^{-3} at Shamrock Mine, Colorado (SHMI1), to 2.29 μg m^{-3} at Point Reyes National Seashore, California (PORE1). On the East Coast, the site at Everglades NP in Florida (EVER1) had an annual mean concentration of 0.60 μg m^{-3}, and Cape Romain NWR in South Carolina (ROMA1) corresponded to a concentration of 0.49 μg m^{-3}. Two sites in Massachusetts had higher concentrations: Martha's Vineyard (0.84 μg m^{-3}, MAVI1) and Cape Cod (0.76 μg m^{-3}, CACO1). The Virgin Islands (VIIS) had a concentration of 1.5 μg m^{-3}. Other than these sites, the rural IMPROVE concentrations were low. The urban IMPROVE site concentrations ranged from 0.19 μg m^{-3} at Washington, D.C. (WASH1), to 0.38 μg m^{-3} at Puget Sound (PUSO1). The sea salt concentrations at CSN urban sites were typically lower than those at IMPROVE sites (Figure 2.2.6b) due to the relative biases between the two estimates (see section 1.4). The minimum concentration of 0.0013 μg m^{-3} occurred in Watford City, North Dakota (#380530002), and the maximum concentration 0f 0.97 μg m^{-3} occurred in Pearl City, Hawaii (#150032004). Nearly all of the CSN sites corresponded to concentrations that were less than 0.4 μg m^{-3}, with the exception of 0.49 μg m^{-3} in Florida (Fort Lauderdale, 120111002) and 0.56 μg m^{-3} in Pennsylvania (Liberty, #420030064) and the maximum concentration at the site in Hawaii.

At the IMPROVE site at Simeonof, Alaska (SIME1), sea salt contributed 46.1% of RCFM, compared to the minimum contribution at Shamrock Mine, Colorado (0.12%, SHMI1) (Figure 2.2.6c). At the CSN site at Pearl City, Hawaii (#150032004), sea salt contributed 26.9% of RCFM, compared to 0.04% at Watford City, North Dakota (#380530002). In general sea salt was not a major contributor to RCFM even in coastal regions; 95% of all IMPROVE sites corresponded to contributions of less than 10%, similar to 99% of all CSN sites (Figure 2.2.6d).

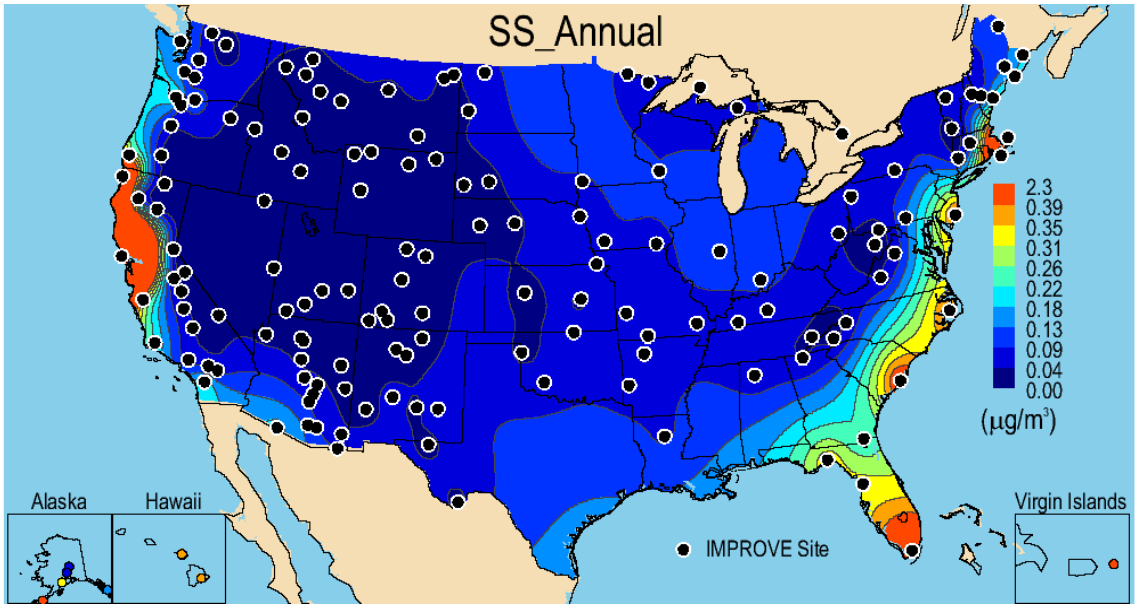

Figure 2.2.6a. IMPROVE (rural) 2005–2008 $PM_{2.5}$ sea salt (SS) annual mean mass concentrations (µg m^{-3}).

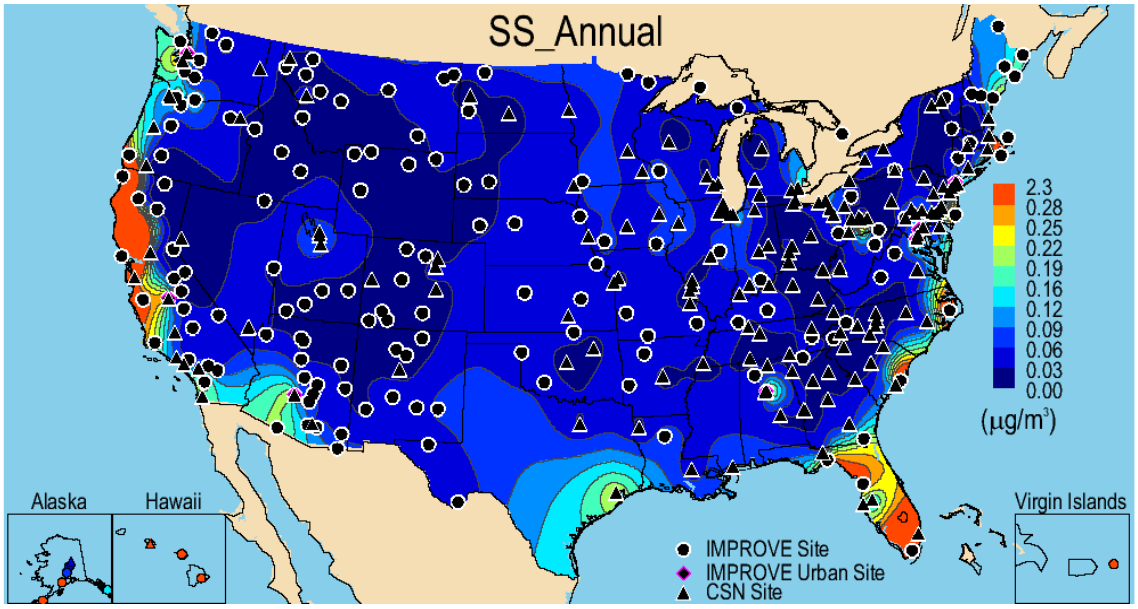

Figure 2.2.6b. IMPROVE and CSN 2005–2008 $PM_{2.5}$ sea salt (SS) annual mean mass concentrations (µg m^{-3}).

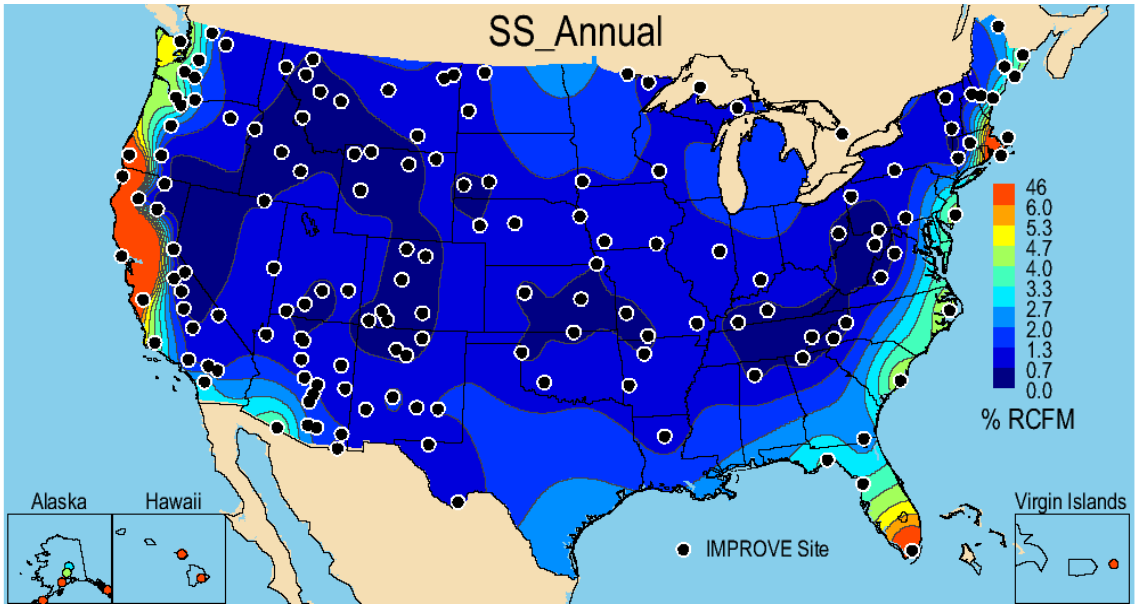

Figure 2.2.6c. IMPROVE (rural) 2005–2008 annual mean percent (%) contributions of sea salt to $PM_{2.5}$ reconstructed fine mass (RCFM).

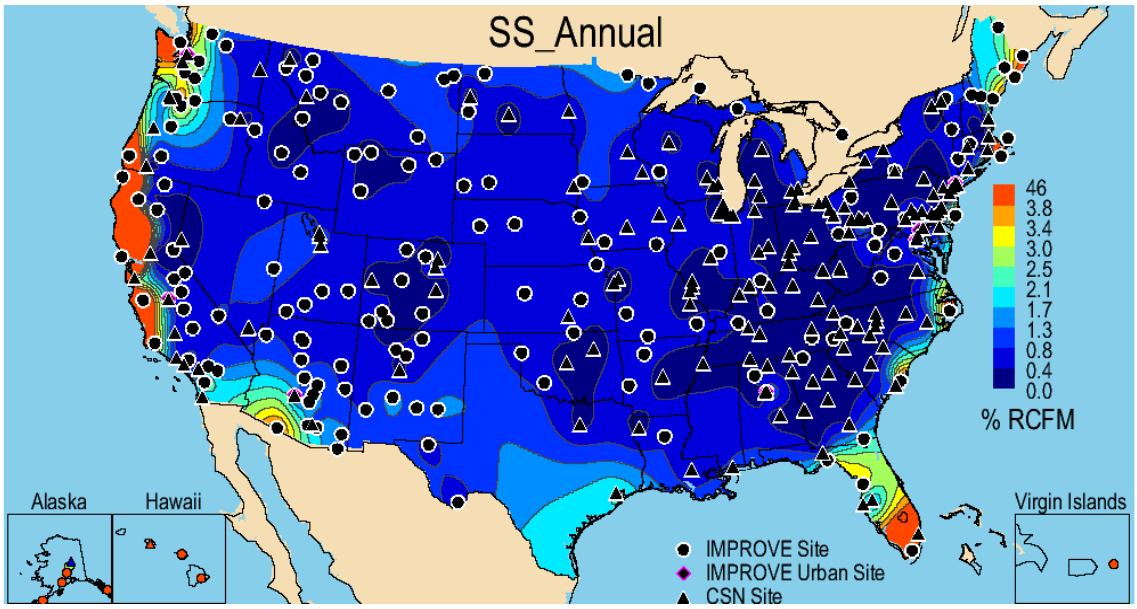

Figure 2.2.6d. IMPROVE and CSN 2005–2008 annual mean percent (%) contributions of sea salt (SS) to $PM_{2.5}$ reconstructed fine mass (RCFM).

2.2.7 $PM_{2.5}$ Gravimetric Fine Mass

The spatial pattern of 2005–2008 annual mean IMPROVE FM concentrations reflected the patterns of both the annual mean concentrations of AS, AN, and POM (compare Figure 2.2.7a to 2.2.1a, 2.2.2a, and 2.2.3a, respectively). High concentrations in the eastern United States (the maximum value of 11.67 μg m^{-3} occurred at Livonia, Indiana, LIVO1) were consistent with high concentrations of AS in this region. The western United States corresponded to lower concentrations (Figure 2.2.7a). The lowest occurred in Petersburg, Alaska (1.29 μg m^{-3}, PETE1). Two regions of higher FM concentrations in the West were associated with urban

IMPROVE sites. Phoenix (PHOE1) had an annual mean concentration of 10.27 μg m^{-3}, and Fresno (FRES1) had an FM concentration of 15.0 μg m^{-3}. The highest urban IMPROVE concentration occurred in Birmingham (17.09 μg m^{-3}, BIRM1), compared with the lowest urban concentration of 6.87 μg m^{-3} in Puget Sound (PUGO1). The urban FM concentrations measured by the CSN network were somewhat higher than the IMPROVE concentrations; only four sites had annual mean concentrations less than 6.0 μg m^{-3} (Figure 2.2.7b). The values ranged from 5.43 μg m^{-3} in Watford City, North Dakota (#380530002) to 21.48 μg m^{-3} in southwestern Pennsylvania (Liberty, #420030064). The same general pattern of high FM in the East compared to the West occurred with the addition of the CSN sites, but the impact of the urban centers, such as Denver, Salt Lake City, Rubidoux, California, Las Vegas, and Libby, Montana, was noticeable.

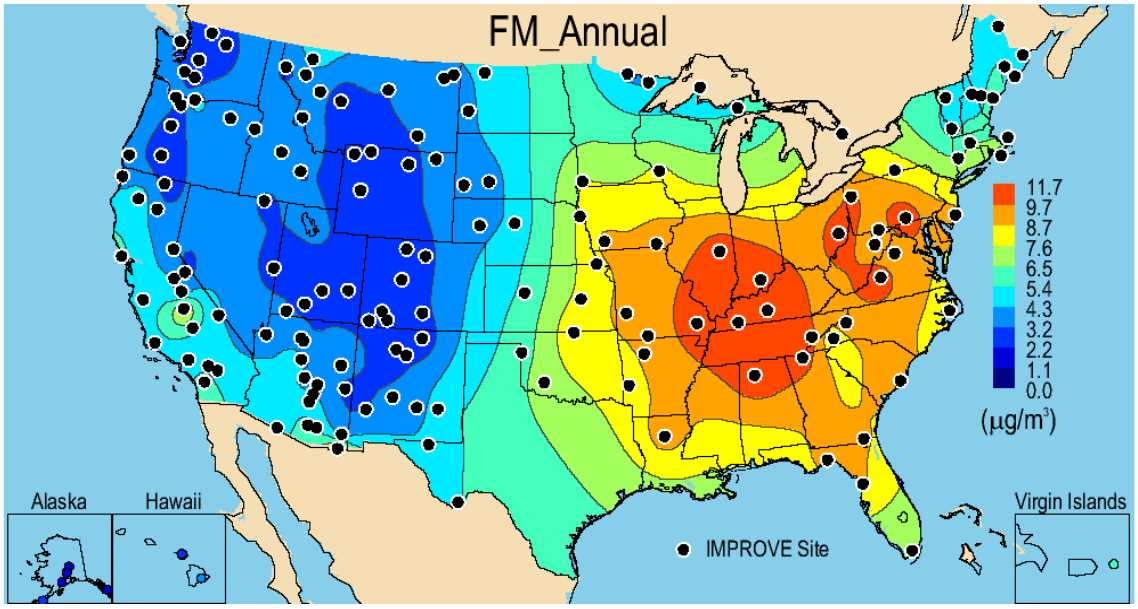

Figure 2.2.7a. IMPROVE (rural) 2005–2008 $PM_{2.5}$ annual mean gravimetric fine mass (FM) concentrations (μg m^{-3}).

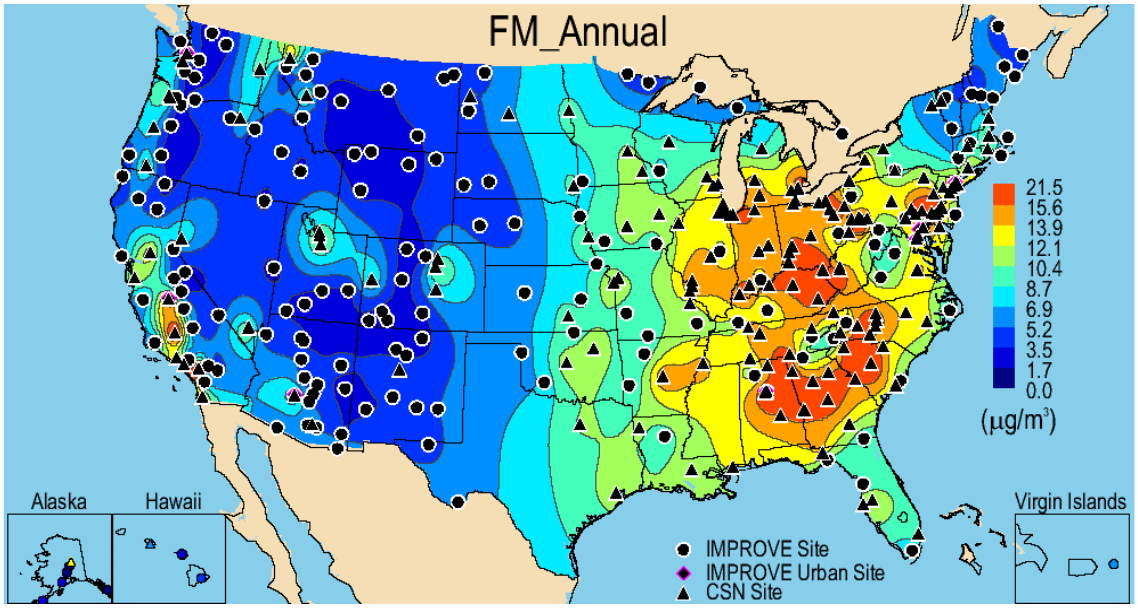

Figure 2.2.7b. IMPROVE and CSN 2005–2008 $PM_{2.5}$ annual mean gravimetric fine mass (FM) concentrations (μg m^{-3}).

2.2.8 $PM_{2.5}$ Reconstructed Fine Mass

If all of the assumptions regarding the molecular species of aerosols included in the calculation of RCFM were appropriate and there were no biases in the FM measurements, then the spatial pattern of RCFM should exactly reproduce the FM spatial pattern. Comparisons of the 2005–2008 annual mean FM and RCFM concentrations for rural IMPROVE (Figures 2.2.7a and 2.2.8a, respectively) show fairly close agreement, although there are some differences. Some of these differences in the patterns also may be due to uncertainties in the interpolation scheme. The maximum rural IMPROVE annual mean RCFM corresponded to the site at Livonia, Indiana (LIVO1, 11.73 μg m^{-3}), where the maximum AS annual mean also occurred. The minimum annual mean RCFM occurred in Petersburg, Alaska (1.18 μg m^{-3}, PETE1). The FM maximum and minimum locations occurred at the same sites, respectively.

The urban annual mean RCFM ranged between 7.77 μg m^{-3} (Puget Sound, PUSO1) and 18.17 μg m^{-3} in Fresno (FRES1), where the maximum AN annual mean also occurred. The maximum annual mean urban FM concentration occurred in Birmingham (BIRM1), not Fresno, possibly because of losses of nitrate species from the Teflon filter. The CSN annual mean RCFM concentration ranged from 3.49 μg m^{-3} at Watford City (#380530002) to 21.28 μg m^{-3} at Rubidoux (#060658001) (Figure 2.2.8b). Similarly to the IMPROVE network, the maximum CSN RCFM occurred at the same location as the maximum AN. Further investigation into the differences between FM and RCFM will be presented in the next section.

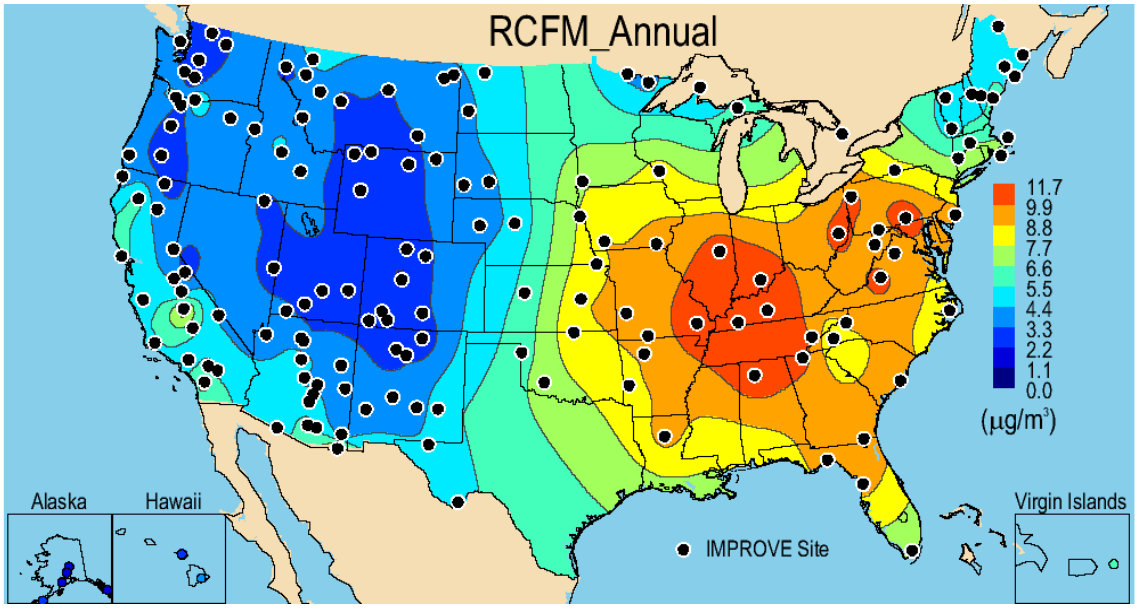

Figure 2.2.8a. IMPROVE (rural) 2005–2008 $PM_{2.5}$ annual mean reconstructed fine mass (RCFM) concentrations (µg m^{-3}).

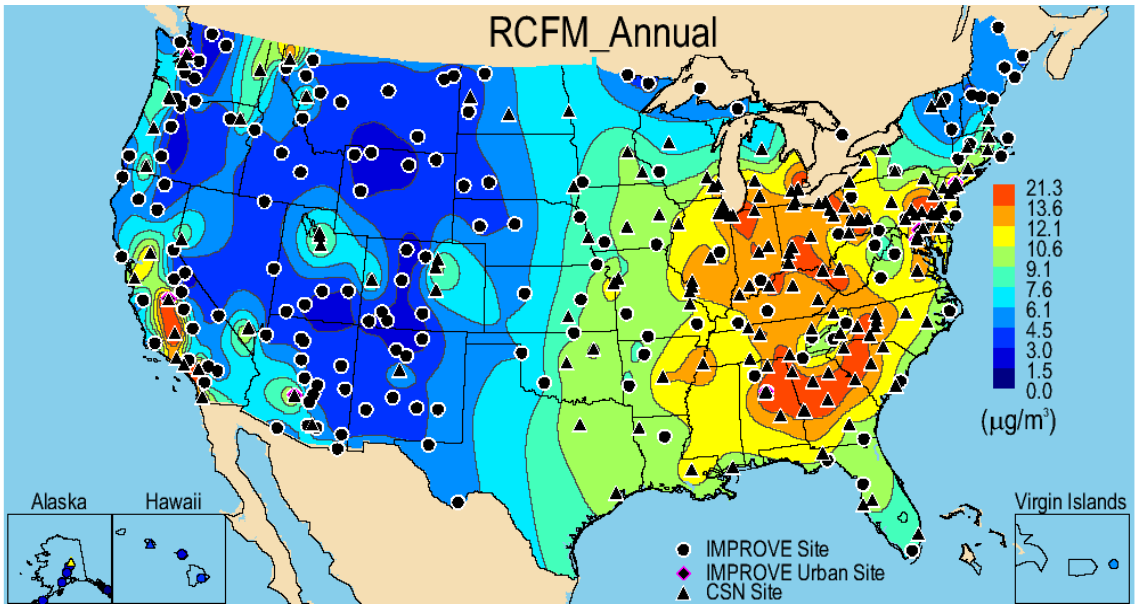

Figure 2.2.8.b. IMPROVE and CSN 2005–2008 $PM_{2.5}$ annual mean reconstructed fine mass (RCFM) concentrations (µg m^{-3}).

2.2.9 Differences in $PM_{2.5}$ Gravimetric and Reconstructed Fine Mass

Differences between 2005−2008 annual mean FM and RCFM (dM = FM - RCFM) for most of the rural IMPROVE sites were fairly low (Figure 2.2.9a). The rural mass difference ranged from -1.14 at Okefenokee, Georgia (OKEF1) to 0.6 µg m^{-3} at Linville Gorge, North Carolina (LIGO1). RCFM overestimated FM (negative dM) at many rural IMPROVE sites and all of the urban IMPROVE sites. The largest overestimate occurred at Fresno (-3.18 µg m^{-3}), most likely due to a loss of nitrate on the fine mass Teflon filter. An inappropriately-high R_{oc} factor may also have contributed. The usual east/west differences in the spatial patterns of dM

were not observed with the IMPROVE rural sites, but this division was more obvious with the addition of urban CSN sites (Figure 2.2.9b). In contrast to the IMPROVE sites, RCFM underestimated FM concentrations at most of the CSN urban sites. The mass difference ranged from -1.37 μg m^{-3} at Los Angeles (#060371103) to 5.25 μg m^{-3} at Columbia, South Carolina (#450790019). For 35% of CSN sites, RCFM was underestimated by more than 2 μg m^{-3}. Sites in the East corresponded to the highest dM. An examination of values of dM at collocated urban IMPROVE and CSN sites revealed negative IMPROVE dM values contrasting positive CSN dM values at the same site. The discrepancy arose from higher CSN FM concentrations compared to IMPROVE FM concentrations (recall the relative biases of 0.04% and 18.4% in RCFM and FM, respectively, reported in Table 1.9). Higher CSN FM concentrations were most likely associated with smaller negative sampling artifacts due to lower filter face velocities of CSN samplers compared with the IMPROVE sampler. Adjusting the CSN OC data to agree with IMPROVE OC data introduced an inconsistency between the CSN RCFM and FM by reducing RCFM concentrations that otherwise would have been consistent with higher FM values. Further investigation of biases associated with FM measurements will be explored in Chapter 8 (Malm et al., 2011).

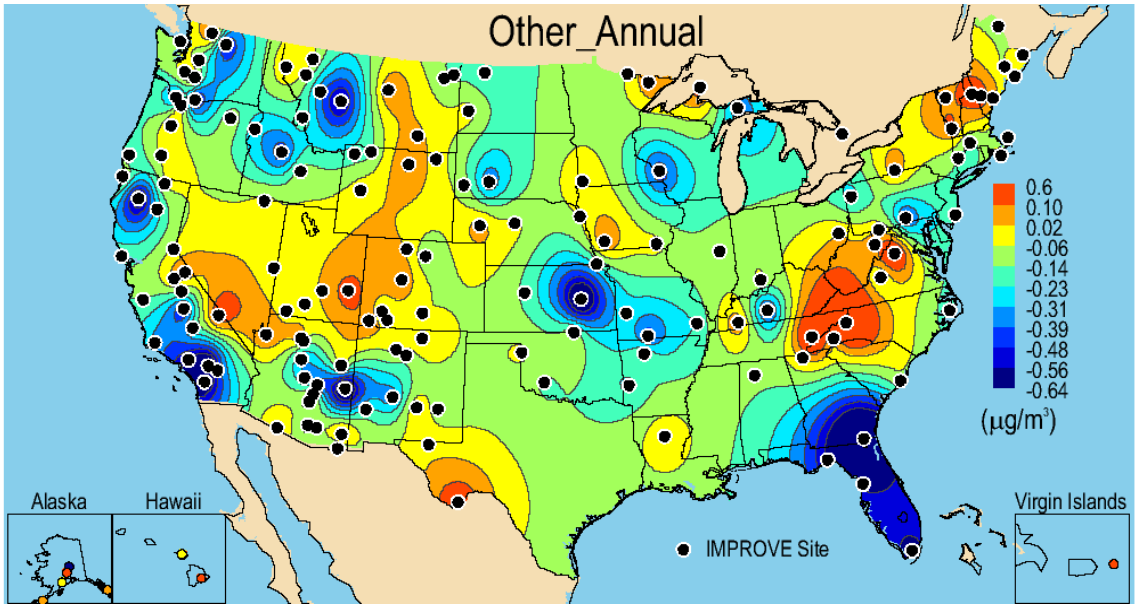

Figure 2.2.9a. IMPROVE (rural) 2005–2008 $PM_{2.5}$ annual mean mass difference (dM = FM - RCFM) between $PM_{2.5}$ gravimetric fine mass (FM) and reconstructed fine mass (RCFM) (μg m^{-3}).

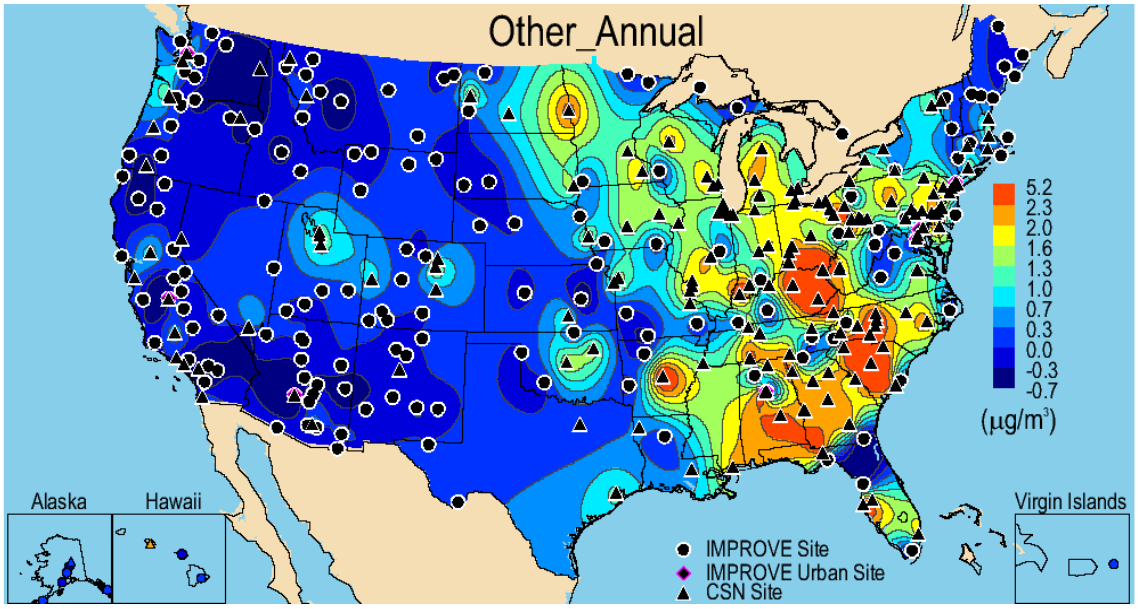

Figure 2.2.9b. IMPROVE and CSN 2005–2008 $PM_{2.5}$ annual mean difference (dM = FM - RCFM) between $PM_{2.5}$ gravimetric fine mass (FM) and reconstructed fine mass (RCFM) (µg m^{-3}).

2.2.10 Coarse Mass

Coarse mass (CM) data were only available for the IMPROVE network and were derived from the difference in PM_{10} and $PM_{2.5}$ gravimetric mass concentrations. The rural CM 2005−2008 annual mean concentration ranged from 1.12 µg m^{-3} in North Cascades, Washington (NOCA1), to 21.12 µg m^{-3} in Douglas, Arizona (DOUG1) (Figure 2.2.10). The high concentration in Douglas was most likely associated with mineral dust. In fact, high concentrations at several sites in the Southwest were observed, similar to soil concentrations (see Figure 2.2.5a). The urban IMPROVE CM ranged from 6.42 µg m^{-3} in Baltimore (BALT1) to 20.51 µg m^{-3} in Phoenix (PHOE1). Twelve sites corresponded to CM greater than 10 µg m^{-3}. With the exception of New York City (NEYO1) and Puget Sound (PUSO1), all of the IMPROVE urban sites had high concentrations (CM > 10 µg m^{-3}). In the central United States higher concentrations most likely corresponded to agricultural activity and fugitive dust (Malm et al., 2007). The annual mean concentration at Cherokee Nation, Oklahoma (CHER1), was 15.70 µg m^{-3}, Mingo, Missouri, had a concentration of 9.02 µg m^{-3} (MING1), and Viking Lake, Iowa, (VILA1) had a concentration of 9.41 µg m^{-3}. Comparisons of annual mean $PM_{2.5}$ soil and CM concentration spatial maps suggested that species other than soil were contributing to CM, especially in the central states. Sites in Iowa and Missouri had high CM concentrations but not necessarily high soil concentrations. In contrast, sites in southern Arizona corresponded to both high fine soil and CM, as would be expected if CM was predominantly soil. High concentrations of CM were also observed at the Virgin Islands site (12.06 µg m^{-3}), probably due to dust and/or sea salt. Lower concentrations were observed along the Appalachian region and in the Northeast, the Rocky Mountain region, the Northwest (with the exception of the Columbia River Gorge, Washington), and northern California.

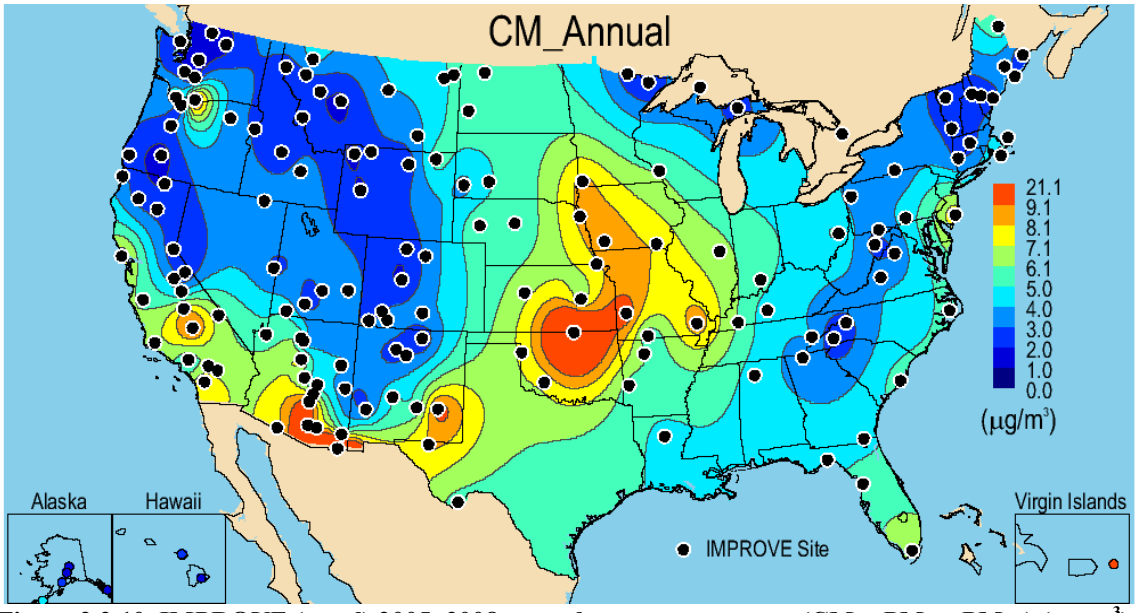

Figure 2.2.10. IMPROVE (rural) 2005–2008 annual mean coarse mass (CM = PM_{10} - $PM_{2.5}$) (μg m^{-3}).

2.2.10 PM_{10} Mass

The spatial pattern of 2005–2008 annual mean rural IMPROVE annual mean PM_{10} mass concentrations reflected the combined CM and FM spatial patterns. The regions of higher PM_{10} concentrations included the eastern half of the United States where $PM_{2.5}$ concentrations were high but also included regions in the Midwest where high CM concentrations were high (Figure 2.2.11a). Sites along the western coast and in the Southwest and California were also associated with high PM_{10} concentrations. The annual mean IMPROVE PM_{10} concentrations ranged from 2.47 μg m^{-3} in Petersburg, Alaska (PETE1), to 29.47 μg m^{-3} in Douglas, Arizona (DOUG1). The high annual mean concentration in Douglas was primarily associated with soil. IMPROVE urban concentrations of PM_{10} were higher than rural concentrations. The urban IMPROVE PM_{10} concentrations ranged from 13.28 μg m^{-3} in Puget Sound (PUSO1) to 34.94 μg m^{-3} in Fresno (FRES1). The site at Fresno also corresponded to high CM as discussed previously. Unfortunately, we have no speciated CM data for Fresno to comment on the major species contributing to CM at that site. The EPA PM_{10} mass concentration spatial map demonstrated much higher spatial variability compared to the IMPROVE data (Figure 2.2.11b). No large regional impacts were observed, with perhaps an exception in the Southwest. Several "hot spots" occurred around the country, with the highest concentration areas in California and the Southwest. The PM_{10} concentrations were also much higher at the EPA sites, suggesting local sources with high spatial variability. The PM_{10} annual mean concentrations ranged from 6.07 μg m^{-3} in Lava Beds National Monument, California (#060930005), to 86.38 μg m^{-3} near Mono Lake, also in California (#060510011). The Mono Lake site location is associated with significant dust emissions from dry lake beds and often has been in nonattainment of EPA air quality standards (e.g., GBUAPCD, 2010). EPA PM_{10} sites are located in both rural and urban locations, and the lack of regional spatial patterns demonstrates the high degree in spatial variability and fairly local impact of many PM_{10} sources.

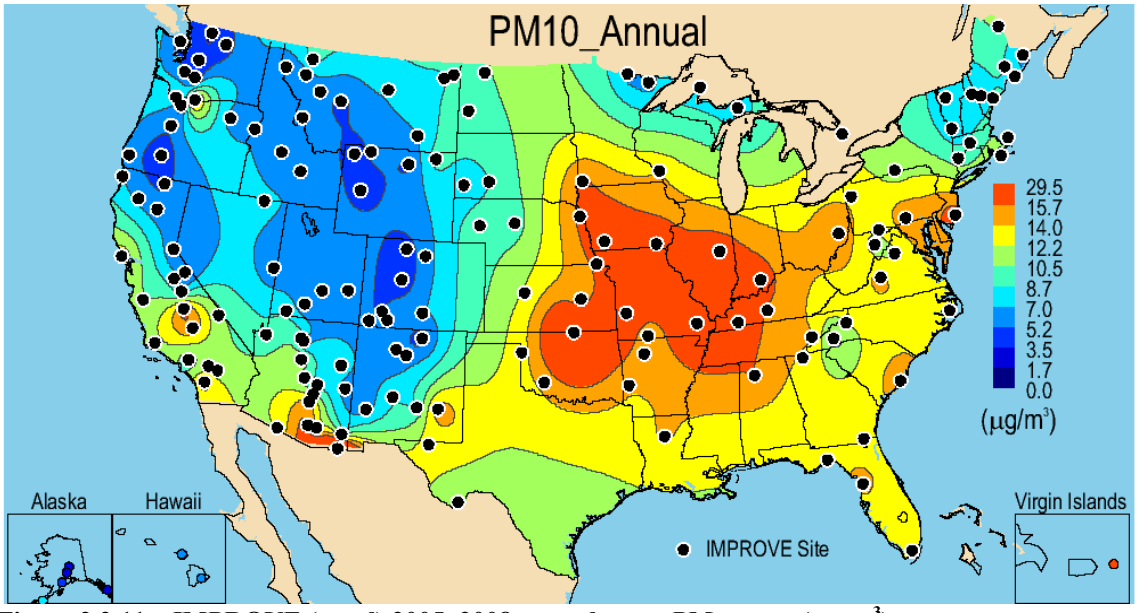

Figure 2.2.11a. IMPROVE (rural) 2005–2008 annual mean PM_{10} mass (µg m^{-3}).

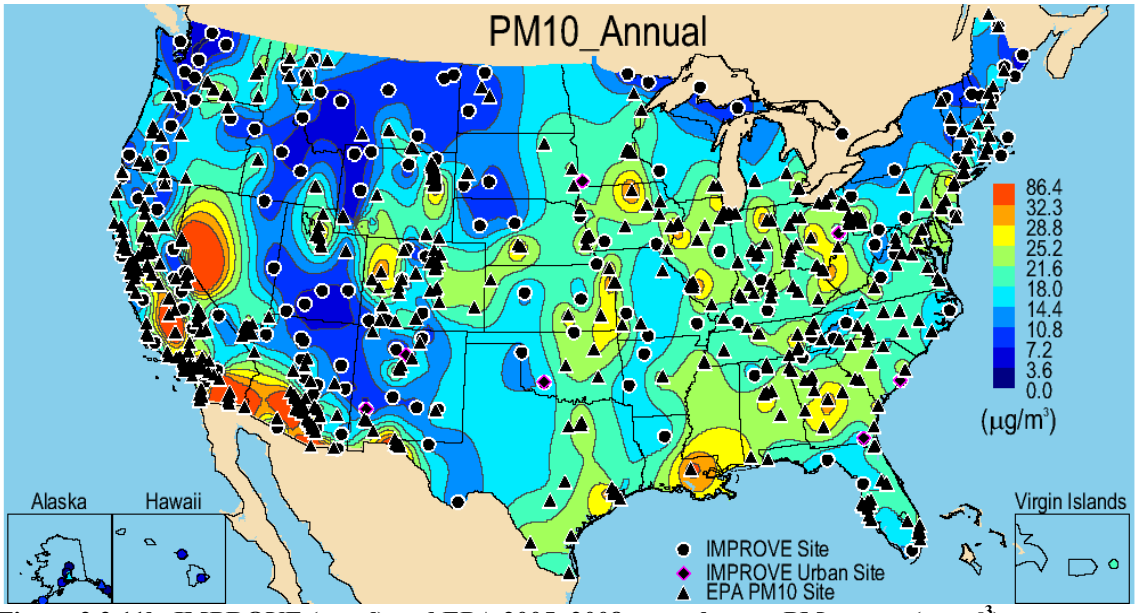

Figure 2.2.11b. IMPROVE (rural) and EPA 2005–2008 annual mean PM_{10} mass (µg m^{-3}).

REFERENCES

Ashbaugh, L. L., and R. A. Eldred (2004), Loss of particle nitrate from Teflon sampling filters: Effects on measured gravimetric mass in California and in the IMPROVE network, *J. Air Waste Manage., 54,* 93-104.

Barna, M. G., K. A. Gebhart, B. A. Schichtel, and W. C. Malm (2006), Modeling regional sulfate during the BRAVO study: Part 1. Base emissions simulation and performance evaluation, *Atmos. Environ. 40,* 2436-2448.

Bench, G., S. Fallon, B. Schichtel, W. Malm, and C. McDade (2007), Relative contributions of fossil and contemporary carbon sources to $PM_{2.5}$ aerosol in nine Interagency Monitoring for Protected Visual Environments (IMPROVE) network sites, *J. Geophys. Res., 112,* D10205, doi:10.1029/2006JD007708.

Bond, T. C., and R. W. Bergstrom (2006), Light absorption by carbonaceous particles: An investigative review, *Aerosol. Sci. Technol.,* 40(1), 27-67.

Chow, J. C., J. G. Watson, L. C. Pritchett, W. R. Pierson, C. A. Frazier, and R. G. Purcell (1993), The DRI thermal/optical reflectance carbon analysis system: Description, evaluation and applications in U.S. air quality studies, *Atmos. Env., 27A(8)*, 1185-1201.

Countess, R. J., G. T. Wolff, and S. H. Cadle (1980), The Denver winter aerosol: A comprehensive chemical characterization, *J. Air Pollution Control Assoc., 30,* 1194-1200.

Chu, S.-H. (2004), $PM_{2.5}$ episodes as observed in the speciation trends network, *Atmos. Environ., 38,* 5237-5246.

Day, D. E., W. C. Malm, and S. M. Kreidenweis (1997), Seasonal variations in aerosol composition and acidity at Shenandoah and Great Smoky Mountains national parks, *J. Air Waste Manage., 47,* 411-418.

Debell, L. J., K. Gebhart, J. L. Hand, W. C. Malm, M. L. Pitchford, B. A. Schichtel, and W. H. White (2006), IMPROVE (Interagency Monitoring of Protected Visual Environments): Spatial and seasonal patterns and temporal variability of haze and its constituents in the United States: Report IV, CIRA Report ISSN: 0737-5352-74, Colo. State Univ., Fort Collins.

Eldred, B. (2002), Carbon artifact on Version 2 IMPROVE Samplers, Doc. # 004, (http://vista.cira.colostate.edu/improve/Publications/GrayLit/004_Quartz_Blanks/004_quartz_blanks.htm).

El-Zanan, H. S., D. H. Lowenthal, B. Zielinska, J. C. Chow, and N. Kumar (2005), Determination of the organic aerosol mass to organic carbon ratio in IMPROVE samples, *Chemosphere, 60(4),* 485-496.

Frank, N. H. (2006), Retained nitrate, hydrated sulfates, and carbonaceous mass in Federal Reference Method fine particulate matter for six eastern U.S. cities, *J. Air & Waste Manage. Assoc., 56,* 500-511.

GBUAPCD (2010), Reasonable further progress report for the Mono Basin PM-10 state implementation plan, http://www.gbuapcd.org/Air%20Quality%20Plans/MONO-SIP/MonoBasinReasonableFurtherProgressReport2010.pdf.

Gebhart, K. A., W. C. Malm, and D. E. Day (1994), Examination of the effects of sulfate acidity and relative humidity on light scattering at Shenandoah National Park, *Atmos. Environ., 28(5),* 841-849.

Gebhart K. A., B. A. Schichtel, M. G. Barna, and W. C. Malm (2006), Quantitative back-trajectory apportionment of sources of particulate sulfate at Big Bend National Park TX, *Atmos. Environ., 40,* 2823-2834.

Grosjean, D., and S. K. Friedlander (1975), Gas-particle distribution factors for organics and other pollutants in the Los Angeles atmosphere, *J. Air Pollution Control Assoc., 25,* 1038-1044.

Hand, J. L. (2001), A new technique for obtaining aerosol size distributions with applications to estimates of aerosol properties, Ph.D. Dissertation, Colorado State University.

Hand, J. L., and S. M. Kreidenweis (2002), A new method for retrieving particle refractive index and effective density from aerosol size distribution data, *Aerosol Sci. Technol., 36,* 1012-1026.

Hand, J. L., S. M. Kreidenweis, D. E. Sherman, J. L. Collett, Jr., S. V. Hering, D. E. Day, W. C. Malm (2002), Aerosol size distributions and visibility estimates during the Big Bend Regional Aerosol Visibility and Observational Study (BRAVO), *Atmos. Environ., 36*, 5043-5055.

Hand, J. L., W. C. Malm, A. Laskin, D. Day, T. Lee, C. Wang, C. Carrico, J. Carrillo, J. P. Cowin, J. Collett, Jr., and M. J. Iedema (2005), Optical, physical, and chemical properties of tar balls observed during the Yosemite Aerosol Characterization Study, *J. Geophys. Res., 110,* D21210, doi:10.1029/2004JD005728.

Hand, J. L., and W. C. Malm (2006), Review of the IMPROVE equation for estimating ambient light extinction coefficients, CIRA Report, ISSN: 0737-5352-71, Colo. State Univ., Fort Collins.

Hering, S., and G. Cass (1999), The magnitude of bias in the measurement of $PM_{2.5}$ arising from volatilization of particulate nitrate from Teflon filters, *J. Air Waste Manage., 49,* 725-733.

Hogrefe O., J. J. Schwab, F. Drewnick, G. G. Lala, S. Peters, K. J. Demerjian, K. Rhoads, H. D. Felton, O. V. Rattigan, L. Husain, and V. A. Dutkiewicz (2004), Semicontinuous $PM_{2.5}$ sulfate and nitrate measurements at an urban and rural location in New York: PMTACS-NY summer 2001 and 2002 campaigns, *J. Air Waste Manage., 54,* 1040-1060.

Husar, R. B., D. M. Tratt, B. A. Schichtel, S. R. Falke, F. Li, D. Jaffe, S. Gasso, T. Gill, N. S. Laulainen, F. Lu, M. C. Reheis, Y. Chun, D. Westphal, B. N. Holben, C. Gueymard, I. McKendry, N. Kuring, G. C. Feldman, C. McClain, R. J. Frouin, J. Merrill, D. DuBois, F. Vignola, T. Murayama, S. Nickovic, W. E. Wilson, K. Sassen, N. Sugimoto, and W. C. Malm (2001), Asian dust events of April, 1998, *J. Geophys. Res., 106*, D16, 18317-18330.

Jaffe, D., J. Snow, and O. Cooper (2003), The April 2001 Asian dust events: Transport and substantial impact on surface particulate matter concentrations across the United States, *Eos, Transactions*, November 18.

Japar, S. M., A. C. Szkarlat, R. A. Gorse, Jr., E. K. Heyerdahl, R. L. Johnson, J. A. Rau, and J. J. Huntzicker (1984), Comparison of solvent extraction and thermal optical carbon analysis methods: Application to diesel vehicle exhaust aerosol, *Environ. Sci. Techonol., 18,* 231-234.

Lee, T., X.-Y. Yu, B. Ayers, S. M. Kreidenweis, W. C. Malm, and J. L. Collett, Jr. (2008), Observations of fine and coarse particle nitrate at several rural locations in the United States, *Atmos. Environ.,42,* 2720-2732.

Lefer, B. L., and R. W. Talbot (2001), Summertime measurements of aerosol nitrate and ammonium at a northeastern U.S. site, *J. Geophys. Res., 106(D17),* 20365-20378.

Liu L.-J. S., R. Burton, W. E. Wilson, and P. Koutrakis (1996), Comparison of aerosol acidity in urban and semi-rural environments, *Atmos. Environ., 30*(8), 1237-1245.

Lowenthal, D. H., J. G. Watson, P. Saxena (2000), Contributions to light extinction during project MOHAVE, *Atmos. Environ., 34,* 2351-2359.

Malm, W. C., J. F. Sisler, D. Huffman, R. A. Eldred, and T. A. Cahill (1994), Spatial and seasonal trends in particle concentration and optical extinction in the United States, *J. Geophys. Res., 99(D1),* 1347-1370.

Malm, W. C., and J. L. Hand (2007), An examination of the physical and optical properties of aerosols collected in the IMPROVE program, *Atmos. Environ., 41,* 3407-3427.

Malm, W. C., M. L. Pitchford, C. McDade, and L. L. Ashbaugh (2007), Coarse particle speciation at selected locations in the rural continental United States, *Atmos. Environ., 41,* 2225-2239.

Malm, W. C., B. A. Schichtel, and M. L. Pitchford (2011), Uncertainties in $PM_{2.5}$ gravimetric and speciation measurements and what we can learn from them, *J. Air Waste Manage,* In press.

Prospero, J. M., P. Ginoux, O. Torres, S. E. Nicholson, and T. E. Gill (2002), Environmental characterization of global sources of atmospheric soil dust identified with the NIMBUS 7 Total Ozone Mapping Spectrometer (TOMS) absorbing aerosol product, *Reviews of Geophysics, 40,* 1-31.

Perry, K. D., T. A. Cahill, R. A. Eldred, and D. D. Dutcher (1997), Long-range transport of North African dust to the eastern United States, *J. Geophys. Res., 102(D10),* 11225-11238.

Quinn, P. K., D. J. Coffman, T. S. Bates, T. L. Miller, J. E. Johnson, K. Voss, E. J. Welton, and C. Neususs (2001), Dominant aerosol chemical components and their contribution to extinction during the Aerosols99 cruise across the Atlantic, *J. Geophys. Res., 106(D18),* 20783-20809.

Quinn, P.K., T. L. Miller, T. S. Bates, J. A. Ogren, E. Andrews, and G. E. Shaw (2002a), A 3-year record of simultaneously measured aerosol chemical and optical properties at Barrow, Alaska, *J. Geophys. Res., 107(D11),* 4130, 10:1029/2001JD001248.

Quinn, P. K., D. J. Coffman, T. S. Bates, T. L. Miller, J. E. Johnson, E. J. Welton, C. Neususs, M. Miller, and P. J. Sheridan (2002b), Aerosol optical properties during INDOEX 1999: Means, variability, and controlling factors, *J. Geophys. Res., 107(D19),* 8020, doi:10.1029/2000JD000037.

Quinn, P. K., D. J. Coffman, T. S. Bates, E. J. Welton, D. S. Covert, T. L. Miller, J. E. Johnson, S. Maria, L. Russell, R. Arimoto, C. M. Carrico, M. J. Rood, and J. Anderson (2004), Aerosol optical properties measured on board the *Ronald H. Brown* during ACE-Asia as a function of aerosol chemical composition and source region, *J. Geophys. Res., 109(D19)*, doi:10.1029/2003JD004010.

Rivera Rivera, N. I., T. E. Gill, K. A. Gebhart, J. L. Hand, M. P. Bleiweiss, and R. M. Fitzgerald (2009), Wind modeling of Chihuahuan Desert dust outbreaks, *Atmos. Environ., 43,* 347-354.

Schichtel B. A., K. A. Gebhart, M. G. Barna and W. C. Malm (2006), Association of airmass transport patterns and particulate sulfur concentrations at Big Bend National Park, Texas, *Atmos. Environ., 40,* 992-1006.

Schwab, J. J., H. D. Felton, and K. L. Demerjian (2004), Aerosol chemical composition in New York state from integrated filter samples: Urban/rural and seasonal contrasts, *J. Geophys. Res., 109(D16),* doi:10.1029/2003JD004078.

Seinfeld, J. H., and S. N. Pandis (1998), *Atmospheric Chemistry and Physics: From Air Pollution to Climate Change,* John Wiley, New York.

Tanner, R. L., W. J. Parkhurst, M. L. Valente, and W. D. Phillips (2004), Regional composition of $PM_{2.5}$ aerosols measured at urban, rural, and "background" sites in the Tennessee valley, *Atmos. Environ., 38,* 3143-3153.

Turpin, B. J., P. Saxena, and E. Andrews (2000), Measuring and simulating particulate organics in the atmosphere: Problems and prospects, *Atmos. Environ., 34,* 2983-3013.

Turpin, B. J., and H.-J. Lim (2001), Species contributions to $PM_{2.5}$ mass concentrations: Revisiting common assumptions for estimating organic mass, *Aerosol Sci. Technol., 35,* 602-610.

VanCuren, R. A., and T. A. Cahill (2002), Asian aerosols in North America: Frequency and concentration of fine dust, *J. Geophys. Res., 107(D24)*, 4804, doi:10.1029/2002JD002204.

VanCuren, R. A. (2003), Asian aerosols in North America: Extracting the chemical composition and mass concentration of the Asian continental aerosol plume from long-term aerosol records in the western United States, *J. Geophys. Res.,108(D20)*, 4623, doi:10.1029/2003JD003459.

Van Vaeck, L., and K. Van Cauwenberghe (1978), Cascade impactor measurements of the size distribution of the major classes of organic pollutants in atmospheric particulate matter, *Atmos. Environ., 12,* 2239.

Vitousek, P. M., J. D. Aber, R. W. Howarth, G. E. Likens, P. A. Matson, D. W. Schindler, W. H. Schlesinger, and D. G. Tilman (1997), Human alteration of the global nitrogen cycle: Sources and consequences, *Ecolog. Applic. 7*(3), 737-750.

White, W. H., and P. T. Roberts (1977), On the nature and origins of visibility-reducing aerosols in the Los Angeles Air Basin, *Atmos. Environ., 11,* 803-812.

White, W. H. (2008), Chemical markers for sea salt in the IMPROVE aerosol data, *Atmos. Environ., 42,* 261-274.

Zhang, Q., M. R. Canagaratna, J. T. Jayne, D. R. Worsnop, and J.-L. Jimenez (2005), Time- and size-resolved chemical composition of submicron particles in Pittsburgh: Implications for aerosol sources and processes, *J. Geophys. Res., 110(D07),* doi:10.1029/2004JD004649.

Chapter 3. Reconstructed Aerosol Light Extinction Coefficients

Light extinction in the atmosphere occurs when incident light is attenuated by the scattering and absorption of particles and gases in the layer through which it travels. The light extinction coefficient (b_{ext}) is the fractional loss of intensity per unit path length. The Beer-Lambert law describes the intensity (F) of an incident flux (F_o) through a layer of thickness (z) as

$$\frac{F}{F_o} = \exp(-b_{ext} z) \quad 3.1$$

The extinction coefficient can be written as the sum of scattering and absorption by particles (b_{sp} and b_{ap}, respectively) and gases (b_{sg} and b_{ag}, respectively) and has units of inverse length:

$$b_{ext} = b_{sp} + b_{ap} + b_{sg} + b_{ag} \quad 3.2$$

Absorption of light by gases is a well-understood phenomenon and straightforward to estimate. Visible light absorption is dominated by nitrogen dioxide (NO_2) and can be estimated by multiplying NO_2 concentrations by an absorption efficiency (Pitchford et al., 2007). Rayleigh scattering theory describes scattering of light by molecules (b_{sg}) and depends on the density of the atmosphere. The highest values occur at sea level (~12 Mm^{-1}), compared to the lowest levels at high elevations (8 Mm^{-1} at ~3.5 km). Rayleigh scattering can vary due to temperature and pressure variations; it can be accurately determined if elevation and meteorological conditions are known.

Light extinction by particles is more complicated and depends strongly on particle size, composition, and hygroscopic properties. All particles scatter light and, if their size and refractive index are known, light scattering coefficients can be computed using Mie theory, assuming spherical particles. Light absorption by particles in the visible wavelengths is due to light absorbing carbon as well as some crustal mineral species. Because the required information necessary for performing Mie calculations is typically unknown (size distribution and concurrent aerosol composition measurements are time intensive and costly), the IMPROVE algorithm was developed to estimate aerosol light extinction coefficients. The algorithm assumes only speciated aerosol composition data are available (Malm et al., 1994).

3.1 IMPROVE AEROSOL LIGHT EXTINCTION COEFFICIENT ALGORITHM

Light extinction coefficients can be computed for an external mixture of aerosols by assuming a linear combination of species mass concentrations:

$$b_{ext} = \sum_j \alpha_j M_j \quad 3.3$$

The species (j) mass concentration is given by M_j ($\mu g\ m^{-3}$) and the extinction efficiency corresponding to that species is given by α_j ($m^2\ g^{-1}$). Equation 3.3 also holds for an internally mixed aerosol where the chemical species are mixed in fixed proportions to each other, the index of refraction is not a function of composition or size, and the aerosol density is independent of volume.

For hygroscopic species (species that absorb water), the linear relationship between light extinction coefficients and mass shown in equation 3.3 will not hold because of the nonlinear behavior of particle growth and b_{ext} with increased relative humidity (RH). To account for this effect, the extinction efficiencies are multiplied by a humidification factor ($f(RH) = b_{sp,RH}/b_{sp,dry}$) that is a ratio of humidified (b_{sp_RH}) to dry (b_{sp_dry}) light scattering coefficients that accounts for the effects of changing RH on extinction coefficients. Humidification factors are computed by assuming a size distribution and composition-dependent growth factor (e.g., Hand et al., 2010).

The original IMPROVE equation has been used extensively to reconstruct b_{ext}, using measured aerosol composition (e.g., Malm et al., 1994; Lowenthal and Kumar, 2003; Malm et al., 2005; Malm and Hand, 2007; Brewer and Moore, 2009), and was adopted by the Environmental Protection Agency (EPA) as a metric for tracking progress in reducing haze levels under the 1999 Regional Haze Rule (RHR) (Pitchford et al., 2007). In 2005 a review was initiated by the IMPROVE steering committee to investigate possible biases in light extinction coefficients as computed by the algorithm (Hand and Malm, 2006; Malm and Hand, 2007). The review resulted in the revised IMPROVE algorithm that is now being used by most states in their state implementation plans (Pitchford et al., 2007). Discussions of the RHR and results using the revised IMPROVE equation are presented in Chapter 9.

The algorithm applied in this report is a combination of the original and revised algorithms and will be referred to here as the "modified original" algorithm. The original algorithm included contributions from ammonium sulfate, ammonium nitrate, particulate organic matter, light absorbing carbon, soil, and coarse mass and a constant Rayleigh scattering term. The modified original algorithm differs from the original in that it included several changes deemed important during the 2005 review. Specifically, sea salt was included and a factor of 1.8 was applied to compute particulate organic matter from organic carbon concentrations. Site-specific Rayleigh scattering was also included, rather than the constant value of 10 Mm^{-1} assumed in the original equation. The modified original algorithm differs from the revised algorithm in that it applies constant mass extinction efficiencies for each species. Mean b_{ext} computed by the modified original algorithm should not differ significantly from b_{ext} computed with the revised algorithm. The modified original algorithm is presented in equation 3.4:

$$b_{ext} = 3f(RH)[\text{ammonium sulfate}] + 3f(RH)[\text{ammonium nitrate}] + 4[\text{particulate organic matter}] + 10[\text{light absorbing carbon}] + 1[\text{soil}] + 1.7f(RH)_{ss}[\text{sea salt}] + 0.6[\text{coarse mass}] + \text{site-specific Rayleigh scattering} \quad (3.4)$$

The units of b_{ext} and Rayleigh scattering are in inverse megameters (Mm^{-1}). Mass concentrations of aerosol species are in $\mu g\ m^{-3}$, and mass scattering and absorption efficiencies have units of $m^2\ g^{-1}$. Dry mass scattering and absorption efficiencies were rounded to one significant digit to represent the degree of uncertainty associated with these values. Values of 3 $m^2\ g^{-1}$ were used for both ammonium sulfate and ammonium nitrate, 4 $m^2\ g^{-1}$ for particulate organic matter, 10 $m^2\ g^{-1}$ for light absorbing carbon, 1 $m^2\ g^{-1}$ for soil, 1.7 $m^2\ g^{-1}$ for sea salt, and 0.6 $m^2\ g^{-1}$ for coarse mass. These values correspond to a wavelength of 550 nm (Hand and Malm, 2007). Comparisons of b_{ext} for IMPROVE and the CSN are limited to $PM_{2.5}$ aerosol b_{ext} because coarse mass is not measured as part of the CSN.

Daily b_{ext} values were computed using equation 3.4; monthly mean values were computed from daily b_{ext}. Daily b_{ext} values that were less than zero were treated as missing data. This treatment was different than the mass concentration analyses that allowed for negative mass values for some species (e.g., blank-corrected ion concentrations could be negative). Therefore, some differences between patterns in mass and b_{ext} values may be due to this difference, most notably for nonhygroscopic species where b_{ext} values are just scaled mass concentrations.

The f(RH) values applied in equation 3.4 were computed using the algorithm outlined in the Regional Haze Rule Guidelines for Tracking Progress (U.S. EPA, 2003) and were the same values applied in previous IMPROVE reports. A lognormal ammonium sulfate mass size distribution with a geometric mass mean diameter of 0.3 μm and a geometric standard deviation of 2.0 was used with Mie theory to compute f(RH). An interpolation between the deliquescence and efflorescence curves was performed to obtain a smoothed f(RH) curve. This same curve was applied to ammonium nitrate. The $f(RH)_{ss}$ applied to sea salt was computed assuming a sea salt geometric mass mean diameter of 2.5 μm and a geometric standard deviation of 2 (Pitchford et al., 2007). We assumed that POM was nonhygroscopic. Figure 3.1 presents the f(RH) curve applied to ammonium sulfate and ammonium nitrate in equation 3.4. Humidification factors are unitless.

Monthly and site-specific f(RH) curves were generated based on monthly climatological mean RH values. These monthly RH values eliminate the effects of interannual variations in RH while maintaining typical regional and seasonal humidity patterns around the United States. The EPA produced recommended monthly f(RH) values for each Class I area, based on analysis of a 10-year record (1988–1997) of hourly RH data from 292 National Weather Service stations across the 50 states and the District of Columbia, as well as from 29 IMPROVE and IMPROVE protocol monitoring sites, 48 Clean Air Status and Trends Network (CASTNet) sites, and 13 additional sites administered by the National Park Service. Values of f(RH) for other IMPROVE sites (non-Class I area sites) were generated using an interpolation scheme with an inverse distance weighting technique (U.S. EPA, 2001). The daily humidified ammonium sulfate and ammonium nitrate and sea salt extinction coefficients for each site were calculated using this lookup table. Values of f(RH) varied significantly depending on time of year and site location. For example, the f(RH) value in Douglas, Arizona (DOUG1), in August was 1.84, compared to 3.88 in Linville Gorge, North Carolina (LIGO1). In April, the f(RH) at DOUG1 was 1.16, compared to 2.65 at LIGO1. For a constant ammonium sulfate mass, its light scattering coefficient can double based only on hygroscopic effects. Estimates of f(RH) for CSN sites were determined similarly to IMPROVE sites by using a lookup table with site locations.

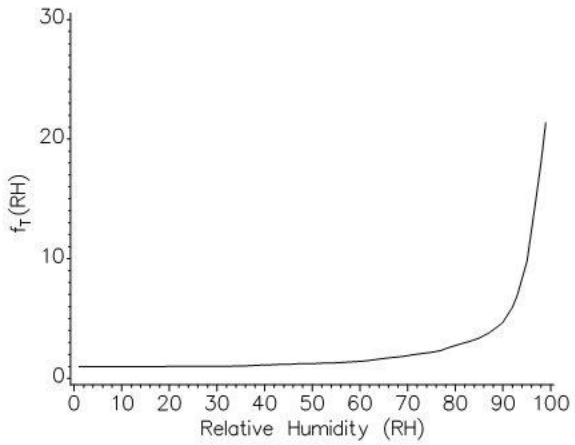

Figure 3.1. Humidification factor (f(RH)) as a function of relative humidity (RH) A lognormal ammonium sulfate mass size distribution with a geometric mass mean diameter of 0.3 µm and a geometric standard deviation of 2.0 was assumed. A wavelength of 550 nm was used.

Visual range and extinction measurements are nonlinear with respect to human perception of visual scene changes caused by haze. The deciview haze index (dv) was derived with a number of assumptions such that uniform changes in haze correspond to approximately uniform incremental changes in visual perception (Pitchford and Malm, 1994). Deciview was calculated from reconstructed b_{ext}, using equation 3.5:

$$dv = 10\ln(b_{ext}/10) \qquad 3.5$$

Deciview corresponds to the total b_{ext}, including the contribution of coarse mass. Because of the absence of coarse mass from the CSN network, dv was computed using only IMPROVE data. In the original IMPROVE equation, dv = 0 for pristine (near-Rayleigh scattering) conditions (elevations ~1.8 km). Now that site-specific Rayleigh scattering is included in equation 3.5 in the place of 10 Mm^{-1}, it is actually possible to have a negative dv for pristine conditions at sites with very low Rayleigh scattering (~3.5 km).

In the following sections we present spatial patterns of 2005–2008 annual mean reconstructed b_{ext} corresponding to ammonium sulfate, ammonium nitrate, particulate organic matter, light absorbing carbon, soil, sea salt, aerosol, coarse mass (IMPROVE only), and deciview (IMPROVE only) for IMPROVE and CSN sites. For many species (those that were considered nonhygroscopic) the b_{ext} maps were similar to the mass concentration maps, but scaled by extinction efficiencies. Percent contributions of each species to $PM_{2.5}$ aerosol b_{ext} are also presented. As with the mass concentration maps, caution should be taken to avoid over-interpreting these maps as they are interpolations of irregularly gridded data and are provided only to reflect general spatial patterns. The top number in the scale of each contour map corresponds to the maximum b_{ext} for all sites, although the contours themselves were created with the highest level set to the 95^{th} percentile in b_{ext}.

3.2 $PM_{2.5}$ AMMONIUM SULFATE LIGHT EXTINCTION COEFFICIENTS

The 2005–2008 annual mean light extinction coefficients corresponding to ammonium sulfate (b_{ext_AS}) ranged from 2.88 Mm^{-1} in Sawtooth National Forest (NF), Idaho (SAWT1), to 65.24 Mm^{-1} in Mammoth Cave, Kentucky (MACA1), for rural IMPROVE sites (Figure 3.2a). The maximum b_{ext_AS} for urban IMPROVE sites was comparable (59.83 Mm^{-1} in Birmingham, Alabama, BIRM1). The minimum IMPROVE urban b_{ext_AS} (5.96 Mm^{-1}, Phoenix, Arizona, PHOE5) was somewhat higher than the rural minimum. Light extinction coefficients from ammonium sulfate were much higher in the eastern United States compared to the western United States. The same east-west division observed for the annual mean ammonium sulfate mass concentrations was observed for b_{ext}, but b_{ext} was more "focused" spatially due to relative humidity effects in the eastern United States. Sites along the Ohio River valley and Appalachian Mountains corresponded to the highest b_{ext_AS}. The magnitude of b_{ext_AS} was comparable to the contribution from Rayleigh scattering (10–12 Mm^{-1}) for 54–60% of all IMPROVE sites, and the majority of these were located in the western United States. The addition of CSN sites did not alter the spatial pattern of b_{ext_AS} significantly, except in Texas and Louisiana, where the addition of sites provided additional spatial detail (Figure 3.2b). The maximum b_{ext_AS} for the CSN network occurred in Liberty, Pennsylvania (74.64 Mm^{-1}, #420030064), compared to the lowest b_{ext_AS} in Reno, Nevada (4.66 Mm^{-1} #320310016). The similarity in the spatial patterns and magnitudes of b_{ext_AS} for the rural and urban sites suggested regional sources of ammonium sulfate and meteorological conditions that contribute to high b_{ext_AS} on regional scales.

In the eastern United States, the IMPROVE aerosol b_{ext} was dominated by ammonium sulfate, with percent contributions to b_{ext} greater than 50% (Figure 3.2c). Overall, ammonium sulfate was a significant contributor to aerosol b_{ext}, with 96% of all IMPROVE sites corresponding to a contribution to aerosol b_{ext} of greater than 20%. The site with the highest contribution of ammonium sulfate to b_{ext} was Hawaii Volcanoes (HAVO1, 86.6%), compared to the minimum at Sawtooth NF, Idaho (15.7%, SAWT1). The IMPROVE urban contribution to b_{ext} from ammonium sulfate ranged from 11.9% (Fresno, California, FRES1) to 58.5% (Baltimore, Maryland, BALT1). The percent contribution of ammonium sulfate to b_{ext} at the CSN sites ranged from 9.5% (Reno, #320310016) to 75.1% (Charleston, West Virginia, #540390011), with very similar spatial patterns as the rural network (Figure 3.2d). However, in general urban aerosol b_{ext} was not as dominated by ammonium sulfate as compared to the rural network. Only 88% of CSN sites corresponded to contributions of ammonium sulfate to b_{ext} of greater than 20%, even though most of the CSN sites are in the eastern United States, where b_{ext_AS} values were the highest.

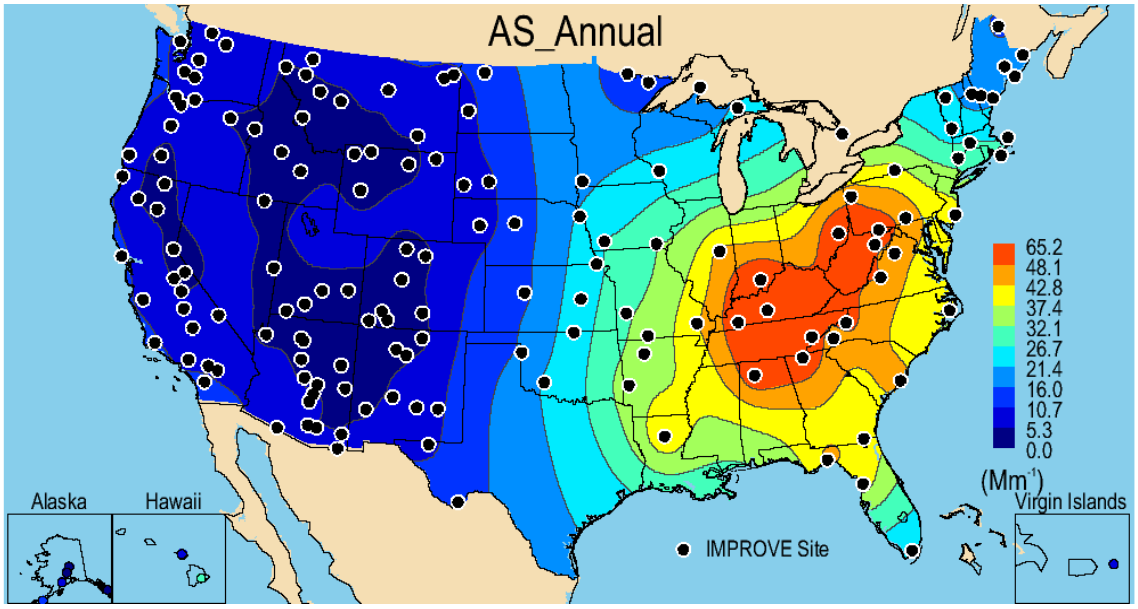

Figure 3.2a. $PM_{2.5}$ reconstructed ambient annual mean light extinction coefficient for ammonium sulfate (b_{ext_AS}, Mm^{-1}) for 2005–2008 for rural IMPROVE sites. The "modified original" IMPROVE algorithm was used (see text). Wavelength corresponds to 550 nm.

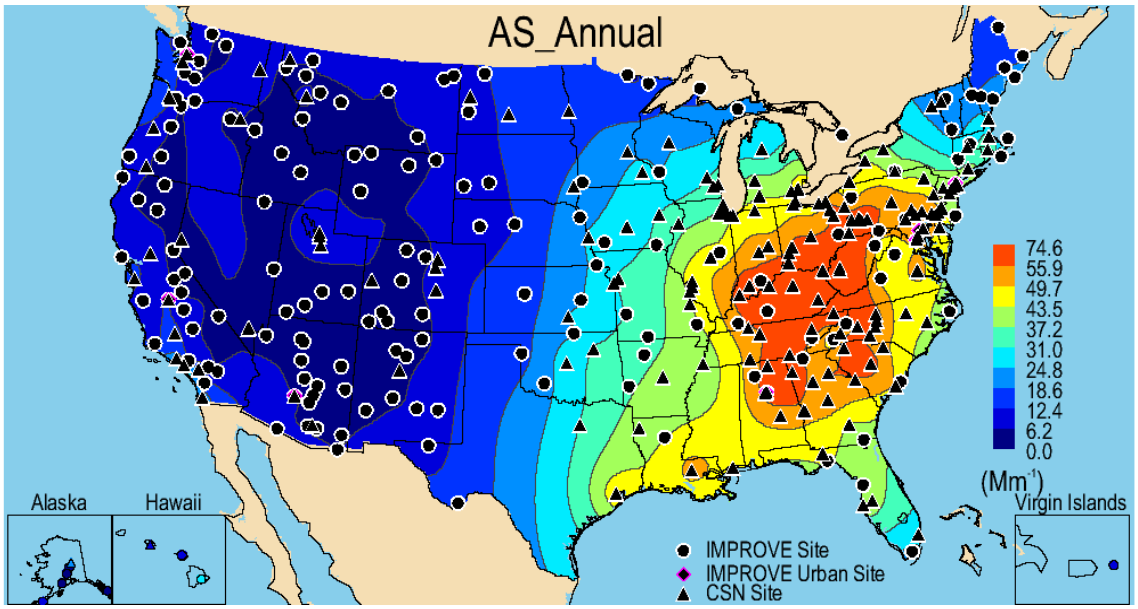

Figure 3.2b. $PM_{2.5}$ reconstructed ambient annual mean light extinction coefficient for ammonium sulfate (b_{ext_AS}, Mm^{-1}) for 2005–2008 for rural IMPROVE and urban CSN sites. The "modified original" IMPROVE algorithm was used (see text). Wavelength corresponds to 550 nm.

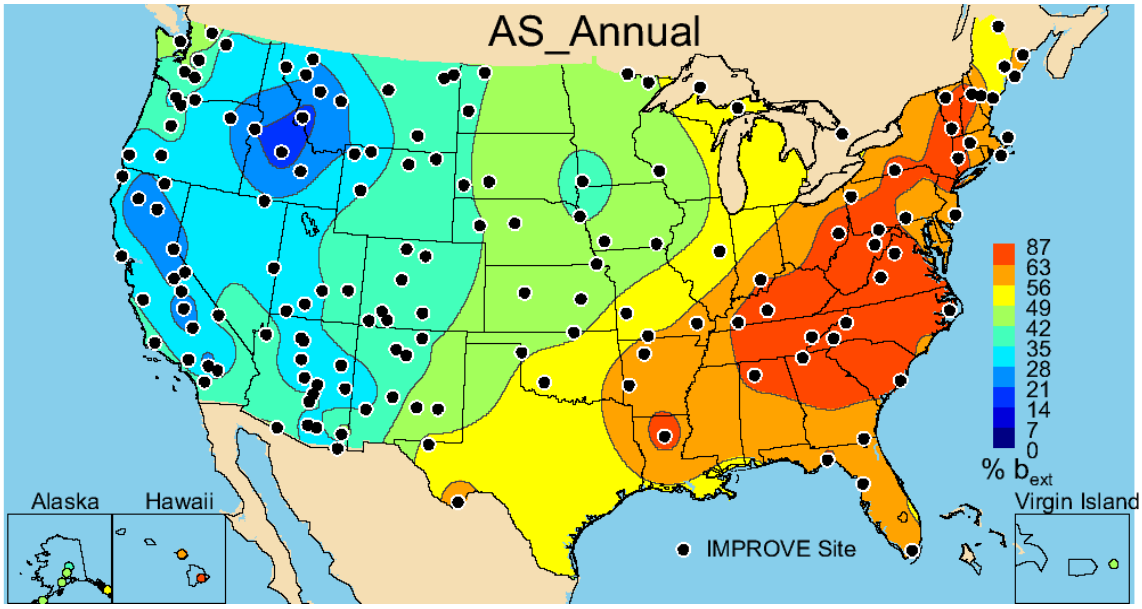

Figure 3.2c. Annual mean percent contribution (%) of ambient ammonium sulfate (AS) light extinction coefficient (b_{ext}) to $PM_{2.5}$ reconstructed aerosol b_{ext} for 2005–2008 for rural IMPROVE sites. The "modified original" IMPROVE algorithm was used (see text). Wavelength corresponds to 550 nm.

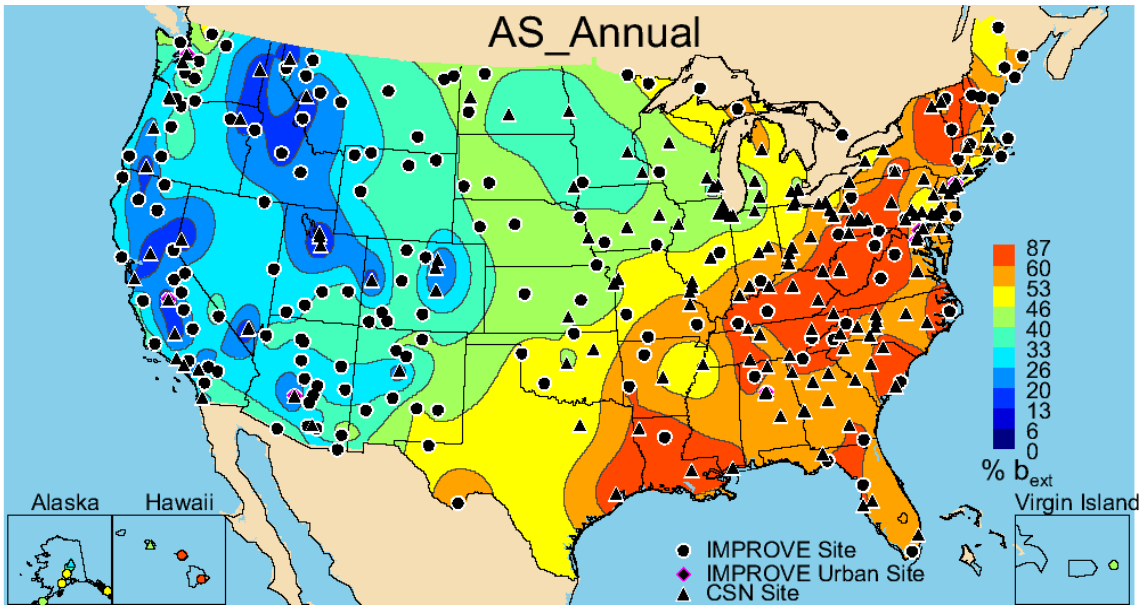

Figure 3.2d. Annual mean percent contribution (%) of ambient ammonium sulfate (AS) light extinction coefficient (b_{ext}) to $PM_{2.5}$ reconstructed aerosol b_{ext} for 2005–2008 for rural IMPROVE and urban CSN sites. The "modified original" IMPROVE algorithm was used (see text). Wavelength corresponds to 550 nm.

3.3 $PM_{2.5}$ AMMONIUM NITRATE LIGHT EXTINCTION COEFFICIENTS

The spatial pattern of the 2005–2008 rural IMPROVE annual mean ammonium nitrate light extinction coefficient (b_{ext_AN}) was nearly identical to the annual mean mass concentration pattern (Figure 3.3a). Regions of elevated b_{ext_AN} were located in the central United States and on the West Coast. Rural IMPROVE estimates ranged from 0.47 Mm^{-1} in Petersburg, Alaska (PETE1), to 27.87 Mm^{-1} in Bondville, Illinois (BOND1), located in the agricultural Midwest. In

general, however, most of the rural sites corresponded to low (< 10 Mm^{-1}) b_{ext_AN}. Not surprisingly, urban IMPROVE sites corresponded to higher b_{ext_AN} (5.68 Mm^{-1}) in Phoenix (PHOE5), to 53.27 Mm^{-1} in Fresno (FRES1). Several urban CSN sites also corresponded to high b_{ext_AN}, including sites in the western United States such as Rubidoux, California (with the highest b_{ext_AN} of 60.49 Mm^{-1}, #060658001), San Francisco, Sacramento, Salt Lake City, and Denver (Figure 3.3b). The central and Midwest sites with high urban b_{ext_AN} stretched eastward, with the inclusion of several sites in Indiana, Michigan, and Ohio. In general the urban sites had higher b_{ext_AN}; only 24% of CSN sites corresponded to b_{ext_AN} less than 10 Mm^{-1}, and 50% of CSN sites had annual b_{ext_AN} greater than 15 Mm^{-1}. The lowest annual mean CSN b_{ext_AN} occurred in Honolulu (1.82 Mm^{-1}, #150032004).

The spatial pattern of the percent contribution of ammonium nitrate to b_{ext} somewhat mirrored the b_{ext_AN} pattern (see Figure 3.3c), except in the Northwest and in California. Although sites in these regions did not correspond to the highest ammonium nitrate mass concentrations, they do correspond to significant contributions of AN to b_{ext}. Also, in the Midwest ammonium nitrate was a significant contributor to b_{ext} at many sites; at 21% of IMPROVE sites, ammonium nitrate contributed over 20% to b_{ext}. In the northern Great Plains, the annual mean percent contribution to b_{ext} was 27.8% at Lostwood, North Dakota (LOST1), 25.7% at Medicine Lake, Montana (MELA1), and 24.9% at Fort Peck, Montana (FOPE1). The highest contribution to the annual mean b_{ext} occurred at Blue Mounds, Minnesota (40.5%), compared to the lowest percent contribution at Hawaii Volcanoes (2.4%, HAVO1). The largest percent contribution to b_{ext} at an urban IMPROVE site occurred at Fresno (FRES1) where 49.3% of the b_{ext} was due to ammonium nitrate. The lowest urban IMPROVE percent contribution occurred at Birmingham, Alabama (8.5%, BIRM1). AN contributed significantly to b_{ext} at CSN sites. At slightly more than half (52%) of all CSN sites, ammonium nitrate contributed over 20% to annual b_{ext} (Figure 3.3d). The impact of urban AN percent contribution to b_{ext} was obvious from the inclusion of those sites in the interpolation. Sites in Utah, Colorado, and California all corresponded to high percent contributions to b_{ext}, as well as additional sites in the central United States (Indiana, Michigan, and Ohio). The highest percent contribution to b_{ext} occurred in Bakersfield, California (53.9%, #060290014), compared to the lowest in Douglas, Georgia (6.3%, #130690002).

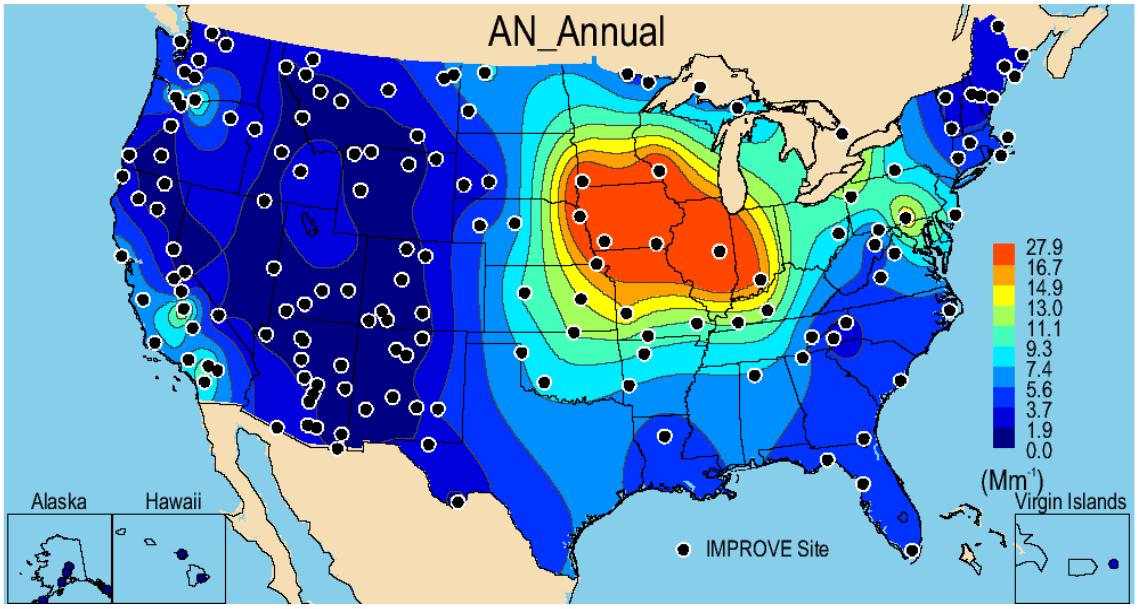

Figure 3.3a. $PM_{2.5}$ reconstructed ambient annual mean light extinction coefficient for ammonium nitrate (b_{ext_AN}, Mm^{-1}) for 2005–2008 for rural IMPROVE sites. The "modified original" IMPROVE algorithm was used (see text). Wavelength corresponds to 550 nm.

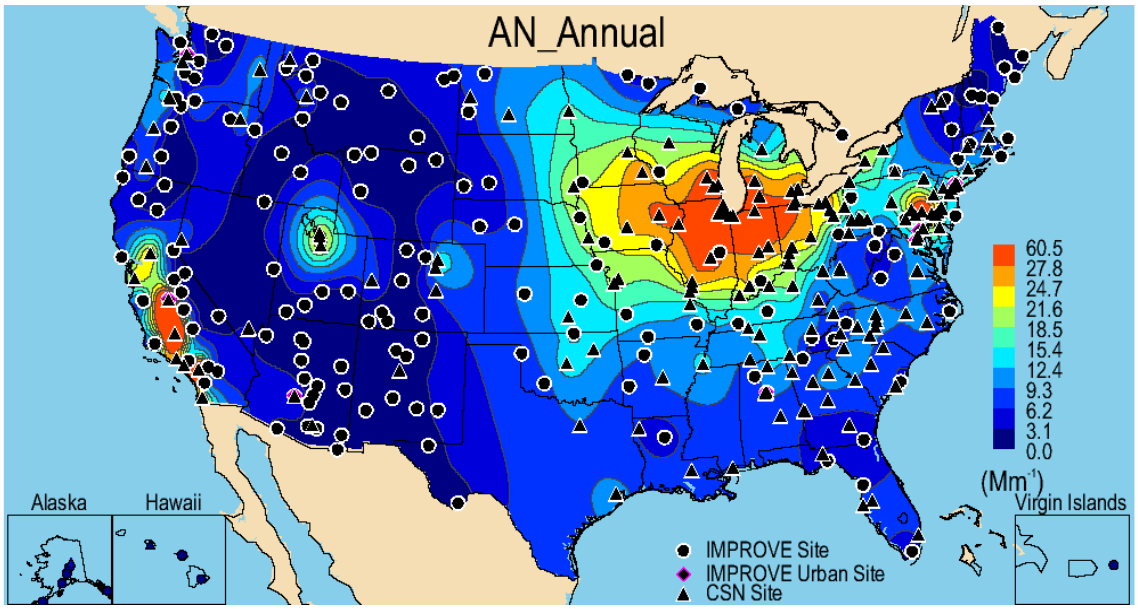

Figure 3.3b. $PM_{2.5}$ reconstructed ambient annual mean light extinction coefficient for ammonium nitrate (b_{ext_AN}, Mm^{-1}) for 2005–2008 for rural IMPROVE and urban CSN sites. The "modified original" IMPROVE algorithm was used (see text). Wavelength corresponds to 550 nm.

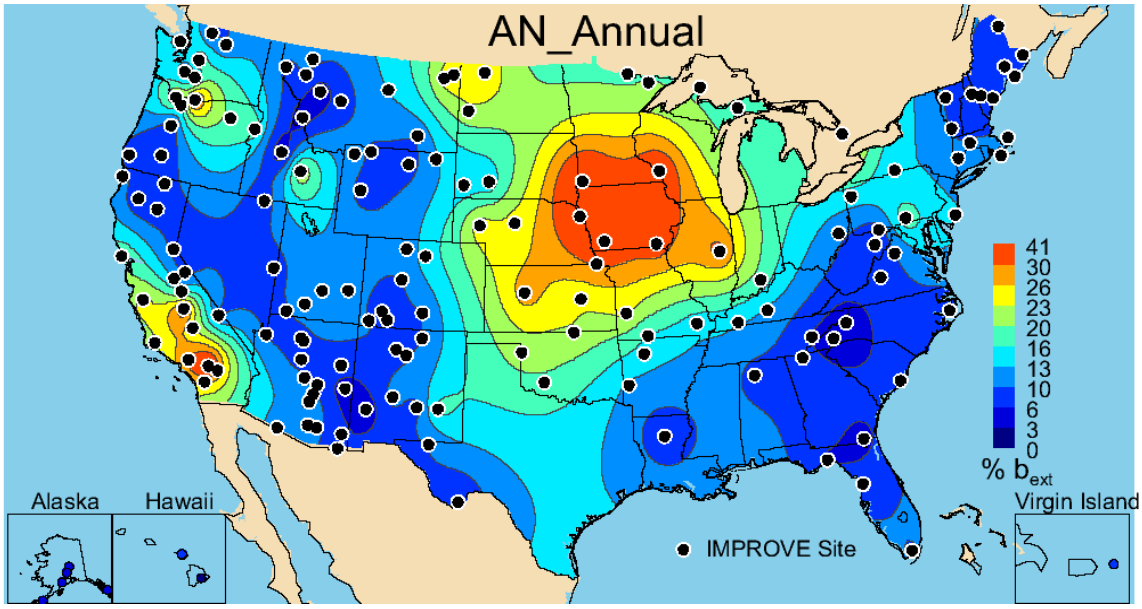

Figure 3.3c. Annual mean percent contribution (%) of ambient ammonium nitrate (AN) light extinction coefficient (b_{ext}) to $PM_{2.5}$ reconstructed aerosol b_{ext} for 2005–2008 for rural IMPROVE sites. The "modified original" IMPROVE algorithm was used (see text). Wavelength corresponds to 550 nm.

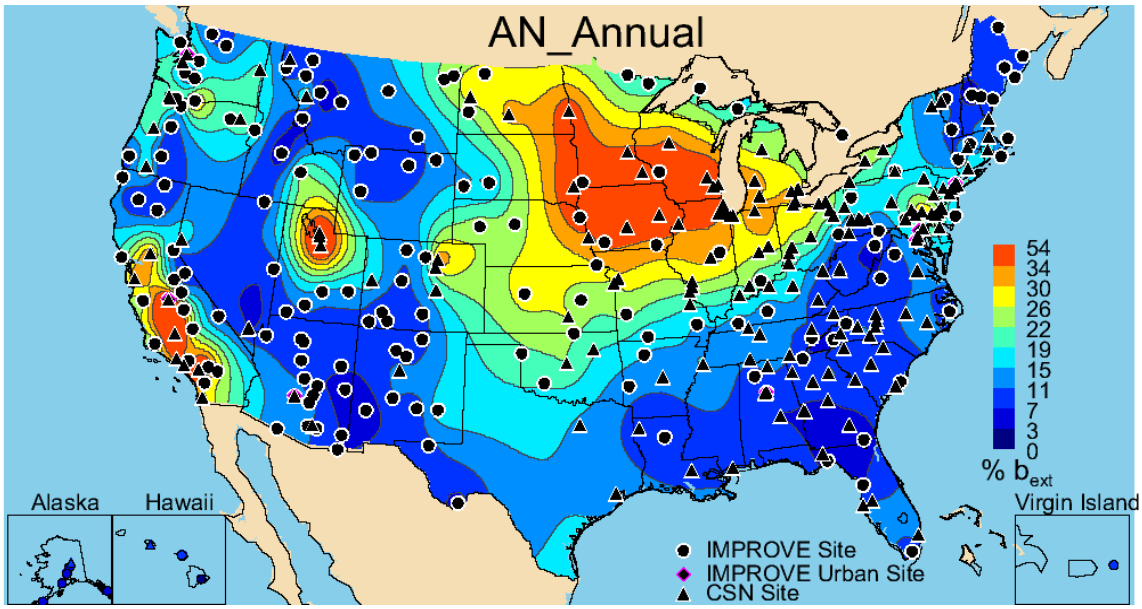

Figure 3.3d. Annual mean percent contribution (%) of ambient ammonium nitrate (AN) light extinction coefficient (b_{ext}) to $PM_{2.5}$ reconstructed aerosol b_{ext} for 2005–2008 for rural IMPROVE and urban CSN sites. The "modified original" IMPROVE algorithm was used (see text). Wavelength corresponds to 550 nm.

3.4 $PM_{2.5}$ PARTICULATE ORGANIC MATTER LIGHT EXTINCTION COEFFICIENTS

The 2005–2008 IMPROVE annual mean light extinction coefficient due to particulate organic matter (b_{ext_POM}) ranged from 1.08 Mm^{-1} (Virgin Islands, VIIS1) to 18.25 Mm^{-1} in Trinity, California (TRIN1), for rural IMPROVE sites, and 14.34 Mm^{-1} (Puget Sound, Washington, PUSO1) to 27.93 Mm^{-1} (Birmingham, BIRM1) for urban IMPROVE sites. POM

was considered nonhygroscopic in the algorithm for computing b_{ext}, so the spatial pattern of b_{ext_POM} reflected that of the POM annual mean mass concentration pattern (Figure 3.4a). High levels of b_{ext_POM} were observed in the southern and southeastern United States and in urban regions in the Southwest (Phoenix) and California (Fresno). Other regions with high levels of b_{ext_POM} were observed in northern California and in Idaho and Montana, most likely due to emissions from wildfires. For most sites, however, b_{ext_POM} was fairly low, which included most sites in the Midwest and western states. The b_{ext_POM} was higher for urban CSN sites, similar to urban POM mass concentrations (Figure 3.4b). Values ranged from 6.69 Mm^{-1} (Fargo, North Dakota, #380171004) to 46.86 Mm^{-1} in Libby, Montana (#300530018). In contrast to the rural sites, most of the urban sites had b_{ext_POM} greater than 10 Mm^{-1}. With the inclusion of urban site data in the interpolation, higher gradients surrounding cities were observed, suggesting local urban sources of organic aerosols. Regional sources (perhaps biogenic or wildfire emissions) seemed more spatially extensive in the Southeast compared to more localized sources for many urban centers in the West. In general, urban b_{ext_POM} was higher than rural b_{ext_POM}.

The rural IMPROVE percent contribution of POM to aerosol b_{ext} is presented in Figure 3.4c. The east-west divide seen in many spatial maps was also observed here but in reverse. Percent contributions of b_{ext_POM} were higher in the West, typically greater than 30%. Regions in northern California, Oregon, Idaho, Montana, and Wyoming were the highest, most likely due to the role of wildfire emissions and relatively low emissions from other major contributors to b_{ext}. Forty-one percent of all IMPROVE sites corresponded to contributions over 30% to b_{ext}, probably due to the density of IMPROVE sites in the West. The maximum percent contribution occurred at Sawtooth, Idaho (70.2%, SAWT1), compared to the lowest at Hawaii Volcano (3.3%, HAVO1). At IMPROVE urban sites the percent contribution ranged from 15.8% (Baltimore, BALT1) to 42.3% (Phoenix, PHOE1). A similar pattern was observed with the addition of the CSN sites, with higher percent contributions in the West (Figure 3.4d). Interestingly, sites in Utah corresponded to lower percent contributions compared to surrounding areas, likely because of the contribution from ammonium nitrate to b_{ext} (see Figure 3.3d) at these sites. The percent contribution ranged from 10.14% (Indianapolis, #180650003) to 66.10% in Libby, Montana (#300530018). Only 10% of CSN sites corresponded to a percent contribution greater than 30%, reflecting the high density of sites in the East where ammonium sulfate is the main contributor to b_{ext}.

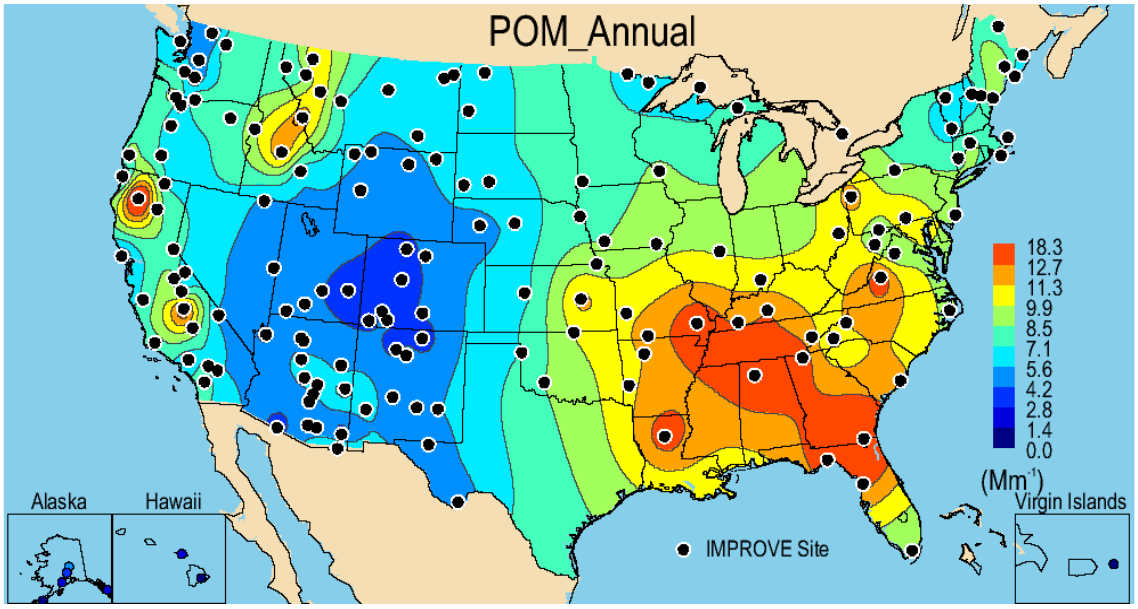

Figure 3.4a. $PM_{2.5}$ reconstructed ambient annual mean light extinction coefficient for particulate organic matter (POM) (b_{ext_POM}, Mm^{-1}) for 2005–2008 for rural IMPROVE sites. The "modified original" IMPROVE algorithm was used (see text). Wavelength corresponds to 550 nm.

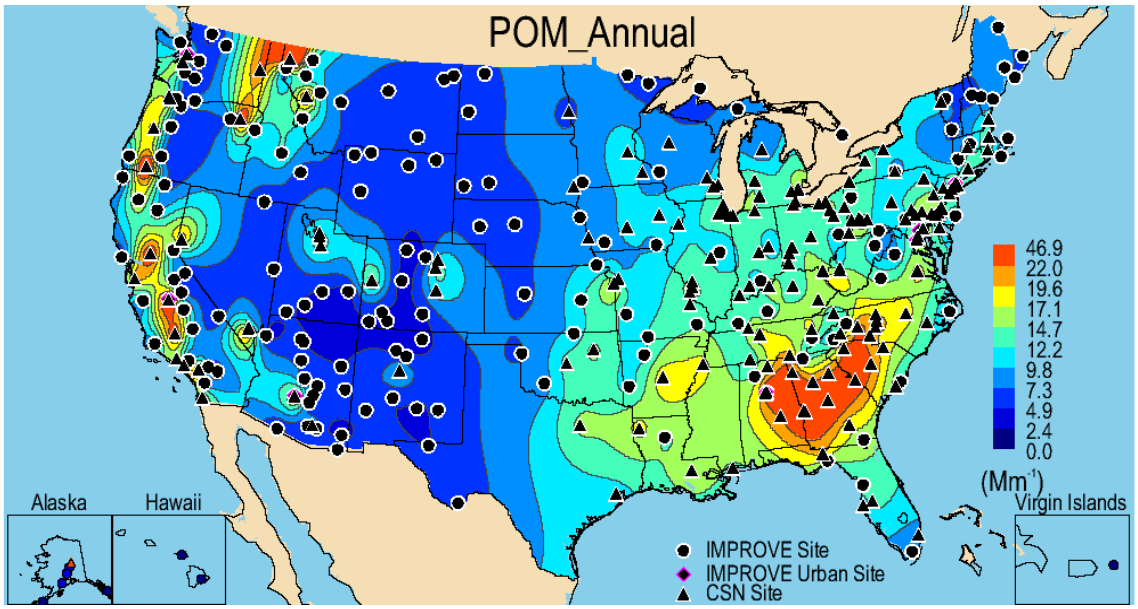

Figure 3.4b. $PM_{2.5}$ reconstructed ambient annual mean light extinction coefficient for particulate organic matter (POM) (b_{ext_POM}, Mm^{-1}) for 2005–2008 for rural IMPROVE and urban CSN sites. The "modified original" IMPROVE algorithm was used (see text). Wavelength corresponds to 550 nm.

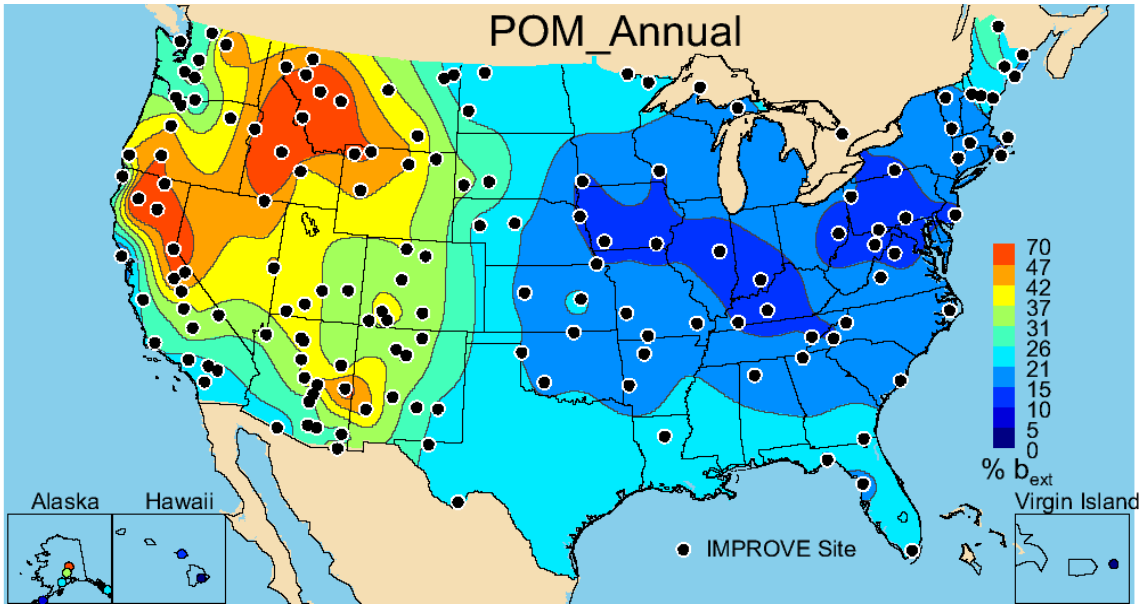

Figure 3.4c. Annual mean percent contribution (%) of ambient particulate organic matter (POM) light extinction coefficient (b_{ext}) to $PM_{2.5}$ reconstructed aerosol b_{ext} for 2005–2008 for rural IMPROVE sites. The "modified original" IMPROVE algorithm was used (see text). Wavelength corresponds to 550 nm.

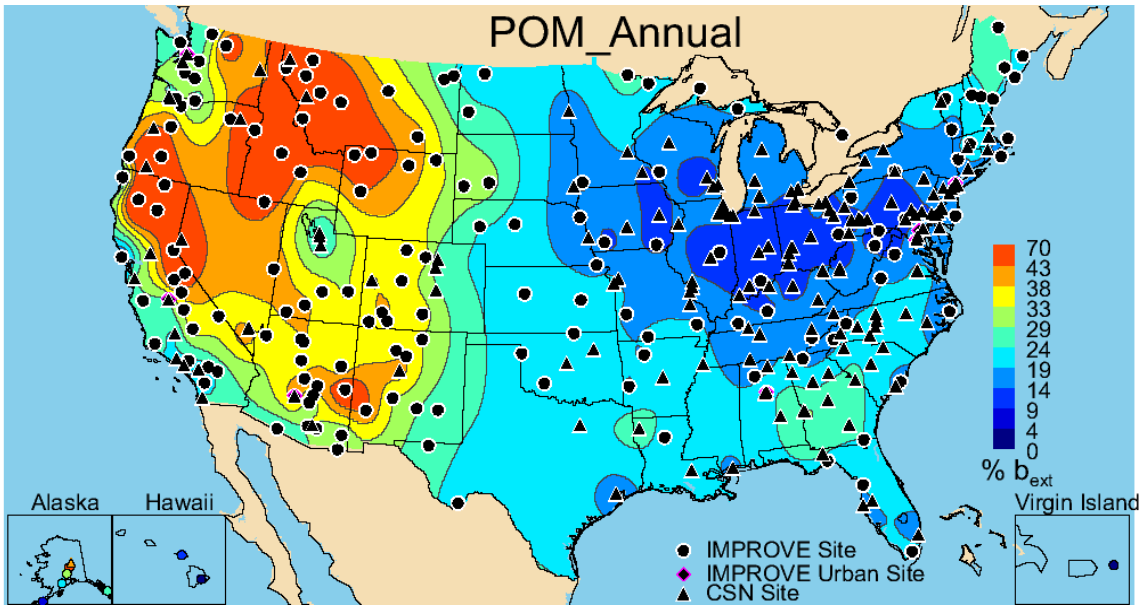

Figure 3.4d. Annual mean percent contribution (%) of ambient particulate organic matter (POM) light extinction coefficient (b_{ext}) to $PM_{2.5}$ reconstructed aerosol b_{ext} for 2005–2008 for rural IMPROVE and urban CSN sites. The "modified original" IMPROVE algorithm was used (see text). Wavelength corresponds to 550 nm.

3.5 $PM_{2.5}$ LIGHT ABSORBING CARBON LIGHT EXTINCTION COEFFICIENTS

The IMPROVE spatial pattern of 2005–2008 annual mean extinction coefficients from light absorbing carbon (b_{ext_LAC}) were similar to the LAC mass concentration patterns, with elevated levels at eastern sites (Figure 3.5a). The maximum annual mean rural b_{ext_LAC} (5.91 Mm^{-1}) occurred at James River Face Wilderness (JARI1) in Virginia, similar to the high

LAC mass concentration. The lowest rural b_{ext_LAC} occurred at Hawaii Volcano (0.36 Mm^{-1}, HAVO1). Most (93%) IMPROVE sites corresponded to very low (< 5 Mm^{-1}) b_{ext_LAC}. The only IMPROVE sites with higher annual mean b_{ext_LAC} corresponded to urban sites as seen in Figure 3.5b. The addition of CSN sites extended the localized impact of LAC on b_{ext} to a number of other sites in major urban centers. Strong gradients surrounding these sites suggested local sources with fairly localized effects on visibility. The minimum urban b_{ext_LAC} was greater than at the maximum rural site (8.50 Mm^{-1} at Puget Sound, PUSO1), and the maximum urban IMPROVE b_{ext_LAC} occurred at Birmingham (16.56 Mm^{-1}, BIRM1). The CSN estimates ranged from 1.34 Mm^{-T} in Watford City, North Dakota (#380530002) to 25.81 Mm^{-1} in Liberty (#420030064). In contrast to the rural sites, only 13% of urban sites corresponded to b_{ext_LAC} less than 5 Mm^{-1}, suggesting the importance of urban sources of LAC to b_{ext} at urban sites.

Although rural b_{ext_LAC} was higher in the East, its percent contribution to b_{ext} was higher in the West (Figure 3.5c). Biomass combustion sources (wildfire and wood burning) in the West were relatively more important, as suggested by the higher percent contribution in the northwestern United States. Rural percent contributions ranged from 1.1% (Hawaii Volcano, HAVO1) to 16.7 % in Petrified Forest, Arizona (PEFO1). IMPROVE urban sites in the Southwest also corresponded to higher percent contributions of LAC to b_{ext}. In urban IMPROVE regions, b_{ext_LAC} ranged from 9.4% (Baltimore, BALT1) to 25.2% (Phoenix, PHOE1). Light-absorbing carbon was an important contributor to b_{ext} for many urban CSN sites in the western United States, specifically. Values ranged from 5.01% (Bonne Terre, Missouri, #291860005) to 36.3% in Nevada (Las Vegas, #320030020) (Figure 3.5d). The spatial gradients in the relative contribution of LAC to b_{ext} were somewhat more diffuse than the spatial gradients in b_{ext_LAC}.

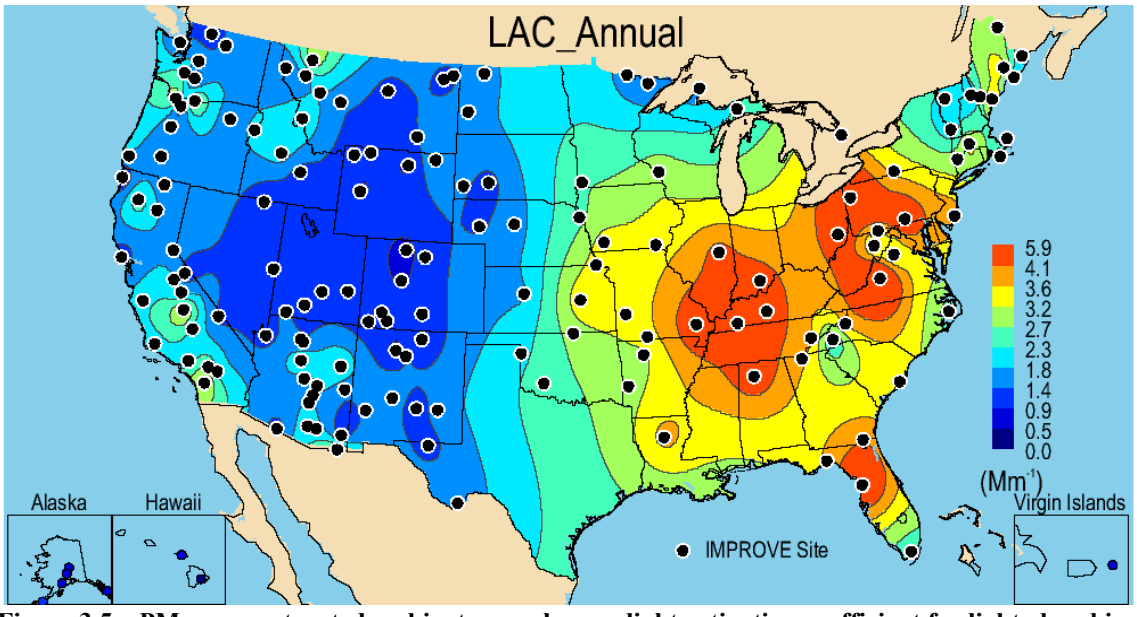

Figure 3.5a. $PM_{2.5}$ reconstructed ambient annual mean light extinction coefficient for light absorbing carbon (b_{ext_LAC}, Mm^{-1}) for 2005–2008 for rural IMPROVE sites. The "modified original" IMPROVE algorithm was used (see text). Wavelength corresponds to 550 nm.

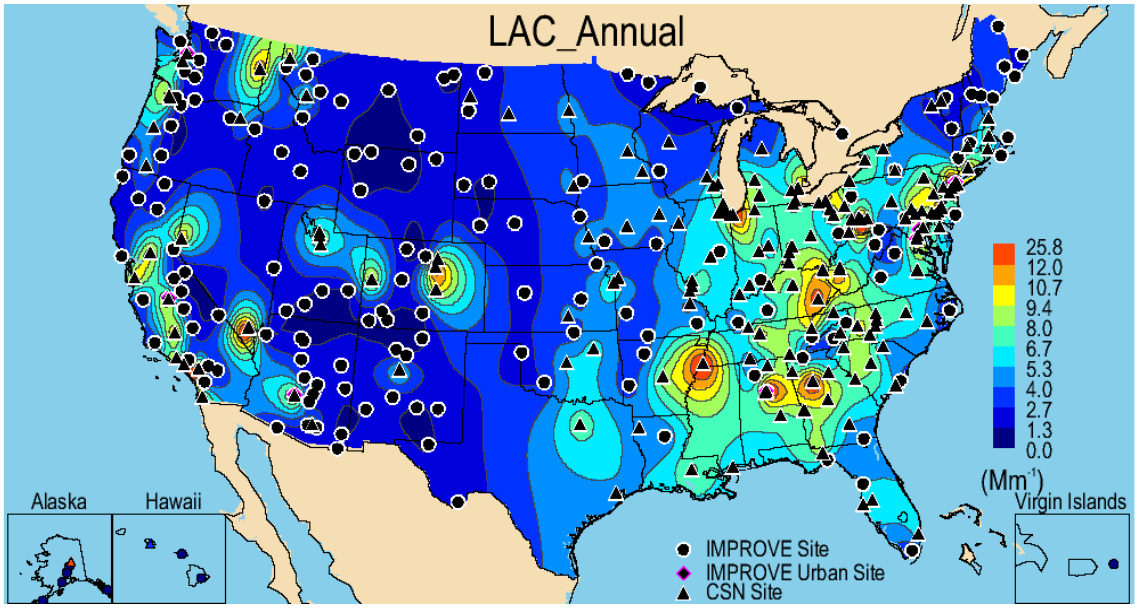

Figure 3.5b. $PM_{2.5}$ reconstructed ambient annual mean light extinction coefficient for light absorbing carbon (b_{ext_LAC}, Mm^{-1}) for 2005–2008 for rural IMPROVE and urban CSN sites. The "modified original" IMPROVE algorithm was used (see text). Wavelength corresponds to 550 nm.

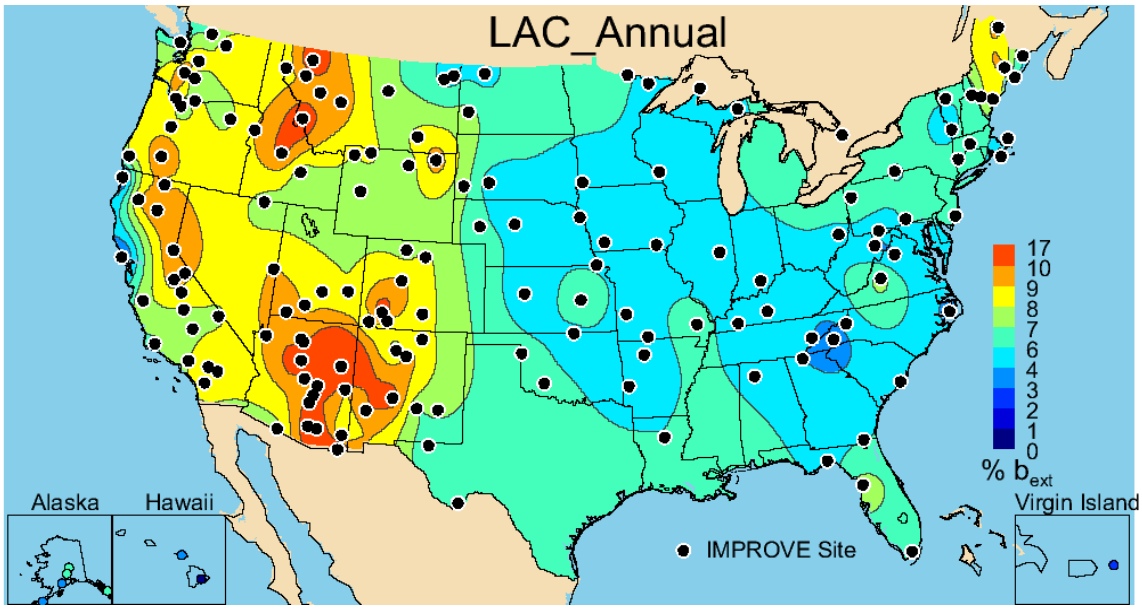

Figure 3.5c. Annual mean percent contribution (%) of ambient light absorbing carbon (LAC) light extinction coefficient (b_{ext}) to $PM_{2.5}$ reconstructed aerosol b_{ext} for 2005–2008 for rural IMPROVE sites. The "modified original" IMPROVE algorithm was used (see text). Wavelength corresponds to 550 nm.

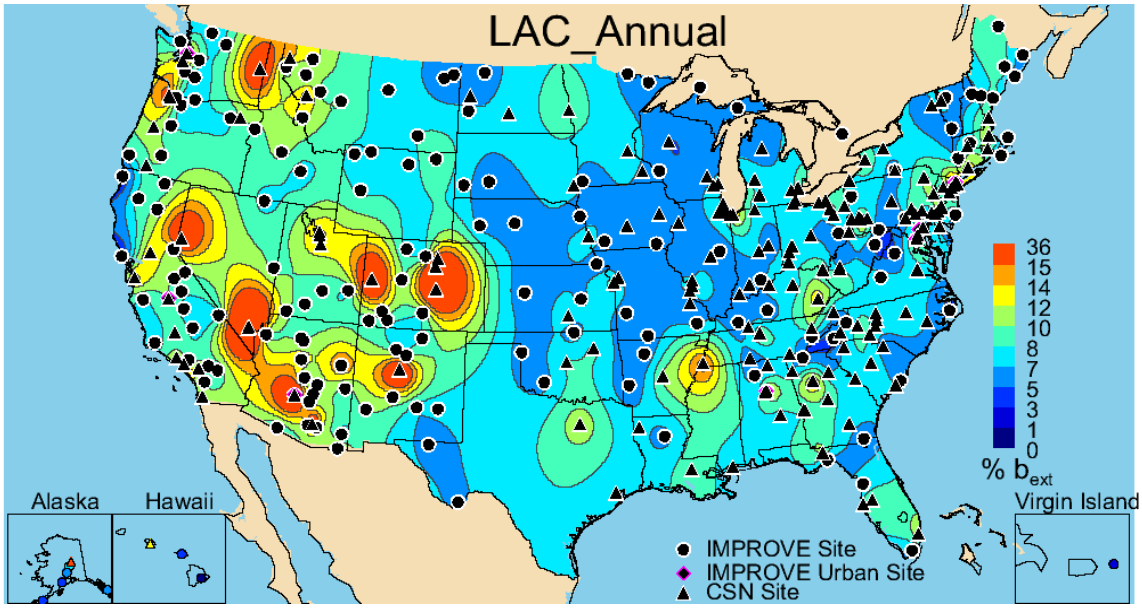

Figure 3.5d. Annual mean percent contribution (%) of ambient light absorbing carbon (LAC) light extinction coefficient (b_{ext}) to $PM_{2.5}$ reconstructed aerosol b_{ext} for 2005–2008 for rural IMPROVE and urban CSN sites. The "modified original" IMPROVE algorithm was used (see text). Wavelength corresponds to 550 nm.

3.6 $PM_{2.5}$ FINE SOIL LIGHT EXTINCTION COEFFICIENTS

The annual mean soil b_{ext} (b_{ext_soil}) spatial pattern was the same as the fine soil mass concentration pattern (Figure 3.6a). The rural IMPROVE b_{ext_soil} ranged from 0.11 Mm^{-1} in Petersburg, Alaska (PETE1), to 4.41 Mm^{-1} in Douglas, Arizona (DOUG1). The urban IMPROVE b_{ext_soil} had a similar range, from 0.49 Mm^{-1} in Puget Sound (PUSO1) to 3.22 Mm^{-1} in Phoenix (PHOE1). Generally the southern half of the United States had higher b_{ext_soil}, but values were relatively low; only ten sites had annual mean b_{ext_soil} greater than 1.5 Mm^{-1}. The addition of data from CSN sites provided further detail to the spatial pattern of b_{ext_soil} (Figure 3.6b) but did not alter it substantially. Sites in Colorado (Denver, 1.61 Mm^{-1}, #080010006), Washington (Spokane, 1.55 Mm^{-1}, #530630016), and Alabama (Birmingham, 1.35 Mm^{-1}, #010730023) had higher b_{ext_soil}. Only nine CSN sites had b_{ext_soil} greater than 1.5 Mm^{-1}.

The largest percent contributions to aerosol b_{ext} from fine soil at rural IMPROVE sites occurred in the West and Southwest (Figure 3.6c). Percent contributions at rural sites ranged from 0.49% (Simeonof, Alaska, SIME1) to 18.4% in Douglas, Arizona (DOUG1). Soil contributed over 10% to b_{ext} for only nine sites; with the exception of Jarbidge, Nevada (JARB1), and the Virgin Islands (VIIS1), all of the sites were in Arizona. The urban IMPROVE percent contributions ranged from 0.65% in Baltimore (BALT1) to 7.5% in Phoenix (PHOE1). A similar range was found for the CSN sites, from 0.30% in Arendtsville, Pennsylvania (#420010001), to 5.2% in Las Vegas (#320030020). Soil was not a major contributor to urban CSN b_{ext} (Figure 3.6d). No CSN sites had contributions greater than 10%.

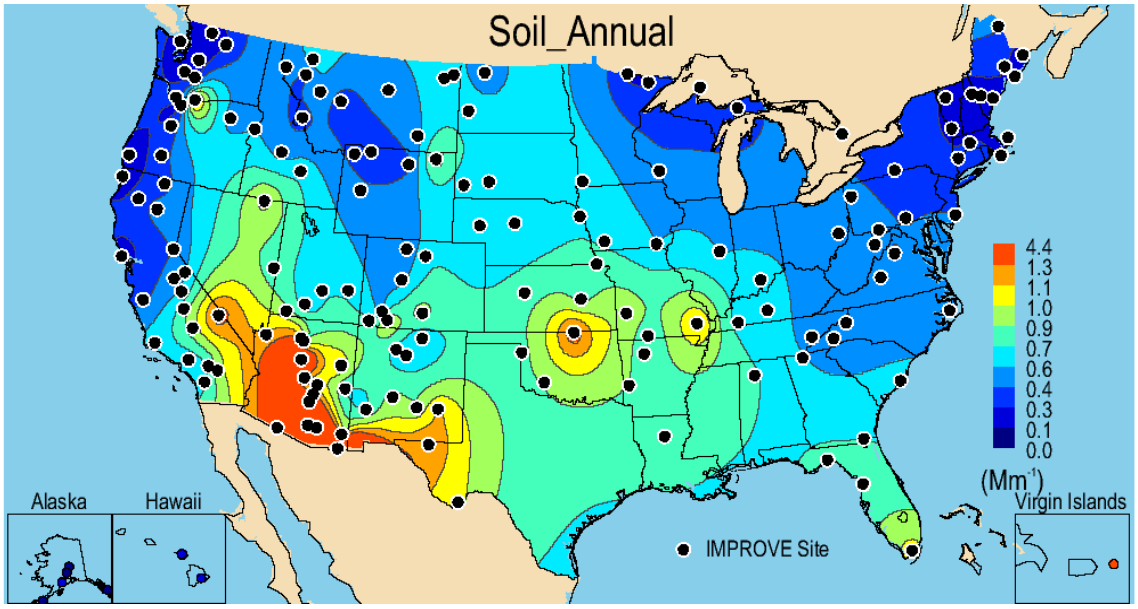

Figure 3.6a. $PM_{2.5}$ reconstructed ambient annual mean light extinction coefficient for soil (b_{ext_soil}, Mm^{-1}) for 2005–2008 for rural IMPROVE sites. The "modified original" IMPROVE algorithm was used (see text). Wavelength corresponds to 550 nm.

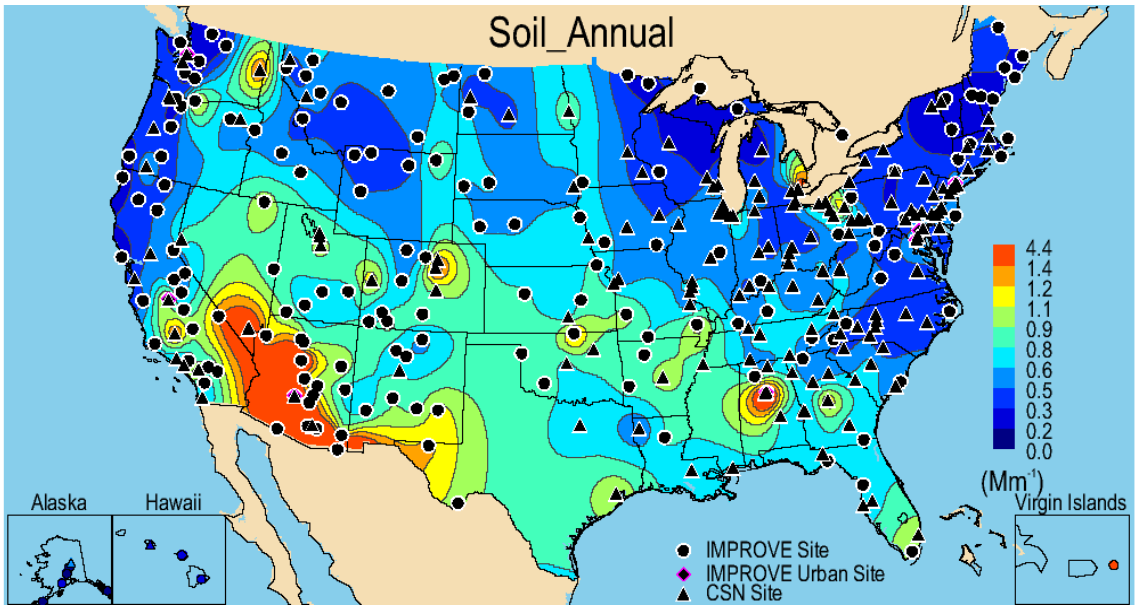

Figure 3.6b. $PM_{2.5}$ reconstructed ambient annual mean light extinction coefficient for soil (b_{ext_soil}, Mm^{-1}) for 2005–2008 for rural IMPROVE and urban CSN sites. The "modified original" IMPROVE algorithm was used (see text). Wavelength corresponds to 550 nm.

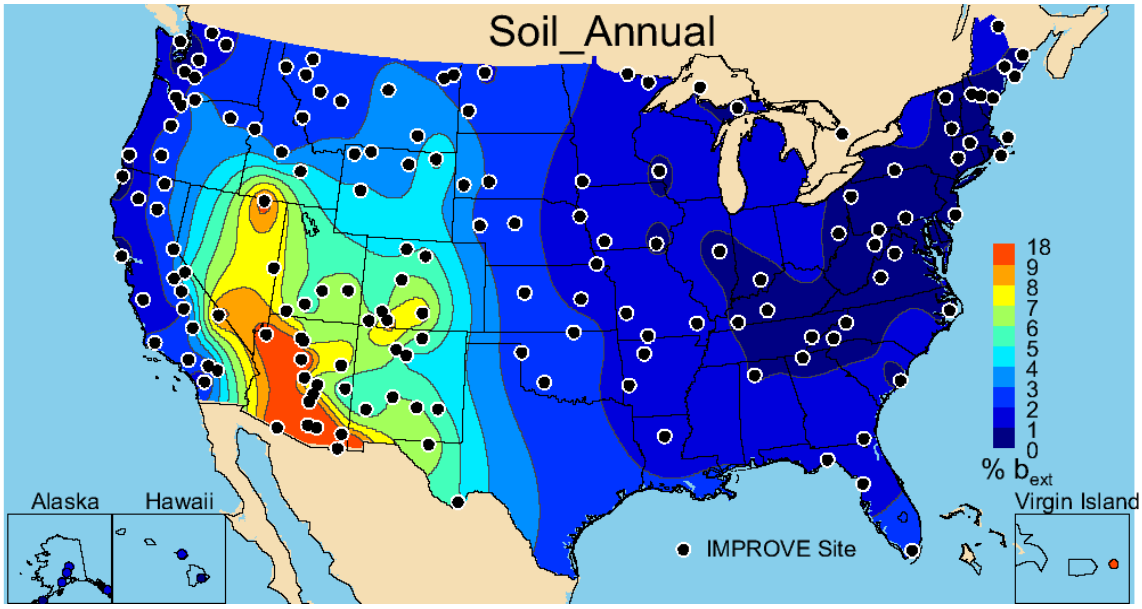

Figure 3.6c. Annual mean percent contribution (%) of ambient soil light extinction coefficient (b_{ext}) to $PM_{2.5}$ reconstructed aerosol b_{ext} for 2005–2008 for rural IMPROVE sites. The "modified original" IMPROVE algorithm was used (see text). Wavelength corresponds to 550 nm.

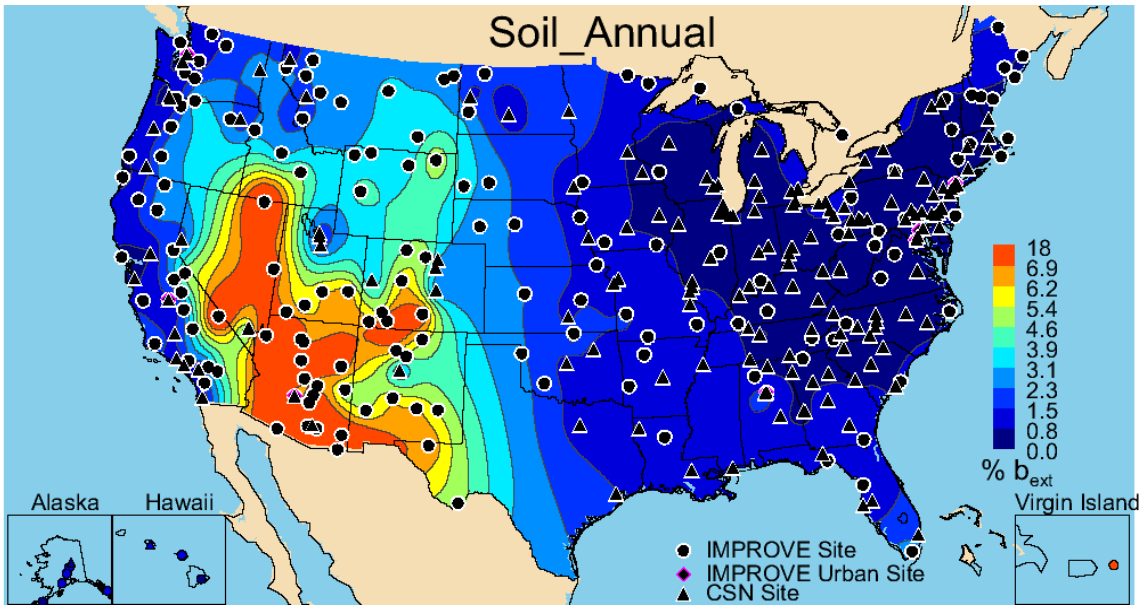

Figure 3.6d. Annual mean percent contribution (%) of ambient soil light extinction coefficient (b_{ext}) to $PM_{2.5}$ reconstructed aerosol b_{ext} for 2005–2008 for rural IMPROVE and urban CSN sites. The "modified original" IMPROVE algorithm was used (see text). Wavelength corresponds to 550 nm.

3.7 $PM_{2.5}$ SEA SALT EXTINCTION COEFFICIENTS

Spatial patterns of IMPROVE 2005–2008 monthly mean light extinction coefficients due to sea salt (b_{ext_SS}) were very similar to sea salt mass concentrations. All IMPROVE values ranged from 0.04 Mm^{-1} (Cloud Peak, Wyoming, CLPE1) to 12.8 Mm^{-1} (Point Reyes National Seashore, California, PORE1). Generally b_{ext_SS} was relatively low; only in coastal regions were estimates non-negligible. Eight sites corresponded to annual mean b_{ext_SS} values greater than 3

Mm^{-1}, and these were located in coastal regions, including the Virgin Islands (VIIS1) (see Figure 3.7a). The coastal pattern of elevated b_{ext_SS} was also observed with the inclusion of CSN sites where only three sites (in Hawaii, Florida, and Pennsylvania) were greater than 3 Mm^{-1} (Figure 3.7b). The maximum b_{ext_SS} occurred at Pearl City, Hawaii (5.33 Mm^{-1}, #150032004), and the minimum b_{ext_SS} occurred at Watford City, North Dakota (0.0075 Mm^{-1}, #380530002).

The IMPROVE percent contribution of sea salt to b_{ext} was typically low on an annual mean basis, except at coastal sites where the maximum IMPROVE contribution (41.1%) occurred at Simeonof, Alaska (SIME1) (Figure 3.7c). The lowest contribution of SS to b_{ext} occurred at Frostberg Reservoir, Maryland (0.29%, FRRE1). Only eighteen sites corresponded to contributions of greater than 5%. The largest percent contribution for CSN occurred at Pearl City, Hawaii (23.0%, #150032004). Besides the Hawaii site, only one other CSN site in Florida had contributions from sea salt to b_{ext} greater than 5% (Fort Lauderdale, #120111002) (Figure 3.7d). The lowest percent contribution occurred at Watford City, North Dakota (0.034%, #380530002)

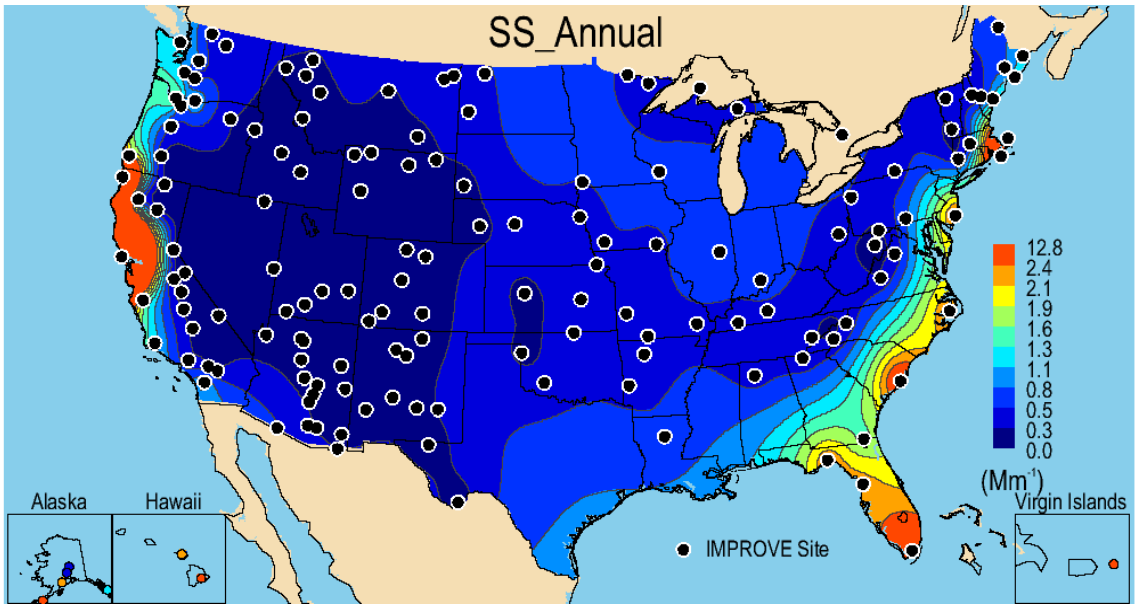

Figure 3.7a. $PM_{2.5}$ reconstructed ambient annual mean light extinction coefficient for sea salt (b_{ext_SS}, Mm^{-1}) for 2005–2008 for rural IMPROVE sites. The "modified original" IMPROVE algorithm was used (see text). Wavelength corresponds to 550 nm.

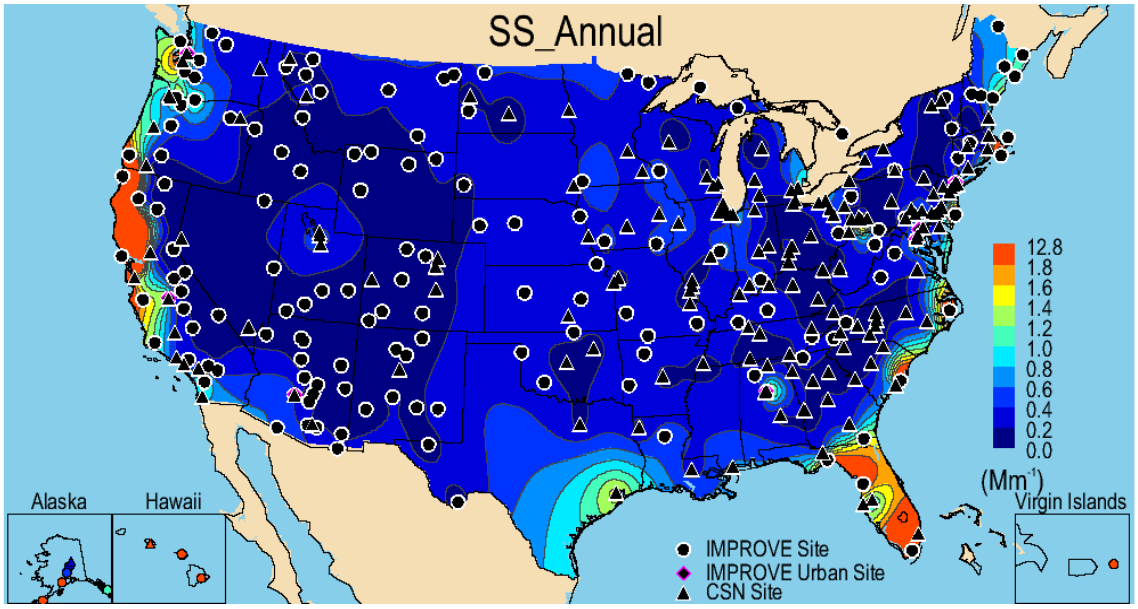

Figure 3.7b. $PM_{2.5}$ reconstructed ambient annual mean light extinction coefficient for sea salt (b_{ext_SS}, Mm^{-1}) for 2005–2008 for rural IMPROVE and urban CSN sites. The "modified original" IMPROVE algorithm was used (see text). Wavelength corresponds to 550 nm.

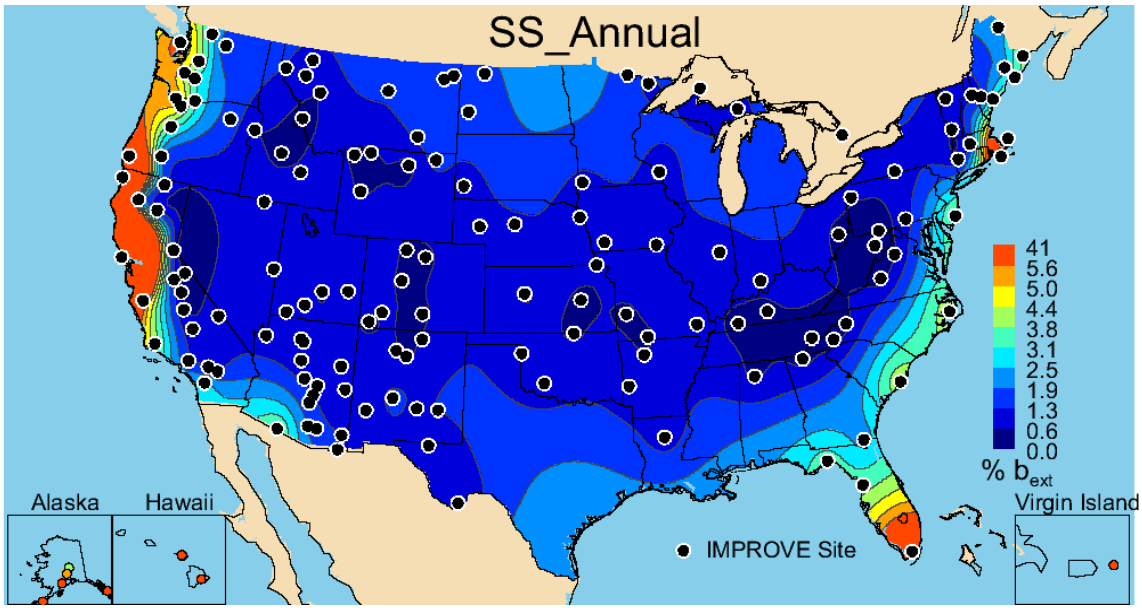

Figure 3.7c. Annual mean percent contribution (%) of ambient sea salt (SS) light extinction coefficient (b_{ext}) to $PM_{2.5}$ reconstructed aerosol b_{ext} for 2005–2008 for rural IMPROVE sites. The "modified original" IMPROVE algorithm was used (see text). Wavelength corresponds to 550 nm.

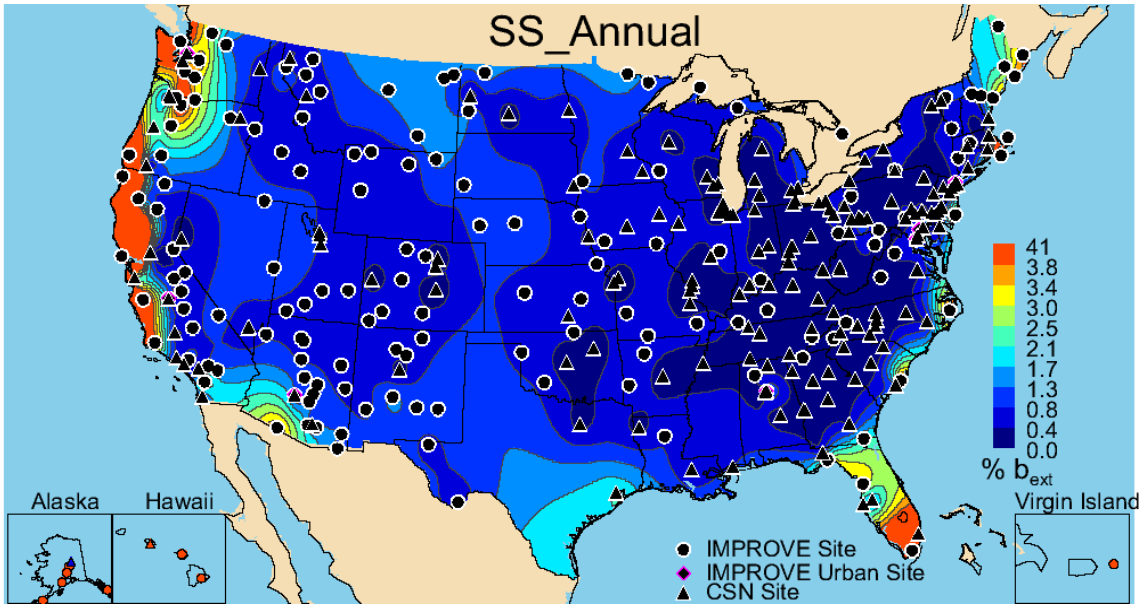

Figure 3.7d. Annual mean percent contribution (%) of ambient sea salt (SS) light extinction coefficient (b_{ext}) to $PM_{2.5}$ reconstructed aerosol b_{ext} for 2005–2008 for rural IMPROVE and urban CSN sites. The "modified original" IMPROVE algorithm was used (see text). Wavelength corresponds to 550 nm.

3.8 $PM_{2.5}$ RECONSTRUCTED AEROSOL LIGHT EXTINCTION COEFFICIENTS

For the purposes of this discussion, $PM_{2.5}$ aerosol b_{ext} (b_{ext_aer}) refers to the sum of $PM_{2.5}$ b_{ext} from ammonium sulfate, ammonium nitrate, particulate organic carbon, light absorbing carbon, fine soil, and sea salt. Rayleigh scattering was not included, and light extinction coefficients due to coarse mass will be investigated separately. The 2005–2008 IMPROVE rural annual mean b_{ext} is presented in Figure 3.8a. The east-west division observed for several species (especially b_{ext_AS}) was preserved in the aggregation of aerosol b_{ext}. Generally the highest rural aerosol b_{ext} occurred in the East and along the Ohio River valley. The values ranged from 8.24 Mm^{-1} in Petersburg, Alaska (PETE1), to 95.54 Mm^{-1} in Mammoth Cave, Kentucky (MACA1). Recall that the major contributor to b_{ext_aer} at this site was ammonium sulfate (68%), and in fact the spatial pattern of b_{ext_aer} is similar to b_{ext_AS} (compare Figures 3.2a and 3.8a). Urban IMPROVE sites corresponded to higher b_{ext_aer} and ranged from 42.05 Mm^{-1} in Phoenix (PHOE5) to 117.65 Mm^{-1} in Birmingham (BIRM1). The addition of CSN sites enhanced the spatial resolution in the East but did not alter the contrast between b_{ext_aer} in the eastern and western United States (Figure 3.8b). Values ranged from 22.17 Mm^{-1} in North Dakota (Watford City, #380530002) to 146.97 Mm^{-1} in Pennsylvania (Liberty, #420030064). Most CSN sites (92%) corresponded to higher b_{ext_aer} (>50 Mm^{-1}), probably due to their location in the eastern United States, where AS was a dominant contributor to b_{ext}. On the West Coast, higher urban b_{ext_aer} was most likely due to the contribution from ammonium nitrate. Recall that the site in Bakersfield corresponded to a 54% contribution from ammonium nitrate to b_{ext}.

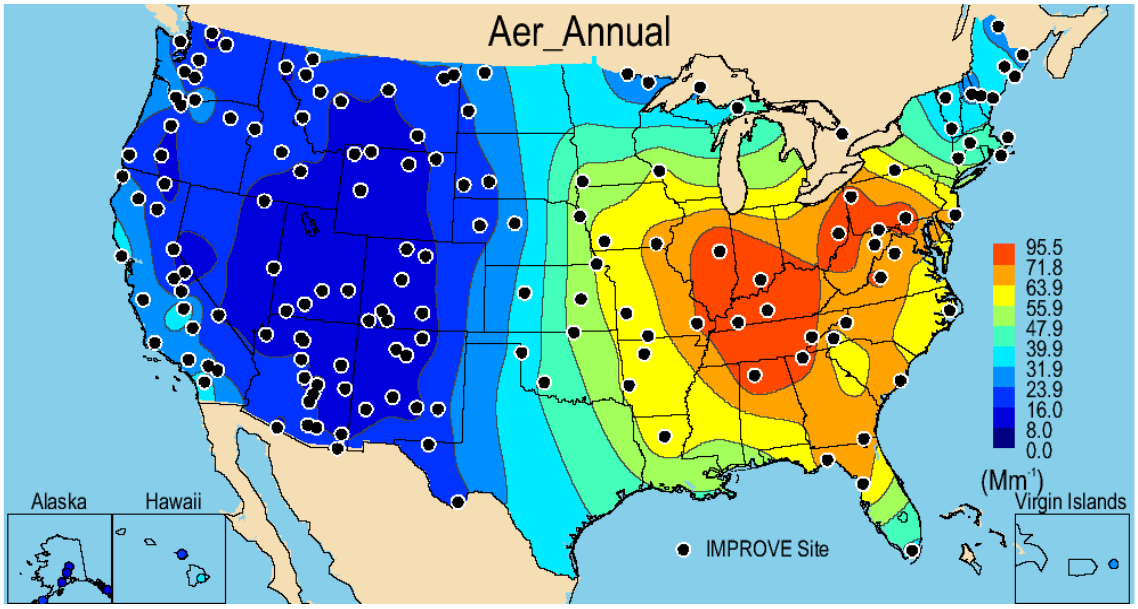

Figure 3.8a. $PM_{2.5}$ reconstructed annual mean light extinction coefficient for ambient aerosol (b_{ext_aer}, Mm^{-1}) for 2005–2008 for rural IMPROVE sites. The "modified original" IMPROVE algorithm was used (see text). Wavelength corresponds to 550 nm.

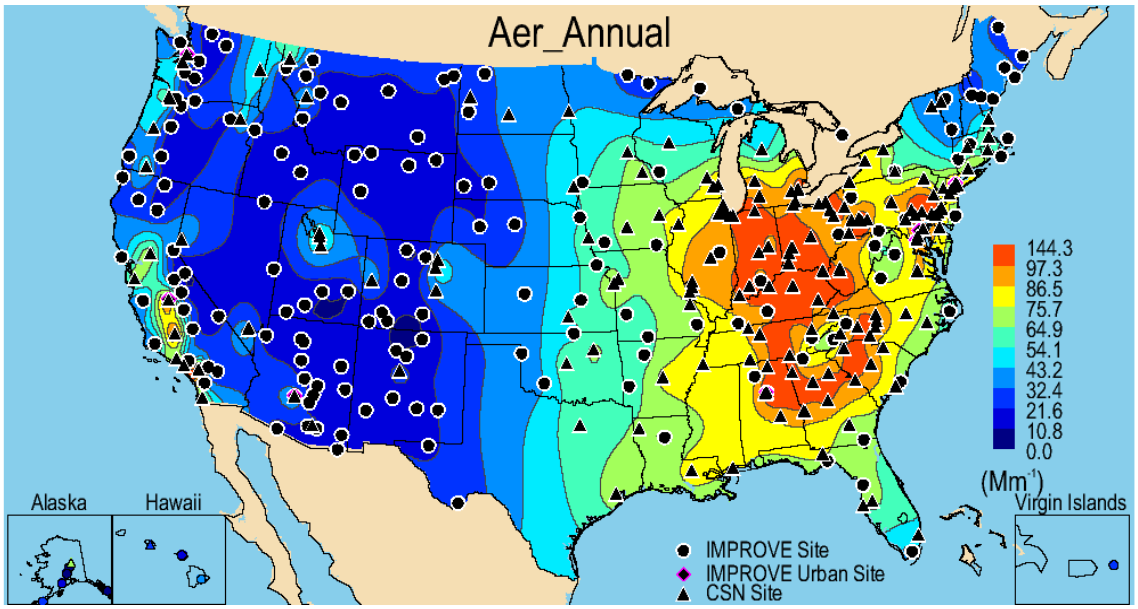

Figure 3.8b. $PM_{2.5}$ reconstructed annual mean light extinction coefficient for ambient aerosol (b_{ext_aer}, Mm^{-1}) for 2005–2008 for rural IMPROVE and urban CSN sites. The "modified original" IMPROVE algorithm was used (see text). Wavelength corresponds to 550 nm.

3.9 COARSE MASS LIGHT EXTINCTION COEFFICIENTS

Although coarse mass was not included in aerosol b_{ext} because it is not measured by the CSN network, we computed light extinction coefficients due to coarse mass (b_{ext_CM}) separately for IMPROVE sites. The spatial pattern of b_{ext_CM} reflected the pattern of the coarse mass concentration distribution (Figure 3.9a). Urban and rural IMPROVE b_{ext_CM} had similar ranges, with the highest nearing that of Rayleigh scattering contributions. The overall maximum

occurred at Douglas, Arizona (12.67 Mm^{-1}, DOUG1), and was most likely associated with soil, as the maximum b_{ext_soil} was also computed for this site. The lowest b_{ext_CM} occurred at North Cascades, Washington (0.68 Mm^{-1}, NOCA1). Regions in the Midwest and Southwest and urban locations in Birmingham (9.37 Mm^{-1}, BIRM1) and Fresno (11.89 Mm^{-1} FRES1) corresponded to higher b_{ext_CM}. In fact, of the four sites with b_{ext_CM} values greater than 10 Mm^{-1}, three of them were urban (Douglas, Arizona; Fresno; and two sites in Phoenix, PHOE1 and PHOE5), which were not included in the map of rural b_{ext_CM} shown in Figure 3.9a. Similar to the discussion of CM mass concentration, elevated b_{ext_CM} occurred at several sites in the Midwest and mid-South. High b_{ext_soil} did not coincide with these site locations, suggesting other CM species were contributing to b_{ext} at these sites. Many IMPROVE sites corresponded to low b_{ext_CM}; 39% of IMPROVE sites had b_{ext_CM} less than 2 Mm^{-1}.

The annual mean IMPROVE fractional contributions of b_{ext_CM} to total aerosol b_{ext} were computed separately from the species discussed above; for this case, total b_{ext} included the contribution from coarse mass. Fractional contributions of b_{ext_CM} ranged from 2.2% at Shining Rock Wilderness, North Carolina (SHRO1) to 34.5% in Douglas, Arizona (DOUG1) (see Figure 3.9b). The contributions of CM to b_{ext} were most important at the Intermountain West and Southwest, where CM contributed 20% or more to total b_{ext}. In the Intermountain West, light extinction due to other species was of similar magnitude to coarse mass b_{ext}, resulting in contributions of b_{ext_CM} to total b_{ext} that were non-negligible. While annual mean b_{ext_CM} was higher in the Central and Midwest regions compared to the Intermountain West region, its contribution to total b_{ext} was not as important, largely due to the relatively higher contributions of ammonium nitrate to b_{ext} in the Midwest. The contribution of CM to b_{ext} was even less important in the eastern United States, where contributions were typically less than 10%.

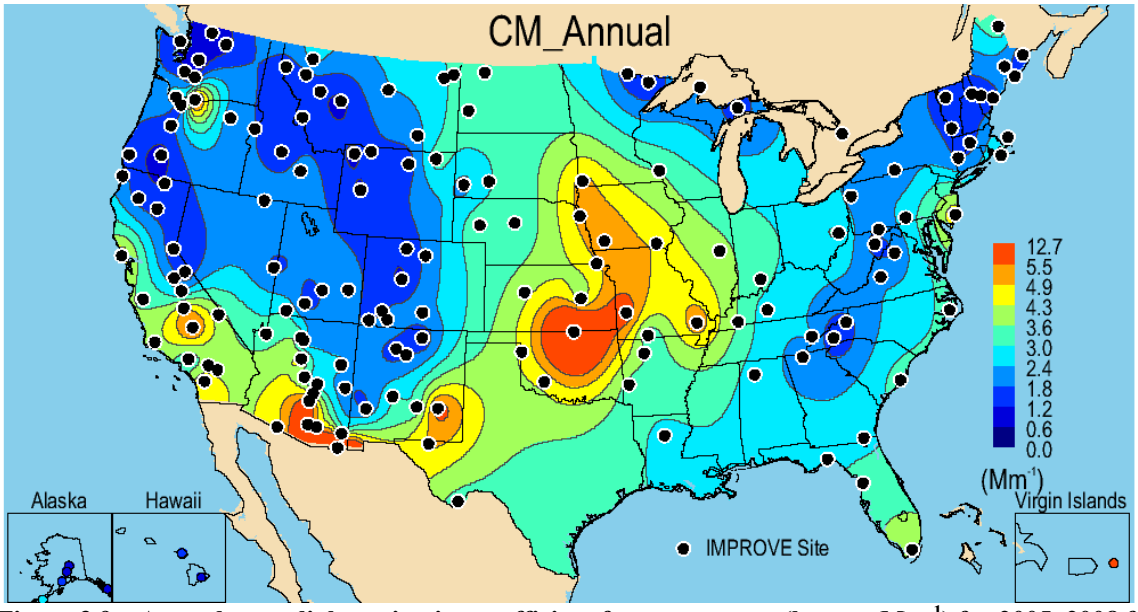

Figure 3.9a. Annual mean light extinction coefficient for coarse mass (b_{ext_CM}, Mm^{-1}) for 2005–2008 for rural IMPROVE sites. The "modified original" IMPROVE algorithm was used (see text). Wavelength corresponds to 550 nm.

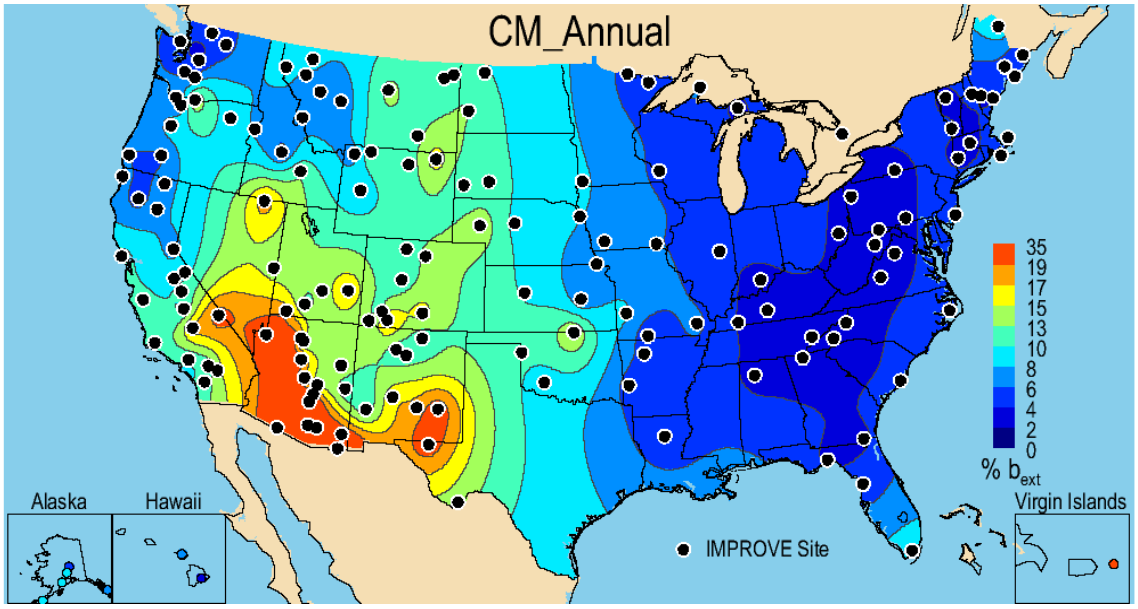

Figure 3.9b. Annual mean percent contribution (%) of coarse mass (CM) light extinction coefficient to total reconstructed aerosol b_{ext} for 2005–2008 for rural IMPROVE sites. The "modified original" IMPROVE algorithm was used (see text). Wavelength corresponds to 550 nm. Rayleigh scattering was not included in total b_{ext}.

3.10 $PM_{2.5}$ DECIVIEW

The 2005–2008 IMPROVE annual mean deciview (dv) spatial pattern was very similar to the b_{ext_aer} pattern, as expected (see Figure 3.10). The main differences were that the contributions of coarse mass and site-specific Rayleigh scattering were included (see equation 3.5). Higher dv values were observed in the eastern United States. Values at rural sites ranged from 4.65 dv at White River NF, Colorado (WHRI1), to 22.19 dv at Mammoth Cave, Kentucky (MACA1). Urban IMPROVE sites corresponded to a similar range, with 17.04 dv in Phoenix (PHOE1) to 24.13 dv in Birmingham (BIRM1). No interpolated map of dv with CSN data was produced because coarse mass data are not available from the CSN network.

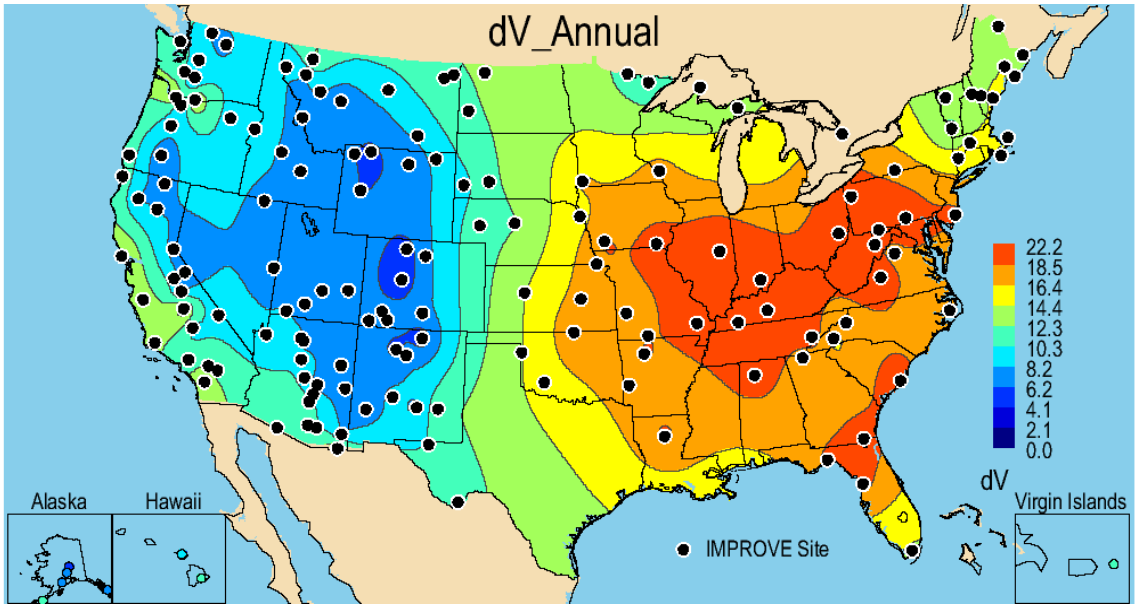

Figure 3.10. Annual mean $PM_{2.5}$ deciview (dv) for 2005–2008 for rural IMPROVE sites. The "modified original" IMPROVE algorithm was used (see text). Wavelength corresponds to 550 nm.

Tables of the 2005–2008 annual mean b_{ext} and b_{ext} fractions are reported for each site in Appendix C.1 (IMPROVE and CSN b_{ext}) and C.2 (IMPROVE and CSN relative b_{ext}).

REFERENCES

Brewer, P., and T. Moore (2009), Source contributions to visibility impairment in the southeastern and western United States, *J. Air & Waste Manage. Assoc., 59*, 1070-1081, doi:10.3155/1047-3289.59.9.1070.

Hand, J. L., and W. C. Malm (2006), Review of the IMPROVE equation for estimating ambient light extinction coefficients, CIRA Report, ISSN: 0737-5352-71, Colo. State Univ., Fort Collins.

Hand, J. L., and W. C. Malm (2007), Review of aerosol mass scattering efficiencies from ground-based measurements since 1990, *J. Geophys. Res., 112,* D16203, doi:10.1029/2007JD008484.

Hand. J. L., D. E. Day, G. R. McMeeking, E. J. T. Levin, C. M. Carrico, S. M. Kreidenweis, W. C. Malm, A. Laskin, and Y. Desyaterik (2010), Measured and modeled humidification factors of fresh smoke particles from biomass burning: role of inorganic constituents, *Atmos. Chem. Phys., 10,* 6179-6194, doi:10.5194/acp-10-6179-2010.

Lowenthal, D. H., and N. Kumar (2003), PM2.5 mass and light extinction reconstruction in IMPROVE, *J. Air & Waste Manage. Assoc., 53,* 1109-1120.

Malm, W. C., J. F. Sisler, D. Huffman, R. A. Eldred, and T. A. Cahill (1994), Spatial and seasonal trends in particle concentration and optical extinction in the United States, *J. Geophys. Res., 99(D1),* 1347-1370.

Malm, W. C., D. E. Day, C. Carrico, S. M. Kreidenweis, J. L. Collett, Jr., G. McMeeking, T. Lee, J. Carrillo, and B. Schichtel (2005), Intercomparison and closure calculations using measurements of aerosol species and optical properties during the Yosemite Aerosol Characterization Study, *J. Geophys. Res., 110,* D14302, doi:10.1029/2004JD005494.

Malm, W. C., and J. L. Hand (2007), An examination of the physical and optical properties of aerosols collected in the IMPROVE program, *Atmos. Environ., 41,* 3407-3427.

Pitchford, M. L., and W. C. Malm (1994), Development and applications of a standard visual index, *Atmos. Environ, 28,* 5, 1049-1054.

Pitchford, M., W. Malm, B. Schichtel, N. Kumar, D. Lowenthal and J. Hand (2007), Revised algorithm for estimating light extinction from IMPROVE particle speciation data, *J. Air & Waste Manage. Assoc., 57,* 1326-1336.

U. S. EPA (2001), Interpolating relative humidity weighting factors to calculate visibility impairment and the effects of IMPROVE monitor outliers, (http://vista.cira.colostate.edu/improve/Publications/GuidanceDocs/DraftReportSept20.pdf).

U.S. EPA (2003), Draft guidance for tracking progress under the Regional Haze Rule, Contract No. 68-D-02-0261, Work Order No. 1-06, http://www.epa.gov/ttn/oarpg/t1/memoranda/rh_tpurhr_gd.pdf.

Chapter 4. Seasonal Distributions of $PM_{2.5}$ Aerosol Mass Concentrations

In the previous chapters we focused only on the annual mean concentrations of several key aerosol species. However, the seasonality of aerosol concentrations can be significant depending on species and region and is a function of the source emissions, meteorological parameters, and local and long-range transport. Examining aerosol concentrations on a regional basis, rather than a site-specific basis, can lead to insights regarding air quality issues on regional scales. In this chapter we examine the differences in the regional seasonal signatures of major aerosol species for rural and urban regions.

IMPROVE and CSN data were grouped and monthly averaged according to previously defined regions. When a specific region is used in this report, it refers to an IMPROVE or CSN region as defined in Figure 1.2 or Figure 1.9, respectively (Chapter 1), not a commonly-used geographical region. For example, the IMPROVE "Northwest" region refers to a specific group of sites, not to the area of the country typically considered as "northwestern United States". We used 35 of the 41 predefined IMPROVE regions (see Table 1.1 and Figure 1.2 in Chapter 1), 28 of which were rural and an additional seven that corresponded to a single urban site per region. Of the rural sites, three regions included only one site (Death Valley, Virgin Islands, and Ontario). The IMPROVE regions were semi-empirically defined based on site location and the seasonal distribution of aerosol concentrations for major species (e.g., Sisler et al., 1993; Sisler et al., 1996; Malm et al., 2000; Malm et al., 2004; Debell, 2006). We did not investigate the variability in the species composition between sites in a given region, nor did we take into account differences in elevation.

We used 29 of the 31 semi-empirically defined regions for the CSN sites based on seasonal distribution of aerosol concentrations. For comparison purposes, we grouped sites in regions similar to those defined for the IMPROVE network. Of the 29 regions, eight had only one site per region. A list of CSN regions and the comprised sites can be found in Chapter 1 (Table 1.8 and Figure 1.9).

We analyzed the monthly and annual mean concentrations of $PM_{2.5}$ ammonium sulfate (AS), ammonium nitrate (AN), particulate organic matter (POM), light absorbing carbon (LAC), soil, sea salt and gravimetric fine mass (FM) and coarse mass (CM). We also evaluated the seasonal distribution in relative contribution (the percent contribution of a species' mass to reconstructed fine mass, RCFM). The evaluation of both the absolute and relative concentrations highlights the importance of the behavior of species mass concentrations relative to each other. For example, a given species might vary on a relative basis although its absolute concentrations are steady (or vice versa), solely based on the seasonal behavior of other species.

The monthly mean IMPROVE and CSN regional data are presented as stacked bar charts. Monthly means are depicted with the first letter of the month, followed by an "A" for annual mean. Seasonality is defined as the ratio of the maximum to minimum monthly mean concentrations for a given region. Seasonal periods correspond to winter (December, January and February) spring (March, April and May), summer (June, July and August), and fall (September, October, and November). Stacked bar charts for monthly mean concentrations are grouped into figures corresponding to four sections of the country: northwestern, southwestern, eastern, and OCONUS (outside the contiguous United States, e.g., Hawaii, Alaska, and Virgin Islands)

United States. Stacked bar charts for monthly mean mass fractions for were also created. Sections 4.1–4.8 present the regional seasonality for the above listed species; a discussion of results is provided in Section 4.9.

4.1 $PM_{2.5}$ AMMONIUM SULFATE MASS CONCENTRATIONS

The IMPROVE maximum 2005–2008 regional monthly mean ammonium sulfate (AS) concentration of 11.29 μg m^{-3} occurred at the urban site of Baltimore in July. The highest concentration in nonurban regions corresponded to the Appalachia region in August (9.94 μg m^{-3}). In fact, bar charts presented in Figure 4.1.1 depict that most of the regions in the eastern United States corresponded to higher AS concentrations in summer, especially the Ohio River Valley, Northeast, East Coast, and Mid South regions. The similar seasonal pattern suggested regional sources of AS. Notice that the scales for each regional bar plot in Figure 4.1.1 (and subsequent figures) are different. The minimum monthly mean AS concentrations occurred in the Oregon/Northern California region in December (0.17 μg m^{-3}). Most regions in the northwestern United States had relatively low AS concentrations compared to other species (typically less than 1 μg m^{-3}) and less-defined summer peaks in concentration (see Figure 4.1.2). AS concentrations in the southwestern United States (Figure 4.1.3) were also low but higher than in the northwestern United States and also demonstrated more of a summer peak (e.g., see the Southern California, Death Valley, and West Texas regions). AS monthly mean concentrations in Alaska and the Virgin Islands were fairly low (less than 2 μg m^{-3}, see Figure 4.1.4) with peaks in the spring. Concentrations of AS in the Hawaii region were very different with higher concentrations (typically greater than 1μg m^{-3}), especially in spring, and lower concentrations in summer.

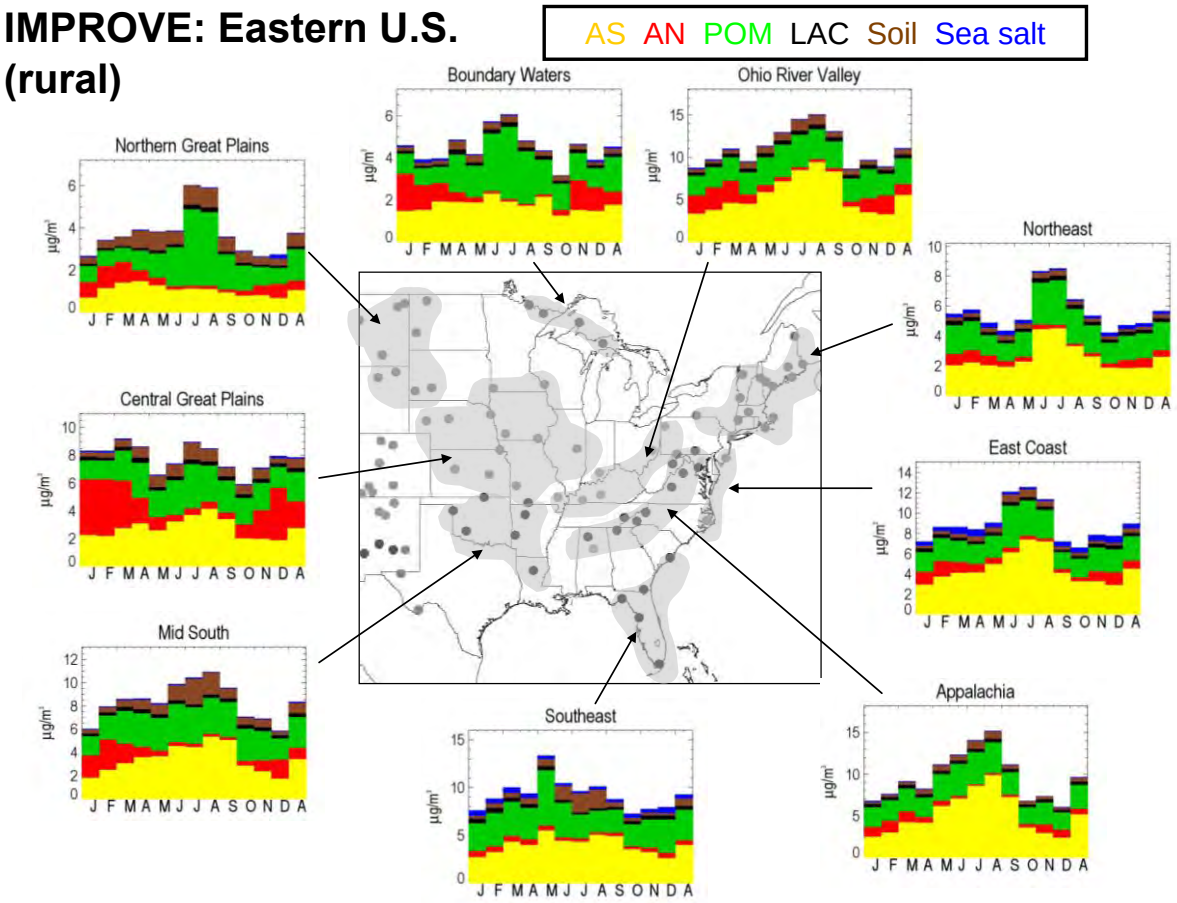

Figure 4.1.1. IMPROVE 2005–2008 regional monthly mean $PM_{2.5}$ mass concentrations (µg m^{-3}) for the eastern United States. The letters on the x-axis correspond to the month and "A" corresponds to "annual" mean. Ammonium sulfate (AS) in yellow, ammonium nitrate (AN) in red, particulate organic matter (POM) in green, light absorbing carbon (LAC) in black, soil in brown, and sea salt in blue. The shaded area corresponds to the regions that comprise the sites used in the analysis, shown as dots.

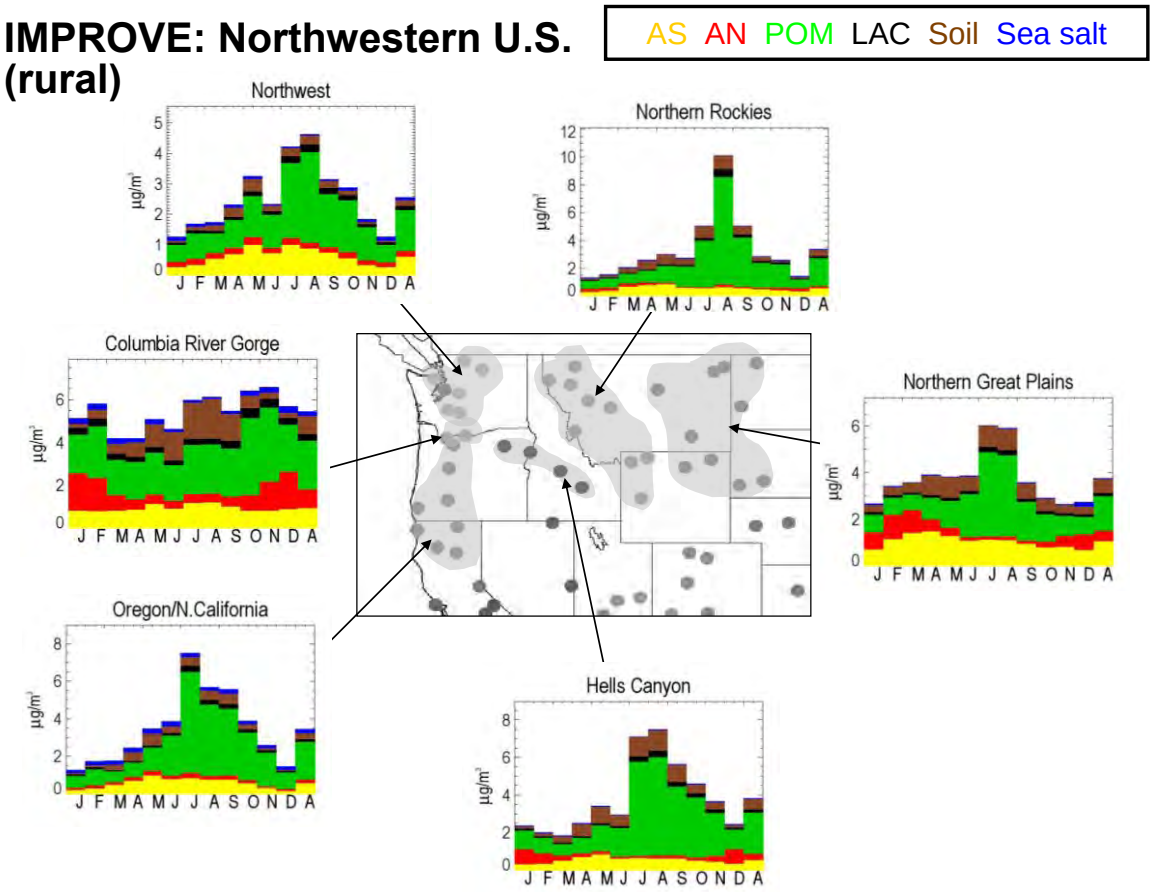

Figure 4.1.2. IMPROVE 2005–2008 regional monthly mean $PM_{2.5}$ mass concentrations (µg m^{-3}) for the northwestern United States. The letters on the x-axis correspond to the month and "A" corresponds to "annual" mean. Ammonium sulfate (AS) in yellow, ammonium nitrate (AN) in red, particulate organic matter (POM) in green, light absorbing carbon (LAC) in black, soil in brown, and sea salt in blue. The shaded area corresponds to the regions that comprise the sites used in the analysis, shown as dots.

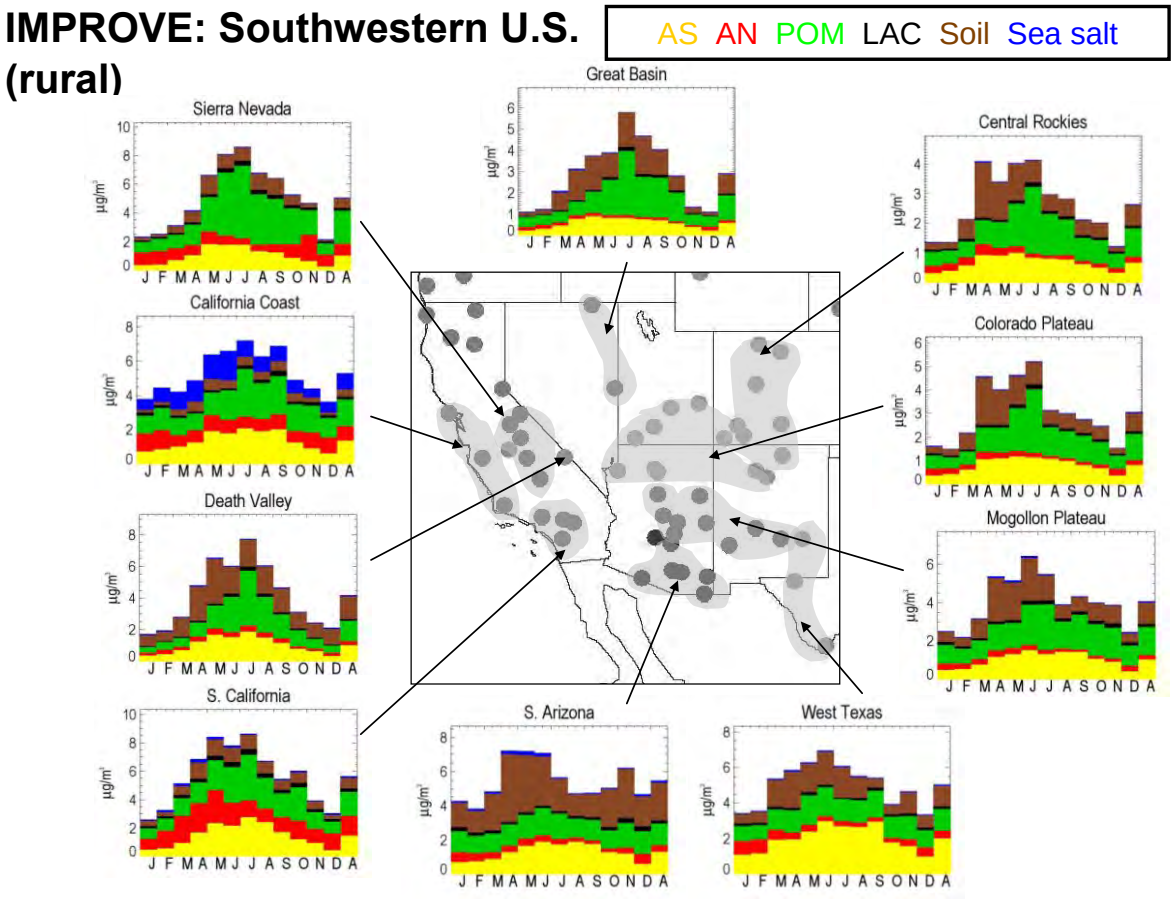

Figure 4.1.3. IMPROVE 2005–2008 regional monthly mean $PM_{2.5}$ mass concentrations (µg m^{-3}) for the southwestern United States. The letters on the x-axis correspond to the month and "A" corresponds to "annual" mean. Ammonium sulfate (AS) in yellow, ammonium nitrate (AN) in red, particulate organic matter (POM) in green, light absorbing carbon (LAC) in black, soil in brown, and sea salt in blue. The shaded area corresponds to the regions that comprise the sites used in the analysis, shown as dots.

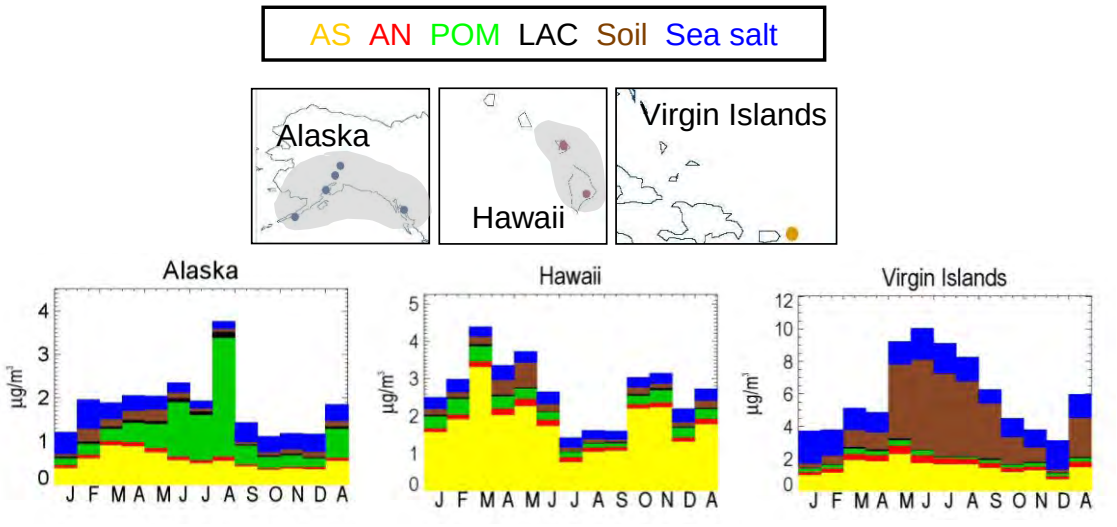

Figure 4.1.4. IMPROVE 2005–2008 regional monthly mean $PM_{2.5}$ mass concentrations (µg m^{-3}) for Hawaii, Alaska, and the Virgin Islands. The letters on the x-axis correspond to the month and "A" corresponds to "annual" mean. Ammonium sulfate (AS) in yellow, ammonium nitrate (AN) in red, particulate organic matter (POM) in green, light absorbing carbon (LAC) in black, soil in brown, and sea salt in blue. The shaded area corresponds to the regions that comprise the sites used in the analysis, shown as dots.

The seasonality of AS is summarized in Figure 4.1.5. Each region is associated with a set of triangles. The color of the upward pointing triangle refers to the season with the maximum monthly mean concentration. The color of the downward pointing triangle refers to the season with the minimum monthly mean concentration. The size of the triangle corresponds to the ratio of maximum to minimum monthly mean concentration such that large triangles represent larger degrees of seasonality. Keep in mind that the location of the triangle represents the region and may not be placed directly over a specific site location. Only three IMPROVE regions had ratios of AS monthly maximum to minimum mean concentrations less than 2, demonstrating a high degree of seasonality (Figure 4.1.5). The highest ratio was computed for the Sierra Nevada region, where the maximum was over six times greater than the minimum, compared to the lowest ratio in the Columbia River Gorge region (maximum was 1.5 times the minimum). The maximum AS mass concentrations predominantly occurred in the summer, especially in the regions in the eastern and southwestern United States and in the Southern California region. In the northwestern United States, the maximum occurred in the spring for many regions. Consistent with the bar charts presented in Figure 4.1.4, the maximum monthly mean concentrations in the OCONUS regions occurred in the spring. The minimum season for almost all regions occurred in winter; fall minimums occurred in the Boundary Waters, Baltimore, Northeast, and Alaska regions. Summer minimum occurred in Hawaii and spring minimum occurred in the Sierra Nevada region.

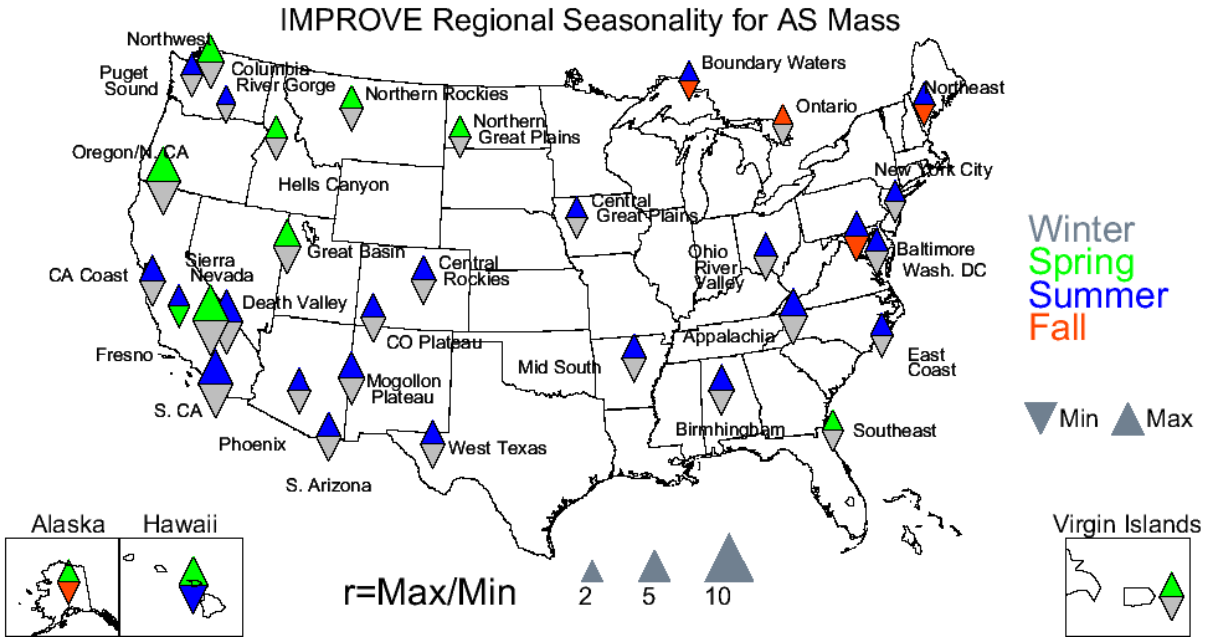

Figure 4.1.5. Seasonal variability for IMPROVE 2005–2008 monthly mean ammonium sulfate (AS) mass concentrations. The color of the upward pointing triangle refers to the season with the maximum monthly mean concentration and the downward pointing triangle refers to the season with the minimum monthly mean concentration. The size of the triangles refers to the magnitude of the ratio of maximum to minimum monthly mean mass concentration.

The CSN maximum monthly mean concentration was 10.82 μg m^{-3} in the Washington D.C./Philadelphia Corridor region in July. Similar to the IMPROVE regions, the CSN regions in the eastern United States corresponded to higher AS monthly mean concentrations that peaked typically in the summer, especially at the Ohio River Valley, Northeast, New York City, Southeast, and Mid South regions, among others (see Figure 4.1.6). The similarity in seasonal patterns of AS concentrations in the eastern United States pointed to regional sources of AS that impact urban and rural regions alike (compare Figures 4.1.1 and 4.1.6). The minimum CSN monthly mean mass concentration was 0.42 μg m^{-3} in the Northwest Nevada region in December (see Figure 4.1.7). The urban AS concentrations in the southwestern United States were lower than in the eastern United States but still peaked in summer for most regions (Figure 4.1.7). In general the southwestern urban concentrations were higher than rural concentrations (compare Figures 4.1.7 and 4.1.3). Regional AS concentrations in the northwestern United States were also lower than in the eastern United States and displayed less of a summer peak (Figure 4.1.8). Urban AS monthly mean concentrations in Alaska were higher than rural concentrations (see Figure 4.1.9) and peaked in winter with a summer minimum. Regional urban concentrations in Hawaii were similar to rural concentrations and demonstrated a similar summer minimum.

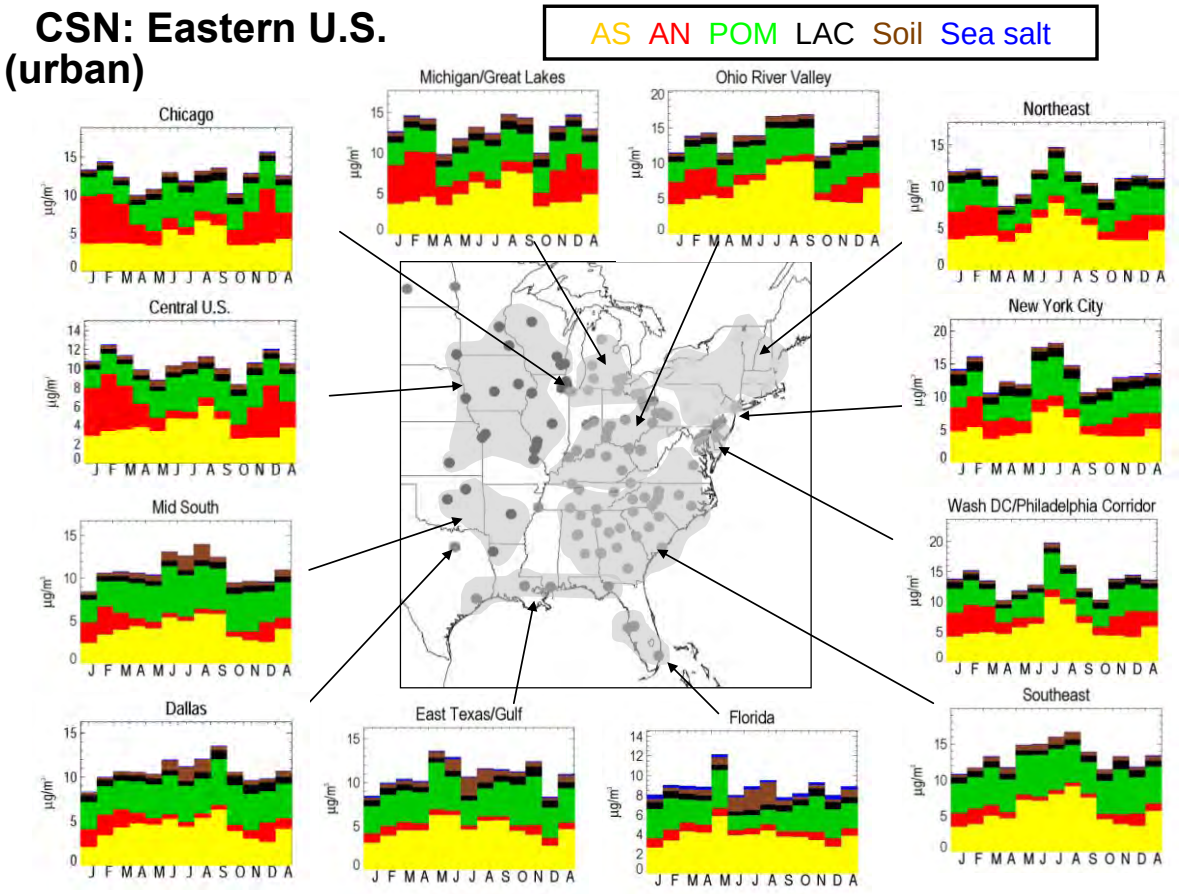

Figure 4.1.6. CSN 2005–2008 regional monthly mean $PM_{2.5}$ mass concentrations (µg m^{-3}) for the eastern United States. The letters on the x-axis correspond to the month and "A" corresponds to "annual" mean. Ammonium sulfate (AS) in yellow, ammonium nitrate (AN) in red, particulate organic matter (POM) in green, light absorbing carbon (LAC) in black, soil in brown, and sea salt in blue. The shaded area corresponds to the regions that comprise the sites used in the analysis, shown as dots.

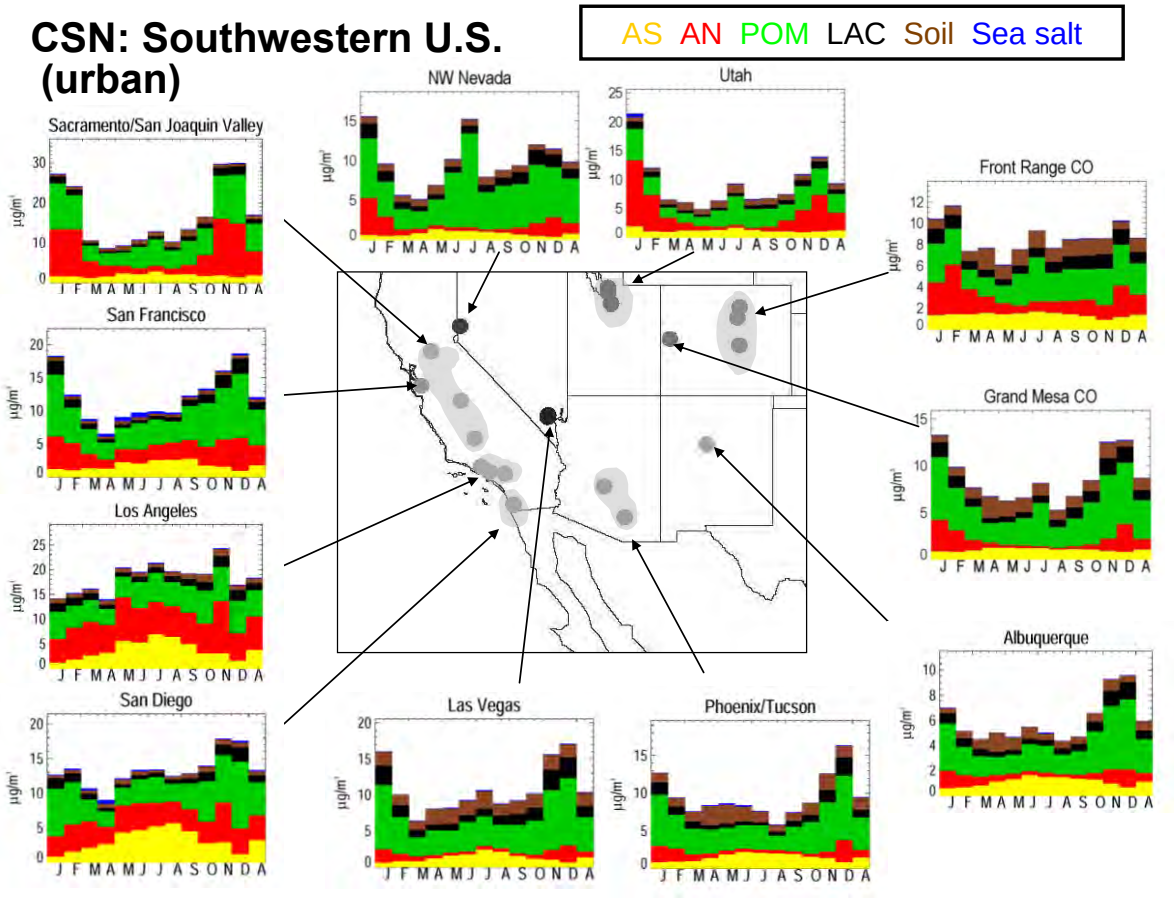

Figure 4.1.7. CSN 2005–2008 regional monthly mean $PM_{2.5}$ mass concentrations (µg m^{-3}) for the southwestern United States. The letters on the x-axis correspond to the month and "A" corresponds to "annual" mean. Ammonium sulfate (AS) in yellow, ammonium nitrate (AN) in red, particulate organic matter (POM) in green, light absorbing carbon (LAC) in black, soil in brown, and sea salt in blue. The shaded area corresponds to the regions that comprise the sites used in the analysis, shown as dots.

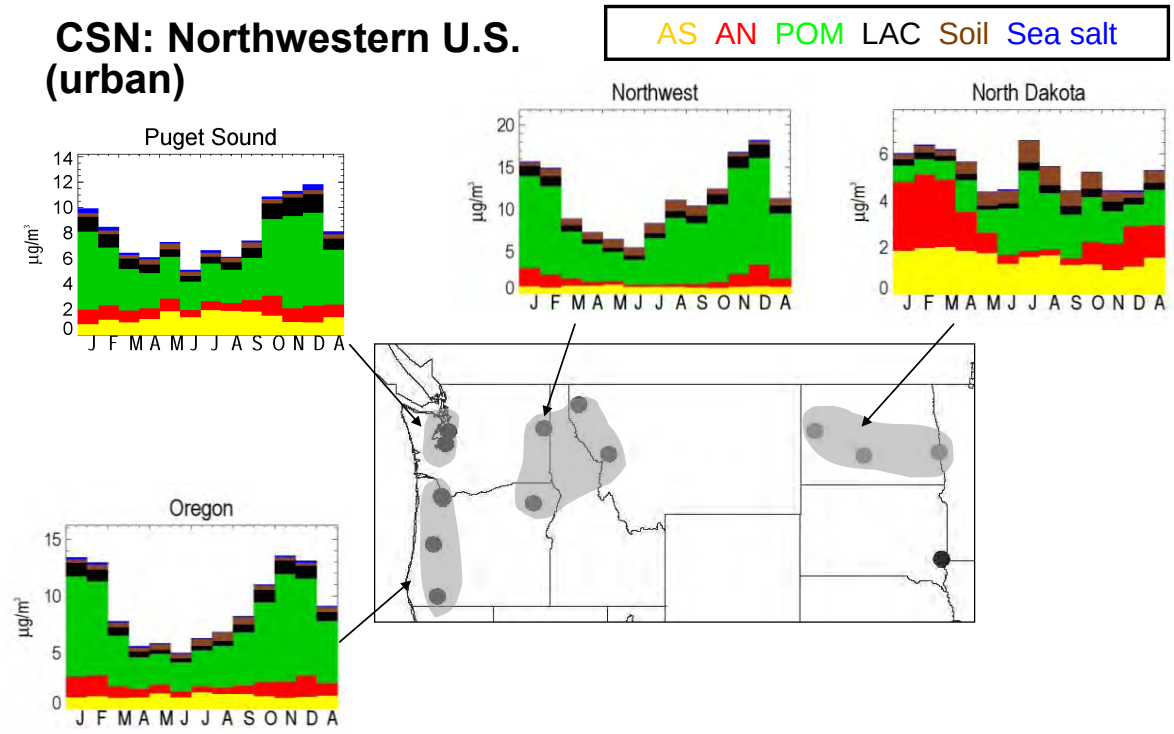

Figure 4.1.8. CSN 2005–2008 regional monthly mean $PM_{2.5}$ mass concentrations (µg m^{-3}) for the northwestern United States. The letters on the x-axis correspond to the month and "A" corresponds to "annual" mean. Ammonium sulfate (AS) in yellow, ammonium nitrate (AN) in red, particulate organic matter (POM) in green, light absorbing carbon (LAC) in black, soil in brown, and sea salt in blue. The shaded area corresponds to the regions that comprise the sites used in the analysis, shown as dots.

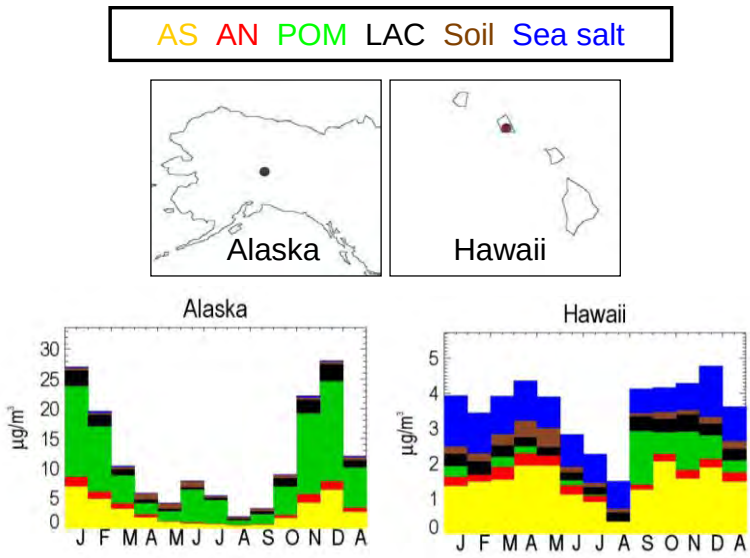

Figure 4.1.9. CSN 2005–2008 regional monthly mean $PM_{2.5}$ mass concentrations (µg m^{-3}) for Hawaii and Alaska. The letters on the x-axis correspond to the month and "A" corresponds to "annual" mean. Ammonium sulfate (AS) in yellow, ammonium nitrate (AN) in red, particulate organic matter (POM) in green, light absorbing carbon (LAC) in black, soil in brown, and sea salt in blue. The shaded area corresponds to the regions that comprise the sites used in the analysis, shown as dots.

Urban regions were somewhat less seasonal than rural regions. Six CSN regions had maximum to minimum ratios less than 2, with the highest and lowest seasonality corresponding to the Alaska (14.6) and Oregon (1.4) regions, respectively. As shown in Figure 4.1.10, there was a higher degree of seasonality in southern part of California, with a summer maximum and winter minimum. Many regions had minimums in the fall (e.g., Central U.S., North Dakota, Utah, Northwest, Oregon, and Michigan/Great Lakes). Regions in the northwestern United States had spring maxima, similar to the IMPROVE regions (see Figure 4.1.5). Spring minima occurred at the Sacramento/San Joaquin Valley, Chicago, Northeast, and New York City regions.

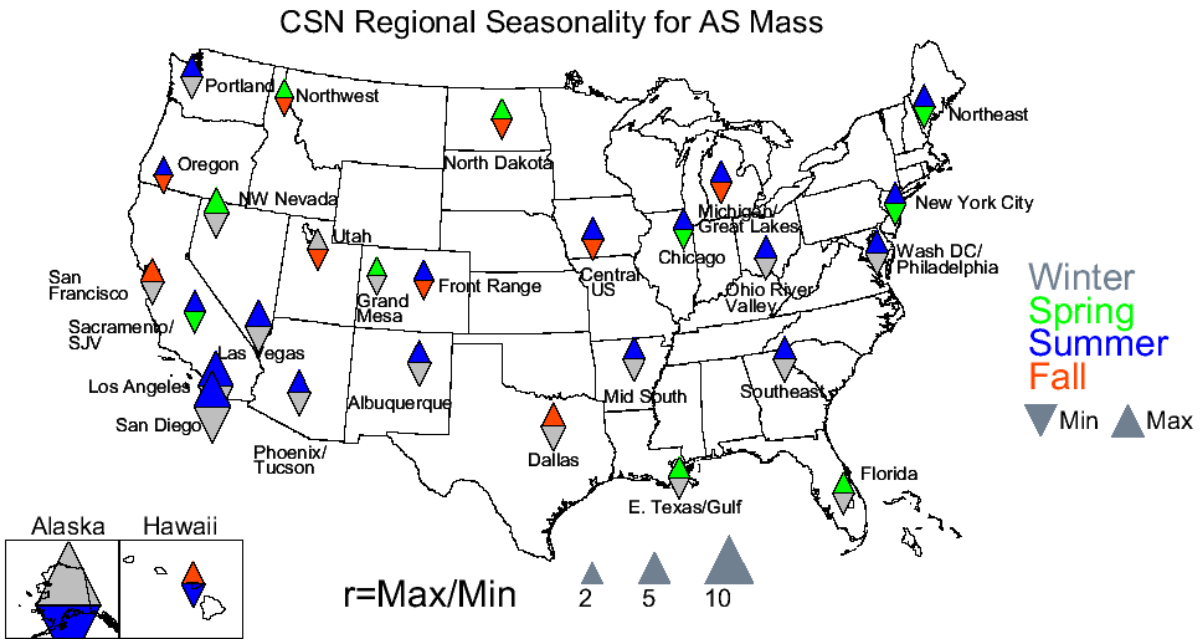

Figure 4.1.10. Seasonal variability for CSN 2005–2008 monthly mean ammonium sulfate (AS) mass concentrations. The color of the upward pointing triangle refers to the season with the maximum monthly mean concentration and the downward pointing triangle refers to the season with the minimum monthly mean concentration. The size of the triangles refers to the magnitude of the ratio of maximum to minimum monthly mean mass concentration.

IMPROVE regional percent contributions of AS to RCFM ranged from 3.9% in Phoenix in December to 75.7% in the Hawaii region in March. AS mass dominated RCFM in summer at many of the rural regions. For example, regions in the eastern United States typically had AS concentrations that contributed 40% or more to RCFM (See Figure 4.1.11) and reached up to 60% in summer (e.g., the Ohio River Valley and East Coast regions). In contrast, contributions of AS to RCFM were typically 20% or less in the northwestern United States (Figure 4.1.12) and did not demonstrate a summer mass fraction maxima; in fact, AS contributed the least to RCFM in the summer in the northwestern United States at many regions (e.g., Northern Rocky Mountains, Northern Great Plains, and Hells Canyon). In the southwestern United States (Figure 4.1.13), the contributions were somewhat higher (20–40%) and often were the highest during summer at regions such as Southern Arizona and West Texas. However, other regions in the southwestern United States, such as Death Valley and Central Rocky Mountains, corresponded to fairly flat seasonal contributions of AS to RCFM. The OCONUS region (Figure 4.1.14) demonstrated different patterns. AS was a large contributor to RCFM in the Hawaii region year round, with 60% or greater contributions and fairly flat seasonal patterns. AS contributions ranged from 20 to 50% and 20 to 40% in the Alaska and Virgin Islands regions, respectively, and peaked in spring months.

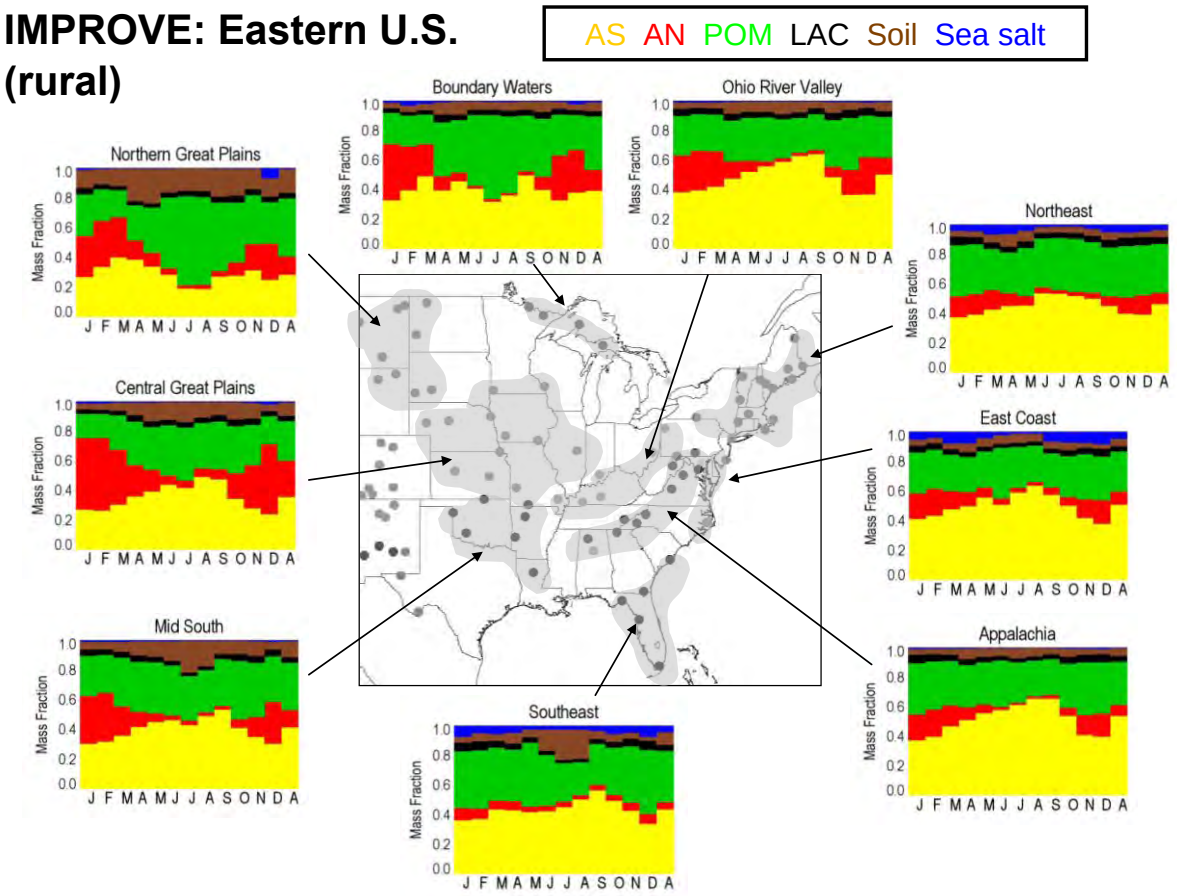

Figure 4.1.11. IMPROVE 2005–2008 regional monthly mean $PM_{2.5}$ reconstructed fine mass fractions for the eastern United States. The letters on the x-axis correspond to the month and "A" corresponds to "annual" mean. Ammonium sulfate (AS) in yellow, ammonium nitrate (AN) in red, particulate organic matter (POM) in green, light absorbing carbon (LAC) in black, soil in brown, and sea salt in blue. The shaded area corresponds to the regions that comprise the sites used in the analysis, shown as dots.

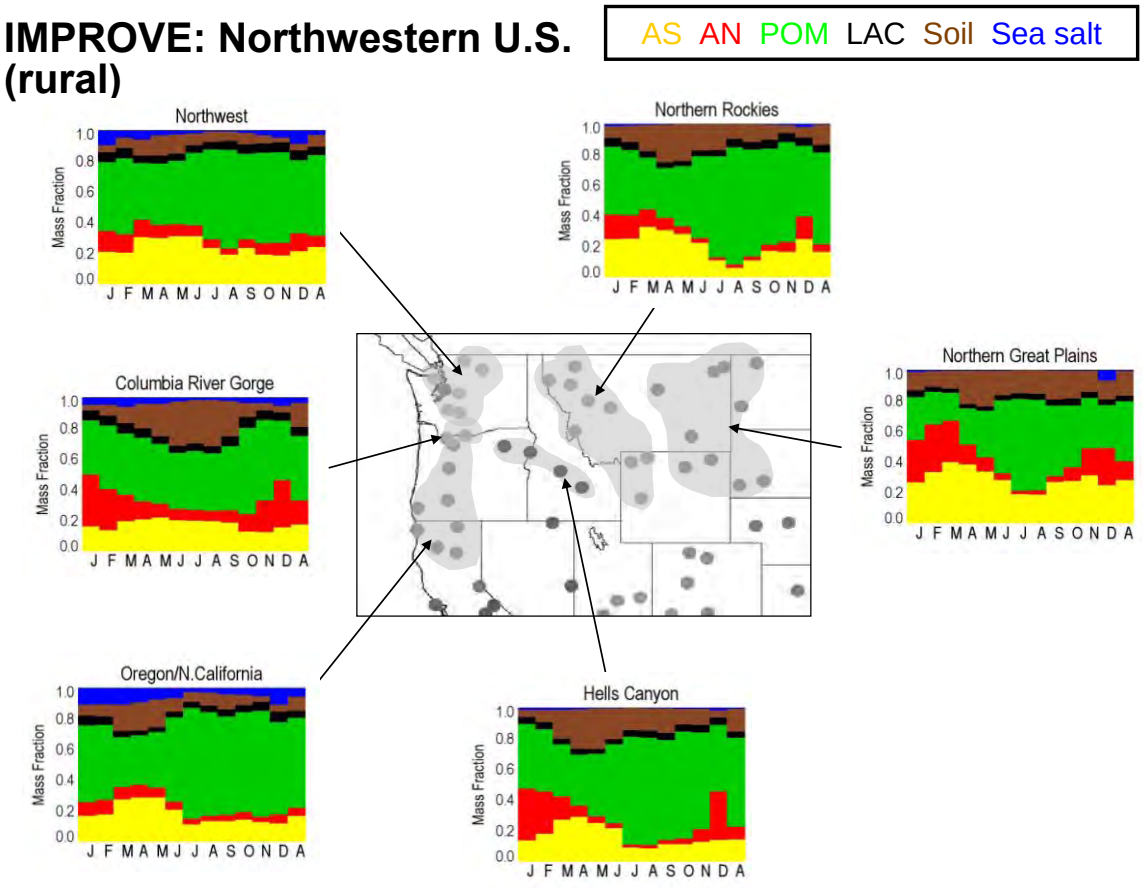

Figure 4.1.12. IMPROVE 2005–2008 regional monthly mean $PM_{2.5}$ reconstructed fine mass fractions for the northwestern United States. The letters on the x-axis correspond to the month and "A" corresponds to "annual" mean. Ammonium sulfate (AS) in yellow, ammonium nitrate (AN) in red, particulate organic matter (POM) in green, light absorbing carbon (LAC) in black, soil in brown, and sea salt in blue. The shaded area corresponds to the regions that comprise the sites used in the analysis, shown as dots.

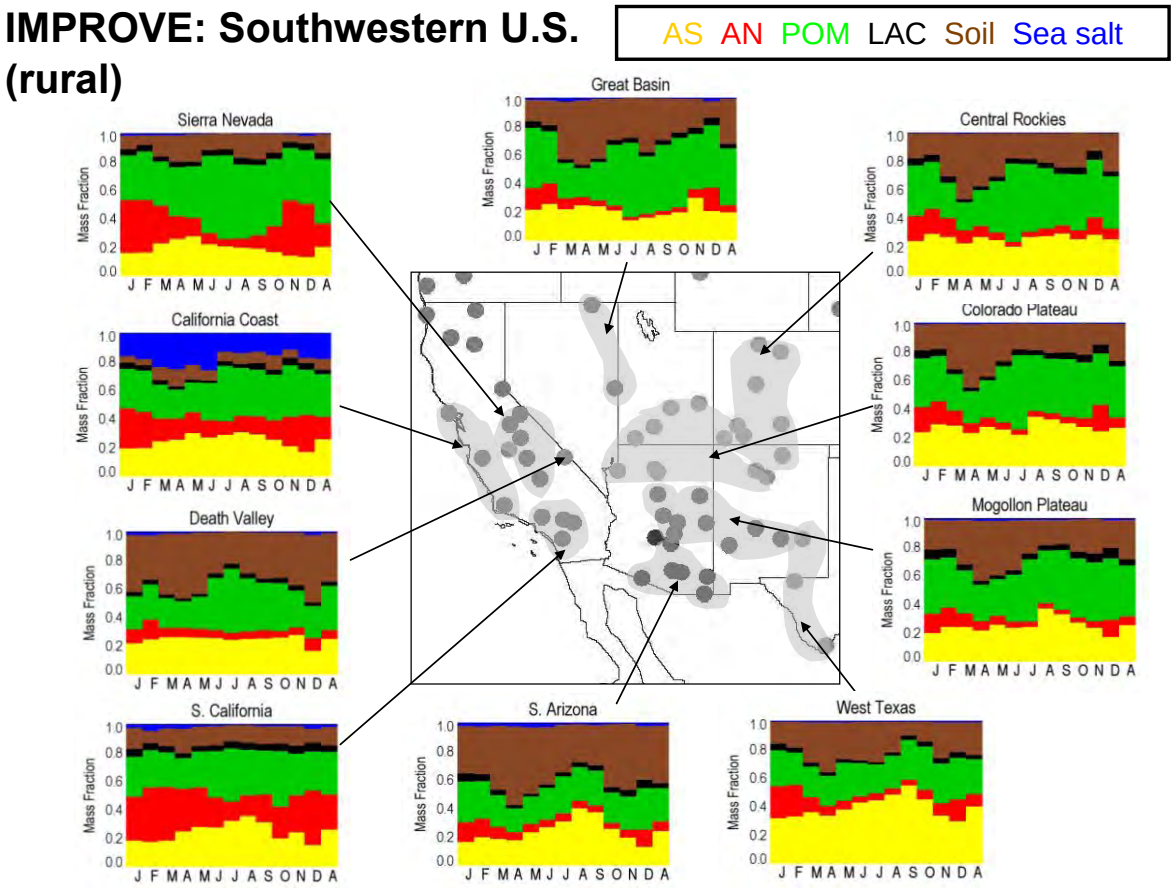

Figure 4.1.13. IMPROVE 2005–2008 regional monthly mean $PM_{2.5}$ reconstructed fine mass fractions for the southwestern United States. The letters on the x-axis correspond to the month and "A" corresponds to "annual" mean. Ammonium sulfate (AS) in yellow, ammonium nitrate (AN) in red, particulate organic matter (POM) in green, light absorbing carbon (LAC) in black, soil in brown, and sea salt in blue. The shaded area corresponds to the regions that comprise the sites used in the analysis, shown as dots.

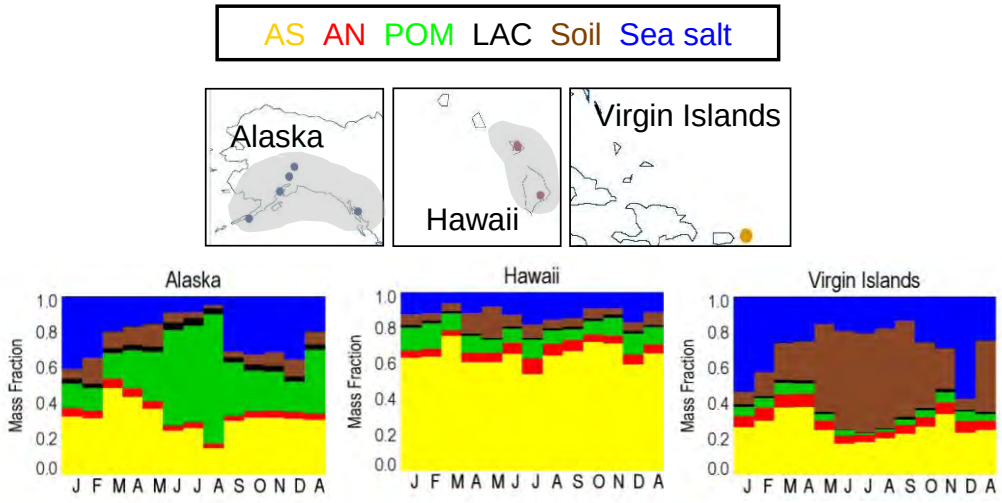

Figure 4.1.14. IMPROVE 2005–2008 regional monthly mean $PM_{2.5}$ reconstructed fine mass fractions for Hawaii, Alaska,and the Virgin Islands. The letters on the x-axis correspond to the month and "A" corresponds to "annual" mean. Ammonium sulfate (AS) in yellow, ammonium nitrate (AN) in red, particulate organic matter (POM) in green, light absorbing carbon (LAC) in black, soil in brown, and sea salt in blue. The shaded area corresponds to the regions that comprise the sites used in the analysis, shown as dots.

Almost half of all the IMPROVE regions demonstrated a small degree of seasonality in which the maximum percent contribution of AS to RCFM was less than twice the minimum percent contribution (Figure 4.1.15). The Hawaii region had the lowest ratio (1.4), suggesting that AS was a consistent contributor to fine mass year round in that region. The largest rural ratio occurred for the Northern Rocky Mountains region, where the maximum percent contribution was 5.2 times larger than the minimum percent contribution. The seasons that corresponded to maximum and minimum were different for mass fractions compared to mass concentrations (compare Figure 4.1.15 to Figure 4.1.5). For example, in the Ohio River Valley region the maximum mass fraction occurred during fall (as did the minimum) while the maximum monthly mean concentration occurred in the summer. Many regions in the southwestern United States had similar seasonality in concentration and mass fraction, such as the Phoenix site and Southern Arizona and Mogollon Plateau regions. In many regions the degree of seasonality for AS mass fractions was less than for mass concentrations (e.g., regions in California and the eastern United States).

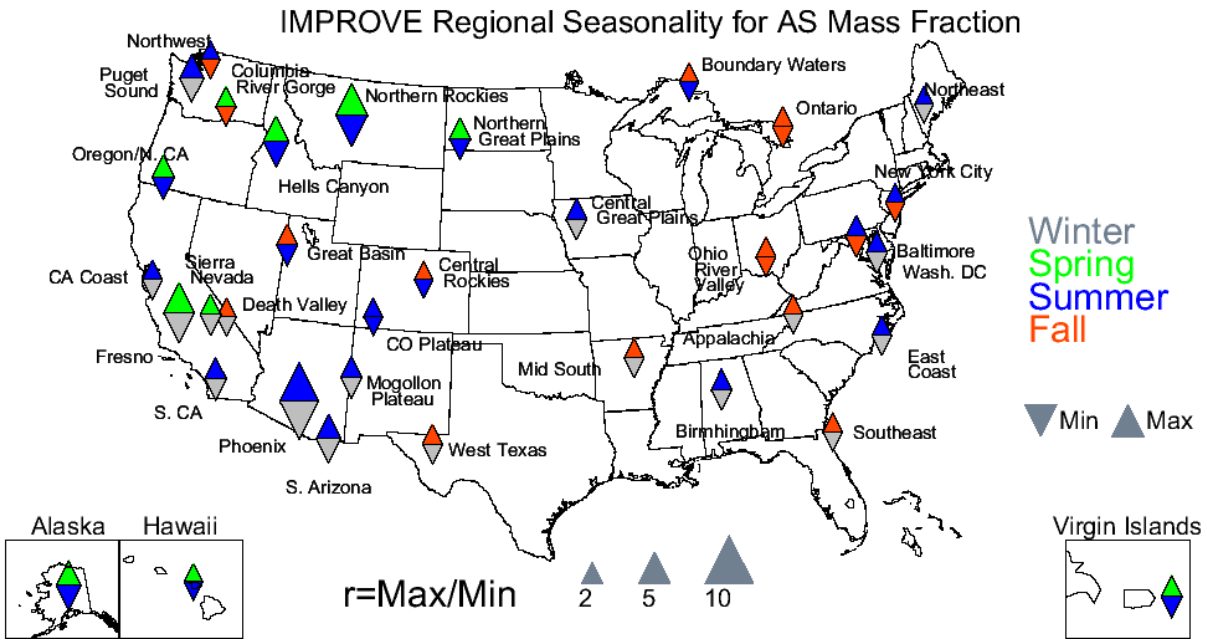

Figure 4.1.15. Seasonal variability for IMPROVE 2005–2008 monthly mean ammonium sulfate (AS) reconstructed fine mass fractions. The color of the upward pointing triangle refers to the season with the maximum monthly mean concentration and the downward pointing triangle refers to the season with the minimum monthly mean concentration. The size of the triangles refers to the magnitude of the ratio of maximum to minimum monthly mean mass concentration.

The CSN AS regional percent contribution to RCFM ranged from 3.6% in the Northwest Nevada region in December to 61.1% in the Ohio River Valley region in August. The Ohio River Valley region was typical of other regions in the eastern United States where AS typically contributed 40% or more to RCFM (see Figure 4.1.16). In the summer relative contributions of AS in many regions almost reached 60%. In contrast, regions in the northwestern United States had AS contributions that were typically 20–30% of RCFM in spring and summer (see Figure 4.1.17). The North Dakota region was the exception, with a fairly flat seasonal pattern in mass fraction. Regions in the southwestern United States exhibited low AS contributions to RCFM (less than 20–30%) and the seasonal pattern showed maxima in the summer (see Figure 4.1.18). Slightly higher contributions were observed in the Alaska region (20–40%) but with a summer minimum (Figure 4.1.19 for OCONUS regions). The Hawaii region had a fairly steady contribution of ~40% to RCFM, with a notable decrease in August.

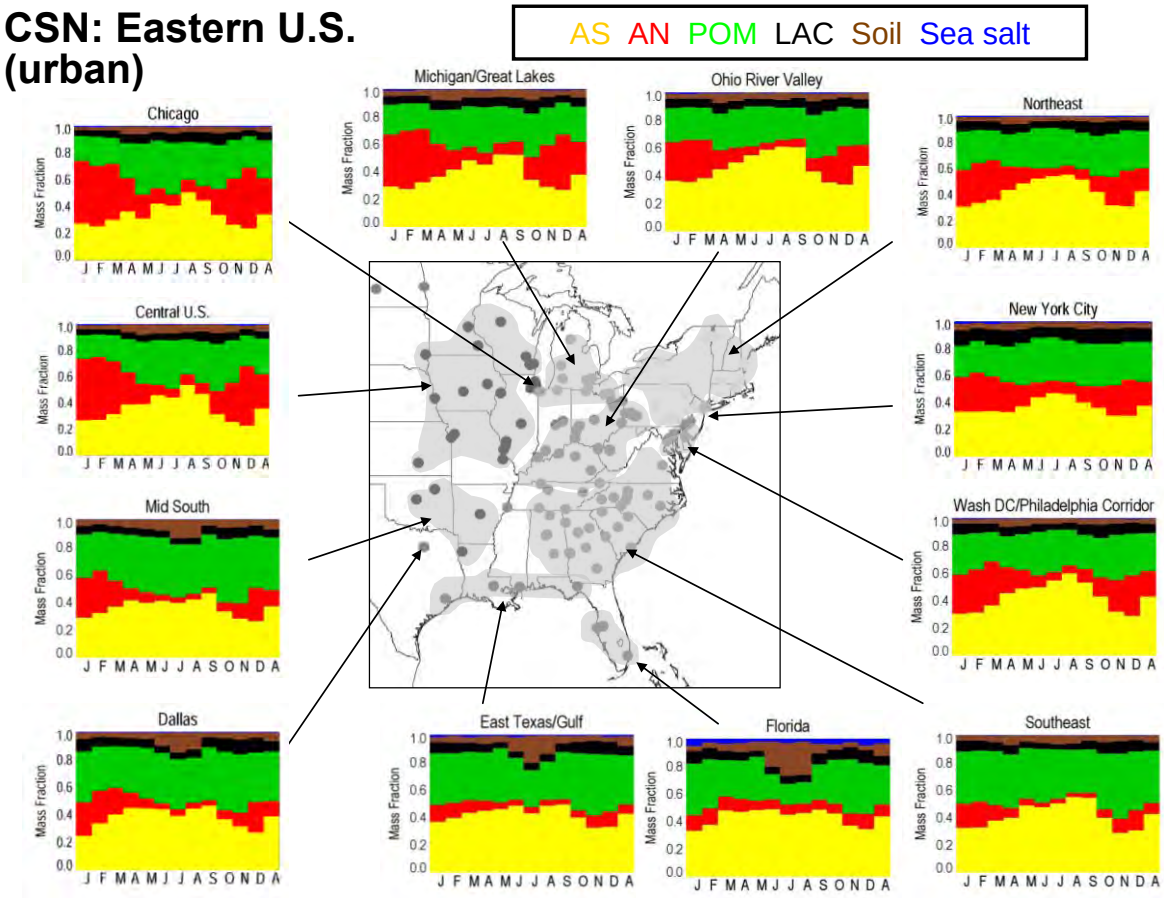

Figure 4.1.16. CSN 2005–2008 regional monthly mean $PM_{2.5}$ reconstructed fine mass fractions for the eastern United States. The letters on the x-axis correspond to the month and "A" corresponds to "annual" mean. Ammonium sulfate (AS) in yellow, ammonium nitrate (AN) in red, particulate organic matter (POM) in green, light absorbing carbon (LAC) in black, soil in brown, and sea salt in blue. The shaded area corresponds to the regions that comprise the sites used in the analysis, shown as dots.

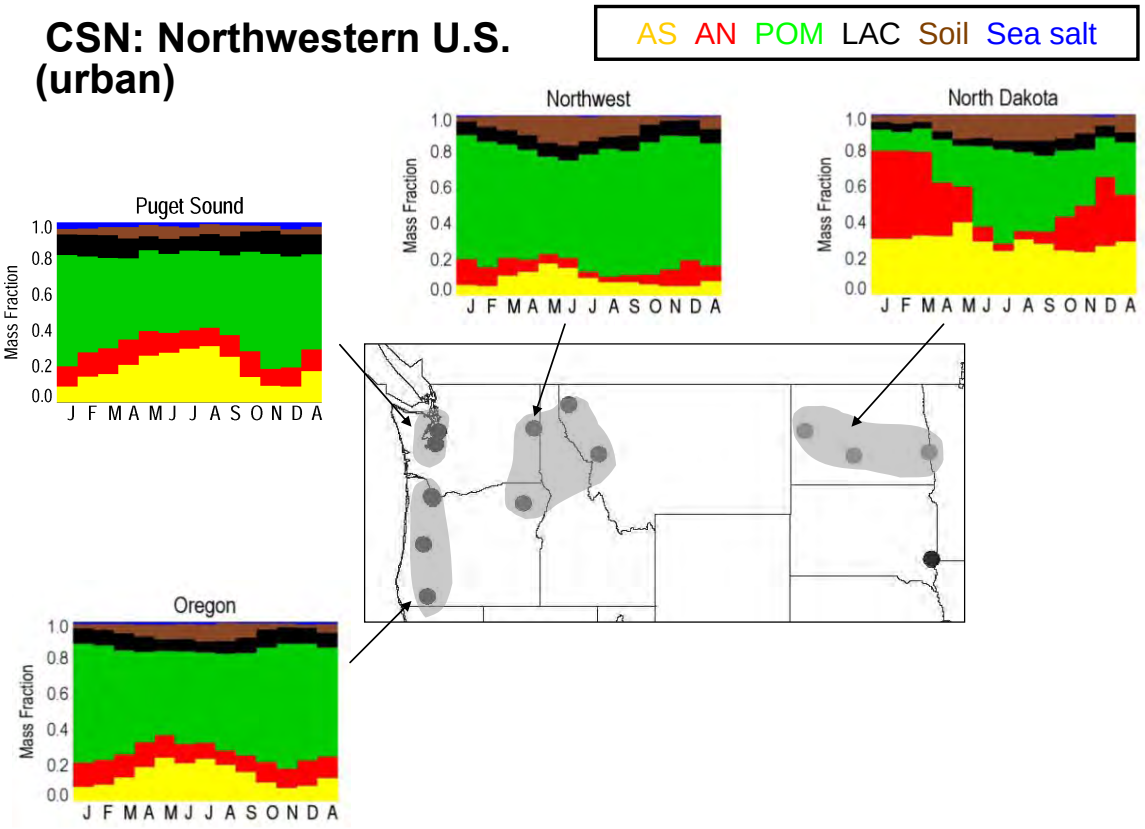

Figure 4.1.17. CSN 2005–2008 regional monthly mean $PM_{2.5}$ reconstructed fine mass fractions for the northwestern United States. The letters on the x-axis correspond to the month and "A" corresponds to "annual" mean. Ammonium sulfate (AS) in yellow, ammonium nitrate (AN) in red, particulate organic matter (POM) in green, light absorbing carbon (LAC) in black, soil in brown, and sea salt in blue. The shaded area corresponds to the regions that comprise the sites used in the analysis, shown as dots.

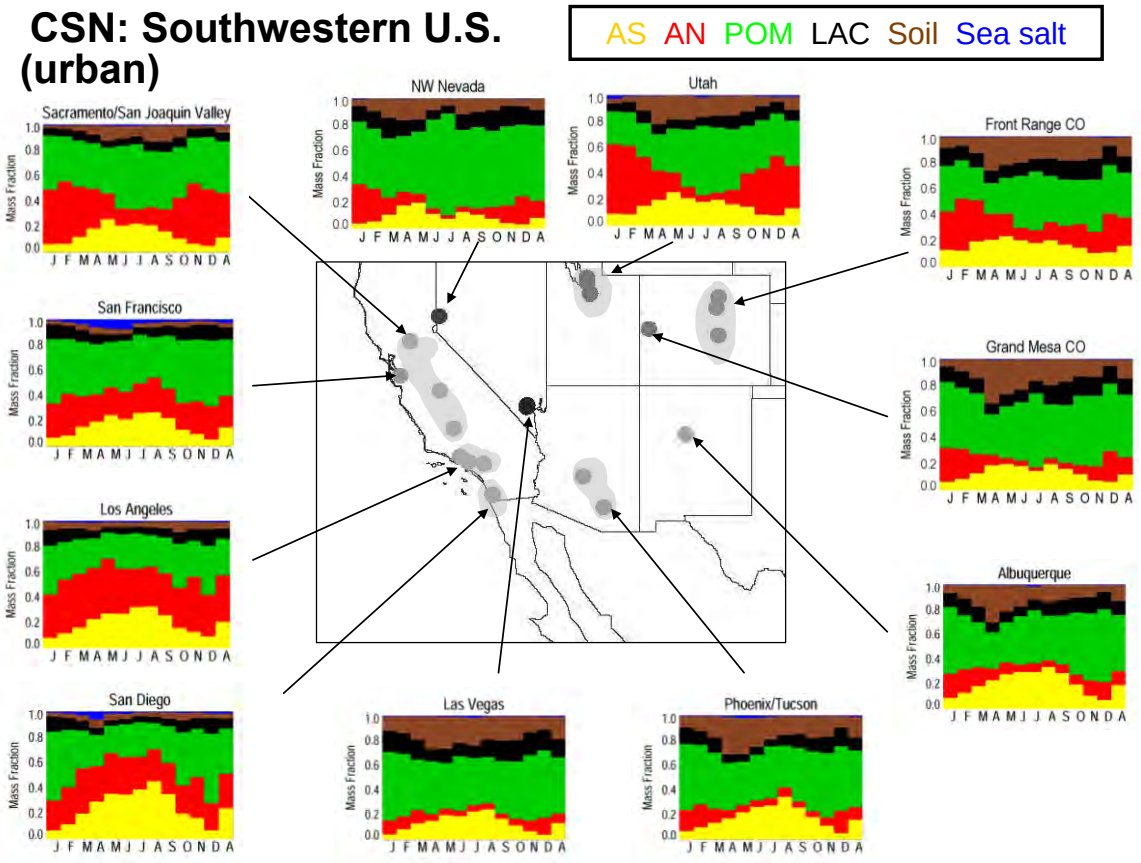

Figure 4.1.18. CSN 2005–2008 regional monthly mean $PM_{2.5}$ reconstructed fine mass fractions for the southwestern United States. The letters on the x-axis correspond to the month and "A" corresponds to "annual" mean. Ammonium sulfate (AS) in yellow, ammonium nitrate (AN) in red, particulate organic matter (POM) in green, light absorbing carbon (LAC) in black, soil in brown, and sea salt in blue. The shaded area corresponds to the regions that comprise the sites used in the analysis, shown as dots.

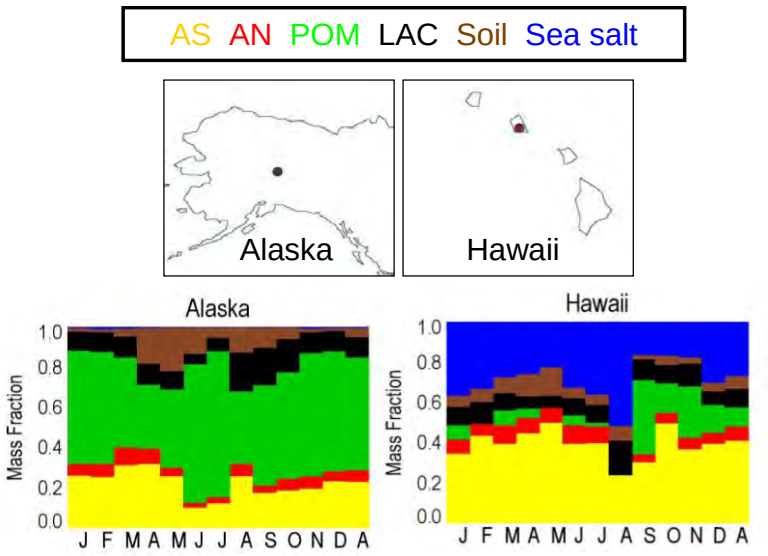

Figure 4.1.19. CSN 2005–2008 regional monthly mean $PM_{2.5}$ reconstructed fine mass fractions for Hawaii and Alaska. The letters on the x-axis correspond to the month and "A" corresponds to "annual" mean. Ammonium sulfate (AS) in yellow, ammonium nitrate (AN) in red, particulate organic matter (POM) in green, light absorbing carbon (LAC) in black, soil in brown, and sea salt in blue. The shaded area corresponds to the regions that comprise the sites used in the analysis, shown as dots.

In contrast to the IMPROVE regions, the seasonality in the CSN mass fraction of AS was actually greater than the seasonality in AS concentration for many regions in the western United States (see Figure 4.1.20). For example, Albuquerque, Phoenix/Tucson, and regions in California had many similar seasons for the maxima and minima in mass fractions compared to concentrations, but the degree of seasonality was greater for the relative contribution (compare Figure 4.1.10 and 4.1.20). Regions in the eastern United States depicted a different scenario, with many regions having lower seasonality in mass fractions compared to concentration and with different seasons corresponding to maxima and minima as well (e.g., the Mid South and Southeast). This lower degree of seasonality for AS mass fractions in the eastern United States suggested AS was a steady contributor to RCFM year round. The seasonality in relative contribution ranged from 1.5 in the East Texas/Gulf region to 6.7 in San Diego.

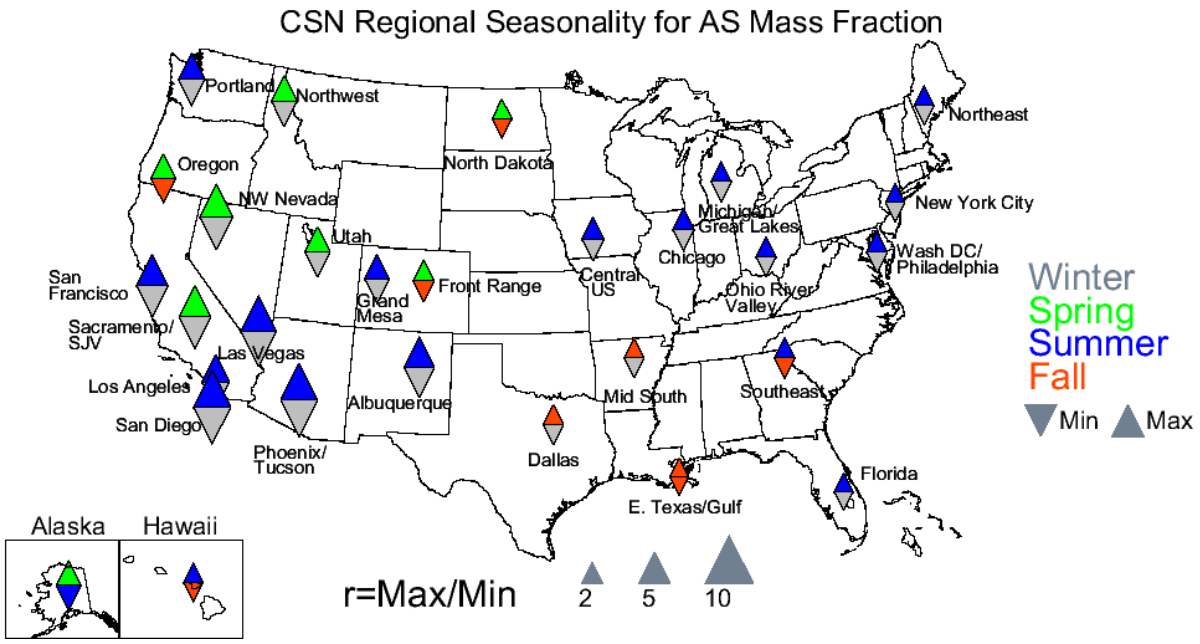

Figure 4.1.20. Seasonal variability for CSN 2005–2008 monthly mean ammonium sulfate (AS) reconstructed fine mass fractions. The color of the upward pointing triangle refers to the season with the maximum monthly mean concentration and the downward pointing triangle refers to the season with the minimum monthly mean concentration. The size of the triangles refers to the magnitude of the ratio of maximum to minimum monthly mean mass concentration.

4.2 $PM_{2.5}$ AMMONIUM NITRATE MASS CONCENTRATIONS

The IMPROVE 2005–2008 regional maximum monthly mean ammonium nitrate (AN) mass concentration (16.19 μg m^{-3}) corresponded to the urban site of Fresno in November and was four times larger than the highest nonurban region (4.08 μg m^{-3}) of the Central Great Plains region in February. A minimum concentration of 0.04 μg m^{-3} was observed in Alaska in October. In regions in the eastern United States, the concentrations were relatively low (see the earlier bar chart in Figure 4.1.1). As one moves west from the east coast, the AN concentrations increased, especially in winter. Other regions of high AN concentrations occurred in the Southern California region in the southwestern United States (see Figure 4.1.3). Concentrations were fairly steady year round in this region. The California Coast and Sierra Nevada regions also corresponded to higher AN concentrations. However, other regions in the southwestern United States had lower concentrations, such as the Colorado Plateau and Mogollon Plateau regions. In the northwestern United States, the Columbia River Gorge and Northern Great Plains regions corresponded to relatively higher concentrations, especially in winter (see Figure 4.1.2). Other regions, such as the Northern Rocky Mountains, had very low concentrations. OCONUS regions all had very low concentrations year round (Figure 4.1.4).

As evidenced from the data presented in these figures, AN concentrations were typically higher in winter due to more favorable conditions of nitrate particle formation in that season. The winter maxima at most regions were very obvious from the depiction of seasonality in Figure 4.2.1. Most of the regions had high seasonality, with only three regions having maximum to minimum ratios less than 2. The maximum ratio was computed for the Boundary Waters region (20.0) and the minimum at the California Coast region (1.7). Several regions in the southwestern

United States had fall minima (e.g., Phoenix, Southern Arizona, and West Texas), and many regions had spring maxima (e.g., Central Rocky Mountains, Colorado Plateau, Mogollon Plateau, Southern California, and Death Valley). Many regions in California had fall maxima and summer minima. In the northwestern United States, most regions corresponded to maxima and minima that occurred in winter and summer, respectively. OCONUS regions had low seasonality. Hawaii and Alaska had spring maxima and fall minima, while the Virgin Islands had a spring maximum and a winter minimum.

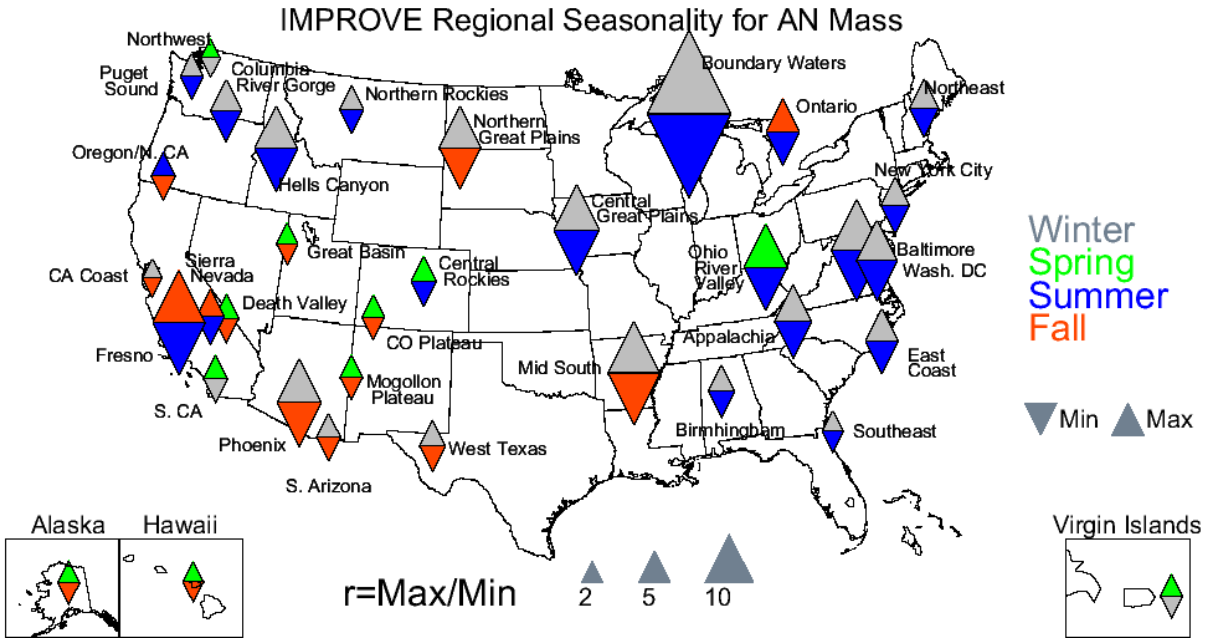

Figure 4.2.1. Seasonal variability for IMPROVE 2005–2008 monthly mean ammonium nitrate (AN) mass concentrations. The color of the upward pointing triangle refers to the season with the maximum monthly mean concentration and the downward pointing triangle refers to the season with the minimum monthly mean concentration. The size of the triangles refers to the magnitude of the ratio of maximum to minimum monthly mean mass concentration.

The maximum CSN monthly mean concentration (14.09 μg m^{-3}) occurred at the Sacramento/San Joaquin Valley region in November. Several regions in the southwestern United States had high AN concentrations, especially compared to IMPROVE regions in this same area (see Figure 4.1.7). Many of the regions in this section showed pronounced winter maxima (e.g., Utah, Sacramento/San Joaquin Valley, and the Front Range CO and Grand Mesa CO regions), while in the southern part of California several regions had fairly flat seasonal AN concentrations. In the northwestern United States, the concentrations decreased but still showed winter maxima, especially in the North Dakota, Northwest, and Oregon regions (Figure 4.1.8). Many regions in the eastern United States had high AN concentrations, especially compared to IMPROVE regions. Winter maxima were obvious at the Chicago, Central U.S., Michigan/Great Lakes, and other regions (Figure 4.1.6). Other regions, such as East Texas/Gulf and Florida, had relatively low concentrations that were fairly flat across all months. The AN concentrations at the Alaska and Hawaii regions were also fairly low and relatively flat year round (Figure 4.1.9). In fact, the minimum regional monthly mean AN concentration occurred at the Alaska region in August (0.11 μg m^{-3}).

CSN regions demonstrated a strong seasonality in AN mass concentrations, with only one region having a maximum to minimum ratio less than or equal to 2 (Florida, 2.0) (see Figure 4.2.2). The largest seasonality was observed in the Utah region (max/min = 32.6). The maximum monthly mean AN concentration occurred in winter for the majority of regions. More urban regions corresponded to winter maxima compared to the IMPROVE regions and were subject to a higher degree of seasonality. Regions in the western United States had a higher seasonality than in the eastern United States, especially in Colorado, Utah, and Nevada. Many regions had minimum concentrations in the fall (e.g., Las Vegas, Phoenix/Tucson, Mid South, East Texas/Gulf, Florida, New York City, and Hawaii).

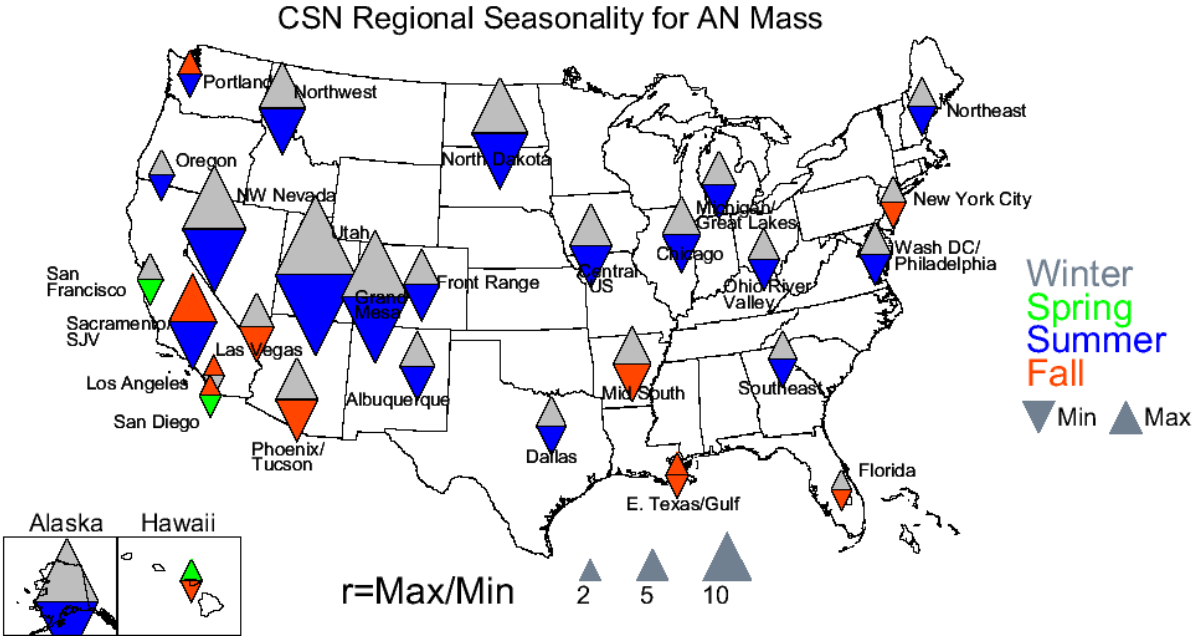

Figure 4.2.2. Seasonal variability for CSN 2005–2008 monthly mean ammonium nitrate (AN) mass concentrations. The color of the upward pointing triangle refers to the season with the maximum monthly mean concentration and the downward pointing triangle refers to the season with the minimum monthly mean concentration. The size of the triangles refers to the magnitude of the ratio of maximum to minimum monthly mean mass concentration.

Rural IMPROVE mass fractions for AN ranged from 1.5% in the Appalachia region in July to 49.1% in the Central Great Plains region in February, similar to the maximum urban IMPROVE site in Fresno in November (50.4%). Many IMPROVE regions on the eastern coast corresponded to fairly low relative contributions (~20% or less), and this contribution was largest in winter when the AS contributions were lower (see Figure 4.1.11). Moving west, the AN mass fraction increased up to 50% in the Central Great Plains region in winter. Other regions, such as Boundary Waters, Northern Great Plains, Mid South, and Ohio River Valley, corresponded to higher contributions compared to coastal regions. These spatial patterns were probably due to the proximity to sources as well as a decrease in AS as the dominant contributor to RCFM. A few regions in the northwestern United States (Figure 4.1.12) also corresponded to considerable AN contributions to RCFM, especially at the Northern Great Plains, Columbia River Gorge, and Hells Canyon regions. Farther west, the contributions of AN decreased, with the exception of the Columbia River Gorge region. In contrast, many regions in the southwestern United States, especially in California, showed considerable AN contributions in winter (4.1.13), such as the

Southern California, Sierra Nevada, and California Coast regions. Regions in Nevada and the Four Corners area tended toward lower AN contributions but still demonstrated winter maxima. The West Texas region had slightly higher contributions. Contributions were low (less than 10%) in the OCONUS region year round (Figure 4.1.14).

As was suggested by the preceding discussion, significant seasonality in AN contributions was observed at IMPROVE regions around the United States (Figure 4.2.3). Only two sites had a ratio of maximum to minimum percent contribution less than 2 (Virgin Islands and Puget Sound). The maximum ratio occurred in the Boundary Waters region (21.0) compared to the minimum in Puget Sound (1.8). Most of the regions had higher AN contributions in winter and lower contributions in summer, following the seasonal pattern of AN concentrations and the formation mechanisms that favor AN formation in winter. Two sites in the eastern United States, Baltimore and Washington, D.C., had spring maxima, and several regions in the western United States corresponded to fall minima. Some California regions had fall maxima and summer minima. The lowest seasonality occurred for regions in the southwestern and northwestern United States.

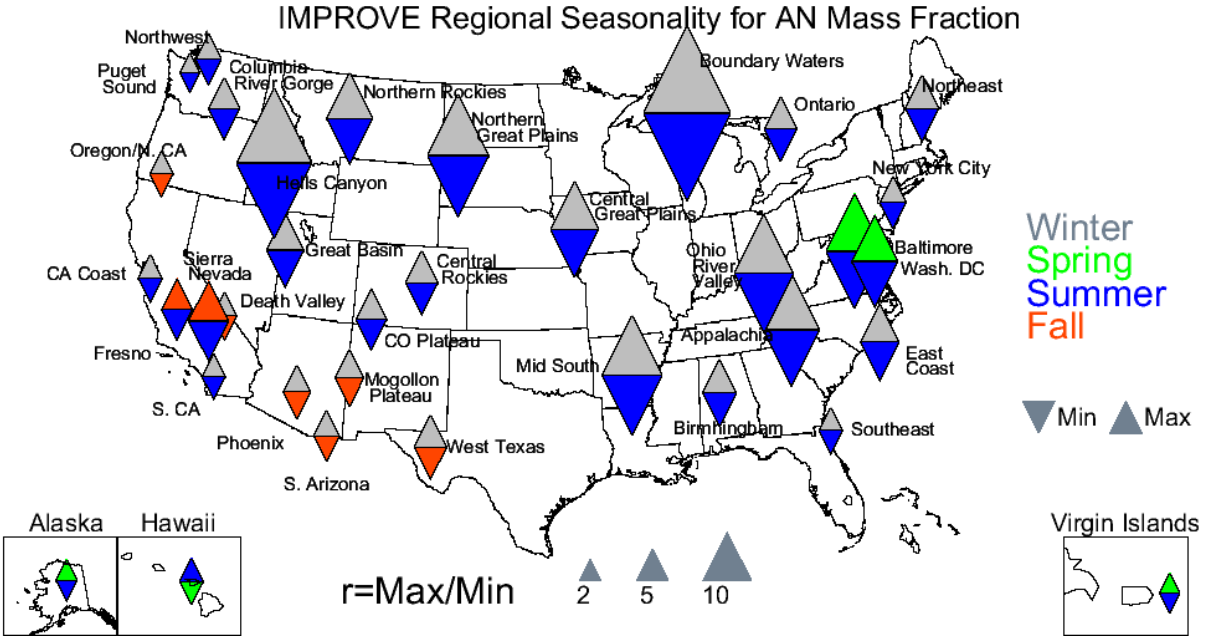

Figure 4.2.3. Seasonal variability for IMPROVE 2005–2008 monthly mean ammonium nitrate (AN) reconstructed fine mass fractions. The color of the upward pointing triangle refers to the season with the maximum monthly mean concentration and the downward pointing triangle refers to the season with the minimum monthly mean concentration. The size of the triangles refers to the magnitude of the ratio of maximum to minimum monthly mean mass concentration.

CSN regional monthly mean AN percent contributions to RCFM ranged from 2.7% in Alaska in June to 53.4% in Utah in January. The southwestern United States included regions with very different seasonal patterns (Figure 4.1.18). For example, the Utah region corresponded to large contributions of AN to RCFM in winter, similar to most regions in Colorado, New Mexico, Arizona, and Nevada but at lower magnitudes. In contrast, regions in the southern part of California corresponded to significant but fairly flat seasonal contributions. At the regions in the northwestern United States, the contributions were fairly flat, except at North Dakota, where

a strong winter maximum and high contributions were observed (Figure 4.1.17). In the eastern United States, AN contributions ranged up to 40% at some regions (Chicago, Central U.S., Michigan/Great Lakes) with strong winter maxima (Figure 4.1.16). Toward the eastern coast, the magnitude of the relative contribution decreased, especially at southern regions like the East Texas/Gulf and Florida regions. This general pattern was also observed with the IMPROVE data. AN contributions at the Hawaii and Alaska regions were also low (~10% or less) and fairly flat seasonally (Figure 4.1.19).

A somewhat higher number of CSN regions demonstrated low seasonality in AN mass fractions compared to the rural regions (six compared to two). The highest ratio corresponded to North Dakota (12.5) compared to the minimum at Los Angeles (1.4), consistent with the monthly mean mass fractions shown in Figure 4.1.18. All of the regions with percent contribution ratios less than 2, with the exception of Florida, corresponded to the western coast (Figure 4.2.4). Most regions corresponded to winter maxima and summer minima, with the exception of several regions with fall minima (Dallas, East Texas/Gulf, Phoenix/Tucson, San Francisco, and Puget Sound). San Diego and Washington D.C./Philadelphia Corridor were the only regions with spring maxima. Overall, regions in the western and central United States had higher seasonality than regions in the eastern United States.

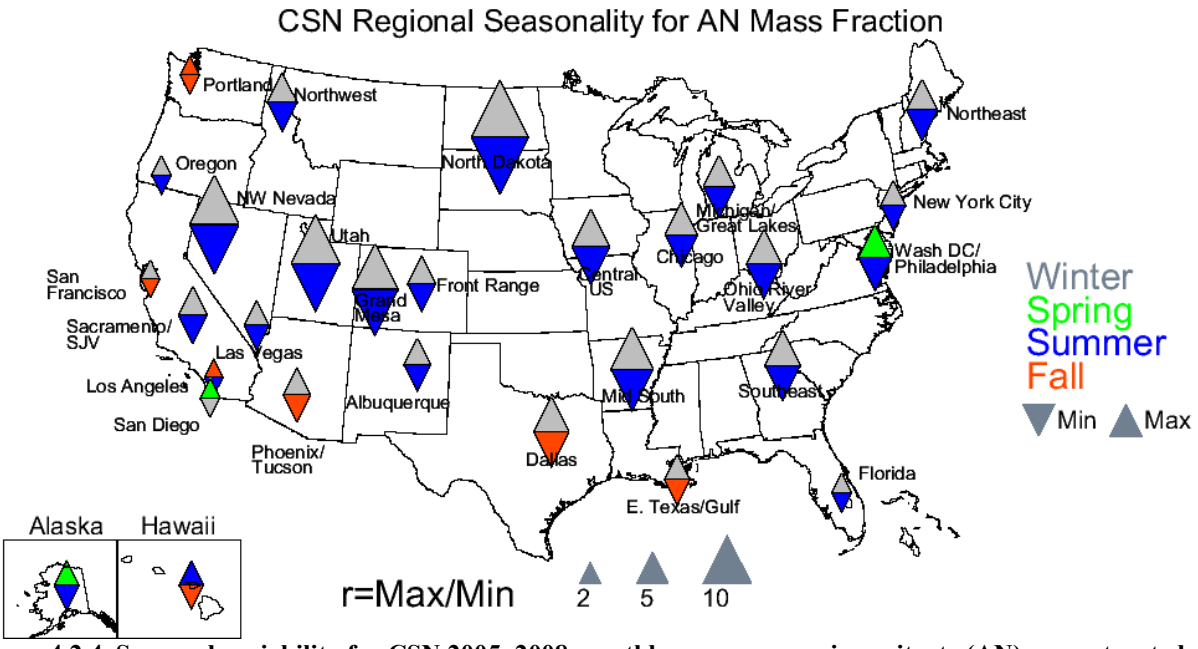

Figure 4.2.4. Seasonal variability for CSN 2005–2008 monthly mean ammonium nitrate (AN) reconstructed fine mass fractions. The color of the upward pointing triangle refers to the season with the maximum monthly mean concentration and the downward pointing triangle refers to the season with the minimum monthly mean concentration. The size of the triangles refers to the magnitude of the ratio of maximum to minimum monthly mean mass concentration.

4.3 $PM_{2.5}$ PARTICULATE ORGANIC MATTER MASS CONCENTRATIONS

IMPROVE 2005–2008 regional monthly mean particulate organic matter (POM) concentrations ranged from 0.08 μg m^{-3} at Virgin Islands in July to 13.02 μg m^{-3} in the urban location of Fresno in December. The maximum nonurban POM concentration was 7.72 μg m^{-3} in

the Northern Rocky Mountains region in August. Most of the regions in the northwestern United States corresponded to significant POM concentrations, especially in summer (e.g., Northern Rocky Mountains, Northwest, Northern Great Plains, Hells Canyon, and Oregon/Northern California, see Figure 4.1.2), most likely associated with biomass burning emissions. More northerly regions in the southwestern United States had similar patterns (e.g., Great Basin and Sierra Nevada), but the magnitude of the concentrations and degree of seasonality decreased moving south (e.g., Southern Arizona and West Texas) (see Figure 4.1.3). For most regions in the eastern United States, POM concentrations were comparable to AS, particularly in non-summer months (e.g., Ohio River Valley, Northeast, East Coast, Appalachia, and Southeast, see Figure 4.1.1). POM monthly mean concentrations were higher in Alaska and peaked in summer, but were relatively low in the Hawaii and Virgin Island regions (Figure 4.1.4).

Most of the IMPROVE regions demonstrated a high level of seasonality with only 6 regions having ratios of maximum to minimum mass concentrations less than 2 (Figure 4.3.1). The largest ratio occurred in the Alaska region (16.9) and the lowest ratio occurred in the Southern Arizona region (1.6). The western United States corresponded to much higher seasonality in POM concentrations compared to the eastern United States, probably because of the impacts from biomass burning in summer. Most western regions had summer maxima and winter minima, with the exception of the urban sites of Fresno, Phoenix, and Puget Sound, all of which had winter maxima. A few regions had spring minima, such as California Coast, Fresno, Oregon and Northern California, Hells Canyon, and Northern Great Plains. In the eastern United States the maxima predominantly occurred in summer, but minima occurred during all seasons. Maximum and minimum both occurred during fall months in Baltimore.

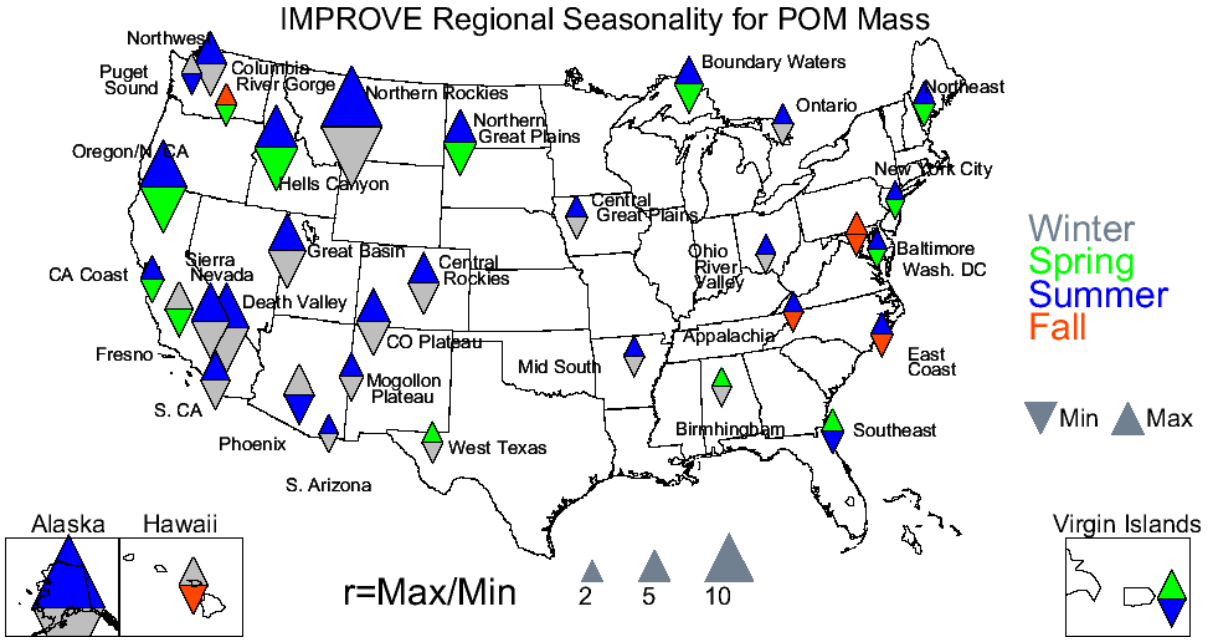

Figure 4.3.1. Seasonal variability for IMPROVE 2005–2008 monthly mean particulate organic matter (POM) mass concentrations. The color of the upward pointing triangle refers to the season with the maximum monthly mean concentration and the downward pointing triangle refers to the season with the minimum monthly mean concentration. The size of the triangles refers to the magnitude of the ratio of maximum to minimum monthly mean mass concentration.

The CSN POM regional monthly mean mass concentrations ranged from 0.66 μg m^{-3} in the North Dakota region in February to 16.74 μg m^{-3} in the Alaska region in December. Eastern regions had comparable POM mass concentrations that were generally seasonally flat (Figure 4.1.6) and comparable in magnitude to AS concentrations, especially in non-summer months. In contrast, POM concentrations were much higher in the northwestern United States (Figure 4.1.8), especially in winter (with the exception of North Dakota). In the Northwest region POM concentrations were much higher than AS concentrations; similar patterns occurred in the Puget Sound and Oregon regions as well. POM concentrations were also larger than AS concentrations in the southwestern United States (Figure 4.1.7). In regions such as Northwest Nevada, Las Vegas, Front Range CO, and others, the POM concentrations were considerably higher than AS concentrations and tended to peak in winter. High POM concentrations were also observed in the Alaska region (Figure 4.1.9), especially in winter. In contrast, concentrations were low in Hawaii although they increased during the fall and early winter.

The seasonality of POM monthly mean concentrations was much different for urban CSN regions compared to rural IMPROVE regions. Lower seasonality was observed in general (eight CSN regions maximum to minimum ratios less than 2) and the winter minima/summer maxima that occurred in most western IMPROVE regions (and Alaska) were replaced with nearly the opposite: winter maxima and spring and summer minima (Figure 4.3.2). In the eastern United States the seasonality varied per region, with several summer maxima and winter and spring minima. Several regions along the eastern coast corresponded to similar summer maxima/spring minima and degree of seasonality as the rural regions. The largest ratio occurred at the Alaska region (24.6) and the lowest in the Southeast region (1.5).

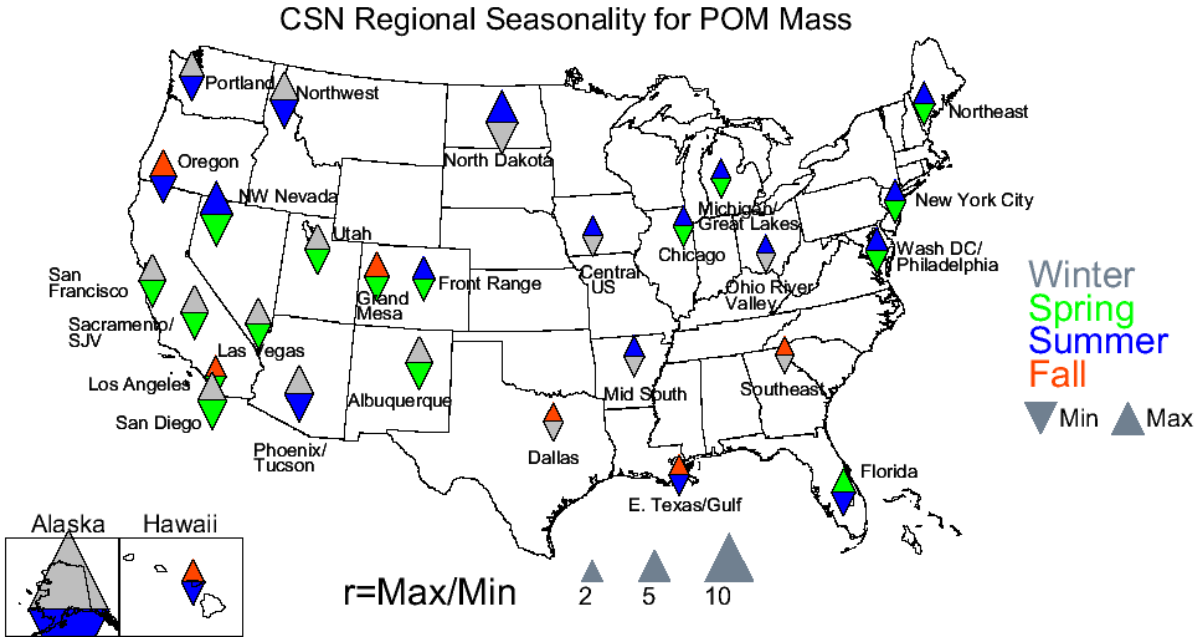

Figure 4.3.2. Seasonal variability for CSN 2005–2008 monthly mean particulate organic matter (POM) mass concentrations. The color of the upward pointing triangle refers to the season with the maximum monthly mean concentration and the downward pointing triangle refers to the season with the minimum monthly mean concentration. The size of the triangles refers to the magnitude of the ratio of maximum to minimum monthly mean mass concentration.

The lowest IMPROVE rural regional monthly mean mass fraction occurred in the Virgin Islands in July (0.9%), compared to the highest (76.3%) in the Northern Rocky Mountains region in August. POM contributions dominated the RCFM in the northwestern United States. Contributions were typically 40–60% and generally higher in summer (see Figure 4.1.12). In the southwestern United States the magnitude and seasonality of POM contributions decreased somewhat (Figure 4.1.13). Contributions were 15–20% at many regions throughout the year (e.g., West Texas, Southern Arizona, and Southern California). In the eastern United States POM relative contributions typically ranged from 20 to 40%, although higher mass fractions occurred at the Boundary Waters and Northern Great Plains regions (Figure 4.1.11). Of the OCONUS regions, Alaska had the highest POM contributions, especially in summer (Figure 4.1.14).

Summer maxima in mass fractions of POM were common for IMPROVE regions. As seen in Figure 4.3.3, most western regions corresponded to summer maxima and spring minima, with the exception of a few regions, such as Puget Sound, Columbia River Gorge, and Southern California. In the eastern United States, many regions had fall maxima, with varying seasons for minima. Relative contributions of POM demonstrated a low degree of seasonality (much lower than POM concentrations), suggesting that the level of contributions of POM to RCFM were fairly steady at most regions. Nearly half of all IMPROVE regions had minimal seasonality (max/min < 2). The maximum ratio occurred at Virgin Islands (7.1) and the lowest occurred at New York City (1.3).

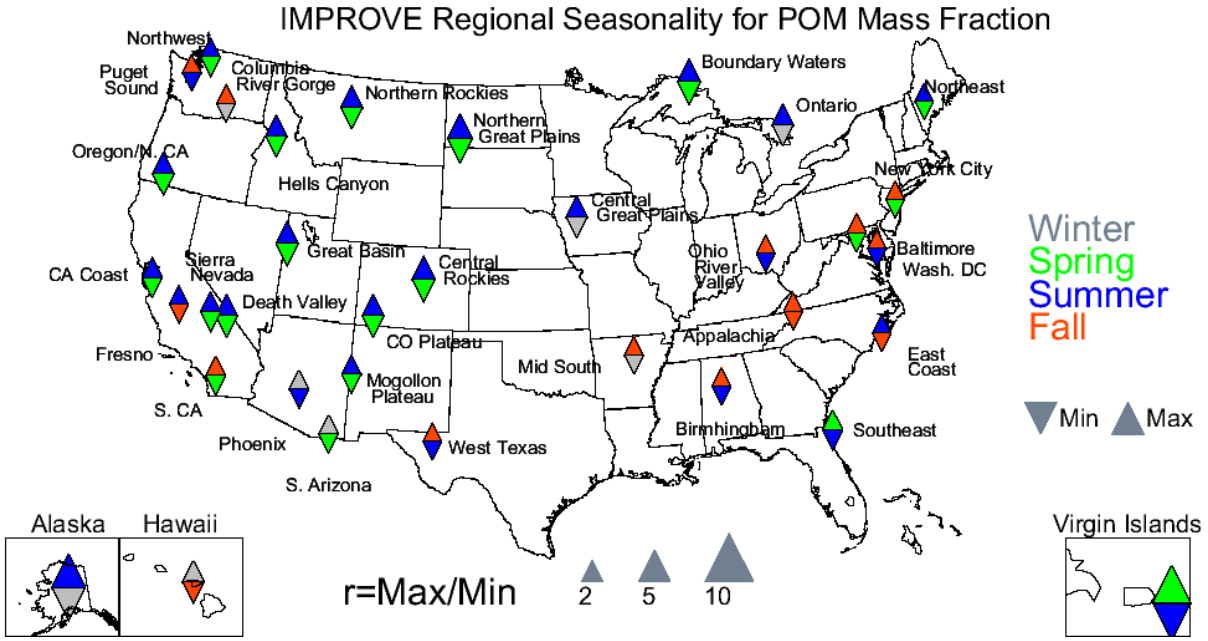

Figure 4.3.3. Seasonal variability for IMPROVE 2005–2008 monthly mean particulate organic matter (POM) reconstructed fine mass fractions. The color of the upward pointing triangle refers to the season with the maximum monthly mean concentration and the downward pointing triangle refers to the season with the minimum monthly mean concentration. The size of the triangles refers to the magnitude of the ratio of maximum to minimum monthly mean mass concentration.

A CSN urban maximum POM mass fraction of 77.8% occurred in the Northwest Nevada region in July compared to a minimum of 10.3% in North Dakota in February. Most regions in the northwestern United States had high POM contributions (see Figure 4.1.17). The seasonal

pattern at North Dakota was markedly different than the other regions in this area. Contributions were largest during winter (70–80%) for Puget Sound, Northwest, and Oregon regions, but at North Dakota the POM contributions were highest in summer. Moving south, the POM contributions decreased to around 40%, depending on region. Northwest Nevada had the highest contributions of POM to RCFM of any region in the southwestern United States (Figure 4.1.18). The contributions of POM to RCFM decreased even further in the eastern United States. Relative contributions of 20–40% were typical at many regions (see Figure 4.1.16) and fairly flat seasonally. Alaska had much higher contributions (60% or more), with the largest in summer. The Hawaii region had a very low POM contribution, but it increased in the fall (Figure 4.1.19).

POM mass fractions in CSN regions were somewhat less seasonal than IMPROVE regions, with 21 of all urban regions having ratios less than 2. The maximum ratio occurred in North Dakota (5.1) compared to the lowest in the Northwest region (1.4). The seasonality also reflected different seasons corresponding to maxima and minima compared to IMPROVE regions, with fewer summer maxima and spring minima in the western United States (Figure 4.3.4). In the northwestern United States the maximum contributions occurred mainly in summer and fall, farther south winter maxima in Arizona, New Mexico, and the southern part of California occurred. In the eastern United States the maxima occurred in the fall for many regions, with minima in the summer for the Southeast, East Texas/Gulf, and Florida regions.

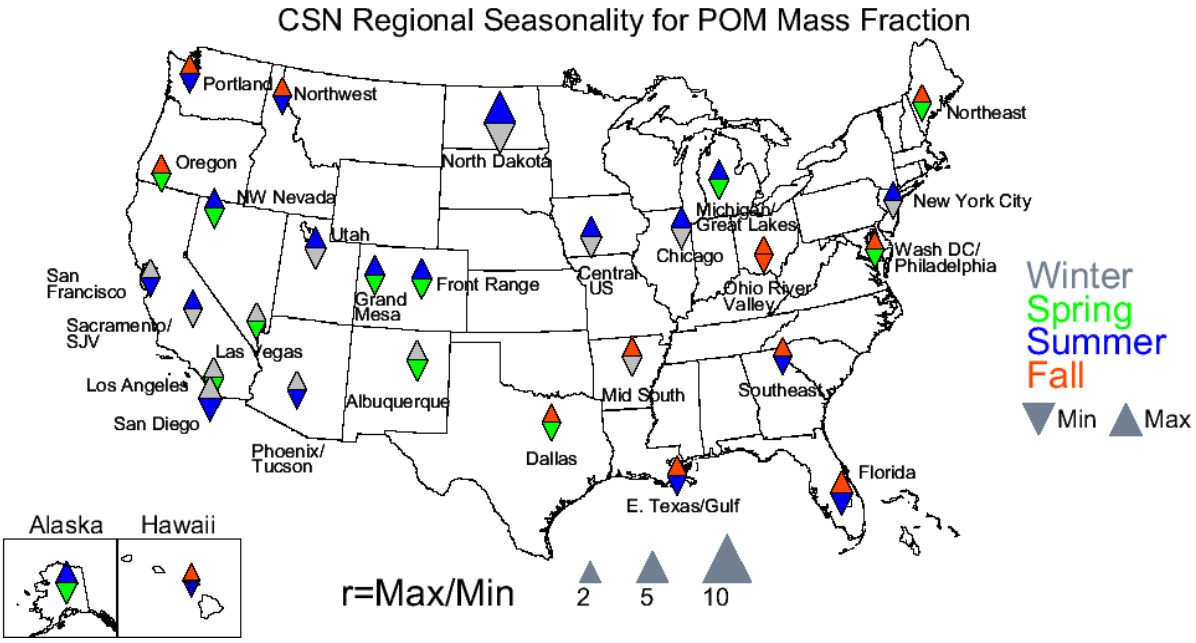

Figure 4.3.4. Seasonal variability for CSN 2005–2008 monthly mean particulate organic matter (POM) reconstructed fine mass fractions. The color of the upward pointing triangle refers to the season with the maximum monthly mean concentration and the downward pointing triangle refers to the season with the minimum monthly mean concentration. The size of the triangles refers to the magnitude of the ratio of maximum to minimum monthly mean mass concentration.

4.4 $PM_{2.5}$ LIGHT ABSORBING CARBON MASS CONCENTRATIONS

The IMPROVE 2005–2008 maximum regional monthly mean light absorbing carbon (LAC) mass concentration of 2.69 μg m^{-3} occurred in the urban location of Phoenix in December

and 0.56 μg m^{-3} in the nonurban locations of the Northern Rocky Mountains region in August. The minimum regional monthly mean mass concentration occurred at the Hawaii region in July (0.012 μg m^{-3}). Compared to other aerosol species, LAC concentrations were so relatively low that they are difficult to discern on bar charts from the eastern (Figure 4.1.1), southwestern (4.1.3), and OCONUS (4.1.4) regions of the United States. Somewhat higher concentrations occurred in the northwestern United States (Figure 4.1.12). For example, the Northern Rocky Mountains, Northwest, and Columbia River Gorge regions had somewhat higher concentrations (i.e., viewable on the charts), especially in summer.

Although difficult to see on the bar charts because of relatively low LAC concentrations compared to other species, IMPROVE LAC concentrations corresponded to some degree of seasonality, although less than POM concentrations. Regions in the western United States had higher seasonality compared to the eastern regions (Figure 4.4.1). Many regions in the western United States corresponded to summer maxima and winter minima. Similar to POM concentrations, some of the urban IMPROVE sites had the opposite seasonality (winter maxima/summer minima), such as Puget Sound and Phoenix. Several eastern regions corresponded to fall maxima. Thirteen regions had maximum to minimum ratios less than 2. The highest ratio in LAC maximum/minimum concentrations occurred at the Northern Rocky Mountain region (7.3) compared to the lowest for the Ohio River Valley region (1.3).

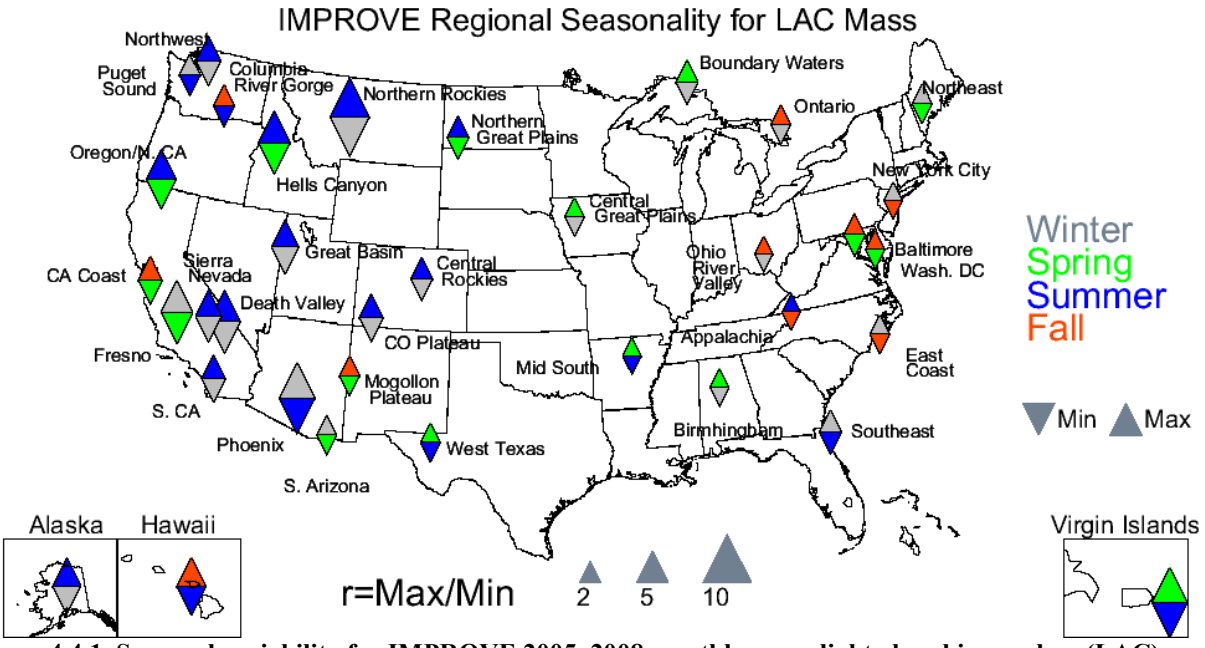

Figure 4.4.1. Seasonal variability for IMPROVE 2005–2008 monthly mean light absorbing carbon (LAC) mass concentrations. The color of the upward pointing triangle refers to the season with the maximum monthly mean concentration and the downward pointing triangle refers to the season with the minimum monthly mean concentration. The size of the triangles refers to the magnitude of the ratio of maximum to minimum monthly mean mass concentration.

The CSN maximum regional monthly mean LAC concentrations ranged from 0.16 μg m^{-3} in North Dakota in May to 2.91 μg m^{-3} in the Alaska region in December. The CSN LAC concentrations were much higher than concentrations in rural IMPROVE regions. For example,

eastern U.S. LAC concentrations are visible on the bar charts in Figure 4.1.6, especially at some locations like New York City. In some southwestern regions the urban LAC concentrations were much larger than rural regions (compare Figure 4.1.7 to 4.1.3). Winter concentrations were higher than during other months at several regions in the southwestern United States, such as Las Vegas, Phoenix/Tucson, San Francisco, Grand Mesa CO, and Albuquerque. Higher LAC concentrations, especially in winter, were observed in the northwestern United States (e.g., Puget Sound region). Higher CSN concentrations were also observed in the Alaska and Hawaii regions (Figure 4.1.9) compared to IMPROVE OCONUS regions.

CSN LAC concentrations demonstrated a similar degree of seasonality as POM concentrations but with different seasons corresponding to maximum and minimum, especially in the eastern United States (Figure 4.4.2 compared to Figure 4.3.2). Several western regions corresponded to winter maxima and spring minima and higher seasonality compared to eastern U.S. regions. In contrast, several eastern regions had fall maxima and summer minima. There were 11 regions with maximum to minimum ratios less than 2 for the CSN network, with the Alaska region demonstrating the highest seasonality (8.0) compared to New York City, which demonstrated the least (1.4).

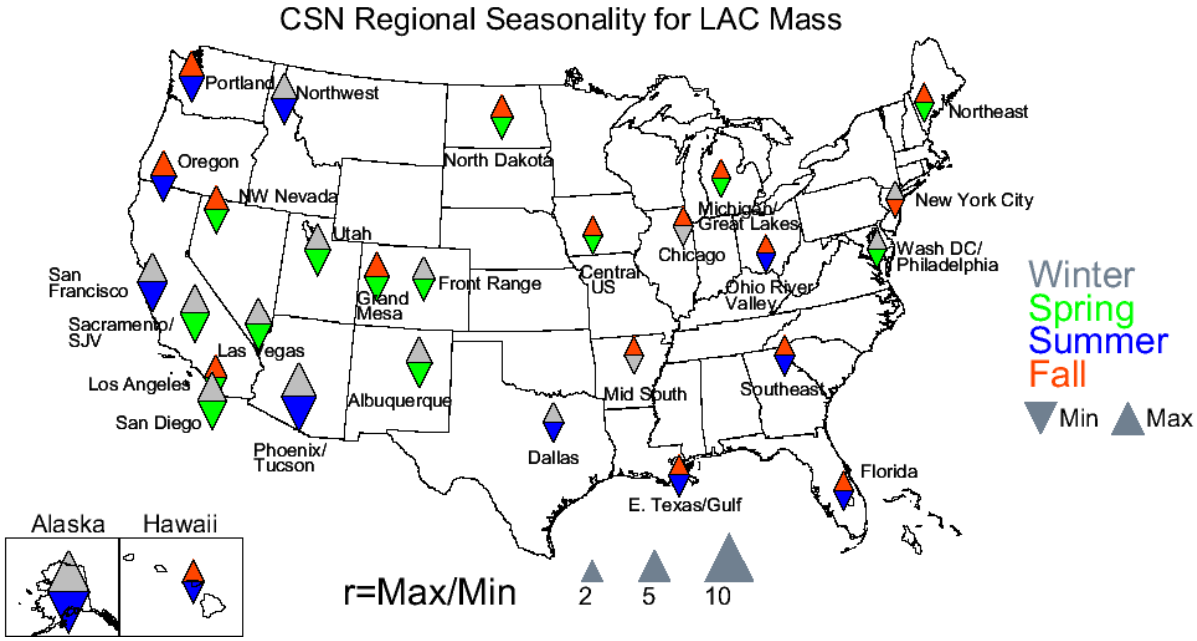

Figure 4.4.2. Seasonal variability for CSN 2005–2008 monthly mean light absorbing carbon (LAC) mass concentrations. The color of the upward pointing triangle refers to the season with the maximum monthly mean concentration and the downward pointing triangle refers to the season with the minimum monthly mean concentration. The size of the triangles refers to the magnitude of the ratio of maximum to minimum monthly mean mass concentration.

As expected from the IMPROVE rural LAC concentrations discussed previously, the relative contribution of LAC to RCFM was low; these low contributions were especially obvious in the eastern United States (see Figure 4.1.11). Somewhat higher contributions occurred in the northwestern United States (e.g., Columbia River Gorge, Northwest, Northern Rocky Mountains, and Oregon/Northern California regions, see Figure 4.1.12). Relative contributions of LAC were low in the southwestern United States also, although they were slightly higher during winter

months at some locations (e.g., Colorado Plateau and Mogollon Plateau, see Figure 4.1.13). LAC relative contributions were higher at Alaska compared to other OCONUS regions (Figure 4.1.14). Rural IMPROVE regional LAC mass fractions ranged from 0.17% in the Virgin Islands to 7.5% in the Mogollon Plateau in December. The maximum monthly mean mass fraction for IMPROVE urban region corresponded to 13.3% in Puget Sound in January.

The IMPROVE LAC mass fractions did not exhibit a high degree of seasonality, with 24 regions having ratios of maximum to minimum mass fractions less than 2. The largest occurred in the Virgin Islands (11.6) compared to the Northwest region (1.4). Relative LAC contributions were lowest in the spring and highest in winter in many western regions. However, in the eastern regions the minimum relative contribution occurred in summer, with maxima in fall and winter (Figure 4.4.3). The seasons corresponding to maxima and minima were quite different for LAC and POM mass fractions, although the degree of seasonality was similar (compare Figures 4.4.3 to 4.3.3).

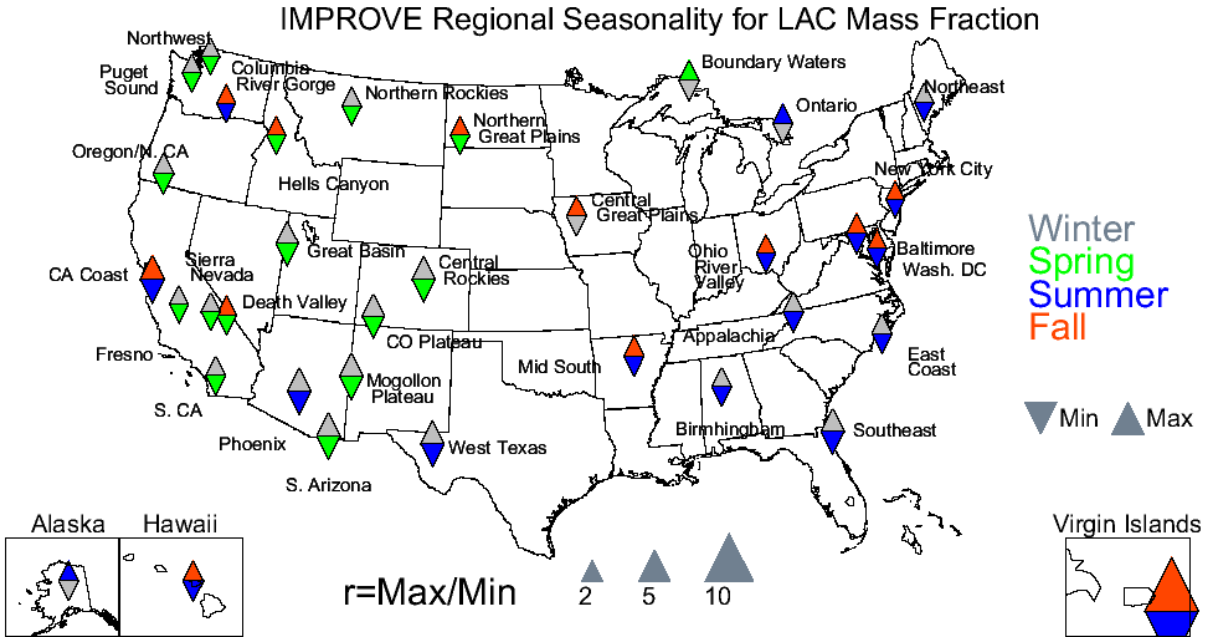

Figure 4.4.3. Seasonal variability for IMPROVE 2005–2008 monthly mean light absorbing carbon (LAC) reconstructed fine mass fractions. The color of the upward pointing triangle refers to the season with the maximum monthly mean concentration and the downward pointing triangle refers to the season with the minimum monthly mean concentration. The size of the triangles refers to the magnitude of the ratio of maximum to minimum monthly mean mass concentration.

CSN regional mass fractions ranged from 3.6% in North Dakota in May to 19.4% in Alaska in August. As seen in Figure 4.1.19, the CSN Hawaii region also corresponded to relatively large LAC mass fractions compared to the IMPROVE Hawaii region (compare Figure 4.1.14). Urban relative contributions were also higher in the northwestern United States (compare Figure 4.1.17 to Figure 4.1.12). For these regions, Puget Sound had the highest LAC mass fractions year round. Relative contributions of urban LAC in the southwestern United States were also higher than rural regions (Figure 4.1.18). Specifically, regions such as Northwest Nevada, Front Range CO, and Phoenix/Tucson corresponded to higher LAC mass fractions compared to nearby rural regions (compare Figure 4.1.18 to Figure 4.1.13). LAC

contributions in the eastern United States appeared somewhat larger than rural regions, but not to the degree as in the western United States (compare Figure 4.1.16 to 4.1.11).

In most CSN regions, LAC did not appear to have a high degree of seasonality. In fact, roughly half (14) of all CSN regions had maximum to minimum mass fraction ratios less than 2. The maximum occurred in Alaska (3.7) compared to the minimum in the Northwest region (1.4). Several regions corresponded to fall maxima, both in the eastern and western United States. However, in the southwestern United States and Dallas, several regions corresponded to winter maxima. Spring and summer minima occurred for most regions around the country, with the exception of winter minima in the Utah, Central U.S., Chicago, and Michigan/Great Lakes regions. LAC relative contributions generally had the same degree of seasonality as POM mass fractions, but maxima and minima seasons differed for most regions (compare Figures 4.3.4 and 4.4.4).

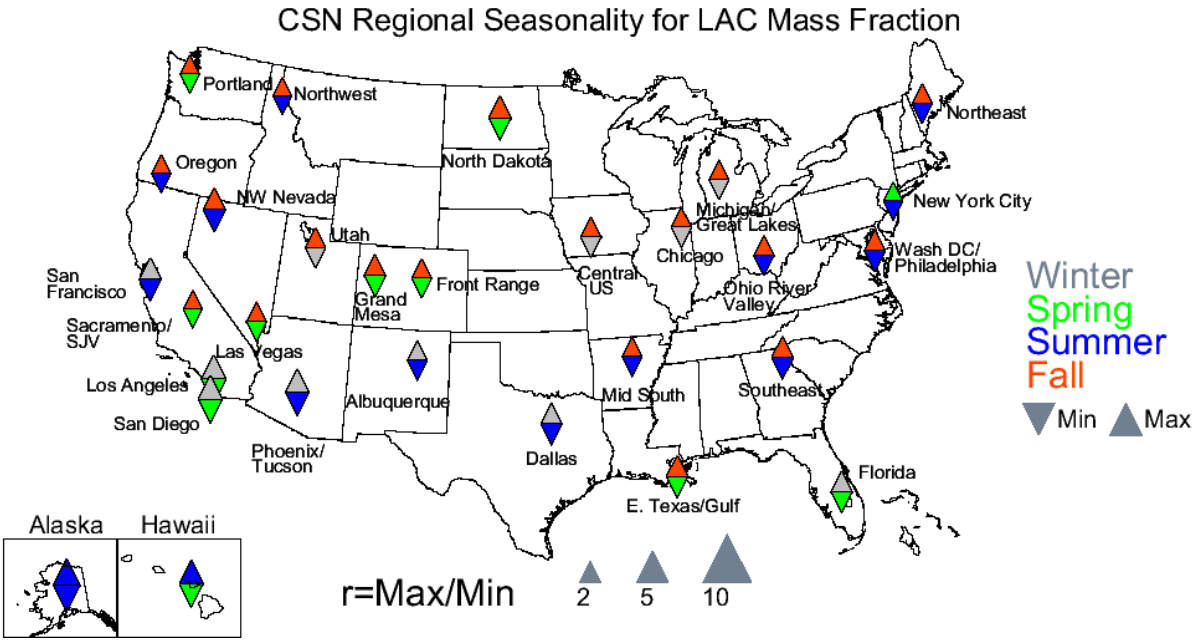

Figure 4.4.4. Seasonal variability for CSN 2005–2008 monthly mean light absorbing carbon (LAC) reconstructed fine mass fractions. The color of the upward pointing triangle refers to the season with the maximum monthly mean concentration and the downward pointing triangle refers to the season with the minimum monthly mean concentration. The size of the triangles refers to the magnitude of the ratio of maximum to minimum monthly mean mass concentration.

4.5 $PM_{2.5}$ SOIL MASS CONCENTRATIONS

A maximum 2005–2008 regional monthly mean IMPROVE soil mass concentration of 5.54 μg m^{-3} was observed in June at Virgin Islands, a site known to have impacts from North African dust transport, especially during summer. The minimum concentration was observed in Alaska in September (0.05 μg m^{-3}) (see Figure 4.1.4). Soil concentrations were highest in the southwestern United States (Figure 4.1.3). Most regions in this area, with the exception of some regions along the coast in California, corresponded to relatively high soil concentrations, such as spring concentrations in the regions of Death Valley, Central Rocky Mountains, Colorado Plateau and Mogollon Plateau, and Southern Arizona. Large differences in monthly

concentrations were observed at some regions, such as Great Basin, where winter soil concentrations were quite low. Concentrations were lower in the northwestern United States and peaked in summer rather than spring but were also quite low in winter (Figure 4.1.2). Concentrations in the eastern United States were also comparatively low compared to the southwestern United States (Figure 4.1.1) and typically were higher in summer for some regions (e.g., Mid South and Southeast regions).

As could be seen in many of the bar charts, IMPROVE soil concentrations were highly seasonal, with only four regions having maximum to minimum ratios less than 2 (all urban regions), consistent with the often episodic impacts of soil emissions. The largest ratio occurred at Virgin Islands (28.9) and the lowest at New York City (1.6) (Figure 4.5.1). Maxima occurred primarily in the spring in the western and southwestern United States and in summer in the most northwestern and eastern regions, and minima often occurred in winter. Southern Arizona and Phoenix were the only regions with summer minima in the country.

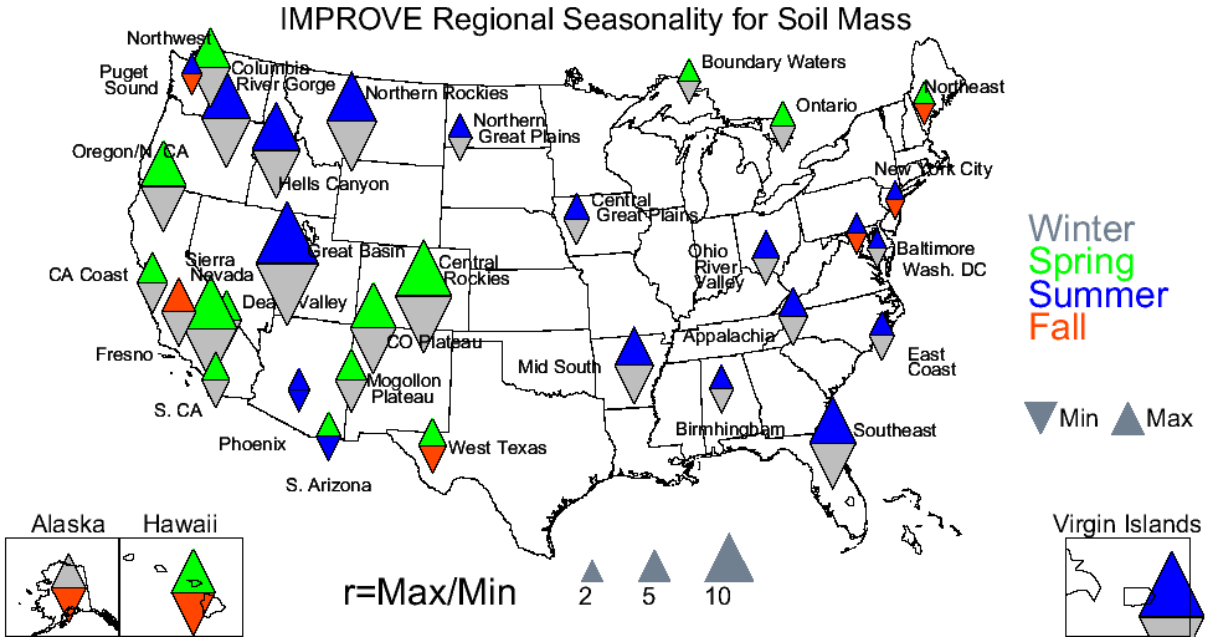

Figure 4.5.1. Seasonal variability for IMPROVE 2005–2008 monthly mean fine soil mass concentrations. The color of the upward pointing triangle refers to the season with the maximum monthly mean concentration and the downward pointing triangle refers to the season with the minimum monthly mean concentration. The size of the triangles refers to the magnitude of the ratio of maximum to minimum monthly mean mass concentration.

Unlike other species, CSN soil concentrations were generally lower than IMPROVE soil concentrations, although recall the relative bias between IMPROVE and CSN data, with higher IMPROVE soil concentrations at collocated sites (Table 1.9). However, spatial patterns in CSN soil concentrations differed from the rural concentrations as demonstrated by data at regions in the southwestern United States. CSN concentrations were noticeably lower than IMPROVE (compare Figure 4.1.7 to 4.1.3) and demonstrated less seasonality, although concentrations increased in spring and summer (e.g., Phoenix/Tucson and Grand Mesa CO). CSN concentrations also were low in the northwestern United States and also increased in summer and

spring (Figure 4.1.8). Low soil concentrations were also characteristic of most eastern urban regions (Figure 4.1.6). Southern regions, such as Florida, East Texas/Gulf, Dallas, and Mid South, had the highest concentrations. The low urban soil concentrations observed in most of the continental United States was also characteristic of the Alaska and Hawaii regions (Figure 4.1.9). The lowest and highest soil concentrations both occurred in summer months in Alaska, while the highest concentrations in Hawaii occurred in spring (Figure 4.1.9). The maximum CSN soil mass concentration was 2.55 μg m^{-3} in Phoenix/Tucson in April, compared to a low value of 0.09 μg m^{-3} in Hawaii in September.

CSN urban regions experienced a much lower degree of seasonality compared to IMPROVE rural regions. (Compare Figure 4.5.2 and 4.5.1), especially in the western United States. While the seasons corresponding to maxima and minima were similar, the range in concentration between minimum and maximum months was much lower. More regions in California had fall maxima compared to spring maxima at IMPROVE regions. Seven regions had maximum to minimum ratios less than 2. The largest ratio occurred in Florida (8.2), perhaps associated with transport of North African dust. The lowest ratio (1.6) occurred in New York City.

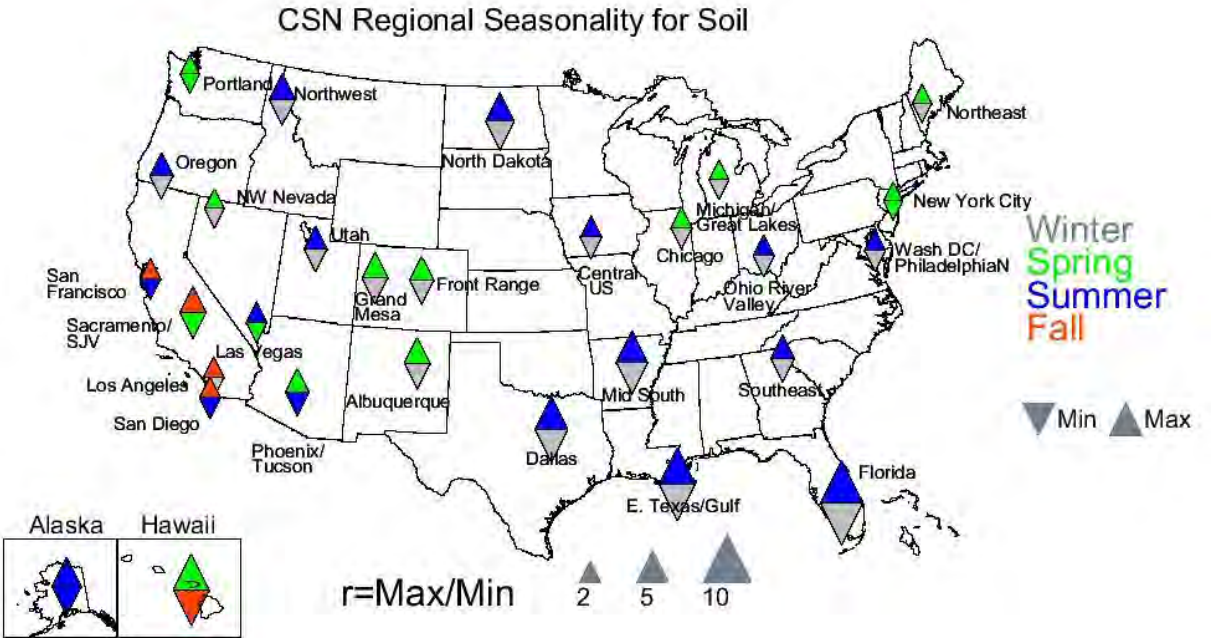

Figure 4.5.2. Seasonal variability for CSN 2005–2008 monthly mean fine soil mass concentrations. The color of the upward pointing triangle refers to the season with the maximum monthly mean concentration and the downward pointing triangle refers to the season with the minimum monthly mean concentration. The size of the triangles refers to the magnitude of the ratio of maximum to minimum monthly mean mass concentration.

Soil mass contributions to RCFM for the IMPROVE rural regions ranged from 1.9% in Alaska in August to 56.3% in the Virgin Islands in August. Given the previous discussions of other aerosol species, it is not surprising that the soil was not a major contributor to RCFM in most eastern regions. However, at the Southeast, Northern Great Plains, and Mid South regions, the relative contributions reached as high as 20% in summer (Figure 4.1.11). The Southeast region most likely experienced the impacts of North African dust transport in summer, as indicated by the high soil mass fractions at the Virgin Islands in summer also (Figure 4.1.14).

The relative contribution of soil to RCFM in the southwestern United States was noticeably higher than in the eastern United States (Figure 4.1.13). Many regions (e.g., Southern Arizona and Death Valley) had contributions of 40% or greater during certain months. The only regions with lower relative contributions were Southern California, California Coast, and Sierra Nevada. Most of the northwestern regions corresponded to ~20% relative contributions of soil (Figure 4.1.12). Soil mass fractions were highest in spring for these regions, with the exception of Columbia River Gorge, which experienced an increase in soil contributions in summer.

IMPROVE soil mass fractions were fairly seasonal for most regions, with only four regions having ratios less than 2 (Figure 4.5.3). The regions with the highest ratios were the urban site of Fresno (12.8) and the rural Virgin Island site (9.2). The lowest ratios occurred at the urban New York City site (1.7) and the rural East Coast region (1.9). Most of the maxima in soil contributions occurred in spring, especially in the western, northern, and eastern areas of the United States. The central and southern United States corresponded to maximum contributions in summer. Winter minima were common for most regions around the country, although there were exceptions (e.g., summer in Phoenix and Death Valley, fall in West Texas and other regions, and spring in Baltimore).

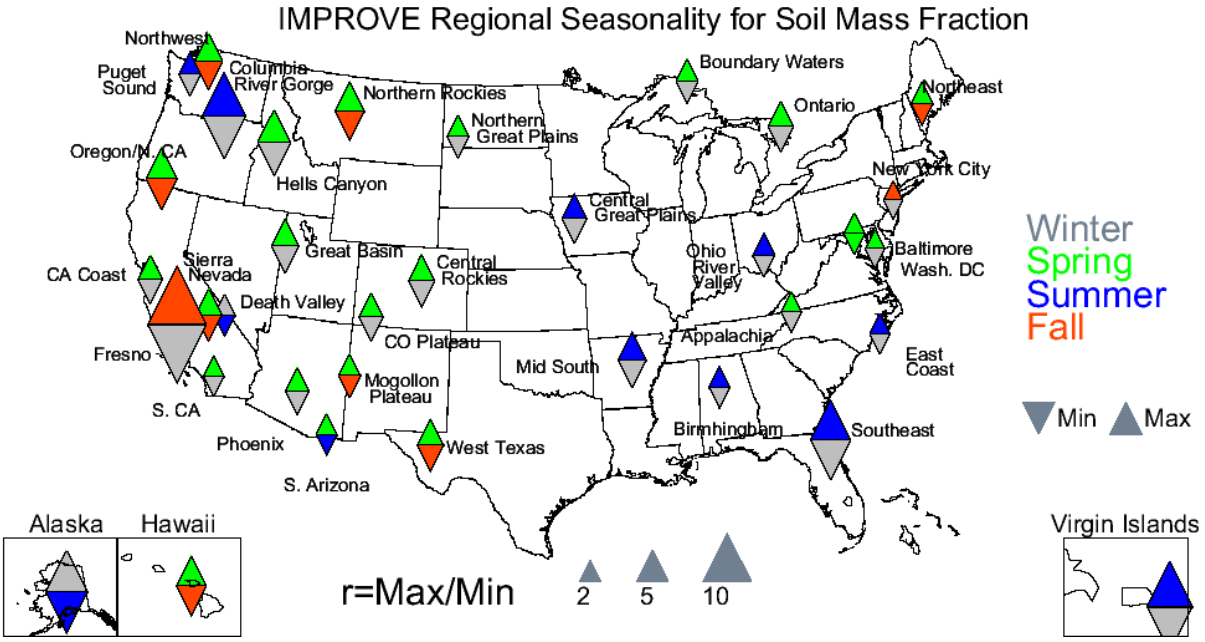

Figure 4.5.3. Seasonal variability for IMPROVE 2005–2008 monthly mean fine soil reconstructed fine mass fractions. The color of the upward pointing triangle refers to the season with the maximum monthly mean concentration and the downward pointing triangle refers to the season with the minimum monthly mean concentration. The size of the triangles refers to the magnitude of the ratio of maximum to minimum monthly mean mass concentration.

The maximum CSN urban mass fraction was lower than for the maximum IMPROVE rural region (33.5% at Grand Mesa CO in April compared to 56.3% in Virgin Islands in August, respectively), but the minimum mass fraction was similar for the rural CSN and IMPROVE regions (1.4% in Alaska in December to 1.9% in Alaska in August, respectively). Low urban soil contributions were observed in the eastern United States (Figure 4.1.16). Contributions of ~10% were common, with exceptions at the Florida and East Texas/Gulf regions in summer. Relative

contributions of soil increased in summer at the Mid South and Dallas regions although to a lesser degree. Contributions of soil to RCFM at urban regions in the southwestern United States were larger than in the eastern regions but lower than many rural regions in the same vicinity (compare Figure 4.1.18 to 4.1.13). Higher contributions in the spring and summer were common for many regions (e.g., Phoenix/Tucson, Albuquerque, and Grand Mesa CO), but regions near to the coast had lower relative contributions with less of a seasonal impact (Figure 4.1.18). In the northwestern United States the urban soil contributions were lower than rural regions and reached up to 10–20% in the North Dakota region and the Northwest region in fall and summer, respectively. Contributions were relatively low in the Puget Sound and Oregon regions (Figure 4.1.17). Relative soil contributions reached up to 20% in the urban Alaska region in spring but were typically lower in Hawaii (Figure 4.1.19).

Most CSN regions experienced some degree of seasonality in soil mass fractions, with only one region having a ratio less than 2 (New York City, 1.6). The maximum ratio occurred in Alaska (15.4). The urban regions mainly experienced spring maxima and winter minima, although, summer maxima occurred in the northwestern, southern, and southeastern United States. The only summer minima occurred in Los Angeles, San Diego, and New York City.

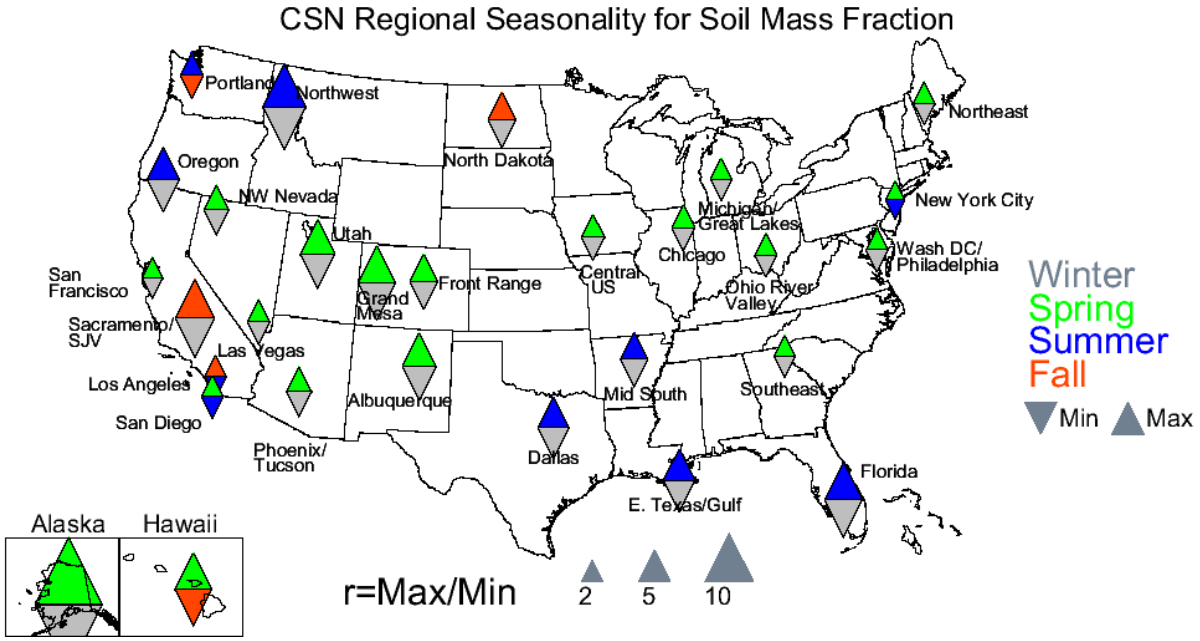

Figure 4.5.4. Seasonal variability for CSN 2005–2008 monthly mean fine soil reconstructed fine mass fractions. The color of the upward pointing triangle refers to the season with the maximum monthly mean concentration and the downward pointing triangle refers to the season with the minimum monthly mean concentration. The size of the triangles refers to the magnitude of the ratio of maximum to minimum monthly mean mass concentration.

4.6 $PM_{2.5}$ SEA SALT MASS CONCENTRATIONS

Estimates of sea salt concentrations were derived from chloride ion (IMPROVE) (White, 2008) and chlorine (CSN) mass concentrations. Because of this difference, the two estimates may not be directly comparable but are the closest approximations available for the two networks. In fact, IMPROVE estimates were biased high relative to CSN estimates at collocated

sites (Table 1.9). In addition, it is well known that chloride concentrations in particle phase can be depleted by a gas-particle exchange of chloride to the atmosphere; estimates of sea salt discussed here are possibly an underestimate. The 2005–2008 regional monthly mean sea salt concentration for the IMPROVE regions ranged from 0.003 μg m^{-3} at the Central Rocky Mountain region in November to 1.98 μg m^{-3} at the Virgin Islands site in January. Sea salt concentrations were visible on the monthly bar charts relative to other species for only a few regions. In the eastern United States, coastal regions such as Northeast, East Coast, and Southeast had noticeable sea salt concentrations relative to other species (Figure 4.1.1). In the northwestern United States, sea salt was noticeable at Columbia River Gorge and Oregon/Northern California (Figure 4.1.2). Higher sea salt concentrations at the California Coast region were obvious in Figure 4.1.3, and non-negligible concentrations occurred at the OCONUS regions (Figure 4.1.4).

IMPROVE sea salt concentrations were highly seasonal, with only three regions (Appalachia, Hawaii, and Oregon/Northern California) having maximum to minimum ratios less than 2 (Figure 4.6.1). Part of the reason for high seasonality of sea salt is its low concentrations in most regions. Many regions corresponded mainly to spring and winter maxima. Spring maxima occurred at regions in the western and coastal (east and west) United States. Winter maxima occurred in the northwestern United States and a few eastern U.S. regions such as Baltimore, Washington D.C., Appalachia, and the Southeast. A few regions corresponded to summer maxima (Oregon/Northern California, California Coast, and Phoenix). Fall minima occurred mainly in the central and southwestern United States and in California.

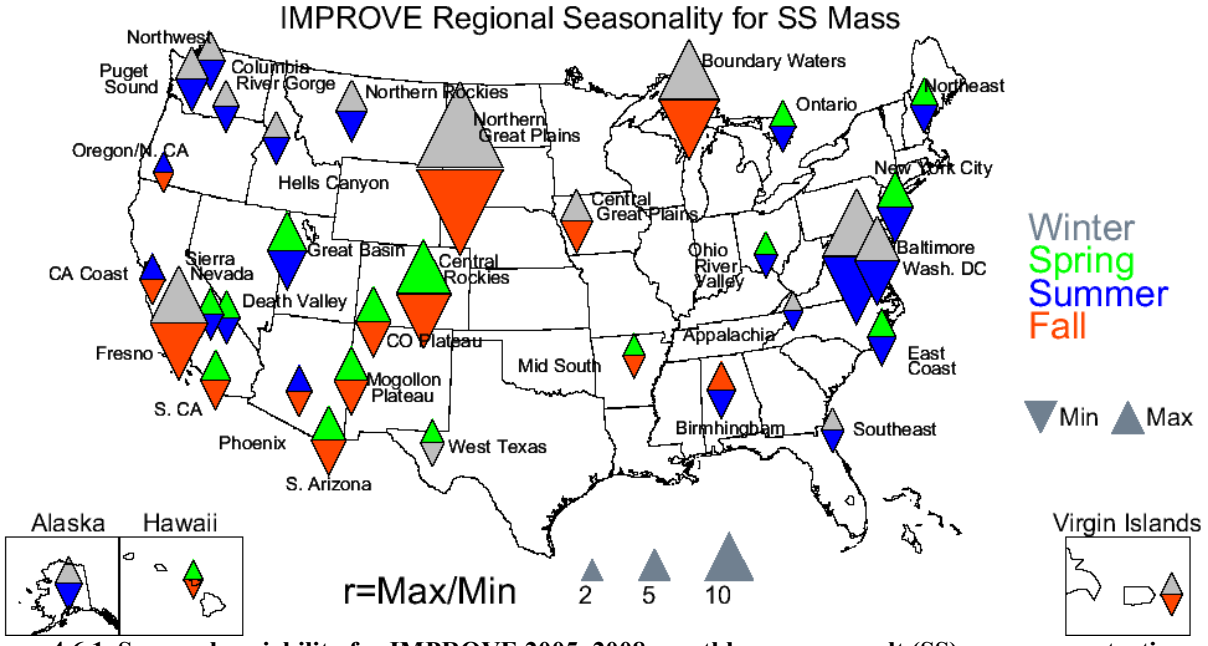

Figure 4.6.1. Seasonal variability for IMPROVE 2005–2008 monthly mean sea salt (SS) mass concentrations. The color of the upward pointing triangle refers to the season with the maximum monthly mean concentration and the downward pointing triangle refers to the season with the minimum monthly mean concentration. The size of the triangles refers to the magnitude of the ratio of maximum to minimum monthly mean mass concentration.

Because the relative concentrations of sea salt to other urban aerosols were so low, sea salt concentrations were difficult to discern in all of the CSN bar charts with the exception of Puget Sound (Figure 4.1.8), Florida (Figure 4.1.6), San Francisco, and San Diego (Figure 4.1.7). However, sea salt concentrations were higher in the Hawaii region relative to other species (Figure 4.1.9). CSN sea salt concentrations ranged from 0.0016 μg m^{-3} at the North Dakota region in September to 1.44 μg m^{-3} at Hawaii in January.

Sea salt concentrations in urban CSN regions were also highly seasonal, with only one region (Southeast) with maximum to minimum ratios less than 2. The maximum ratio of monthly mean sea salt concentrations occurred at Alaska (94.9) compared to the Southeast (1.9). Western regions corresponded to higher seasonality compared to eastern regions (Figure 4.6.2). Many regions, especially in the northern United States, had winter maxima that were perhaps associated with road salt applied during winter months. Summer and spring maxima were common for southern regions (e.g., Las Vegas, San Diego, Phoenix/Tucson, Albuquerque, Dallas, and East Texas/Gulf). Minima occurred for all seasons, although many northern regions corresponded to summer minima.

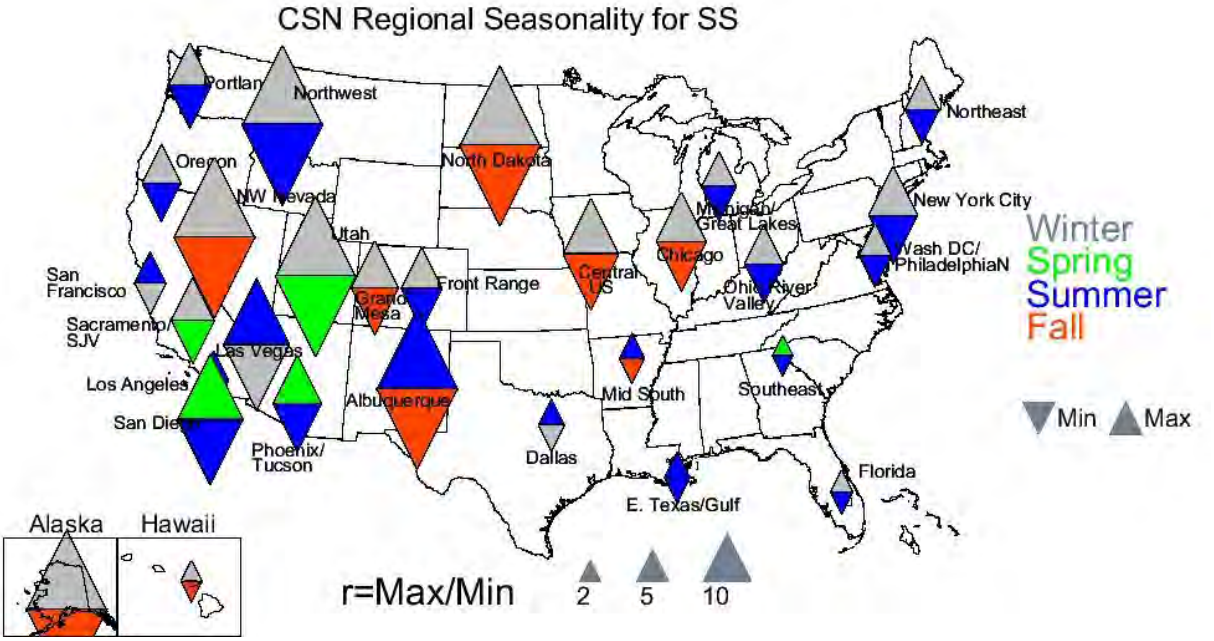

Figure 4.6.2. Seasonal variability for CSN 2005–2008 monthly mean sea salt (SS) mass concentrations. The color of the upward pointing triangle refers to the season with the maximum monthly mean concentration and the downward pointing triangle refers to the season with the minimum monthly mean concentration. The size of the triangles refers to the magnitude of the ratio of maximum to minimum monthly mean mass concentration.

Because of the low concentrations of sea salt relative to other species, its contributions were more easily viewed as mass fractions. IMPROVE sea salt mass fractions ranged from 0.11% in the Northern Rocky Mountains region in August to 57.2% in the Virgin Islands in December. The only eastern regions with noticeable contributions of sea salt to RCFM were the Northeast, East Coast, and Southeast (all coastal regions) (Figure 4.1.11). Other coastal regions in the northwestern United States had noticeable sea salt contributions, such as the Northwest, Columbia River Gorge, and Oregon/Northern California regions. Interestingly, Northern Great

Plains showed contributions of sea salt in December, possibly associated with long-range transport of sea salt (White et al., 2010) (Figure 4.1.12). The California Coast region had the highest contribution of sea salt to RCFM of any southwestern region; mass fractions of 20% or less were typical year round (Figure 4.1.13). The regions of Alaska, Hawaii, and the Virgin Islands all corresponded to higher sea salt mass fractions also. The Hawaii region experienced year-round contributions of 10–20%, and the Alaska and Virgin Island regions had typical contributions of 40–50%, with higher values in winter (Figure 4.1.14).

The contribution of sea salt to fine mass at IMPROVE regions was highly seasonal, with only one region with a ratio less than 2 (West Texas, 1.7). The maximum ratio occurred in the Northern Great Plains region (36.1). Relative contributions of sea salt had greater seasonality than sea salt concentrations (compare Figures 4.6.3 to 4.6.1), with many western regions having high seasonality. The seasons corresponding to maxima and minima were similar for mass fractions and mass concentrations for most regions, with the exception of some regions on the western coast.

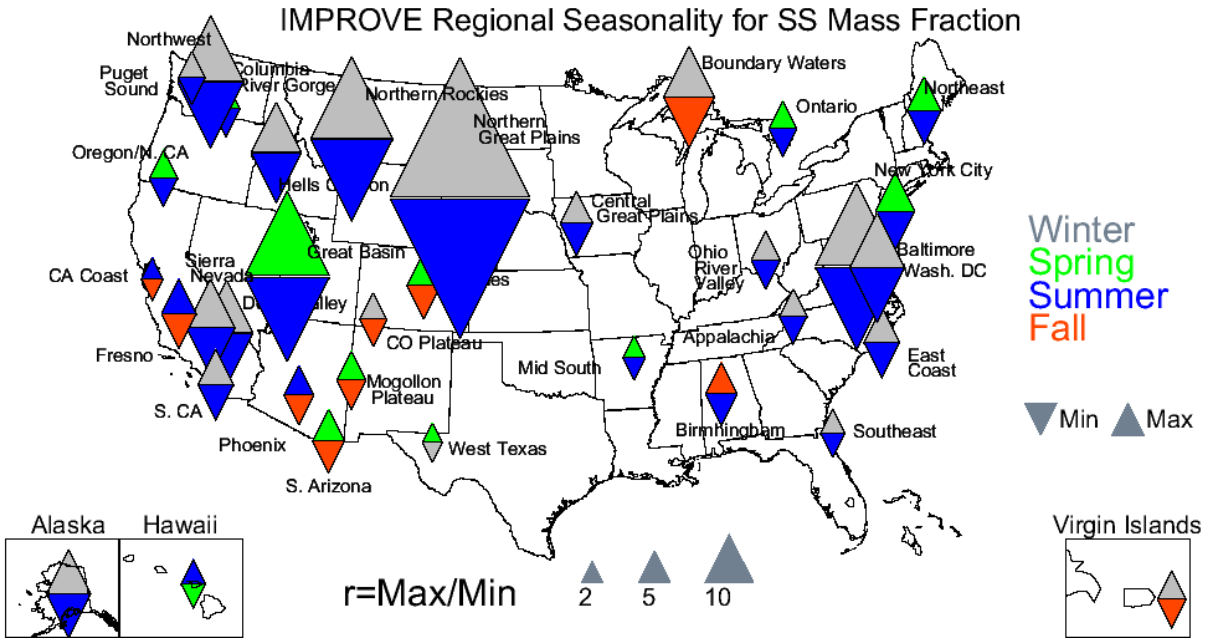

Figure 4.6.3. Seasonal variability for IMPROVE 2005–2008 monthly mean sea salt (SS) reconstructed fine mass fractions. The color of the upward pointing triangle refers to the season with the maximum monthly mean concentration and the downward pointing triangle refers to the season with the minimum monthly mean concentration. The size of the triangles refers to the magnitude of the ratio of maximum to minimum monthly mean mass concentration.

The range of sea salt contributions to RCFM were similar for the urban CSN regions compared to rural regions, with a high of 51.5% in Hawaii in August and a low of 0.04% in North Dakota in September. The CSN regions with noticeable sea salt contributions were San Diego and San Francisco in the southwestern United States (Figure 4.1.18), Puget Sound in the northwestern United States (Figure 4.1.17), and the Florida region in the eastern United States (Figure 4.1.16). In contrast to the rural Alaska regions, the urban Alaska regions corresponded to only negligible contributions from sea salt. However, the CSN Hawaii region had much higher sea salt contributions compared to the IMPROVE Hawaii region (Figure 4.1.19).

The seasonal patterns of CSN sea salt mass fractions were very similar to sea salt mass concentrations (compare Figures 4.6.4 to 4.6.1). Mass fractions had a slightly lower degree of seasonality for many regions, but overall they were comparable. The seasons corresponding to maxima and minima varied for some regions, such as the Northeast, New York City, Mid South, Phoenix/Tucson, and Sacramento/San Joaquin Valley, to name a few. No regions had ratios less than 2, suggesting all CSN regions experienced seasonal contributions of sea salt to RCFM.

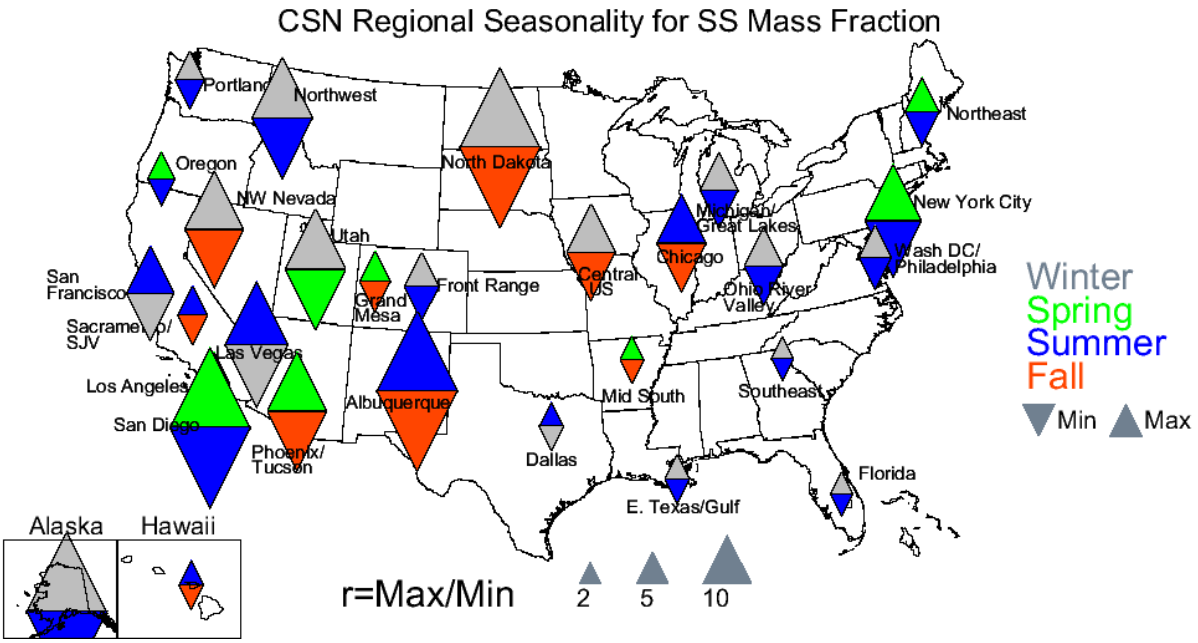

Figure 4.6.4. Seasonal variability for CSN 2005–2008 monthly mean sea salt (SS) reconstructed fine mass fractions. The color of the upward pointing triangle refers to the season with the maximum monthly mean concentration and the downward pointing triangle refers to the season with the minimum monthly mean concentration. The size of the triangles refers to the magnitude of the ratio of maximum to minimum monthly mean mass concentration.

4.7 $PM_{2.5}$ GRAVIMETRIC FINE MASS CONCENTRATIONS

IMPROVE regional monthly mean gravimetric $PM_{2.5}$ fine mass (FM) concentrations ranged from 0.93 μg m^{-3} in the Great Basin region in January to 26.0 μg m^{-3} in the urban site of Fresno in November. The highest concentrations in a nonurban region occurred at the Appalachian region in August (16.41 μg m^{-3}). Most of the regions corresponded to summer maxima and winter minima, with the exception of several regions along the eastern coast that had summer maxima and fall minima (Figure 4.7.1). Western summer maxima were most likely associated with the seasonal dominance of POM concentrations in the northwestern and southwestern United States (see Figures 4.1.2 and 4.1.3, respectively). Regional maxima in the eastern United States were most likely associated with summer peaks in AS concentrations (see Figure 4.1.1). There was less seasonality in FM compared to individual species, with nine regions having maximum to minimum ratios less than 2. The maximum ratio occurred at the Northern Rocky Mountains region (7.3) compared to the minimum region at Ontario (1.3). Higher seasonality occurred in the western compared to the eastern United States.

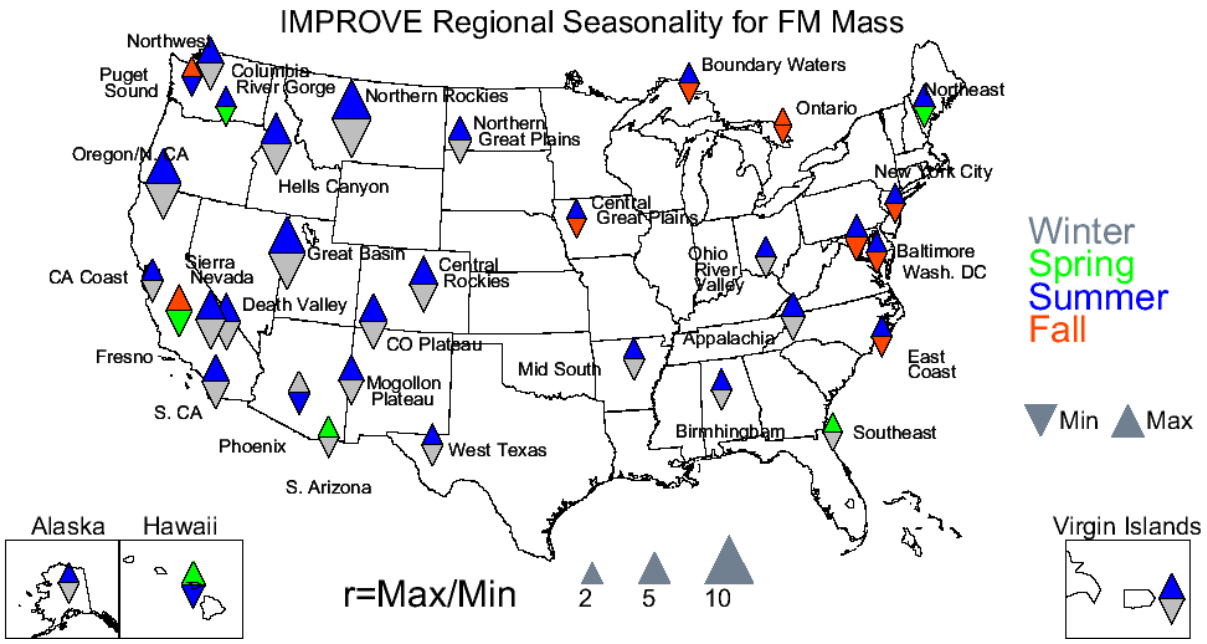

Figure 4.7.1. Seasonal variability for IMPROVE 2005–2008 monthly mean $PM_{2.5}$ gravimetric fine mass (FM) concentrations. The color of the upward pointing triangle refers to the season with the maximum monthly mean concentration and the downward pointing triangle refers to the season with the minimum monthly mean concentration. The size of the triangles refers to the magnitude of the ratio of maximum to minimum monthly mean mass concentration.

FM concentrations were higher at the CSN urban regions, ranging from 3.52 μg m^{-3} in Alaska in August to 34.1 μg m^{-3} in Sacramento/San Joaquin Valley in December. In contrast to the IMPROVE network, many regions corresponded to winter maxima and spring minima. The regional seasonal patterns of CSN FM concentrations were very different from the IMPROVE regional seasonal patterns (Figure 4.7.2). Many western U.S. regions corresponded to winter maxima and spring minima, most likely due to the prevalence of peaks in AN and POM concentrations in winter (see Figures 4.1.7 and 4.1.8). Regions in the East corresponded to summer maxima and winter and fall minima, and probably were associated with summer peaks in AS concentrations since it dominates FM in summer in this area (Figure 4.1.6). In general the urban regions demonstrated a lower degree of seasonality compared to FM concentrations in the rural regions. Fifteen regions had maximum to minimum ratios less than 2; the maximum ratio occurred at Alaska (7.5), compared to the minimum at the Central U.S. region (1.5).

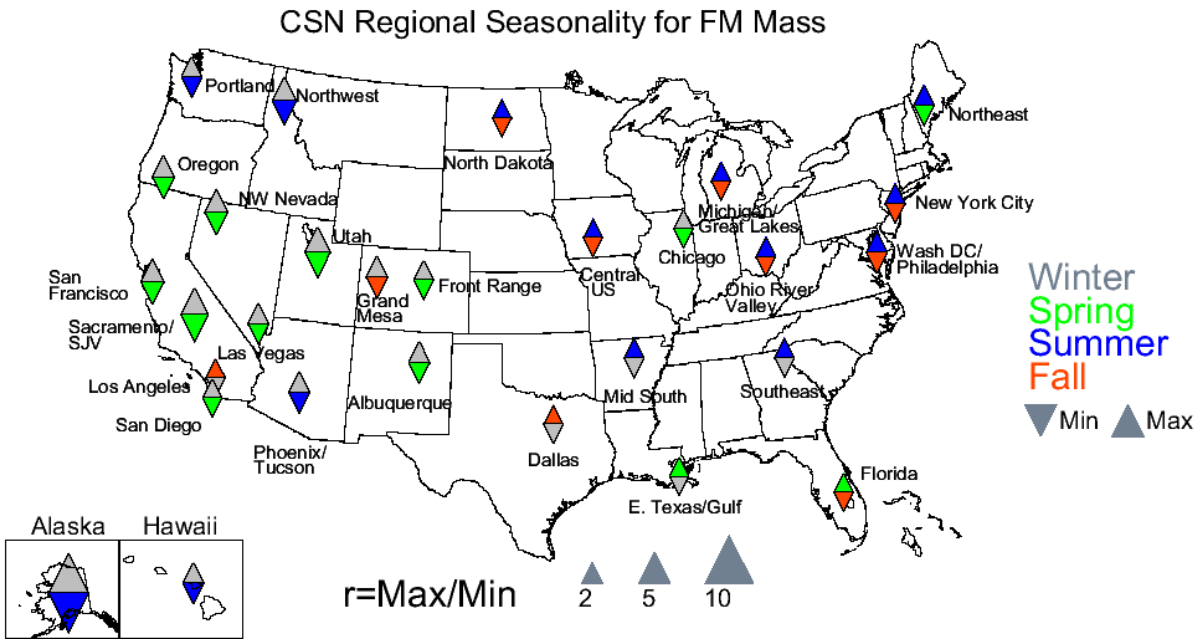

Figure 4.7.2. Seasonal variability for CSN 2005–2008 monthly mean $PM_{2.5}$ gravimetric fine mass (FM) concentrations. The color of the upward pointing triangle refers to the season with the maximum monthly mean concentration and the downward pointing triangle refers to the season with the minimum monthly mean concentration. The size of the triangles refers to the magnitude of the ratio of maximum to minimum monthly mean mass concentration.

4.8 COARSE MASS CONCENTRATIONS

IMPROVE 2005–2008 regional monthly mean coarse mass (CM) concentrations ranged from 0.46 μg m^{-3} in the Northwest region in December to 19.56 μg m^{-3} in the rural site of Virgin Islands in July and 39.79 μg m^{-3} in the urban Fresno site in September. The seasonal distribution of coarse mass concentrations was fairly similar for northwestern regions (see Figure 4.8.1). Although the magnitude of coarse mass concentrations varied, they were highest in July and August for all of the regions in the northwestern United States, with the exception of the Oregon/Northern California region. The Columbia River Gorge region had the highest concentration in the northwestern United States, compared to the lowest concentrations in the Northwest region. In the southwestern United States the summer maxima associated with the Sierra Nevada and Great Basin regions shifted toward the spring months for regions farther south (e.g., Colorado Plateau, Southern Arizona, and West Texas, see Figure 4.8.2). A bimodal distribution corresponding to peaks in concentration in spring/summer and late fall was associated with the Southern Arizona, West Texas, and Mogollon Plateau regions, perhaps related to soil, as dust source regions in Mexico and predominant meteorological conditions correspond to dust episodes in those seasons (Rivera Rivera et al., 2008). The Great Basin, Central Rocky Mountains, and Colorado Plateau and Mogollon Plateau regions corresponded to the lowest monthly mean CM concentrations in the southwestern United States, compared to the regions farther south and in California, where the peak concentrations were twice as high.

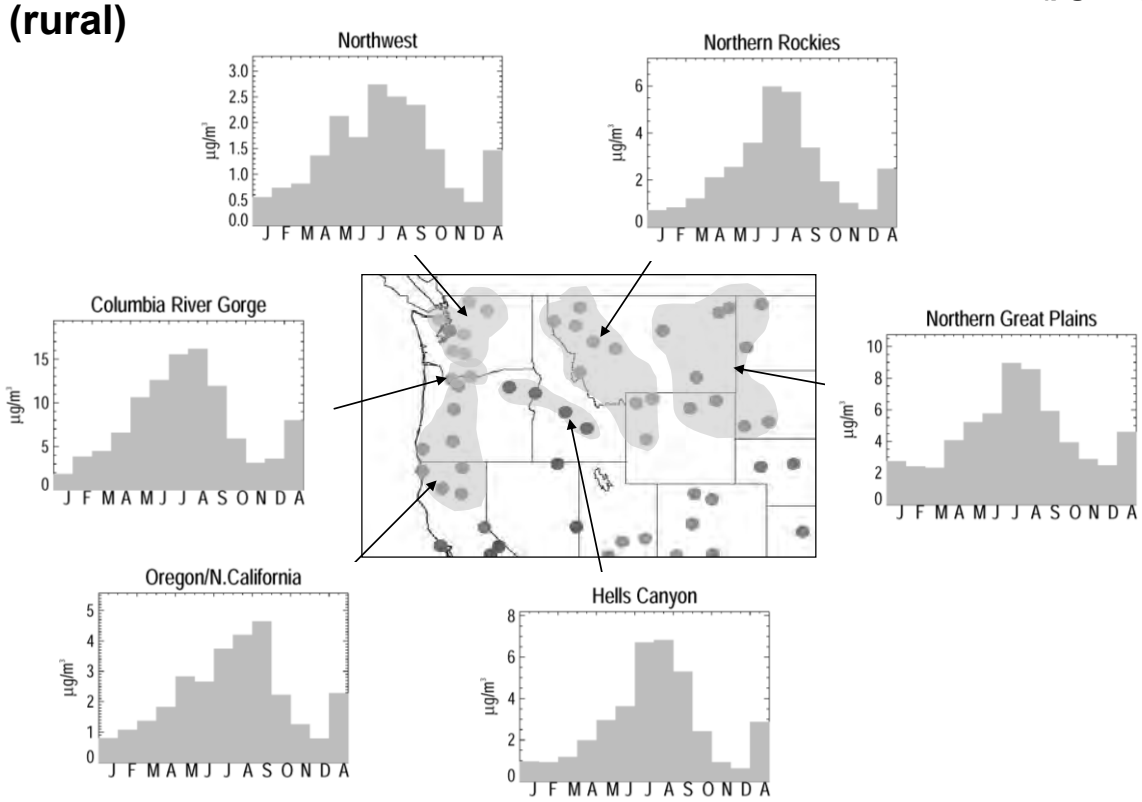

Figure 4.8.1. IMPROVE 2005–2008 regional monthly mean coarse mass concentrations (µg m^{-3}) for the northwestern United States. The letters on the x-axis correspond to the month and "A" corresponds to "annual" mean. The shaded area corresponds to the regions that comprise the sites used in the analysis, shown as dots.

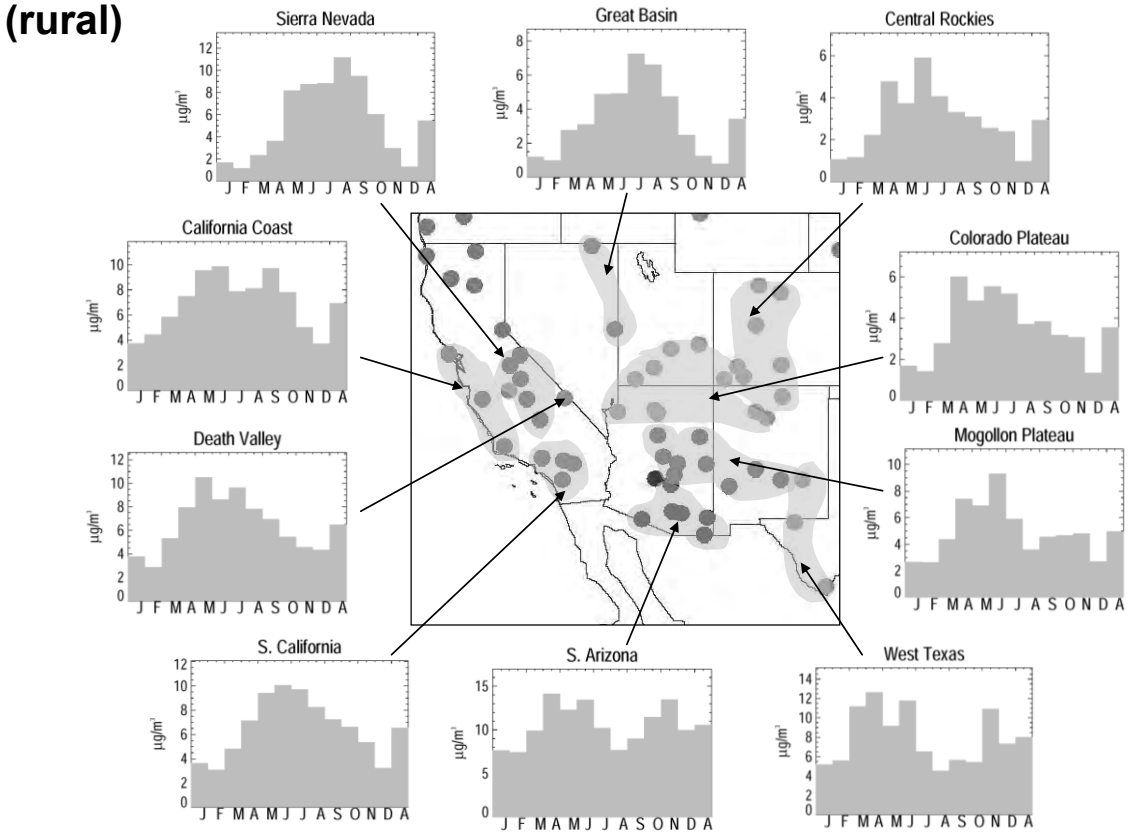

Figure 4.8.2. IMPROVE 2005–2008 regional monthly mean coarse mass concentrations (µg m^{-3}) for the southwestern United States. The letters on the x-axis correspond to the month and "A" corresponds to "annual" mean. The shaded area corresponds to the regions that comprise the sites used in the analysis, shown as dots.

CM concentrations increased during summer months at regions in the eastern United States, such as Northeast, East Coast, Appalachia, and Ohio River Valley (see Figure 4.8.3). Regions toward the central United States were associated with summer peaks. CM concentrations were fairly well distributed across months in the eastern compared to the western United States, with less-defined peaks of concentrations in any one month. The Virgin Island site corresponded to a large peak in CM concentration in summer months compared to other months (Figure 4.8.4) that was probably associated with the transport of North African dust. The CM concentrations at the Virgin Islands region were nearly ten times greater than the other OCONUS regions of Hawaii and Alaska. Those regions did not exhibit strong peaks in monthly concentrations, but concentrations did increase somewhat in spring months.

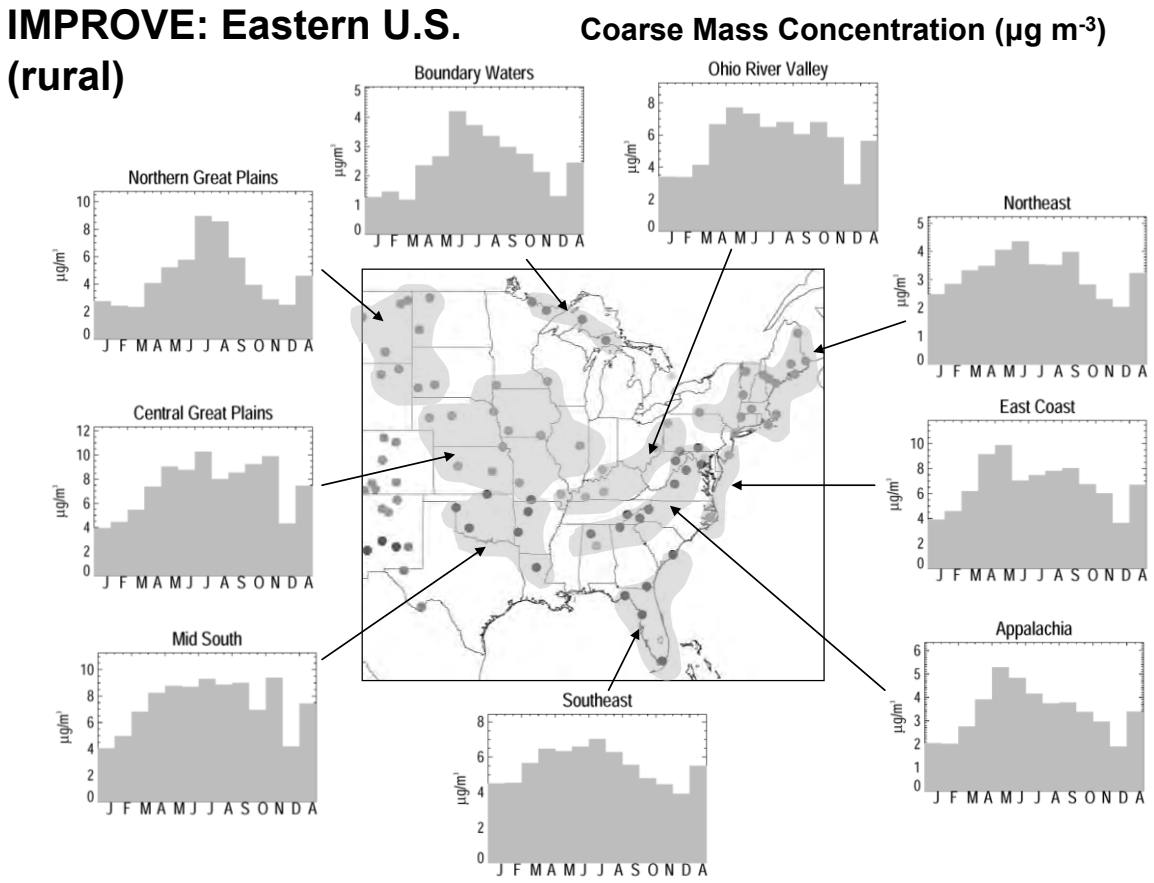

Figure 4.8.3. IMPROVE 2005–2008 regional monthly mean coarse mass concentrations (μg m^{-3}) for the eastern United States. The letters on the x-axis correspond to the month and "A" corresponds to "annual" mean. The shaded area corresponds to the regions that comprise the sites used in the analysis, shown as dots.

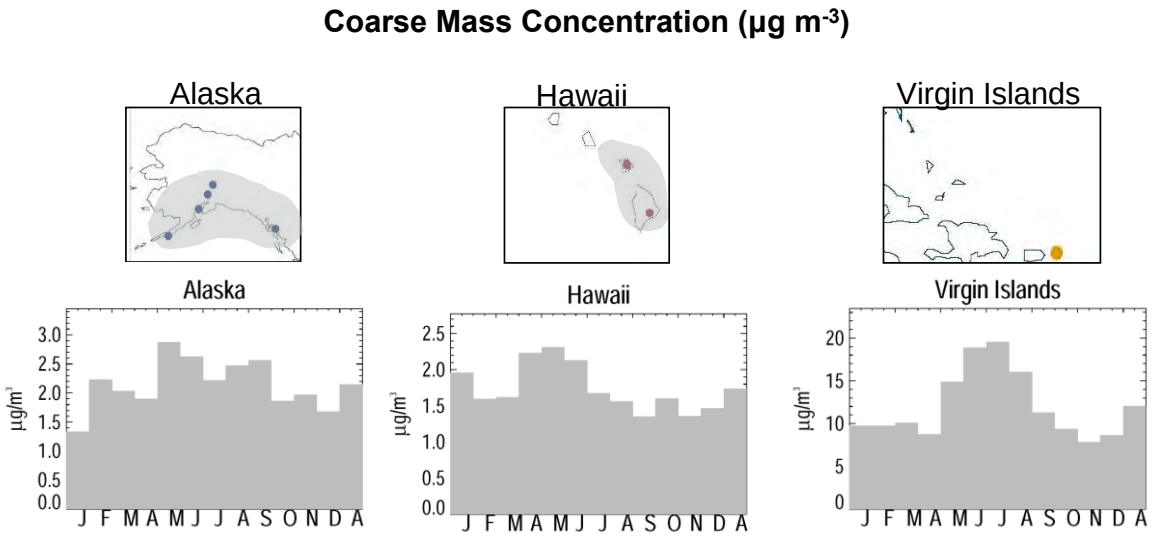

Figure 4.8.4. IMPROVE 2005–2008 regional monthly mean coarse mass concentrations (µg m^{-3}) for OCONUS U.S. The letters on the x-axis correspond to the month and "A" corresponds to "annual" mean. The shaded area corresponds to the regions that comprise the sites used in the analysis, shown as dots.

Most regions demonstrated some seasonality in monthly mean CM concentrations, with only four regions having maximum to minimum ratios less than 2. The highest ratio occurred at Hells Canyon (11.0) and the lowest was in Washington, D.C. (1.6). The seasonality was higher in the western United States. Most regions corresponded to winter minima, with the exception of a few regions (e.g., West Texas, Puget Sound, Northern Great Plains, Boundary Waters, and Washington, D.C., see Figure 4.8.5). Summer maxima occurred for over half of the regions and many of them were located in the northwestern United States, in California, and in the Southeast region. Spring maxima occurred for many eastern U.S. regions, as well as Southern Arizona, West Texas, and the Colorado Plateau.

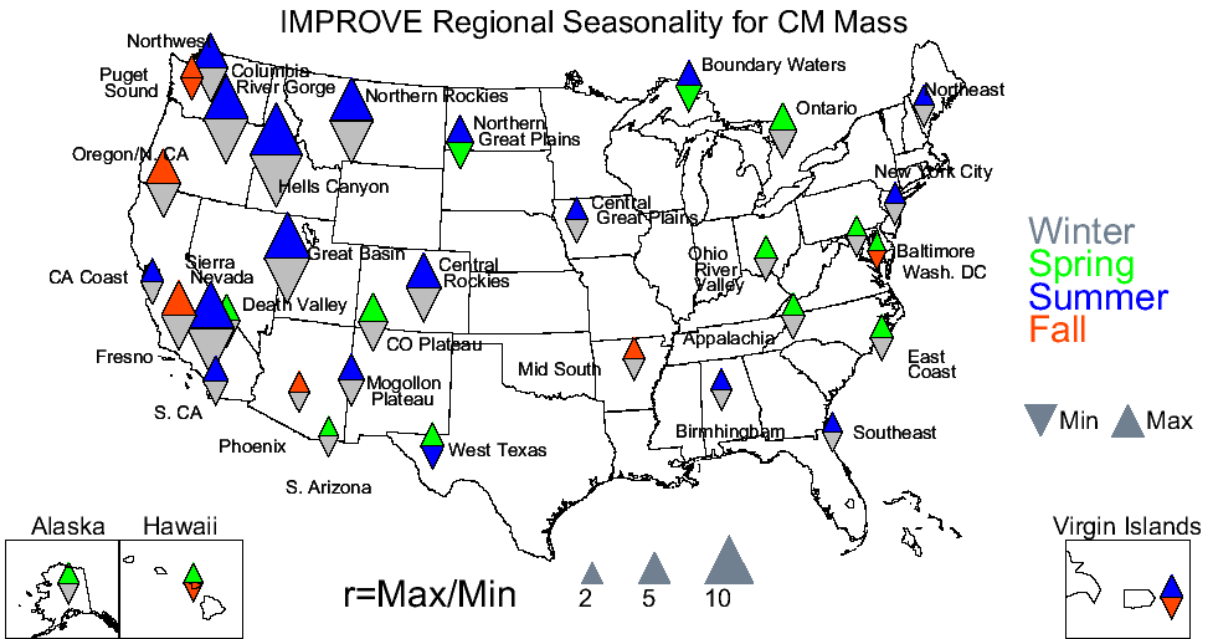

Figure 4.8.5. Seasonal variability for IMPROVE 2005–2008 monthly mean coarse mass (CM) concentrations. The color of the upward pointing triangle refers to the season with the maximum monthly mean concentration and the downward pointing triangle refers to the season with the minimum monthly mean concentration. The size of the triangles refers to the magnitude of the ratio of maximum to minimum monthly mean mass concentration.

4.9 DISCUSSION

The differences observed in the seasonal and spatial patterns in species concentrations for the rural regions of the IMPROVE network and the urban/suburban locations in the CSN network were indicative of the spatial extent of aerosol sources, atmospheric processes, regional transport, and sinks. For example, AS seasonal patterns and concentrations were similar for both the IMPROVE rural and CSN urban regions, with summer maxima in the eastern half of the country. This pattern reflected the higher emissions of SO_2 in this region and favorable conditions for aerosol formation in summer. Seasonal patterns in AN were consistent between CSN and IMPROVE regions. Winter maxima were observed for urban locations and in the central United States, demonstrating the regional impacts of agricultural sources in that area and favorable aerosol formation conditions during that season. CSN urban nitrate concentrations were considerably higher than rural IMPROVE concentrations. Maximum contributions of AN to fine mass occurred in winter for both rural and urban regions.

The strong summer maxima in POM concentrations at western rural regions (Figure 4.3.1) contrasted with the summer/fall/winter maxima observed at CSN urban regions (Figure 4.3.2), suggesting that wildfire activity is a major contributor to POM concentrations in rural areas especially in the western and northwestern United States in summer. Biogenic secondary organic aerosol also could have contributed significantly to high summer POM concentrations as well. Winter urban maxima at some urban regions were probably due in part to meteorological conditions but also to local sources. LAC concentrations followed similar patterns as POM concentrations, although summer maxima rural LAC concentrations were not as dominant as POM concentrations. CSN LAC concentrations corresponding to fall/winter urban maxima were

probably associated with local sources like residential heating and transportation. Both CSN POM and LAC concentrations were considerably higher than those measured in rural IMPROVE regions. The maximum percent contribution of POM to RCFM was highest in summer for most rural regions compared to both summer and fall in urban regions. LAC percent contributions displayed a somewhat different seasonal pattern compared to POM. LAC maximum percent contributions at rural regions occurred in winter, while regional urban maximum contributions occurred in fall, followed by winter.

Soil concentrations were influenced by both local and long-range transport. Major regions of higher dust concentrations were evident in the urban and rural regions, especially in the southwestern United States in spring/summer and IMPROVE Southeast and CSN East Texas/Gulf regions in summer. Both networks had many "hot spots" of high soil that were similar in some seasons and not others, suggesting fairly localized fugitive dust sources (Kavouras et al., 2007; 2009). The maximum contributions of soil to fine mass occurred in spring for many rural and urban regions, perhaps associated with agricultural sources. While the seasons corresponding to maxima and minima for CM and fine soil concentrations agreed in some regions (e.g., in the northwestern United States, see Figures 4.5.1 and 4.8.1), for most regions these seasons did not coincide. One would expect that if soil was the main contributor to CM, their seasonality would be similar. However, based on work by Malm et al. (2007), who investigated the speciation of CM at select IMPROVE sites for a year, the speciation of CM varied significantly depending on region and month. For example, the Mount Rainier site corresponded to POM-dominated CM either year round or for select months, as did the sites at Sequoia National Park in California, Bridger Wilderness Area in Wyoming, Bondville, Illinois, and Great Smoky Mountains National Park in Tennessee. The only regions with consistent seasonal maxima and minima between soil and CM were Columbia River Gorge, Hells Canyon, Northern Rocky Mountains, Great Basin, Death Valley, and the Colorado Plateau. It is possible and probably quite likely that the seasonality of CM was impacted by the variability of species other than soil.

Sea salt concentrations and percent contributions were negligible at most regions for both the urban and rural networks. Coastal regions (including both the east and west coasts, including OCONUS regions) were the only regions to correspond to non-negligible impacts from sea salt on RCFM. Sea salt corresponded to a high degree of seasonality, probably in part because of its very low concentrations.

FM concentrations were noticeably higher in urban regions than rural regions. The highest concentrations of FM for the CSN network occurred in California, in the Sacramento/San Joaquin Valley region during December, where AN and POM composed the majority of the RCFM. Similarly, the urban IMPROVE site of Fresno had the highest FM concentrations in November, again dominated by AN and POM. The highest IMPROVE nonurban FM concentration corresponded to the Appalachia region in August, where AS dominated the RCFM composition in summer.

Tables with regional monthly mean concentrations listed a function of species, month and region are provided in Appendix D.1 for IMPROVE and CSN values. Regional monthly mean mass fractions are listed in Appendix D.2 for IMPROVE and CSN. Stacked bar charts of

monthly mean concentrations for individual sites for IMPROVE and the CSN are provided in Appendix D.3, while mass fractions for IMPROVE and the CSN are provided in Appendix D.4.

REFERENCES

Kavouras, I. G., V. Etyemezian, J. Xu, D. W. Dubois, M. Green, and M. Pitchford (2007), Assessment of the local windblown component of dust in the western United States, *J. Geophys. Res., 112,* D08211, doi:10.1029/2006JD007832.

Kavouras, I. G., V. Etyemezian, D. W. Dubois, J. Xu, and M. Pitchford (2009), Source reconciliation of atmospheric dust causing visibility impairment in Class I areas of the western United States, *J. Geophys. Res., 114,* D02308, doi:10.1029/2008JD009923.

White, W. H., B. P. Perley, R. L. Poirot, T. F. Dann, and E. Dabek-Zlotorzynska, 2010, Continental-scale transport of sea salt aerosol, Abstract A43C-0245 presented at the 2010 Fall Meeting, AGU, San Francisco, California, 13-17 December 2010.

Chapter 5. Seasonal Distribution of $PM_{2.5}$ Reconstructed Aerosol Light Extinction Coefficients

Along with the 2005–2008 annual mean $PM_{2.5}$ reconstructed light extinction coefficients (b_{ext}) presented in Chapter 3, we computed monthly mean b_{ext} for major aerosol species including ammonium sulfate (AS), ammonium nitrate (AN), particulate organic matter (POM), light absorbing carbon (LAC), soil, sea salt and coarse mass. These monthly mean b_{ext} values were averaged to regional means based on the IMPROVE and CSN regions discussed in Chapter 4. In this chapter regional monthly and annual mean b_{ext} values are presented as stacked bar charts, similar to the regional mean mass concentrations presented in the previous chapter. For nonhygroscopic species, the seasonality of b_{ext} should be the same as the seasonality in mass concentrations; however, this may not be the case in some instances and is due to the treatment of negative mass concentrations in the calculation of b_{ext} (see Chapter 3). Monthly means are depicted with the first letter of the month, followed by an "A" for annual mean. The seasonal distributions in percent contribution of major $PM_{2.5}$ aerosol species to b_{ext} are also presented. Seasonal periods are defined as winter (December, January, and February), spring (March, April, and May), summer (June, July, and August) and fall (September, October, and November). Seasonal stacked bar charts for monthly mean concentrations are grouped into figures corresponding to four areas of the country: northwestern, southwestern, eastern, and OCONUS (outside the contiguous United States, e.g., Hawaii, Alaska, and Virgin Islands) United States. Regional seasonality is summarized in terms of the ratio of maximum to minimum monthly mean b_{ext} and presented in separate maps for each species. Each region is associated with a set of triangles. The color of the upward pointing triangle refers to the season with the maximum monthly mean concentration. The color of the downward pointing triangle refers to the season with the minimum monthly mean concentration. The size of the triangle corresponds to the ratio of maximum to minimum monthly b_{ext} such that large triangles represent higher levels of seasonality. Recall that most regions comprise many sites; therefore the positions of the triangles on the map are meant to represent the general location of the region. Sections 5.1–5.6 present regional monthly mean b_{ext} for the species listed above. In addition, monthly mean aerosol b_{ext} (b_{ext_aer}), coarse mass b_{ext} (b_{ext_CM}), and deciview are presented in sections 5.7, 5.8, and 5.9, respectively.

5.1 $PM_{2.5}$ AMMONIUM SULFATE LIGHT EXTINCTION COEFFICIENTS

Reconstructed extinction coefficients from ammonium sulfate, b_{ext_AS}, were computed using a dry extinction efficiency of 3 m^2g^{-1} and a humidification factor (f(RH)) to account for hygroscopic effects. The b_{ext_AS} may closely resemble AS mass concentrations, but differences will arise due to its hygroscopic nature. The IMPROVE 2005–2008 regional monthly mean rural b_{ext_AS} ranged from 1.69 Mm^{-1} in the Great Basin region in December to 105.44 Mm^{-1} in the Appalachia region in August. Recall that the eastern United States corresponded to high AS mass concentrations in summer (Chapter 4 and Figure 4.1.1). A similarly high value of 106.33 Mm^{-1} in the IMPROVE urban location of Birmingham demonstrated that the regional influence of AS mass concentrations in conjunction with increased relative humidity in the summer leads to decreased visibility on regional scales. Many of the eastern IMPROVE regions corresponded to high b_{ext_AS} in summer, but values were highest in the Appalachia and Ohio River Valley regions (Figure 5.1.1). Extinction coefficients in the Northeast and Southeast regions were considerably lower, as were values towards the central United States, such as the Central Great Plains and Mid

South regions. Regardless of the magnitude of b_{ext_AS}, it still peaked in the summer at most eastern regions. In the northwestern United States, the b_{ext_AS} was comparable or less than typical values of Rayleigh scattering (~10 Mm^{-1}) (Figure 5.1.2) and only a fraction of the b_{ext_AS} in eastern regions. Values up to 10 Mm^{-1} occurred at the Northern Great Plains, Oregon/Northern California, Columbia River Gorge, and Northwest regions and usually peaked during spring months. Somewhat higher values occurred for some southwestern regions, but values of b_{ext_AS} at many regions were still comparable or less than contributions from Rayleigh scattering (Figure 5.1.3). The West Texas region corresponded to the highest b_{ext_AS}, with values near 20 Mm^{-1} in September. Spring and summer peaks in b_{ext_AS} were common for most of the southwestern regions. Values of b_{ext_AS} were higher at the OCONUS regions compared to the western United States, but not as high as in the eastern United States (Figure 5.1.4).

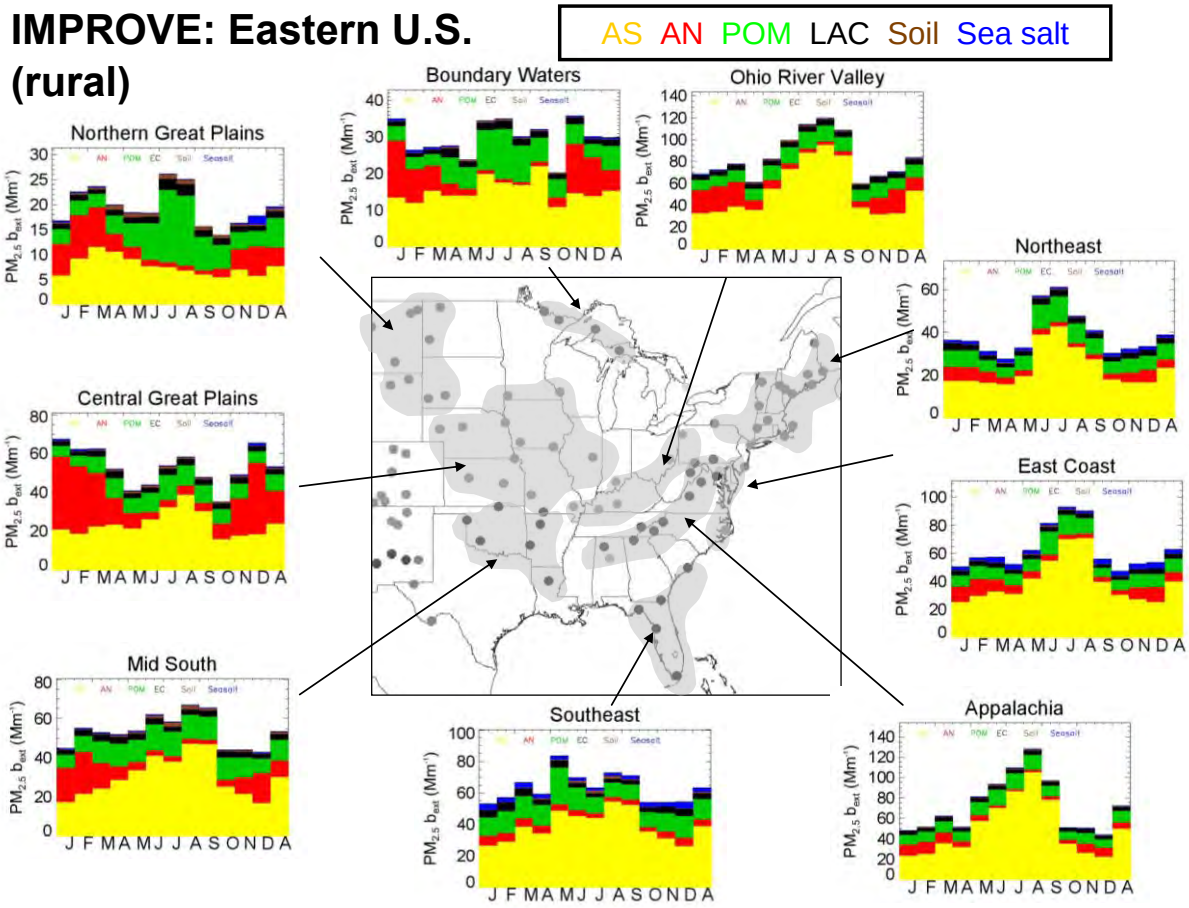

Figure 5.1.1. IMPROVE 2005–2008 regional monthly mean $PM_{2.5}$ reconstructed light extinction coefficients (b_{ext}, Mm^{-1}) for the eastern United States. The letters on the x-axis correspond to the month and "A" corresponds to "annual" mean. Ammonium sulfate (AS) in yellow, ammonium nitrate (AN) in red, particulate organic matter (POM) in green, light absorbing carbon (LAC) in black, soil in brown, and sea salt in blue. The shaded area corresponds to the regions that comprise the sites used in the analysis, shown as dots. The "modified original" IMPROVE algorithm was used (see text). Wavelength corresponds to 550 nm.

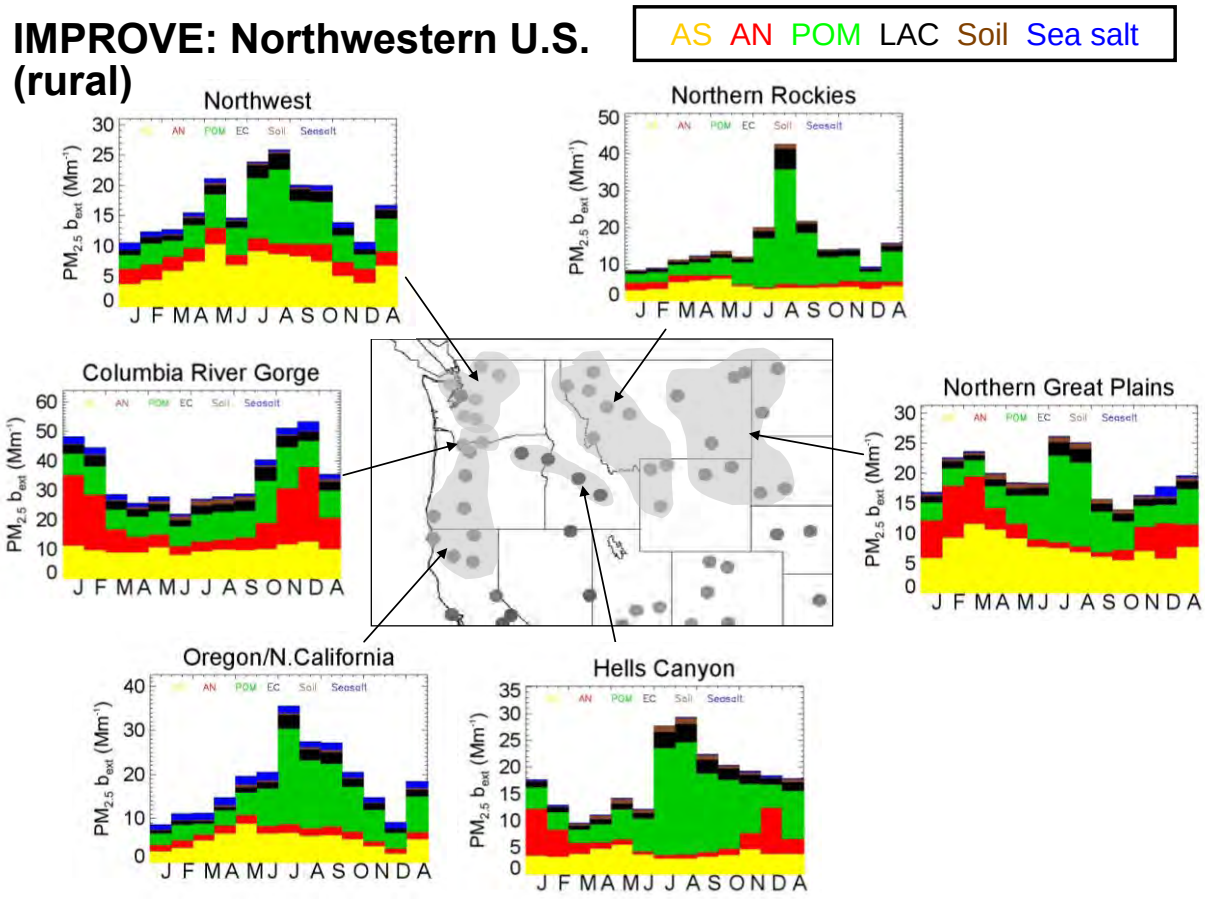

Figure 5.1.2. IMPROVE 2005–2008 regional monthly mean $PM_{2.5}$ reconstructed light extinction coefficients (b_{ext}, Mm^{-1}) for the northwestern United States. The letters on the x-axis correspond to the month and "A" corresponds to "annual" mean. Ammonium sulfate (AS) in yellow, ammonium nitrate (AN) in red, particulate organic matter (POM) in green, light absorbing carbon (LAC) in black, soil in brown, and sea salt in blue. The shaded area corresponds to the regions that comprise the sites used in the analysis, shown as dots. The "modified original" IMPROVE algorithm was used (see text). Wavelength corresponds to 550 nm.

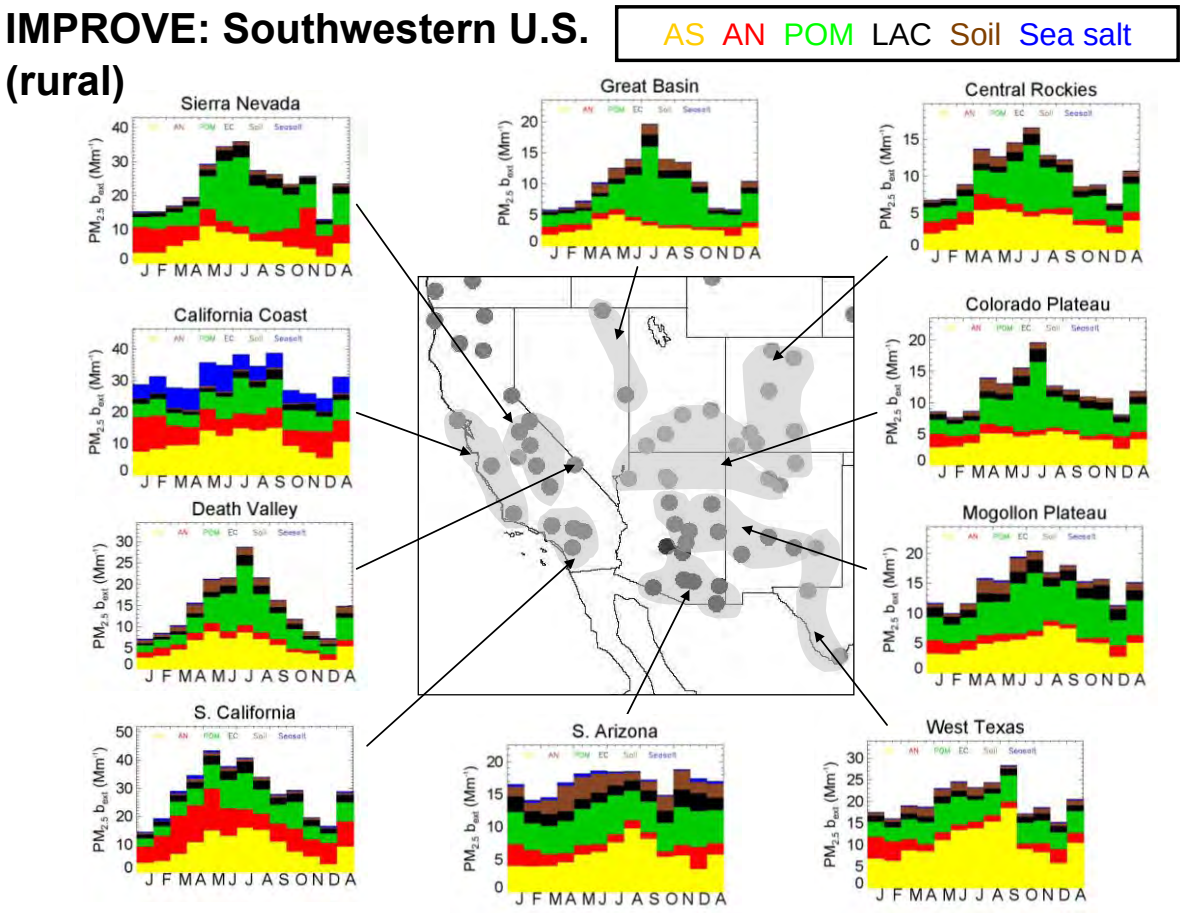

Figure 5.1.3. IMPROVE 2005–2008 regional monthly mean $PM_{2.5}$ reconstructed light extinction coefficients (b_{ext}, Mm^{-1}) for the southwestern United States. The letters on the x-axis correspond to the month and "A" corresponds to "annual" mean. Ammonium sulfate (AS) in yellow, ammonium nitrate (AN) in red, particulate organic matter (POM) in green, light absorbing carbon (LAC) in black, soil in brown, and sea salt in blue. The shaded area corresponds to the regions that comprise the sites used in the analysis, shown as dots. The "modified original" IMPROVE algorithm was used (see text). Wavelength corresponds to 550 nm.

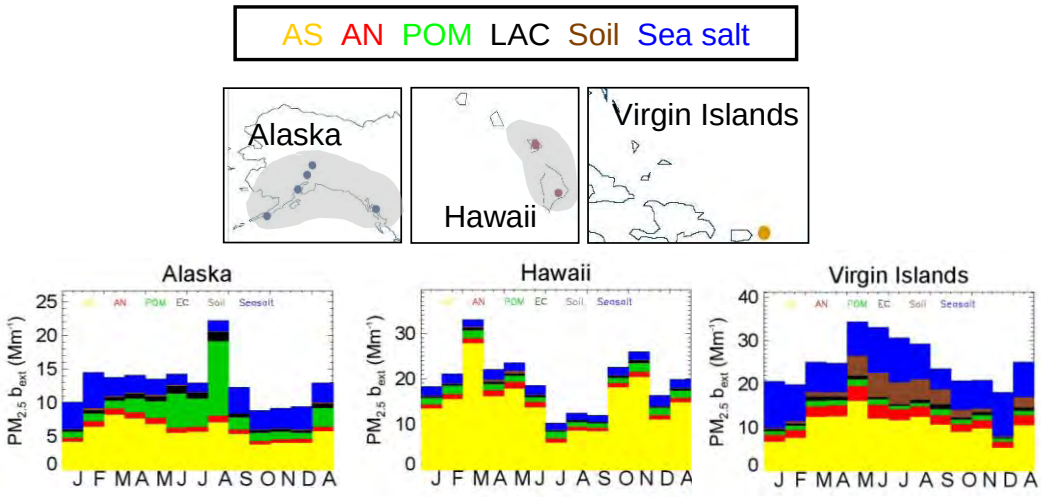

Figure 5.1.4. IMPROVE 2005–2008 regional monthly mean $PM_{2.5}$ reconstructed light extinction coefficients (b_{ext}, Mm^{-1}) for Hawaii, Alaska, and the Virgin Islands. The letters on the x-axis correspond to the month and "A" corresponds to "annual" mean. Ammonium sulfate (AS) in yellow, ammonium nitrate (AN) in red, particulate organic matter (POM) in green, light absorbing carbon (LAC) in black, soil in brown, and sea salt in blue. The shaded area corresponds to the regions that comprise the sites used in the analysis, shown as dots. The "modified original" IMPROVE algorithm was used (see text). Wavelength corresponds to 550 nm.

Only six IMPROVE regions had maximum to minimum b_{ext} ratios less than 2, suggesting a fairly high degree of seasonality in b_{ext_AS}. The largest ratio occurred for the Southern California region (5.2) compared to the lowest in the Colombia River Gorge region (1.6) (Figure 5.1.5). The majority of IMPROVE regions corresponded to summer maxima in b_{ext_AS} (similar to AS mass concentrations), including several regions in the southwestern and eastern United States.

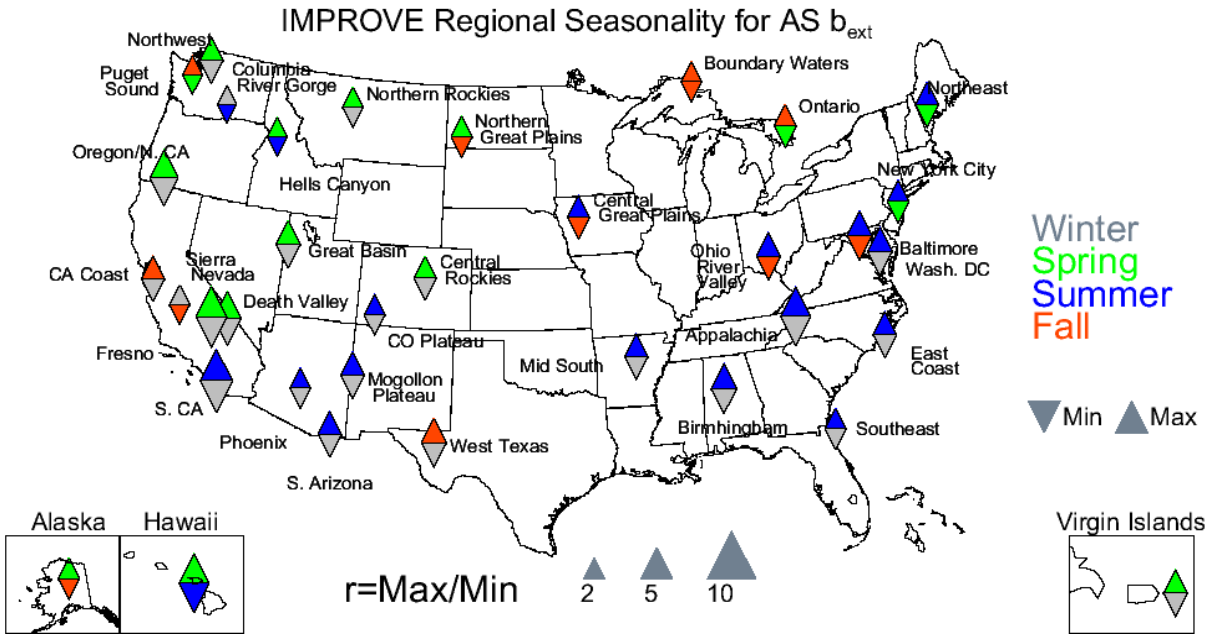

Figure 5.1.5. Seasonal variability for 2005–2008 monthly mean regional IMPROVE ammonium sulfate (AS) light extinction coefficients (b_{ext}). The color of the upward pointing triangle refers to the season with the maximum monthly mean concentration and the downward pointing triangle refers to the season with the minimum monthly mean concentration. The size of the triangles refers to the magnitude of the ratio of maximum to minimum monthly mean mass concentration.

The highest CSN urban b_{ext_AS} occurred at the Ohio River Valley region in September (106.94 Mm^{-1}) and was comparable to the rural regional monthly mean maximum. The lowest urban b_{ext_AS} (3.08 Mm^{-1}) occurred in Las Vegas in December. With the exception of Los Angeles and San Diego, the b_{ext_AS} at the other southwestern regions were similar to the low values at the Las Vegas region (Figure 5.1.6) and also reflected the low AS mass concentrations (Figure 4.1.7). Although AS mass concentrations were similar for the regions in the southwestern and northwestern United States (Figure 4.1.7 and Figure 4.1.8, respectively), the b_{ext_AS} values were higher in the northwestern compared to the southwestern United States for many regions (compare Figure 5.1.7 and Figure 5.1.6, respectively). Much higher b_{ext_AS} values corresponded to eastern regions, especially at the Ohio River Valley, Washington D.C./Philadelphia Corridor, and Southeast regions in summer (and fall for the Ohio River Valley region) (Figure 5.1.8). The b_{ext_AS} values decreased at central U.S. regions but still peaked during summer and fall months. Extinction values were higher in Alaska compared to Hawaii, especially during winter months (Figure 5.1.9).

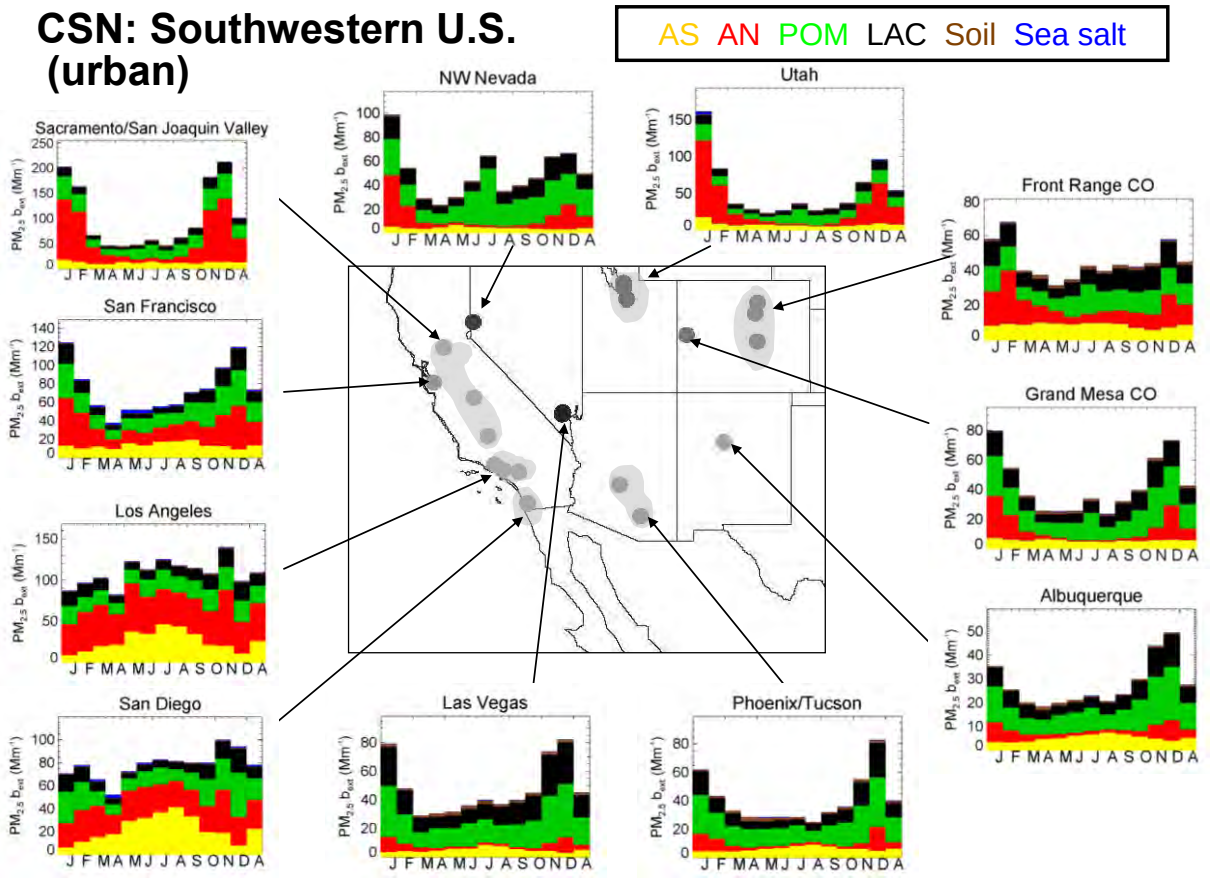

Figure 5.1.6. CSN 2005–2008 regional monthly mean $PM_{2.5}$ reconstructed light extinction coefficients (b_{ext}, Mm^{-1}) for the southwestern United States. The letters on the x-axis correspond to the month and "A" corresponds to "annual" mean. Ammonium sulfate (AS) in yellow, ammonium nitrate (AN) in red, particulate organic matter (POM) in green, light absorbing carbon (LAC) in black, soil in brown, and sea salt in blue. The shaded area corresponds to the regions that comprise the sites used in the analysis, shown as dots. The "modified original" IMPROVE algorithm was used (see text). Wavelength corresponds to 550 nm.

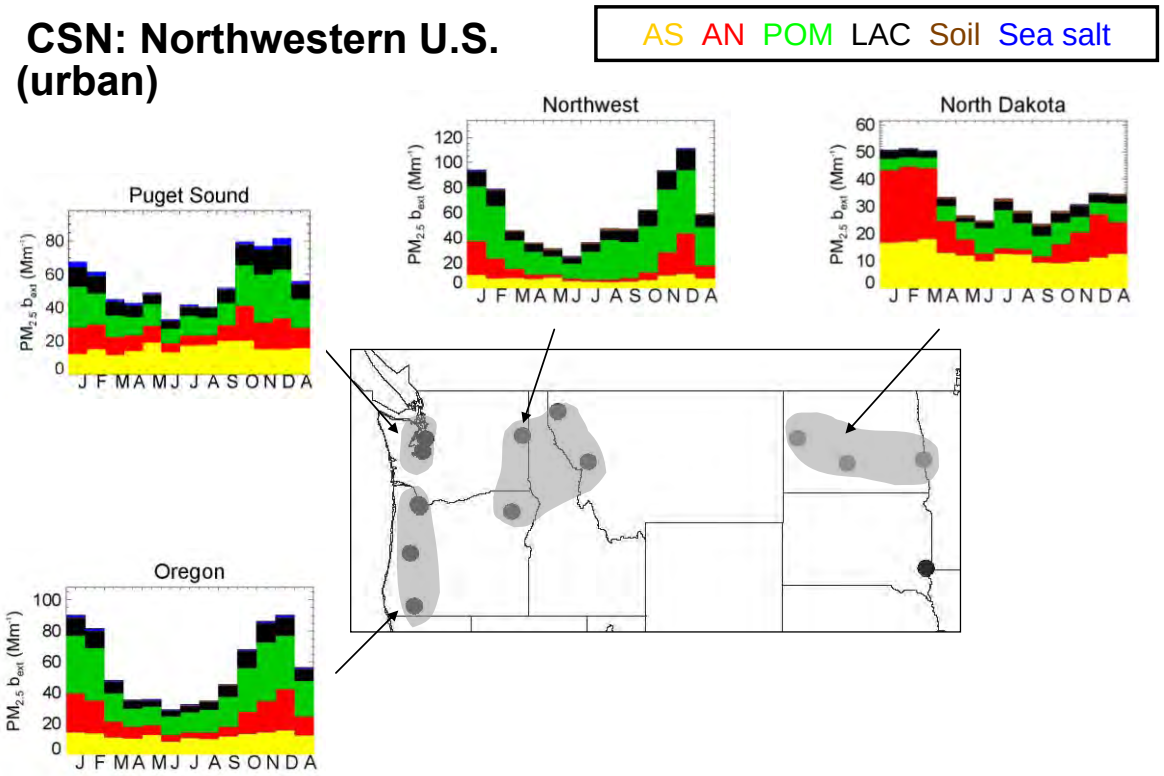

Figure 5.1.7. CSN 2005–2008 regional monthly mean $PM_{2.5}$ reconstructed light extinction coefficients (b_{ext}, Mm^{-1}) for the northwestern United States. The letters on the x-axis correspond to the month and "A" corresponds to "annual" mean. Ammonium sulfate (AS) in yellow, ammonium nitrate (AN) in red, particulate organic matter (POM) in green, light absorbing carbon (LAC) in black, soil in brown, and sea salt in blue. The shaded area corresponds to the regions that comprise the sites used in the analysis, shown as dots. The "modified original" IMPROVE algorithm was used (see text). Wavelength corresponds to 550 nm.

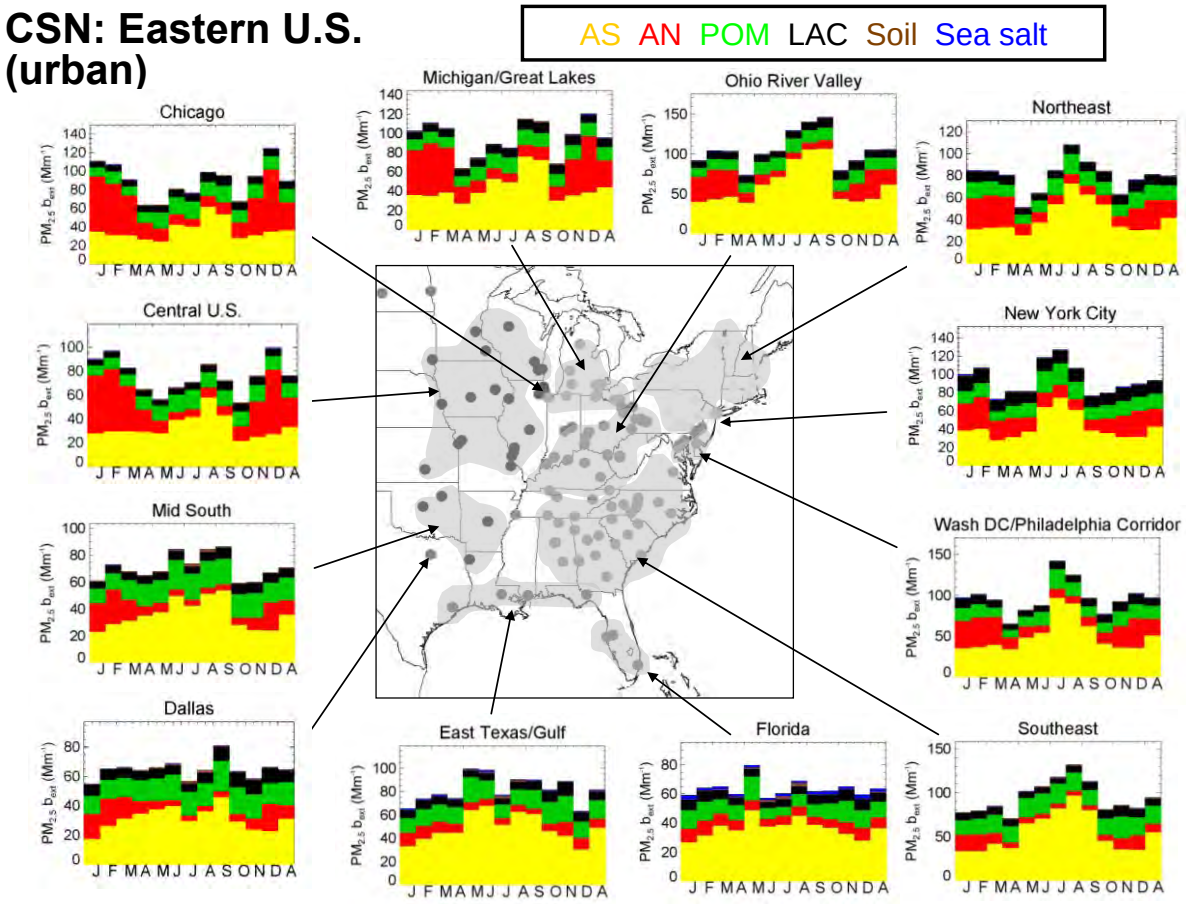

Figure 5.1.8. CSN 2005–2008 regional monthly mean reconstructed light extinction coefficients (b_{ext}, Mm^{-1}) for the eastern United States. The letters on the x-axis correspond to the month and "A" corresponds to "annual" mean. Ammonium sulfate (AS) in yellow, ammonium nitrate (AN) in red, particulate organic matter (POM) in green, light absorbing carbon (LAC) in black, soil in brown, and sea salt in blue. The shaded area corresponds to the regions that comprise the sites used in the analysis, shown as dots. The "modified original" IMPROVE algorithm was used (see text). Wavelength corresponds to 550 nm.

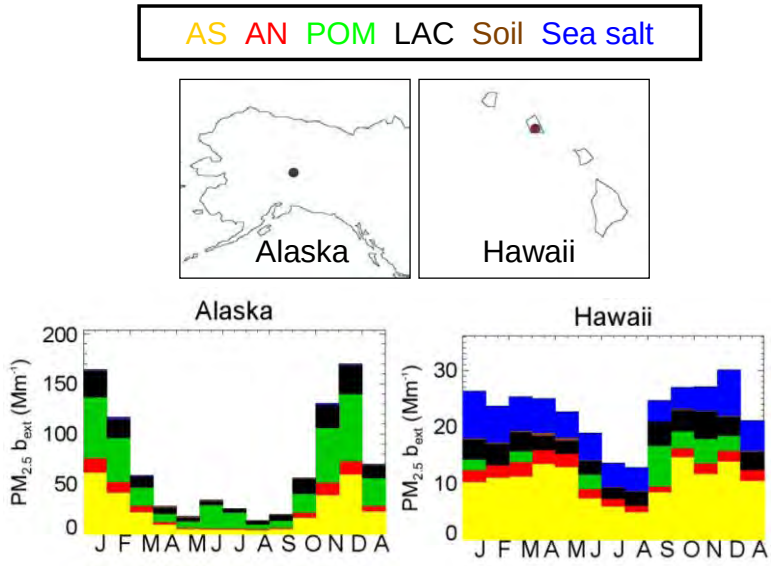

Figure 5.1.9. CSN 2005–2008 regional monthly mean $PM_{2.5}$ reconstructed light extinction coefficients (b_{ext}, Mm^{-1}) for Hawaii and Alaska. The letters on the x-axis correspond to the month and "A" corresponds to "annual" mean. Ammonium sulfate (AS) in yellow, ammonium nitrate (AN) in red, particulate organic matter (POM) in green, light absorbing carbon (LAC) in black, soil in brown, and sea salt in blue. The shaded area corresponds to the regions that comprise the sites used in the analysis, shown as dots. The "modified original" IMPROVE algorithm was used (see text). Wavelength corresponds to 550 nm.

CSN regions corresponded to similar degrees of seasonality for monthly mean b_{ext_AS} and AS mass concentrations (Figures 5.1.10 and 4.1.10, respectively). Regions in southern California and Alaska had the highest degrees of seasonality across the United States. The highest ratio occurred in Alaska (14.0) compared to the lowest in Grand Mesa CO (1.5). Many regions corresponded to summer b_{ext_AS} maxima but may correspond to different regions from those for summer mass concentration maxima (e.g., the Puget Sound, Oregon, Sacramento/San Joaquin Valley, Front Range CO, Mid South, East Texas/Gulf, and Ohio River Valley regions).

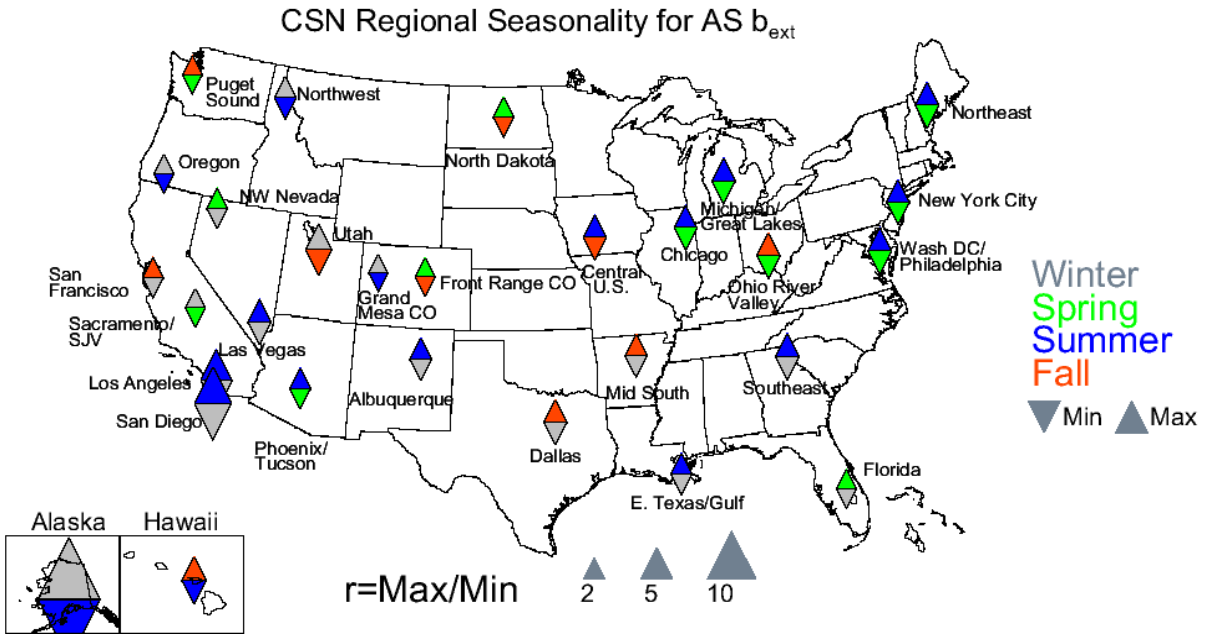

Figure 5.1.10. Seasonal variability for 2005–2008 monthly mean regional CSN ammonium sulfate (AS) light extinction coefficients (b_{ext}). The color of the upward pointing triangle refers to the season with the maximum monthly mean concentration and the downward pointing triangle refers to the season with the minimum monthly mean concentration. The size of the triangles refers to the magnitude of the ratio of maximum to minimum monthly mean mass concentration.

The IMPROVE fractional b_{ext} contribution from AS ranged from 4.6% in Phoenix in December (8.6% in the Northern Rocky Mountains for rural IMPROVE regions) to 84.6% in Hawaii in March, most likely due to volcanic emissions. Other OCONUS regions also had high AS contributions to b_{ext}. Both the Alaska and Virgin Islands regions corresponded to percent contributions of 40% or higher year round, while contributions of AS to b_{ext} at the Hawaii region were 60% or greater year round (Figure 5.1.11). Percent contributions of AS dominated b_{ext} in the eastern United States, ranging from 40% up to ~80% in the Ohio River Valley, East Coast, and Appalachia regions during summer (Figure 5.1.12). The percent contributions of AS to b_{ext} decreased in the southwestern United States to 20–40% at most regions (Figure 5.1.13) but were slightly higher than the AS mass fractions in the same regions (Figure 4.1.13). A similar pattern was observed (higher b_{ext_AS} fractions compared to AS mass fractions) at the northwestern U.S. regions (Figure 5.1.14). Percent contributions of AS to b_{ext} ranged from 15 to 50% and decreased during the summer months at every region except Columbia River Gorge.

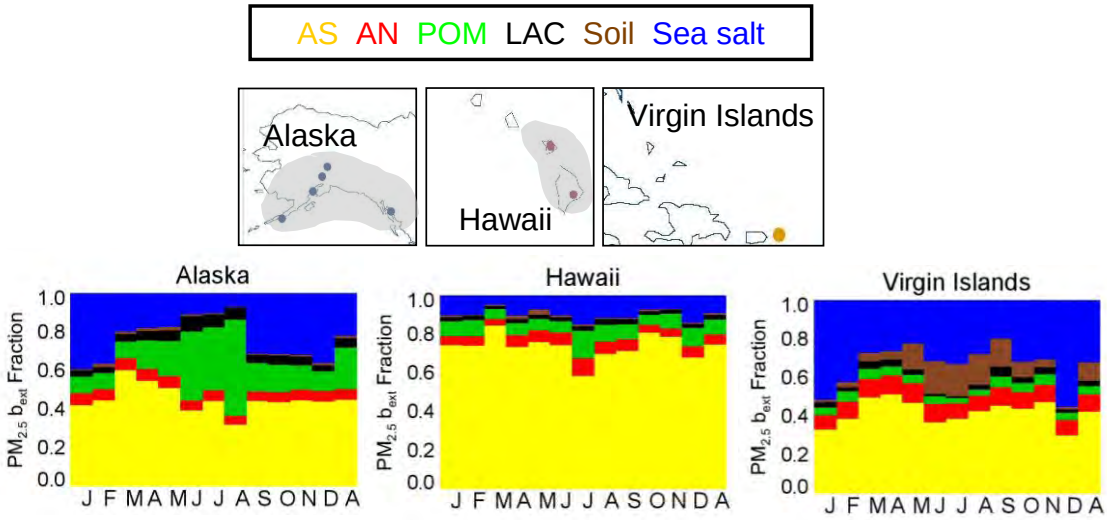

Figure 5.1.11. IMPROVE 2005–2008 regional monthly mean $PM_{2.5}$ light extinction coefficient (b_{ext}) fractions for Hawaii, Alaska, and the Virgin Islands. The letters on the x-axis correspond to the month and "A" corresponds to "annual" mean. Ammonium sulfate (AS) in yellow, ammonium nitrate (AN) in red, particulate organic matter (POM) in green, light absorbing carbon (LAC) in black, soil in brown, and sea salt in blue. The shaded area corresponds to the regions that comprise the sites used in the analysis, shown as dots.

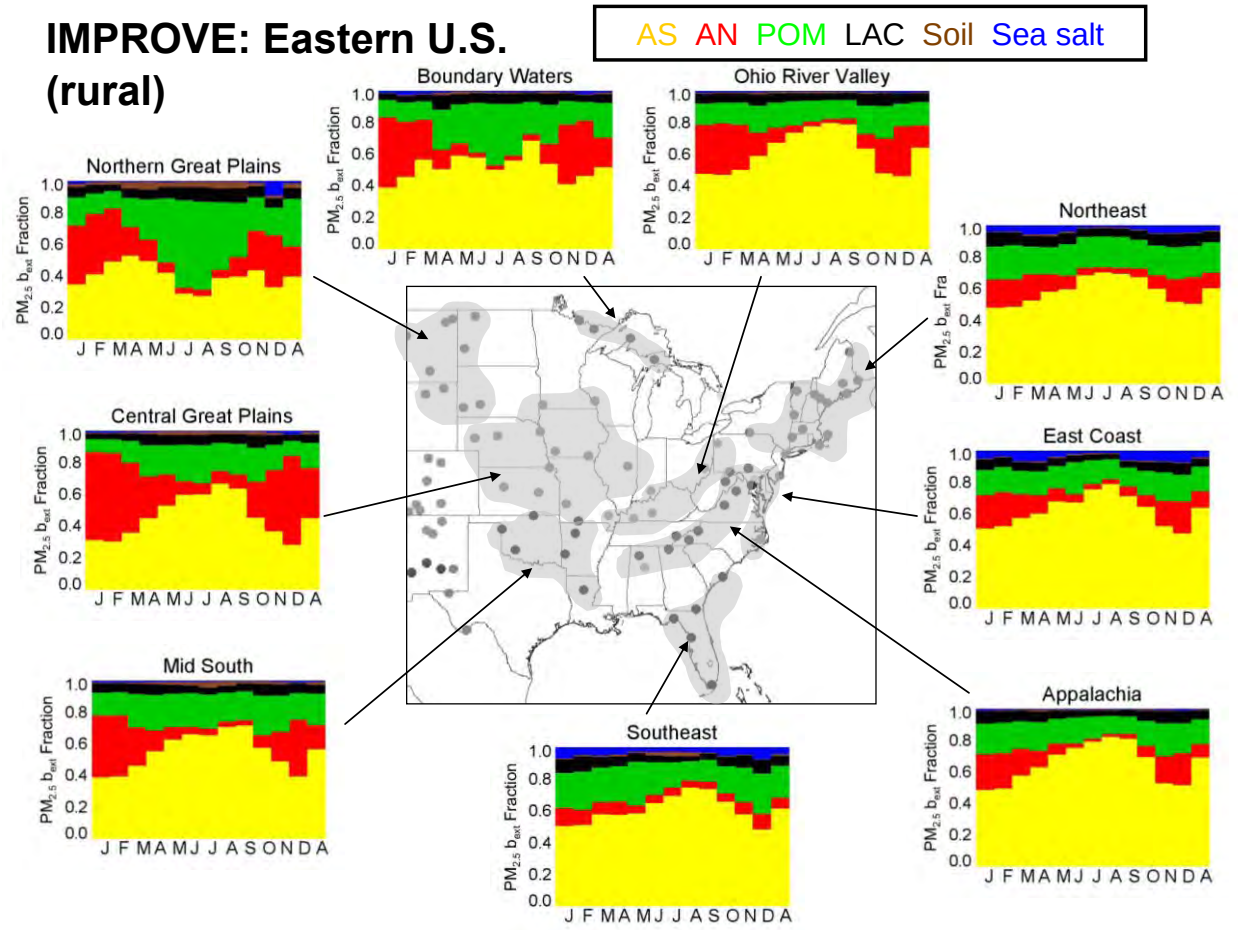

Figure 5.1.12. IMPROVE 2005–2008 regional monthly mean $PM_{2.5}$ light extinction coefficient (b_{ext}) fractions for the eastern United States. The letters on the x-axis correspond to the month and "A" corresponds to "annual" mean. Ammonium sulfate (AS) in yellow, ammonium nitrate (AN) in red, particulate organic matter (POM) in green, light absorbing carbon (LAC) in black, soil in brown, and sea salt in blue. The shaded area corresponds to the regions that comprise the sites used in the analysis, shown as dots.

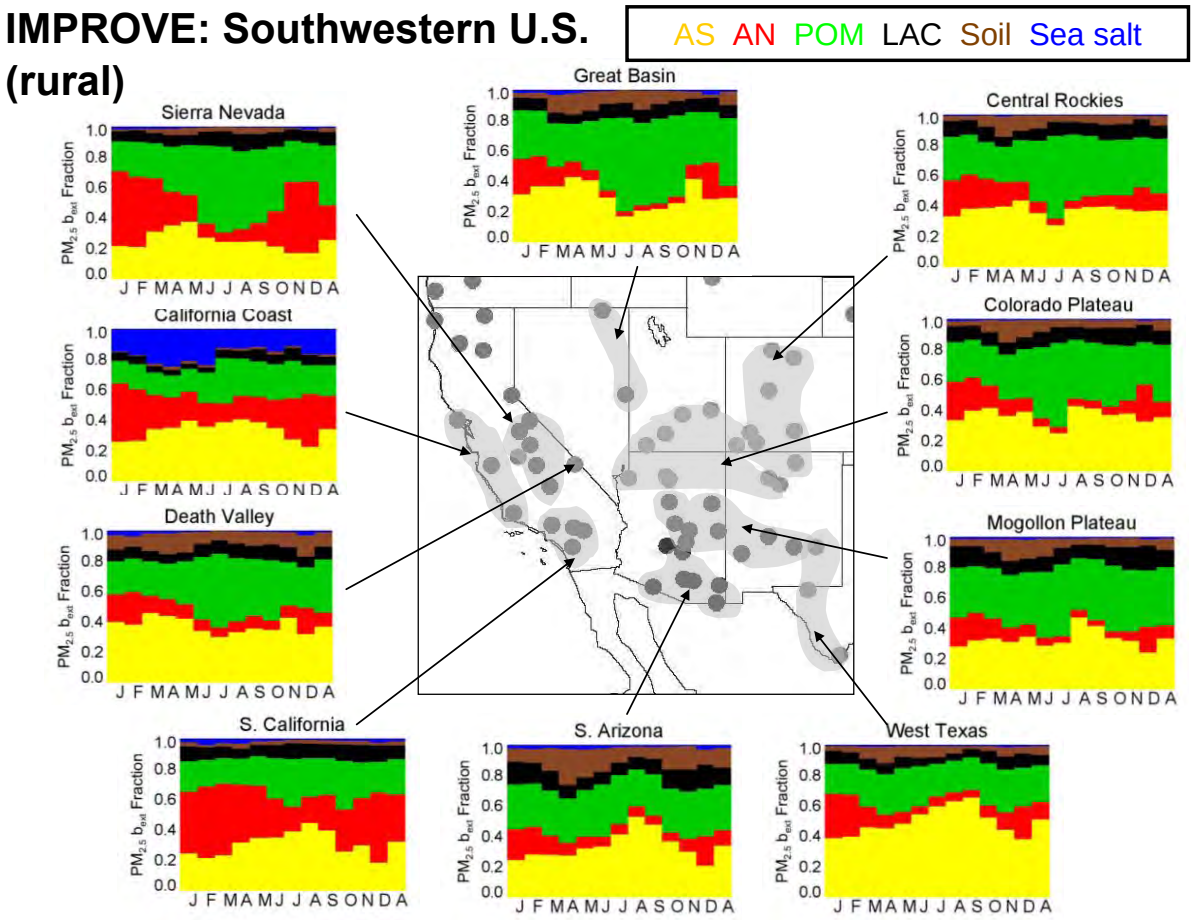

Figure 5.1.13. IMPROVE 2005–2008 regional monthly mean $PM_{2.5}$ light extinction coefficient (b_{ext}) fractions for the southwestern United States. The letters on the x-axis correspond to the month and "A" corresponds to "annual" mean. Ammonium sulfate (AS) in yellow, ammonium nitrate (AN) in red, particulate organic matter (POM) in green, light absorbing carbon (LAC) in black, soil in brown, and sea salt in blue. The shaded area corresponds to the regions that comprise the sites used in the analysis, shown as dots.

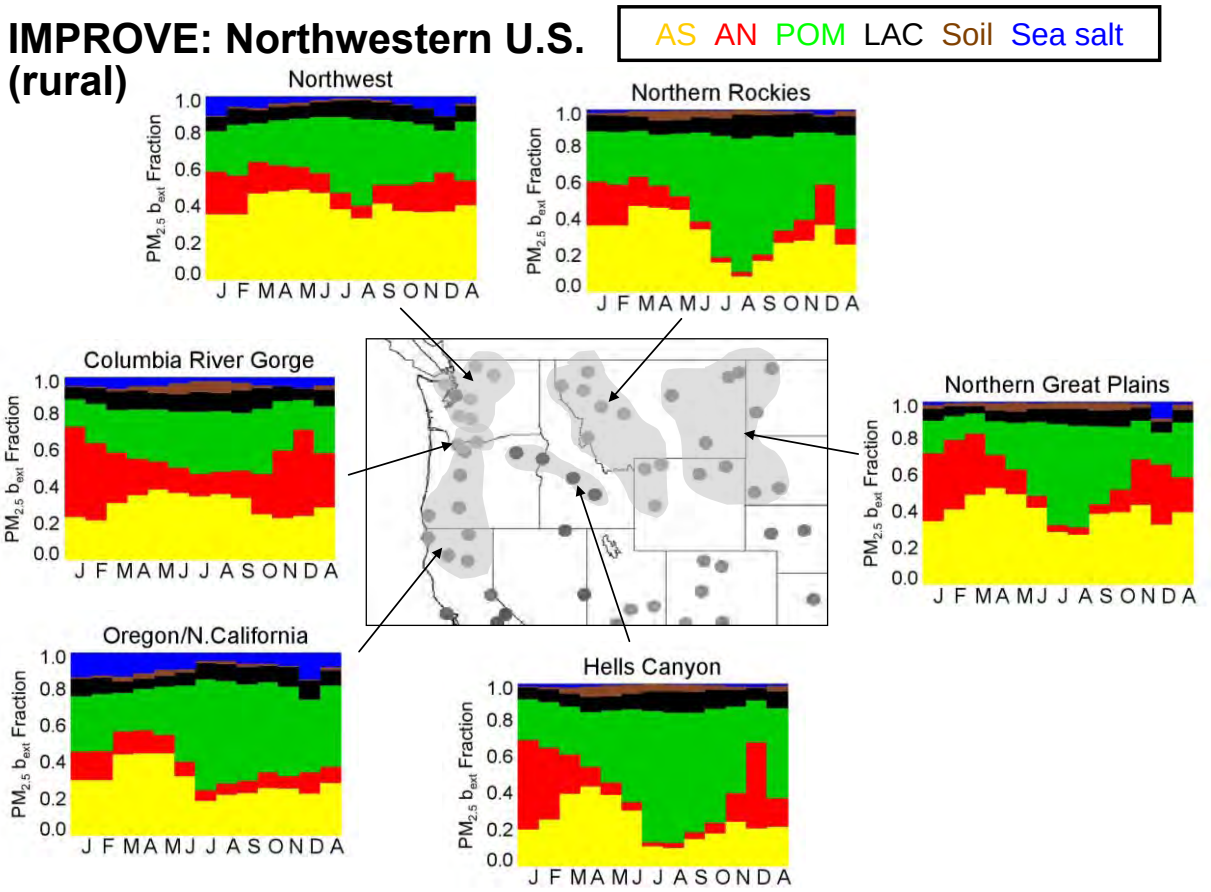

Figure 5.1.14. IMPROVE 2005–2008 regional monthly mean $PM_{2.5}$ light extinction coefficient (b_{ext}) fractions for the northwestern United States. The letters on the x-axis correspond to the month and "A" corresponds to "annual" mean. Ammonium sulfate (AS) in yellow, ammonium nitrate (AN) in red, particulate organic matter (POM) in green, light absorbing carbon (LAC) in black, soil in brown, and sea salt in blue. The shaded area corresponds to the regions that comprise the sites used in the analysis, shown as dots.

Most regions did not experience highly seasonal contributions of AS to b_{ext}; twenty-one regions had maximum to minimum contributions less than 2, suggesting that AS was a consistent contributor to b_{ext} year round. The maximum ratio occurred in Phoenix (7.0, 5.5 for Northern Rocky Mountains) compared to 1.5 in Hawaii. Comparisons of seasonality maps for relative contributions of AS to b_{ext} (Figure 5.1.15) and absolute b_{ext_AS} (Figure 5.1.5) demonstrated interesting differences. The seasonality of the percent contribution of AS to b_{ext} appeared greater than that for absolute b_{ext_AS} for many western U.S. regions (e.g., Northern Rocky Mountains, Hells Canyon, Phoenix, and Fresno). This pattern was reversed in the eastern United States, where b_{ext_AS} had higher seasonality compared to the relative contribution of AS to b_{ext} at many regions. The seasons corresponding to the maximum and minimum absolute b_{ext} and relative b_{ext} also differed for many regions, especially in the western and northeast United States. The seasonality in relative contribution depends on the sources, meteorology, atmospheric processes, and transport that control species concentrations in the atmosphere, but it also depends on the behavior of other species. For example, the minimum absolute b_{ext_AS} values in the western United States occurred during winter for many regions (e.g., Northern Rocky Mountains, Great Basin, and Central Rocky Mountains), but the minimum relative b_{ext_AS} occurred in summer at

those same regions, similar to the patterns in AS mass and mass fractions (Figures 4.1.5 and 4.1.15, respectively). While absolute b_{ext_AS} did not decrease considerably in summer in the western United States, the increase in b_{ext_POM} during summer acted to decrease the relative contribution to b_{ext_AS}.

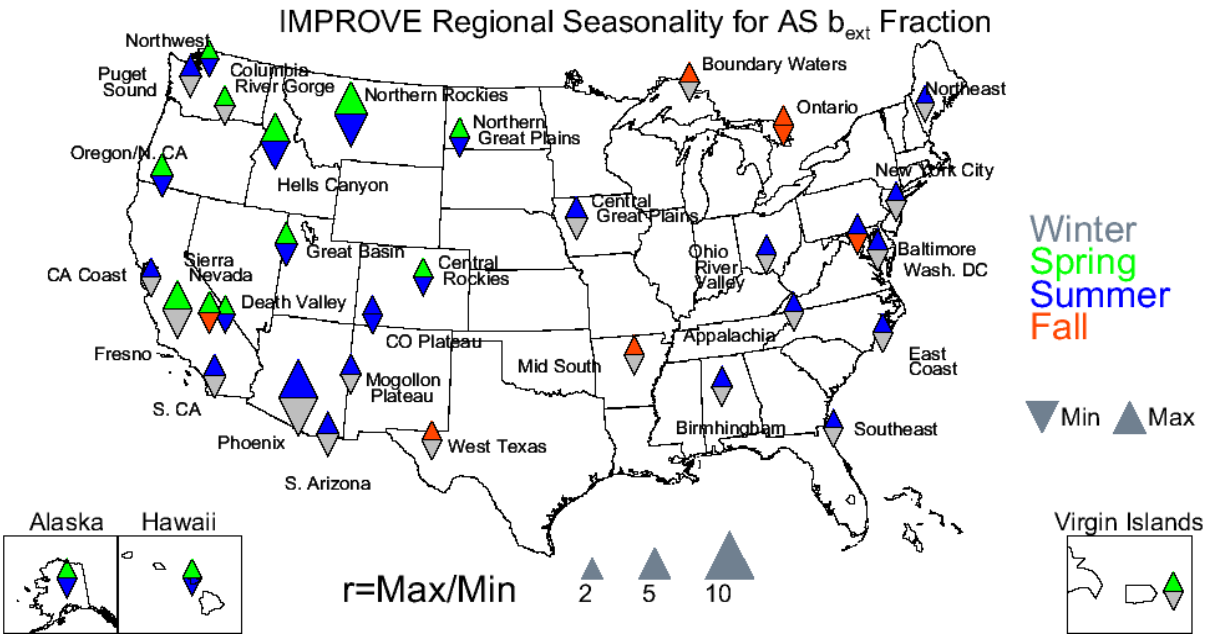

Figure 5.1.15. Seasonal variability for IMPROVE 2005–2008 monthly mean regional ammonium sulfate (AS) light extinction coefficient (b_{ext}) fractions. The color of the upward pointing triangle refers to the season with the maximum monthly mean concentration and the downward pointing triangle refers to the season with the minimum monthly mean concentration. The size of the triangles refers to the magnitude of the ratio of maximum to minimum monthly mean mass concentration.

Urban CSN regional mean b_{ext_AS} fraction ranged from 3.8% in Las Vegas in December to 75.4% in the Ohio River Valley in August. Large contributions of AS to b_{ext} were common for eastern regions (Figure 5.1.16). Contributions ranged from 40 to 75% and increased during summer months for most regions, except the East Texas/Gulf and Florida regions, where the seasonal distribution was flatter. The relative contribution of AS to b_{ext} decreased considerably in the western United States. For example, in the eastern United States the monthly mean fractional b_{ext_AS} rarely dropped below 40%; however, in the northwestern United States 40% was the highest fractional b_{ext_AS} (e.g., the Puget Sound and North Dakota regions, Figure 5.1.17). The summer maxima were not as dominant in the northwestern United States either. In the Puget Sound and Oregon regions, relative b_{ext_AS} increased during summer months, compared to an increase in relative b_{ext_AS} during spring months at the Northwest region and the fairly flat seasonal distribution in the North Dakota region. Higher values of relative b_{ext_AS} during summer months were common for most southwestern regions (Figure 5.1.18), but the magnitudes were consistent with northwestern regions, with fractional b_{ext_AS} less than 40% year round at most regions. The OCONUS regions had similar contributions of AS to b_{ext} (Figure 5.1.19). In the Alaska region the relative b_{ext_AS} was ~40%, except during summer when it decreased to ~20%. In the Hawaii region the contribution of AS to b_{ext} was ~40% but increased to near 60% in May and October.

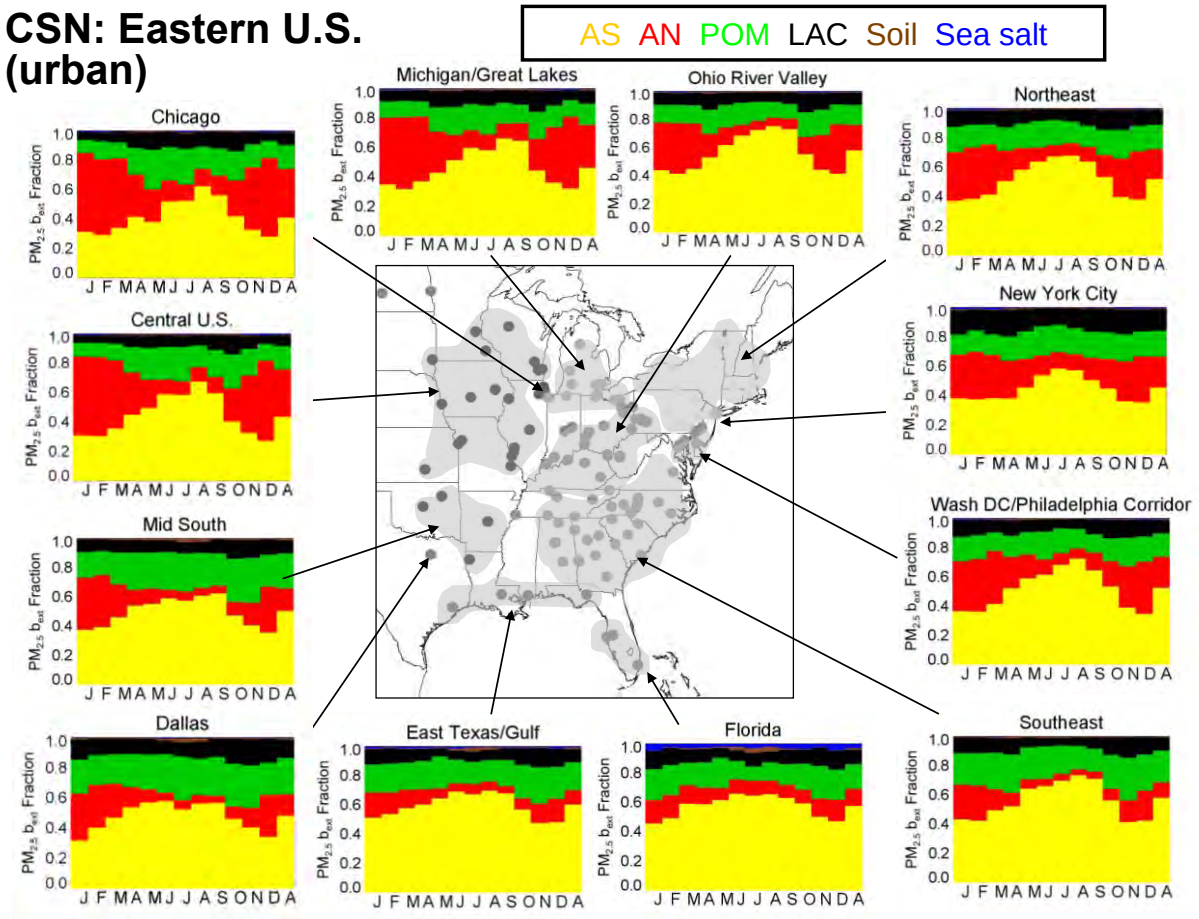

Figure 5.1.16. CSN 2005–2008 regional monthly mean $PM_{2.5}$ light extinction coefficient (b_{ext}) fractions for the eastern United States. The letters on the x-axis correspond to the month and "A" corresponds to "annual" mean. Ammonium sulfate (AS) in yellow, ammonium nitrate (AN) in red, particulate organic matter (POM) in green, light absorbing carbon (LAC) in black, soil in brown, and sea salt in blue. The shaded area corresponds to the regions that comprise the sites used in the analysis, shown as dots.

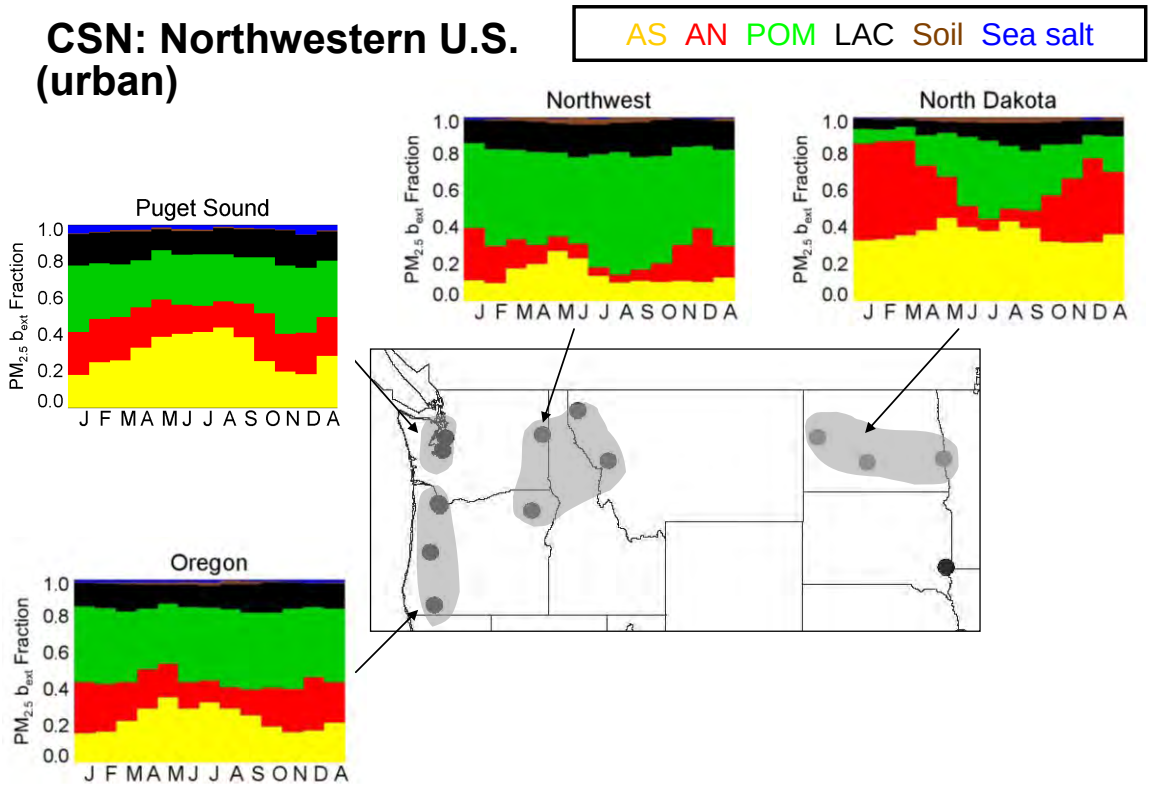

Figure 5.1.17. CSN 2005–2008 regional monthly mean $PM_{2.5}$ light extinction coefficient (b_{ext}) fractions for the northwestern United States. The letters on the x-axis correspond to the month and "A" corresponds to "annual" mean. Ammonium sulfate (AS) in yellow, ammonium nitrate (AN) in red, particulate organic matter (POM) in green, light absorbing carbon (LAC) in black, soil in brown, and sea salt in blue. The shaded area corresponds to the regions that comprise the sites used in the analysis, shown as dots.

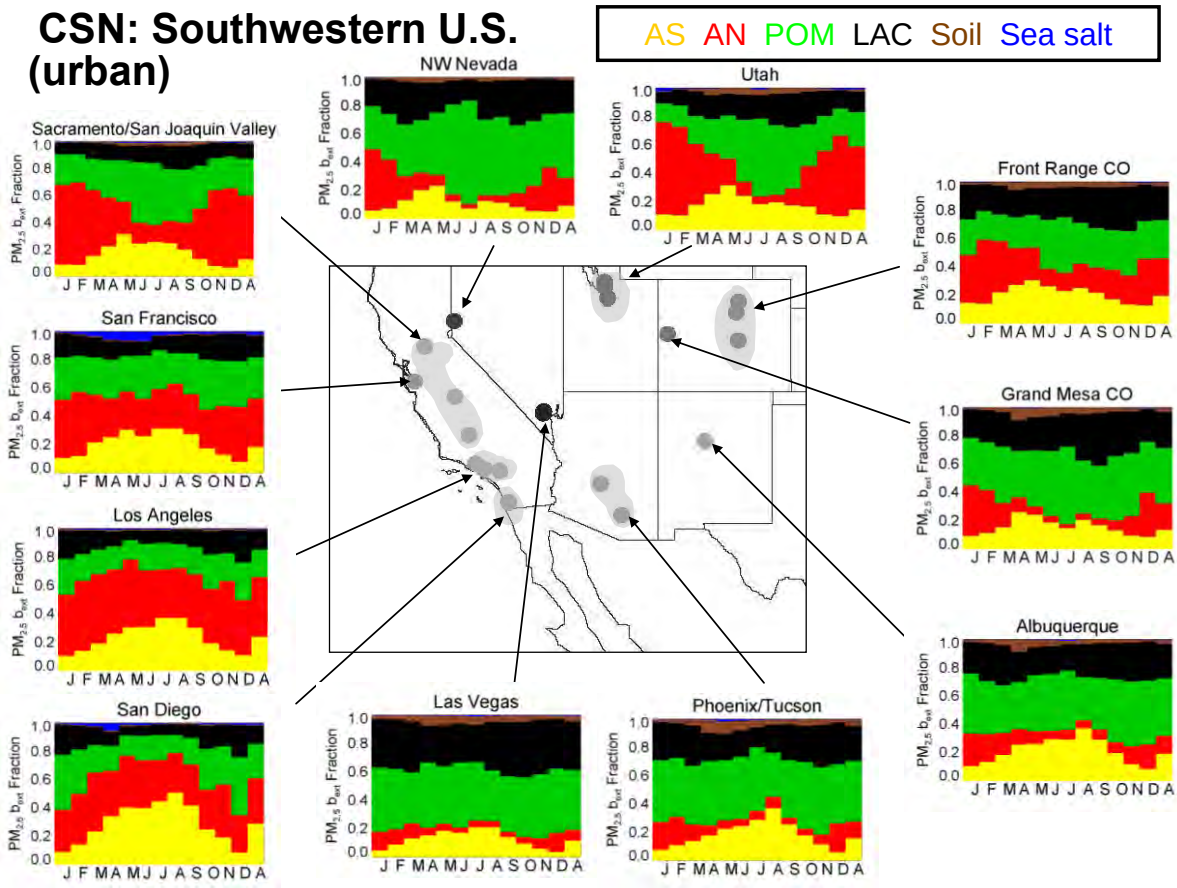

Figure 5.1.18. CSN 2005–2008 regional monthly mean $PM_{2.5}$ light extinction coefficient (b_{ext}) fractions for the southwestern United States. The letters on the x-axis correspond to the month and "A" corresponds to "annual" mean. Ammonium sulfate (AS) in yellow, ammonium nitrate (AN) in red, particulate organic matter (POM) in green, light absorbing carbon (LAC) in black, soil in brown, and sea salt in blue. The shaded area corresponds to the regions that comprise the sites used in the analysis, shown as dots.

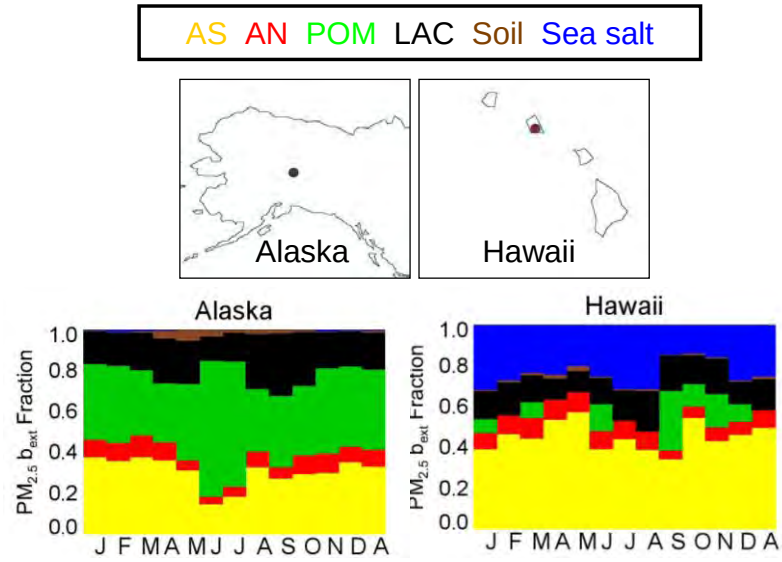

Figure 5.1.19. CSN 2005–2008 regional monthly mean $PM_{2.5}$ light extinction coefficient (b_{ext}) fractions for Hawaii and Alaska. The letters on the x-axis correspond to the month and "A" corresponds to "annual" mean. Ammonium sulfate (AS) in yellow, ammonium nitrate (AN) in red, particulate organic matter (POM) in green, light absorbing carbon (LAC) in black, soil in brown, and sea salt in blue. The shaded area corresponds to the regions that comprise the sites used in the analysis, shown as dots.

Ten of the CSN regions had ratios of maximum to minimum percent contributions less than 2 (Figure 5.1.20). The largest ratio occurred in the Phoenix/Tucson region (6.3) compared to the lowest in the North Dakota region (1.4). Western regions had the highest level of seasonality, with the highest in the southwestern United States (e.g., the Albuquerque, Phoenix/Tucson, Las Vegas, and San Diego regions). These regions were also associated with summer maxima and winter minima. The seasons of maxima and minima shifted in the northwestern United States to spring maxima and winter minima. The winter maxima at urban regions contrasted with the summer maxima that occurred for rural regions. Lower degrees of seasonality corresponding to eastern U.S. regions suggested that AS was a consistent contributor to b_{ext} year round at those regions.

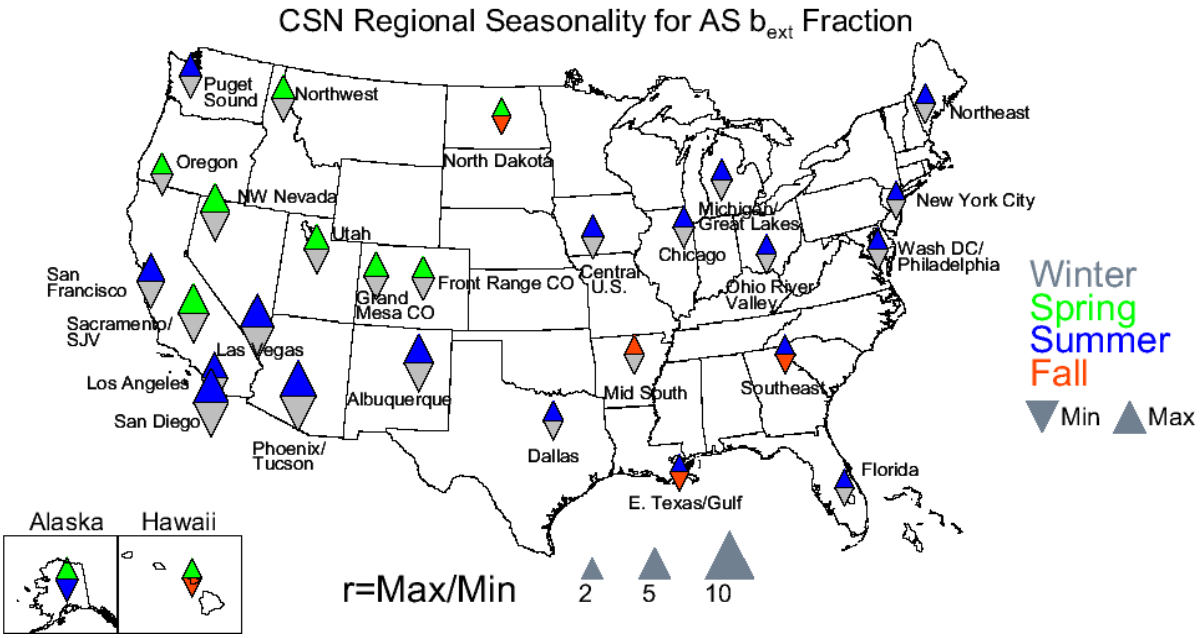

Figure 5.1.20. Seasonal variability for CSN 2005–2008 monthly mean regional ammonium sulfate (AS) light extinction coefficient (b_{ext}) fractions. The color of the upward pointing triangle refers to the season with the maximum monthly mean concentration and the downward pointing triangle refers to the season with the minimum monthly mean concentration. The size of the triangles refers to the magnitude of the ratio of maximum to minimum monthly mean mass concentration.

5.2 $PM_{2.5}$ AMMONIUM NITRATE LIGHT EXTINCTION COEFFICIENTS

The extinction efficiency and f(RH) values used to compute reconstructed light extinction coefficients from ammonium nitrate, b_{ext_AN}, were the same as those used to compute b_{ext_AS}. In a similar manner, while general patterns of b_{ext_AN} mostly follow AN mass concentrations, differences may occur due to hygroscopic effects. Winter maxima in 2005–2008 regional monthly mean b_{ext_AN} were common at many IMPROVE regions, consistent with favorable AN formation in winter conditions. In fact, the maximum b_{ext_AN} at urban and rural IMPROVE regions occurred in winter. In addition, the urban IMPROVE regional monthly mean maximum b_{ext_AN} (149.46 Mm^{-1} at Fresno in December) was almost four times higher than the rural IMPROVE regional monthly mean maximum (37.56 Mm^{-1} in the Central Great Plains region in January). The minimum IMPROVE regional monthly mean b_{ext_AN} was in 0.44 Mm^{-1} in the Great Basin region in October. The b_{ext_AN} values at the Central Great Plains region were larger than most regions in the eastern half of the United States (Figure 5.1.1), especially with respect to other species. Higher values of b_{ext_AN} also occurred during winter at the Northern Great Plains, Boundary Waters, and Mid South regions, due to their proximity to source regions. In contrast, regions farther east corresponded to relatively low values of b_{ext_AN}, especially in comparison to other species (e.g., the Southeast, Appalachia, East Coast, and Northeast regions). The values of b_{ext_AN} varied considerably between regions in the northwestern United States (Figure 5.1.2). The Northern Great Plains, Hells Canyon, and Columbia River Gorge regions corresponded to relatively higher values with strong winter maxima. In contrast, values in the Oregon/Northern California and Northern Rocky Mountain regions were fairly low and did not have strong winter maxima. Extinction coefficients due to AN in the southwestern United States were typically less than contributions from Rayleigh scattering (~10 Mm^{-1}) at most regions

(Figure 5.1.3). The exceptions included the Sierra Nevada and California Coast regions; these regions corresponded to higher winter b_{ext_AN}. In addition, the Southern California region experienced relatively high b_{ext_AN} year round, similar to monthly mean AN mass concentrations (Figure 4.1.3). Monthly mean AN mass concentrations and b_{ext_AN} at OCONUS regions also had very similar patterns (Figures 4.1.4 and 5.1.4, respectively), except at the Virgin Islands site where b_{ext_AN} increased relative to other species, probably due to its hygroscopic nature and higher extinction efficiency compared to other species (e.g., soil).

Most IMPROVE regions demonstrated a high degree of seasonality, with only two regions having a maximum to minimum b_{ext_AN} ratio less than 2. The largest ratios occurred in the Fresno (21.2, urban) and Boundary Waters regions (17.9, rural), and the lowest ratio occurred in the Northwest region (1.8). Most of the IMPROVE regions corresponded to winter maxima (Figure 5.2.1), although fall maxima occurred at the Ontario, Northwest, and Sierra Nevada regions. Spring maxima occurred at the Virgin Islands, Hawaii, Southern California, Death Valley, and Central Rocky Mountain regions. Summer and fall minima were common for most regions. In general, b_{ext_AN} exhibited a higher degree of seasonality compared to monthly mean AN mass concentrations (see Figure 4.2.1), and for many regions the seasons corresponding to maximum and minimum shifted (especially at southwestern U.S. regions).

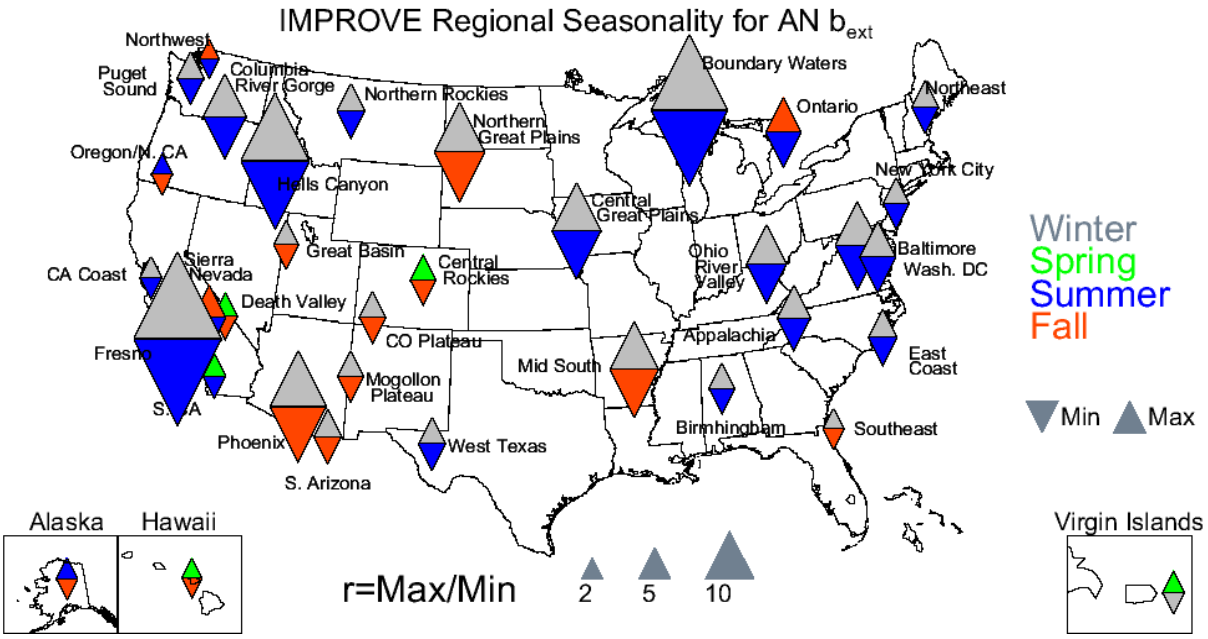

Figure 5.2.1. Seasonal variability for IMPROVE 2005–2008 monthly mean regional ammonium nitrate (AN) light extinction coefficients (b_{ext}). The color of the upward pointing triangle refers to the season with the maximum monthly mean concentration and the downward pointing triangle refers to the season with the minimum monthly mean concentration. The size of the triangles refers to the magnitude of the ratio of maximum to minimum monthly mean mass concentration.

The CSN urban regional monthly mean b_{ext_AN} ranged from 0.92 Mm^{-1} in the Alaska region in May to 125.28 Mm^{-1} in the Sacramento/San Joaquin Valley region in December. Values of b_{ext_AN} at urban regions were considerably higher than at rural regions in the southwestern United States (compare Figures 5.1.6 and 5.1.3). Regions in California, Nevada, Utah, and Colorado corresponded to b_{ext_AN} values that were several times higher than Rayleigh

scattering (~10 Mm^{-1}). Values of b_{ext_AN} increased considerably during winter months at most regions except Los Angeles and San Diego, where they were high year round. Compared to AN mass concentrations, b_{ext_AN} was higher relative to other species, especially at the San Francisco, Sacramento/San Joaquin Valley, Northwest Nevada, and Utah regions. Values of b_{ext_AN} decreased in the northwestern United States compared to regional values in the southwestern United States but were still much larger than those at rural northwestern U.S. regions. Values near 20 Mm^{-1} during winter months were common at most regions (Figure 5.1.7) and similar in seasonal pattern to AN mass concentrations (Figure 4.1.8), although higher relative to other species. Extinction coefficients near 40 Mm^{-1} were common at eastern U.S. regions, especially during winter months (Figure 5.1.8). Regions closer to the central United States corresponded to higher b_{ext_AN} values compared to estimates at regions near the eastern or in the southeastern United States. Values of b_{ext_AN} at the Florida and Southeast regions were actually similar to estimates at rural regions in the same vicinity (Figure 5.1.6). Values of b_{ext_AN} were much higher at the Alaska region compared to the Hawaii region (Figure 5.1.9), similar to patterns in monthly mean AN mass concentrations. Urban b_{ext_AN} values at the Hawaii region were much higher than rural regional Alaska b_{ext_AN} values.

Urban b_{ext_AN} was highly seasonal, with only two sites having ratios less than 2. The majority of regions corresponded to winter maxima (Figure 5.2.2). The highest ratio occurred in the Utah region (75.12) and the lowest occurred in the Los Angeles region (1.8). The degree of seasonality for b_{ext_AN} was noticeably higher than that for AN mass concentrations (compare Figure 5.2.2 to Figure 4.2.2). Western U.S. regions corresponded to the greatest degree of seasonality. Most seasons corresponded to maximum and minimum b_{ext_AN} in winter and summer, respectively. The differences in seasonality between rural and urban b_{ext_AN} were also quite noticeable, with more winter maxima and summer minima associated with urban regions, especially in the southwestern United States.

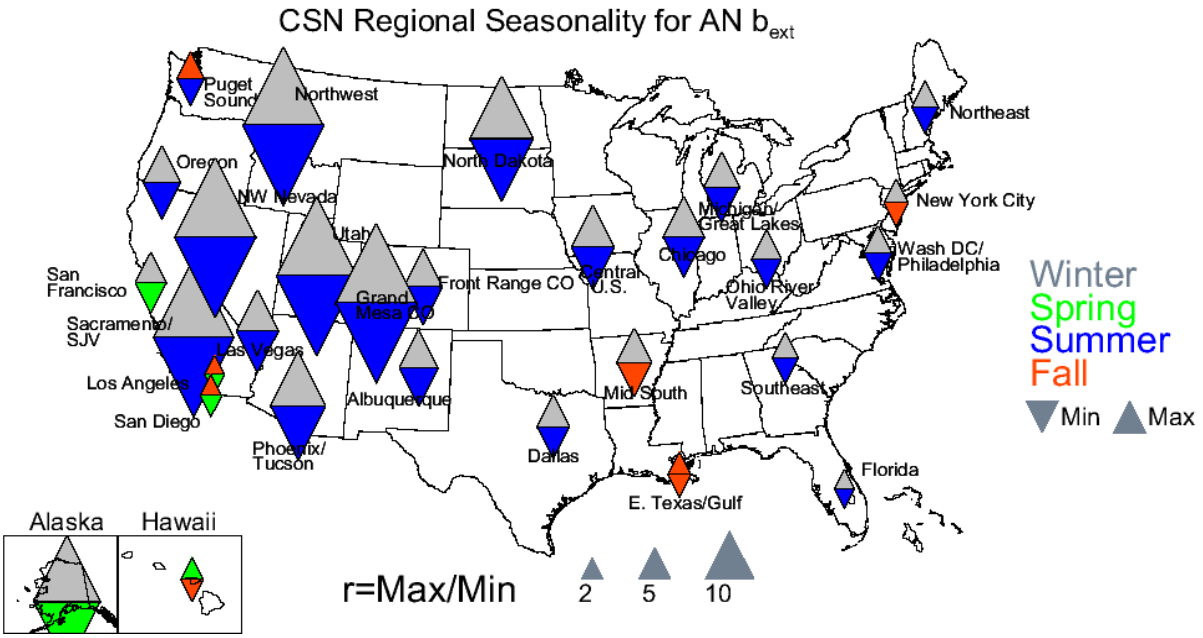

Figure 5.2.2. Seasonal variability for CSN 2005–2008 monthly mean regional ammonium nitrate (AN) light extinction coefficients (b_{ext}). The color of the upward pointing triangle refers to the season with the maximum monthly mean concentration and the downward pointing triangle refers to the season with the minimum monthly mean concentration. The size of the triangles refers to the magnitude of the ratio of maximum to minimum monthly mean mass concentration.

AN dominated the IMPROVE b_{ext} in Fresno (61.3%) in February and in the Central Great Plains region (56.2%) in December. The lowest monthly mean AN contributions to b_{ext} occurred in the Appalachia region in August (1.8%), similar to the other eastern U.S. regions (Figure 5.1.12) with values reaching up to 20% during winter months at the Ohio River Valley, Northeast, and East Coast regions. The contributions of AN to b_{ext} increased toward the central United States, with values near 40% or more in winter at regions such as Central Great Plains, Boundary Waters, Northern Great Plains, and the Mid South. Contributions of AN to b_{ext} were even higher than its contributions to reconstructed fine mass (RCFM) (Figure 4.1.11) at these regions, in part due to its hygroscopic properties and higher extinction efficiencies relative to other species (e.g., soil). Percent contributions of AN to b_{ext} of 40% were common at northwestern U.S. rural IMPROVE regions (Figure 5.1.14). The Colombia River Gorge, Hells Canyon, and Northern Great Plains regions all corresponded to large AN b_{ext} fractions, especially during winter months. While the Northwest, Northern Rocky Mountains, and Oregon/Northern California regions did not experience as high a b_{ext_AN} fraction, these regions did experience high values during winter months. AN contributed more to b_{ext} than it did to RCFM (see Figure 5.1.14 compared to Figure 4.1.12), especially at the Northern Great Plains and Columbia River Gorge regions. The relative contribution of AN to b_{ext} was somewhat lower in the southwestern United States (Figure 5.1.13). Values near 20% were more common for regions in this area, although higher contributions in the winter still occurred. Somewhat elevated contributions (~40%) occurred at the Sierra Nevada and Southern California regions. These regions also experienced higher contributions of AN to b_{ext} compared to RCFM (compare Figures 4.1.13 and 5.1.13) but not to the same degree as other U.S. regions. Compared to other regions, the AN contributions to b_{ext} in the OCONUS regions were relatively low (<10%) (Figure 5.1.11).

Most IMPROVE regions showed a high degree of seasonality for the contribution of AN to b_{ext}, with only two regions having ratios less than 2 (Virgin Islands was the lowest with 1.4). The highest ratio occurred at the Hells Canyon region (21.4). Most regions corresponded to winter maxima and summer minima (Figure 5.2.3). Only two regions in the continental United States had spring maxima (Baltimore and Southern California), and only five regions had fall minima. The OCONUS regions had very different seasonal patterns and had a lower degree of seasonality. In general, the degree of seasonality was higher for relative b_{ext_AN} compared to absolute b_{ext_AN} (compare Figure 5.2.1). In addition, more regions had winter maxima and summer minima. The degree of seasonality of relative b_{ext_AN} was actually quite similar to that of AN mass fraction (Figure 4.2.3), although the seasons corresponding to maximum and minimum varied for some regions.

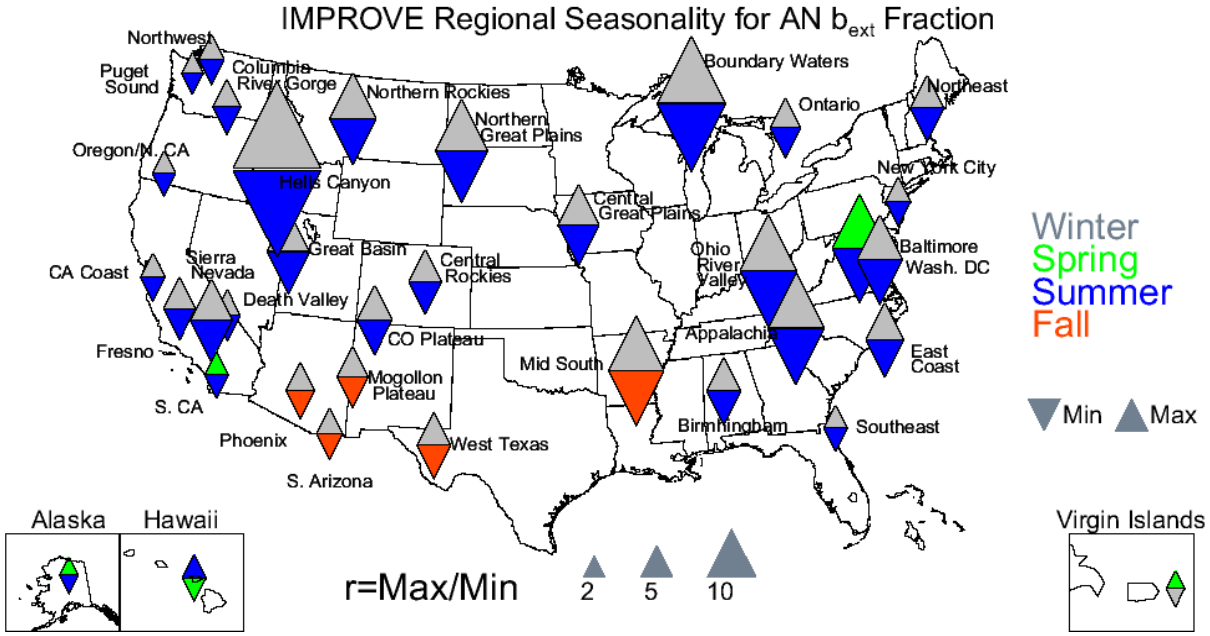

Figure 5.2.3. Seasonal variability for IMPROVE 2005–2008 monthly mean regional ammonium nitrate (AN) light extinction coefficient (b_{ext}) fractions. The color of the upward pointing triangle refers to the season with the maximum monthly mean concentration and the downward pointing triangle refers to the season with the minimum monthly mean concentration. The size of the triangles refers to the magnitude of the ratio of maximum to minimum monthly mean mass concentration.

CSN urban monthly mean b_{ext_AN} fractions ranged from 2.7% at the Grand Mesa CO region in July to 64.8% at the Utah region in January. The southwestern United States was home to many regions where AN contributed significantly to b_{ext} (Figure 5.1.18). Contributions of 40% or higher were common at many regions (e.g., Utah, Northwest Nevada, Sacramento/San Joaquin Valley, San Francisco, Los Angeles, and San Diego). Contributions were much lower at regions farther south, such as the Las Vegas, Phoenix/Tucson, and Albuquerque regions. Although most regions did exhibit higher AN contributions to b_{ext} during winter months, some regions, such as San Diego and Los Angeles, had fairly flat seasonal patterns. In general, urban regions experienced a much higher contribution of AN to b_{ext} than did rural regions in the southwestern United States. Contributions of AN to b_{ext} reached ~20% at northwestern U.S. regions, except at the North Dakota region where relative b_{ext_AN} during winter months reached up to ~40% (Figure 5.1.17). The relative b_{ext} at central U.S. regions was similar to the North

Dakota region in that they reached up to 40% of b_{ext} during winter months (e.g., the Chicago, Central U.S., and Michigan/Great Lakes regions, Figure 5.1.16). AN contributions to b_{ext} at regions farther east were somewhat lower. Twenty percent contributions were common during winter months, though they were somewhat lower during winter months at southern regions (e.g., East Texas/Gulf, Florida, and Southeast). Urban regions experienced much higher contributions of AN to b_{ext} compared to rural regions in the eastern United States (see Figure 5.1.12). The lowest urban relative contributions occurred at the OCONUS regions (Figure 5.1.19) and were more comparable to rural regions.

Most CSN regions had the highest contributions of AN to b_{ext} in winter, as was observed in the bar charts of monthly mean b_{ext_AN} fraction. Only five regions had ratios of maximum to minimum contributions less than 2; the highest occurred in the Northwest Nevada region (14.8) and the lowest in the Los Angeles region (1.5) (Figure 5.2.4). The highest maximum to minimum ratios occurred in the western United States, including the Utah, Grand Mesa CO, Northwest Nevada, North Dakota, and Northwest regions. Most regions corresponded to winter maxima and summer minima, with the exception of several southern U.S. regions (e.g., East Texas/Gulf, Dallas TX, Mid South, Phoenix/Tucson, and Las Vegas). The degree of seasonality of the relative contributions of AN to b_{ext} was lower than the degree of seasonality of absolute b_{ext_AN}, especially in the western United States (see Figure 5.2.2). The seasonality of relative b_{ext_AN} suggested that the contributions of AN to b_{ext} were consistent year round for many western U.S. regions. The seasonality pattern of fractional b_{ext_AN} followed that of the AN mass fraction (see Figure 4.2.4).

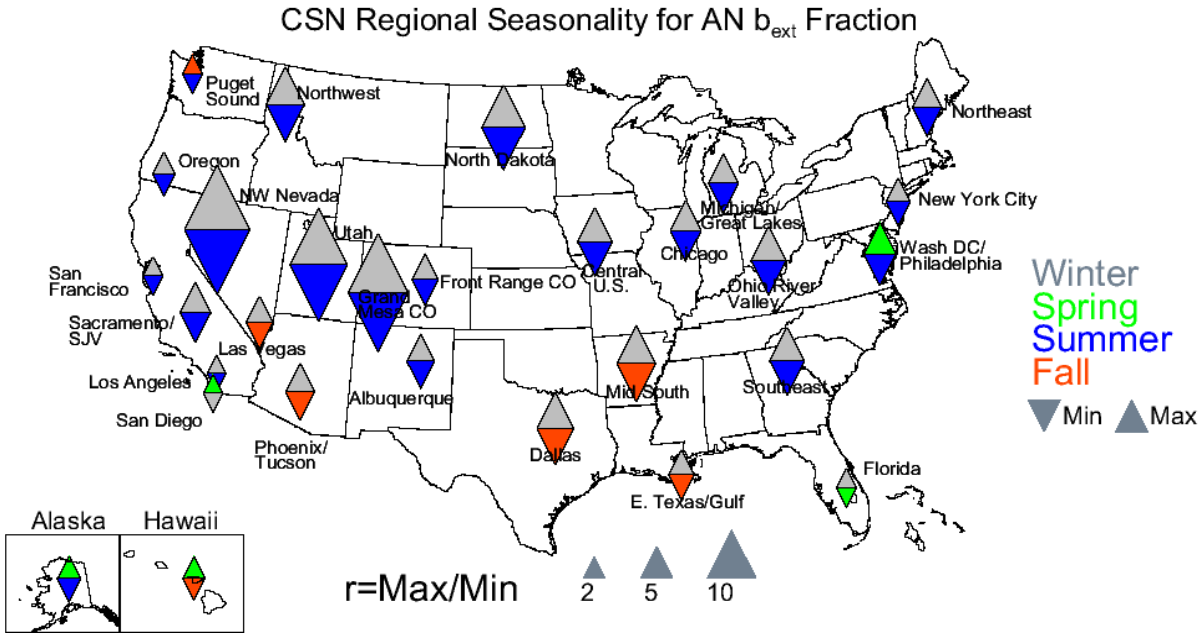

Figure 5.2.4. Seasonal variability for CSN 2005–2008 monthly mean regional ammonium nitrate (AN) light extinction coefficient (b_{ext}) fractions. The color of the upward pointing triangle refers to the season with the maximum monthly mean concentration and the downward pointing triangle refers to the season with the minimum monthly mean concentration. The size of the triangles refers to the magnitude of the ratio of maximum to minimum monthly mean mass concentration.

5.3 $PM_{2.5}$ PARTICULATE ORGANIC MATTER LIGHT EXTINCTION COEFFICIENTS

POM light extinction coefficients (b_{ext_POM}) were scaled to POM mass because, unlike AS and AN, POM was considered nonhygroscopic in reconstructed b_{ext} calculations (section 3.1). On a similar dry mass basis, b_{ext_POM} would be higher than b_{ext_AS} or b_{ext_AN} because its extinction efficiency is higher (4 m^2 g^{-1} compared to 3 m^2 g^{-1}; see section 3.1).

The minimum IMPROVE 2005–2008 regional monthly mean b_{ext_POM} occurred at the Virgin Islands in December (0.68 Mm^{-1}). The urban IMPROVE maximum b_{ext_POM} was considerably higher than the rural maximum; b_{ext_POM} in Fresno was 52.06 Mm^{-1} in December compared to 31.03 Mm^{-1} in the Northern Rocky Mountains region in August. Relatively high values of b_{ext_POM} during summer months were common at several northwestern U.S. regions (Figure 5.1.2), probably related to wildfire or biogenic emissions. The Columbia River Gorge region was the exception to this pattern, with fairly constant b_{ext_POM} year round. Similar regional and seasonal patterns of b_{ext_POM} and POM mass were observed as expected (Figure 4.1.2). The northerly regions in the southwestern United States had somewhat higher b_{ext_POM} values compared to regions farther south (Figure 5.1.3). For example, the Sierra Nevada, Great Basin, Central Rocky Mountains, Colorado Plateau, Mogollon Plateau, and Hells Canyon regions all corresponded to values near or greater than 10 Mm^{-1}, especially during summer. However, the Southern California, Southern Arizona, and West Texas regions corresponded to values on the order of Rayleigh scattering (10 Mm^{-1}). Values of b_{ext_POM} in the eastern United States ranged from 10 to 20 Mm^{-1} at many regions (Figure 5.1.1). Higher b_{ext_POM} during summer months occurred at the Northern Great Plains and Boundary Water regions, probably also related to biomass burning or biogenic emissions. Distinct seasonal patterns were not as obvious at regions along the eastern coast. Of the OCONUS regions, the Alaska region was the only one with considerable b_{ext_POM}, especially during summer (Figure 5.1.4).

The seasonal patterns in IMPROVE b_{ext_POM} (Figure 5.3.1) were similar to the seasonal patterns in POM mass (Figure 4.3.1). Most rural regions corresponded to summer maxima and winter or spring minima. Summer maxima were most likely associated with biomass burning emissions (especially in the western United States) or biogenic emissions. Only six regions had maximum to minimum contributions less than 2. The ratios ranged from 1.6 in the Southern Arizona region to 13.3 in the Northern Rocky Mountains region.

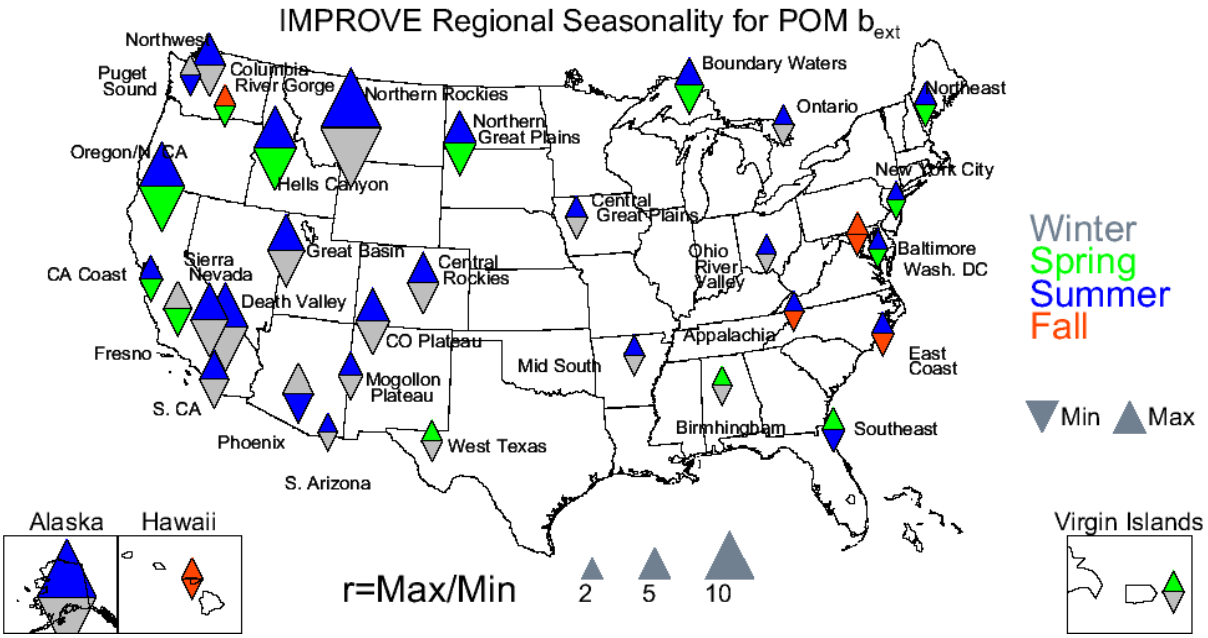

Figure 5.3.1. Seasonal variability for IMPROVE 2005–2008 monthly mean regional particulate organic matter (POM) light extinction coefficients (b_{ext}). The color of the upward pointing triangle refers to the season with the maximum monthly mean concentration and the downward pointing triangle refers to the season with the minimum monthly mean concentration. The size of the triangles refers to the magnitude of the ratio of maximum to minimum monthly mean mass concentration.

CSN urban regions were associated with higher b_{ext_POM} compared to rural regions. In the eastern United States the b_{ext_POM} values approached 20 Mm^{-1} or higher and were fairly steady year round (Figure 5.1.8). However, in the southwestern United States b_{ext_POM} increased during winter months at several regions (e.g., Albuquerque, Phoenix/Tucson, Las Vegas, San Diego, San Francisco, Sacramento/San Joaquin Valley, Figure 5.1.6). Estimates of urban b_{ext_POM} in the southwestern United States were also higher than in rural regions in the same area. The magnitudes of urban b_{ext_POM} were often greater than rural b_{ext_POM} in the northwestern United States also (Figure 5.1.7), but seasonal patterns were very different. Values of urban b_{ext_POM} increased during winter months for most regions, with the exception of the North Dakota region. Different seasonal patterns also occurred at urban versus rural OCONUS regions (Figure 5.1.9), as did higher magnitudes of b_{ext_POM}. Higher b_{ext_POM} corresponded to winter months in the Alaska region and during fall in the Hawaii region. The range in b_{ext_POM} at CSN regions was similar to the urban IMPROVE regions, with a minimum of 1.83 Mm^{-1} in the Hawaii region in January and a maximum of 66.94 Mm^{-1} in the Alaska region in December.

The seasonality for CSN regions did not correspond to high summer maxima as did IMPROVE rural regions. In fact, many regions actually corresponded to winter maxima, just as did the CSN POM monthly mean mass concentrations (Figure 5.3.2). The urban regions corresponded to a lower degree of seasonality in b_{ext_POM} compared to the rural regions (compare Figure 5.3.2 and Figure 5.3.1). Seven regions did not experience significant seasonality (ratio < 2). The maximum to minimum ratios ranged from 1.5 in the Ohio River Valley region to 16.13 in the Alaska region. The urban and rural differences in the seasons corresponding to the maximum b_{ext_POM} suggested different sources contributing to POM, with rural summer maxima most likely

associated with wildfire and biogenic emissions and urban winter maxima likely associated with local urban sources.

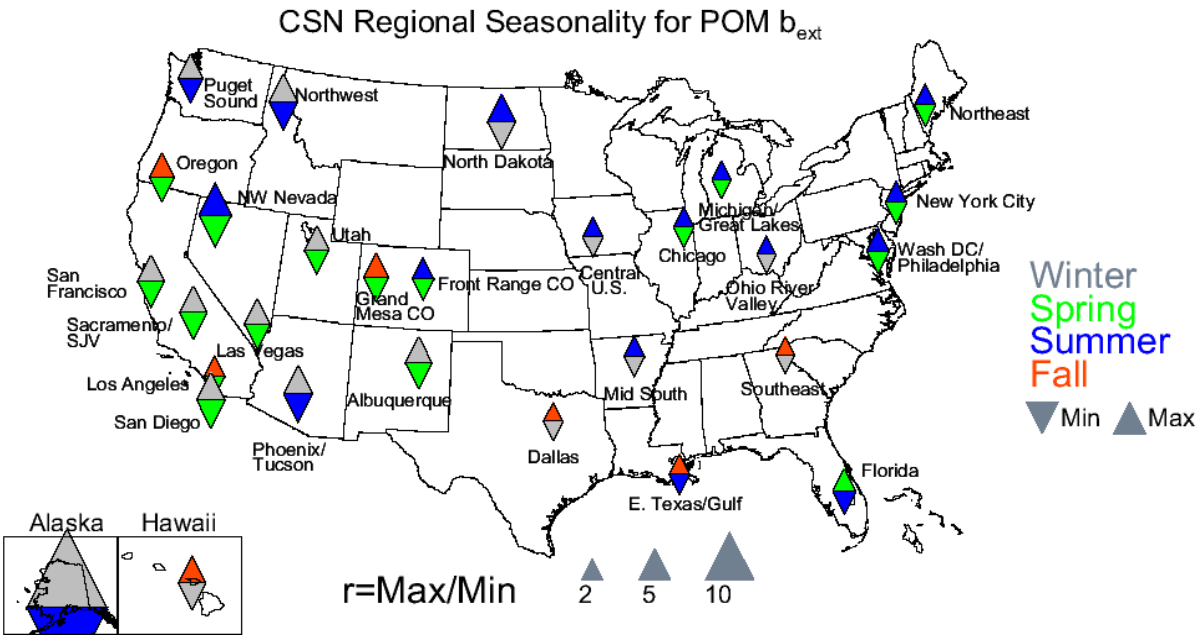

Figure 5.3.2. Seasonal variability for CSN 2005–2008 monthly mean regional particulate organic matter (POM) light extinction coefficients (b_{ext}). The color of the upward pointing triangle refers to the season with the maximum monthly mean concentration and the downward pointing triangle refers to the season with the minimum monthly mean concentration. The size of the triangles refers to the magnitude of the ratio of maximum to minimum monthly mean mass concentration.

Although the patterns of b_{ext_POM} were similar to those of POM mass concentrations, its relative contributions to reconstructed b_{ext} were not because of the hygroscopic and optical properties of other species contributing to b_{ext}. For example, in the eastern United States the b_{ext_POM} fraction was generally lower than the POM mass fraction at several IMPROVE regions (compare Figures 5.1.12 and 4.1.11), probably due to the increased importance of hygroscopic AS on b_{ext}. The percent contribution of POM to b_{ext} was fairly constant year round at most eastern regions, except for the Boundary Waters, Northern Great Plains, and Central Great Plains regions, which had higher contributions during summer. Contributions of POM to b_{ext} were significant for many northwestern U.S. regions. The relative b_{ext_POM} values were generally lower than POM mass fraction for these regions (compare Figure 5.1.14 to Figure 4.1.12). In the summer, POM was the dominant contributor to b_{ext} at the Hells Canyon, Northern Rocky Mountains, Northern Great Plains, and Oregon/Northern California regions. POM contributions to b_{ext} were typically 20–30% at most southwestern U.S. regions (Figure 5.1.13). Higher fractions during summer months occurred at the Sierra Nevada, Great Basin, Central Rocky Mountains, Colorado Plateau, Mogollon Plateau, and Death Valley regions. Other regions, such as the West Texas, Southern Arizona, Southern California, and California Coast regions corresponded to relatively flat seasonal patterns. The Alaska region was the only OCONUS region that had considerable contributions of POM to b_{ext}. These contributions peaked in summer and dropped off fairly rapidly in fall (Figure 5.1.11). Relative contributions of POM to b_{ext} were fairly low (~10% or less) in the Hawaii and Virgin Islands regions. The IMPROVE mean

fractional contribution of POM to b_{ext} ranged from 2.6% in the Virgin Islands in July to 72.9% in the Northern Rocky Mountains region in August.

The rural IMPROVE POM b_{ext} fraction did not exhibit a high degree of seasonality (Figure 5.3.3). Nearly half of the regions had maximum to minimum ratios less than 2. The maximum ratio occurred in the IMPROVE Alaska region (6.0) and the minimum in the Puget Sound (1.2) and Northeast regions (1.2). The relative b_{ext_POM} had a much lower degree of seasonality compared to absolute b_{ext_POM} (see Figure 5.3.1), especially in the western United States. Summer maxima were still the most common, but in some rural regions, such the Hawaii, Southern California, Mid South, Appalachia, Ohio River Valley, and Virgin Islands and many northwestern U.S. regions, the seasons corresponding to the maximum relative b_{ext_POM} changed from the maximum seasons corresponding to absolute b_{ext_POM}.

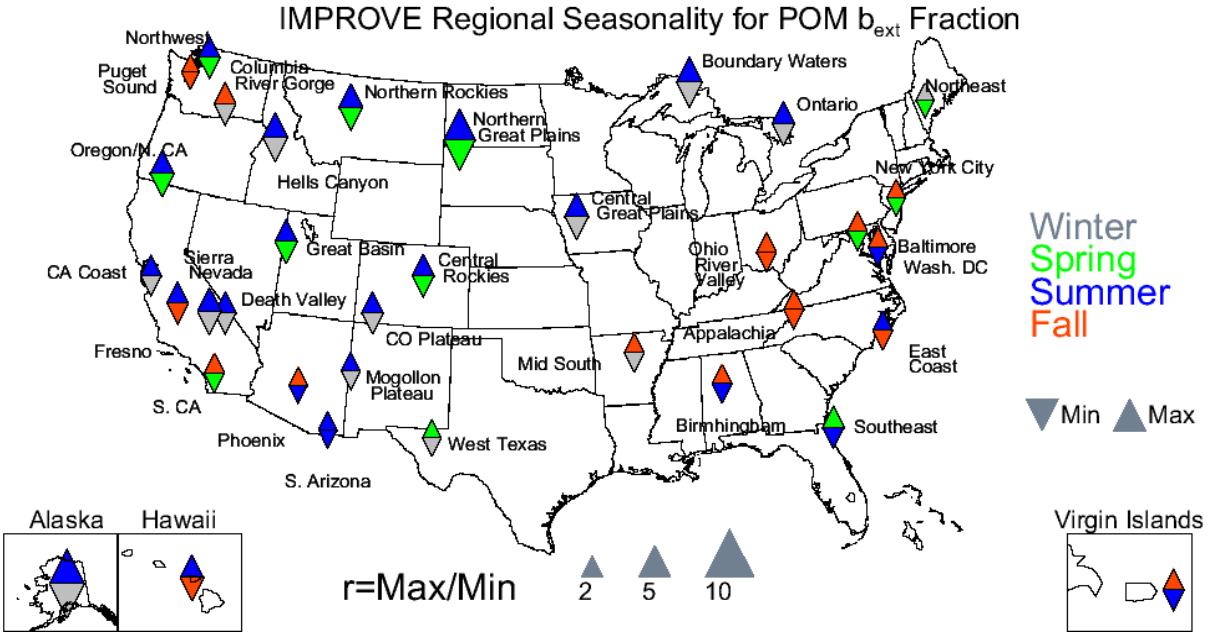

Figure 5.3.3. Seasonal variability for IMPROVE 2005–2008 monthly mean regional particulate organic matter (POM) light extinction coefficient (b_{ext}) fractions. The color of the upward pointing triangle refers to the season with the maximum monthly mean concentration and the downward pointing triangle refers to the season with the minimum monthly mean concentration. The size of the triangles refers to the magnitude of the ratio of maximum to minimum monthly mean mass concentration.

Of the CSN urban regions, the contribution of POM to b_{ext} was 6.6% in the North Dakota region in February compared to the highest at the Northwest Nevada region in July (73.2%). POM contributed significantly to b_{ext} at many southwestern urban regions (Figure 5.1.18). Percent contributions of 40% year round were typical at the Las Vegas, Phoenix/Tucson, Albuquerque, and Grand Mesa CO regions. Contributions of POM to b_{ext} were less (~20%) farther west, such as at regions in California. Contributions increased during summer months in the Sacramento/San Joaquin Valley, Northwest Nevada, and Utah regions; elsewhere the contributions were fairly constant year round. POM contributions to b_{ext} at urban regions were higher than at rural regions (compare to Figure 5.1.13). Urban POM contributions to b_{ext} in the northwestern United States were similar to the regions in the southwest United States, with values of ~40% or less (Figure 5.1.17). The Northwest region was the exception where

contributions reached up to 60% during summer months. The North Dakota region had the most pronounced seasonal variability; contributions were fairly flat in the other northwestern U.S. regions. POM contributions to b_{ext} generally were lower than its contributions to RCFM in the northwestern United States (compare to Figure 4.1.12). Relative b_{ext_POM} values were lower at eastern U.S. regions compared to northwestern and southwestern U.S. regions (Figure 5.1.16). Values of 20% or less were typical and, with the exception of regions toward the central United States (e.g., Chicago and Central U.S.), the contributions were fairly flat seasonally. AS was the main contributor to b_{ext} in the eastern United States, followed by POM or AN, depending on the month. Finally, contributions of POM to b_{ext} were much higher at the Alaska region compared to the Hawaii region (Figure 5.1.19). Values near 40% were typical during most months at the Alaska region, except during summer when they increased to ~60%. This pattern was in contrast to the seasonal pattern in absolute b_{ext_POM}, with higher values during winter months.

More than half of the CSN regions did not experience significant seasonality with the contribution of POM to b_{ext}. The largest ratio occurred in the North Dakota region (6.5) compared to smallest in the Las Vegas region (1.3). The seasons corresponding to the maximum and minimum were different for many regions when comparing the seasonal patterns in relative b_{ext_POM} (Figure 5.3.4) to absolute b_{ext_POM} (Figure 5.3.2). While many urban regions corresponded to winter maxima in absolute b_{ext_POM}, the maximum in relative b_{ext_POM} switched to summer at many regions (such as in the previous example of the Alaska region).

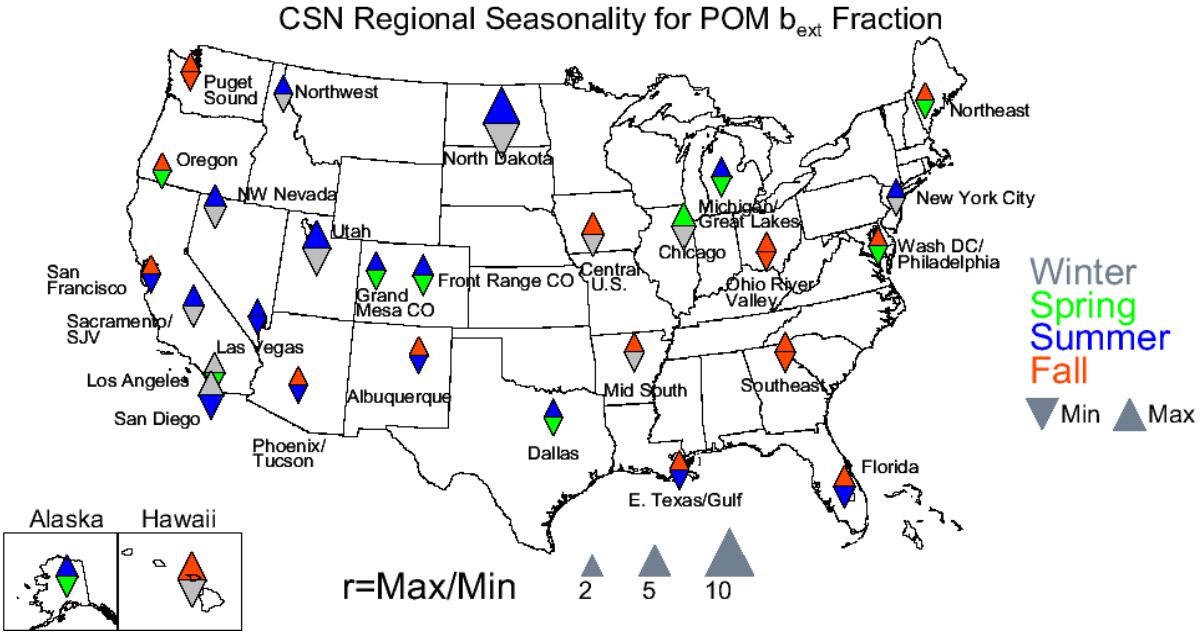

Figure 5.3.4. Seasonal variability for CSN 2005–2008 monthly mean regional particulate organic matter (POM) light extinction coefficient (b_{ext}) fractions. The color of the upward pointing triangle refers to the season with the maximum monthly mean concentration and the downward pointing triangle refers to the season with the minimum monthly mean concentration. The size of the triangles refers to the magnitude of the ratio of maximum to minimum monthly mean mass concentration.

5.4 $PM_{2.5}$ LIGHT ABSORBING CARBON LIGHT EXTINCTION COEFFICIENT

As we saw in the Chapter 4, the monthly mean LAC mass concentrations were relatively low compared to other species, and urban concentrations were generally higher than rural concentrations. Recall that LAC light extinction coefficients (b_{ext_LAC}) were computed by scaling the LAC mass by its extinction efficiency (10 m^2 g^{-1}), which is higher than the other species, due to its ability to both scatter and absorb visible light. This higher extinction efficiency increased LAC's relative contribution to b_{ext} compared to RCFM.

The rural IMPROVE 2005–2008 regional monthly mean LAC light extinction coefficient (b_{ext_LAC}) ranged from 0.24 Mm^{-1} in the Hawaii region in July to 5.67 Mm^{-1} in the Northern Rocky Mountain region in August (roughly half of the contribution by Rayleigh scattering). The maximum urban IMPROVE regional mean b_{ext_LAC} was considerably higher (26.88 Mm^{-1} in Phoenix in December). Values of b_{ext_LAC} at rural southwestern U.S. regions were much lower (<5 Mm^{-1}) than at the urban site of Phoenix (Figure 5.1.3). However, the magnitudes of b_{ext_LAC} were greater relative to other species compared to that for LAC mass concentrations (Figure 4.1.3). Higher b_{ext_LAC} values during summer months were common (e.g., the Sierra Nevada, Great Basin, Central Rocky Mountains, Colorado Plateau, and Death Valley regions), but a few regions lacked strong seasonality (e.g., Southern California, Southern Arizona, and West Texas). Values of b_{ext_LAC} for regions in the northwestern United States were similar in magnitude to regions in the southwestern United States (Figure 5.1.2). Higher b_{ext_LAC} occurred during summer months for all of the regions with the exception of the Columbia River Gorge region. Relatively high b_{ext_LAC} values during summer months, such as those at the Northern Rocky Mountains and Hells Canyon regions, were most likely associated with wildfire emissions. LAC extinction coefficients were also relatively low in the eastern U.S. regions (~5 Mm^{-1} or less, Figure 5.1.1). The higher values of b_{ext_LAC} in summer months that occurred for many western U.S. regions did not occur for regions in the eastern United States; in fact, b_{ext_LAC} increased during fall and winter months. In addition, b_{ext_LAC} values were fairly constant year round. With the exception of the Alaska region during summer, the b_{ext_LAC} values were negligible at the OCONUS regions (Figure 5.1.4).

The seasons corresponding to maximum and minimum monthly mean b_{ext_LAC} at IMPROVE regions were the same as for LAC mass concentrations (compare Figure 5.4.1 to Figure 4.4.1), with the exception of the Virgin Islands region due to treatment of missing data in the calculation of b_{ext} (see Chapter 3). LAC mass concentrations and b_{ext_LAC} also demonstrated the same level of seasonality. Just over a third of the regions did not exhibit significant seasonality. The largest maximum to minimum ratio occurred in the Northern Rocky Mountains region (7.4), compared to the smallest in the Ohio River Valley region (1.3).

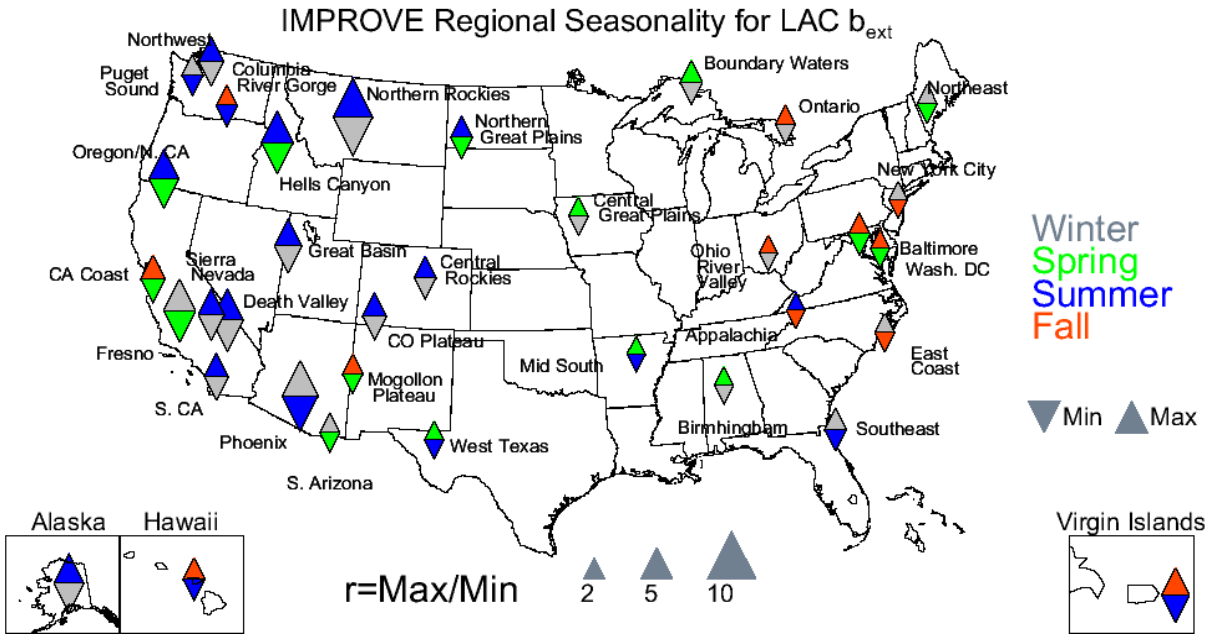

Figure 5.4.1. Seasonal variability for IMPROVE 2005–2008 monthly mean regional light absorbing carbon (LAC) light extinction coefficients (b_{ext}). The color of the upward pointing triangle refers to the season with the maximum monthly mean concentration and the downward pointing triangle refers to the season with the minimum monthly mean concentration. The size of the triangles refers to the magnitude of the ratio of maximum to minimum monthly mean mass concentration.

Urban CSN regional mean b_{ext_LAC} values were similar to the urban IMPROVE regions, ranging from 1.59 Mm^{-1} in the North Dakota region in May to 29.15 Mm^{-1} in the Alaska region in December. The CSN b_{ext_LAC} values in the Alaska region were much higher than those in the IMPROVE regions and peaked in winter months rather than in summer months (Figure 5.1.9). Values of b_{ext_LAC} at the urban Hawaii region were also considerably higher than at the rural regions. The highest b_{ext_LAC} values in the eastern United States occurred at the New York City region (~20 Mm^{-1}, Figure 5.1.8). However, in general the b_{ext_LAC} values were near 10 Mm^{-1} at most eastern regions and fairly constant year round. Urban b_{ext_LAC} values were higher than rural b_{ext_LAC} at most regions in the same vicinity. LAC extinction coefficients were around 10 Mm^{-1} and generally peaked in winter months at regions in the northwestern United States (Figure 5.1.7). This seasonal pattern was opposite to that for rural regions, where b_{ext_LAC} peaked during summer months, and suggested urban sources of LAC that were mostly likely localized and related to combustion emissions. Values of b_{ext_LAC} in the southwestern United States were comparable to b_{ext} from other species at several regions (e.g., Front Range CO, Grand Mesa CO, Albuquerque, Phoenix/Tucson, and Las Vegas, Figure 5.1.6). In contrast, LAC mass concentrations were typically much lower than mass concentrations of other species (see Figure 4.1.7). Winter months were often associated with higher b_{ext_LAC}, and urban b_{ext_LAC} values were higher than rural b_{ext_LAC} values in the southwestern United States (compare to rural b_{ext_LAC} in Figure 5.1.3).

The seasons corresponding to maximum and minimum monthly mean urban b_{ext_LAC} were exactly the same as for urban LAC mass concentrations (compare Figure 5.4.2 to Figure 4.4.2). However, the urban versus rural seasonal patterns were very different. Most urban maxima occurred in fall or winter, most likely associated with residential heating or other urban

emissions. These regions did not exhibit a high degree of seasonality; the highest levels of seasonality occurred in western U.S. regions and in the Alaska region, where the maximum b_{ext_LAC} was 8.0 times higher than the minimum. The lowest ratio occurred in New York City, where the maximum was only 1.4 times higher than the minimum b_{ext_LAC}.

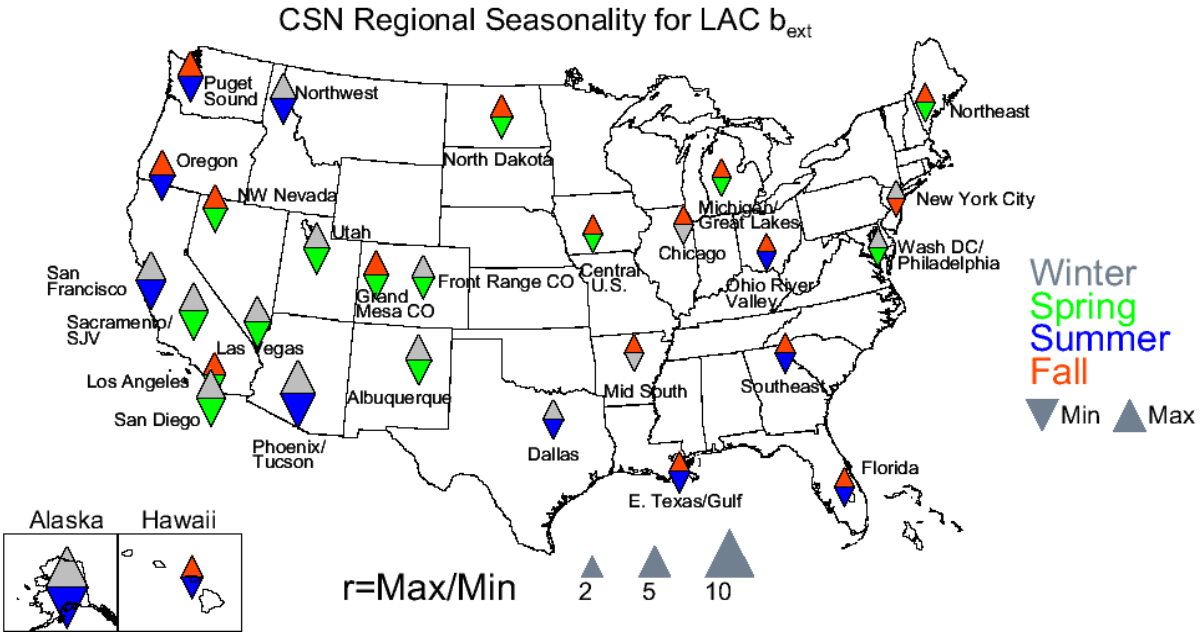

Figure 5.4.2. Seasonal variability for CSN 2005–2008 monthly mean regional light absorbing carbon (LAC) light extinction coefficients (b_{ext}). The color of the upward pointing triangle refers to the season with the maximum monthly mean concentration and the downward pointing triangle refers to the season with the minimum monthly mean concentration. The size of the triangles refers to the magnitude of the ratio of maximum to minimum monthly mean mass concentration.

The contribution of LAC to b_{ext} was higher than its contribution to RCFM at most IMPROVE eastern U.S. regions (compare Figure 5.1.12 to Figure 4.1.11). The higher contribution to b_{ext} was due to the high extinction efficiency of LAC compared to the extinction efficiencies of other relatively low mass concentration species (e.g., soil). Contributions were less than 10% at most eastern IMPROVE regions (e.g., Appalachia, Southeast, and East Coast, among others) and higher in fall and winter. Somewhat higher LAC contributions to b_{ext} occurred for southwestern U.S. regions (Figure 5.1.13), including the highest in the United States at the rural Mogollon Plateau region (16.2% in December) and the urban Phoenix site in November (29.1%). Lower contributions also occurred at southwestern U.S. regions, such as California Coast and West Texas. LAC contributions to b_{ext} were considerably higher than its contributions to RCFM at regions in the southwestern United States (Figure 4.1.13). LAC contributed more significantly to b_{ext} than RCFM in the northwestern United States as well (e.g., the Northern Rocky Mountains, Hells Canyon, and Oregon/Northern California regions, Figure 5.1.14). Relative b_{ext_LAC} contributions of 10% or more were common at most regions and fairly steady year round. Contributions of LAC to b_{ext} were greater than its contributions to RCFM in the eastern United States also (Figure 5.1.12). Estimates of 10% or less were typical at most regions. Of the OCONUS regions, the Alaska region had the highest b_{ext_LAC} contributions (Figure 5.1.11). The Hawaii and Virgin Islands regions had the lowest b_{ext_LAC} contributions of any in the

United States; in fact, the smallest contribution occurred at the Virgin Islands region in July (0.97%).

The relative b_{ext_LAC} had a much lower degree of seasonality compared to absolute b_{ext_LAC}, especially in the western United States (e.g., the Northern Rocky Mountains region, compare Figure 5.4.3 to Figure 5.4.1). The maximum ratio occurred in the Virgin Islands (5.2) and the minimum ratio occurred at the Puget Sound (1.4) and Northwest regions (1.5). Summer minima were common in the eastern and some southwestern U.S. regions. Although the degree of seasonality of relative b_{ext_LAC} was similar to its relative contribution to RCFM (Figure 4.4.3), the seasons corresponding to maxima and minima were different for many regions, especially in the western United States. While LAC mass fractions were typically higher in winter months for many regions, the b_{ext_LAC} fraction was highest in summer, as was absolute b_{ext_LAC} (e.g., the Great Basin, Fresno, Sierra Nevada, Northwest, and Hells Canyon regions). These differences were mostly likely a reflection of the changes in seasonal behavior of other species as well. For example, species that may be more important on a mass basis, like soil, may be less important optically.

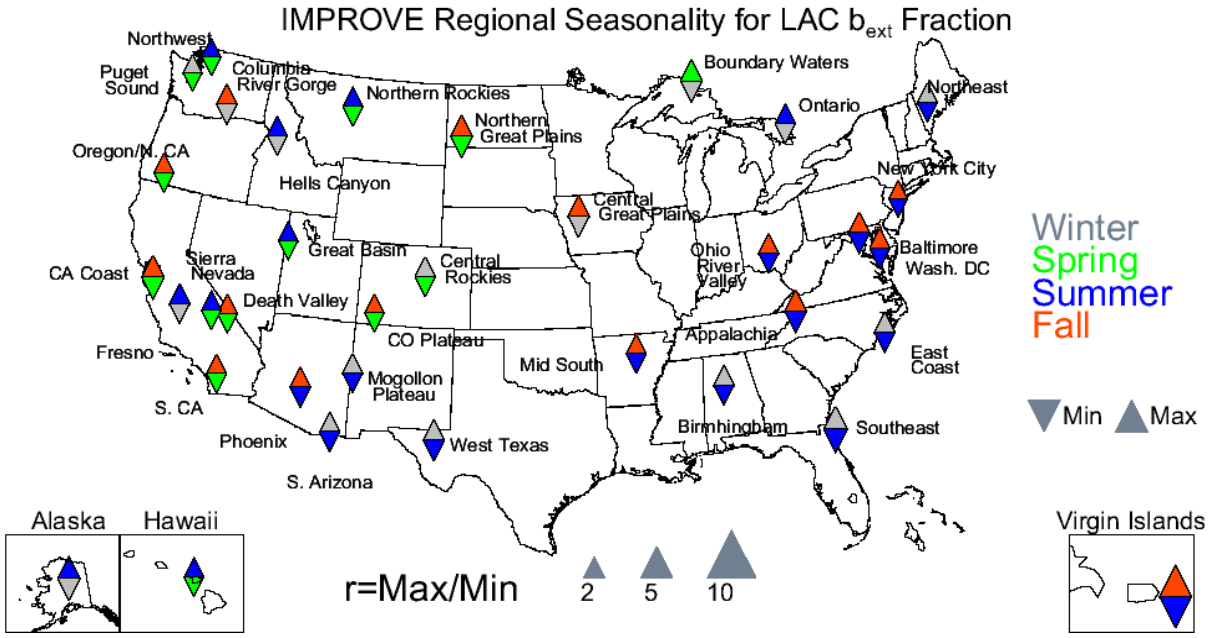

Figure 5.4.3. Seasonal variability for IMPROVE 2005–2008 monthly mean regional light absorbing carbon (LAC) light extinction coefficient (b_{ext}) fractions. The color of the upward pointing triangle refers to the season with the maximum monthly mean concentration and the downward pointing triangle refers to the season with the minimum monthly mean concentration. The size of the triangles refers to the magnitude of the ratio of maximum to minimum monthly mean mass concentration.

CSN urban contributions of LAC to b_{ext} were considerably higher than rural contributions to b_{ext}. For example, in the southwestern United States, contributions of 20% or greater were common at most regions (Figure 5.1.18). The highest contribution in the United States occurred at the Las Vegas region in October (39.2%). In comparison, rural contributions were ~10% or less in the southwestern United States. Regions in California (e.g., Sacramento, San Francisco, Los Angeles, and San Diego) had lower contributions compared to those regions farther east, such as the Northwest Nevada, Front Range CO, Grand Mesa CO, Albuquerque, Las Vegas, and

Phoenix/Tucson regions. Contributions of LAC to b_{ext} were somewhat lower in the northwestern United States, with values less than 20% year round (Figure 5.1.17). However, relative b_{ext_LAC} values were still higher than its contributions to RCFM in the northwestern United States (Figure 4.1.17). The lowest contributions in the United States occurred at the North Dakota region in March (4.5). Urban b_{ext_LAC} contributions at eastern U.S. regions were lower than other sections in the United States. Estimates of relative b_{ext_LAC} were typically 10% or less (Figure 5.1.16). LAC contributions to b_{ext} were higher than its contributions to RCFM in the eastern United States but not to the same degree as in other regions, probably because of the dominance of other species such as AS, AN, and POM. Urban OCONUS regions corresponded to significantly higher relative b_{ext_LAC} values compared to rural regions (Figure 5.1.19 compared to Figure 5.1.11). In the Alaska region the contributions were greater than 20% in spring and fall. In the Hawaii region the contributions ranged from 10 to 20%.

The urban contributions to b_{ext} from LAC did not exhibit a strong seasonality (Figure 5.4.4). The lowest maximum to minimum ratio occurred at the Las Vegas region (1.5) compared to the largest at the North Dakota region (3.5). The relative contribution of b_{ext_LAC} was less seasonal than absolute b_{ext_LAC} for several regions in the western United States, suggesting LAC had fairly steady contributions to b_{ext} for many regions. The contributions of LAC to b_{ext} generally were highest in the fall and lowest during winter, spring and summer.

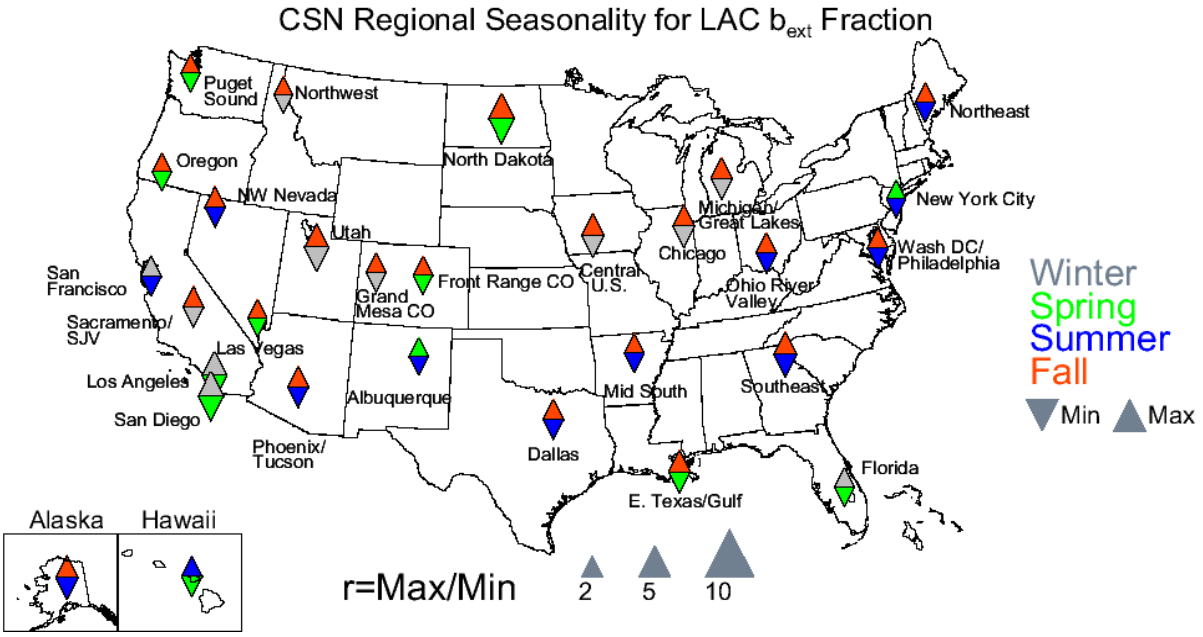

Figure 5.4.4. Seasonal variability for CSN 2005–2008 monthly mean regional light absorbing carbon (LAC) light extinction coefficient (b_{ext}) fractions. The color of the upward pointing triangle refers to the season with the maximum monthly mean concentration and the downward pointing triangle refers to the season with the minimum monthly mean concentration. The size of the triangles refers to the magnitude of the ratio of maximum to minimum monthly mean mass concentration.

5.5 $PM_{2.5}$ SOIL LIGHT EXTINCTION COEFFICIENTS

Recall from section 3.1 that the soil extinction efficiency used to compute b_{ext_soil} in the IMPROVE algorithm was 1 m^2 g^{-1}. The soil extinction efficiency is lower than for most other

species and soil is nonhygroscopic; therefore light extinction coefficients from soil, b_{ext_soil}, were the same as the soil mass concentrations, as were its seasonal and regional patterns. However, the magnitude of b_{ext} might change relative to other species, as well as its relative contribution to b_{ext}. The IMPROVE 2005–2008 regional monthly mean b_{ext_soil} ranged from 0.049 Mm^{-1} in the Alaska region in September to 5.54 Mm^{-1} in the Virgin Islands in June. Long-distance transport of dust from North Africa in summer is well documented and the likely reason for high soil concentrations and consequent light extinction in summer in the Virgin Islands. Light extinction coefficients due to soil were negligible at other OCONUS regions (Figure 5.1.4). However, several regions in the southwestern United States were associated with non-negligible b_{ext_soil}, especially relative to b_{ext} from other species (Figure 5.1.3). The highest values of b_{ext_soil} in the southwestern United States were at the Southern Arizona region, due to high soil mass concentrations at that region. The Death Valley, Central Rocky Mountains, Great Basin, and Colorado Plateau and Mogollon Plateau regions all had higher b_{ext_soil}, especially during spring months. Regions farther west, such as the Sierra Nevada, California Coast, and Southern California regions, had relatively low b_{ext_soil}, less than 5 Mm^{-1}. Light extinction coefficients due to soil at northwestern U.S. regions were lower still, only 1–2 Mm^{-1} at most regions (Figure 5.1.2). The Northwest and Oregon/Northern California regions had the lowest values year round. Similar to the northwestern United States, values of b_{ext_soil} in the eastern United States were negligible compared to other species. With the exception of the Northern Great Plains, Mid South, and Southeast regions, the values were not visible on the bar charts (Figure 5.1.1).

The highest monthly mean b_{ext_soil} occurred most frequently in summer for IMPROVE regions (Figure 5.5.1). These regions were located in the central and eastern United States, as well as a few regions in the western United States (e.g., Puget Sound, Columbia River Gorge, Hells Canyon, Northern Rocky Mountains, Great Basin, Northern Great Plains, and Phoenix). Spring maxima occurred at regions along the western coast and in the southwestern United States. Winter maxima occurred at the Alaska region, but generally most regions were associated with winter minima. As expected, the seasons corresponding to the maximum and minimum b_{ext_soil} were exactly the same as for the soil mass concentrations (Figure 4.5.1). Light extinction coefficients from soil were strongly seasonal, with only four regions having maximum to minimum ratios less than 2. The largest ratio occurred in the Virgin Islands (28.9) compared to the lowest in the New York City region (1.6) (2.3 in the rural Northeast region). In general IMPROVE regions in the eastern United States had lower degrees of seasonality (with the exception of the Southeast region) compared to most western U.S. regions.

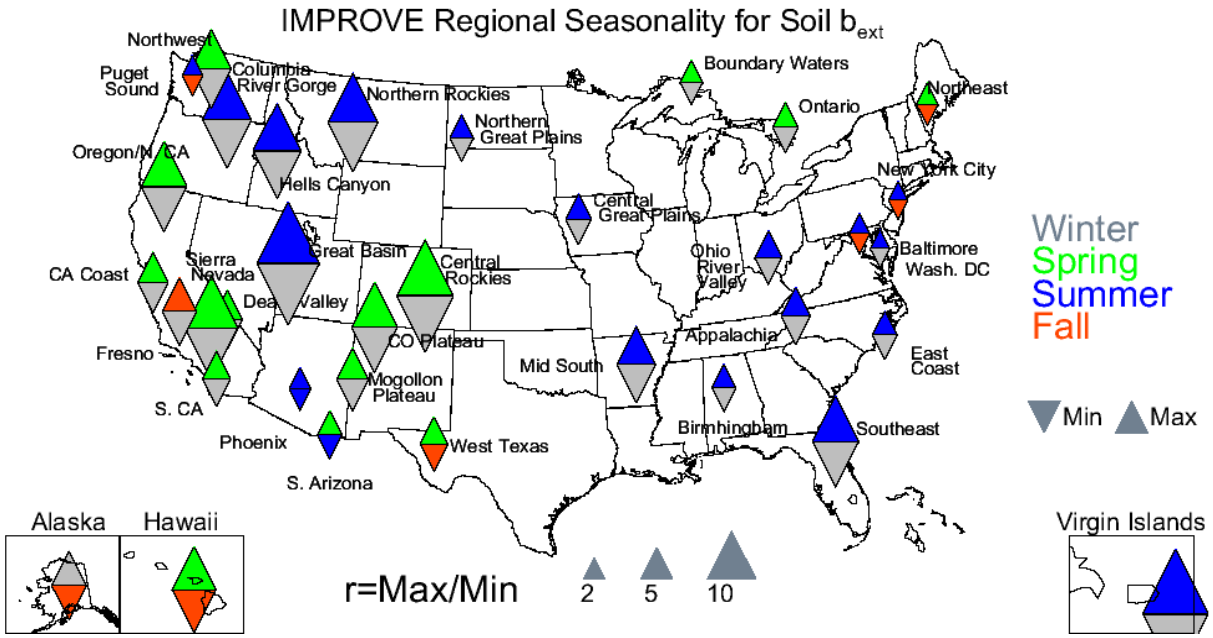

Figure 5.5.1. Seasonal variability for IMPROVE 2005–2008 monthly mean regional soil light extinction coefficients (b_{ext}). The color of the upward pointing triangle refers to the season with the maximum monthly mean concentration and the downward pointing triangle refers to the season with the minimum monthly mean concentration. The size of the triangles refers to the magnitude of the ratio of maximum to minimum monthly mean mass concentration.

The CSN maximum regional monthly mean b_{ext_soil} was lower than the maximum value for the IMPROVE network (recall the relative bias in soil mass concentrations between the two networks, with IMPROVE having higher soil concentrations; see section 1.4). The CSN maximum value of 2.55 Mm^{-1} occurred in the Phoenix region in April compared to the lowest value of 0.089 Mm^{-1} in the Hawaii region in September. Similar to the rural regions, b_{ext_soil} was negligible at eastern U.S. regions (Figure 5.1.8). Only at the Florida, East Texas/Gulf, Dallas, and Mid South regions were the values of b_{ext_soil} even visible on the bar charts. Light extinction coefficients due to soil at these regions were most likely due to long-range transport of dust during summer. The relative values of b_{ext} for all species in the southwestern United States demonstrated that, while a species may contribute significantly to RCFM, it may not contribute as significantly to b_{ext} because it is not as optically efficient as other species. For example, recall that soil mass concentrations were fairly significant and comparable to or larger than LAC mass concentrations at some urban regions in the southwestern United States (Figure 4.1.7). The effects of the larger extinction efficiency for LAC compared to that for soil were obvious in magnitudes of b_{ext} in Figure 5.1.6. For most regions, the b_{ext_soil} values were much lower than b_{ext_LAC}. A similar pattern was observed at the regions in the northwestern United States (Figure 5.1.7). Soil mass concentrations that were easily viewed on the bar charts for the North Dakota and Northwest regions were no longer visible on the associated b_{ext_soil} bar charts. Of the OCONUS regions, very low b_{ext_soil} values occurred at the Hawaii region during spring months, but values of b_{ext_soil} were not even visible on the Alaska region bar chart (Figure 5.1.9).

Many CSN regions had maximum b_{ext_soil} in summer in the eastern United States, as well as at a few western U.S. regions (e.g., North Dakota, Utah, Las Vegas, Oregon, and Northwest, Figure 5.5.2). A few spring maxima occurred for eastern U.S. regions (e.g., Northeast, New York

City, Michigan/Great Lakes, and Chicago) and in the western United States (Grand Mesa CO, Front Range CO, Albuquerque, Phoenix/Tucson, Northwest Nevada, Puget Sound, and Hawaii). Only a few regions in California corresponded to fall maxima. Most regions corresponded to winter minima. Urban regions were also strongly seasonal, with only seven regions having maximum to minimum monthly mean b_{ext_soil} ratios less than 2. The maximum ratio occurred in the Florida region (8.2) compared to 1.5 in the New York City region. In general urban regions corresponded to a lower degree of seasonality compared to the rural regions, especially in the West (see Figure 5.5.1).

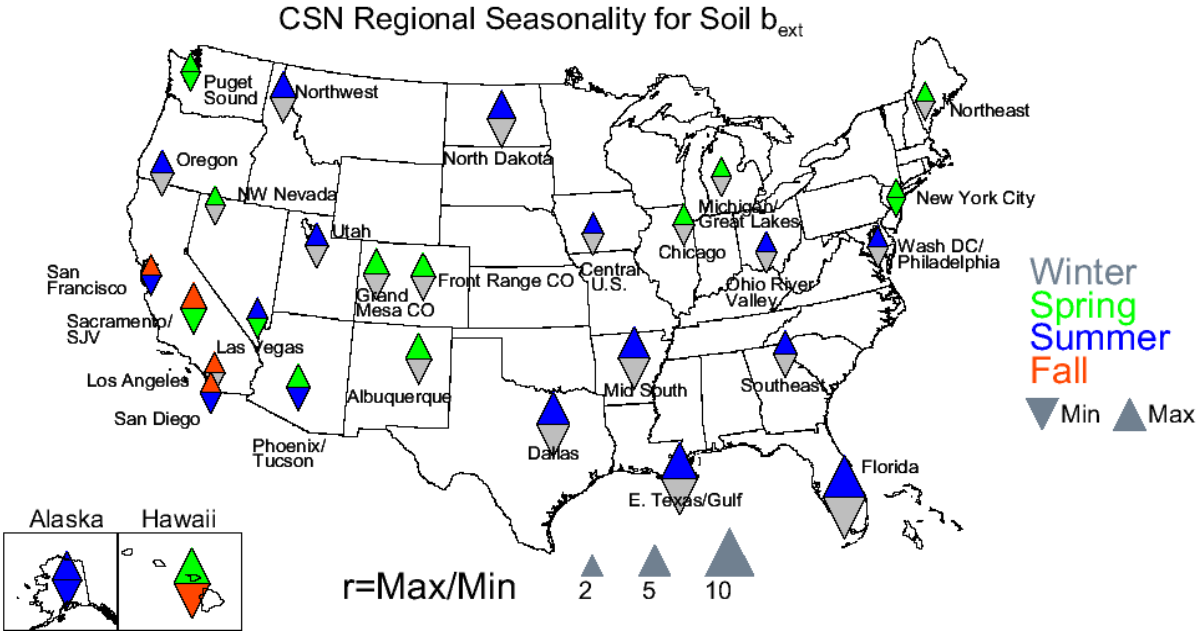

Figure 5.5.2. Seasonal variability for CSN 2005–2008 monthly mean regional soil light extinction coefficients (b_{ext}). The color of the upward pointing triangle refers to the season with the maximum monthly mean concentration and the downward pointing triangle refers to the season with the minimum monthly mean concentration. The size of the triangles refers to the magnitude of the ratio of maximum to minimum monthly mean mass concentration.

As was expected from the discussion of Figure 5.1.1, relative contributions of soil to b_{ext} in the eastern United States were negligible at most rural regions. Relative b_{ext_soil} reached a few percent at the Southeast, Mid South, Central Great Plains, and Northern Great Plains IMPROVE regions (Figure 5.1.12). In contrast, soil mass contributions to RCFM reached 10–20% at these same regions, depending on time of year (Figure 4.1.11). Compared to the eastern United States, soil contributions to b_{ext} were higher in the southwestern United States and reached up to 15–20%, especially during spring months at the Death Valley, Southern Arizona, West Texas, Mogollon Plateau, Colorado Plateau, Central Rocky Mountains, and Great Basin regions (Figure 5.1.13). However, at these same regions soil mass contributed up to 50% to RCFM. At the Sierra Nevada, California Coast, and Southern California regions the relative b_{ext_soil} values were comparable to regional mean values in the eastern United States. Contributions of only a few percent were common at northwestern U.S. regions. The highest relative b_{ext_soil} occurred at the Hells Canyon, Northern Great Plains, Northern Rocky Mountains, and Columbia River Gorge regions, where contributions of 5–10% were more likely during spring and summer months (Figure 5.1.14). Soil contributions to b_{ext} increased to ~20% at the Virgin Islands region during

summer (Figure 5.1.11); however, its contribution to RCFM was near 60% during the same months (Figure 4.1.14). Relative b_{ext_soil} values were low at other OCONUS regions. The maximum contribution of soil to b_{ext} in rural regions occurred in the Southern Arizona region in April (23.7%). The lowest contribution occurred at the Ontario (Egbert) region (0.26% in December).

Contributions to b_{ext} from soil were typically highest in the spring for IMPROVE regions. The seasons corresponding to the maximum and minimum in monthly mean relative b_{ext_soil} were different than for its maximum and minimum contributions to RCFM at some regions (compare Figure 5.5.3 to 4.5.3). Although the seasons at the OCONUS regions remained the same, many other regions shifted when comparing the seasonality of relative b_{ext_soil} to soil mass fractions (e.g., the Fresno, Phoenix, Birmingham, Ohio River Valley, and East Coast regions). However, the shift in seasons occurred at a larger number of regions for relative b_{ext_soil} compared to absolute b_{ext_soil} (e.g., the Hells Canyon, Northern Rocky Mountains, and Great Basin regions, among others; compare Figures 5.5.3 and 5.5.1). Many regions shifted from summer maxima in absolute b_{ext_soil} to spring maxima for relative b_{ext_soil}. Most regional minima still occurred during winter for relative b_{ext_soil}. Strong seasonality in relative b_{ext_soil} was associated with IMPROVE regions, with only three regions having maximum to minimum ratios less than 2. The highest occurred in the IMPROVE urban site of Fresno (22.4) and the rural Columbia River Gorge region (17.5). The lowest occurred in the rural East Coast region (1.9) and New York City region (1.6). The regions with the highest degrees of seasonality changed for absolute b_{ext_soil} compared to relative b_{ext_soil}, especially for southwestern U.S. regions (e.g., Fresno, Colombia River Gorge, and Great Basin, among others).

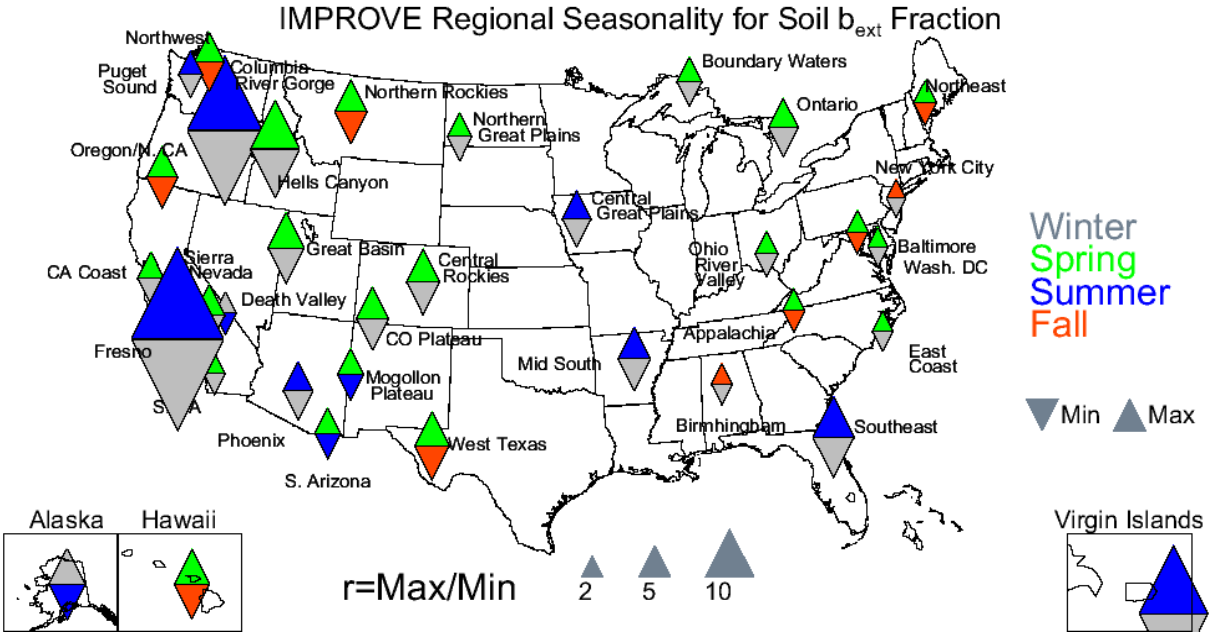

Figure 5.5.3. Seasonal variability for IMPROVE 2005–2008 monthly mean regional soil light extinction coefficient (b_{ext}) fractions. The color of the upward pointing triangle refers to the season with the maximum monthly mean concentration and the downward pointing triangle refers to the season with the minimum monthly mean concentration. The size of the triangles refers to the magnitude of the ratio of maximum to minimum monthly mean mass concentration.

The highest urban CSN contribution of soil to b_{ext} also occurred in the Phoenix/Tucson region in April (8.9%), a factor of 2.5 less than the maximum contribution at rural regions. The lowest contribution occurred in the Alaska region in December (0.23%). During spring months in the Alaska region, the soil contribution to b_{ext} was a few percent, larger than at any time of the year in the Hawaii region (Figure 5.1.19). Low relative contributions were also common at eastern U.S. regions. With the exception of the Florida, East Texas/Gulf, Dallas, and Mid South regions, the contributions were not visible on the bar charts (Figure 5.1.16). In contrast, soil contributions to RCFM of up to 20% in summer occurred at the Florida region and were ~10% at other eastern U.S. regions (Figure 4.1.16). Soil contributed only a few percent to b_{ext} in the northwestern United States (Figure 5.1.17). The bar charts associated with the Northwest and North Dakota regions had the most visible fractional b_{ext_soil}, but only 1–2%. In contrast, the soil mass fractions approached 20% at the same locations (Figure 4.1.17). Of all the urban regions, those in the southwestern United States corresponded to the highest contributions of soil to b_{ext} (Figure 5.1.18), but the contributions were still less than 10% for most regions. The Las Vegas, Phoenix/Tucson, Albuquerque, Grand Mesa CO, Front Range CO, and Utah regions corresponded to the highest contributions, compared to regions along the western coast, where relative b_{ext_soil} was not visible on the associated bar charts.

Similar to IMPROVE regions, many CSN regions had maximum relative b_{ext_soil} in spring. Many regions shifted to spring maxima for relative b_{ext_soil} compared to the summer maxima common for absolute b_{ext_soil}. For example, the Southeast, Ohio River Valley, Washington DC/Philadelphia Corridor, Las Vegas, San Francisco, San Diego, Puget Sound, Utah, and Alaska regions all corresponded to spring maxima (Figure 5.5.4). Minima in relative b_{ext_soil} occurred mainly in winter except for fall minima at the Hawaii, Puget Sound, and Southeast regions and a few regions with summer minima (New York City, Los Angeles, and San Diego). All but one region demonstrated strong seasonality in the contribution of soil to b_{ext}. The lowest ratio occurred in the New York City region (1.6) compared to the highest ratio in the Alaska region (21.7). The relative contributions of soil to b_{ext} generally displayed a higher degree of seasonality than did absolute b_{ext_soil} (Figure 5.5.2) or soil mass fraction (Figure 4.5.4). In addition, the western U.S. regions generally corresponded to higher seasonality in relative b_{ext_soil} compared to the eastern U.S. regions.

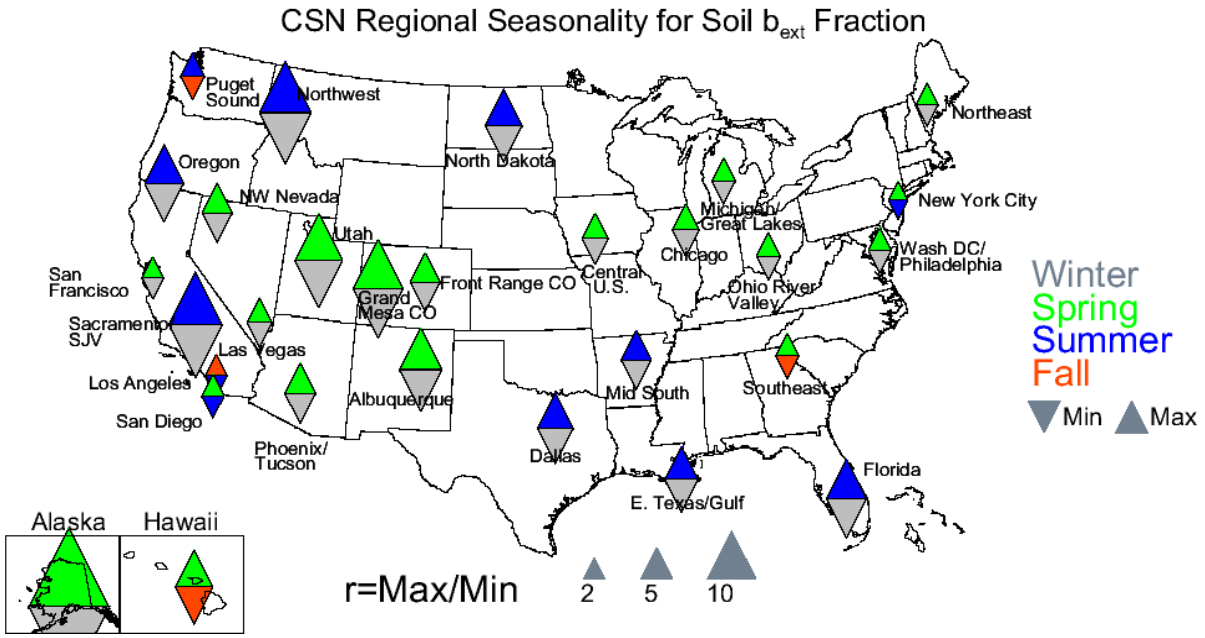

Figure 5.5.4. Seasonal variability for CSN 2005–2008 monthly mean regional soil light extinction coefficient (b_{ext}) fractions. The color of the upward pointing triangle refers to the season with the maximum monthly mean concentration and the downward pointing triangle refers to the season with the minimum monthly mean concentration. The size of the triangles refers to the magnitude of the ratio of maximum to minimum monthly mean mass concentration.

5.6 $PM_{2.5}$ SEA SALT LIGHT EXTINCTION COEFFICIENTS

Recall from section 3.1 that sea salt is a hygroscopic species and was treated as such in the algorithm for computing reconstructed light extinction coefficient for sea salt (b_{ext_SS}). While sea salt mass concentrations were relatively low, except at coastal regions, values of b_{ext_SS} were significant at some regions due to hygroscopic effects. We point to some of these cases in the discussion below.

IMPROVE 2005–2008 regional monthly mean light extinction from sea salt ranged from 0.033 Mm^{-1} in the Central Rocky Mountains region in December to 10.65 Mm^{-1} in January in the Virgin Islands region. Sea salt b_{ext} was fairly significant year round at the Virgin Islands region, with estimates near 10 Mm^{-1} (Figure 5.1.4). While soil mass concentrations were higher than sea salt mass concentrations at the Virgin Island region (see Figure 4.1.4), b_{ext_SS} was higher than b_{ext_soil} by a factor of 2 or more due to hygroscopic effects of sea salt, as well as a higher sea salt dry extinction efficiency. Light extinction coefficients from sea salt were lower at the Hawaii region (<5 Mm^{-1}) and the Alaska region (5-10 Mm^{-1}) compared to the Virgin Islands region. In the eastern United States, b_{ext_SS} was significantly lower than b_{ext} from other species at most regions (~5 Mm^{-1}) and was barely visible on the bar charts associated with the East Coast, Southeast, Northeast, and the Northern Great Plains (December) regions. Light extinction from sea salt was non-negligible at the California Coast region in the southwestern United States (Figure 5.1.3), as was sea salt mass (Figure 4.1.3); values of b_{ext_SS} at the California Coast region were still relatively low (5–10 Mm^{-1}). Some of the northwestern U.S. coastal regions corresponded to b_{ext_SS} values of a few inverse megameters. With the exception of the higher b_{ext_SS} at the Northern Great Plains region in December, most non-coastal regions had negligible

b_{ext_SS} (Figure 5.1.2). The winter high in b_{ext_SS} at the Northern Great Plains region was associated with one sample day in December (14 December 2008), when all of the sites within the region corresponded to historically high chloride ion concentrations. The event may have been associated with transport of Arctic air (White et al., 2010), but is such a rare event that its contribution could be treated as an outlier.

The seasons corresponding to maxima and minima in IMPROVE b_{ext_SS} (Figure 5.6.1) were very similar to those corresponding to rural sea salt mass concentrations (Figure 4.6.1), except at the Death Valley, Phoenix, West Texas, Ohio River Valley, Appalachia, New York City, and East Coast regions. Most regions experienced winter maxima that were possibly associated with road salt. A strong seasonality was observed in rural regions, with only three regions having maximum to minimum ratios less than 2. The highest occurred in the Northern Great Plains region (28.9) and the lowest in the Hawaii region (1.7). The degree of seasonality increased for some regions, with high ratios for b_{ext_SS} compared to sea salt mass (e.g., the Northern Great Plains and Fresno regions). The degree of seasonality was lower for a few regions on the eastern coast (e.g., Baltimore and Washington, D.C., regions) for b_{ext_SS} compared to sea salt mass.

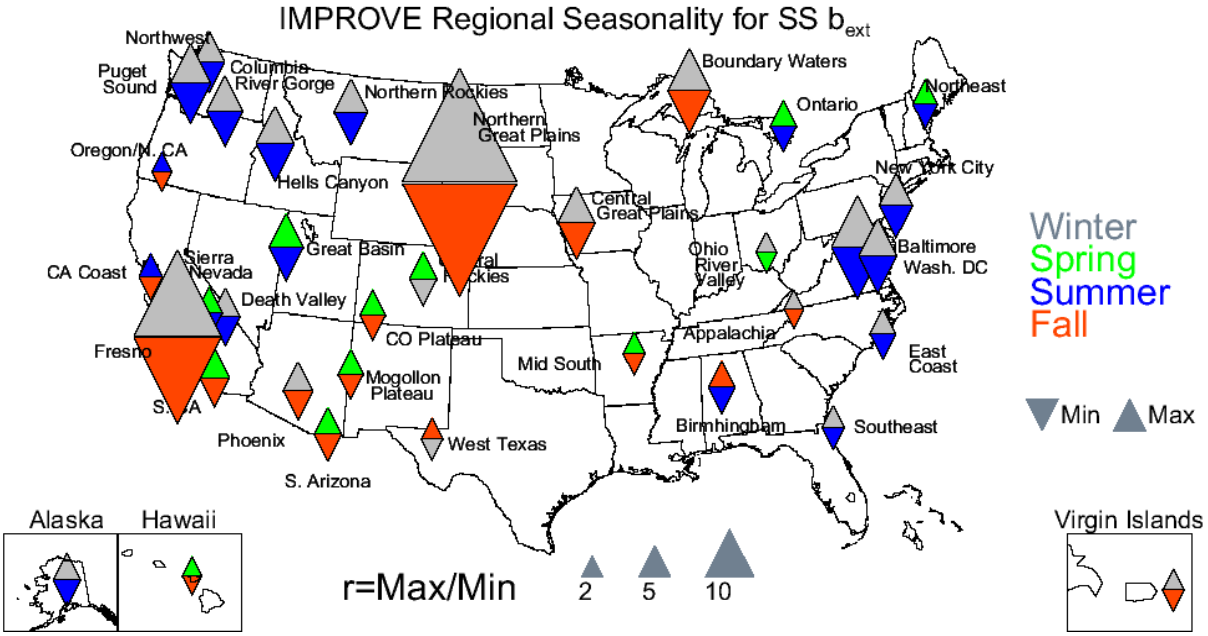

Figure 5.6.1. Seasonal variability for IMPROVE 2005–2008 monthly mean regional sea salt (SS) light extinction coefficients (b_{ext}). The color of the upward pointing triangle refers to the season with the maximum monthly mean concentration and the downward pointing triangle refers to the season with the minimum monthly mean concentration. The size of the triangles refers to the magnitude of the ratio of maximum to minimum monthly mean mass concentration.

The range in b_{ext_SS} in CSN regions was similar to the range for IMPROVE regions, with the lowest in Albuquerque in October (0.0079 Mm^{-1}) and the highest regional mean in the Hawaii region in January (8.31 Mm^{-1}). Values of b_{ext_SS} were higher at the urban Hawaii region compared to the rural Hawaii region (Figure 5.1.9) (recall the large bias in sea salt mass concentrations between IMPROVE and CSN, with higher IMPROVE concentrations, Table 1.9 in Chapter 1). Estimates of b_{ext_SS} were negligible compared to b_{ext} from other species at the

Alaska region. Extinction coefficients for sea salt were relatively insignificant at eastern U.S. urban regions, except at the Florida region, where it was barely visible on the corresponding bar chart (Figure 5.1.8). Similar magnitudes of b_{ext_SS} occurred in the southwestern (Figure 5.1.6) and northwestern United States (Figure 5.1.7). Values of b_{ext_SS} of 5 Mm^{-1} occurred at the Puget Sound region, mostly during winter months.

The majority of urban regions had maximum b_{ext_SS} in winter (Figure 5.6.2). Recall that rural regions also corresponded mainly to winter maxima. The seasons corresponding to maximum and minimum sea salt mass concentrations were different for some regions for b_{ext_SS} (e.g., San Francisco, Sacramento/San Joaquin Valley, Las Vegas, Phoenix/Tucson, Chicago, and Southeast). The urban regions also experienced a strong seasonality in b_{ext_SS}, with only one region having maximum to minimum ratios less than 2 (Southeast, 1.7). The highest ratio was observed in the Utah region (93.8). Most of the western U.S. regions experienced a higher degree of seasonality compared to the eastern U.S. regions. Regions in the southeastern United States corresponded to the lowest degree of seasonality (e.g., Dallas, Mid South, East Texas/Gulf, and Florida).

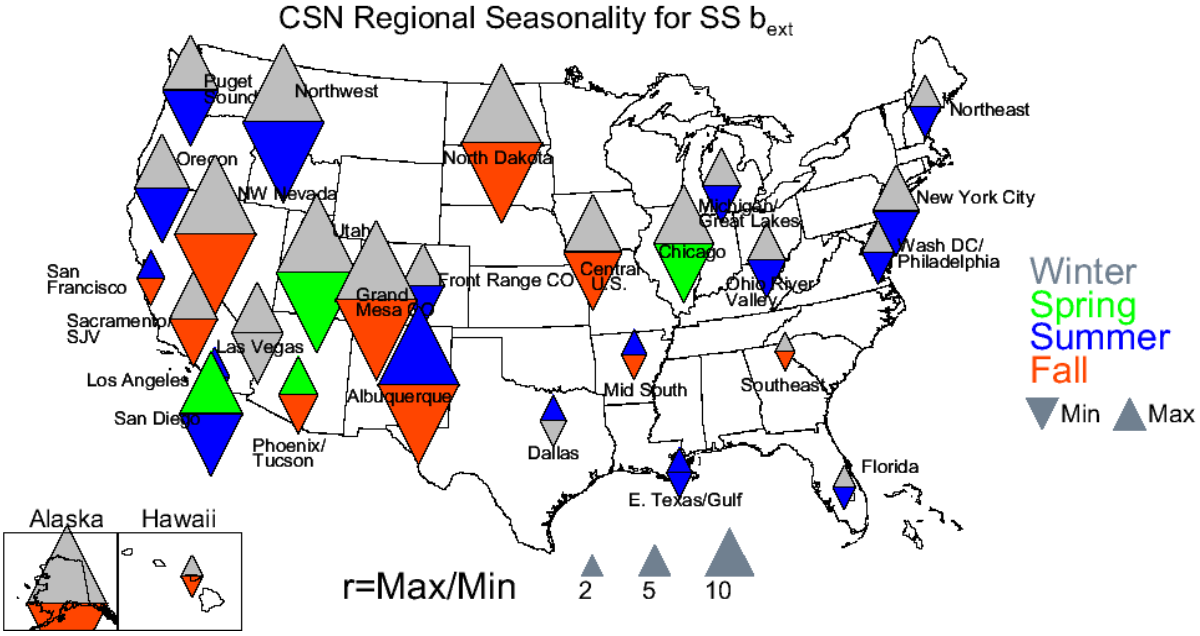

Figure 5.6.2. Seasonal variability for CSN 2005–2008 monthly mean regional sea salt (SS) light extinction coefficients (b_{ext}). The color of the upward pointing triangle refers to the season with the maximum monthly mean concentration and the downward pointing triangle refers to the season with the minimum monthly mean concentration. The size of the triangles refers to the magnitude of the ratio of maximum to minimum monthly mean mass concentration.

The fractional contribution of sea salt to b_{ext} in rural regions ranged from 0.0015% in the IMPROVE Northern Rocky Mountains region in August to 55.2% in the Virgin Islands in December. The major contributions to b_{ext} at the Virgin Islands region were sea salt and AS (Figure 5.1.11), in contrast to the major contributors to RCFM (AS, soil, and sea salt). In the Alaska region the contributions of sea salt to b_{ext} were near 40% during winter months. Contributions at the Hawaii region were lower (~10%). Contributions of sea salt to b_{ext} in the eastern United States were 10% or lower at the coastal locations of the Southeast, East Coast,

and Northeast regions and negligible at other regions (Figure 5.1.12). The only southwestern U.S. region with non-negligible contributions of sea salt to b_{ext} (~20%) was the California Coast region (Figure 5.1.13). The northwestern U.S. coastal regions, such as Oregon/Northern California, Columbia River Gorge, and Northwest, corresponded to contributions of 10% or less.

The seasons corresponding to maximum and minimum b_{ext_SS} fraction and sea salt mass fractions were fairly similar for most regions (Figure 5.6.3 and Figure 4.6.3, respectively). However, the California Coast, West Texas, Hells Canyon, Colorado Plateau, Central Rocky Mountains, Boundary Waters, Mid South, and Southeast regions all shifted seasons. The maps of seasonality for relative and absolute b_{ext_SS} were quite different (compare Figure 5.6.3 to Figure 5.6.1). Both the maximum and minimum seasons and the degree of seasonality changed for many regions. Most regions experienced the greatest contribution from sea salt to b_{ext} in winter. Only one region did not experience strong seasonality: West Texas had a maximum to minimum ratio of 1.99. The greatest ratio occurred in the Northern Great Plains region (31.0).

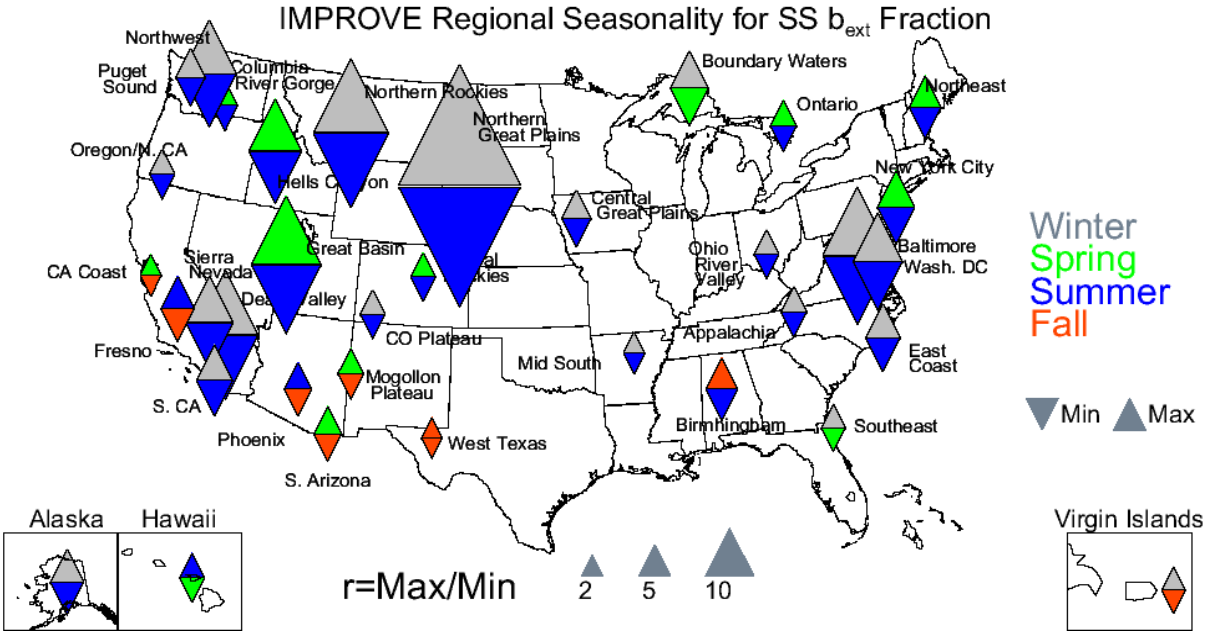

Figure 5.6.3. Seasonal variability for IMPROVE 2005–2008 monthly mean regional sea salt (SS) light extinction coefficients (b_{ext}) fraction. The color of the upward pointing triangle refers to the season with the maximum monthly mean concentration and the downward pointing triangle refers to the season with the minimum monthly mean concentration. The size of the triangles refers to the magnitude of the ratio of maximum to minimum monthly mean mass concentration.

Contributions of sea salt to b_{ext} in CSN urban regions ranged from 0.026% in the Albuquerque region in October to 31.6% in January in the Hawaii region. The contributions of sea salt to b_{ext} at the Hawaii region were 20% or greater year round but negligible at the Alaska region (Figure 5.1.19). Of all the urban regional bar charts associated with the eastern United States, only the Florida region corresponded to visible relative b_{ext_SS}, and those contributions were less than 5% (Figure 5.1.16). In the southwestern United States, relative b_{ext_SS} values were visible in the Southern California and San Francisco regional bar charts (Figure 5.1.18). Of the northwestern U.S. regions, Puget Sound was the only region with visible b_{ext_SS} values on the bar chart (Figure 5.1.17).

Similar to IMPROVE regions, most CSN regions also experienced maxima b_{ext_SS} in winter (Figure 5.6.4). The seasons corresponding to maximum and minimum were fairly similar for sea salt mass fractions and relative sea salt b_{ext} (compare Figures 4.6.4 and 5.6.4). Differences in seasons between relative and absolute b_{ext_SS} occurred at the Hawaii, Oregon, Utah, Grand Mesa CO, Mid South, and Northwest regions. Unlike the rural regions, the seasons corresponding to relative b_{ext_SS} and absolute b_{ext_SS} were fairly similar for most urban regions (Figure 5.6.4 and Figure 5.6.2, respectively). Shifts in seasons occurred at the Alaska, San Francisco, Sacramento/San Joaquin Valley, Las Vegas, Utah, East Texas/Gulf, Southeast, Chicago, and New York City regions. Generally, urban regions had a similar degree of seasonality for relative b_{ext_SS} compared to absolute b_{ext_SS}, although it varied for individual regions (e.g., Grand Mesa CO). Several regions exhibited strong seasonality. The highest ratio of maximum to minimum percent contribution occurred in the Albuquerque region (30.8) and the lowest occurred in the Hawaii region (2.3). The high degree of seasonality in b_{ext_SS} and relative b_{ext_SS} compared to other species may have been partly due to the very low sea salt mass concentrations that occurred at most regions year round.

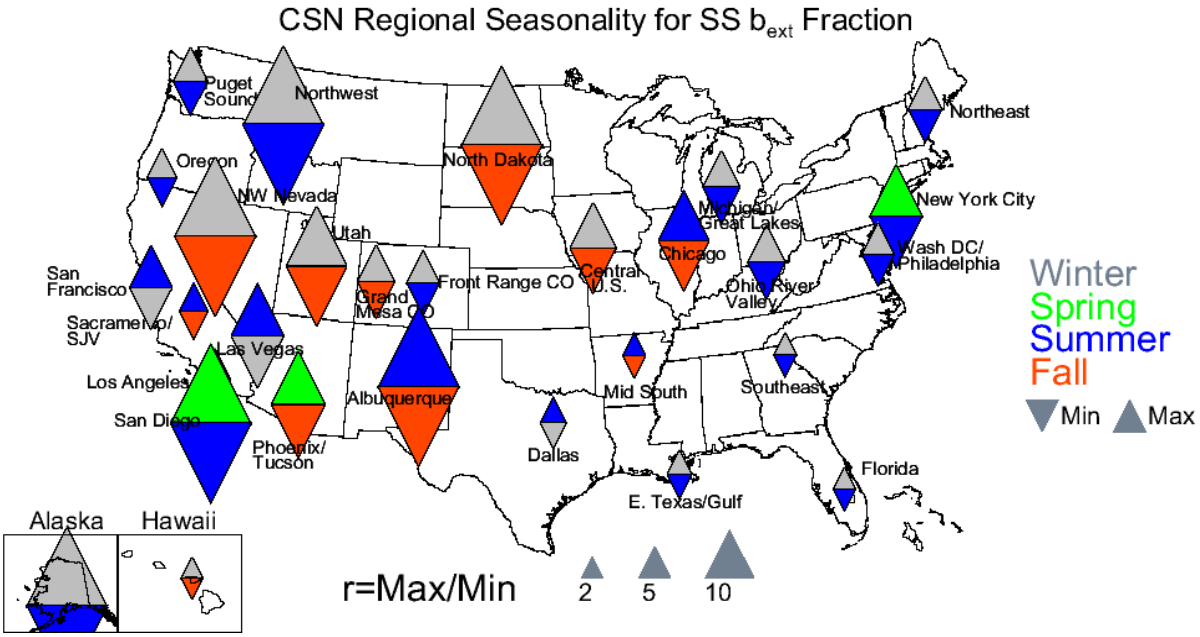

Figure 5.6.4. Seasonal variability for CSN 2005–2008 monthly mean regional sea salt (SS) light extinction coefficient (b_{ext}) fractions. The color of the upward pointing triangle refers to the season with the maximum monthly mean concentration and the downward pointing triangle refers to the season with the minimum monthly mean concentration. The size of the triangles refers to the magnitude of the ratio of maximum to minimum monthly mean mass concentration.

5.7 $PM_{2.5}$ RECONSTRUCTED AEROSOL LIGHT EXTINCTION COEFFICIENTS

The $PM_{2.5}$ reconstructed aerosol light extinction coefficient (b_{ext_aer}) is the sum of light extinction coefficients from the previous $PM_{2.5}$ components discussed above, namely, AS, AN, POM, LAC, soil, and sea salt. The range in 2005–2008 regional monthly mean IMPROVE b_{ext_aer} was from 5.73 Mm^{-1} in the Great Basin region in January to 127.26 Mm^{-1} in the Appalachia region in August (rural) and 246.09 Mm^{-1} in the urban region of Fresno in December. Given the discussion regarding b_{ext} from individual species in the previous sections, it

is reasonable to assume that the high b_{ext_aer} in the Appalachian region in August was due to AS and the high b_{ext_aer} in Fresno CA in December was due to AN. Most of the maximum b_{ext_aer} occurred in summer (Figure 5.7.1), probably also associated with AS in the eastern and POM in the western United States. Regions with fall maxima corresponded to the Puget Sound, California Coast, Phoenix, West Texas, Boundary Waters, and Ontario regions. Spring maxima corresponded to the Hawaii, Virgin Islands, Southern California, and the Southeast regions. Minima at most regions were associated with fall and winter, although summer minima did occur (Hawaii, Puget Sound, Columbia River Gorge, Phoenix, and Ontario regions). Most (21 regions) of all IMPROVE regions experienced some degree of seasonality. The highest occurred in Fresno (5.7) and the Northern Rocky Mountains regions (5.0) compared to the Southern Arizona region (1.3). Higher degrees of seasonality tended to occur for western U.S. regions. In general, however, the degree of seasonality in b_{ext_aer} was lower than for individual species.

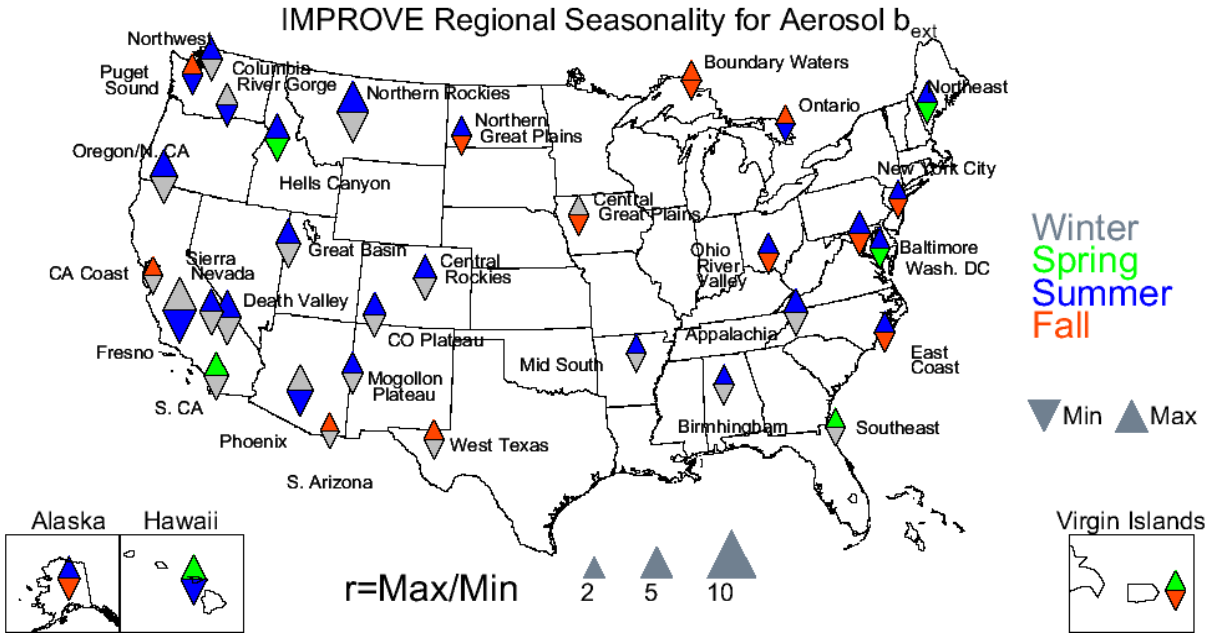

Figure 5.7.1. Seasonal variability for IMPROVE 2005–2008 monthly mean regional $PM_{2.5}$ aerosol light extinction coefficients (b_{ext}). The color of the upward pointing triangle refers to the season with the maximum monthly mean concentration and the downward pointing triangle refers to the season with the minimum monthly mean concentration. The size of the triangles refers to the magnitude of the ratio of maximum to minimum monthly mean mass concentration.

The urban CSN regional mean b_{ext_aer} ranged from 12.43 Mm^{-1} in the Alaska region in August to 204.41 Mm^{-1} in the Sacramento/San Joaquin Valley region in December, most likely from AN. In contrast to rural regions, most urban regional maxima occurred in winter, consistent with winter peaks in AN and POM (Figure 5.7.2). Spring minima were common for many U.S. regions. Summer minima occurred at the Puget Sound, Northwest, Oregon, Phoenix/Tucson, Hawaii, Alaska, Grand Mesa CO, and Florida regions, while summer maxima occurred for many regions along the eastern coast. Eleven regions had maximum to minimum ratios less than 2, suggesting that many regions experienced some degree of seasonality; these regions were predominantly in the western United States. The seasonality in urban b_{ext_aer} was greater for urban compared to rural regions. The highest ratio occurred at the Alaska region (13.7) compared to the lowest in the Florida region (1.4).

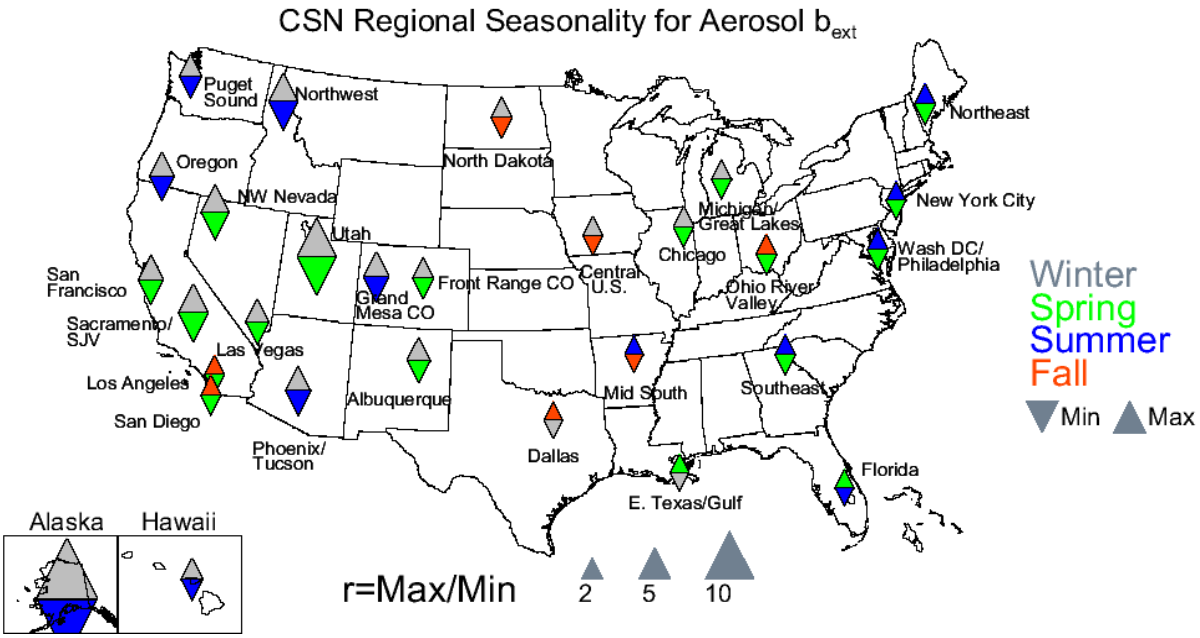

Figure 5.7.2. Seasonal variability for CSN 2005–2008 monthly mean regional $PM_{2.5}$ aerosol light extinction coefficients (b_{ext}). The color of the upward pointing triangle refers to the season with the maximum monthly mean concentration and the downward pointing triangle refers to the season with the minimum monthly mean concentration. The size of the triangles refers to the magnitude of the ratio of maximum to minimum monthly mean mass concentration.

5.8 COARSE MASS LIGHT EXTINCTION COEFFICIENTS

Coarse mass (CM=PM_{10} - $PM_{2.5}$) concentrations are measured routinely by the IMPROVE network only; therefore this discussion covers only IMPROVE 2005–2008 regional monthly mean light extinction coefficients from CM (b_{ext_CM}). The extinction efficiency for CM is 0.6 m^2 g^{-1}, and since CM is considered nonhygroscopic, b_{ext_CM} is scaled to CM concentrations (see section 3.1). Values of regional b_{ext_CM} ranged from 0.31 Mm^{-1} in the Northwest region in December to 11.73 Mm^{-1} in the Virgin Islands in June (rural) and 23.87 Mm^{-1} in Fresno in September (urban). The high b_{ext_CM} in the Virgin Islands was consistent with the high b_{ext_SS} observed for that location during that same month, suggesting that the CM contributions to b_{ext} were mostly likely sea salt, and perhaps soil, related. High extinction due to CM at the Virgin Islands site was roughly ten times greater than other OCONUS sites and corresponded to a more defined seasonal peak (see Figure 5.8.1). Well-defined seasonal peaks were also common for northwestern U.S regions, usually in summer (Figure 5.8.2). The exception was the Oregon/Northern California region, which was associated with a peak in b_{ext_CM} in fall. The Columbia River Gorge region corresponded to the highest b_{ext_CM} in that area and was roughly double or greater than at other areas.

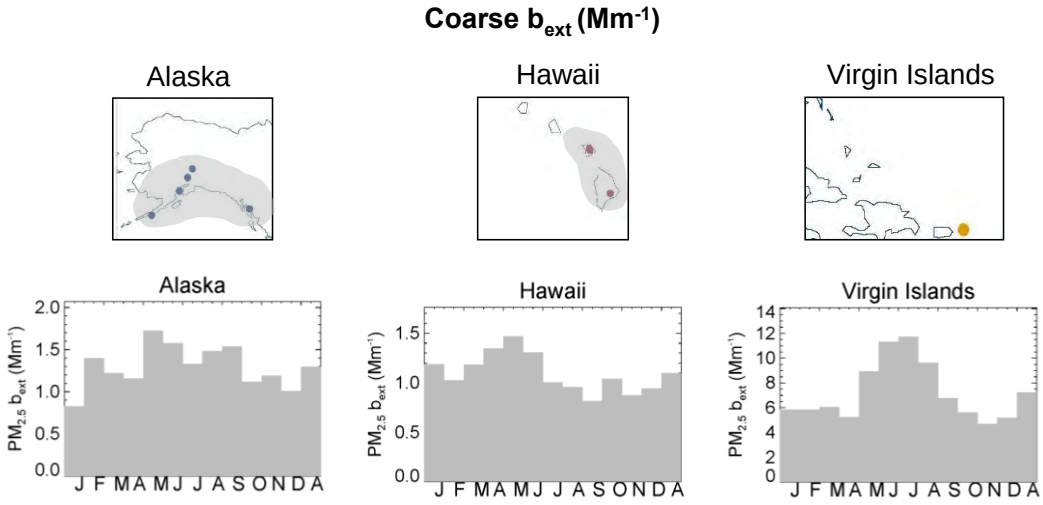

Figure 5.8.1. IMPROVE 2005–2008 regional monthly mean coarse mass reconstructed light extinction coefficients (b_{ext}, Mm^{-1}) for Hawaii, Alaska and the Virgin Islands. The letters on the x-axis correspond to the month and "A" corresponds to "annual" mean. The shaded area corresponds to the regions that comprise the sites used in this analysis, shown as dots. The "modified original" IMPROVE algorithm was used (see text). Wavelength corresponds to 550 nm.

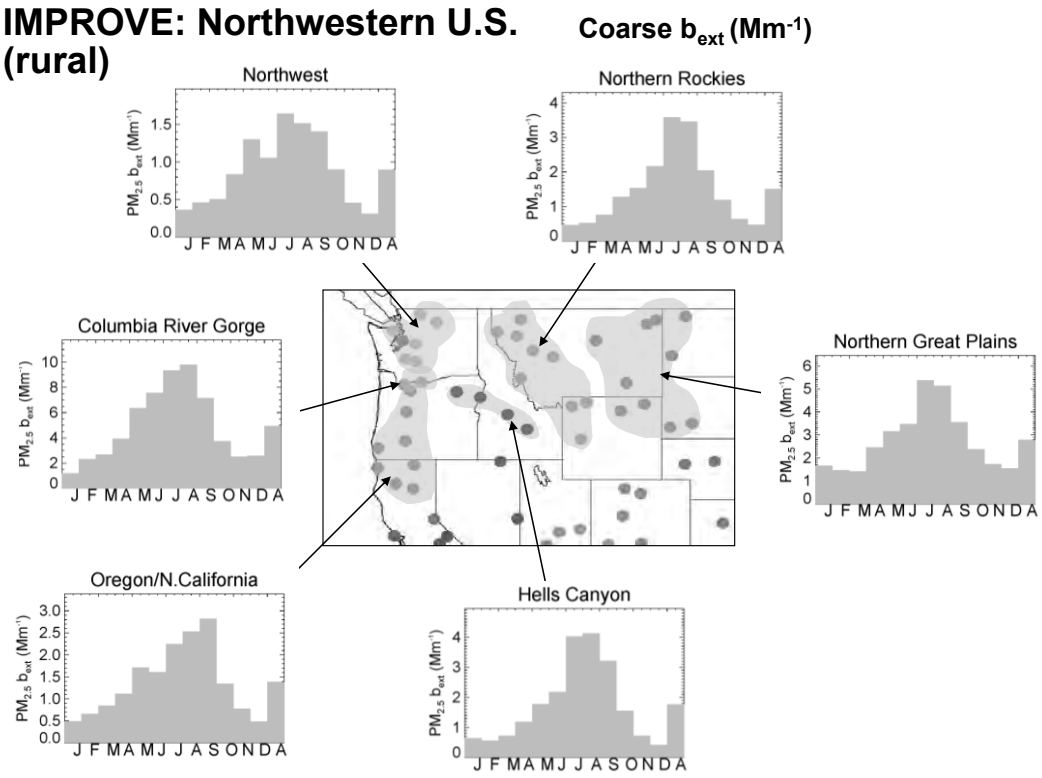

Figure 5.8.2. IMPROVE 2005–2008 regional monthly mean coarse mass reconstructed light extinction coefficients (b_{ext}, Mm^{-1}) for the northwestern United States. The letters on the x-axis correspond to the month and "A" corresponds to "annual" mean. The shaded area corresponds to the regions that comprise the sites used in this analysis, shown as dots. The "modified original" IMPROVE algorithm was used (see text). Wavelength corresponds to 550 nm.

Peaks in b_{ext_CM} during summer also occurred for southwestern U.S. regions that were typically located farther north (e.g., Sierra Nevada and Great Basin; see Figure 5.8.3). Most of the other regions were associated with spring peaks in b_{ext_CM} that were generally well defined. Bimodal distributions in seasonal b_{ext_CM} (spring and fall) occurred at the Southern Arizona, West Texas, and Mogollon Plateau regions. The Sierra Nevada, Southern Arizona, and West Texas regions were associated with the highest values of b_{ext_CM} in the southwestern United States. Seasonal distributions of b_{ext_CM} in the eastern United States were broader than most U.S. regions. Light extinction coefficients from CM peaked in spring for regions such as the Northeast, East Coast, Appalachia and Ohio River Valley regions. Toward the central United States, the peak months shifted toward summer months (see Figure 5.8.4).

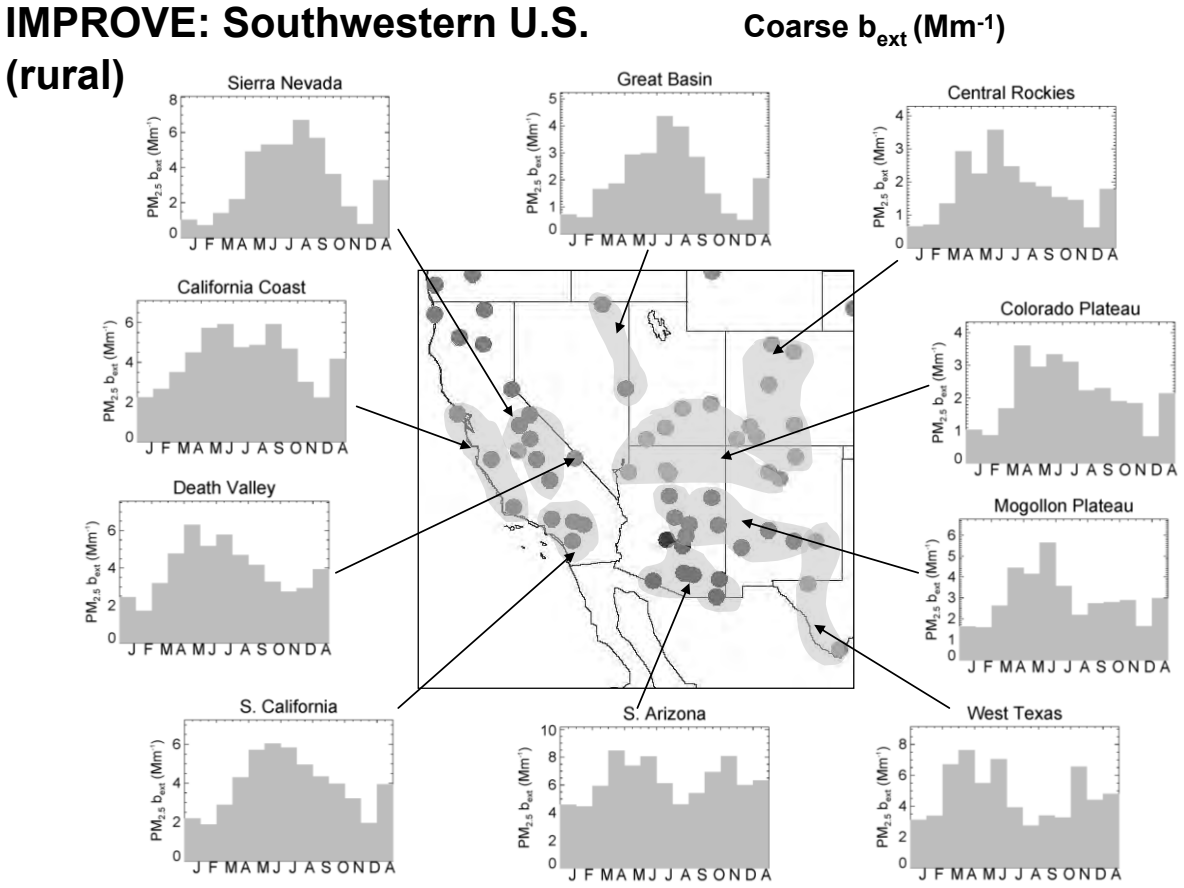

Figure 5.8.3. IMPROVE 2005–2008 regional monthly mean coarse mass reconstructed light extinction coefficients (b_{ext}, Mm^{-1}) for the southwestern United States. The letters on the x-axis correspond to the month and "A" corresponds to "annual" mean. The shaded area corresponds to the regions that comprise the sites used in this analysis, shown as dots. The "modified original" IMPROVE algorithm was used (see text). Wavelength corresponds to 550 nm.

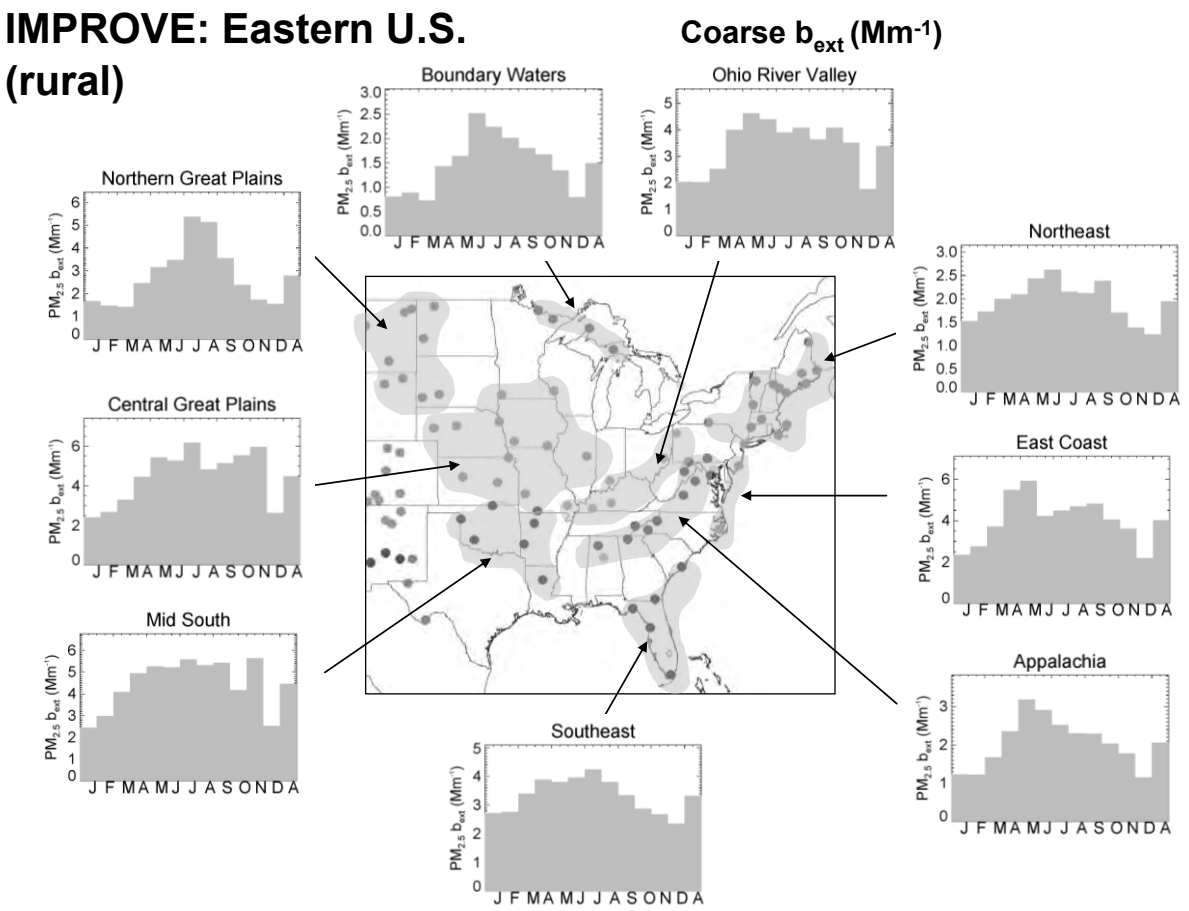

Figure 5.8.4. IMPROVE 2005–2008 regional monthly mean coarse mass reconstructed light extinction coefficients (b_{ext}, Mm^{-1}) for the eastern United States. The letters on the x-axis correspond to the month and "A" corresponds to "annual" mean. The shaded area corresponds to the regions that comprise the sites used in this analysis, shown as dots. The "modified original" IMPROVE algorithm was used (see text). Wavelength corresponds to 550 nm.

The majority of IMPROVE regions had maximum b_{ext_CM} in summer. Many regions corresponding to summer maxima were in the western United States, and spring maxima were common in the northeastern United States and some southwestern regions (e.g., Death Valley, Colorado Plateau, Southern Arizona, West Texas, Hawaii, and Alaska, Figure 5.8.5). Winter minima were common for many regions, although a few regions corresponded to fall minima (e.g., Hawaii, Virgin Islands, Puget Sound, and Washington, D.C., regions). Because CM could be associated with a variety of species (e.g., soil, sea salt, POM, and coarse nitrate species), it is difficult to comment specifically on sources without additional information. Most regions exhibited strong seasonality, with only four regions having ratios less than 2. The highest occurred in the Hells Canyon region (9.9) compared to the lowest at the Washington, D.C. (1.6), and Southeast regions (1.8).

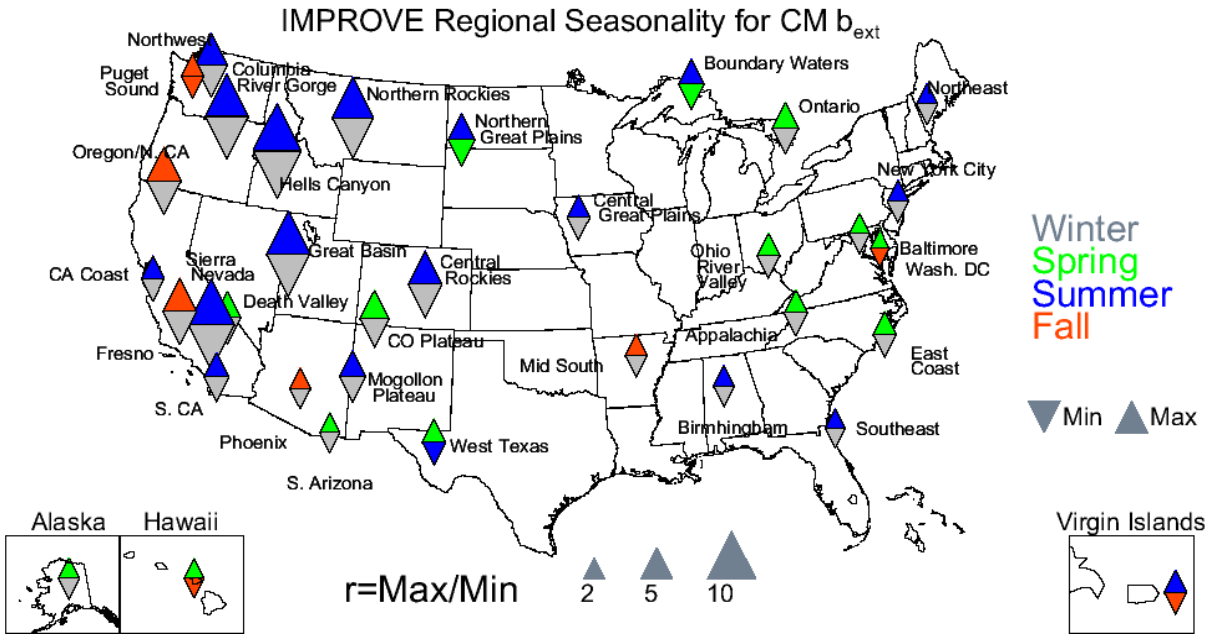

Figure 5.8.5. Seasonal variability for IMPROVE 2005–2008 monthly mean regional coarse mass (CM) light extinction coefficients (b_{ext}). The color of the upward pointing triangle refers to the season with the maximum monthly mean concentration and the downward pointing triangle refers to the season with the minimum monthly mean concentration. The size of the triangles refers to the magnitude of the ratio of maximum to minimum monthly mean mass concentration.

5.9 $PM_{2.5}$ DECIVIEW

Recall from section 3.1 that the estimates of deciview (dv) take into account the site-specific Rayleigh scattering coefficient and CM scattering coefficients and therefore were computed for IMPROVE data only. Because of these additions, the regions corresponding to maximum and minimum dv may differ from b_{ext_aer} described in the previous section. The seasons corresponding to maximum and minimum did in fact shift from b_{ext_aer} to dv (e.g., the Alaska, Virgin Islands, Columbia River Gorge, California Coast, Fresno, Southern Arizona, West Texas, Central Great Plains, Boundary Waters, Ontario, Southeast, Baltimore, New York City, and Northeast regions; see Figure 5.9.1). The regional IMPROVE dv ranged from 3.16 in the Central Rocky Mountains region in December to 24.45 in the rural Ohio River Valley region in August and 30.26 in the urban region of Fresno in December. The maximum values in the Ohio River Valley and Fresno regions were probably due to AS and AN, respectively. Maximum dv occurred in summer for most of the IMPROVE regions, but winter maxima also occurred (e.g., the Fresno, Phoenix, Boundary Waters, New York City, and Ontario regions), as did spring maxima (the Hawaii, Southern California, Central Great Plains, and Southeast regions). Fall maxima occurred only at the Puget Sound region. Winter and fall minima were common for most regions. The seasonality in dv was generally low.

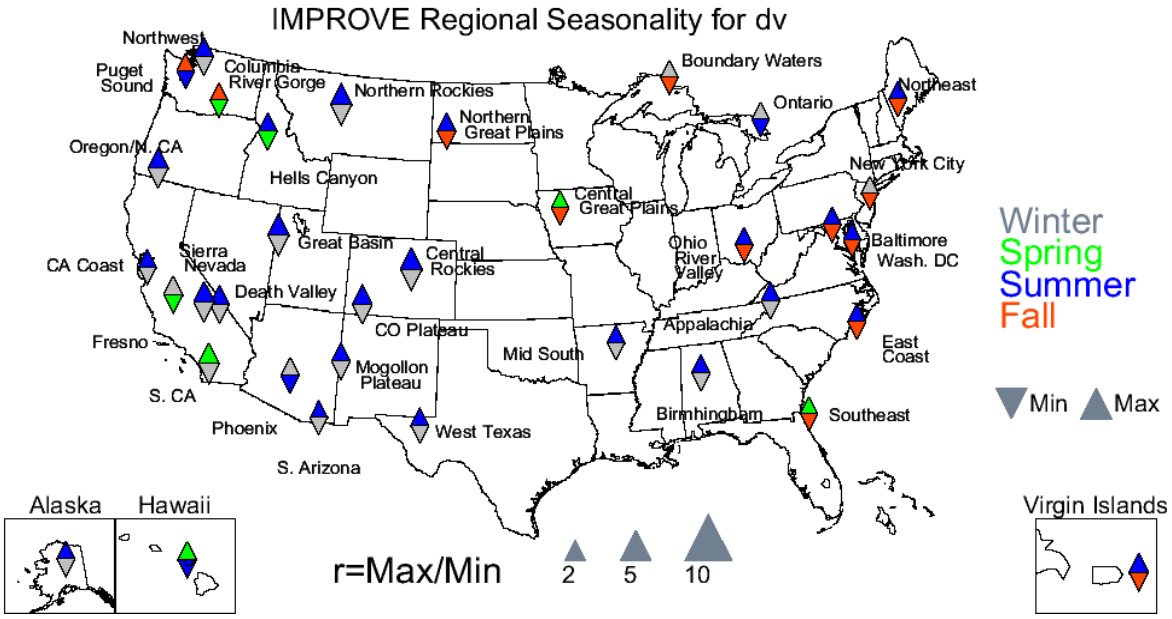

Figure 5.9.1. Seasonal variability for IMPROVE 2005–2008 monthly mean regional deciview (dv) light extinction coefficients (b_{ext}). The color of the upward pointing triangle refers to the season with the maximum monthly mean concentration and the downward pointing triangle refers to the season with the minimum monthly mean concentration. The size of the triangles refers to the magnitude of the ratio of maximum to minimum monthly mean mass concentration.

5.10 SUMMARY

The seasonal patterns in light extinction coefficients corresponding to major aerosol species were similar to the seasonal distributions in mass concentrations presented in the Chapter 4. This similarity was expected for most species because mass concentrations were converted to b_{ext}, with mass extinction efficiencies that essentially just scaled the values to inverse megameter units. However, for AS, AN, and sea salt, the conversion to b_{ext} accounted for relative humidity effects and hygroscopic growth that can be considerable in environments with high relative humidity. No significant differences were observed between the seasonal distributions in mass compared to b_{ext}. Occasionally, the season that corresponded to the majority of the maximum and minimum regional absolute b_{ext} or relative b_{ext} changed for many of the species examined here. In addition, some species that were important for their contributions to RCFM were less important in reconstructed b_{ext} (e.g., soil), while others became more important (e.g., LAC, POM, and hygroscopic species).

Appendices associated with this chapter include tables of regional monthly mean b_{ext} for IMPROVE and the CSN (E.1), and tables of relative b_{ext} for IMPROVE and the CSN (E.2). Figures include monthly mean b_{ext} bar charts for individual IMPROVE sites and CSN sites (E.3), as well as individual site bar charts of relative b_{ext} for IMPROVE and CSN sites (E.4).

REFERENCES

White, W. H., B. P. Perley, R. L. Poirot, T. F. Dann, and E. Dabek-Zlotorzynska, 2010, Continental-scale transport of sea salt aerosol, Abstract A43C-0245 presented at the 2010 Fall Meeting, AGU, San Francisco, California, 13-17 December 2010.

Chapter 6. Trends in IMPROVE Speciated Aerosol Concentrations

Trend analyses of aerosol concentrations are performed for a variety of purposes. Evaluating temporal changes in aerosol concentrations assists in determining whether emission mitigation strategies are effective in improving air quality. For example, the Regional Haze Rule, promulgated by the U.S. Environmental Protection Agency, addresses visibility impairment in Class I areas. The rule requires states and tribes to establish strategies to improve visibility in 156 national parks and wilderness areas by reducing emissions of visibility-impairing particulate matter (U.S. EPA, 1999). In addition, health effects standards, such as the National Ambient Air Quality Standards (NAAQS), require that states and tribes meet standards for criteria pollutants, including $PM_{2.5}$ and PM_{10} particulate matter (www.epa.gov/air/particlepollution/standards.html). Trend analyses provide information as to whether mitigation strategies are successful in meeting these types of goals.

On a global scale, trend analyses of global aerosol optical depth, a column-integrated light extinction coefficient, provide important information on "global dimming", a term used to describe the decrease of incoming solar radiation to the Earth's surface, due in part to changes in aerosol concentrations (Wild et al., 2005; Mishchenko and Geogdzhayev, 2007; Mishchenko et al., 2007). While trends in remote sensing products, such as aerosol optical depth or Ångstrom exponent, provide information related to the changes in the transmittance of the atmosphere, they do not inform as to the specific species responsible. Modeling studies have been used to investigate this particular issue by investigating effects of changing emissions, meteorology, and atmospheric processes that affect aerosol concentrations in the atmosphere (e.g., Streets et al., 2009). To this end, long-term trend analyses of speciated aerosol concentrations provide constraints for global models (e.g., Bahadur et al., 2009; Streets et al., 2009).

While long-term trend analyses of speciated aerosol concentrations are important, few have been performed because long-term speciated datasets are not widely available. However, trend analyses have been performed for precipitation chemistry data from the National Atmospheric Deposition Program (NADP) and have provided important results regarding changes in aerosol chemistry in wet deposition around the United States (e.g., Holland et al., 1995; Lynch et al., 1995; Walker et al., 2000; Nilles and Conley, 2001; Lehmann et al., 2007; Lloyd, 2010). Analyses of aerosol data from high latitude locations in the North American continent, such as Arctic sites in Canada and Alaska, have provided long-term trends in aerosol species such as sulfate and black carbon in an effort to understand Arctic haze (e.g., Polissar et al., 1999; Sirois and Barrie, 1999; Quinn et al., 2007; Gong et al., 2010; Hirdman et al., 2010). The IMPROVE network is an important source of data for trend analyses in the United States because of its duration (observations initiated in 1988), spatial distribution of sites, and consistent sampling methodology for all sites in the network. Previous trends studies were reviewed by Malm et al. (2002), who also demonstrated through trend analyses that IMPROVE sulfate concentrations were decreasing at most sites over a period of 10 years (1988–1999). More recently, Murphy et al. (2011) investigated trends in light absorbing carbon (LAC) and found that LAC concentrations were decreasing at most IMPROVE sites in the United States. In addition, a comprehensive trend analysis on IMPROVE reconstructed aerosol visibility (deciview) at national parks was reported in the most recent *Air Quality in National Parks 2009 Annual Performance and Progress Report* for the 1999–2008 time period (NPS, 2010).

The analyses of IMPROVE data presented in the previous chapters focused on spatial and seasonal patterns in aerosol species from 2005 through 2008 but did not investigate trends in aerosol concentrations over longer periods. In this chapter we present trend analyses over "short-term" (20 years, 2000–2008) and "long-term" (9 years, 1989–2008) time periods. We did not perform trend analyses with CSN data because trends are sensitive to changes in CSN sampling methodology (e.g., sampler and analytical methodology vary from site to site and over time) and because of CSN's shorter history (network established in 2000 with additional sites coming online over a period of several years).

Trends were computed for a total of eight parameters: annual mean, 10^{th}, 50^{th}, and 90^{th} percentiles, and four seasons (winter included December, January, February; spring included March, April, May; summer included June, July, August; fall included September, October, November). Fifty percent of yearly data was required for a given site to be included in the trend analysis. In addition, long-term and short-term trends were computed with the requirement that data for 70% of the years were complete for a trend analysis to be performed at a given site (i.e., 6 out of 9 years for short-term trends and 14 out of 20 years for long-term trends). A Theil regression was performed with the concentration data as the dependent variable and the year as the independent variable. An advantage to the Theil regression is that heavy influence by outliers on the regression results is avoided (Theil, 1950). Slopes for every possible combination of data at a given site were computed and the median slope ($\mu g\ m^{-3}\ yr^{-1}$) was computed from all possible slopes. Kendall tau statistics were used to determine the significance by using the difference in each combination of data points at a given site. A positive difference was assigned a + 1, a negative difference was assigned a - 1, and the sum of values was computed. The sum was used to determine the probability that the differences occurred by chance. We assumed that a trend was statistically significant at 5% ($p \leq 0.05$), meaning that there was a 95% chance that the slope was not due to random chance. We also present trends that were significant at 15% ($0.05 < p \leq 0.15$). We refer to "trend" as percent change per year (% yr^{-1}) and computed it by dividing the slope derived from the Theil regression by the median concentration value over the time period of the trend, multiplied by 100%. Reporting trend instead of slope reflects the relative change in concentration at a given site. However, trends can be quite large (>100%) when median concentrations are very low (e.g., 10^{th} percentile).

We present long-term trends for sulfate ion, total carbon (TC = organic carbon + light absorbing carbon), fine soil, fine mass (FM), coarse mass (CM), and PM_{10} concentrations. In addition to the species listed above, short-term trends were computed for nitrate ion concentrations. No trends were computed for sea salt because of issues with chloride measurements (White, 2008). In an effort to condense this discussion, not all of the trend results will be presented here but are available in Appendix F. Instead, we identify interesting trends for given species and parameters, as well as individual sites. Percent change per year for each site and species is presented on a map of the United States. Sites with positive trends with significance levels of 95% and greater ($p \leq 0.05$) correspond to solid red, upward-pointing triangles. Positive trends with significance levels of 85–95% ($0.05 < p \leq 0.15$) correspond to red, unfilled, upward-pointing triangles. A similar methodology was applied to sites with decreasing trends but in blue. The size of the triangle corresponds to the magnitude of the trend, with the same scale maintained for all species and parameters for comparison purposes. Sites with no significant trends ($p > 0.15$) but with complete data are represented as black triangles with size

scaled by the magnitude and orientation by the direction of the trend. We present both long- and short-term trends within the discussion of a given species.

Summaries of network-wide long-term and short-term trend information for all of the major components are provided in Tables 6.1 and 6.2, respectively. The first five columns of these tables provide a useful overview of particulate mass trends at IMPROVE sites that are described in greater detail in the sections that follow. For example, notice that the large majority of sites with statistically significant long-term trends (Table 6.1) have negative (i.e., improving) trends for all components, except for fine soil which has positive trends at half or more of the sites with significant trends. The situation is similar for the short-term trends (Table 6.2) at an expanded number of sites, except that coarse mass joins fine soil as having half or more positive trends, with all other components having generally decreasing trends at the large majority of sites. This seems to suggest that emissions controls applied in the United States over the last two decades have been successful in reducing particulate mass concentrations.

6.1 SULFATE ION TRENDS

Decreasing trends in sulfate ion concentrations were typical for most IMPROVE sites, regardless of the percentile, season, or time period. The 10^{th} percentile and winter periods were associated with some of the negative trends. A map of the 10^{th} percentile, long-term sulfate ion trends is shown in Figure 6.1.1. Decreasing trends occurred at sites in the southwestern United States (e.g., Gila Wilderness, New Mexico, GICL1, -5.6% yr^{-1}; Guadalupe Mountains, Texas, GUMO1, -3.6% yr^{-1}; Petrified Forest, Arizona, PEFO1,-3.7% yr^{-1}) and in the eastern United States (e.g., Acadia, Maine, ACAD1,
-4.0% yr^{-1}; Lye Brook, Vermont, LYBR1, -3.9% yr^{-1}; Dolly Sods, West Virginia, DOSO1, -4.2% yr^{-1}; Shenandoah, Virginia, SHEN1, -3.3% yr^{-1}; Washington, D.C., WASH1, -4.2% yr^{-1}). As shown in Figure 6.1.2, large decreasing trends occurred during winter months at sites in the southwestern United States, such as Canyonlands, Utah (CANY1, -5.7% yr^{-1}), Bryce Canyon, Utah (BRCA1, -4.6% yr^{-1}), Indian Gardens, Arizona (INGA1, -5.2% yr^{-1}), Petrified Forest, Arizona (PEFO1, -4.7% yr^{-1}), Tonto, Arizona (TONT1, -4.7% yr^{-1}), and the northwestern United States (e.g., Snoqualmie Pass, Washington, SNPA1, -5.0% yr^{-1}; Mount Rainier, Washington, MORA1, -5.0% yr^{-1}) and a few sites in the Northeast United States (Acadia, Maine, ACAD1, -4.4% yr^{-1}; Lye Brook, Vermont, LYBR1, -4.2% yr^{-1}). Recall from Chapter 4.1.1 that the lowest concentrations in regional mean ammonium sulfate (derived from sulfate ion concentrations) from 2005 through 2008 occurred during winter in the southwestern United States (Figure 4.1.5). The long-term trends suggested that the lowest sulfate ion concentration days in winter have been decreasing for several years at many sites. An example of decreasing long-term sulfate ion concentrations during winter is shown for Denali, Alaska (DENA1, -4.7% yr^{-1}), in Figure 6.1.3.

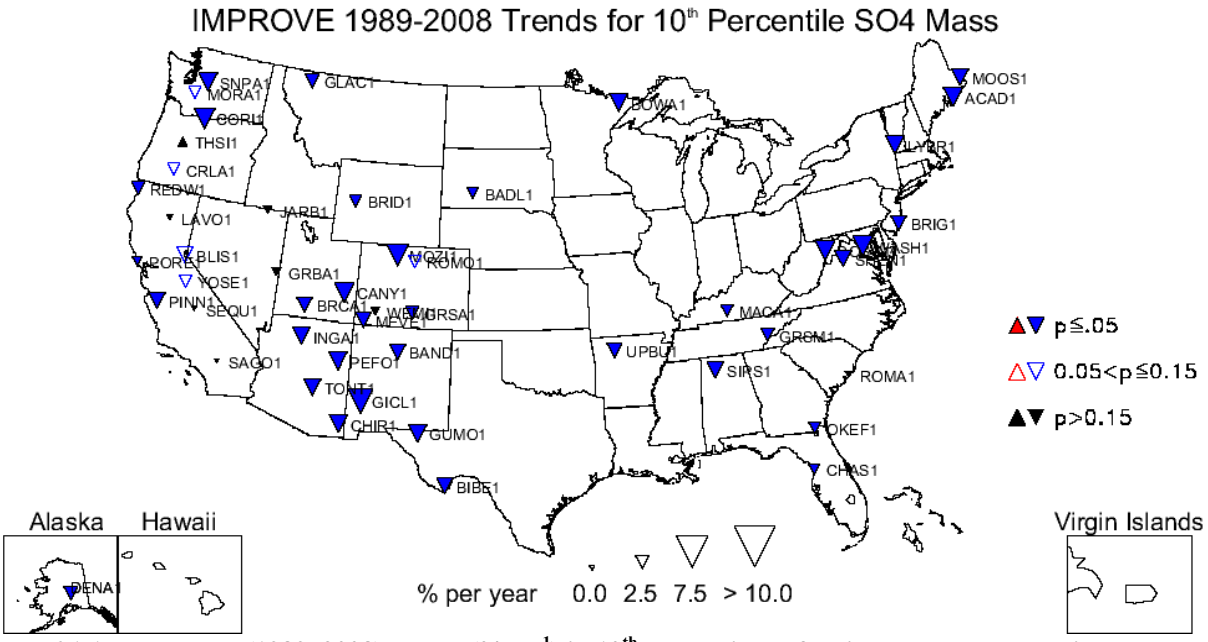

Figure 6.1.1. Long-term (1989–2008) trends (% yr^{-1}) in 10th percentile sulfate ion mass concentrations.

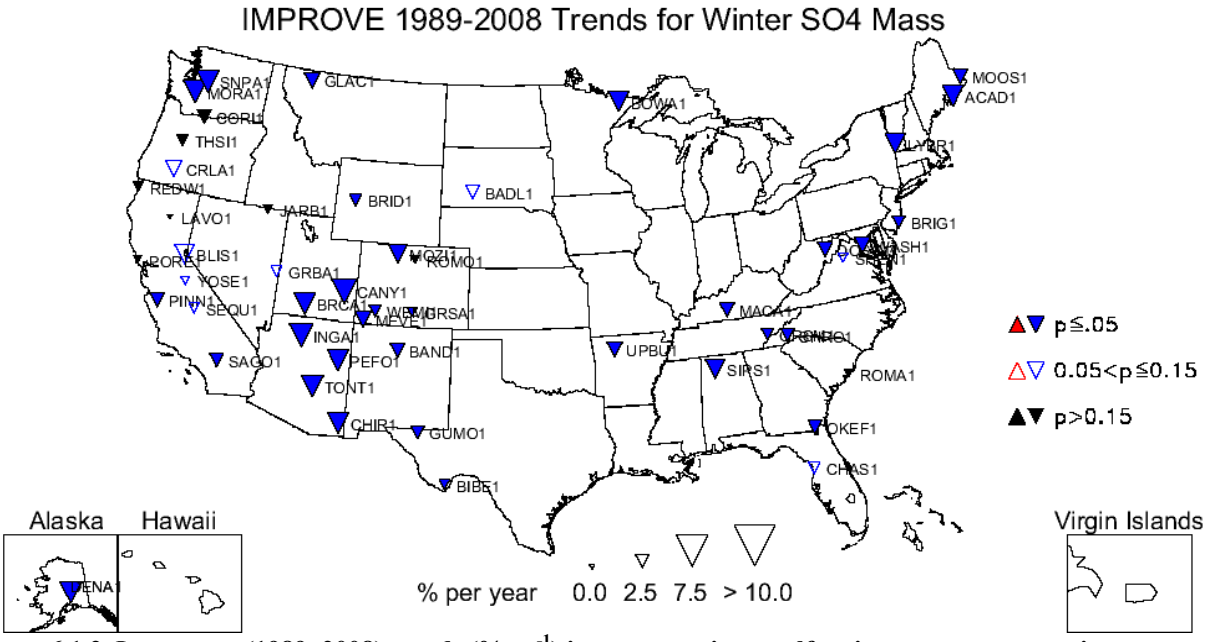

Figure 6.1.2. Long-term (1989–2008) trends (% yr^{-1}) in average winter sulfate ion mass concentrations.

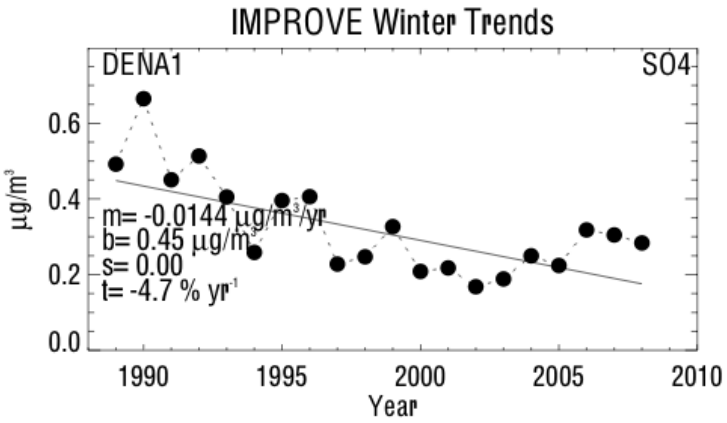

Figure 6.1.3. Average winter sulfate ion mass concentrations (µg m^{-3}) for Denali, Alaska (DENA1). Regression results, including Theil slope (m, µg m^{-3} yr^{-1}), intercept (b, µg m^{-3}), significance (s), and trend (t, % yr^{-1}) are included. The trend line is plotted as a solid line. The intercept corresponds to the initial year of data.

In contrast to the 10th percentile map, the 90th percentile map presented much lower trends in sulfate ion concentrations, especially in the southwestern United States (Figure 6.1.4). Positive long-term trends occurred at Big Bend, Texas (BIBE1), for the 90th percentile and spring season (1.5% yr^{-1} and 1.3% yr^{-1}, respectively) and at Lassen Volcanic NP, California (LAVO1), during summer (1.4% yr^{-1}). The increase in the 90th percentile sulfate ion concentrations at BIBE1 is shown in Figure 6.1.5; concentrations increased slowly but steadily since 1989. The sites listed above were the only IMPROVE locations that corresponded to positive trends for any long-term-trend parameter investigated. The largest negative long-term, 90th percentile trend occurred at Snoqualmie Pass, Washington (SNPA1), during summer (-6.3% yr^{-1}). Of the parameters investigated, approximately fifty sites typically met the completeness criteria for trend analyses and of these, 25–45 sites corresponded to significant trends ($p \leq 0.15$), depending on the parameter (see Table 6.1).

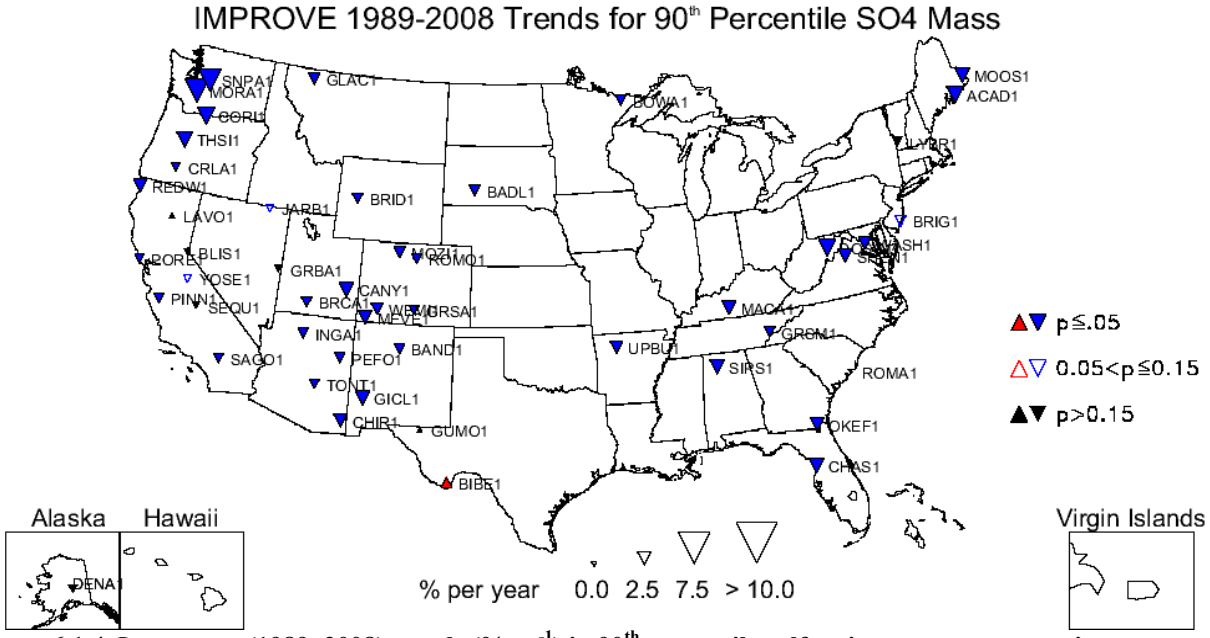

Figure 6.1.4. Long-term (1989–2008) trends (% yr^{-1}) in 90th percentile sulfate ion mass concentrations.

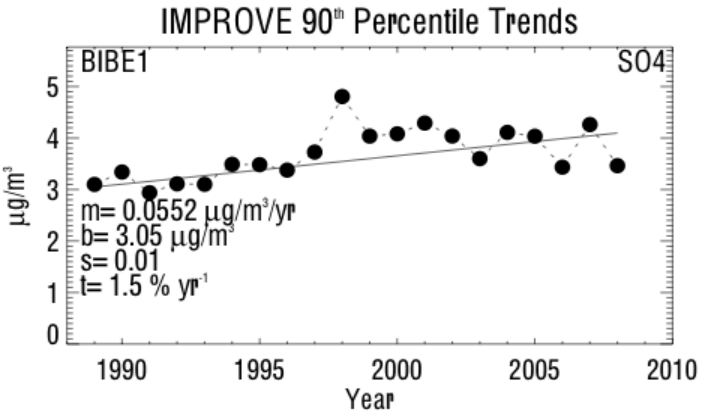

Figure 6.1.5. 90th percentile sulfate ion mass concentrations (µg m^{-3}) for Big Bend, Texas (BIBE1). Regression results, including Theil slope (m, µg m^{-3} yr^{-1}), intercept (b, µg m^{-3}), significance (s), and trend (t, % yr^{-1}) are included. The trend line is plotted as a solid line. The intercept corresponds to the initial year of data.

Table 6.1. Results from long-term (1989–2008) trend analyses for sulfate ion, total carbon (organic carbon + light absorbing carbon), fine soil, gravimetric fine mass, coarse mass, and PM_{10}. The minimum and maximum slope (μg m^{-3} yr^{-1}) and trend (% yr^{-1}) are provided, along with the site corresponding to the maximum and minimum.

Parameter	N_{tot}	N_{sig}	N_{neg}	N_{pos}	Slope (min.) (μg m^{-3} yr^{-1})	Site (min)	Slope (max.) (μg m^{-3} yr^{-1})	Site (max)	Trend (min.) (% yr^{-1})	Site (min)	Trend (max.) (% yr^{-1})	Site (max)
Sulfate Ion												
10th	49	41	41	0	-0.078	WASH1	-0.001	CRLA1	-5.6	GICL1	-1.4	PORE1
50th	49	43	43	0	-0.124	WASH1	-0.003	JARB1	-5.4	ACAD1	-1.1	JARB1
90th	49	41	40	1	-0.297	DOSO1	0.055	BIBE1	-5.2	MORA1	1.5	BIBE1
Mean	50	45	45	0	-0.140	DOSO1	-0.003	DENA1	-4.6	SNPA1	-0.9	DENA1
Winter	49	41	41	0	-0.114	WASH1	-0.002	YOSE1	-5.7	CANY1	-1.1	YOSE1
Spring	50	25	24	1	-0.119	WASH1	0.027	BIBE1	-4.5	ACAD1	1.3	BIBE1
Summer	51	39	37	2	-0.291	DOSO1	0.019	BIBE1	-6.3	SNPA1	1.4	LAVO1
Fall	50	36	36	0	-0.121	DOSO1	-0.003	DENA1	-4.6	ACAD1	-0.9	TONT1
Total Carbon												
10th	48	46	46	0	-0.046	WASH1	-0.003	BAND1	-14.6	THSI1	-0.7	BAND1
50th	48	45	45	0	-0.090	WASH1	-0.005	GRSA1	-5.0	MORA1	-0.8	GRSA1
90th	48	25	23	2	-0.172	WASH1	0.027	BRID1	-4.5	MORA1	1.6	BRID1
Mean	49	29	29	0	-0.103	WASH1	-0.009	CANY1, GUMO1	-4.7	MORA1	-1.0	PEFO1
Winter	49	44	44	0	-0.130	WASH1	-0.004	BRID1	-6.8	MORA1	-1.3	GRSM1
Spring	50	35	35	0	-0.094	WASH1	-0.009	CANY1	-4.6	MORA1	-1.3	TONT1
Summer	50	27	21	6	-0.064	GRGU1	0.045	BRID1	-3.9	REDW1	3.8	BRID1
Fall	50	30	29	1	-0.158	WASH1	0.030	CRLA1	-4.3	MORA1	3.2	CRLA1
Fine Soil												
10th	57	18	16	2	-0.003	MOZI1	0.006	TONT1	-5.0	DENA1	3.2	TONT1
50th	57	16	9	7	-0.035	VIIS1	0.025	DEVA1	-5.3	VIIS1	3.3	DEVA1
90th	57	18	4	14	-0.357	VIIS1	0.128	DEVA1	-4.3	VIIS1	6.9	CORI1
Mean	59	14	6	8	-0.081	VIIS1	0.060	DEVA1	-3.2	VIIS1	5.3	DEVA1
Winter	56	14	7	7	-0.006	BOWA1	0.025	CHIR1	-5.9	SNPA1	5.7	CHIR1
Spring	57	15	2	13	-0.013	SNPA1	0.085	DEVA1	-4.2	SNPA1	5.6	DEVA1
Summer	60	17	8	9	-0.181	VIIS1	0.103	CORI1	-4.3	CHAS1	12.4	CORI1
Fall	58	11	5	6	-0.112	VIIS1	0.041	DEVA1	-8.1	SAGO1	4.8	DEVA1
Gravimetric Fine Mass												
10th	57	49	49	0	-0.195	SIPS1	-0.013	CRLA1	-6.1	CRMO1	-0.9	CHAS1
50th	57	55	55	0	-0.376	WASH1	-0.027	MEVE1	-4.1	SNPA1	-0.6	BIBE1
90th	57	33	32	1	-0.698	DOSO1	0.202	SAWT1	-3.9	MORA1	3.3	SAWT1
Mean	59	47	45	2	-0.384	WASH1	0.071	SAWT1	-4.2	MORA1	2.4	SAWT1

Parameter	N_{tot}	N_{sig}	N_{neg}	N_{pos}	Slope (min.) ($\mu g\ m^{-3}\ yr^{-1}$)	Site (min)	Slope (max.) ($\mu g\ m^{-3}\ yr^{-1}$)	Site (max)	Trend (min.) (% yr^{-1})	Site (min)	Trend (max.) (% yr^{-1})	Site (max)
Winter	56	52	52	0	-0.395	WASH1	-0.027	BRID1	-6.5	MORA1	-1.0	EVER1
Spring	57	33	32	1	-0.334	SAGO1	0.125	DEVA1	-5.1	SNPA1	2.5	DEVA1
Summer	60	33	29	4	-0.584	DOSO1	0.242	SAWT1	-4.1	GRGU1	5.0	SULA1
Fall	58	36	35	1	-0.407	WASH1	0.111	SAWT1	-4.9	ACAD1	3.4	SAWT1
Coarse Mass												
10^{th}	50	42	42	0	-0.234	BRIG1	-0.023	ACAD1	-44.0	SNPA1	-2.2	BADL1
50^{th}	50	41	41	0	-0.377	BRIG1	-0.047	MEVE1	-12.7	SNPA1	-1.4	BADL1
90^{th}	50	34	34	0	-0.624	BRIG1	-0.121	BRCA1	-8.2	SNPA1	-1.6	YOSE1
Mean	50	40	40	0	-0.420	BRIG1	-0.055	MEVE1	-11.7	SNPA1	-1.4	GLAC1
Winter	48	42	42	0	-0.363	SEQU1	-0.062	JARB1	-18.7	SNPA1	-1.8	UPBU1
Spring	49	29	28	1	-0.242	REDW1	0.129	UPBU1	-7.7	MOOS1	1.7	UPBU1
Summer	51	31	29	2	-0.436	ROMA1	0.862	CORI1	-7.2	SNPA1	8.5	CORI1
Fall	51	37	37	0	-0.394	SAGO1	-0.049	BLIS1	-8.7	SNPA1	-1.1	PORE1
PM_{10}												
10th	50	50	50	0	-0.416	BRIG1	-0.046	THSI1	-9.9	MOZI1	-1.2	MACA1
50th	50	46	46	0	-0.569	BRIG1	-0.087	CHIR1	-8.0	SNPA1	-0.8	UPBU1
90th	50	26	26	0	-1.016	BRIG1	-0.126	BRID1	-4.6	SNPA1	-1.0	PORE1
Mean	50	44	44	0	-0.656	BRIG1	-0.058	MEVE1	-5.6	SNPA1	-0.9	UPBU1
Winter	49	46	46	0	-0.594	ROMA1	-0.118	ROMO1	-9.0	SNPA1	-1.7	TONT1
Spring	49	33	33	0	-0.511	SAGO1	-0.093	WEMI1	-4.9	MORA1	-1.2	GRSM1
Summer	51	29	28	1	-0.899	DOSO1	0.763	CORI1	-5.0	GRGU1	4.6	CORI1
Fall	51	39	39	0	-0.688	BRIG1	-0.075	CHIR1	-5.2	ACAD1	-0.9	CHIR1

N_{tot} refers to the total number of sites in the analysis
N_{sig} refers to the number of sites with significant trends ($p \leq 0.15$)
N_{pos} refers to the number of significant positive trends
N_{neg} refers to the number of significant negative trends

Examining shorter time periods (2000–2008) resulted in additional sites that met completeness criteria (usually > 150 sites, depending on the parameter, see Table 6.2); however, typically, 40–50% of the sites were significant. Negative 10th percentile trends at sites in the southwestern United States were relatively large (see Figure 6.1.6), as well as sites in the northwestern and eastern United States. Many of these same sites corresponded to significantly large negative trends during winter also, but fewer sites were significant for winter trends (Figure 6.1.7), compared to trends for 10th percentile. The largest negative short-term trend occurred at Martha's Vineyard, Massachusetts, in spring (MAVI1, -13.6% yr^{-1}), although El Dorado Springs, Missouri (ELDO1,
-13.2% yr^{-1}, 90th percentile), and Snoqualmie Pass, Washington (SNPA1, -13.1% yr^{-1} in summer), were similar. The spring sulfate ion concentrations at MAVI1 are shown in Figure 6.1.8. Concentrations have decreased from 2.8 µg m^{-3} to 1.9 µg m^{-3} in 9 years.

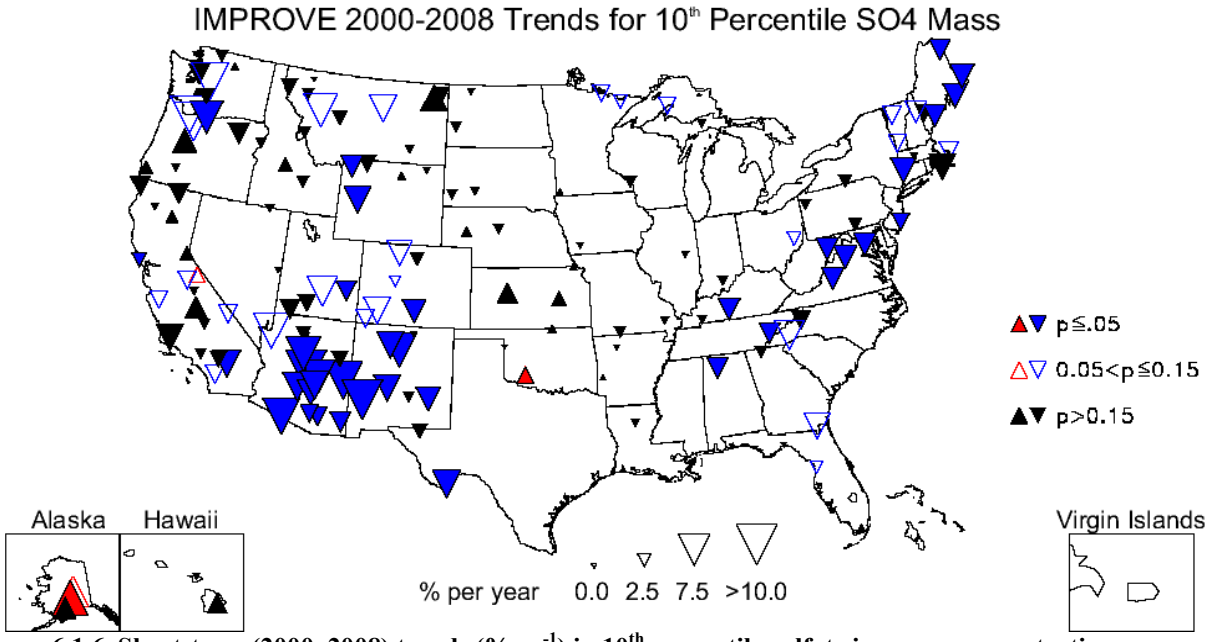

Figure 6.1.6. Short-term (2000–2008) trends (% yr^{-1}) in 10th percentile sulfate ion mass concentrations.

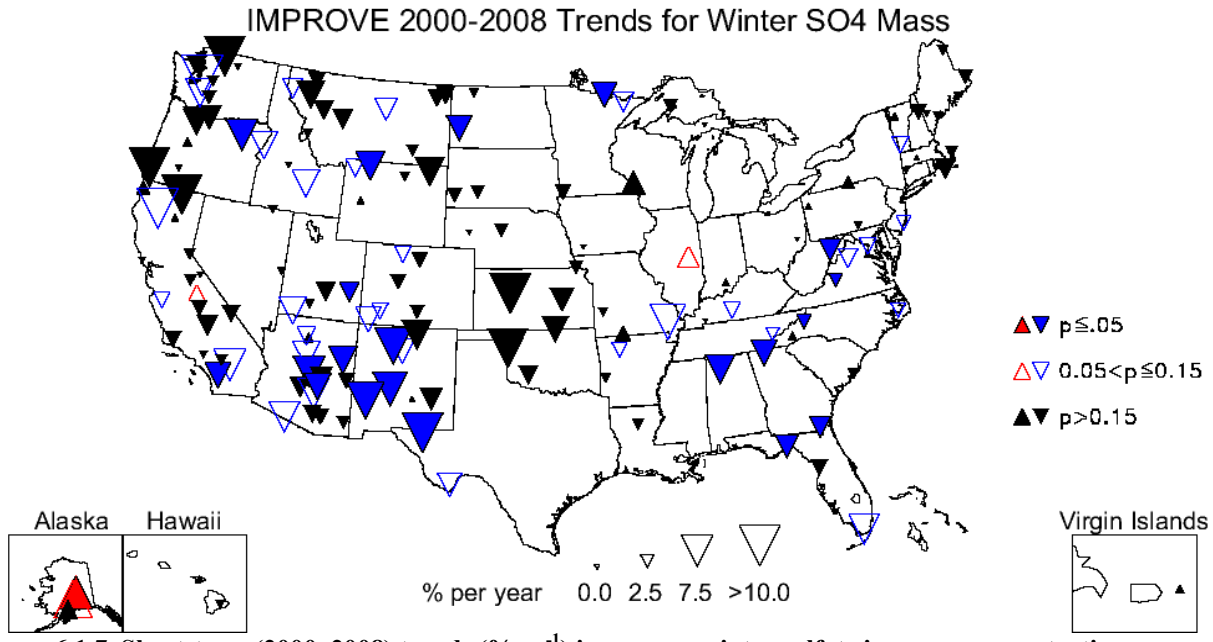

Figure 6.1.7. Short-term (2000–2008) trends (% yr^{-1}) in average winter sulfate ion mass concentrations.

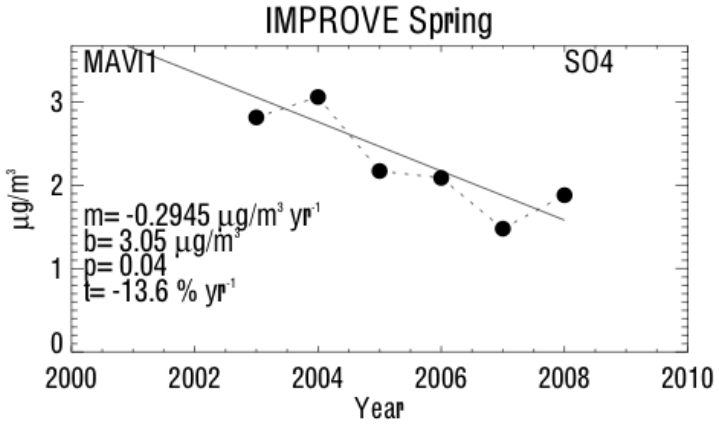

Figure 6.1.8. Average spring sulfate ion mass concentrations (µg m^{-3}) for Martha's Vineyard, Massachusetts (MAVI1). Regression results, including Theil slope (m, µg m^{-3} yr^{-1}), intercept (b, µg m^{-3}), significance (p), and trend (t, % yr^{-1}) are included. The trend line is plotted as a solid line. The intercept corresponds to the initial year of data.

Table 6.2. Results from short-term (2000–2008) trend analyses for sulfate ion, nitrate ion, total carbon (organic carbon + light absorbing carbon), fine soil, gravimetric fine mass, coarse mass, and PM_{10}. The minimum and maximum slope (μg m^{-3} yr^{-1}) and trend (% yr^{-1}) are provided, along with the site corresponding to the maximum and minimum.

Parameter	N_{tot}	N_{sig}	N_{neg}	N_{pos}	Slope (min.) (μg m^{-3} yr^{-1})	Site (min)	Slope (max.) (μg m^{-3} yr^{-1})	Site (max)	Trend (min.) (% yr^{-1})	Site (min)	Trend (max.) (% yr^{-1})	Site (max)
Sulfate Ion												
10th	153	67	63	4	-0.078	WASH1	0.018	WIMO1	-11.7	GICL1	8.7	TRCR1
50th	153	75	67	8	-0.165	SHEN1	0.020	HOOV1	-8.8	COGO1	6.8	TRCR1
90th	153	61	58	3	-0.706	JARI1	0.817	HAVO1	-13.2	ELDO1	11.8	HAVO1
Mean	155	91	87	4	-0.260	JARI1	0.229	HAVO1	-9.3	MAVI1	10.7	HAVO1
Winter	153	55	51	4	-0.197	MING1	0.106	BOND1	-11.9	TRIN1	9.4	TRCR1
Spring	155	43	30	13	-0.295	MAVI1	0.481	HAVO1	-13.6	MAVI1	16.8	HAVO1
Summer	155	54	52	2	-0.464	MKGO1	0.134	HAVO1	-13.1	SNPA1	14.1	HAVO1
Fall	154	46	41	5	-0.204	WASH1	0.206	HAVO1	-11.2	ACAD1	10.2	HAVO1
Nitrate Ion												
10th	153	116	116	0	-0.022	WASH1	-0.001	DENA1	-18.8	SAGO1	-2.3	BOND1
50th	153	97	97	0	-0.146	SAGO1	-0.002	HAVO1	-15.0	TALL1	-1.4	SIKE1
90th	153	62	62	0	-0.314	SAFO1	-0.005	THSI1	-16.8	HECA1	-1.0	SAGU1
Mean	155	90	90	0	-0.140	SAGO1	-0.002	CABI1	-10.0	SAGA1	-1.3	CABI1
Winter	153	40	38	2	-0.251	ELDO1	0.012	JARB1	-25.5	TRIN1	11.9	JARB1
Spring	155	31	27	4	-0.149	SAGA1	0.039	MELA1	-12.9	CRES1	8.9	VIIS1
Summer	155	77	77	0	-0.126	SAGO1	-0.002	CABI1	-19.9	VILA1	-2.1	CHIR1
Fall	154	81	81	0	-0.177	SAGO1	-0.002	DENA1	-21.0	ZICA1	-2.9	KALM1
Total Carbon												
10th	153	95	95	0	-0.073	CHER1	-0.004	BALD1	-125.3	TUXE1	-1.3	QUVA1
50th	153	92	92	0	-0.129	STAR1	-0.008	THRO1,WEMI1	-25.2	HAVO1	-1.1	THRO1
90th	153	59	59	0	-0.456	PUSO1	-0.018	GUMO1	-15.4	GICL1	-1.1	JARI1
Mean	155	70	70	0	-0.172	PHOE1	-0.008	CANY1	-23.3	HAVO1	-1.5	CANY1
Winter	151	67	67	0	-0.289	PHOE1	-0.005	WHPE1	-21.7	STAR1	-1.6	WHPE1
Spring	154	59	58	1	-0.324	CHER1	0.136	COHU1	-25.6	HAVO1	6.0	COHU1
Summer	155	36	31	5	-0.225	MOMO1	0.209	DOME1	-23.0	SIME1	8.8	GAMO1
Fall	154	58	56	2	-0.324	MING1	0.182	SAWT1	-30.4	HAVO1	11.0	ZICA1
Fine Soil												
10th	153	26	19	7	-0.022	SAGU1	0.013	FOPE1 SWAN1	-13.5	MONT1	15.2	SWAN1
50th	153	38	22	16	-0.114	VIIS1	0.035	PEFO1	-22.1	VIIS1	7.3	FOPE1
90th	153	16	8	8	-0.261	BIBE1	0.282	CHER1	-10.1	BIBE1	8.5	CHER1
Mean	154	15	9	6	-0.144	SYCA1	0.084	CHER1	-10.5	COHI1	7.2	FOPE1

Parameter	N_{tot}	N_{sig}	N_{neg}	N_{pos}	Slope (min.) ($\mu g\ m^{-3}\ yr^{-1}$)	Site (min)	Slope (max.) ($\mu g\ m^{-3}\ yr^{-1}$)	Site (max)	Trend (min.) (% yr^{-1})	Site (min)	Trend (max.) (% yr^{-1})	Site (max)
Winter	152	12	10	2	-0.142	BIBE1	0.009	MKGO1	-20.8	BIBE1	2.7	MKGO1
Spring	154	15	8	7	-0.147	BIBE1	0.339	ZICA1	-13.5	CACO1	25.1	ZICA1
Summer	154	26	9	17	-0.079	COHI1	0.197	CHER1	-13.4	COHI1	14.3	INGA1
Fall	154	21	7	14	-0.070	THBA1	0.181	CHER1	-8.6	MEVE1	20.8	ZICA1
Gravimetric Fine Mass												
10th	153	47	42	5	-0.210	SIPS1	0.063	WIMO1	-12.2	STAR1	11.9	TRCR1
50th	153	60	57	3	-0.453	ELDO1	0.059	PEFO1	-7.2	STAR1	4.6	DENA1
90th	153	40	38	2	-0.887	GRSM1	1.438	HAVO1	-7.7	TUXE1	12.8	HAVO1
Mean	154	57	54	3	-0.457	QUCI1	0.296	HAVO1	-6.1	STAR1	7.3	HAVO1
Winter	152	47	43	4	-0.591	PHOE1	0.078	TRCR1	-14.6	STAR1	9.1	TRCR1
Spring	154	36	32	4	-1.049	TALL1	0.740	COHU1	-12.0	TALL1	12.0	HAVO1
Summer	154	39	37	2	-0.721	ADPI1	0.552	DOME1	-7.9	WHPE1	6.6	DOME1
Fall	154	44	33	11	-0.483	AREN1	0.386	ZICA1	-6.5	MOOS1	12.3	ZICA1
Coarse Mass												
10th	153	32	17	15	-0.246	VIIS1	0.173	QUCI1	-40.0	SNPA1	40.0	PASA1
50th	153	45	26	19	-0.730	VILA1	0.345	INGA1	-16.3	FLAT1	11.6	COHU1
90th	153	34	24	10	-1.374	GUMO1	0.809	DOME1	-8.8	MONT1	8.6	COHU1
Mean	154	35	23	12	-0.860	ELDO1	0.392	INGA1	-13.5	HOOV1	9.5	LYBR1
Winter	152	37	28	9	-0.831	BIBE1	0.310	THBA1	-18.2	HOOV1	12.7	SULA1
Spring	154	28	18	10	-0.662	WIMO1	0.933	CORI1	-16.4	MONT1	16.4	COHU1
Summer	154	44	17	27	-1.210	ELDO1	2.066	DOME1	-9.6	OLYM1	12.9	INGA1
Fall	154	25	13	12	-0.737	SAFO1	1.817	CHER1	-8.7	MONT1	12.9	SHRO1
PM_{10}												
10th	154	37	34	3	-0.707	CHER1	0.125	NEBR1	-15.1	STAR1	12.1	TRCR1
50th	154	50	48	2	-1.191	CHER1	0.424	INGA1	-9.9	STAR1	5.6	INGA1
90th	154	38	33	5	-1.566	SAFO1	1.630	HAVO1	-8.1	TUXE1	12.5	HAVO1
Mean	155	47	43	4	-1.140	ELDO1	0.429	DOME1	-6.8	MONT1	6.0	HAVO1
Winter	153	42	40	2	-1.656	VILA1	0.242	BOND1	-12.9	STAR1	1.7	BOND1
Spring	155	30	25	5	-1.361	VILA1	1.642	COHU1	-8.2	MONT1	12.3	COHU1
Summer	155	34	29	5	-1.802	ELDO1	2.701	DOME1	-7.1	ELDO1	13.4	INGA1
Fall	154	37	29	8	-0.733	SAFO1	2.177	CHER1	-6.0	GICL1	10.0	ZICA1

N_{tot} refers to the total number of sites in the analysis
N_{sig} refers to the number of sites with significant trends ($p \leq 0.15$)
N_{pos} refers to the number of significant positive trends
N_{neg} refers to the number of significant negative trends

A greater number of sites had positive short-term trends compared to positive long-term trends. In fact, some sites with decreasing long-term trends had positive short-term trends. For example, sulfate ion concentrations at the Denali, Alaska, site (DENA1) started increasing in later years. Notice the upward-trending sulfate concentrations for the most recent 10 years on the timeline for DENA1 in Figure 6.1.3, which was the period evaluated for the short-term trends analyses.

The 50th percentile and spring season corresponded to the highest number of significant positive short-term sulfate ion trends for all of the parameters investigated. Short-term sulfate trends during spring were very interesting (Figure 6.1.9). Many sites in the western United States corresponded to positive trends in the spring, the only season to exhibit such patterns. Recall that many western U.S. regions corresponded to maximum ammonium sulfate mean concentrations (2005–2008) during spring (Figure 4.5.1). The Hawaii Volcanoes HI site (HAVO1) corresponded to positive trends for the 50th, 90th, spring, summer, and fall seasons (10th percentile and winter trends were not significant). In fact, out of all significant short-term trends, the largest positive short-term trends in the United States occurred at HAVO1 for spring, summer, fall, and 90th percentile (16.8% yr^{-1}, 14.1% yr^{-1}, 10.2% yr^{-1}, and 11.8% yr^{-1}, respectively). The 90th percentile concentrations at HAVO1 are shown in Figure 6.1.10. High sulfate ion concentrations in 2008 were likely associated with volcanic activity. The maximum short-term sulfate ion trends for other percentiles and seasons were associated with the Trapper Creek site in Alaska (TRCR1, 8.7% yr^{-1}, 6.8% yr^{-1}, and 9.4% yr^{-1} for 10th percentile, 50th percentile, and winter, respectively).

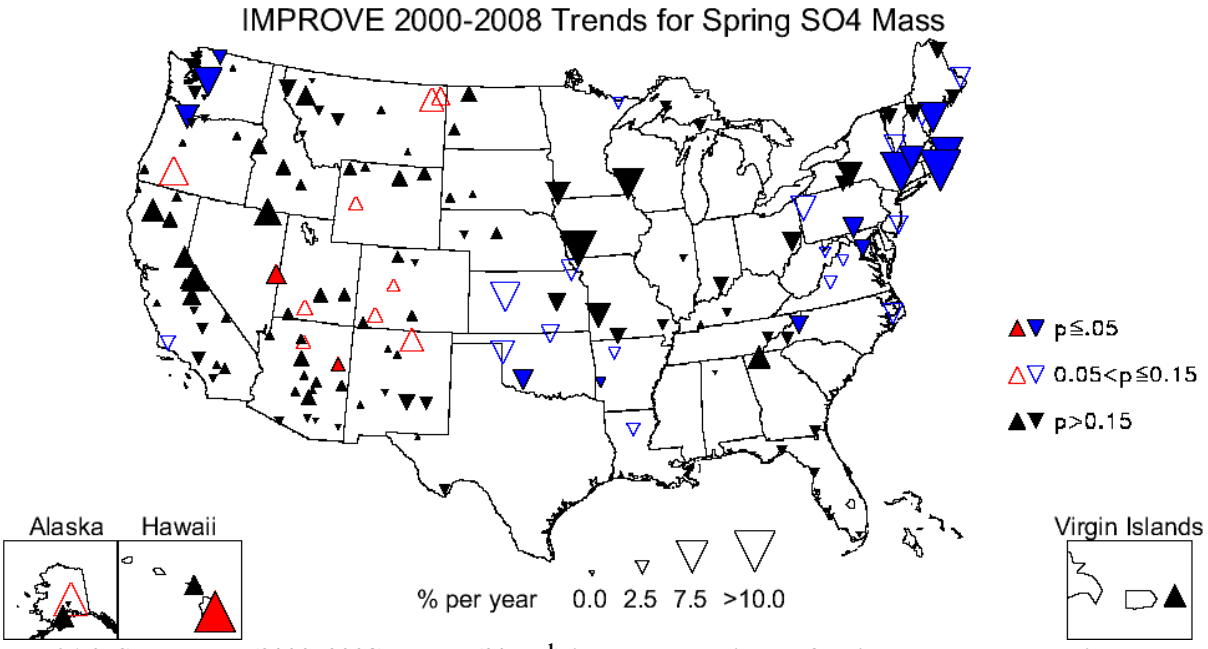

Figure 6.1.9. Short-term (2000–2008) trends (% yr^{-1}) in average spring sulfate ion mass concentrations.

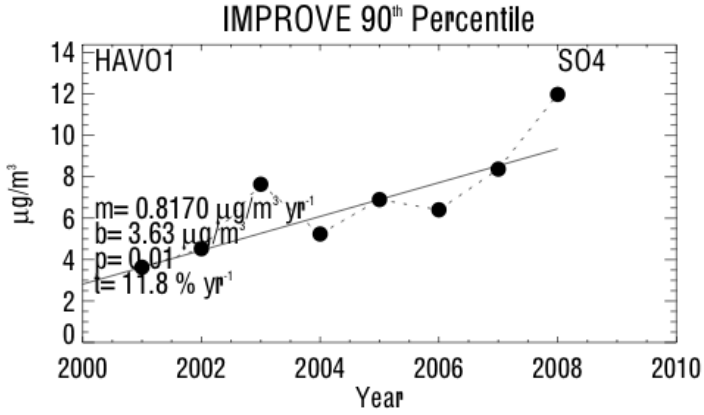

Figure 6.1.10. Average spring sulfate ion mass concentrations (µg m^{-3}) for Hawaii Volcanoes (HAVO1). Regression results, including Theil slope (m, µg m^{-3} yr^{-1}), intercept (b, µg m^{-3}), significance (p), and trend (t, % yr^{-1}) are included. The trend line is plotted as a solid line. The intercept corresponds to the initial year of data.

6.2 NITRATE ION TRENDS

During the late 1990s, IMPROVE nitrate ion concentrations at many sites fell below historical values during winter months. Investigations into a period from 1996 through 2000 revealed lower than usual concentrations during winter months and the cause remains unknown (McDade, 2007). Concentrations returned to normal levels after 2000, after which the data were deemed valid. Given these uncertainties, we computed short-term trends only for nitrate concentrations.

Approximately 155 sites met the completeness criteria for the nitrate ion short-term trend analysis, and only 31–116 of those (20–75%) were determined to be significant, depending on parameter. The 10^{th} percentile had the highest number of significant sites, while the average spring concentrations had the lowest. The map corresponding to the 10^{th} percentile trends is presented in Figure 6.2.1. Recall that the scale used to represent the magnitude of the trend was kept the same for all species. The 10^{th} percentile nitrate ion trends at most sites were relatively large compared to the short-term sulfate ion trends and highly significant ($p \leq 0.05$) at most sites around the United States. No sites were associated with positive 10^{th} percentile trends. The largest negative short-term nitrate ion trend for any percentile or season occurred at Trinity, California, in winter (TRIN1, -25.5% yr^{-1}). Winter nitrate ion concentrations at TRIN1 are shown in Figure 6.2.2. Concentrations decreased from 0.4 µg m^{-3} to 0.03 µg m^{-3} from 2000 to 2008. The individual site trends for the fall season, which corresponded to the season with the largest number of sites with significant trends, are shown in Figure 6.2.3. Large decreasing trends occurred for sites all around the United States during fall months, and no positive trends occurred at any site. Summer was the only other season that had no sites with positive trends.

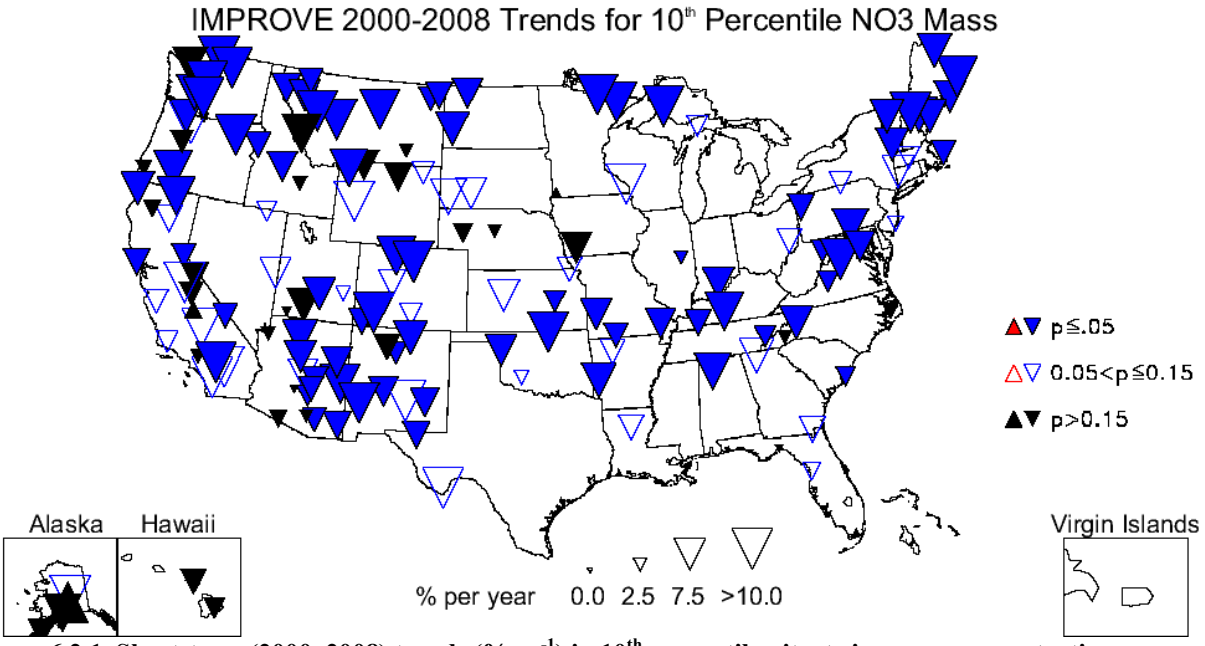

Figure 6.2.1. Short-term (2000–2008) trends (% yr^{-1}) in 10th percentile nitrate ion mass concentrations.

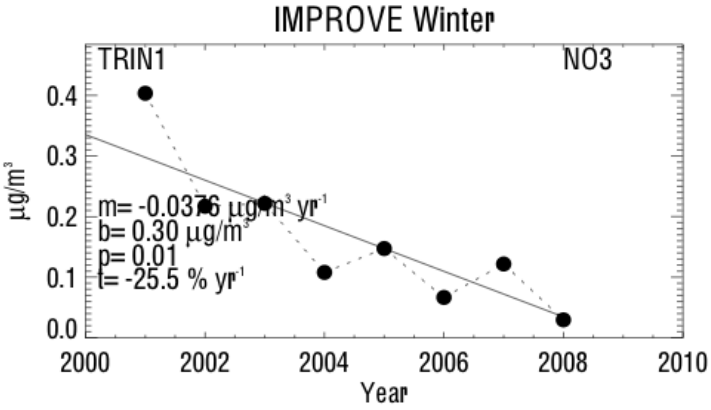

Figure 6.2.2. Average winter nitrate ion mass concentrations (µg m^{-3}) for Trinity, California (TRIN1). Regression results, including Theil slope (m, µg m^{-3} yr^{-1}), intercept (b, µg m^{-3}), significance (p), and trend (t, % yr^{-1}) are included. The trend line is plotted as a solid line. The intercept corresponds to the initial year of data.

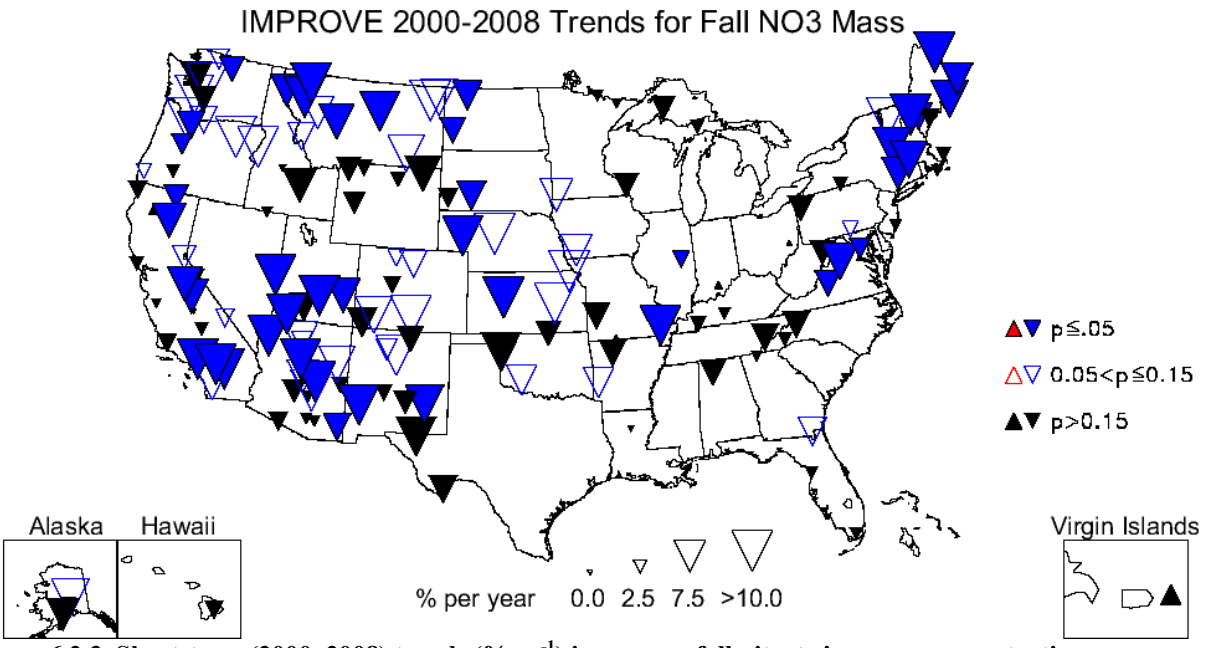

Figure 6.2.3. Short-term (2000–2008) trends (% yr^{-1}) in average fall nitrate ion mass concentrations.

The map for the 50th percentile, short-term nitrate ion trends is shown in Figure 6.2.4. As was the case with the trends for the 10th percentile and fall season, the magnitude of 50th percentile trends was fairly consistent for most sites across the United States, although several sites in the Mountain West corresponded to less significant ($p \leq 0.15$) negative trends. The map for spring nitrate ion trends at individual sites is shown in Figure 6.2.5. Only 20% of the sites with complete data corresponded to significant trends for spring. Positive trends in spring occurred at the Virgin Islands site (VIIS1, 8.9% yr^{-1}), Medicine Lake, Montana (MELA1, 6.0% yr^{-1}), Fort Peck, Montana (FOPE1, 6.6% yr^{-1}), and Denali, Alaska (DENA1, 6.2% yr^{-1}). Recall from Figure 4.2.1 that both the Virgin Islands and Alaska regions corresponded to maximum monthly mean ammonium nitrate concentrations during spring months. Positive trends also occurred for winter months, such as at Great Basin, Nevada (GRBA1, 3.8% yr^{-1}), and Jarbidge, Nevada (JARB1, 11.9%), which had the largest positive trend of any site for any percentile or season. The timeline of mean winter concentrations at JARB1 is shown in Figure 6.2.6 and demonstrates variable concentrations from year to year.

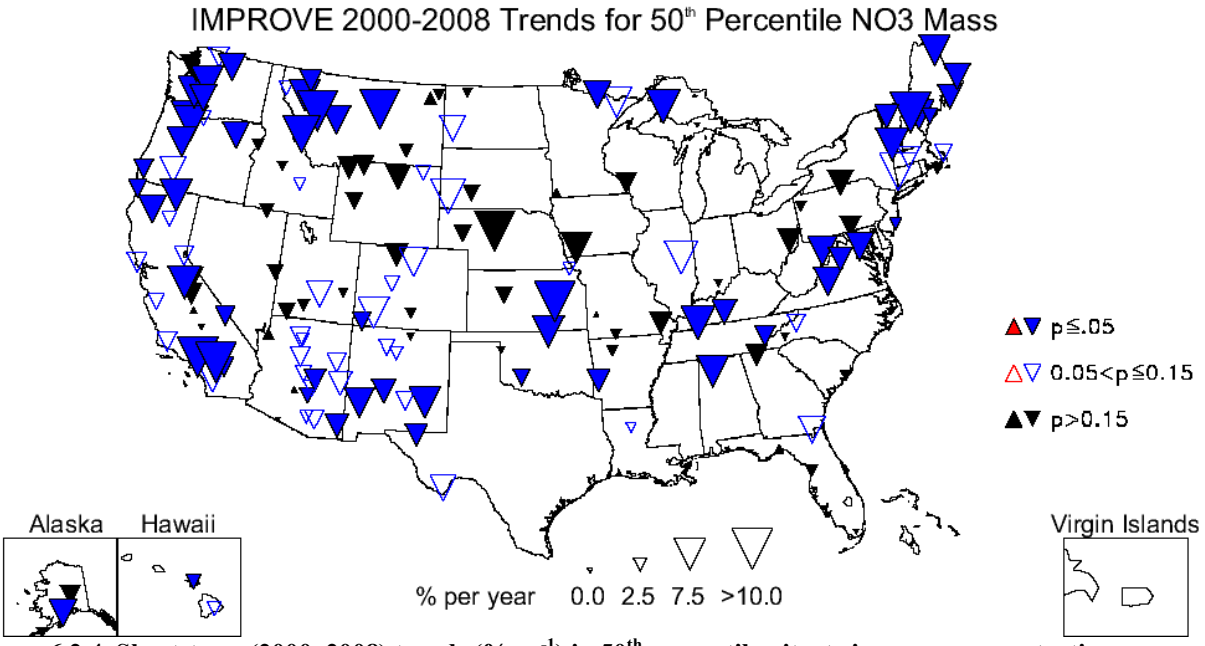

Figure 6.2.4. Short-term (2000–2008) trends (% yr^{-1}) in 50th percentile nitrate ion mass concentrations.

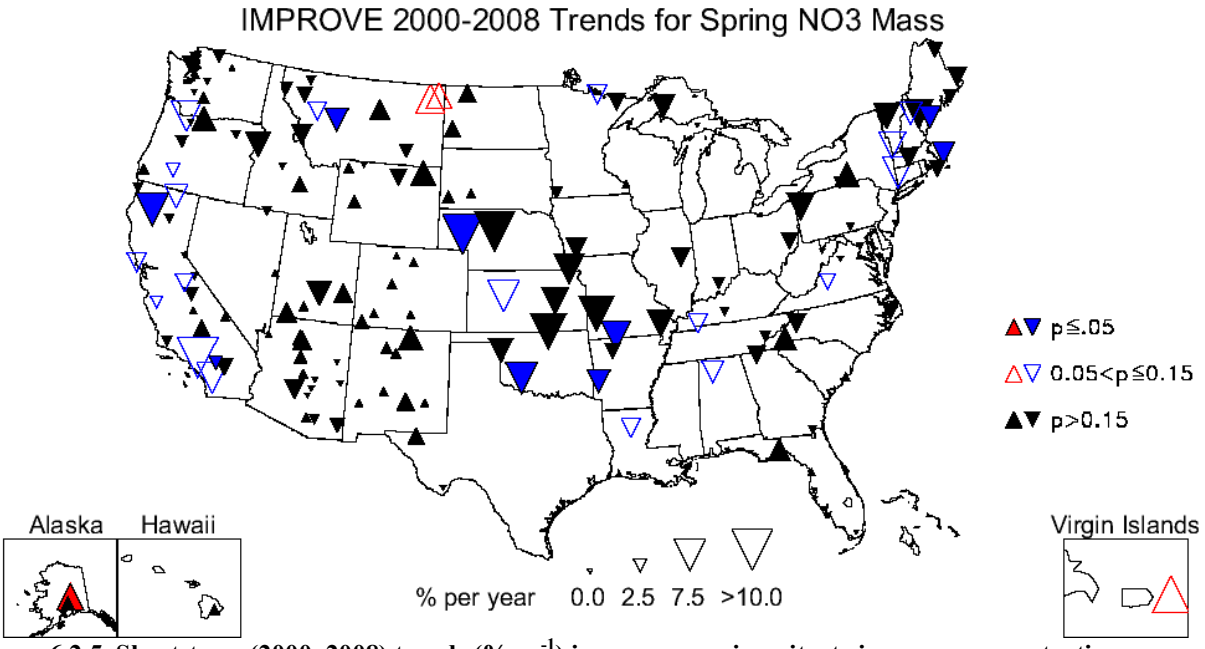

Figure 6.2.5. Short-term (2000–2008) trends (% yr^{-1}) in average spring nitrate ion mass concentrations.

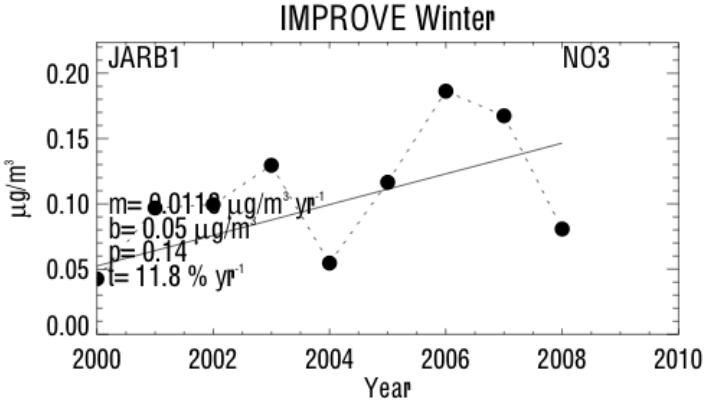

Figure 6.2.6. Average winter nitrate ion mass concentrations (µg m^{-3}) for Jarbidge NV (JARB1). Regression results, including Theil slope (m, µg m^{-3} yr^{-1}), intercept (b, µg m^{-3}), significance (p), and trend (t, % yr^{-1}) are included. The trend line is plotted as a solid line. The intercept corresponds to the initial year of data.

6.3 TOTAL CARBON TRENDS

We computed trends on total carbon, rather than on OC and LAC individually, because changes in analytical methods due to hardware upgrades on 1 January 2005 resulted in changes in the split between OC and LAC that introduced uncertainty to trend analyses (Chow et al., 2007; White, 2007). Higher LAC/TC ratios were reported after the change in analytical methods, but no changes in total carbon were detected (see Chapter 1.3.1.1).

Evaluating long-term trends in TC typically resulted in roughly 50 sites with complete data; 25–46 of these sites were associated with significant trends depending on the parameter (see Table 6.1). The 10^{th} percentile, long-term trends corresponded to the highest number of significant trends (46) for any parameter. A map of the 10^{th} percentile, TC long-term trends is shown in Figure 6.3.1. Sites with larger negative trends were located along the western coast. The least negative 10^{th} percentile trend occurred at Redwood, California (REDW1, -3.9% yr^{-1}), and the largest negative 10^{th} percentile trend occurred at Three Sisters, Oregon (THSI1, -14.6% yr^{-1}). The timeline of the 10^{th} percentile TC concentrations at the THSI1 site is presented in Figure 6.3.2 and shows a large decrease in low TC concentrations since the mid-1990s. No positive trends were associated with any site for 10^{th} percentile concentrations. The winter season was also associated with large, decreasing, long-term trends and corresponded to sites in the western United States (Figure 6.3.3). The largest negative trend during winter occurred at the Mount Rainier, Washington, site (MORA1, -6.8% yr^{-1}), and the least negative trend occurred at Great Smoky Mountains, Tennessee (GRSM1, -1.3% yr^{-1}). It is possible that the low TC concentrations associated with the 10^{th} percentile occurred mainly in winter; recall that in the western United States both OC and LAC minimum monthly mean concentrations (2005–2008) occurred during winter months for many regions (see Figure 4.3.1 and Figure 4.4.1, respectively). Concentrations on these already low concentration days in winter appear to be decreasing. For example, see the timeline of winter concentrations for the MORA1 site (Figure 6.3.4). Winter concentrations decreased from 2.3 µg m^{-3} to 0.7 µg m^{-3} from 1989 to 2008.

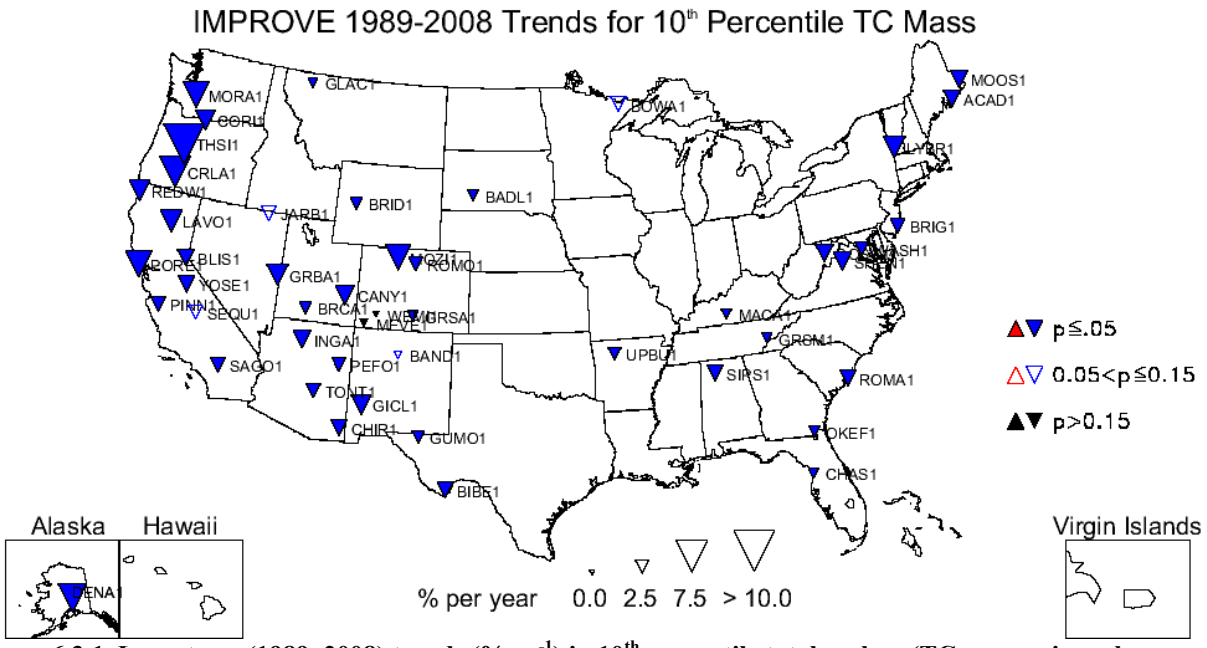

Figure 6.3.1. Long-term (1989–2008) trends (% yr^{-1}) in 10th percentile total carbon (TC = organic carbon + light absorbing carbon) mass concentrations.

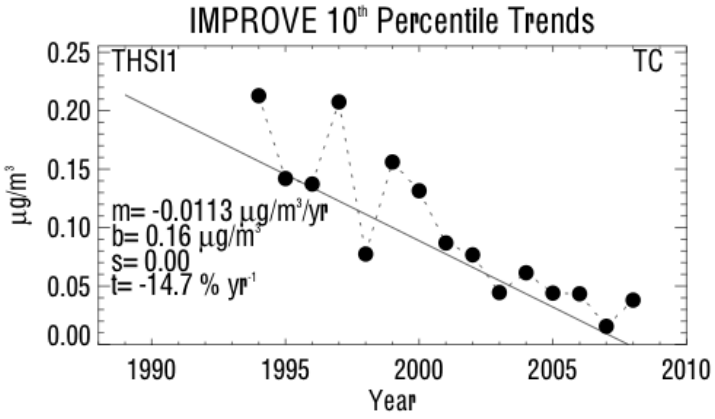

Figure 6.3.2. 10th percentile total carbon (TC = organic carbon + light absorbing carbon) mass concentrations (µg m^{-3}) for Three Sisters, Oregon (THSI1). Regression results, including Theil slope (m, µg m^{-3} yr^{-1}), intercept (b, µg m^{-3}), significance (s), and trend (t, % yr^{-1}) are included. The trend line is plotted as a solid line. The intercept corresponds to the initial year of data.

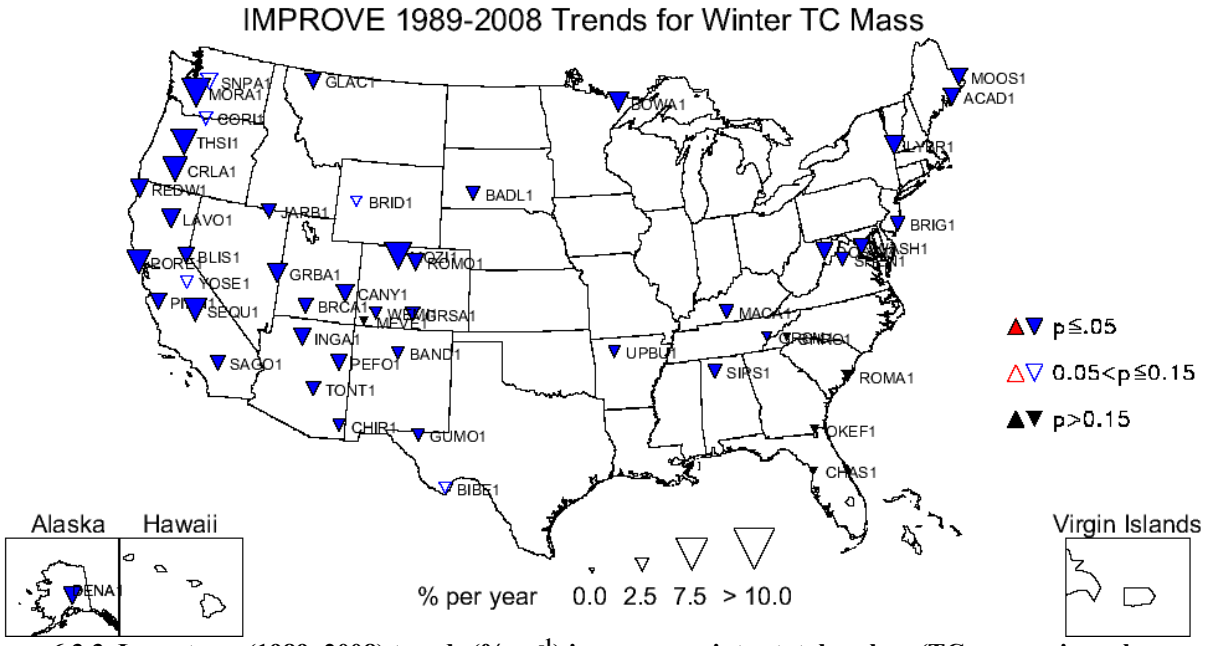

Figure 6.3.3. Long-term (1989–2008) trends (% yr^{-1}) in average winter total carbon (TC = organic carbon + light absorbing carbon) mass concentrations.

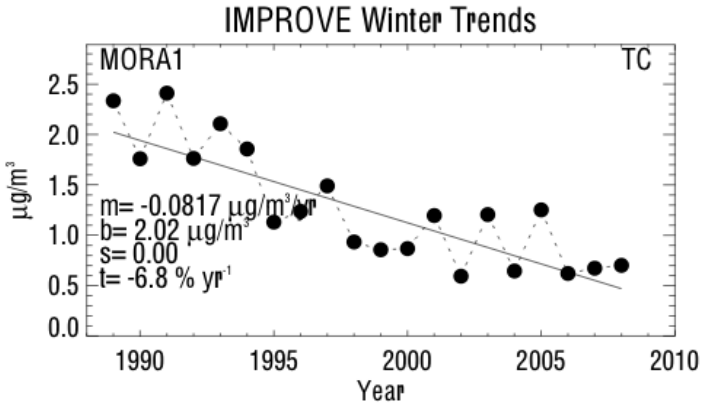

Figure 6.3.4. Average winter total carbon (TC = organic carbon + light absorbing carbon) mass concentrations (µg m^{-3}) for Mount Rainier, Washington (MORA1). Regression results, including Theil slope (m, µg m^{-3} yr^{-1}), intercept (b, µg m^{-3}), significance (s), and trend (t, % yr^{-1}) are included. The trend line is plotted as a solid line. The intercept corresponds to the initial year of data.

The individual site trends for the 90th percentile concentration were less negative or insignificant, especially at sites along the western coast, compared to the 10th percentile trends (compare Figure 6.3.5 to Figure 6.3.1). Sites with positive 90th percentile, long-term TC trends corresponded to Bridger, Wyoming (BRID1, 1.7% yr^{-1}), and Bryce Canyon, Utah (BRCA1, 1.2% yr^{-1}). The BRID1 timeline of 90th percentile concentration is shown in Figure 6.3.6. The variability in the increasing TC concentration may be related to sporadic emissions from biomass burning. Of the 10th, 50th, and 90th percentiles, positive trends occurred only for the 90th percentile (see Table 6.1).

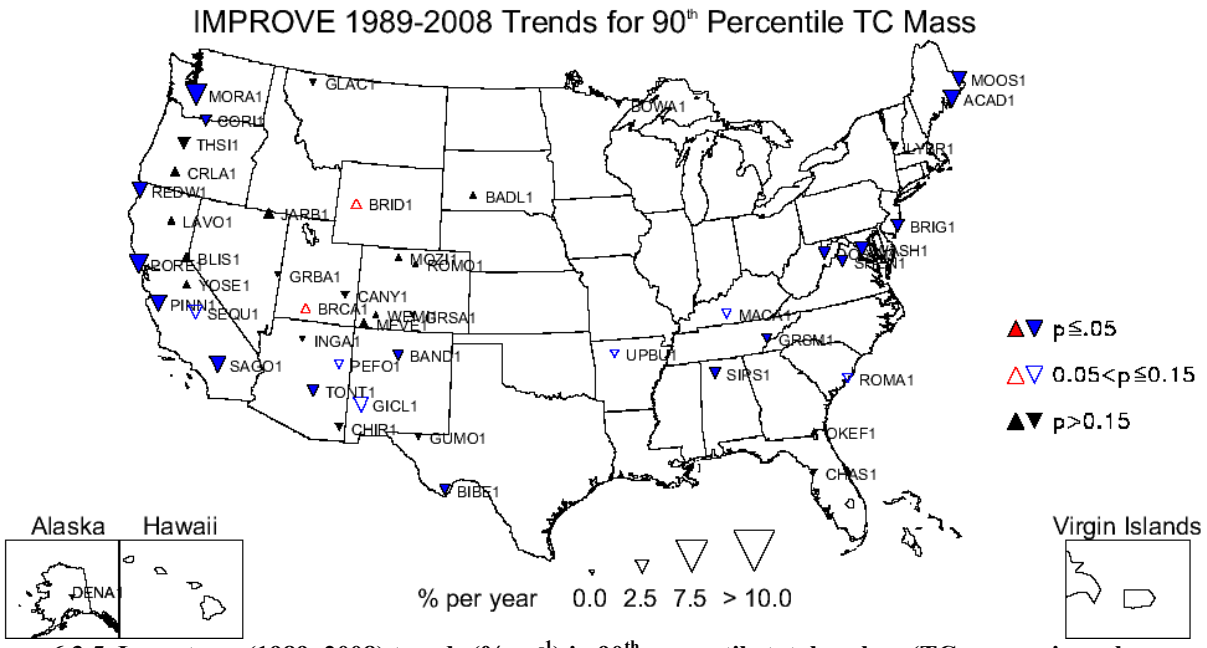

Figure 6.3.5. Long-term (1989–2008) trends (% yr^{-1}) in 90th percentile total carbon (TC = organic carbon + light absorbing carbon) mass concentrations.

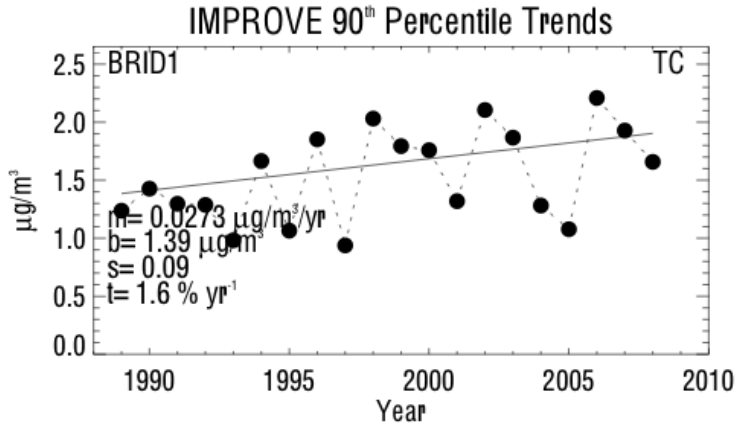

Figure 6.3.6. 90th percentile total carbon (TC = organic carbon + light absorbing carbon) mass concentrations (μg m^{-3}) for Bridger, Wyoming (BRID1). Regression results, including Theil slope (m, μg m^{-3} yr^{-1}), intercept (b, μg m^{-3}), significance (s), and trend (t, % yr^{-1}) are included. The trend line is plotted as a solid line. The intercept corresponds to the initial year of data.

Long-term, summer TC trends were associated with the largest number of sites (six) with positive trends of all the parameters investigated, although many sites corresponded to insignificant trends. In general, magnitudes of summer trends were fairly consistent (and low) around the United States (see Figure 6.3.7). The largest negative summer, long-term trend occurred at Redwood, California (REDW1, -3.9% yr^{-1}), and the largest positive summer trend occurred at Bridger, Wyoming (BRID1, 3.8% yr^{-1}). The other five sites associated with positive trends were Bliss, California (BLIS1, 2.3% yr^{-1}), Great Basin, Nevada (GRBA1, 2.1% yr^{-1}), Bryce Canyon, Utah (BRCA1, 2.4% yr^{-1}), Rocky Mountain National Park, Colorado (ROMO1, 1.04% yr^{-1}), and Great Sand Dunes, Colorado (GRSA1, 1.3% yr^{-1}). The timeline of summer TC

concentrations for BRID1 is shown in Figure 6.3.8. The variable summer concentrations were similar to the 90th percentile TC concentration shown in Figure 6.3.6, and suggested contributions from biomass burning emissions. Recall from Chapters 4.3 and 4.4 that most regions in the western United States corresponded to summer maxima in both OC and LAC (Figures 4.3.1 and 4.4.1, respectively). Unlike the strongly decreasing TC 10th percentile concentrations that likely occurred during winter days, the highest concentrations that were likely associated with summer months were decreasing to a much lower degree and in some cases actually increasing.

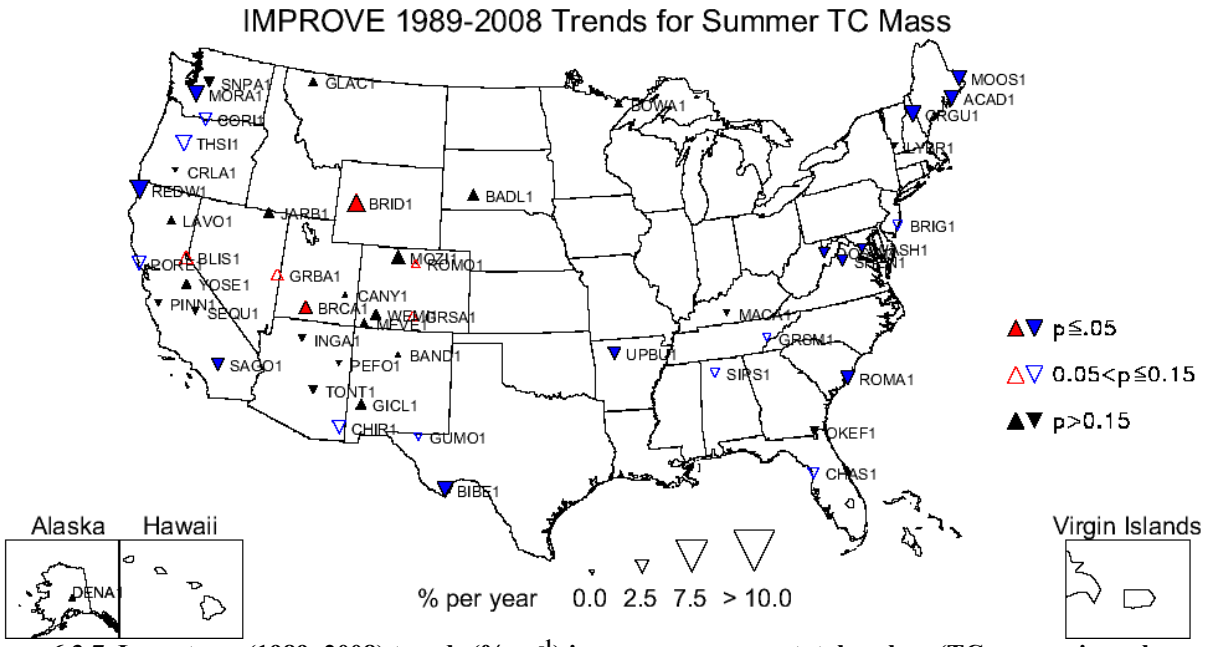

Figure 6.3.7. Long-term (1989–2008) trends (% yr^{-1}) in average summer total carbon (TC = organic carbon + light absorbing carbon) mass concentrations.

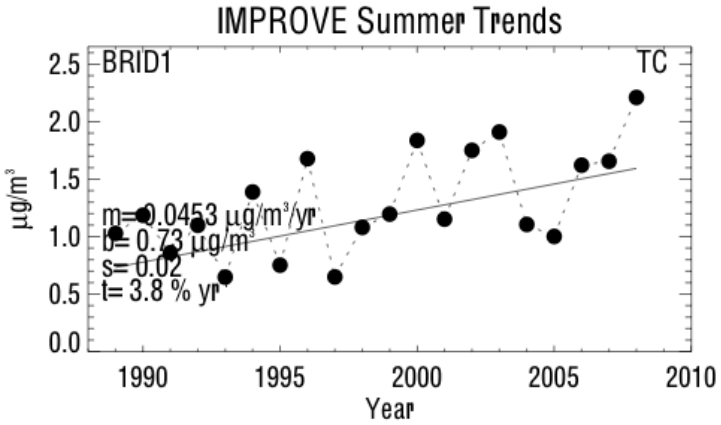

Figure 6.3.8. Average summer total carbon (TC = organic carbon + light absorbing carbon) mass concentrations (µg m^{-3}) for Bridger, Wyoming (BRID1). Regression results, including Theil slope (m, µg m^{-3} yr^{-1}), intercept (b, µg m^{-3}), significance (s), and trend (t, % yr^{-1}) are included. The trend line is plotted as a solid line. The intercept corresponds to the initial year of data.

Short-term trend analyses were performed on a much larger number of sites compared to the long-term trend analyses (150–155 sites, depending on parameter); roughly 20–60% of the sites were determined to be significant. The later time period allowed for more sites with complete data to be included in the analyses. The 10th percentile trends corresponded to the largest number of significant trends for the parameters investigated (see Table 6.2). The short-term, 10th percentile trends in TC for individual sites are shown in Figure 6.3.9. Short-term trends were much larger for many sites around the United States compared to long-term trends. Trends generally were less negative at sites in the eastern compared to the western United States. One of the largest negative 10th percentile trends occurred at Three Sisters, Oregon (THSI1, -22.9% yr^{-1}). The timeline for the 10th percentile TC concentration at THSI1 is shown in Figure 6.3.10 and demonstrates the downward trend of already low TC concentrations. The least negative 10th percentile trend occurred at Queen Valley, Arizona (QUVA1, -1.3% yr^{-1}). There were no sites associated with positive short-term trends for any of the percentiles. The large negative trends in winter for individual sites are presented in Figure 6.3.11. Although there were fewer sites with significant trends compared to the 10th percentile trends, the magnitudes were comparable. No positive short-term winter trends were associated with any site. The largest decreasing winter trend was associated with the Starkey, Oregon, site (STAR1, -21.7% yr^{-1}). The smallest decreasing trend in winter concentrations occurred at the Wheeler Peak, New Mexico, site (WHPE1, -1.6% yr^{-1}).

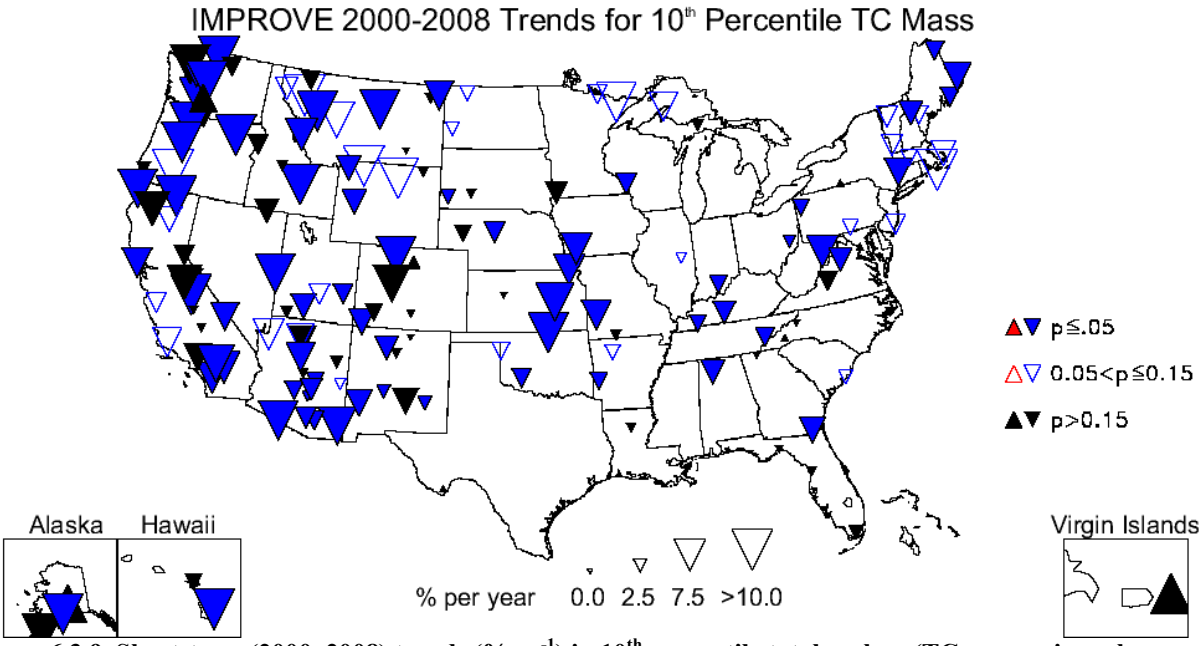

Figure 6.3.9. Short-term (2000–2008) trends (% yr^{-1}) in 10th percentile total carbon (TC = organic carbon + light absorbing carbon) mass concentrations.

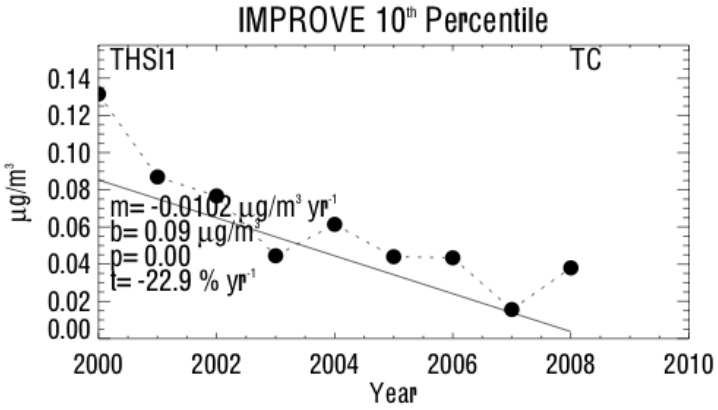

Figure 6.3.10. 10th percentile total carbon (TC = organic carbon + light absorbing carbon) mass concentrations (µg m^{-3}) for Three Sisters, Oregon (THSI1). Regression results, including Theil slope (m, µg m^{-3} yr^{-1}), intercept (b, µg m^{-3}), significance (p), and trend (t, % yr^{-1}) are included. The trend line is plotted as a solid line. The intercept corresponds to the initial year of data.

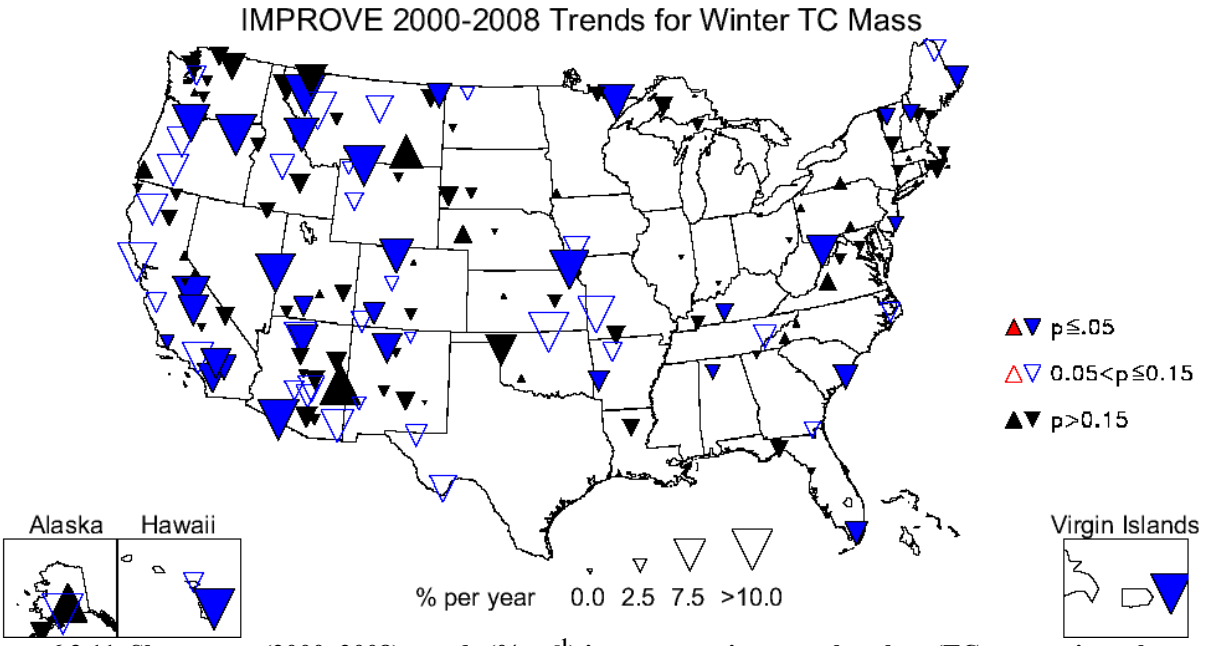

Figure 6.3.11. Short-term (2000–2008) trends (% yr^{-1}) in average winter total carbon (TC = organic carbon + light absorbing carbon) mass concentrations.

Although the number of sites with significant trends corresponding to the 10th and 50th percentiles was similar (95 versus 92, respectively), the 50th percentile trends were generally less negative. A map of 50th percentile trends is shown in Figure 6.3.12. Trends corresponding to sites in the eastern United States generally were less negative than trends for western sites. The largest decreasing 50th percentile, short-term trend occurred at Hawaii Volcanoes (HAVO1, -25.16% yr^{-1}), and the least negative 50th percentile trend occurred at James River Face Wilderness, Virginia (JARI1, -1.07% yr^{-1}). A timeline showing the decrease in 50th percentile TC concentrations at HAVO1 is presented in Figure 6.3.13. A precipitous drop in the 50th percentile TC concentrations occurred around 2003, after which concentrations decreased slowly. Results for short-term summer trends included five sites with positive trends (Figure 6.3.14). The sites at

Gates of the Mountains, Montana (GAMO1, 8.8% yr^{-1}), Dome Lands Wilderness, California (DOME1, 8.1% yr^{-1}), Hells Canyon, Oregon (HECA1, 5.4% yr^{-1}), Craters of the Moon, Idaho (CRMO1, 3.6% yr^{-1}), and Shenandoah, Virginia (SHEN1, 3.2% yr^{-1}), all corresponded to positive trends in summer concentrations. The trend line of summer concentration at GAMO1 is shown in Figure 6.3.15. High concentrations in 2003 and 2007 were most likely related to wildfire emissions. The trend line plotted alongside the data demonstrated that these outliers were not heavily weighted in the regression. Positive short-term TC trends also occurred during other seasons. In spring, a positive trend was associated with Cohutta, Georgia (COHU1, 6.0% yr^{-1}), and in fall the sites of Sawtooth, Idaho (SAWT1, 10.9% yr^{-1}), and Zion Canyon, Utah (ZICA1, 11.0% yr^{-1}), were associated with positive trends.

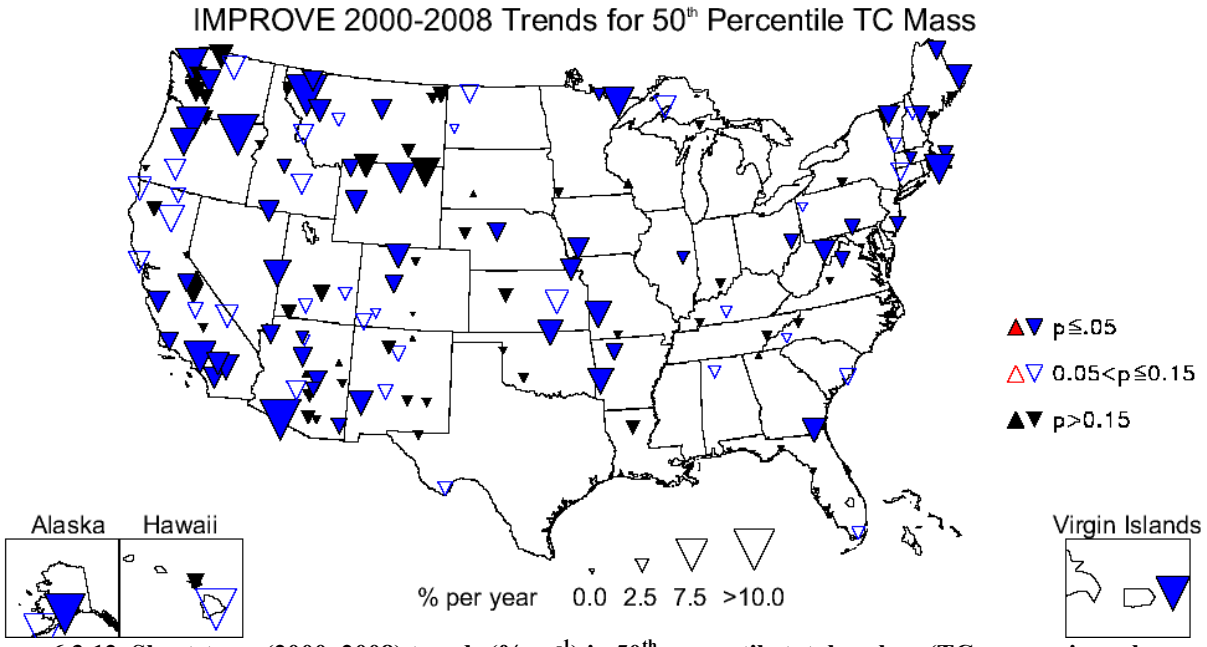

Figure 6.3.12. Short-term (2000–2008) trends (% yr^{-1}) in 50th percentile total carbon (TC = organic carbon + light absorbing carbon) mass concentrations.

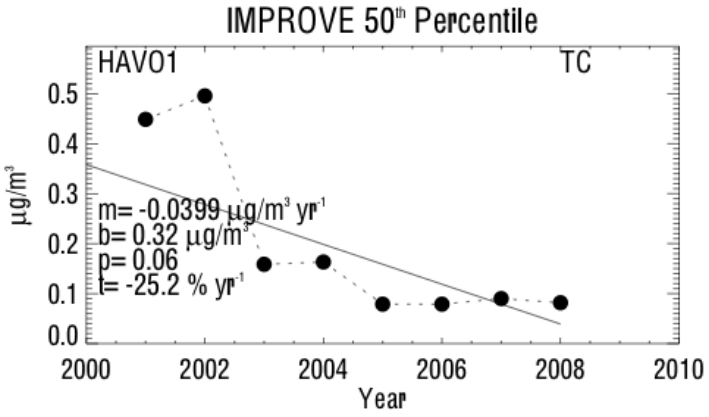

Figure 6.3.13. 50th percentile total carbon (TC = organic carbon + light absorbing carbon) mass concentrations (µg m^{-3}) for Hawaii Volcanoes (HAVO1). Regression results, including Theil slope (m, µg m^{-3} yr^{-1}), intercept (b, µg m^{-3}), significance (p), and trend (t, % yr^{-1}) are included. The trend line is plotted as a solid line. The intercept corresponds to the initial year of data.

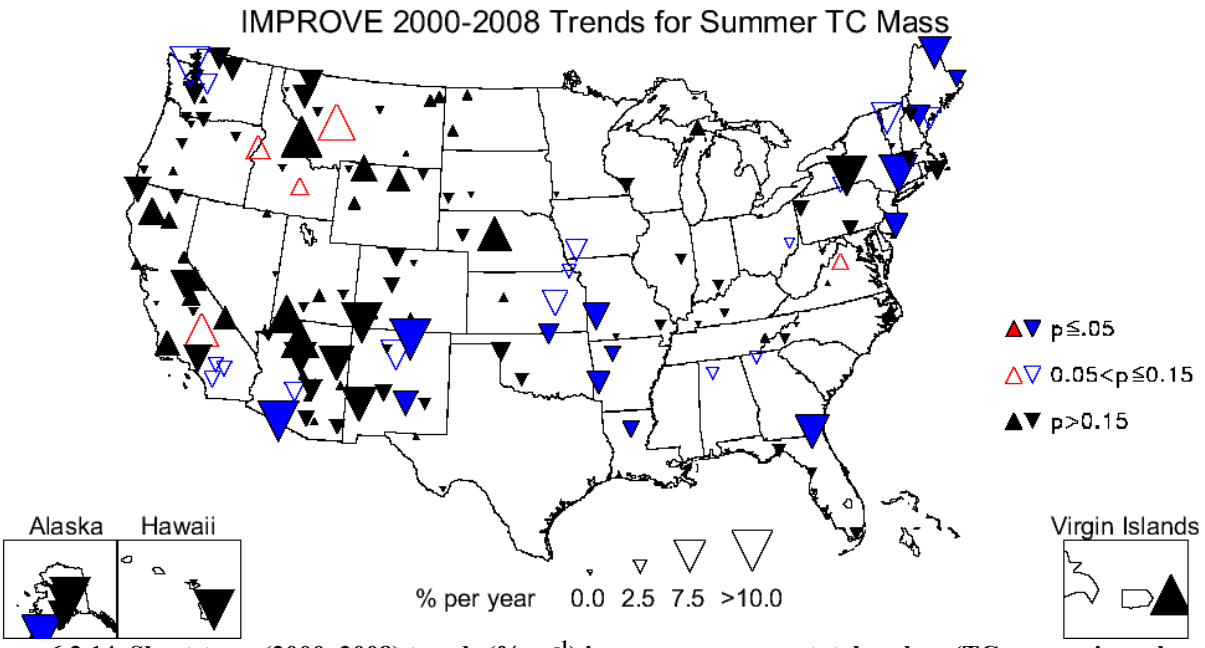

Figure 6.3.14. Short-term (2000–2008) trends (% yr^{-1}) in average summer total carbon (TC = organic carbon + light absorbing carbon) mass concentrations.

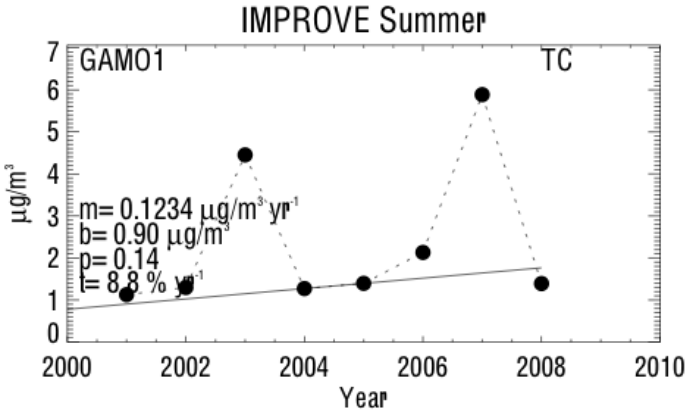

Figure 6.3.15. Average summer total carbon (TC = organic carbon + light absorbing carbon) mass concentrations (µg m^{-3}) for Gates of the Mountains, Montana (GAMO1). Regression results, including Theil slope (m, µg m^{-3} yr^{-1}), intercept (b, µg m^{-3}), significance (p), and trend (t, % yr^{-1}) are included. The trend line is plotted as a solid line. The intercept corresponds to the initial year of data.

6.4 $PM_{2.5}$ SOIL TRENDS

Recall from Chapter 2.1 that $PM_{2.5}$ soil mass concentrations were determined by combining the oxides of elemental mass concentrations of Al, Si, Ca, Fe, and Ti (see Table 2.1). The analytical methods used to determine these species have evolved over time and included PIXE (proton induced X-ray emission) and XRF (X-ray fluorescence) techniques. The transitions from PIXE to XFR methods, the change in XRF anodes from Mo to Cu, as well as different calibration procedures affect the data by changing minimum detection limits (see Chapters 1.3.1.2-1.3.1.5). No corrections to the elemental data were performed to account for changes in analytical methods as part of this trend analysis. These results should be interpreted with some

caution as the trends are sensitive to variability in analytical methods. Changes in analytical methods may not equally affect data for each soil species; therefore the integrated soil concentration may be less susceptible to possible variability introduced by the analytical methods, although this has not been specifically demonstrated. A thorough trend analysis that removed variability in the data due to analytical changes was beyond the scope of this report.

Trends in soil concentrations were quite different than trend results for the previous species and included a much higher number of sites with significant positive trends for all parameters. However, the number of sites with significant long-term soil trends was generally lower. Only 11–18 sites were significant (out of ~57), depending on the parameter. The map of sites for the 10^{th} percentile trends demonstrated the low number of sites and fairly low magnitude trends (Figure 6.4.1). Most of the sites with significant trends were in the western and the northeastern United States. The largest decreasing 10^{th} percentile trend occurred at the Denali, Alaska, site (DENA1, -5.0% yr^{-1}). A decrease in the very low 10^{th} percentile soil concentrations at DENA1 is shown in Figure 6.4.2. Only two sites corresponded to positive 10^{th} percentile trends: Tonto, Arizona (TONT1, 3.16% yr^{-1}), and Everglades, Florida (EVER1, 1.17% yr^{-1}). Long-term trends in average winter soil concentrations are shown for individual sites in Figure 6.4.3. Only 14 sites corresponded to statistically significant trends, and half of them were positive. The largest negative winter trend occurred at Snoqualmie Pass, Washington (SNPA1, -5.9% yr^{-1}), and the largest positive trend occurred at Chiricahua, Arizona (CHIR1, 5.7% yr^{-1}). Two sites in the southeastern United States with increasing winter trends (Okefenokee, Georgia, OKEF1, and Everglades, Florida, EVER1) were actually associated with minimum mean soil concentrations in winter (for 2005–2008, see Figure 4.5.1), suggesting that the lowest soil concentrations at these sites has increased over the last 20 years. Long-term soil trends at OKEF1 and EVER1 were negative during summer, when soil concentrations were typically highest and long-range transport of dust is a well-known phenomenon. An example of decreasing soil concentrations in summer is shown for the Virgin Islands site (VIIS1, -3.6yr^{-1}) in Figure 6.4.4. Soil concentrations are typically highest in summer at VIIS but are decreasing.

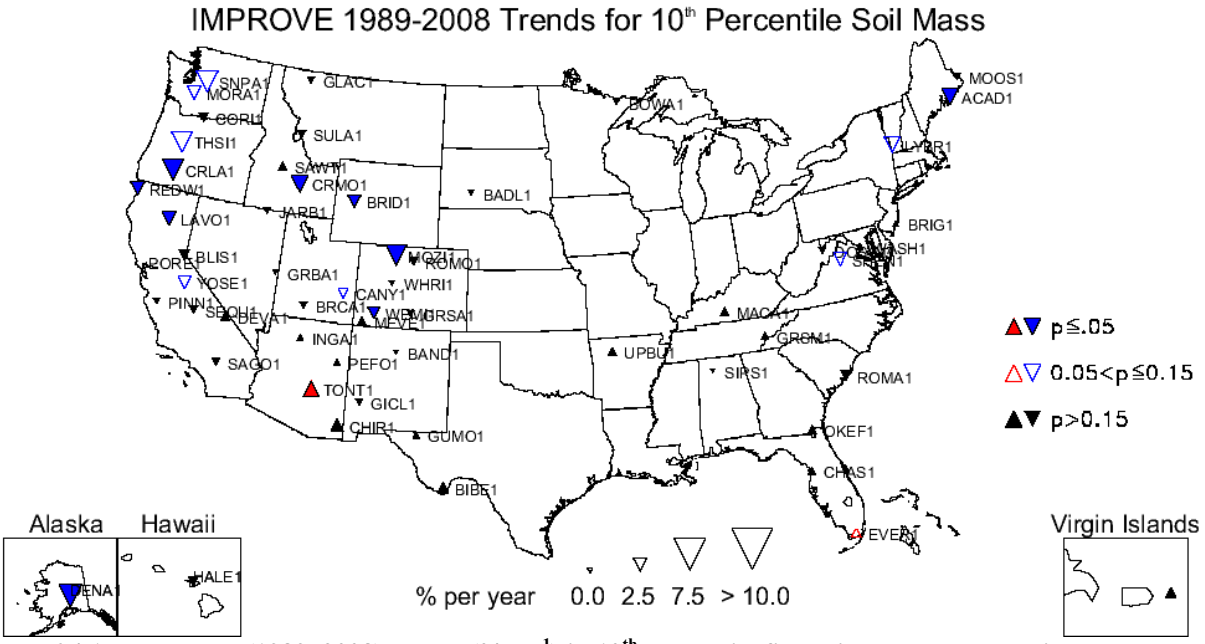

Figure 6.4.1. Long-term (1989–2008) trends (% yr^{-1}) in 10th percentile fine soil mass concentrations.

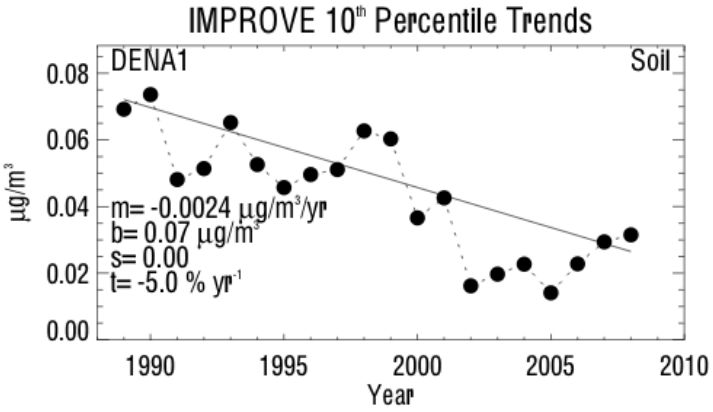

Figure 6.4.2. 10th percentile fine soil mass concentrations (µg m^{-3}) for Denali, Alaska (DENA1). Regression results, including Theil slope (m, µg m^{-3} yr^{-1}), intercept (b, µg m^{-3}), significance (s), and trend (t, % yr^{-1}) are included. The intercept corresponds to the initial year of data.

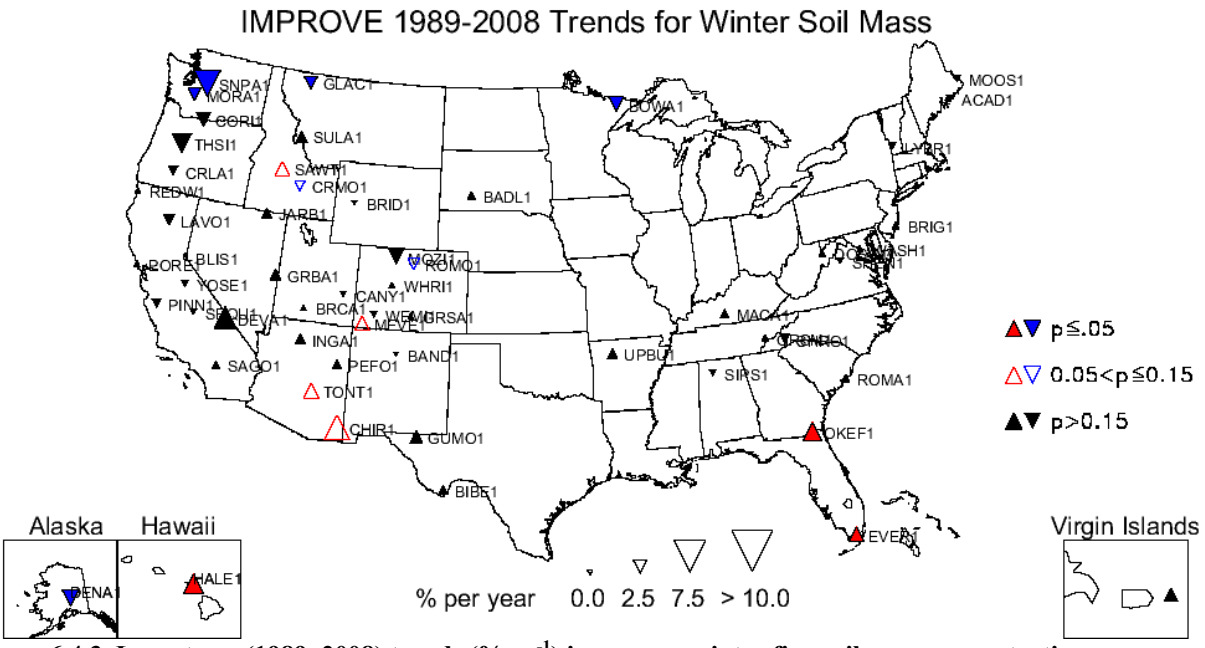

Figure 6.4.3. Long-term (1989–2008) trends (% yr^{-1}) in average winter fine soil mass concentrations.

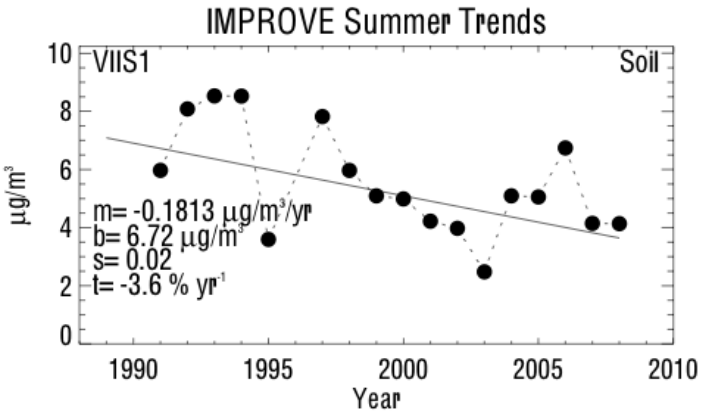

Figure 6.4.4. Average summer fine soil mass concentrations (µg m^{-3}) for Virgin Islands (VIIS1). Regression results, including Theil slope (m, µg m^{-3} yr^{-1}), intercept (b, µg m^{-3}), significance (s), and trend (t, % yr^{-1}) are included. The trend line is plotted as a solid line. The intercept corresponds to the initial year of data.

The 10th and 90th percentile trends corresponded to the highest number of sites with significant long-term soil trends of all the parameters investigated. Most of the 18 sites with statistically significant 90th percentile trends were in the western United States, and most were associated with positive trends (see Figure 6.4.5). Only four sites were associated with negative 90th percentile trends (Snoqualmie Pass, Washington, SNPA1, -2.4% yr^{-1}; San Gorgonio, California, SAGO1, -2.7% yr^{-1}; Virgin Islands, VIIS1, -4.3% yr^{-1}, and Denali, Alaska, DENA1, -2.9% yr^{-1}). The largest positive trend corresponded to the Columbia River Gorge, Washington, site (CORI1, 6.9% yr^{-1}). The timeline of 90th percentile soil concentrations at CORI1 shows variable but increasing soil concentrations (Figure 6.4.6). Contrasted to this timeline is the decreasing 90th percentile soil concentrations at Denali (DENA1, see Figure 6.4.7). With the exception of the concentration in 1990, the soil concentrations at DENA1 have been fairly steady

and slowly decreasing, unlike the variability seen in the much larger magnitude concentrations measured at the CORI1 site. Spring trends were associated with the second highest number of sites with positive trends. Individual trends for spring concentrations are presented in Figure 6.4.8. The largest spring trend occurred at Death Valley, California (DEVA1, 5.6% yr^{-1}), and most negative trend occurred at SNPA1 (-4.2% yr^{-1}). Of the 15 sites with statistically significant trends, only two were negative and corresponded to SNPA1 and DENA1 (-2.3% yr^{-1}). For many regions in the western United States, the 2005–2008 monthly mean maximum soil concentrations were associated with spring months (recall Figure 4.5.1). Trend results suggested that the highest soil concentrations are increasing, such as shown by the timeline of spring soil concentrations at DEVA1 (Figure 6.4.9). Spring concentrations increased from 1.2 µg m^{-3} to 3.2 µg m^{-3} from 1994 to 2008.

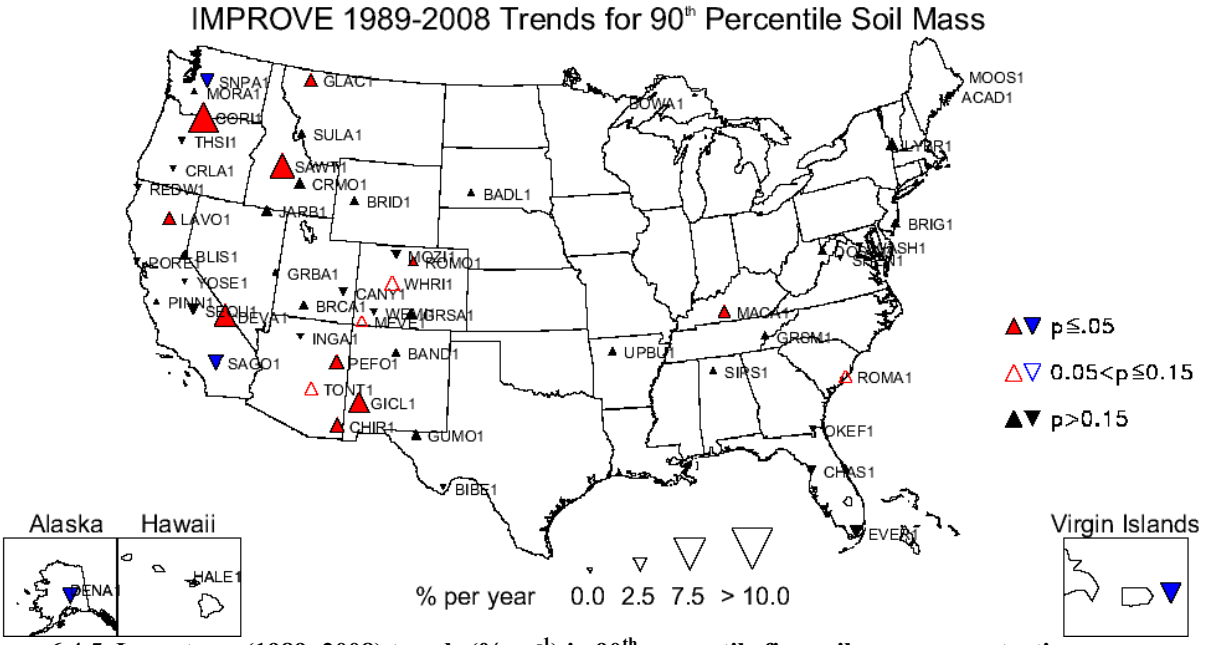

Figure 6.4.5. Long-term (1989–2008) trends (% yr^{-1}) in 90th percentile fine soil mass concentrations.

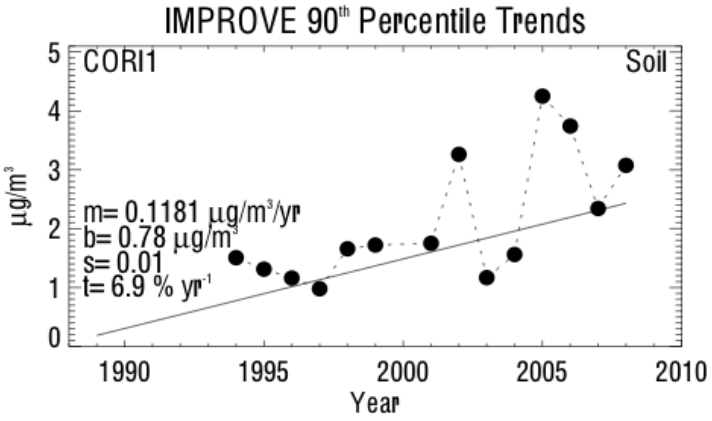

Figure 6.4.6. 90th percentile fine soil mass concentrations (µg m^{-3}) for Columbia River Gorge, Washington (CORI1). Regression results, including Theil slope (m, µg m^{-3} yr^{-1}), intercept (b, µg m^{-3}), significance (s), and trend (t, % yr^{-1}) are included. The intercept corresponds to the initial year of data.

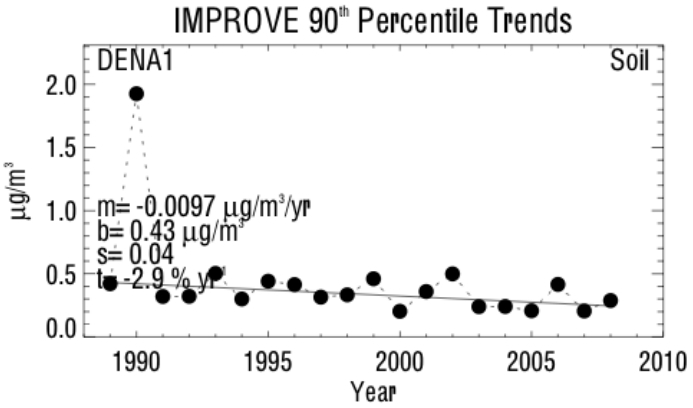

Figure 6.4.7. 90th percentile fine soil mass concentrations (µg m^{-3}) for Denali, Alaska (DENA1). Regression results, including Theil slope (m, µg m^{-3} yr^{-1}), intercept (b, µg m^{-3}), significance (s), and trend (t, % yr^{-1}) are included. The trend line is plotted as a solid line. The intercept corresponds to the initial year of data.

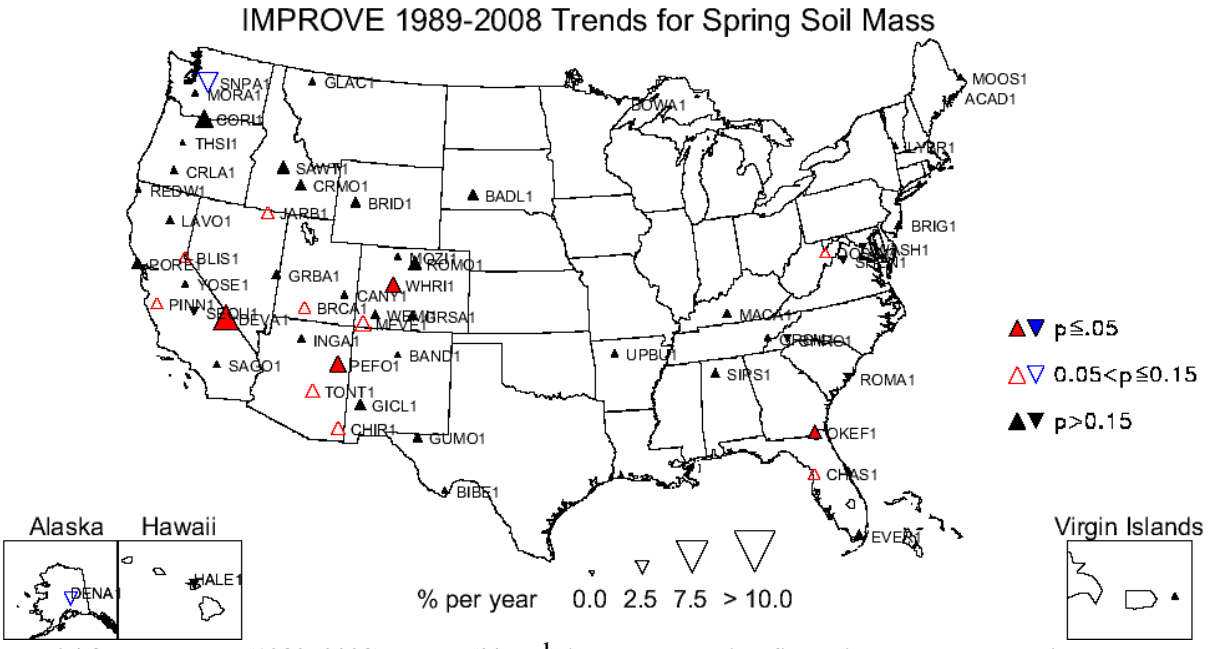

Figure 6.4.8. Long-term (1989–2008) trends (% yr^{-1}) in average spring fine soil mass concentrations.

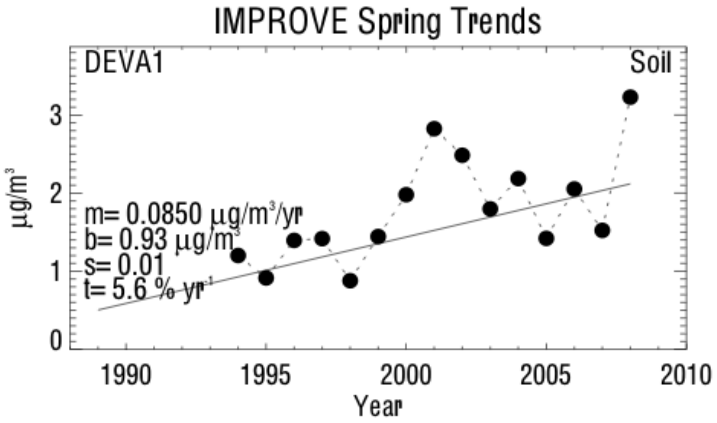

Figure 6.4.9. Average spring fine soil mass concentrations (µg m^{-3}) for Death Valley, California (DEVA1). Regression results, including Theil slope (m, µg m^{-3} yr^{-1}), intercept (b, µg m^{-3}), significance (s), and trend (t, % yr^{-1}) are included. The trend line is plotted as a solid line. The intercept corresponds to the initial year of data.

A much smaller percentage of sites corresponded to significant short-term soil trends compared to long-term soil trends (see Table 6.2). Both the 10^{th} and 50^{th} percentile, short-term soil trends corresponded to the highest number of sites with significant decreasing trends for all the parameters. Maps of 10^{th} and 50^{th} percentile trends are shown in Figures 6.4.10 and 6.4.11, respectively. Many sites in the western United States had negative (or insignificant) 10^{th} percentile trends compared to positive 50^{th} percentile trends in similar areas. In contrast, sites in the eastern United States had similar positive trends (but different magnitudes) for the 10^{th} and 50^{th} percentile concentrations. The largest positive 10^{th} and 50^{th} percentile, short-term soil trends corresponded to the Swanquarter, North Carolina (SWAN1, 15.2% yr^{-1}), and Fort Peck, Montana (FOPE1, 7.3% yr^{-1}), sites, respectively. The largest negative 10^{th} and 50^{th} percentile, short-term soil trends occurred at Monture, Montana (MONT1, -13.5% yr^{-1}), and the Virgin Islands (VIIS1, -22.10% yr^{-1}), respectively. Only 12 sites corresponded to statistically significant winter short-term soil trends (Figure 6.4.12). Two of these sites had positive trends (M.K. Goddard, Pennsylvania, MKGO1, 2.7% yr^{-1} and Brigantine, New Jersey, BRIG1, 1.8% yr^{-1}). The largest negative short-term, winter trend occurred at Big Bend, Texas (BIBE1, -20.8% yr^{-1}). The winter soil concentrations at BIBE1 have decreased significantly since 2000. The timeline of winter soil concentrations at BIBE1 is shown in Figure 6.4.13.

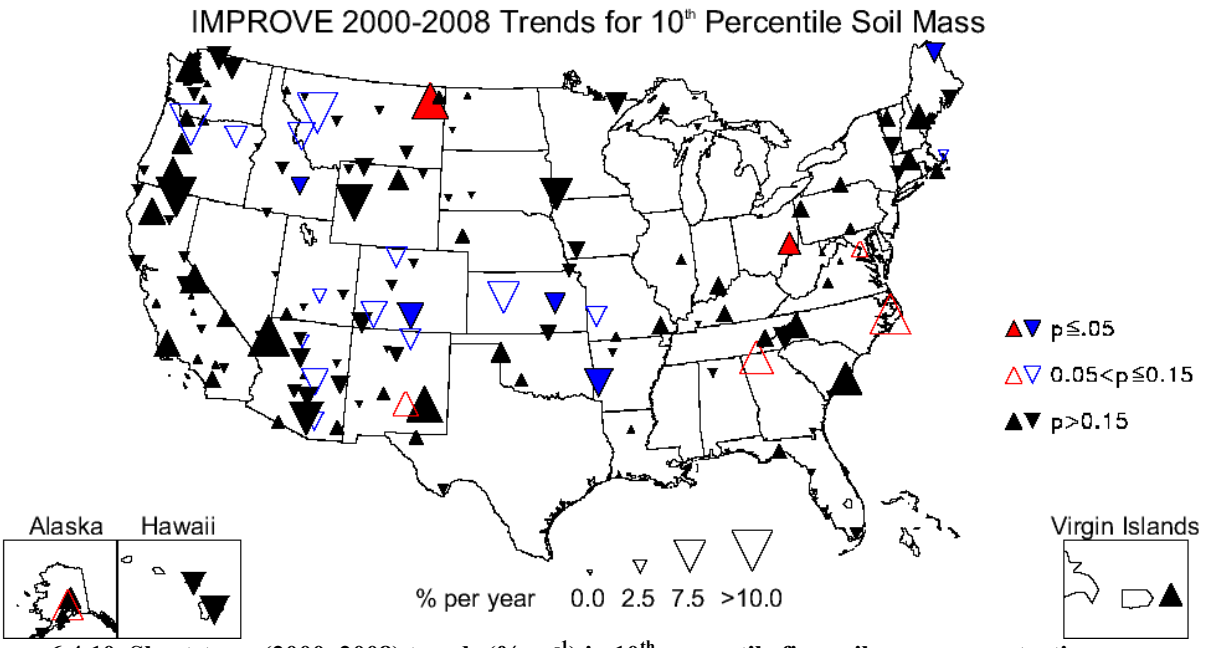

Figure 6.4.10. Short-term (2000–2008) trends (% yr^{-1}) in 10th percentile fine soil mass concentrations.

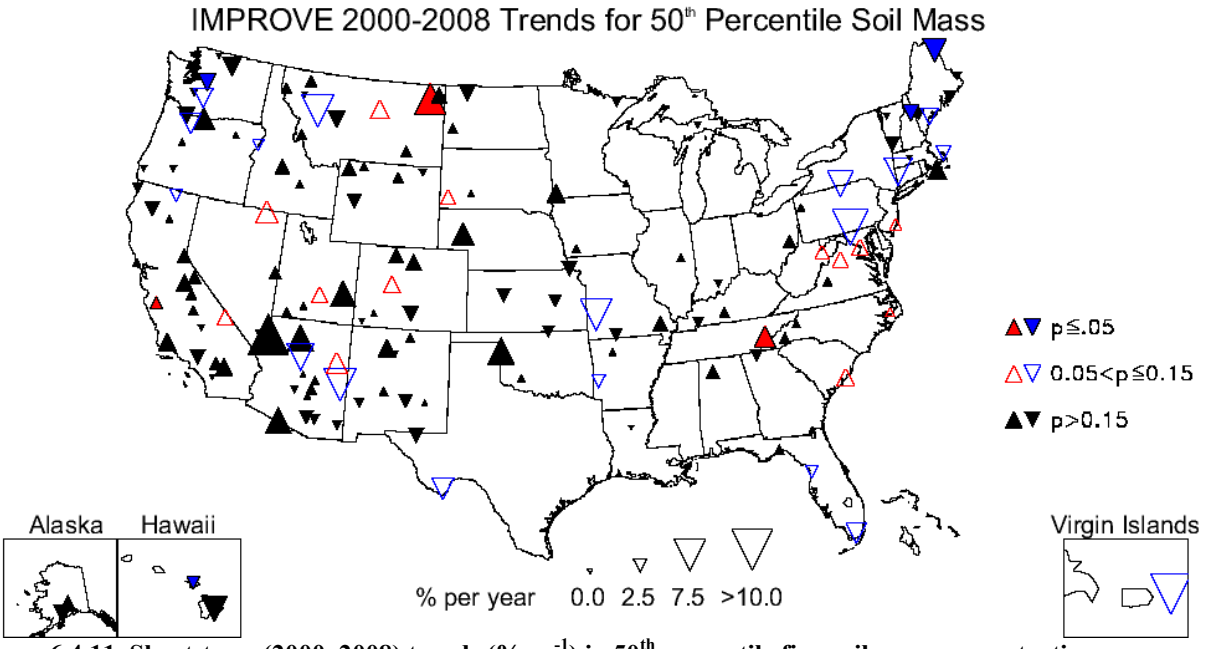

Figure 6.4.11. Short-term (2000–2008) trends (% yr^{-1}) in 50th percentile fine soil mass concentrations.

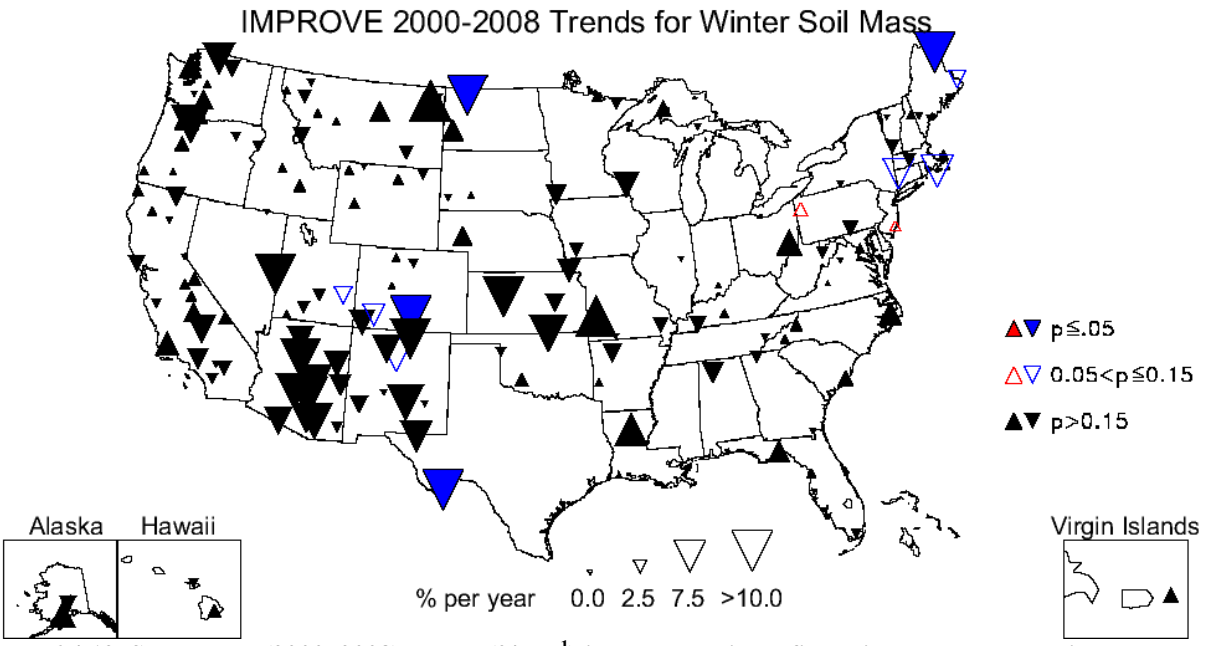

Figure 6.4.12. Short-term (2000–2008) trends (% yr^{-1}) in average winter fine soil mass concentrations.

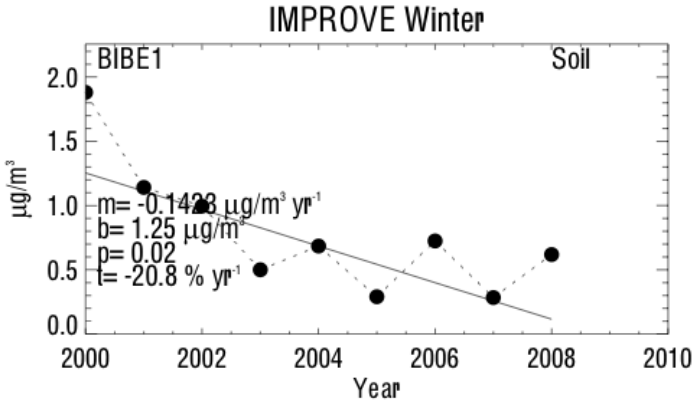

Figure 6.4.13. Average winter fine soil mass concentrations (µg m^{-3}) for Big Bend, Texas (BIBE1). Regression results, including Theil slope (m, µg m^{-3} yr^{-1}), intercept (b, µg m^{-3}), significance (p), and trend (t, % yr^{-1}) are included. The trend line is plotted as a solid line. The intercept corresponds to the initial year of data.

Of the sites with significant short-term trends, 50% or more were positive for the 90th percentile and summer and fall seasons. Several sites in the western United States corresponded to positive 90th percentile trends (Figure 6.4.14), while many sites in the northeastern United States were associated with negative trends. The map showing short-term fall soil trends is presented in Figure 6.4.15. Many sites at central latitudes were associated with positive trends. The largest positive fall trend was associated with Zion Canyon, Utah (ZICA1, 20.8% yr^{-1}). The timeline for fall soil concentrations at ZICA1 is shown in Figure 6.4.16 and demonstrates that soil concentrations increased steadily until 2007, when the concentrations dropped. In contrast, the largest decreasing trend occurred at Mesa Verde, Colorado (MEVE1, -8.6% yr^{-1}). An example of the mean fall soil concentrations at MEVE1 is given in Figure 6.4.17. While the fall soil concentrations at ZICA1 and MEVE1 were similar in magnitude, they displayed very different temporal patterns.

As was stated at the beginning of this section, trends in soil concentrations should be interpreted with some caution, and the trend analyses suggested that only a very few sites were associated with statistically significant trends (11–18 sites for long-term and 12–38 sites for short-term trends, depending on parameter). However, trend results at these sites suggested interesting patterns that should be investigated in further detail.

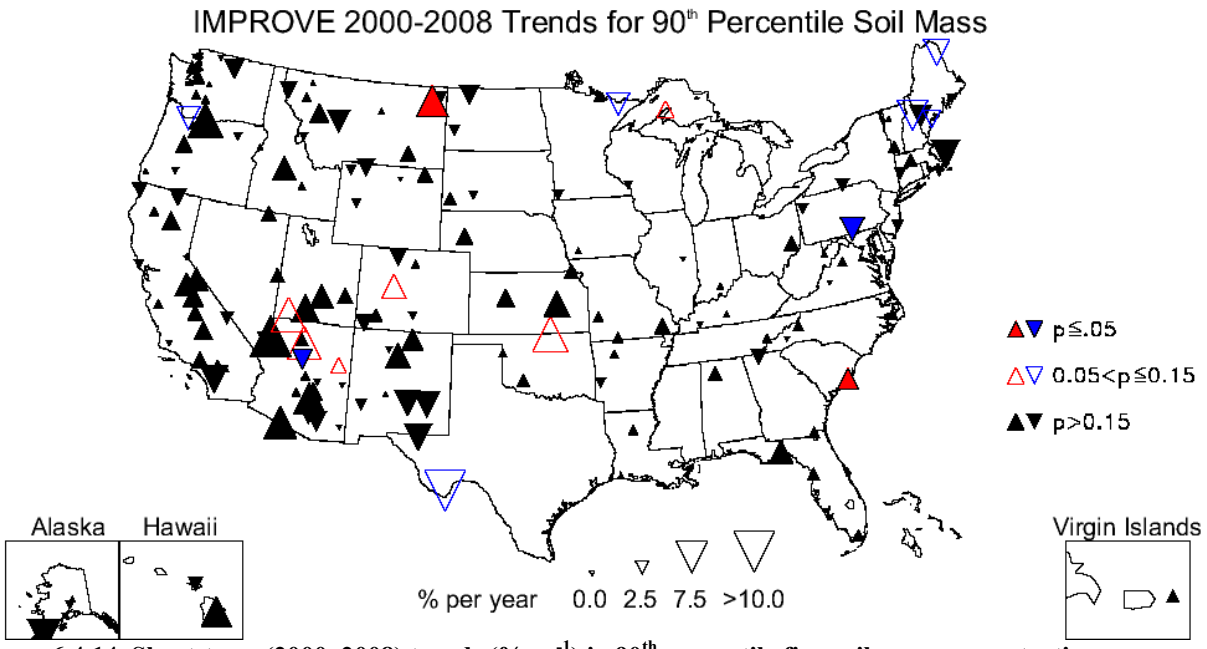

Figure 6.4.14. Short-term (2000–2008) trends (% yr^{-1}) in 90th percentile fine soil mass concentrations.

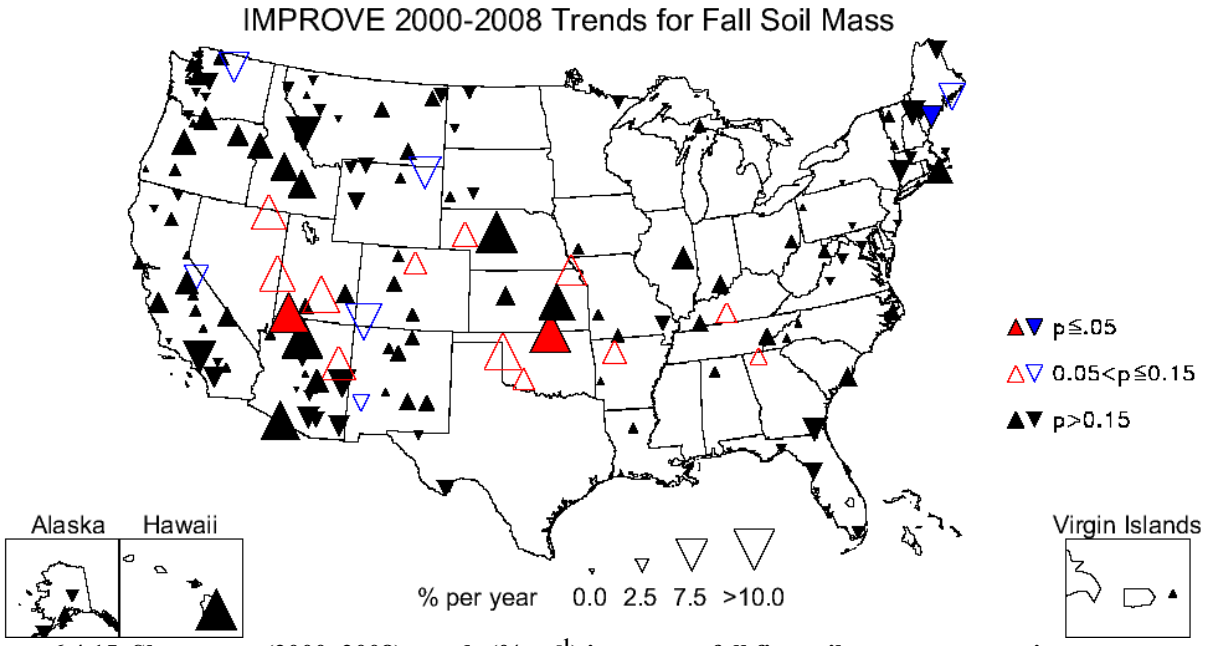

Figure 6.4.15. Short-term (2000–2008) trends (% yr^{-1}) in average fall fine soil mass concentrations.

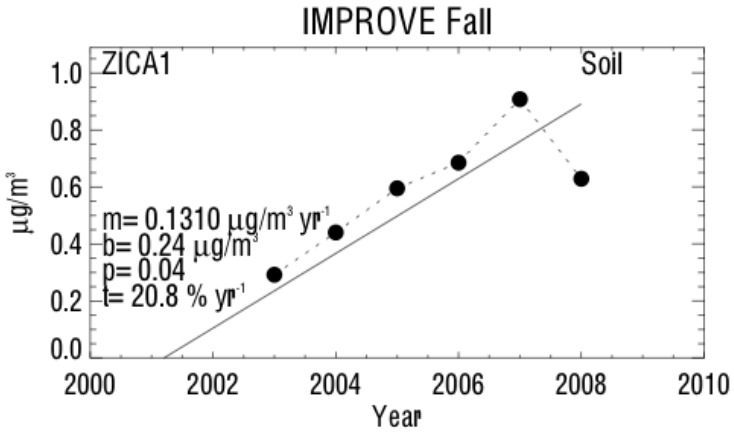

Figure 6.4.16. Average fall fine soil mass concentrations (µg m^{-3}) for Zion Canyon, Utah (ZICA1). Regression results, including Theil slope (m, µg m^{-3} yr^{-1}), intercept (b, µg m^{-3}), significance (p), and trend (t, % yr^{-1}) are included. The trend line is plotted as a solid line. The intercept corresponds to the initial year of data.

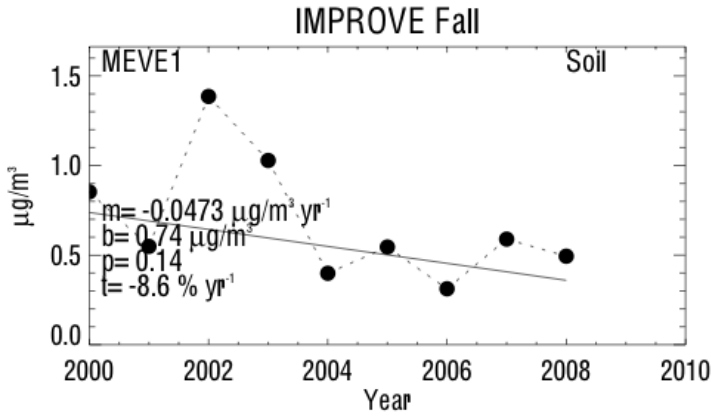

Figure 6.4.17. Fall fine soil mass concentrations (µg m^{-3}) for Mesa Verde, Colorado (MEVE1). Regression results, including Theil slope (m, µg m^{-3} yr^{-1}), intercept (b, µg m^{-3}), significance (p), and trend (t, % yr^{-1}) are included. The trend line is plotted as a solid line. The intercept corresponds to the initial year of data.

6.5 GRAVIMETRIC $PM_{2.5}$ FINE MASS TRENDS

Given the previous discussions, we might have some expectation of the trends in $PM_{2.5}$ fine mass (FM) since it is composed of the species presented in previous sections. However, inferring FM trends based on the trends of other species is complicated because of the difference in the behavior and seasonality of a specific species in relation to each other. In addition, the significance level of trends at a given site differs for each species and for FM trends, complicating comparisons of trends at a specific location. Due to sampling artifacts like those discussed in Chapter 8, FM does not equal the simple sum of all species. We did not discuss all of the species that compose fine mass, nor do we attempt to comment on the behavior of missing mass, both of which could impact the behavior of FM. However, when possible, we comment on an FM trend based on the behavior of trends of other species, including comparisons of timelines of data.

The number of sites with statistically significant long-term FM trends ranged from 33 (spring, summer, 90th percentile) to 49 (10th percentile), depending on parameter. The 10th percentile and winter long-term FM trend results were associated with a large number of sites with significantly decreasing trends. Trends for the 10th percentile for individual sites are shown in Figure 6.5.1. The magnitudes of trends were fairly similar across the United States, although sites in the southeastern United States had less-negative trends, similar to the sulfate ion and total carbon 10th percentile maps (Figures 6.1.1 and 6.3.1, respectively). No sites were associated with positive 10th percentile trends. The largest negative 10th percentile trend occurred at Craters of the Moon, Idaho (CRMO1, -6.1% yr^{-1}), and the least negative trend occurred at Chassahowitzka, Florida (CHAS1, -1.0% yr^{-1}). A timeline of 10th percentile FM concentrations at CRMO1 is shown in Figure 6.5.2. Concentrations decreased steadily until 2004, after which they flattened. Winter trends were larger in magnitude (more negative) at most sites compared to 10th percentile trends, and no sites were associated with positive trends (Figure 6.5.3). Recall that fine mass monthly mean concentrations (2005–2008) were at a minimum during winter months for many regions in the United States (Figure 4.7.1). The negative winter trends suggested that the days with the lowest FM concentrations were getting cleaner. The largest long-term, negative winter trend occurred at Mount Rainier, Washington (MORA1, -6.5% yr^{-1}), as did the largest negative winter trend in total carbon (see Section 6.3). The least-negative winter trend occurred at Everglades, Florida (EVER1, -1.0% yr^{-1}).

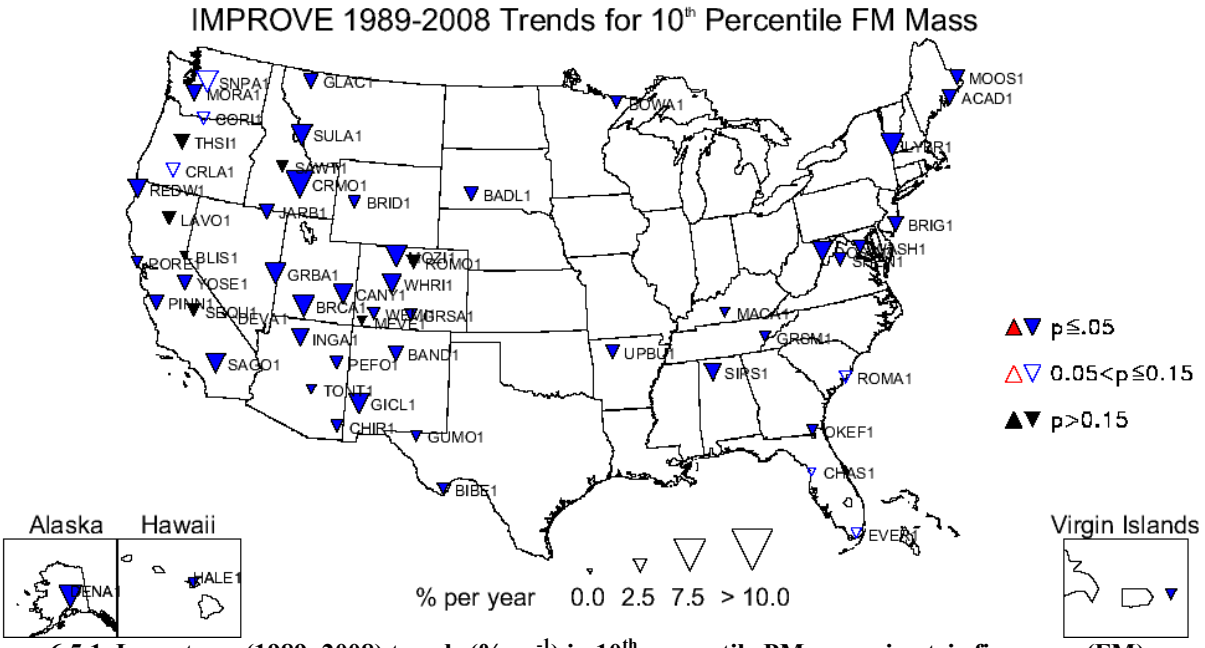

Figure 6.5.1. Long-term (1989–2008) trends (% yr^{-1}) in 10th percentile $PM_{2.5}$ gravimetric fine mass (FM) concentrations.

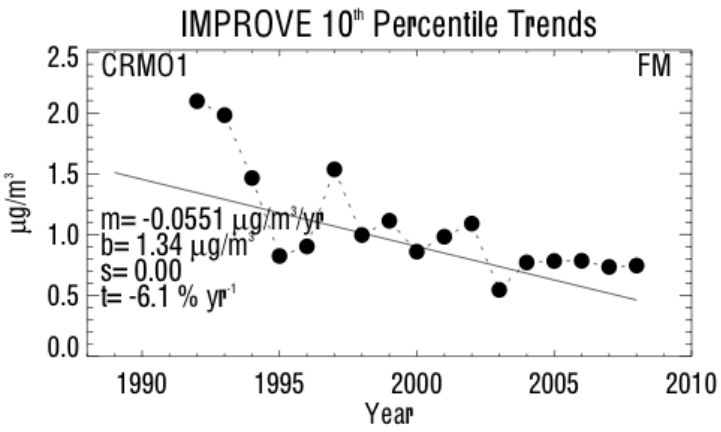

Figure 6.5.2. 10th percentile $PM_{2.5}$ gravimetric fine mass (FM) concentrations (µg m^{-3}) for Craters of the Moon, Idaho (CRMO1). Regression results, including Theil slope (m, µg m^{-3} yr^{-1}), intercept (b, µg m^{-3}), significance (s), and trend (t, % yr^{-1}) are included. The trend line is plotted as a solid line. The intercept corresponds to the initial year of data.

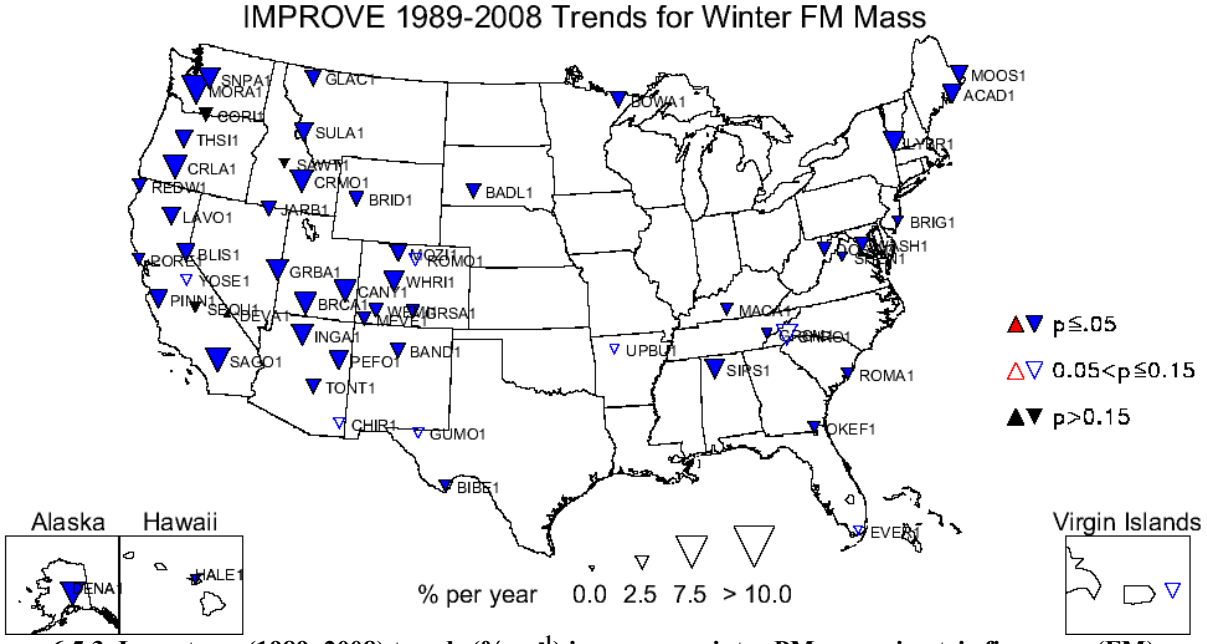

Figure 6.5.3. Long-term (1989–2008) trends (% yr^{-1}) in average winter $PM_{2.5}$ gravimetric fine mass (FM) concentrations.

Although there were fewer sites with significant 90th percentile, long-term FM trends compared to the 10th percentile trends (see Table 6.1), only 25 (out of 48) sites were associated with statistically significant trends in the 90th percentile FM concentrations. In general, the magnitude of long-term, 90th percentile, FM trends at many sites was less negative than the 10th percentile trends (See Figure 6.5.4). Several sites in the southwestern United States that were associated with significant 10th percentile trends did not have significant 90th percentile trends. The largest negative 90th percentile, long-term FM trend occurred at Mount Rainier, Washington (MORA1, -3.9% yr^{-1}), and the only positive 90th percentile trend occurred at Sawtooth, Idaho (SAWT1, 3.3% yr^{-1}). An example of increasing 90th percentile FM concentrations at SAWT1 is

shown in Figure 6.5.5. The high concentration in 2007 was most likely associated with biomass burning emissions as summer fine mass and total carbon concentrations were also high then. SAWT1 was one of the four sites with positive trends during summer (Sula Peak, Montana, SULA1, 5.0% yr^{-1}; Sawtooth, Idaho, SAWT1, 4.8% yr^{-1}; Death Valley, California, DEVA1, 1.3% yr^{-1}; and Bridger, Wyoming, BRID1, 1.10% yr^{-1}) (se Figure 6.5.6). The largest negative FM summer trend occurred at Great Gulf, New Hampshire (GRGU1, -4.10% yr^{-1}). Fine mass trends in the summer in the eastern United States were decreasing at most sites. Many western U.S. sites were associated with either low negative summer trends or trends that were statistically insignificant. Recall that most regions in the United States were associated with maximum FM monthly mean concentrations in the summer months (see Figure 4.7.1), probably due to total carbon concentrations; trend results suggested that these summer FM concentrations appeared to be decreasing less over time compared to other seasons.

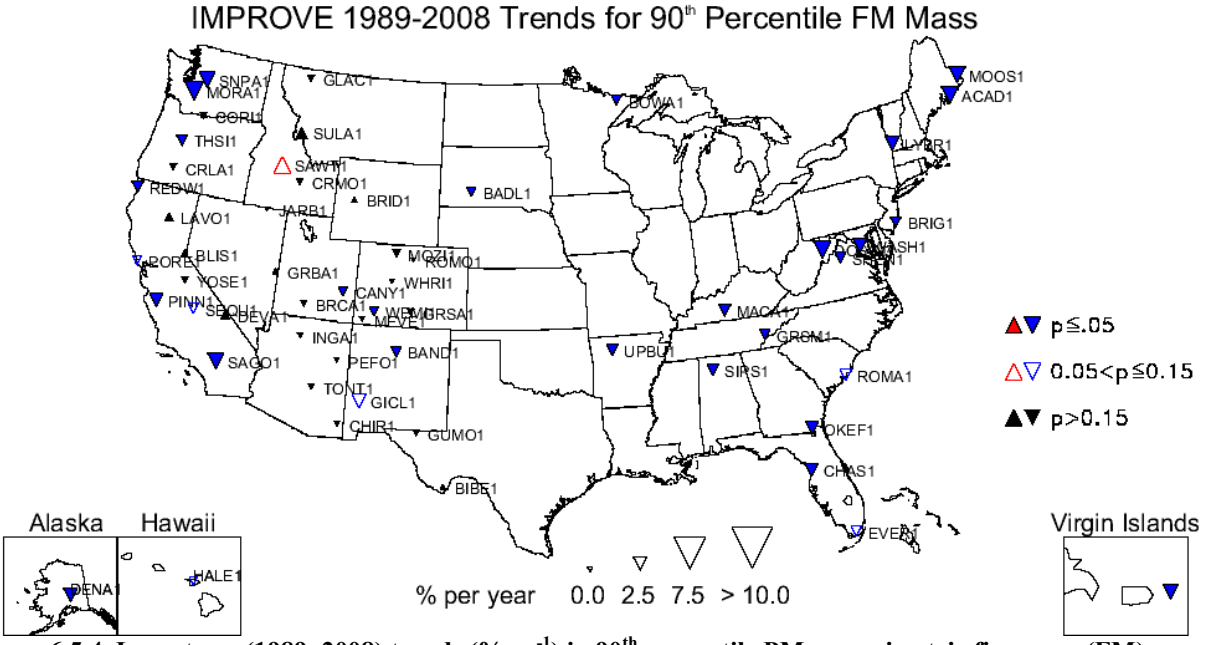

Figure 6.5.4. Long-term (1989–2008) trends (% yr^{-1}) in 90th percentile $PM_{2.5}$ gravimetric fine mass (FM) concentrations.

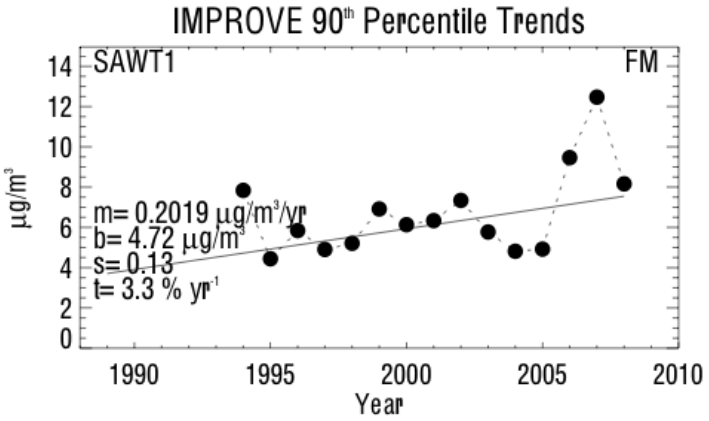

Figure 6.5.5. 90th percentile $PM_{2.5}$ gravimetric fine mass (FM) concentrations (µg m^{-3}) for Sawtooth, Idaho (SAWT1). Regression results, including Theil slope (m, µg m^{-3} yr^{-1}), intercept (b, µg m^{-3}), significance (s), and trend (t, % yr^{-1}) are included. The trend line is plotted as a solid line. The intercept corresponds to the initial year of data.

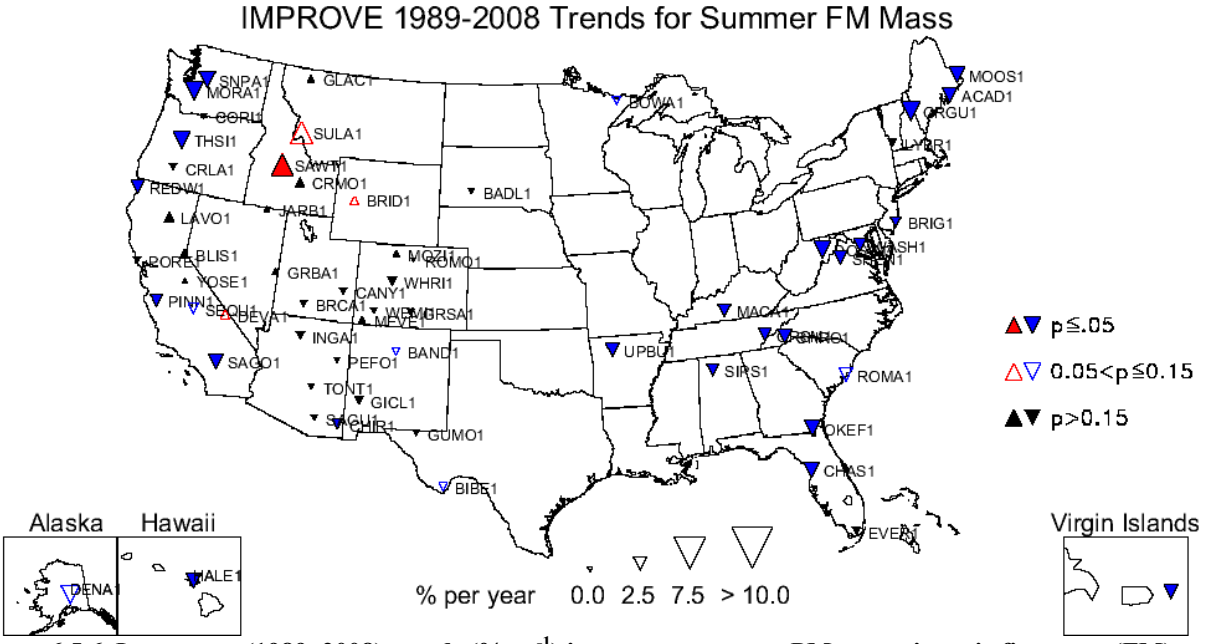

Figure 6.5.6. Long-term (1989–2008) trends (% yr^{-1}) in average summer $PM_{2.5}$ gravimetric fine mass (FM) concentrations.

The number of sites with statistically significant short-term FM trends ranged from 36 in spring to 60 for 50th percentile concentrations (out of ~153, see Table 6.2). Only two sites corresponded to positive short-term FM trends for both the summer season and the 90th percentile (the lowest for all parameters). A map of the 90th percentile, short-term trends is shown in Figure 6.5.7. The largest negative 90th percentile trend was associated with Tuxedni, Alaska (TUXE1, -7.7%), and the largest positive trend occurred at Hawaii Volcanoes (HAVO1, 12.8%). A timeline of the 90th percentile FM concentrations at HAVO1 is shown in Figure 6.5.8. High concentrations in 2008 were mostly likely associated with volcanic eruptions, as the 90th percentile concentrations of sulfate ion displayed similar behavior (Figure 6.1.10). The other

positive trend in the 90th percentile FM concentrations corresponded to Capitol Reef, Utah (CAPI1, 2.0% yr^{-1}).

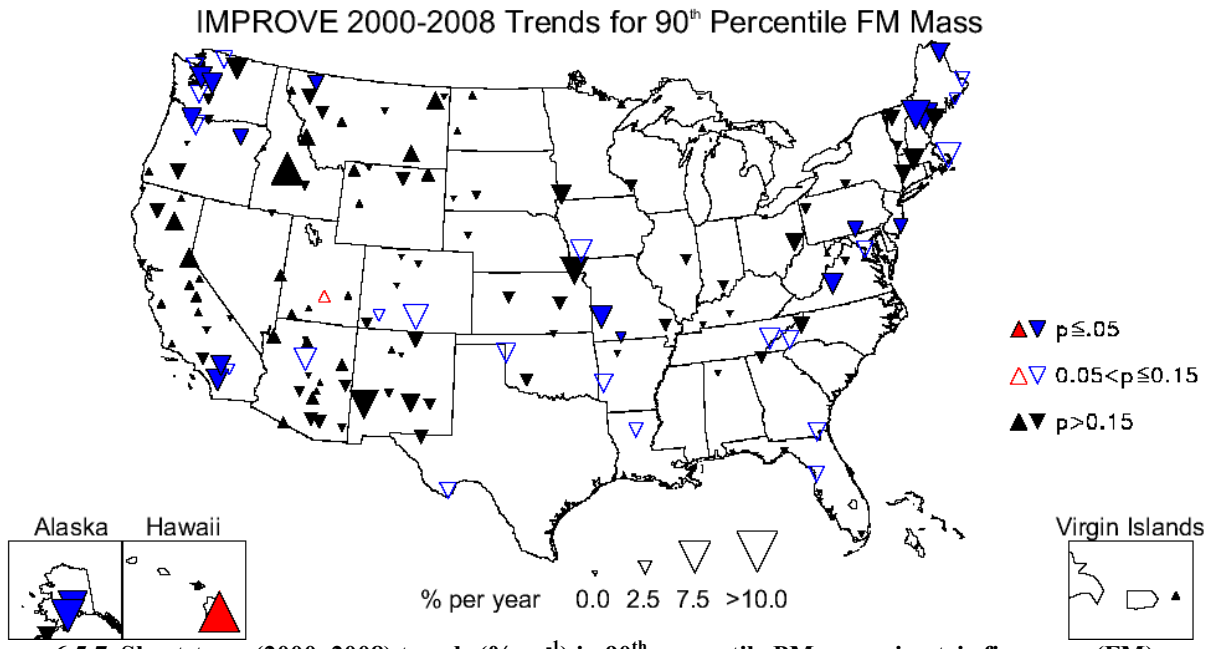

Figure 6.5.7. Short-term (2000–2008) trends (% yr^{-1}) in 90th percentile $PM_{2.5}$ gravimetric fine mass (FM) concentrations.

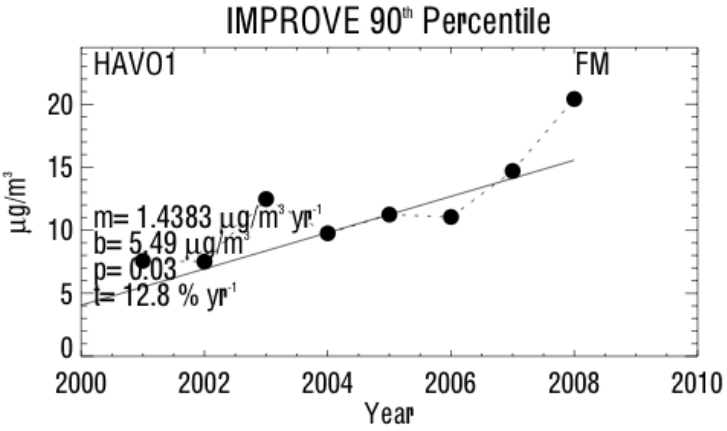

Figure 6.5.8. 90th percentile $PM_{2.5}$ gravimetric fine mass (FM) concentrations (µg m^{-3}) for Hawaii Volcanoes (HAVO1). Regression results, including Theil slope (m, µg m^{-3} yr^{-1}), intercept (b, µg m^{-3}), significance (p), and trend (t, % yr^{-1}) are included. The trend line is plotted as a solid line. The intercept corresponds to the initial year of data.

Many western U.S. sites were associated with relatively large negative short-term winter FM trends (Figure 6.5.9). The largest negative winter trend occurred at Starkey, Oregon (STAR1, -14.6% yr^{-1}), similar to total carbon. Sites in southern California were also associated with relatively large negative trends. The timeline showing steadily decreasing FM winter concentrations at STAR1 is shown in Figure 6.5.10. Winter concentrations dropped from 6.3 µg m^{-3} to 1.3 µg m^{-3} from 2001 to 2008. Four sites corresponded to positive, short-term, winter FM

trends, with the largest at Trapper Creek, Alaska (TRCR1, 9.1% yr^{-1}). An example of the increasing FM winter concentration at TRCR1 is shown in Figure 6.5.11. Notice the lowest concentrations at this site compared to the STAR1 site. The highest winter FM concentration at TRCR1 was comparable to the lowest winter FM concentration at STAR1.

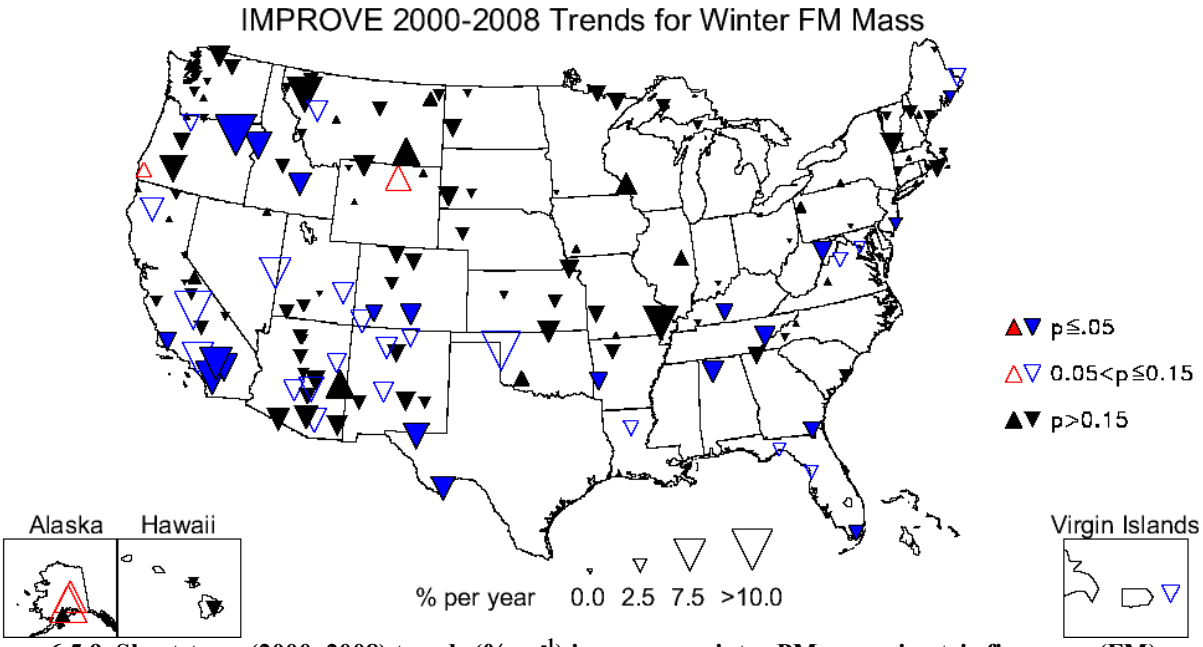

Figure 6.5.9. Short-term (2000–2008) trends (% yr^{-1}) in average winter $PM_{2.5}$ gravimetric fine mass (FM) concentrations.

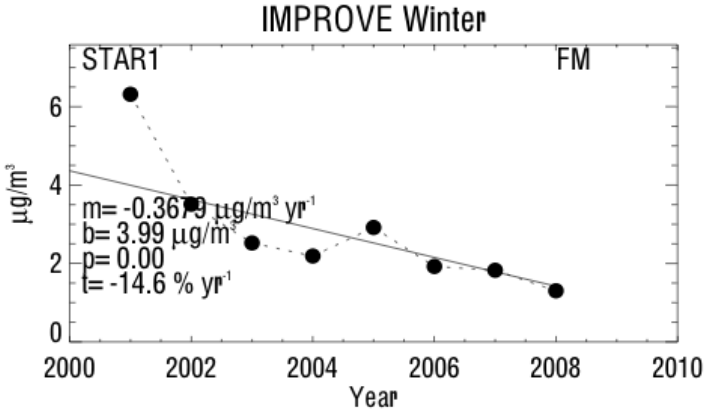

Figure 6.5.10. Average winter $PM_{2.5}$ gravimetric fine mass (FM) concentrations (µg m^{-3}) for Starkey, Oregon (STAR1). Regression results, including Theil slope (m, µg m^{-3} yr^{-1}), intercept (b, µg m^{-3}), significance (p), and trend (t, % yr^{-1}) are included. The trend line is plotted as a solid line. The intercept corresponds to the initial year of data.

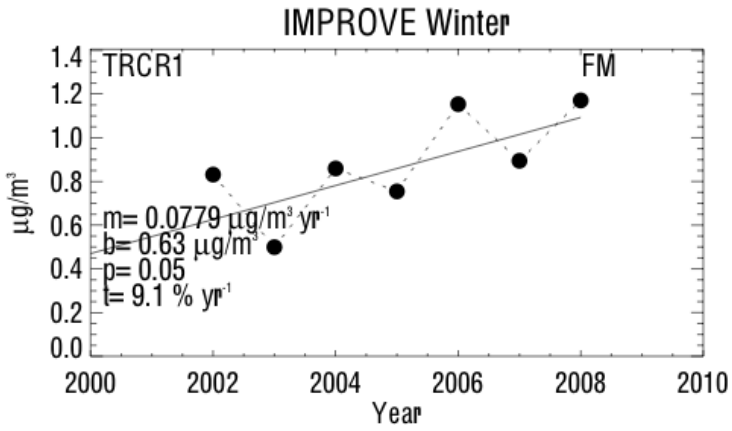

Figure 6.5.11. Average winter $PM_{2.5}$ gravimetric fine mass (FM) concentrations (µg m^{-3}) for Trapper Creek, Alaska (TRCR1). Regression results, including Theil slope (m, µg m^{-3} yr^{-1}), intercept (b, µg m^{-3}), significance (p), and trend (t, % yr^{-1}) are included. The trend line is plotted as a solid line. The intercept corresponds to the initial year of data.

The largest number of sites with significant positive short-term trends corresponded to the fall season. A map of the fall FM trends is shown in Figure 6.5.12. Most of the sites with positive, short-term fall trends were located in the western United States and in Alaska and Hawaii. No eastern U.S. sites were associated with positive fall trends. The largest positive fall trend occurred at Zion Canyon, Utah (ZICA1, 12.3% yr^{-1}), and the largest decreasing fall trend occurred at Moosehorn, Maine (MOOS1, -6.5% yr^{-1}). A timeline showing the steady increase in fall FM concentrations at ZICA1 is shown in Figure 6.5.13. The fine soil trend in fall at ZICA1 was also positive (see Figure 6.4.16 and discussion in Section 6.4). The only species to be associated with positive, short-term, fall trends in the western United States were sulfate (in Alaska, Hawaii, and Arizona), soil (several western U.S. sites), and total carbon at a couple of western sites; therefore the fall positive trends in FM in the western United States were most likely driven by different species, depending on the site.

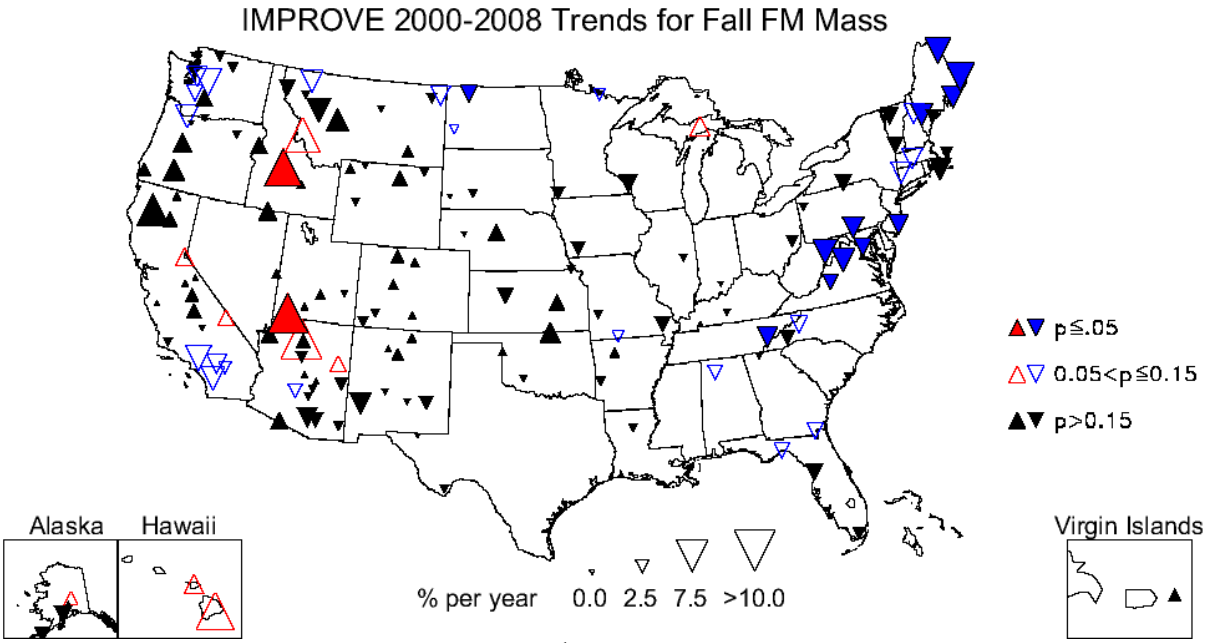

Figure 6.5.12. Short-term (2000–2008) trends (% yr^{-1}) in average fall $PM_{2.5}$ gravimetric fine mass (FM) concentrations.

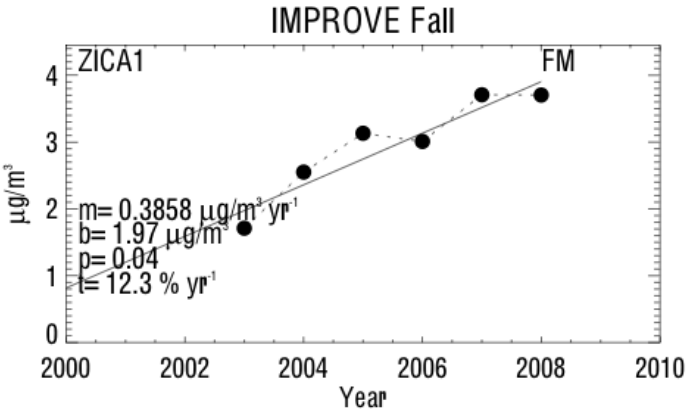

Figure 6.5.13. Average fall $PM_{2.5}$ gravimetric fine mass (FM) concentrations (μg m^{-3}) for Zion Canyon, Utah (ZICA1). Regression results, including Theil slope (m, μg m^{-3} yr^{-1}), intercept (b, μg m^{-3}), significance (p), and trend (t, % yr^{-1}) are included. The trend line is plotted as a solid line. The intercept corresponds to the initial year of data.

6.6 COARSE MASS TRENDS

The 10th percentile and winter, long-term CM trends were generally the most negative of the parameters. The map in Figure 6.6.1 shows sites with largely negative long-term CM trends, especially in the western United States, including Denali, Alaska (DENA1). A timeline of 10th percentile CM concentrations at Mount Zirkel, Colorado (MOZI1), provides an example of a site with one of the largest negative 10th percentile trends (-20.5% yr^{-1}, Figure 6.6.2). The CM 10th percentile concentration was near 1.4 μg m^{-3} in 1995 and decreased to 0.17 μg m^{-3} in 2008. The least negative 10th percentile, long-term trend occurred at Badlands, South Dakota (BADL1, -2.2% yr^{-1}).

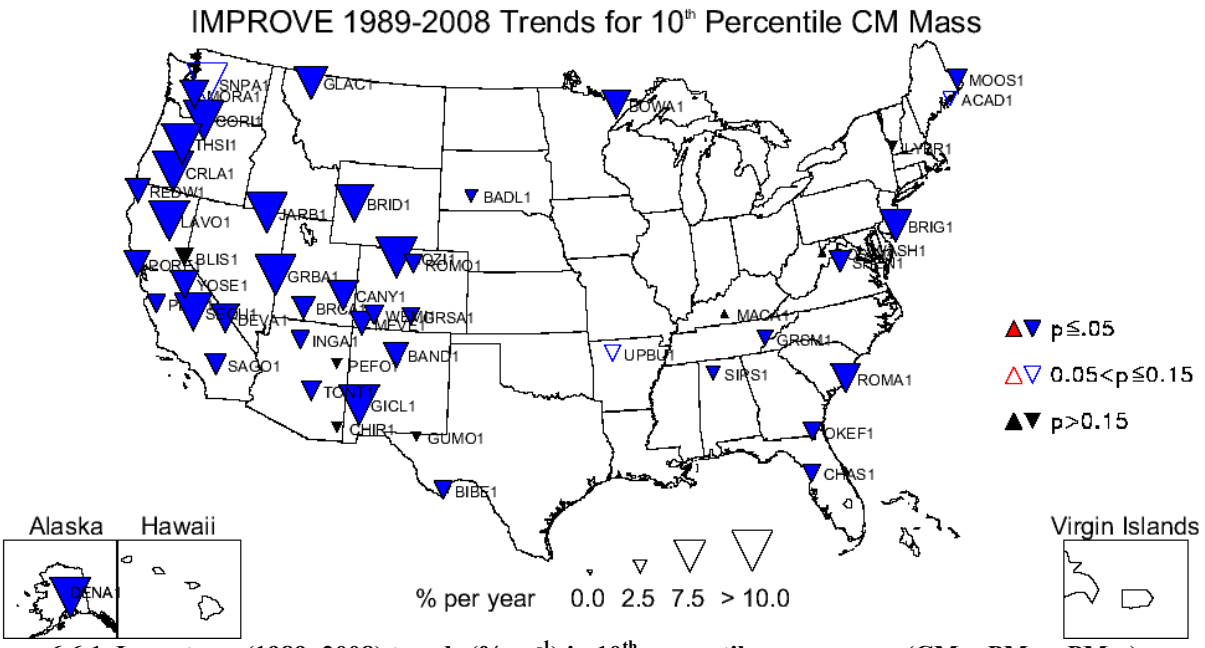

Figure 6.6.1. Long-term (1989–2008) trends (% yr^{-1}) in 10th percentile coarse mass (CM = PM_{10} - $PM_{2.5}$) concentrations.

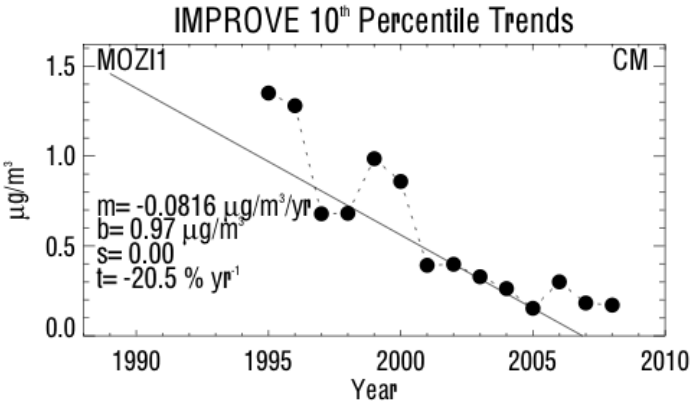

Figure 6.6.2. 10th percentile coarse mass (CM = PM_{10} - $PM_{2.5}$) concentrations (µg m^{-3}) for Mount Zirkel, Colorado (MOZI1). Regression results, including Theil slope (m, µg m^{-3} yr^{-1}), intercept (b, µg m^{-3}), significance (s), and trend (t, % yr^{-1}) are included. The trend line is plotted as a solid line. The intercept corresponds to the initial year of data.

The map of long-term winter trends in CM was very similar to the 10th percentile map (Figure 6.6.3). This similarity was not surprising given that the lowest CM concentration occurred during winter months for regions around the United States (Figure 4.8.1). The largest negative winter trend corresponded to the site at Snoqualmie Pass, Washington (SNPA1, -18.7% yr^{-1}), and Figure 6.6.4 shows the strong decrease in CM over time at that site. Winter CM concentrations decreased considerably in 2001 at SNPA and remained fairly steady through 2008. The least negative, winter, CM long-term trend occurred at Upper Buffalo, Arkansas (ULBU1, -1.8% yr^{-1}).

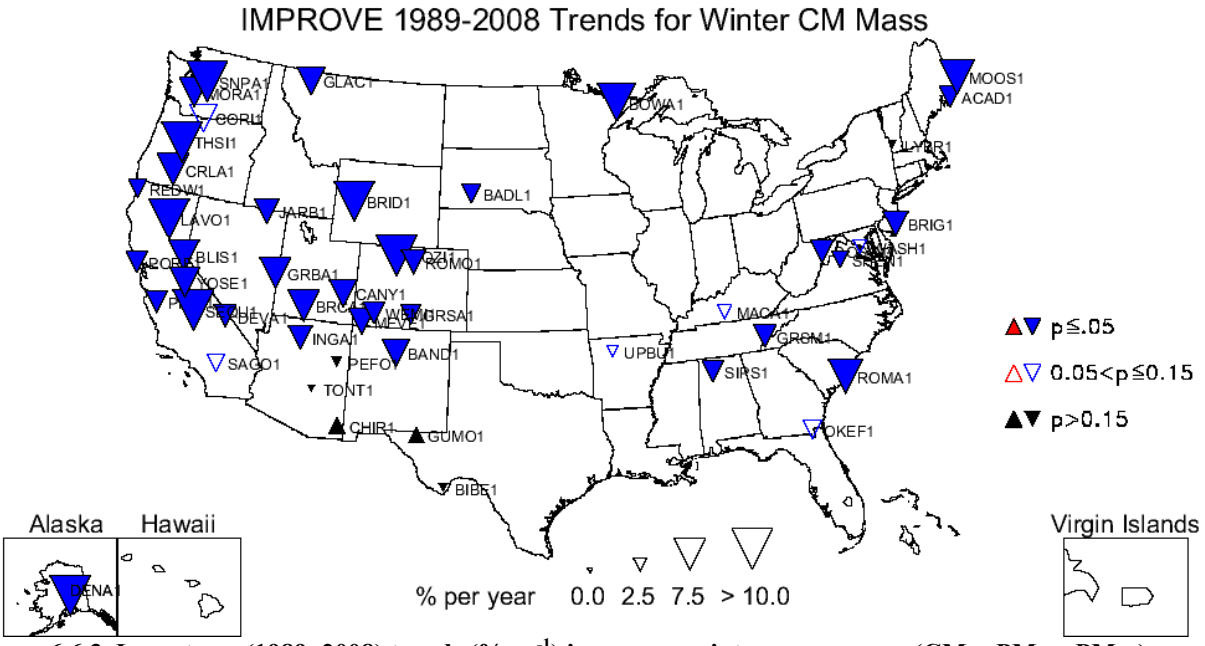

Figure 6.6.3. Long-term (1989–2008) trends (% yr^{-1}) in average winter coarse mass (CM = PM_{10} - $PM_{2.5}$) concentrations.

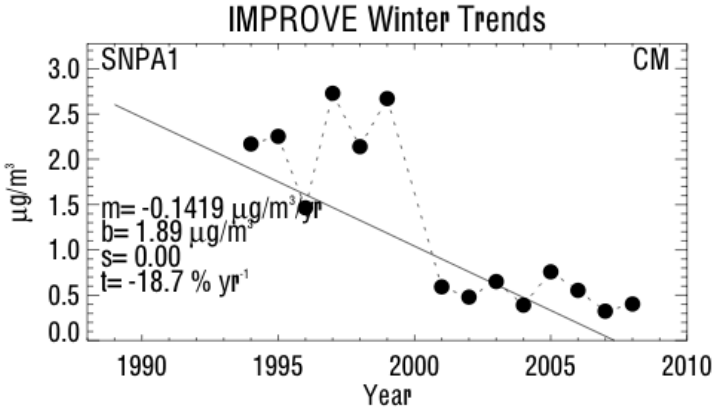

Figure 6.6.4. Average winter coarse mass (CM = PM_{10} - $PM_{2.5}$) concentrations (µg m^{-3}) for Snoqualmie Pass, Washington (SNPA1). Regression results, including Theil slope (m, µg m^{-3} yr^{-1}), intercept (b, µg m^{-3}), significance (s), and trend (t, % yr^{-1}) are included. The trend line is plotted as a solid line. The intercept corresponds to the initial year of data.

The 90th percentile, long-term CM trends corresponded to fewer statistically significant sites compared to the 10th percentile trends (34 versus 42, respectively), especially in the western United States (Figure 6.6.5). In addition, the magnitudes of 90th percentile trends were noticeably lower (less negative) than 10th percentile trends. No sites corresponded to positive 90th percentile CM trends. The largest negative 90th percentile, CM long-term trend occurred at Snoqualmie Pass, Washington (SNPA1, -8.2% yr^{-1}), and the least negative trend corresponded to Yosemite, California (YOSE1, -1.6% yr^{-1}). The timeline of the 90th percentile CM concentrations at YOSE1 is presented in Figure 6.6.6. Concentrations at YOSE1 were slowly decreasing, in contrast to the large decrease in CM concentrations at SNPA1 (see Figure 6.6.7). CM concentrations at SNPA1

were also significantly lower than those at YOSE1. Long-term summer trends in CM at individual sites are shown in Figure 6.6.8. Significant trends were negative at most sites, except at Badlands, South Dakota (BADL1, 2.2% yr^{-1}), and Columbia River Gorge, Washington (CORI1, 8.5% yr^{-1}). Like the previously discussed parameters, the largest negative summer long-term trend occurred at (SNPA1, -7.2% yr^{-1}).

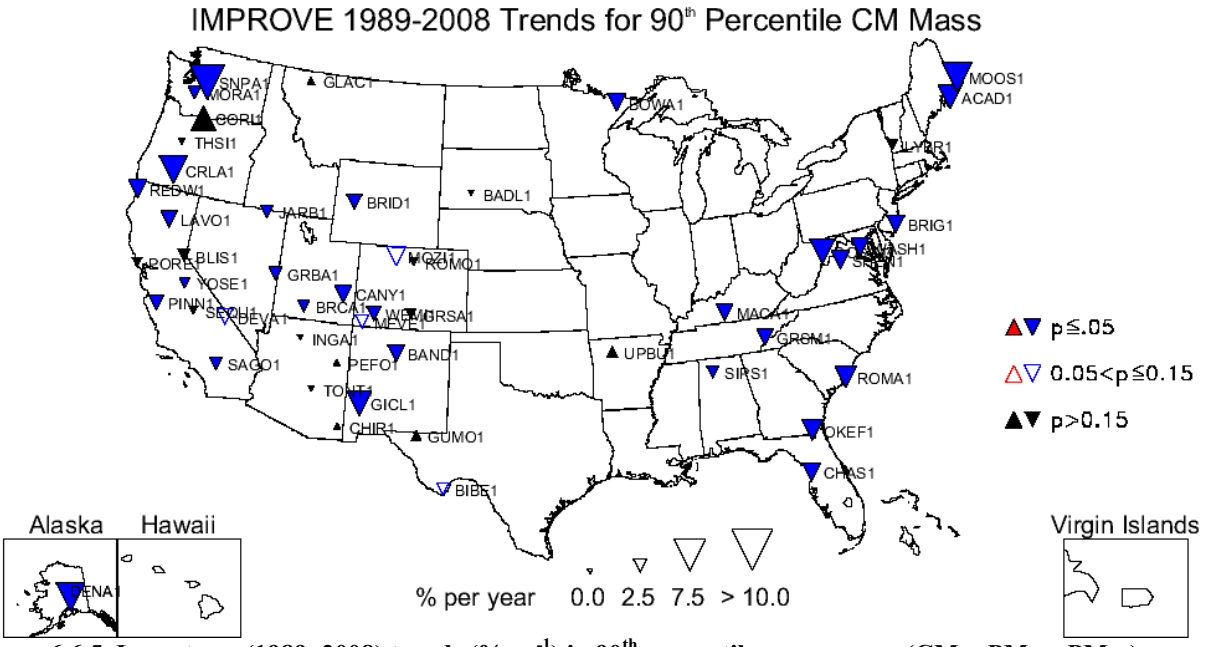

Figure 6.6.5. Long-term (1989–2008) trends (% yr^{-1}) in 90th percentile coarse mass (CM = PM_{10} - $PM_{2.5}$) concentrations.

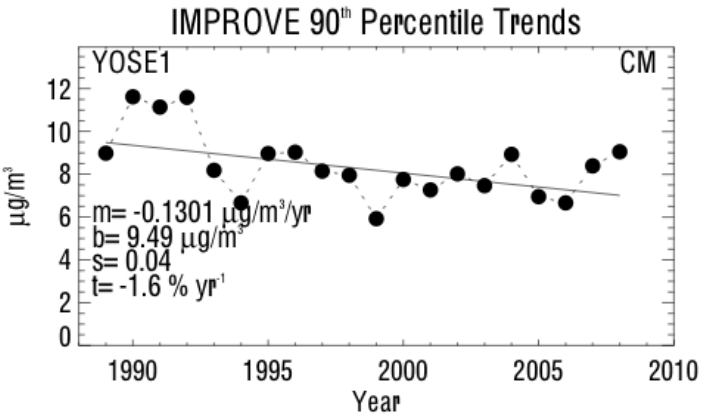

Figure 6.6.6. 90th percentile coarse mass (CM = PM_{10} - $PM_{2.5}$) concentrations (µg m^{-3}) for Yosemite, California (YOSE1). Regression results, including Theil slope (m, µg m^{-3} yr^{-1}), intercept (b, µg m^{-3}), significance (s), and trend (t, % yr^{-1}) are included. The trend line is plotted as a solid line. The intercept corresponds to the initial year of data.

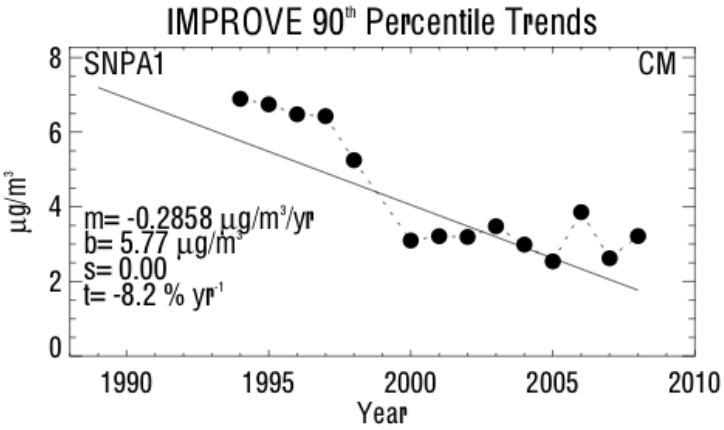

Figure 6.6.7. 90th percentile coarse mass (CM = PM_{10} - $PM_{2.5}$) concentrations (µg m^{-3}) for Snoqualmie Pass, Washington (SNPA1). Regression results, including Theil slope (m, µg m^{-3} yr^{-1}), intercept (b, µg m^{-3}), significance (s), and trend (t, % yr^{-1}) are included. The intercept corresponds to the initial year of data.

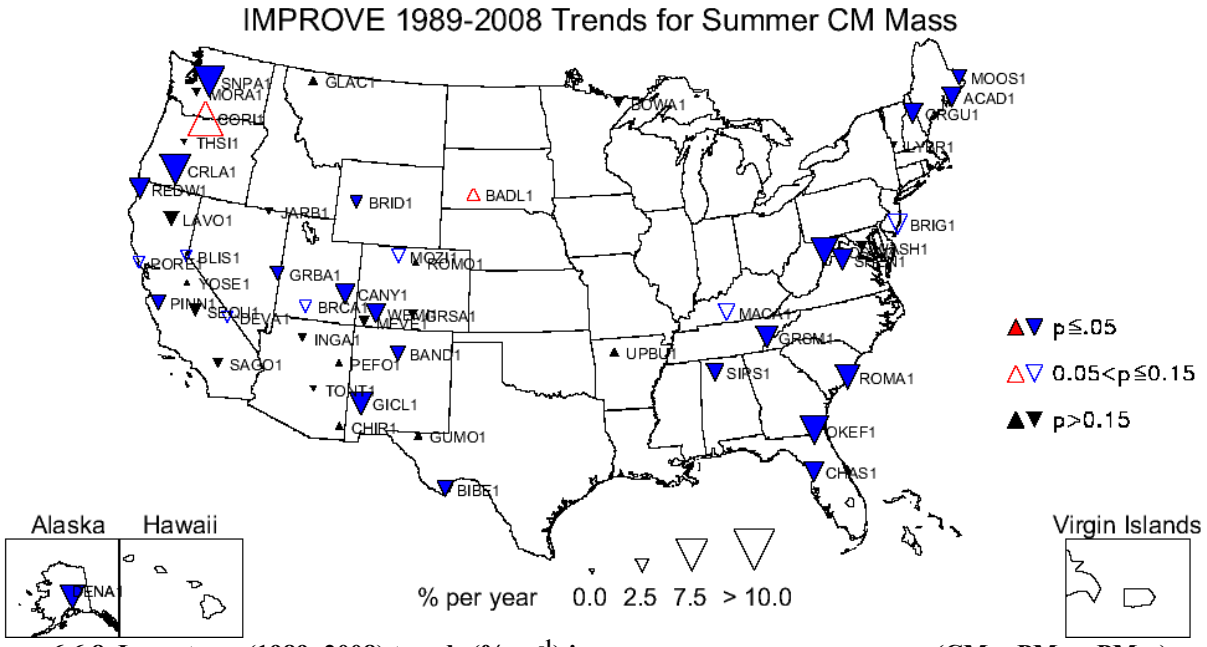

Figure 6.6.8. Long-term (1989–2008) trends (% yr^{-1}) in average summer coarse mass (CM = PM_{10} - $PM_{2.5}$) concentrations.

Of the ~153 sites used to investigate short-term CM trends, sites with significant trends ranged from 25 (fall) to 45 (50th percentile) (see Table 6.2). In addition, many more sites were associated with positive short-term trends compared to long-term CM trends. Short-term trends in the 90th percentile CM concentrations for individual sites are shown in Figure 6.6.9. Unlike the long-term, 90th percentile trends, short-term trends at several sites were positive (10 out of 34 statistically significant trends). The largest 90th percentile negative trend occurred at Monture, Montana (MONT1, -8.8% yr^{-1}), compared to the largest positive trend at Cohutta, Georgia (COHU1, 8.6% yr^{-1}). Decreasing 90th percentile CM concentrations at MONT1 are shown in Figure 6.6.10. High CM concentrations in 2000 decreased and remained steady through 2008. Relatively large negative short-term trends in winter CM concentrations are presented in Figure

6.6.11. Several southwestern sites corresponded to negative trends, compared to increasing trends in Idaho, Montana, Wyoming, and the northeastern United States. The largest negative winter CM trend corresponded to Hoover, California (HOOV1, -18.3% yr^{-1}), and the largest positive winter CM trend corresponded to Sula Peak, Montana (SULA1, 12.7% yr^{-1}). The winter CM concentrations at HOOV1 dropped considerably after 2002, from 4.8 µg m^{-3} to 0.5 µg m^{-3} from 2002 to 2008 (Figure 6.6.12).

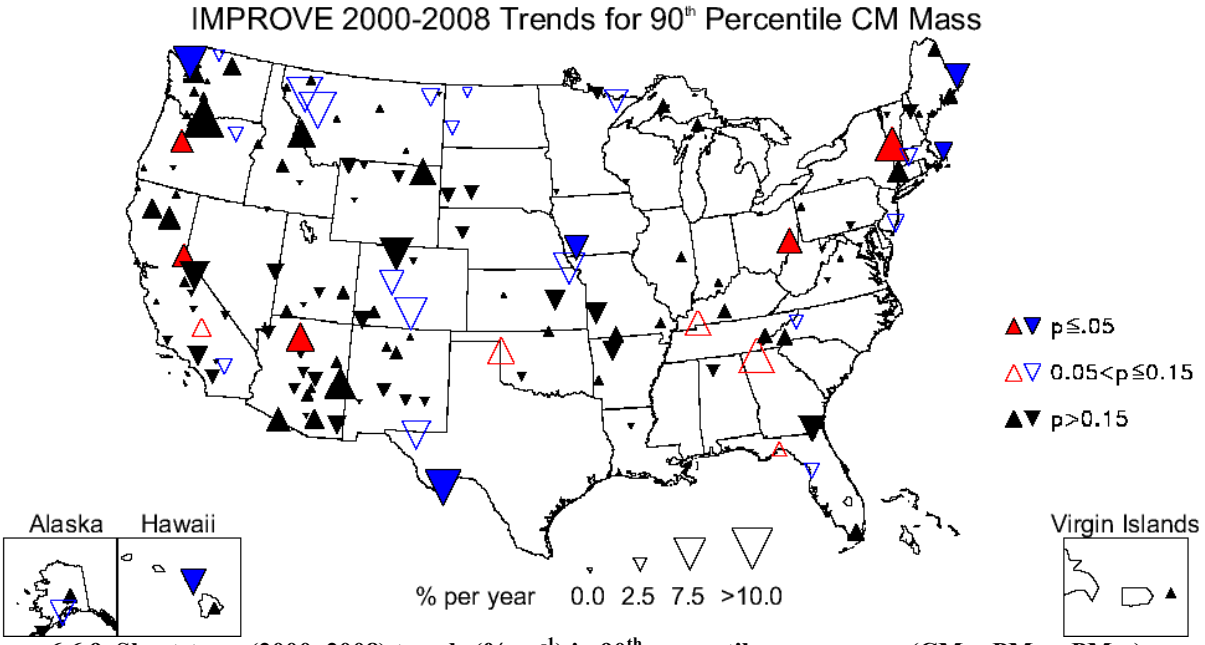

Figure 6.6.9. Short-term (2000–2008) trends (% yr^{-1}) in 90th percentile coarse mass (CM = PM_{10} - $PM_{2.5}$) concentrations.

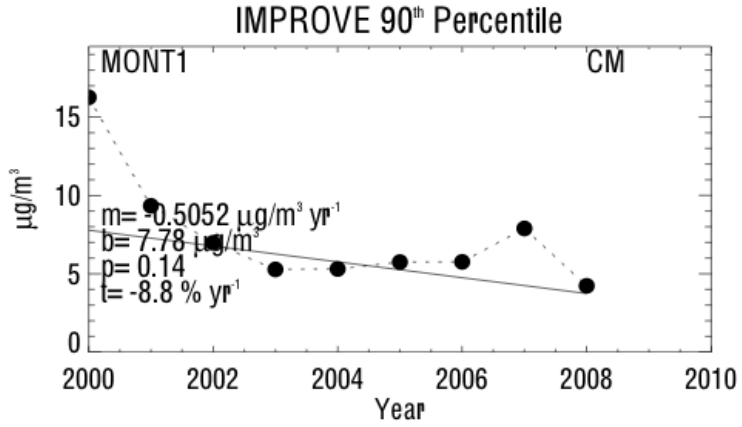

Figure 6.6.10. 90th percentile coarse mass (CM = PM_{10} - $PM_{2.5}$) concentrations (µg m^{-3}) for Monture, Montana (MONT1). Regression results, including Theil slope (m, µg m^{-3} yr^{-1}), intercept (b, µg m^{-3}), significance (p), and trend (t, % yr^{-1}) are included. The trend line is plotted as a solid line. The intercept corresponds to the initial year of data.

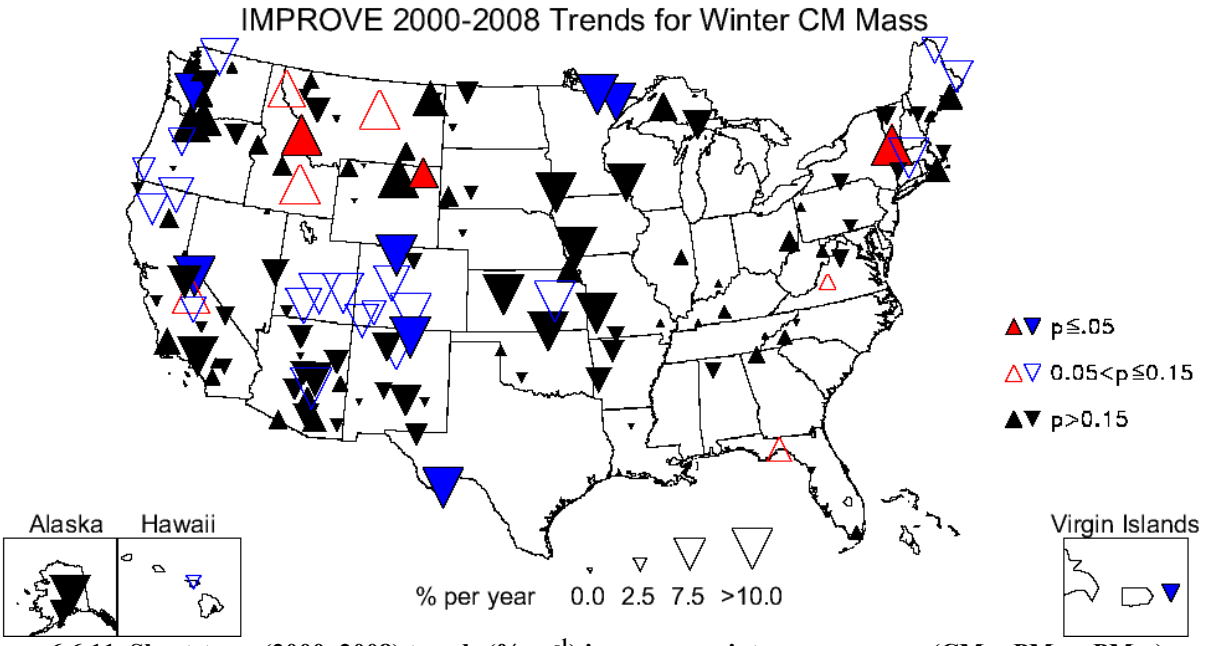

Figure 6.6.11. Short-term (2000–2008) trends (% yr^{-1}) in average winter coarse mass (CM = PM_{10} - $PM_{2.5}$) concentrations.

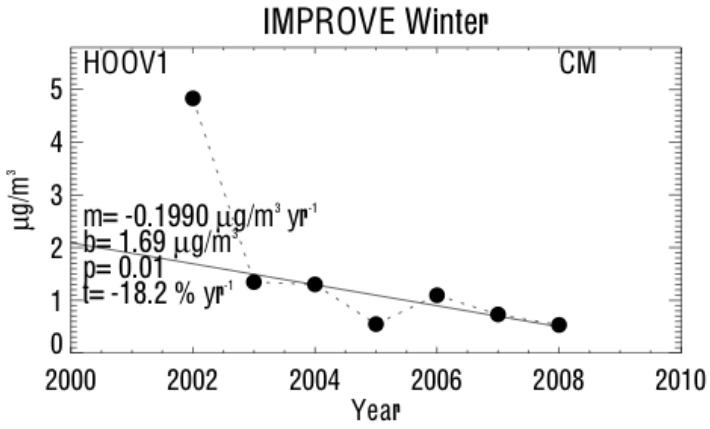

Figure 6.6.12. Average winter coarse mass (CM = PM_{10} - $PM_{2.5}$) concentrations (µg m^{-3}) for Hoover, California (HOOV1). Regression results, including Theil slope (m, µg m^{-3} yr^{-1}), intercept (b, µg m^{-3}), significance (p), and trend (t, % yr^{-1}) are included. The trend line is plotted as a solid line. The intercept corresponds to the initial year of data.

The 50th percentile and summer season were associated with the highest number of sites with significant short-term positive trends (Table 6.2). The 50th percentile trends included 19 sites with positive trends, several of which were in the eastern United States (Figure 6.6.13). The largest positive, 50th percentile trend occurred at Cohutta, Georgia (COHU1, 11.6% yr^{-1}), compared to the largest negative 50th percentile trend at Flathead, Montana (FLAT1, -16.3% yr^{-1}). Individual summer trends for CM are shown in Figure 6.1.14. Most eastern sites were associated with positive summer trends, as well as sites in the southwestern and northwestern United States. Of the 44 sites with significant summer trends, 27 were associated with positive trends. The largest positive short-term, summer trend occurred at Indian Gardens, Arizona

(INGA1, 12.9% yr^{-1}), and the largest negative trend occurred at Olympic, Washington (OLYM1, -9.6% yr^{-1}). Coarse mass summer concentrations at INGA1 (Figure 6.6.15) were much larger and increased steadily compared to the steadily decreasing low CM concentrations in summer at OLYM1 (Figure 6.1.16).

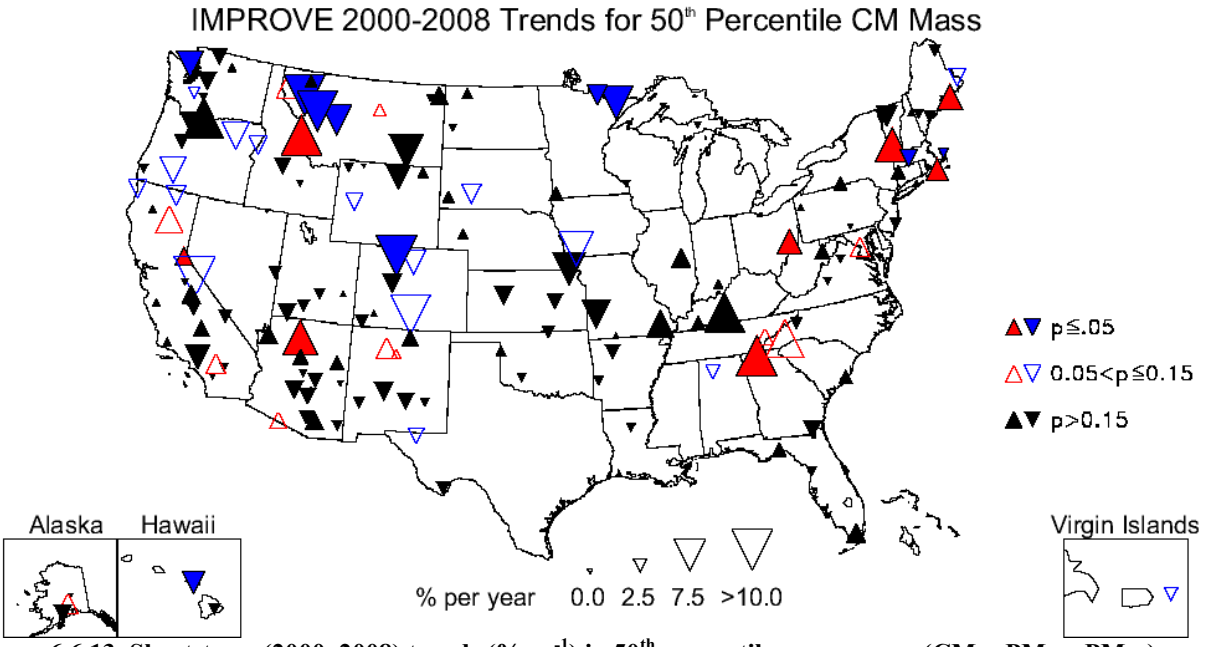

Figure 6.6.13. Short-term (2000–2008) trends (% yr^{-1}) in 50th percentile coarse mass (CM = PM_{10} - $PM_{2.5}$) concentrations.

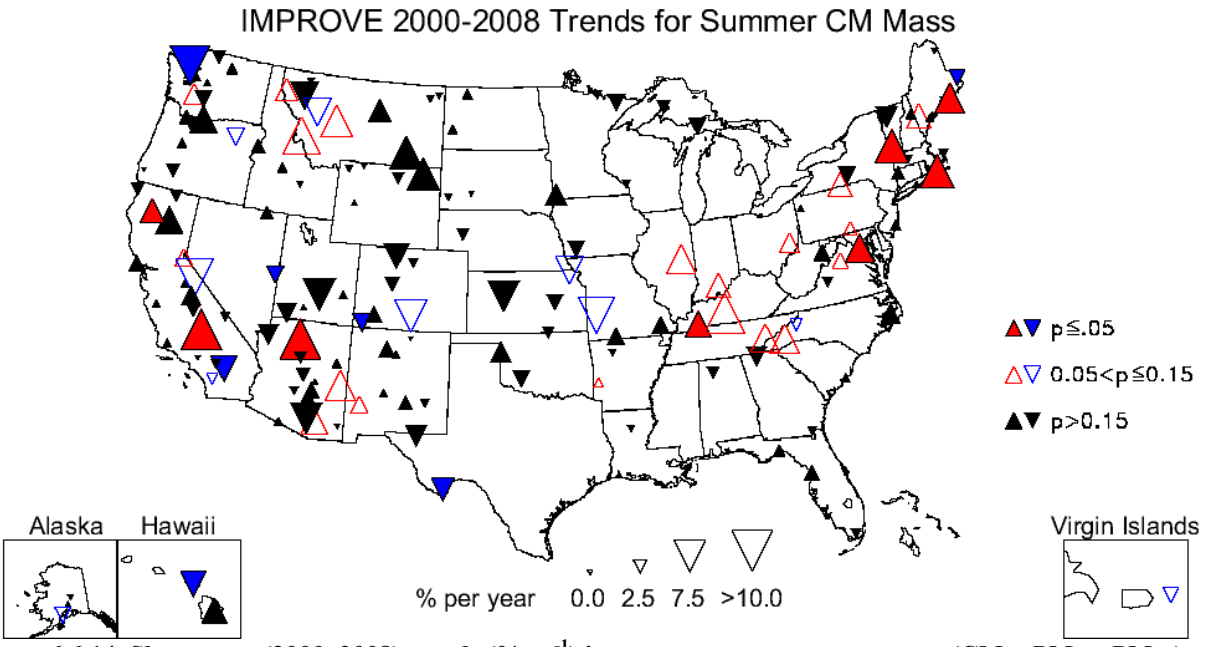

Figure 6.6.14. Short-term (2000–2008) trends (% yr^{-1}) in average summer coarse mass (CM = PM_{10} - $PM_{2.5}$) concentrations

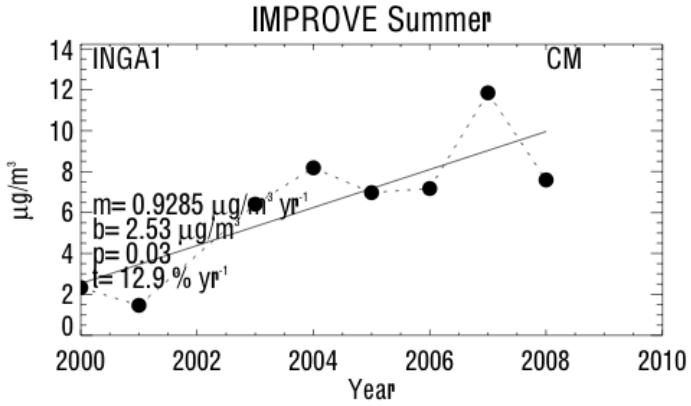

Figure 6.6.15. Average summer coarse mass (CM = PM_{10} - $PM_{2.5}$) concentrations (µg m^{-3}) for Indian Gardens, Arizona (INGA1). Regression results, including Theil slope (m, µg m^{-3} yr^{-1}), intercept (b, µg m^{-3}), significance (p), and trend (t, % yr^{-1}) are included. The trend line is plotted as a solid line. The intercept corresponds to the initial year of data.

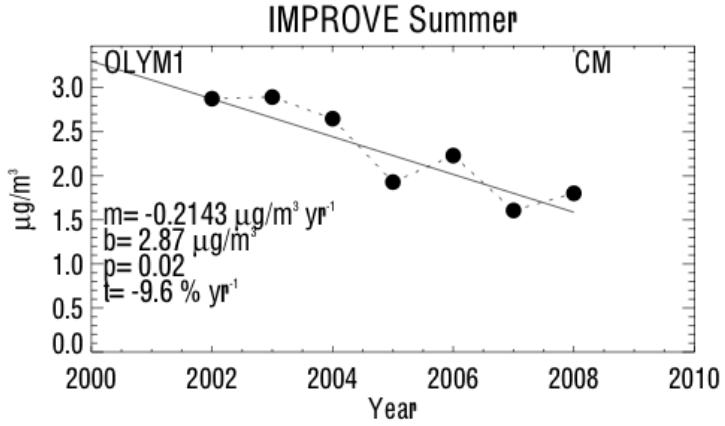

Figure 6.6.16. Average summer coarse mass (CM = PM_{10} - $PM_{2.5}$) concentrations (µg m^{-3}) for Olympic, Washington (OLYM1). Regression results, including Theil slope (m, µg m^{-3} yr^{-1}), intercept (b, µg m^{-3}), significance (p), and trend (t, % yr^{-1}) are included. The trend line is plotted as a solid line. The intercept corresponds to the initial year of data.

The interpretation of CM trends is complicated by the fact that the speciation of CM was unknown. For regions where CM concentrations were suspected to be dominated by soil (e.g., southwestern United States), we might expect the CM trends to be similar to the soil trends. Although some seasonal short-term trends suggest similarities, in general, comparisons of soil and CM trends between similar parameters were inconclusive. Reasons for discrepancies between soil and CM trends include the possibilities that soil trends may be more questionable than realized, CM trends were driven by species other than soil, or CM trends were questionable. Any changes in the cut points for the $PM_{2.5}$ and PM_{10} samplers over time could produce questionable trends in CM, although we have no specific evidence to support this possibility. Additionally, sites with statistically significant trends in soil may not have statistically significant trends in CM, further complicating comparisons between trends.

6.7 PM_{10} GRAVIMETRIC MASS TRENDS

PM_{10} concentrations are determined gravimetrically and correspond to particles with an aerodynamic diameter (D_{ae}) less than 10 μm. PM_{10} mass concentrations include all the species presented in the previous sections, and trends for PM_{10} concentrations represent the temporal behavior in the total (D_{ae} < 10 μm) aerosol mass concentration. Not surprisingly, the long-term trends were generally negative (see Figure 6.7.1), with the largest negative trends corresponding to the 10th percentile and winter season. The individual site trends for PM_{10}, 10th percentile concentrations are shown in Figure 6.7.1. All 50 sites with complete data corresponded to statistically significant 10th percentile trends, and the largest negative 10th percentile trend occurred at Mount Zirkel, Colorado (MOZI1, -9.9% yr^{-1}). The least negative 10th percentile trend corresponded to Mammoth Cave, Kentucky (MACA1, -1.2% yr^{-1}). Winter trends in PM_{10} concentrations are shown in Figure 6.7.2. Sites along the western United States were associated with relatively large negative winter trends, with the largest corresponding to Snoqualmie Pass, Washington (SNPA1, -9.0% yr^{-1}), similar to winter CM trends. The least negative winter trend occurred at Tonto, Arizona (TONT1, -1.7% yr^{-1}), and no sites were associated with positive winter trends. Winter PM_{10} concentrations at SNPA1 decreased after 2000 and remained fairly flat (Figure 6.7.3).

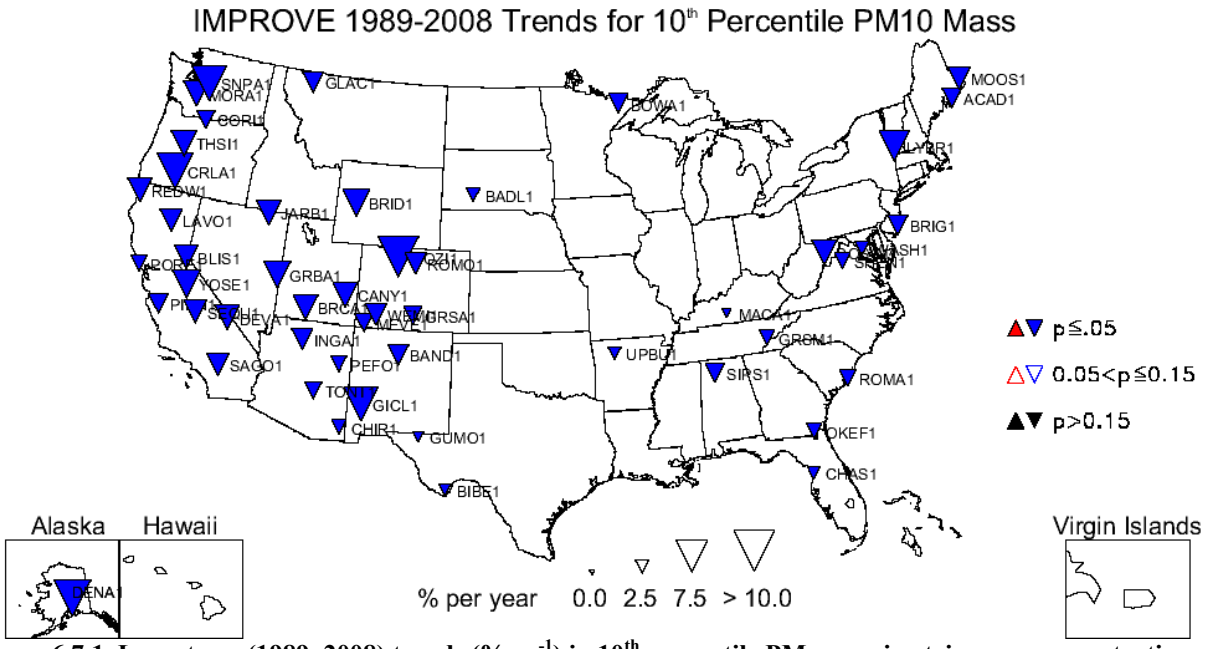

Figure 6.7.1. Long-term (1989–2008) trends (% yr^{-1}) in 10th percentile PM_{10} gravimetric mass concentrations.

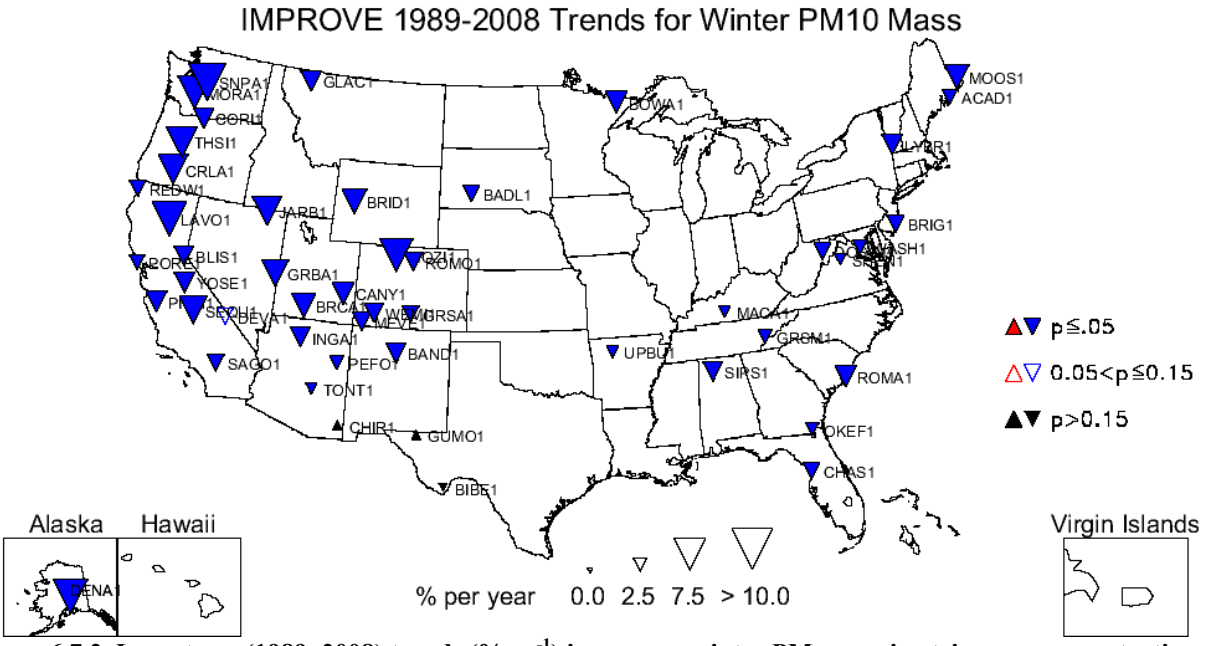

Figure 6.7.2. Long-term (1989–2008) trends (% yr^{-1}) in average winter PM_{10} gravimetric mass concentrations.

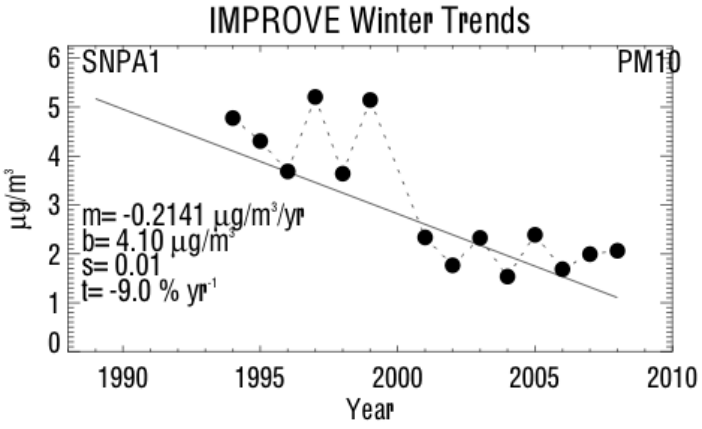

Figure 6.7.3. Average winter PM_{10} gravimetric mass concentrations (µg m^{-3}) for Snoqualmie Pass, Washington (SNPA1). Regression results, including Theil slope (m, µg m^{-3} yr^{-1}), intercept (b, µg m^{-3}), significance (s), and trend (t, % yr^{-1}) are included. The trend line is plotted as a solid line. The intercept corresponds to the initial year of data.

PM_{10} trends for the 90th percentile were considerably lower, or insignificant, compared to the 10th percentile trends (Figure 6.7.4). No sites corresponded to positive, 90th percentile, PM_{10} trends. Many eastern sites corresponded to negative summer PM_{10} trends, and many western sites were associated with insignificant summer trends (Figure 6.7.5). The largest negative summer trend occurred at Great Gulf, New Hampshire (GRGU1, -5.0% yr^{-1}), similar to FM summer trends. Only one significant positive trend occurred for long-term PM_{10} trends, and it was for summer concentrations at Columbia River Gorge, Washington (CORI1, 4.6% yr^{-1}). Recall that CORI1 was also associated with a large positive trend in soil in summer.

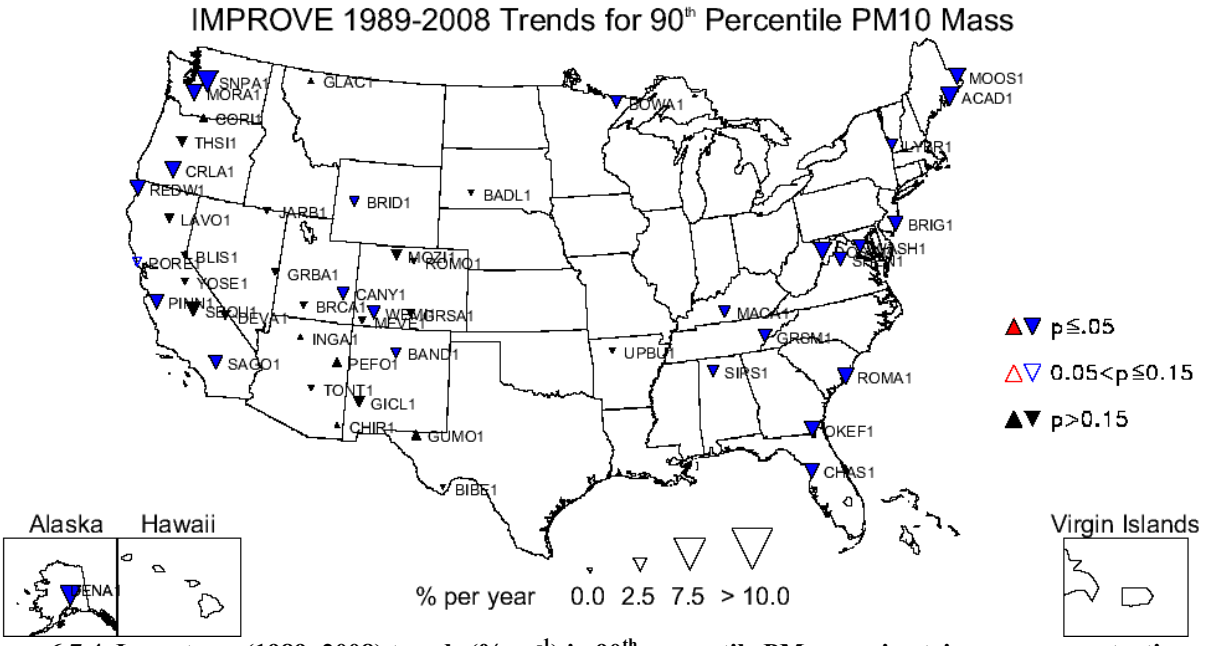

Figure 6.7.4. Long-term (1989–2008) trends (% yr^{-1}) in 90th percentile PM_{10} gravimetric mass concentrations.

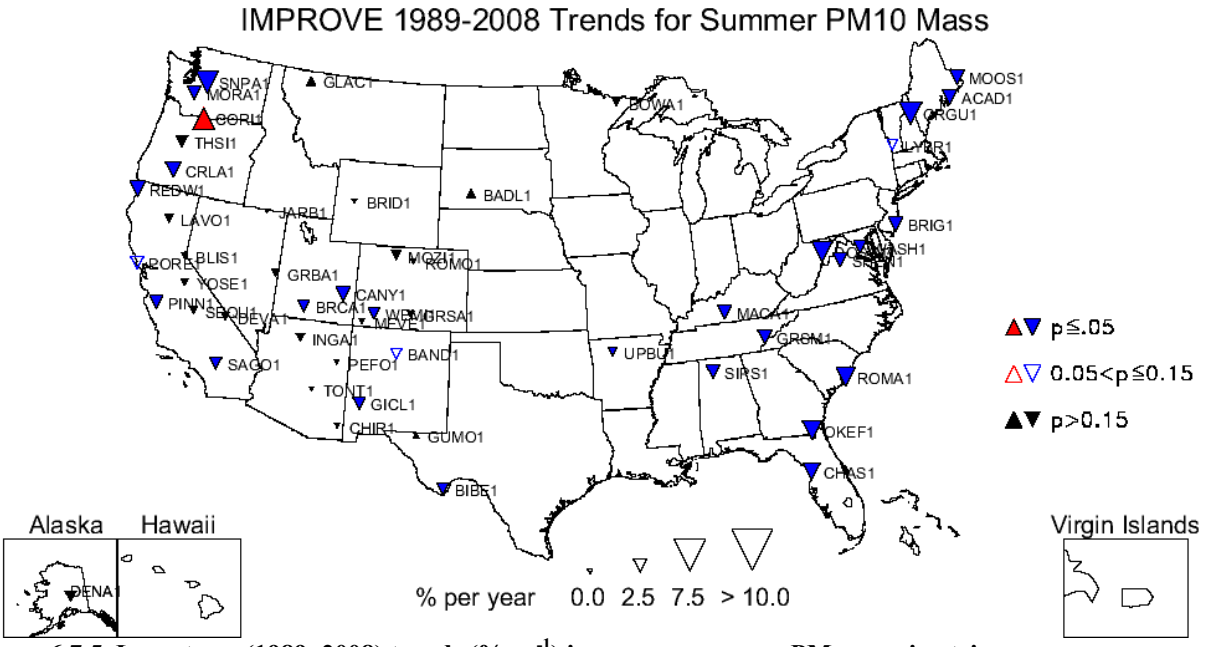

Figure 6.7.5. Long-term (1989–2008) trends (% yr^{-1}) in average summer PM_{10} gravimetric mass concentrations.

Although short-term PM_{10} trends were associated with more sites with positive significant trends compared to long-term PM_{10} trends, they still were dominated by sites with negative trends (see Table 6.2). The map of sites for short-term 10th percentile PM_{10} trends suggested that statistically significant trends were more negative in the central, western, and northwestern United States (Figure 6.7.6). The largest negative 10th percentile, short-term PM_{10} trend was associated with Starkey, Oregon (STAR1, -15.10% yr^{-1}), similar to FM trends. The

largest positive 10th percentile, short-term, PM_{10} trend corresponded to Trapper Creek, Alaska (TRCR1, 12.10% yr^{-1}), also similar to FM trends. In addition to the TRCR1 site, two sites were associated with positive trends: Nebraska NF, Nebraska (NEBR1, 3.8% yr^{-1}), and Denali, Alaska (DENA1, 8.7% yr^{-1}). Winter PM_{10} short-term trends were most negative in the western United States (Figure 6.7.7). The largest negative winter, PM_{10} trend occurred at Starkey, Oregon (STAR1, -12.9% yr^{-1}), similar to FM trends. The largest positive winter trend occurred at Bondville, Illinois (BOND1, 1.7% yr^{-1}). Figure 6.7.8 shows a slow but steady increase in the winter PM_{10} concentrations at BOND1.

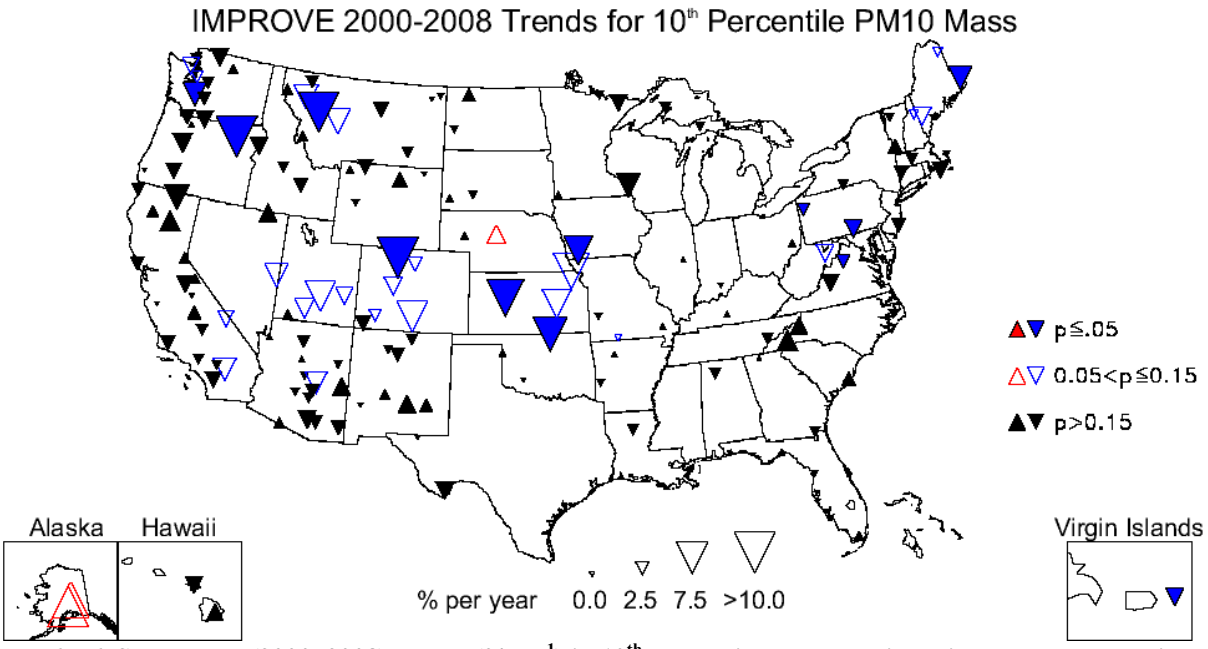

Figure 6.7.6. Short-term (2000–2008) trends (% yr^{-1}) in 10th percentile PM_{10} gravimetric mass concentrations.

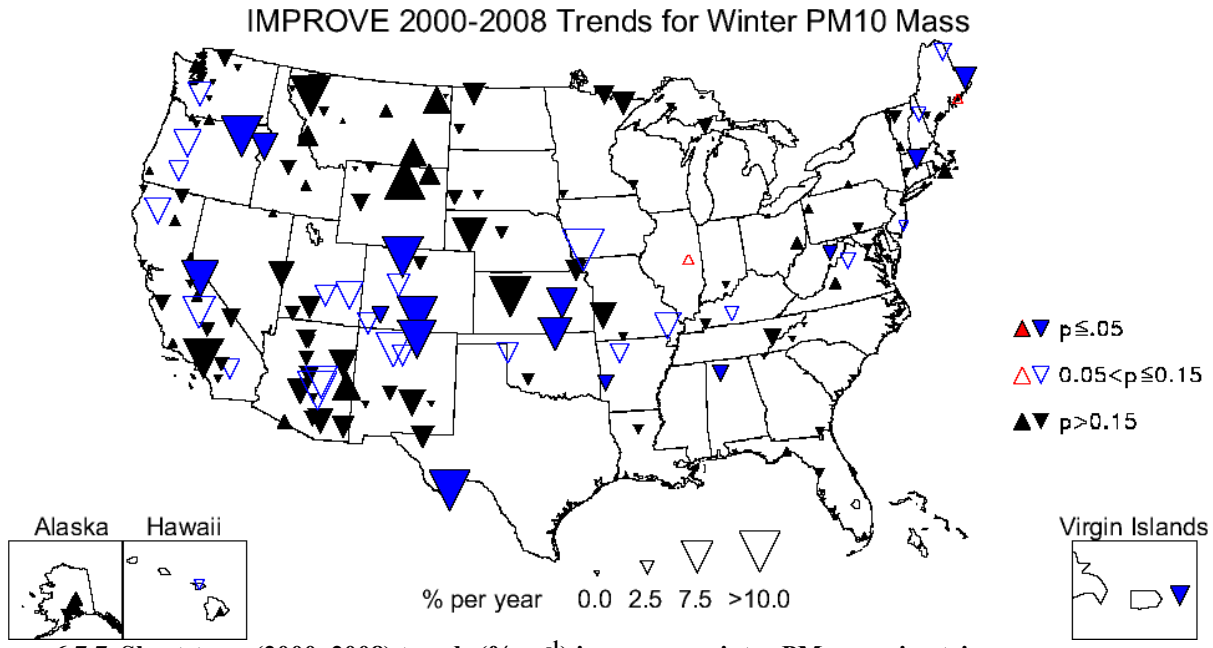

Figure 6.7.7. Short-term (2000–2008) trends (% yr^{-1}) in average winter PM_{10} gravimetric mass concentrations.

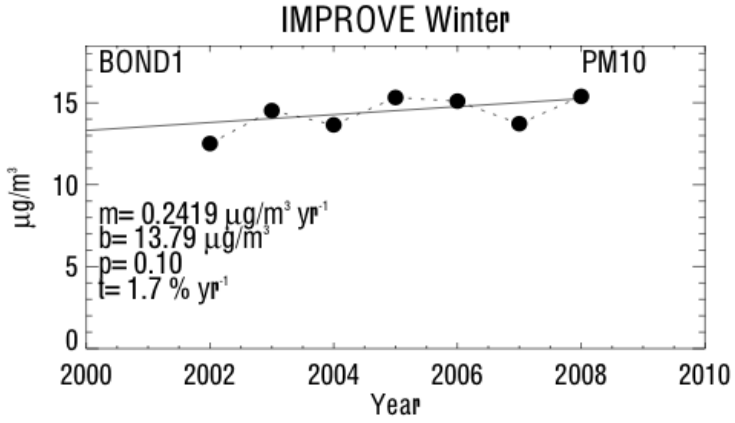

Figure 6.7.8. Average winter PM_{10} gravimetric mass concentrations (µg m^{-3}) for Bondville, Illinois (BOND1). Regression results, including Theil slope (m, µg m^{-3} yr^{-1}), intercept (b, µg m^{-3}), significance (p), and trend (t, % yr^{-1}) are included. The trend line is plotted as a solid line. The intercept corresponds to the initial year of data.

The parameters associated with the largest number of positive trend sites were the 90th percentile and fall season. A map of 90th percentile, short-term PM_{10} trends is shown in Figure 6.7.9. Five sites were associated with positive 90th percentile trends, including the site at Hawaii Volcanoes (HAVO1) with the largest positive trend (12.5% yr^{-1}). The HAVO1 site was also associated with the largest FM and sulfate 90th percentile trends. The largest negative, short-term trend in 90th percentile PM_{10} concentrations corresponded to Tuxedni, Alaska (TUXE1, -8.10% yr^{-1}), which also corresponded to the largest negative, FM, 90th percentile trend. Fall PM_{10} trends were associated with eight positive trends, none of which were located in the eastern United States (Figure 6.7.10). The largest positive fall, PM_{10}, short-term trend corresponded to the Zion

Canyon, Utah, site (ZICA1, 10.0% yr^{-1}), similar to the fall FM and soil trends, and the largest negative fall, PM_{10} trend occurred at Gila, New Mexico (GICL1, -6.0% yr^{-1}). A timeline of fall PM_{10} concentrations at GICL1 is shown in Figure 6.7.11 and demonstrates a decrease in PM_{10} concentrations from 9.5 µg m^{-3} to 4.3 µg m^{-3} from 2000 to 2008. The fall PM_{10} concentration in 2000 was the largest concentration in 20 years, so the short-term fall trend at GICL1 was somewhat larger than the long-term trend (-4.5% yr^{-1}).

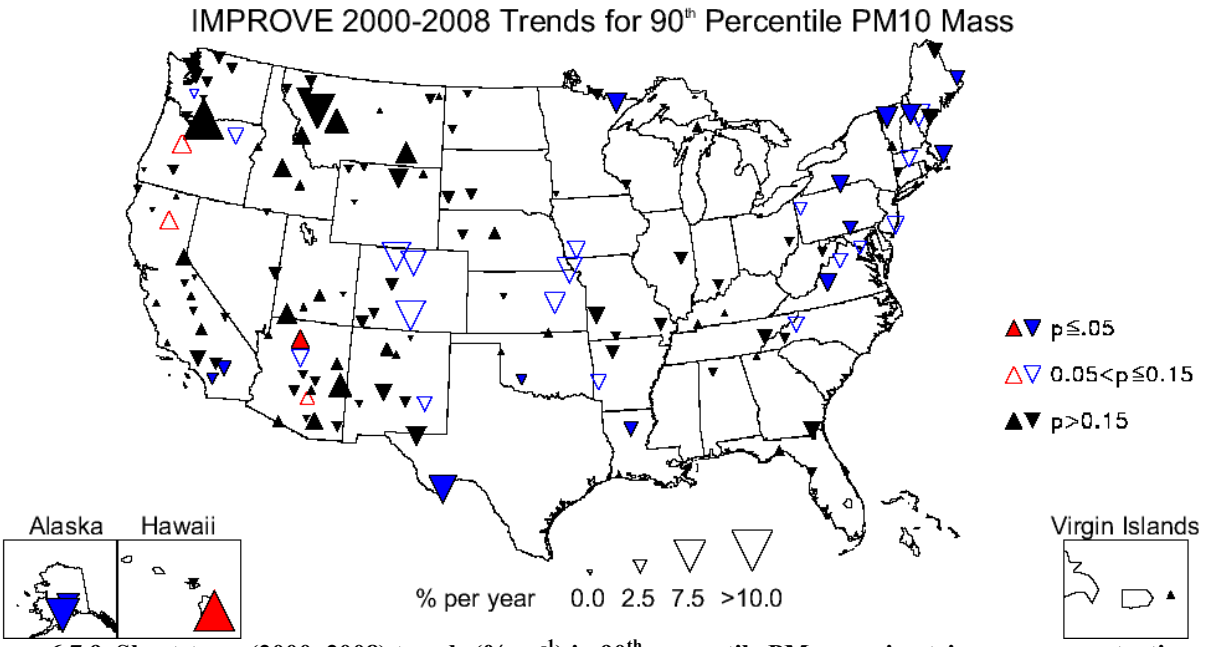

Figure 6.7.9. Short-term (2000–2008) trends (% yr^{-1}) in 90th percentile PM_{10} gravimetric mass concentrations.

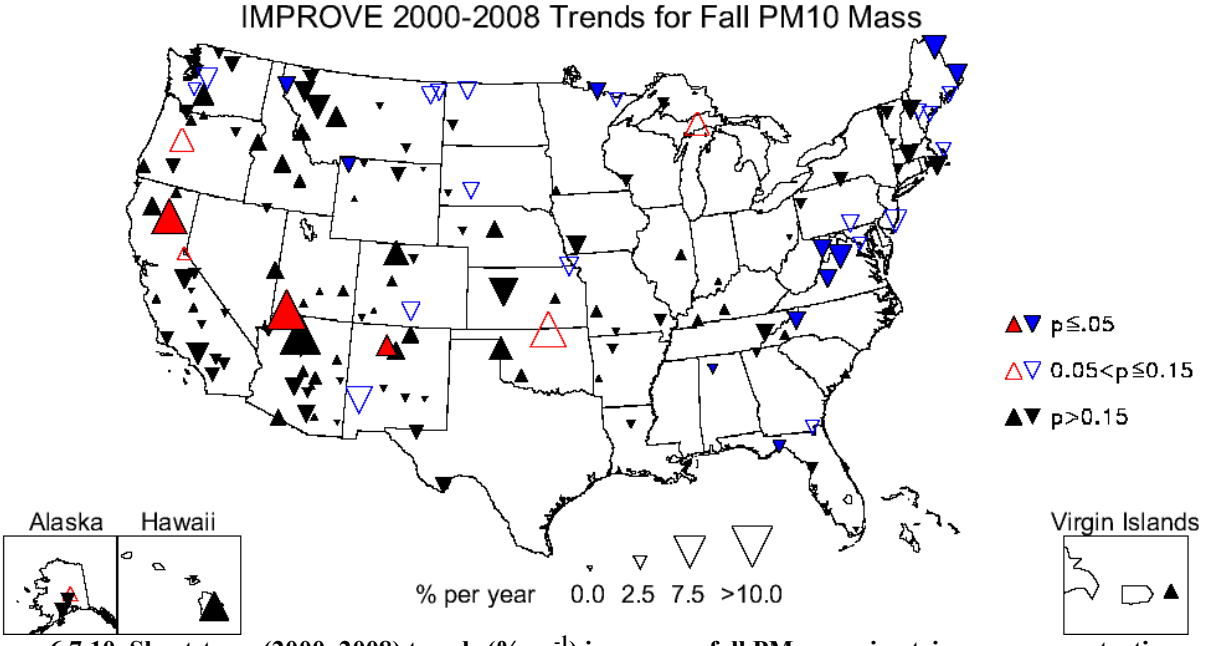

Figure 6.7.10. Short-term (2000–2008) trends (% yr^{-1}) in average fall PM_{10} gravimetric mass concentrations.

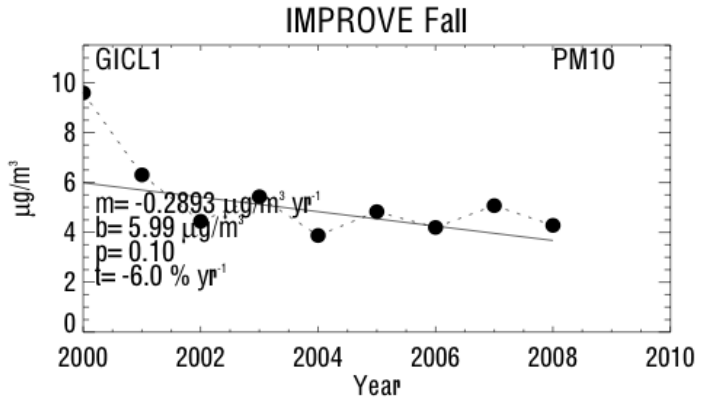

Figure 6.7.11. Average fall PM_{10} gravimetric mass concentrations (µg m^{-3}) for Gila, New Mexico (GICL1). Regression results, including Theil slope (m, µg m^{-3} yr^{-1}), intercept (b, µg m^{-3}), significance (p), and trend (t, % yr^{-1}) are included. The trend line is plotted as a solid line. The intercept corresponds to the initial year of data.

The trend results presented in this chapter were intended as a summary of the temporal changes in the mass concentrations of major aerosol species over short and long time periods. Results suggested that for most species, concentrations were decreasing at IMPROVE sites around the United States, and these decreasing trends were largest for the lowest concentrations and during winter seasons. Because we present normalized trends, it is not surprising that the 10th percentile trends were typically the largest in magnitude because they were normalized with the lowest concentrations. This general result may not hold for individual sites or for given species (e.g., soil), but overall this consistent pattern emerged. A similar pattern was presented in recent progress report for air quality in national parks (NPS, 2010) that demonstrated larger decreasing trends in deciview on the clearest days compared to the haziest days.

To demonstrate the visibility conditions associated with the trends in particle concentrations presented in this chapter, we used WinHaze 2.9.9 (Air Resource Specialists, 2011) to model the view of scenic areas with specified air quality levels. WinHaze is a computer software program that simulates visibility conditions from user-specified scenes and speciated aerosol concentrations or visibility levels. For our applications we chose scenes for parks and wilderness areas with speciated aerosol concentrations measured from the IMPROVE network. We specified 50th percentile aerosol concentrations for "beginning" and "end" periods corresponding to our trend analyses. We used default optical properties (i.e. "original" IMPROVE algorithm) and assumed an 80% relative humidity for all simulations. An example of results from WinHaze is shown in the split-image of a scene at Linville Gorge NC (LIVO) for aerosol levels in 2000 and 2008 (Figure 6.7.12). A noticeable improvement in visibility levels occurred due to the decrease in aerosol concentrations over the 9-year span. The cover of this report showing the scene in Acadia, ME is another example of split-images that represent the visibility conditions associated with the measured aerosol concentrations over the trend period. Winhaze is a powerful tool for visualizing the impact of aerosol trends on visibility conditions over time.

Figure 6.7.12. Split-image of visibility conditions in Linville Gorge, NC (LIVO) for 50th percentile speciated aerosol levels in 2000 (left-side) and 2008 (right-side). Images were generated using WinHaze 2.9.9.

Appendix F includes additional figures showing long-term and short-term trends for other percentiles and seasons that were not included in this discussion. The appendix also includes WinHaze images, like the one shown in Figure 6.7.12, for approximately fifty additional sites.

REFERENCES

Air Resource Specialists, Inc. (2011), WinHaze visual air quality modeler version 2.9.9, Fort Collins CO (http://www.air-resource.com/resources/downloads.html).

Bahadur, R., G. Habib, and L. M. Russell (2009), Climatology of PM2.5 organic carbon concentrations from a review of ground-based atmospheric measurements by evolved gas analysis, *Atmos. Environ, 43,* 1591-1602.

Chow, J. C., J. G. Watson, L.-W. A. Chen, M. C. O. Chang, N. F. Robinson, D. Trimble, and S. Kohl (2007), The IMPROVE_A temperature protocol for thermal/optical carbon analysis: Maintaining consistency with a long-term database, *J. Air & Waste Manage. Assoc., 57,* 1014-1023.

Gong, S. L., T. L. Zhao, S. Sharma, D. Toom-Sauntry, D. Lavoué, X. B. Zhang, W. R. Leaitch, and L. A. Barrie (2010), Identification of trends and interannual variability of sulfate and black carbon in the Canadian High Artic: 1981-2007, *J. Geophys. Res., 115,* D07305, doi:10.1029/2009JD012943.

Hirdman, D., J. F. Burkhart, H. Sodemann, S. Eckhardt, A. Jefferson, P. K. Quinn, S. Sharma, J. Ström, and A. Stohl (2010), *Atmos. Chem. Phys*., *10*, 9351–9368, doi:10.5194/acp-10-9351-2010.

Holland, D., C. Simmons, L. Smith, T. Cohn, G. Baier, J. Lynch, J. Grimm, G. Oehlert, and S. Lindberg (1995), Long-term trends in NADP/NTN precipitation chemistry data: Results of different statistical analyses, *Water Air Soil Pollut, 85,* 595-601.

Lehmann, C. M. B., V. C. Bowersox, R. S. Larson, and S. M. Larson (2007), Monitoring long-term trends in sulfate and ammonium in U.S. precipitation: Results from the National Atmospheric Deposition Program/National Trends Network, *Water Air Soil Pollut: Focus, 7,* 59-66, doi:10.1007/s11267-006-9100-z.

Lloyd, P. J., (2010), Changes in the wet precipitation of sodium an chloride over the continental United States, 1984-2006, *Atmos. Environ., 44,* 3196-3206.

Lynch, J. A., J. W. Grimm, and V. C. Bowersox (1995), Trends in precipitation chemistry in the United States: A national perspective, 1980-1992, *Atmos. Environ., 29,*11, 1231-1246.

Malm, W. C., B. A. Schichtel, R. B. Ames, and K. A. Gebhart (2002), A 10-year spatial and temporal trend of sulfate across the United States, *J. Geophys. Res*., 107(D22), 4627, doi:10.1029/2002JD002107.

Malm, W. C., B. A. Schichtel, and M. L. Pitchford (2011), Uncertainties in PM2.5 gravimetric and speciation measurements and what we can learn from them, *J. Air Waste Manage,* In press.

McDade, C. E. (2007), Diminished wintertime nitrate concentrations in late 1990s, Doc. # da0002, http://vista.cira.colostate.edu/improve/Data/QA_QC/Advisory/da0002/da0002_WinterNO3.pdf.

Mishchenko, M. I., I. V. Geogdzhayev, W. B. Rossow, B. Cairns, B. E. Carlson, A. A. Lacis, L. Liu, and L. D. Travis (2007), Long-term satellite record reveals likely recent aerosol trend, *Science*, *315*, 1543.

Mishchenko, M. I., and I. V. Geogdzhayev (2007), Satellite remote sensing reveals regional tropospheric aerosol trends, *Optics Express, 15,* 12, 7423-7438.

Nilles, M. A., and B. E. Conley (2001), Changes in the chemistry of precipitation in the United States, 1981-1998, *Water, Air and Soil Pollut., 130,* 409-414.

NPS (2010), Air quality in National Parks, 2009 Annual Performance and Progress Report, Natural Resource Report NPS/NRPC/ARD/NRR-2010/266.

Polissar, A. V., P. K. Hopke, P. Paatero, Y. J. Kaufmann, D. K. Hall, B. A. Bodhaine, E. G. Dutton, and J. M. Harris (1999), The aerosol at Barrow, Alaska: long term trends and source locations, *Atmos. Environ., 33,* 2441-2458.

Quinn, P. K., G. Shaw, E. Andrews, E. G. Dutton, T. Ruoho-Airola, and S. L. Gong (2007), Artic haze: current trends and knowledge gaps, *Tellus, 59B,* 99-114.

Sirois, A., and L. A. Barrie (1999), Artic lower tropospheric aerosol trends and composition at Alert, Canada: 1980-1995, *J. Geophys. Res., 104,* D9, 11599-11618.

Streets, D. G., F. Yan, M. Chin, T. Diehl, N. Mahowald, M. Schultz, M. Wild, Y. Wu, and C. Yu (2009), Anthropogenic and natural contributions to regional trends in aerosol optical depth, 1980–2006, *J. Geophys. Res*., *114*, D00D18, doi:10.1029/2008JD011624.

Theil, H. (1950), A rank-invariant method of linear and polynomial regression analysis, *Proc. Kon. Ned. Akad. V. Wetensch. A., 53,* 386-392, 521-525, 1397-1412.

U.S. EPA (1999), Regional Haze Regulations; Final Rule, 40 CFR 51, Federal Register, 64, 35714-35774.

Wild, M., H. Gilgen, A. Roesch, A. Ohmura, C. N. Long, E. G. Dutton, B. Forgan, A. Kallis, V. Russak, and A. Tsvetkov (2005), From dimming to brightening: decadal changes in solar radiation at the Earth's surface, *Science, 308,* 847-850.

White, W. H. (2007), Shift in EC/OC split with 1 January 2005 TOR hardware upgrade, Doc. # da0016, http://vista.cira.colostate.edu/improve/Data/QA_QC/Advisory/da0016/da0016_TOR2005.pdf.

White, W. H. (2008), Chemical markers for sea salt in IMPROVE aerosol data, *Atmos. Environ., 42,* 261-274.

Chapter 7. Urban Excess in $PM_{2.5}$ Speciated Aerosol Concentrations

7.1 INTRODUCTION AND METHOD

Regulatory efforts designed to reduce aerosol concentrations in the atmosphere, such as the EPA's (Environmental Protection Agency) National Ambient Air Quality Standards (www.epa.gov/air/particlepollution/standards.html) or Regional Haze Rule (U.S. EPA, 1999), rely on an understanding of the sources, lifetimes, and sinks of aerosols in the atmosphere. Emission sources of primary aerosols, secondary aerosol production through atmospheric processes, and aerosol transport are all important considerations for characterizing the impacts of aerosol concentrations on local, regional, and global scales. Primary or secondary aerosols can be transported hundreds or thousands of kilometers from their source region and impact air quality at distant locations. The average regional impact of aerosol sources can be inferred from the spatial distribution of aerosol concentrations; emissions from local sources produce sharper spatial gradients, while emissions from more distant or dispersed sources (e.g., biogenic emissions from vegetation) produce more homogeneous regional spatial patterns. Separating background or regional aerosol concentrations from those emitted locally is important for regulating aerosol sources, especially for meeting air quality standards in nonattainment areas where the regional or background concentrations of a given aerosol species are similar to the standard itself.

We define urban excess as the difference or ratio in aerosol mass concentrations in urban regions compared to nearby remote and rural regions. A schematic depiction of the impact of urban sources on background aerosol concentrations is shown in Figure 7.1. Aerosol concentrations within the city are higher than aerosol concentrations surrounding the city due to the increase in aerosols emitted from anthropogenic activities within the urban corridor. Urban impacts on background or regional aerosol concentrations are influenced by wind direction and mesoscale or synoptic meteorological patterns. We assume that the rural background concentrations refer to the lowest concentrations in a region but may include some impacts from urban emissions. Remote or background aerosol concentrations tend to be aged, well mixed, and regional in extent (depending on the species), whereas urban aerosols tend to originate from local sources, correspond to a younger aerosol, and tend to dilute after some distance from their sources. Both vary as a function of season and region. We also assume that regional contributions to aerosol concentrations of a given species affect the background and urban concentrations similarly, resulting in similar concentrations in the absence of additional urban sources to that species. Urban excess studies provide estimates of the relative magnitude of local versus regional contributions to aerosol concentrations and subsequently increase our understanding of aerosol sources, atmospheric processes, and lifetimes in the atmosphere.

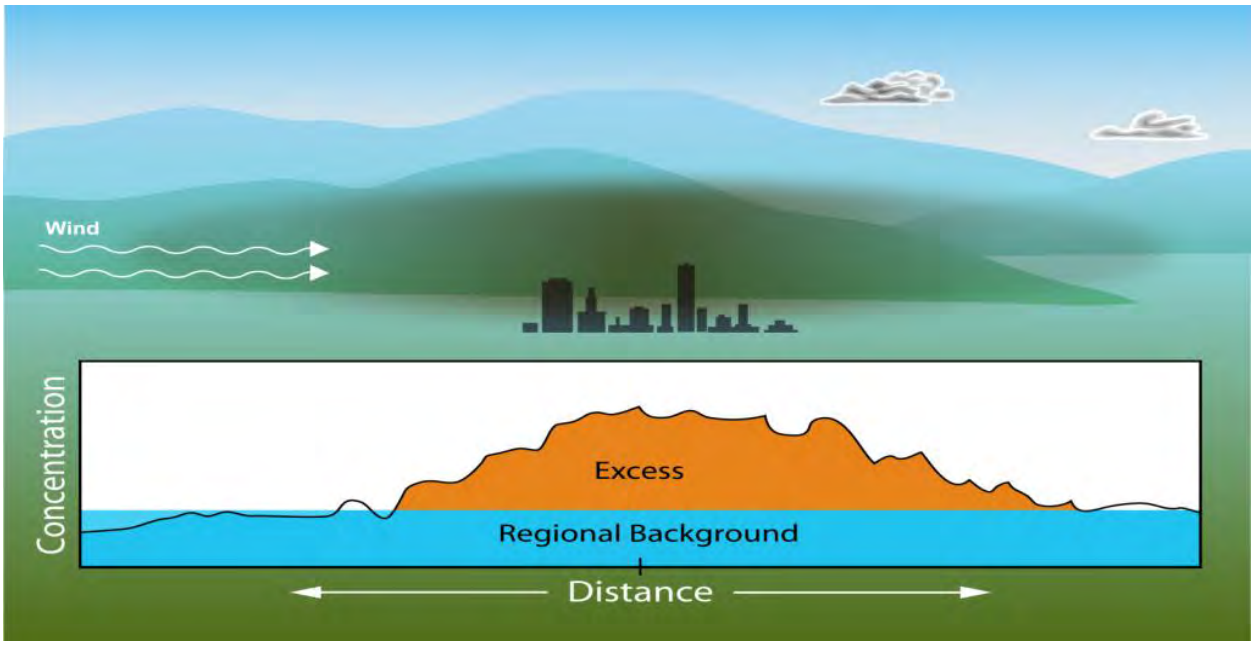

Figure 7.1. Schematic showing urban sources of aerosol concentrations and their impact on surrounding rural concentrations. An arbitrary concentration scale is on the y-axis and distance is on the x-axis. The concentrations levels depicted in orange represent levels above a rural background, depicted as blue.

Different aerosol species correspond to a range in urban excess values, depending on their sources and lifetimes. For example, secondary aerosols, such as sulfate or secondary organic aerosols, form through atmospheric processes that depend not only on sources of precursors, but other meteorological and chemical parameters (e.g., clouds, solar radiation, available reactive aerosol species, chemical equilibrium, etc.). These aerosols can be dispersed over large regions and undergo chemical transformations during their transport. In contrast, primary aerosols, such as light absorbing carbon, are produced from distinct sources, emitted directly, and therefore tend to have the highest concentrations near their source locations. Clearly, both types of aerosols can be entrained in episodic weather patterns that transport them long distances; in general, however, regional aerosols correspond to secondary formation processes, while primary aerosols tend to be associated with local sources.

Urban excess is often characterized by examining the ratios and differences of aerosol concentrations at an urban site and associated remote or rural site(s). One of major challenges to estimating urban excess is determining the rural background concentration at an urban location. One method for computing urban excess is to use data from combinations of urban and nearby rural sites (within a defined elevation or distance). Rao et al. (2003) applied this approach and analyzed urban excess at thirteen CSN sites for one year of data (March 2001- February 2002). They chose nearby IMPROVE sites and performed an inverse-distance-weighted average of the rural concentrations to compare with data from the CSN sites. This approach is straightforward but does depend on the choice of sites and spatial averaging method used to characterize a rural concentration. Additional studies of urban excess were reviewed by Allen and Turner (2008) and the NARSTO (North American Research Strategy for Tropospheric Ozone and Aerosols) Assessment of Fine Particulate Matter Science for Policy Makers (2004). Many of the studies reviewed by Allen and Turner (2008) applied positive matrix factorization (e.g., Liu et al., 2003, 2005; Dutkiewicz et al., 2004; Eatough et al., 2006; Pekney et al., 2006) to data from urban and

rural sites to determine source contribution functions. Comparisons of sources at both sites led to the determination of regional versus local sources. Other studies reviewed by Allen and Turner (2008) and the NARSTO assessment used simpler analyses on data for paired sites to evaluate the relative urban and rural concentrations and determine an urban excess. Most of these studies focused on individual sites or regions (e.g., Kim et al, 2000; Hansen et al, 2003; Rao et al., 2003; U.S. EPA, 2004; Russell et al., 2004; Chow et al. 2006); very few, studies examined urban excess on a continental scale.

The choice of rural site(s) used in the above types of analyses is limited by logistical constraints such as availability and location of nearby sites. These types of issues can be avoided by using spatially-interpolated aerosol concentrations for both the urban and rural values, such as those presented in Chapter 2. Interpolations provide regularly gridded data through a sophisticated weighted averaging technique (a Kriging algorithm was used in Chapter 2). From the interpolated fields a rural aerosol concentration can be obtained at a location corresponding to an urban sampling site that reflects the background concentrations surrounding the site, not just at one or two locations. One major advantage to this method, over choosing a handful of sites in the analyses, is that the rural concentrations are determined from an interpolation scheme that incorporates data from all available nearby sites. The interpolation of both rural and urban data provides gridded urban and rural aerosol fields that can be combined to provide gridded estimates of urban excess for high resolution maps. However, these maps must be interpreted with some caution. Uncertainties introduced by interpolation schemes may bias the results. For example, interpolation schemes tend to smooth concentrations such that high urban concentrations could be biased low, and regions with sparse data may result in gridded concentrations with higher uncertainties.

A third option for estimating urban excess is a combination of the first two. Interpolated fields of rural aerosol concentrations can be used to determine a rural concentration at an urban site location. Measured data from an urban site can be used to compute a ratio or difference between urban and rural concentrations at the site location. These ratios and differences are then interpolated with a Kriging algorithm to provide isopleths of urban excess. An advantage to this method is avoiding the issues surrounding the subjective nature of choosing rural site locations, or the possibility that the chosen sites may not be representative of a regional background. In addition, urban site data are incorporated directly, avoiding the possibility of smoothed data from the interpolation scheme. We apply the third method as a compromise to incorporate actual urban data while retaining the detail in spatial patterns.

Rural concentrations were determined from the interpolated 2005–2008 annual mean IMPROVE data at the grid cell corresponding to the urban CSN site and limited to urban sites with at least one IMPROVE site within 150 km. The urban sites investigated for urban excess were chosen from the 174 CONUS (Contiguous United States) sites that met the completeness criteria outlined in Chapter 2 (sites in Alaska and Hawaii were not included in these analyses). Of these, 114 had a ~~–e~~omplete" IMPROVE rural site within 150 km. The 60 sites that did not meet the distance limit were located in Alabama, Georgia, Illinois, Indiana, Iowa, Kentucky, Louisiana, Michigan, Missouri, New York, North Carolina, North Dakota, Ohio, Pennsylvania, South Carolina, Tennessee, Texas, West Virginia, and Wisconsin.

CSN sites are designated as "urban", "suburban", and "rural" by the EPA. We assumed all CSN sites were "urban" for this analysis as the designation of "rural" can have very different meanings than that for the IMPROVE network. No elevation corrections (standard pressure and temperature) were applied to the urban and rural data, with the assumption that if the sites were typically within 150 km, the corrections based on elevation differences would be negligible (it is unlikely that a site at sea level would be 150 km from a site at an elevation of 3 km). In fact, Rao et al. (2003) showed that elevation effects were negligible in their analyses. A more important elevation issue is the possibility that urban and rural sites with a significant elevation difference were actually sampling different air masses, as some IMPROVE monitors could be above the boundary layer in many cases (e.g. Denver and Rocky Mountain National Park).

Caveats to this approach include the uncertainties associated with interpolated aerosol concentrations and other fields. Isopleths serve to guide the eye in observing spatial patterns but obviously are only representations of reality. Site locations are not regularly spaced; regions with high site density from only one network, like in the eastern United States, could affect the derived results. In addition, characterization of "rural" aerosol concentrations assumed that the concentrations at rural sites were not significantly influenced by nearby urban regions, which is likely not the case.

Urban excess was investigated for 2005–2008 annual mean ammonium sulfate (AS), ammonium nitrate (AN), particulate organic matter (POM), light absorbing carbon (LAC), and $PM_{2.5}$ gravimetric fine mass (FM). Sea salt or fine soil were not included because of the relative biases derived for those species from analyses of data from collocated IMPROVE and CSN sites (see Table 1.8). Coarse mass also was not included, as CSN does not monitor for it. We computed differences and ratios in annual mean urban and rural concentrations from 2005 to 2008, although urban excess undoubtedly varies temporally, as the seasonal aerosol concentration for urban and rural sources can be very distinct (see Chapter 4). Differences in urban and rural concentrations emphasized relatively higher concentrations, while ratios revealed patterns in both low and high concentrations. For example, urban and rural LAC concentrations of 0.2 $\mu g\ m^{-3}$ and 0.1 $\mu g\ m^{-3}$, respectively, resulted in a difference of 0.1 $\mu g\ m^{-3}$ and a ratio of 2, while urban and rural FM concentrations of 20 $\mu g\ m^{-3}$ and 10 $\mu g\ m^{-3}$, respectively, result in a difference of 10 $\mu g\ m^{-3}$ but the same ratio of 2.

Isopleths maps of aerosol concentrations for both the IMPROVE and CSN networks are presented to remind the reader of the spatial patterns and magnitudes in concentrations for the species under consideration. The urban and rural aerosol concentration isopleths were created with the same scales to emphasize the differences in urban and rural concentrations. Maps of ratios and differences in urban and rural concentrations are also presented. Finally, results are summarized by comparing urban excess estimates for each species.

7.2. AMMONIUM SULFATE

Recall from Chapter 2.2.1 that the 2005–2008 annual mean AS concentrations were fairly regional in spatial extent. Figure 7.2.1 shows interpolated annual mean AS concentrations for rural IMPROVE sites, compared to the isopleths for IMPROVE plus CSN sites in Figure 7.2.2. The maximum concentration level listed on the scale corresponds to the 95th percentile for the combined IMPROVE and CSN data. Both maps were created with the same scale. The spatial

extent of AS concentrations was similar, with higher AS concentrations in the eastern United States for both networks. Higher urban concentrations in the eastern United States were associated with the Ohio River valley and Appalachian Mountains. Notice the difference in site density between the IMPROVE and CSN networks, with many additional eastern CSN sites that provide enhanced detail to the spatial patterns of AS in this area.

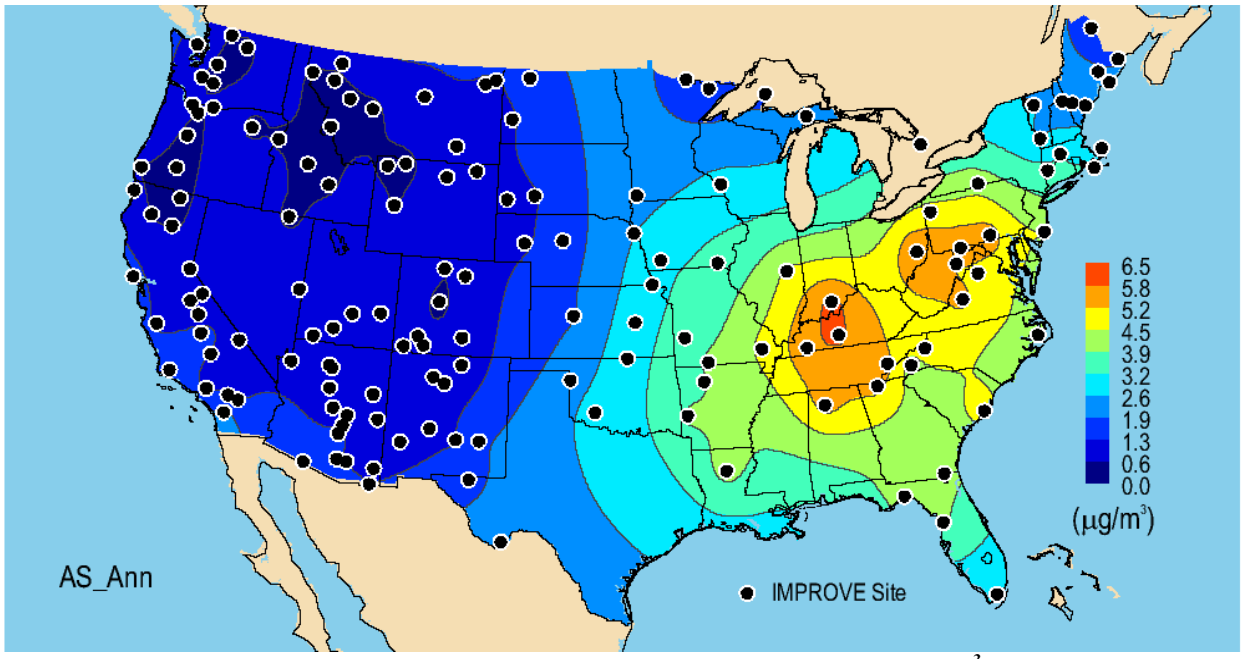

Figure 7.2.1. Interpolated annual mean ammonium sulfate (AS) concentrations (µg m^{-3}) for the rural IMPROVE network for 2005–2008. IMPROVE site locations are shown as black circles.

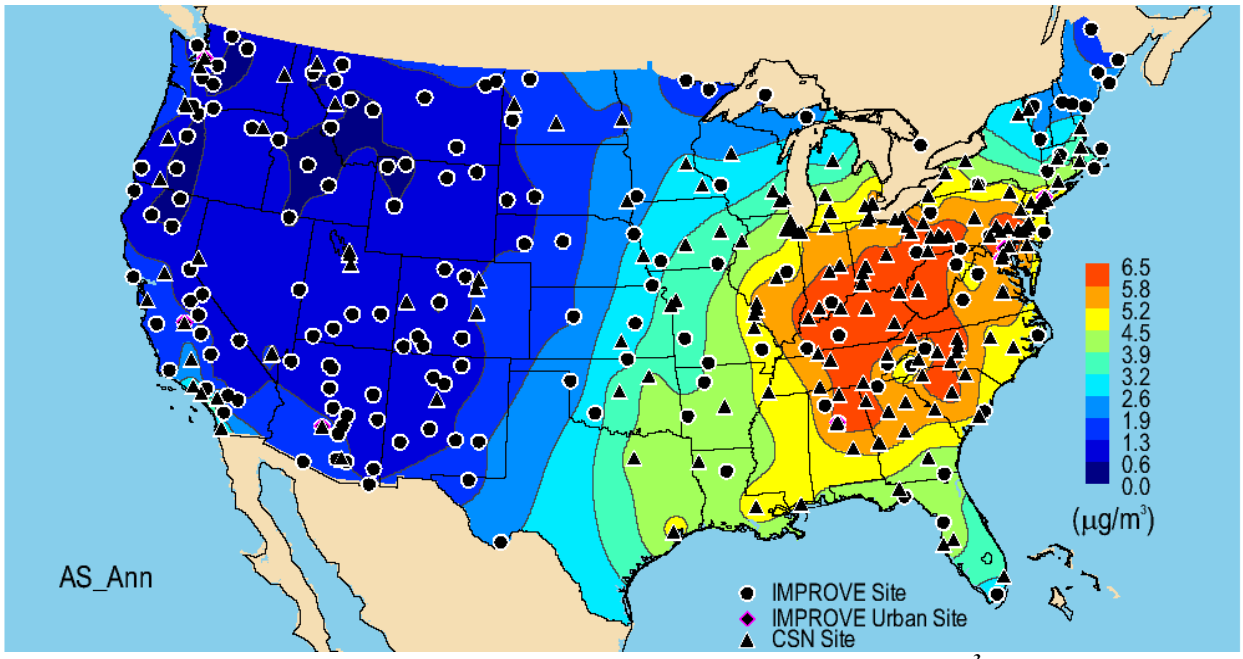

Figure 7.2.2. Interpolated annual mean ammonium sulfate (AS) concentrations (µg m^{-3}) for the rural IMPROVE and urban CSN networks for 2005–2008. IMPROVE site locations are shown as black circles, CSN sites are shown as black triangles, and urban IMPROVE sites are shown as magenta diamonds.

The ratio of urban to rural AS concentrations is shown in Figure 7.2.3. CSN site locations with an IMPROVE monitor within 150 km are depicted as black squares, and CSN sites that were not used in the analyses are shown as black triangles. The isopleth scale ranges from <1.26 to >2.0. The ratios ranged from 0.6 in Spokane (#530630016) to 2.9 in Los Angeles (#060371103). In addition to the southern California area, higher ratios occurred for a swath of area southeast of the Appalachian Mountains and the Ohio River valley. The lowest ratios occurred in the central, western, northwestern, and northeastern United States. The mean and one standard deviation in the ratio was 1.4 ± 0.3. Recall the relative bias of 7% in AS concentrations between CSN and the IMPROVE network, with CSN having larger concentrations (Table 1.9).

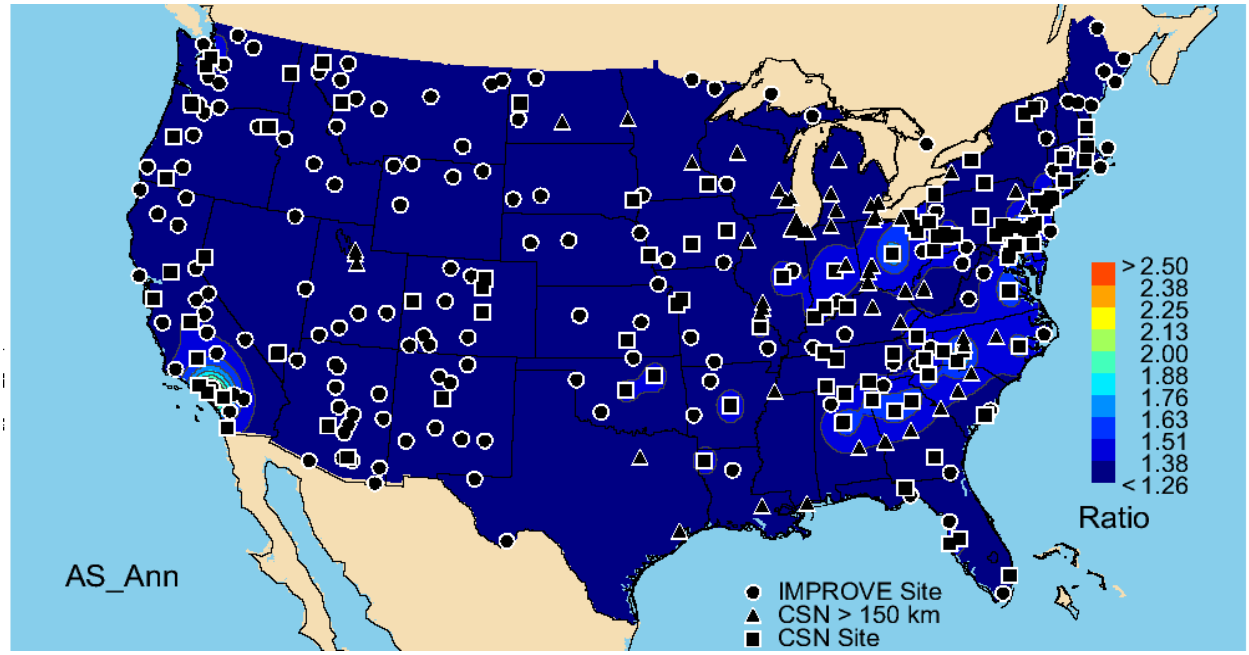

Figure 7.2.3. Interpolated ratios of urban (CSN) to rural (IMPROVE) annual mean ammonium sulfate (AS) concentrations for 2005–2008. IMPROVE sites are shown as circles, CSN sites with an IMPROVE monitor within 150 km are depicted as squares, and CSN sites not used in the analyses are shown as triangles.

The difference between urban and rural annual mean AS concentrations is shown in Figure 7.2.4. The scale ranges from <0.82 to >2.50 μg m^{-3}. Differences ranged from -0.7 μg m^{-3} in Spokane to 3.4 μg m^{-3} in Liberty, Pennsylvania (#420030064), with a mean of 1.3 ± 0.9 μg m^{-3}. Patterns in urban-rural differences highlight regions in the eastern United States, most likely because AS concentrations were higher there compared to the Southern California region. Higher differences corresponded to the Ohio River valley and Washington, D.C./Philadelphia Corridor and southeast of the Appalachian Mountains. Differences in these regions were ~2 μg m^{-3} or less. Most of the United States corresponded to differences less than 1 μg m^{-3}. The higher differences in the eastern United States may reflect the impact of site density and location on this type of analysis. While we focused on urban sites within 150 km of rural sites, the location of those sites could be important. For example, notice that the urban sites near the Appalachia Mountains region have rural sites to the north and west but no nearby sites in the southeast, corresponding to where ratios and differences were highest.

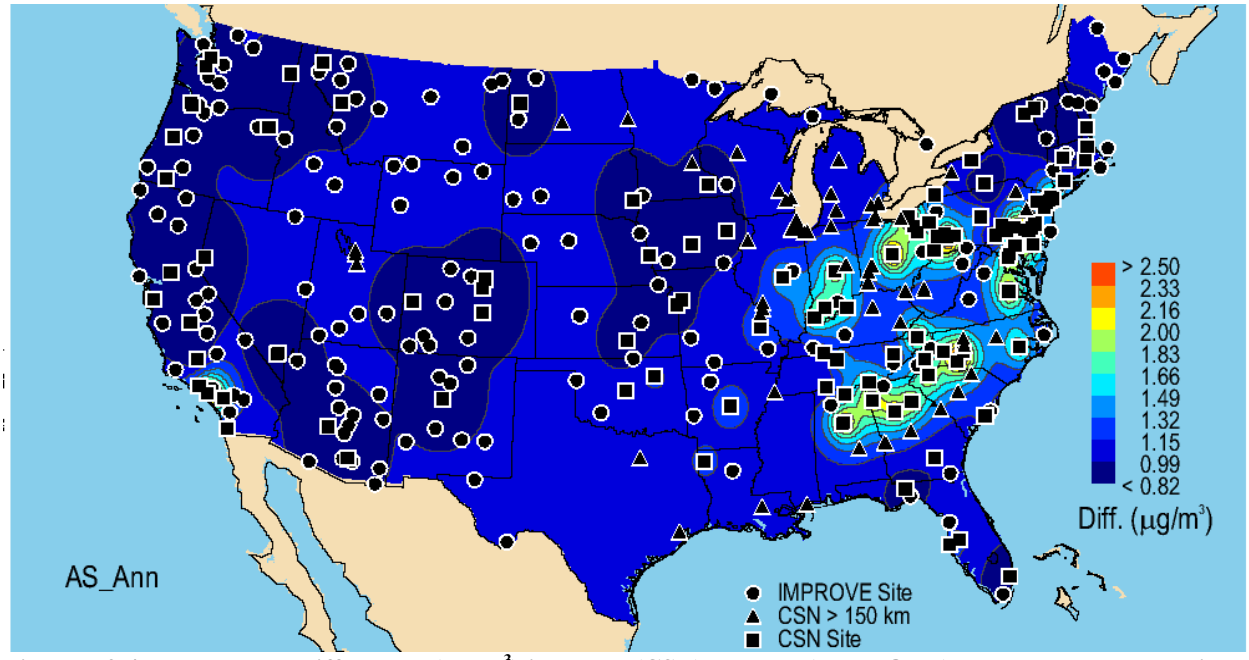

Figure 7.2.4. Interpolated differences (µg m^{-3}) in urban (CSN) to rural (IMPROVE) annual mean ammonium sulfate (AS) concentrations for 2005–2008. IMPROVE sites are shown as circles, CSN sites with an IMPROVE monitor within 150 km are depicted as squares, and CSN sites not used in the analyses are shown as triangles.

Rao et al. (2003) reported lower differences compared to those we derived; the over-all mean difference for the thirteen sites they investigated was 0.41 µg m^{-3} (we converted their sulfate ion mass difference to AS mass difference) and ranged from 0 to 1.4 µg m^{-3}. Our values at the same cities (although different time periods) ranged from -0.6 µg m^{-3} to 2.7 µg m^{-3}, with a mean of 1.8 ± 1.1 µg m^{-3}. We assumed we were using data from the same sites, although they did not list specific site ID. They also computed higher differences in sulfate ion mass for three western sites compared to ten eastern sites. In contrast, our analyses demonstrated larger differences in the eastern United States. Some of the discrepancy between our estimates and that of Rao et al. (2003) includes the different time periods of data used in the analysis and the calculation of rural aerosol concentration, as we applied a Kriging algorithm and they used a simple inverse weighting technique. The NARSTO (2004) assessment suggested that sulfate was strongly regional in the eastern United States. Urban excess ratios ranging from 1.05 to 1.33 were reported by the NARSTO assessment in a review of Hansen et al. (2003) for four urban-rural pairs of SEARCH (Southeastern Aerosol Research and Characterization Study) sites in Mississippi, Alabama, Georgia, and Florida from 1999 to 2001, consistent with our results. Allen and Turner (2008) also reported an urban to rural sulfate ratio of 1.05 in Saint Louis in 2001.

7.3 AMMONIUM NITRATE

Emissions of precursors to AN are higher in agricultural regions in the Midwest, resulting in the highest 2005–2008 annual mean concentrations of AN for rural sites (Figure 7.3.1). Elevated rural AN concentrations are also found in southern California in the West and near Baltimore and Washington, D.C. in the East, perhaps due to urban sources. Urban concentrations (Figure 7.3.2) were also higher in the Midwest and were considerably higher than rural concentrations in the same region. Relatively high urban AN concentrations in the Midwest

extended farther east to include several sites in Michigan, Indiana, Ohio, and Wisconsin. In addition, urban sources resulted in several localized areas with relatively high AN concentrations, such as cities in southern California, Salt Lake City, Denver, and cities in the northeastern United States.

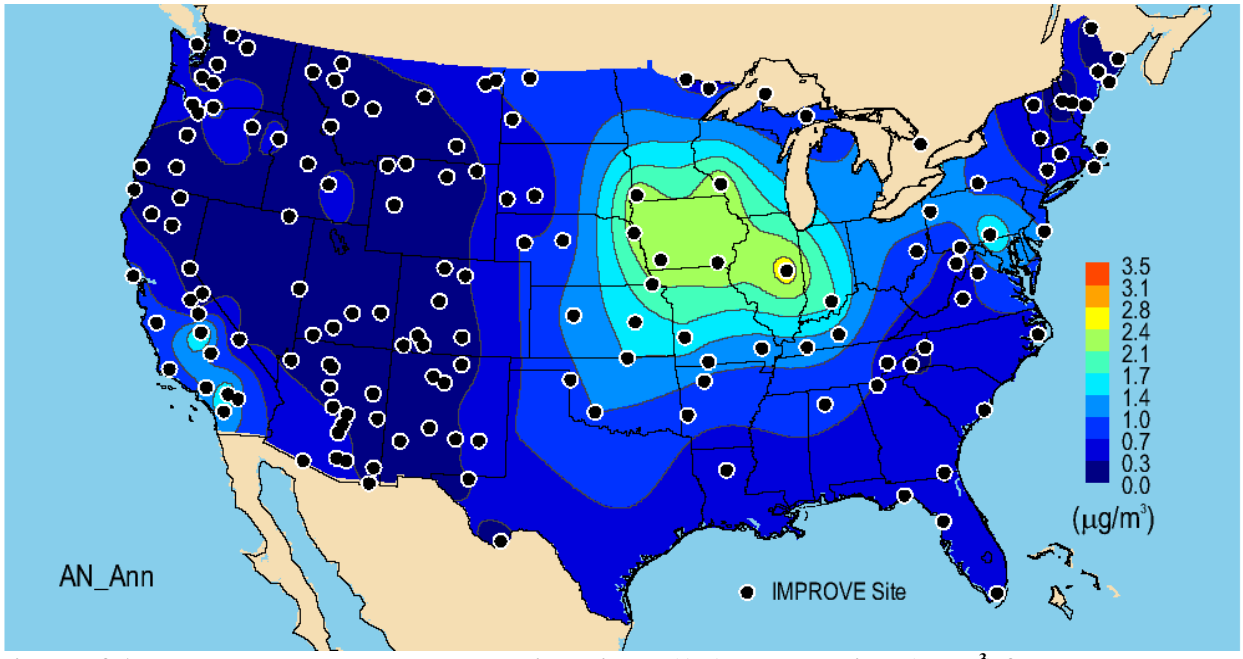

Figure 7.3.1. Interpolated annual mean ammonium nitrate (AN) concentrations (µg m^{-3}) for the rural IMPROVE network for 2005–2008. IMPROVE site locations are shown as black circles.

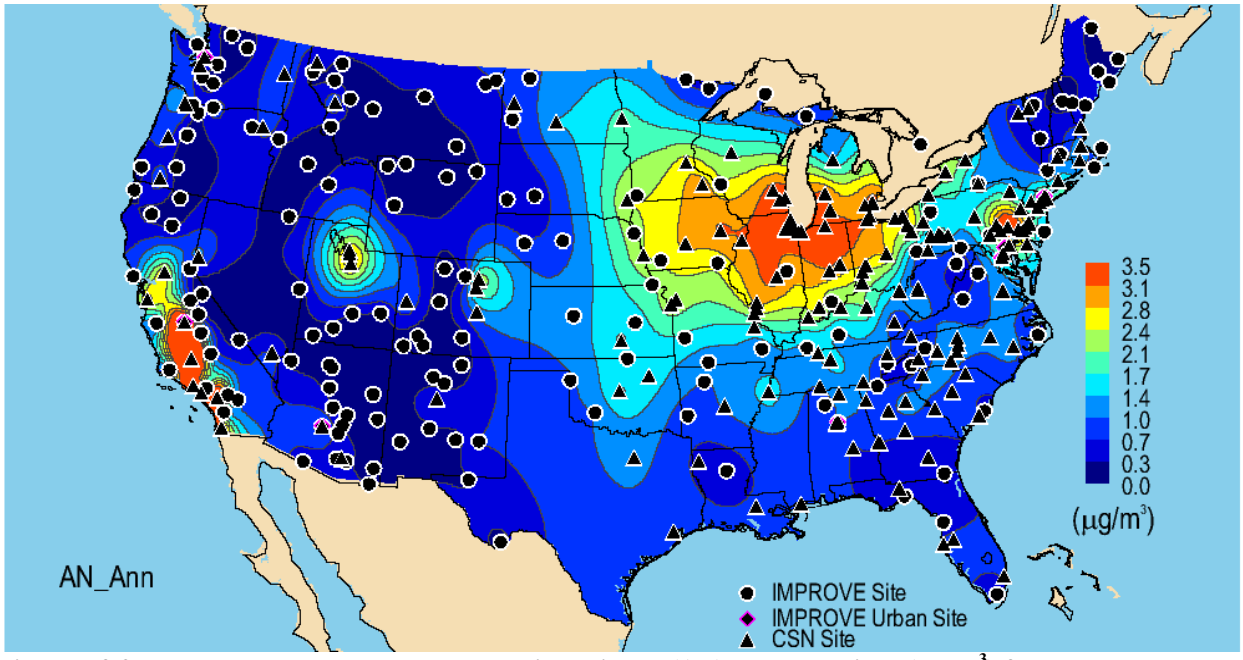

Figure 7.3.2. Interpolated annual mean ammonium nitrate (AN) concentrations (µg m^{-3}) for the rural IMPROVE and urban CSN networks for 2005–2008. IMPROVE site locations are shown as black circles, CSN sites are shown as black triangles, and urban IMPROVE sites are shown as magenta diamonds.

The impacts of urban sources of AN to surrounding rural regions were apparent by examining the ratio of urban to rural AN concentrations as shown in Figure 7.3.3. Western cities such as Denver, Missoula, and Medford, Oregon, corresponded to relatively high ratios with sharp spatial gradients. Most of California corresponded to higher ratios. Based on the differences in the rural and urban concentrations in the Great Lakes region of the Midwest presented in Figures 7.3.1 and 7.3.2, respectively, one would expect significant urban excess in that region. However, none of the urban sites in that area were associated with rural sites within 150 km (notice the sites depicted as triangles in that region); therefore low urban excess in that area was most likely due to lack of data. The urban to rural ratio ranged from 0.8 in Wilmington, New York, (#360310003) to 7.9 in Bakersfield, California (#060290014). The mean ratio (one standard deviation) was 2.5±1.3. Recall the relative bias in AN concentrations of 17.2% with CSN having higher concentrations.

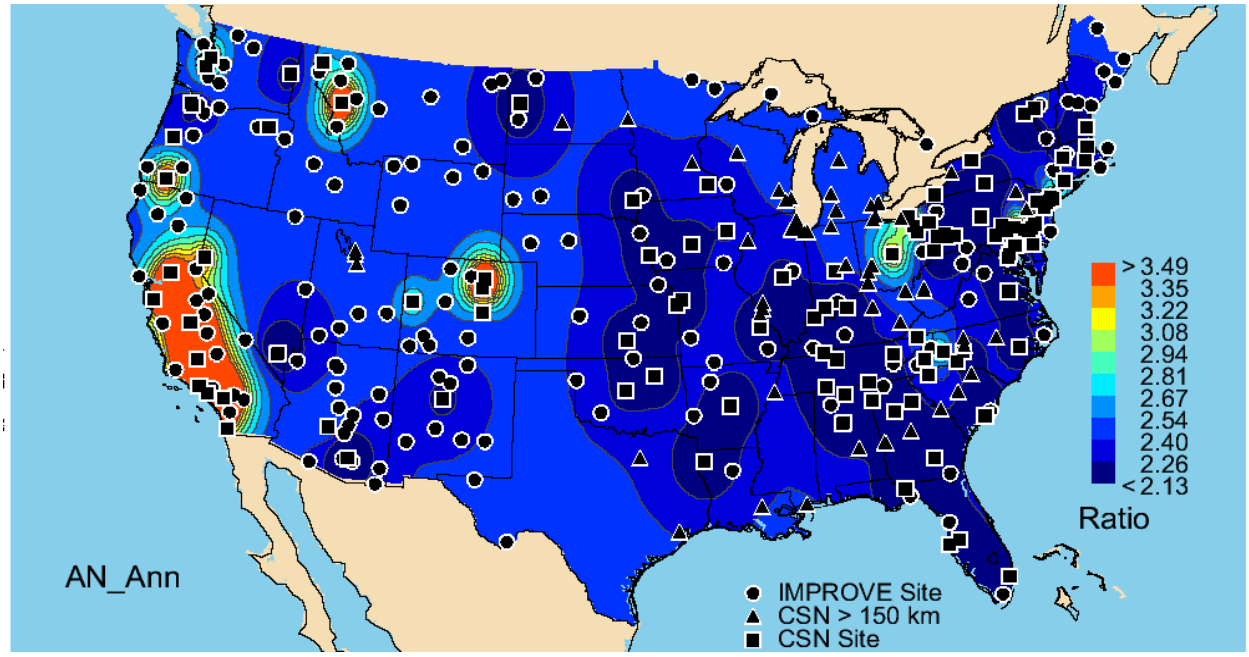

Figure 7.3.3. Interpolated ratios of urban (CSN) to rural (IMPROVE) annual mean ammonium nitrate (AN) concentrations for 2005–2008. IMPROVE sites are shown as circles, CSN sites with an IMPROVE monitor within 150 km are depicted as squares, and CSN sites not used in the analyses are shown as triangles.

The difference in urban and rural AN ranged from -0.11 μg m^{-3} in Wilmington to 7.8 μg m^{-3} in Rubidoux, California (#060658001). The mean difference was 1.2 ± 1.3 μg m^{-3}. The spatial pattern in the urban-rural difference is shown in Figure 7.3.4. Higher differences were associated with Denver, Rochester, Minnesota, Cedar Rapids, Iowa, Decatur, Illinois, Indianapolis, Columbus, Ohio, and New York City. Unlike urban to rural ratios, the differences in Medford, Oregon, were relatively low, probably because concentrations there were also relatively low (see Figure 7.3.2). Most of central and southern California corresponded to differences in AN concentrations around 1.9 μg m^{-3} or greater.

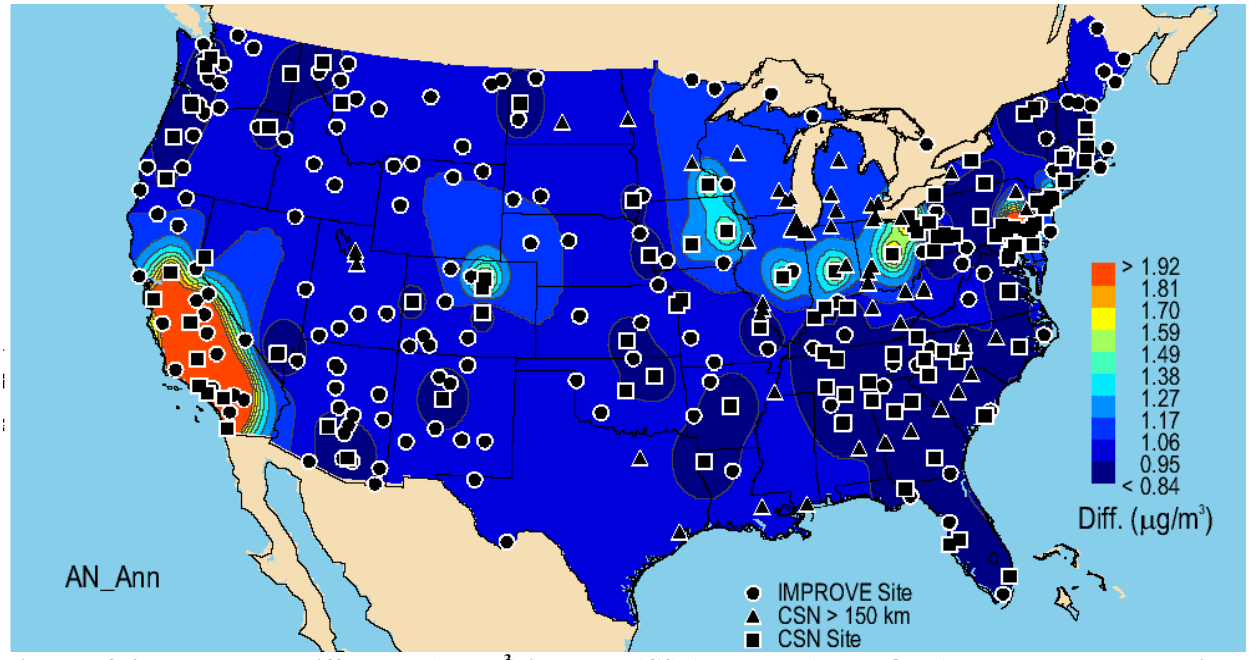

Figure 7.3.4. Interpolated differences (µg m^{-3}) in urban (CSN) to rural (IMPROVE) annual mean ammonium nitrate (AN) concentrations for 2005–2008. IMPROVE sites are shown as circles, CSN sites with an IMPROVE monitor within 150 km are depicted as squares, and CSN sites not used in the analyses are shown as triangles.

A similar range in urban to rural difference was computed by Rao et al. (2003). Their values ranged from 0.52 µg m^{-3} to 8.4 µg m^{-3}, with an average of 1.9 µg m^{-3} for thirteen sites. They found that higher values corresponded to western U.S. cities (Fresno and Salt Lake City) and in the central (Cleveland) and northeastern United States (Baltimore and the Bronx), similar to the spatial patterns shown in Figure 7.3.4. For the same cities we computed a difference range from 0.3 µg m^{-3} to 6.0 µg m^{-3} with a mean of 1.6 ± 1.5 µg m^{-3}. These estimates were in closer agreement than those for AS. Recall that estimates by Rao et al. (2003) correspond to a different time period.

Other studies in the central Midwest suggested regional-scale nitrate events with smaller urban excess (Allen and Turner, 2008, and references therein). In addition, the region-wide nitrate influence in the San Joaquin Valley in California was also observed during the CRPAQS study (Central California Regional PM10/PM2.5 Air Quality Study, Chow et al. 2006; Turkiewicz et al. 2006). While AN is secondary in nature, its spatial extent may be limited by its specific sources or equilibrium behavior in the atmosphere.

7.4 PARTICULATE ORGANIC MATTER

Urban excess estimates for POM did not account for different types of organic aerosols known to exist in urban versus rural settings. Urban organic aerosols from local sources are less aged and correspond to lower molecular weight per carbon weight ratios compared to rural aerosols (e.g., Turpin and Lim, 2001). We did not account for differences in the organic carbon multiplier for urban versus rural aerosols in this analysis (a value of 1.8 was applied to both), although Malm et al. (2011) suggested that the urban organic multiplier was 5–15% lower than

that for rural sites after investigating biases in fine mass data from the IMPROVE network and the CSN (also see Chapter 8).

The highest 2005–2008 rural annual mean POM concentrations corresponded to a large regional area in the southeastern United States (Figure 7.4.1), most likely associated with biogenic emissions and perhaps biomass smoke emissions (Tanner et al., 2004; Bench et al., 2007). The western United States was associated with more localized regions of higher rural POM concentrations. The impact of urban POM sources on local and regional POM concentrations was significant, as shown in Figure 7.4.2. In the southeastern United States, the regional extent of higher rural POM concentrations increased and the spatial pattern became more resolved with the addition of urban sites, especially to the southeast of the Appalachian Mountains. Higher POM concentrations and more localized impacts of urban POM sources were apparent in the western United States, such as for cities in Colorado, Utah, Nevada, Arizona, California, Oregon, Idaho, Montana, and Washington, with sharper gradients compared to the eastern United States.

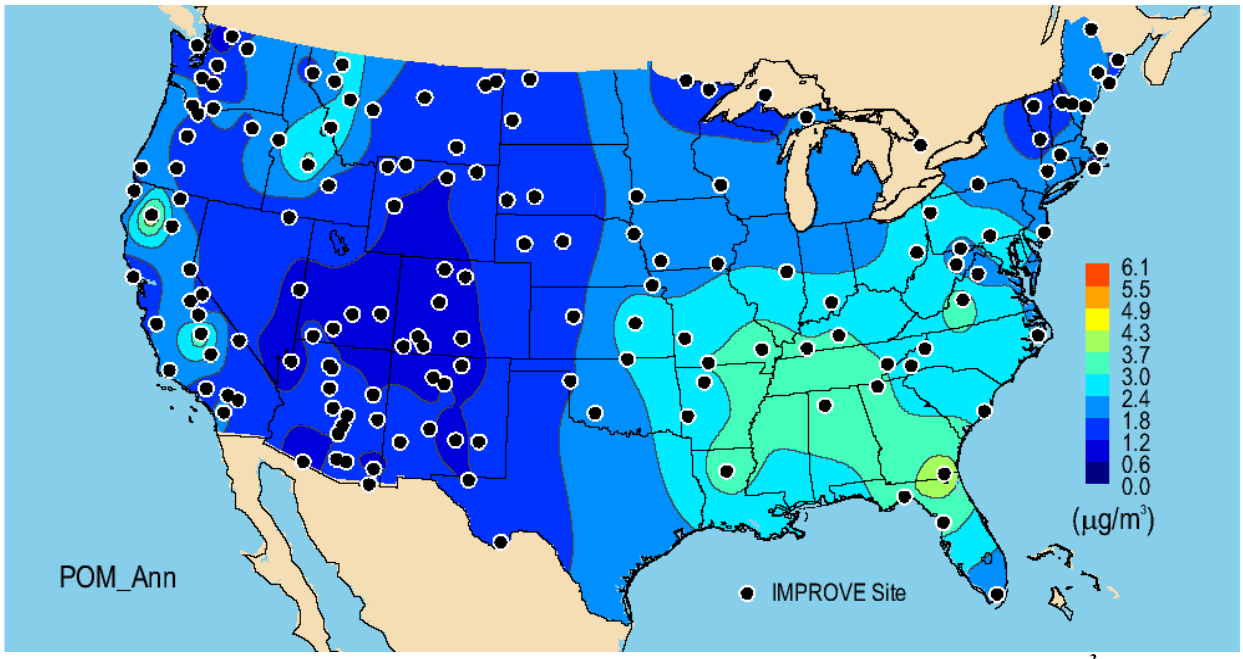

Figure 7.4.1. Interpolated annual mean particulate organic matter (POM) concentrations (µg m^{-3}) for the rural IMPROVE network for 2005–2008. IMPROVE site locations are shown as black circles.

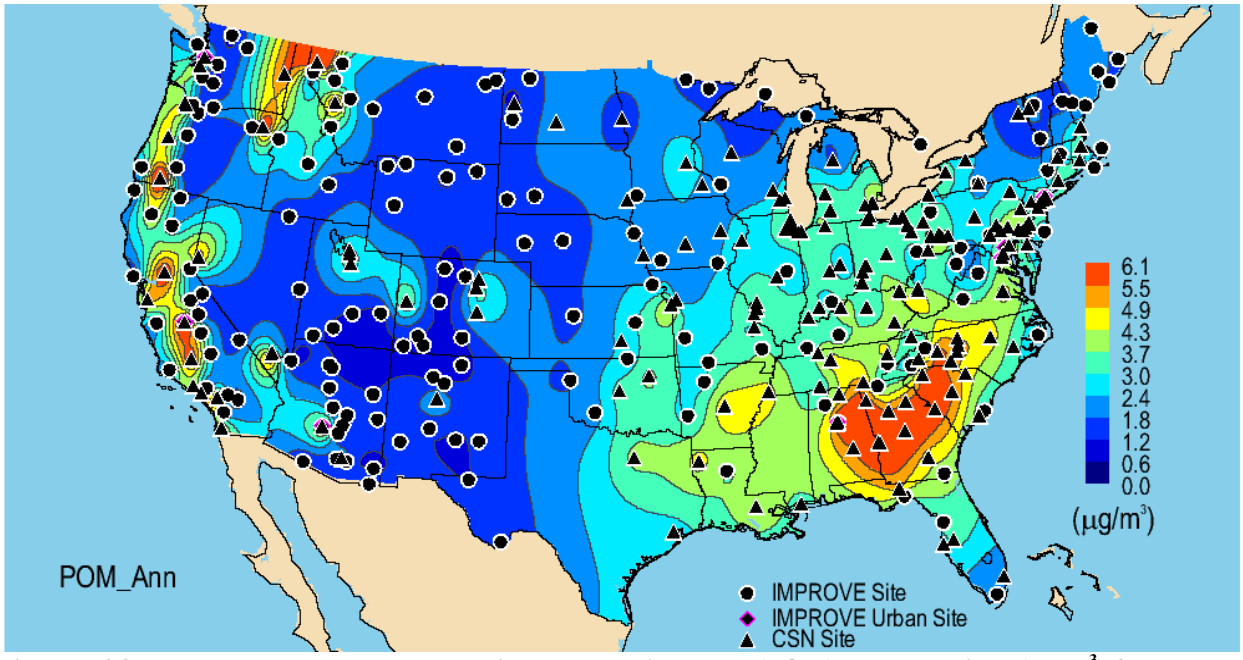

Figure 7.4.2. Interpolated annual mean particulate organic matter (POM) concentrations (µg m^{-3}) for the rural IMPROVE and urban CSN networks for 2005–2008. IMPROVE site locations are shown as black circles, CSN sites are shown as black triangles, and urban IMPROVE sites are shown as magenta diamonds.

This pattern of localized influence is displayed more clearly as the urban to rural concentration ratio in Figure 7.4.3. Several western cities were associated with higher ratios (urban concentrations over 2.5 times higher than rural concentrations), including Denver, Grand Junction, Phoenix, and Las Vegas. Several northwestern U.S. sites as well as most of California were associated with higher ratios. In the southeastern United States, a swath of area to the southeast of the Appalachian Mountains corresponded to ratios of ~2.3. This area was associated with the highest POM urban concentrations and the fewest number of rural IMPROVE sites. Urban concentrations were 1.9 ± 0.9 higher than rural concentrations on average. Ratios ranged from 0.6 in Wilmington, New York (#360310003, designated as a ~~r~~ural" site), to 6.7 in Libby, Montana (#300530018).

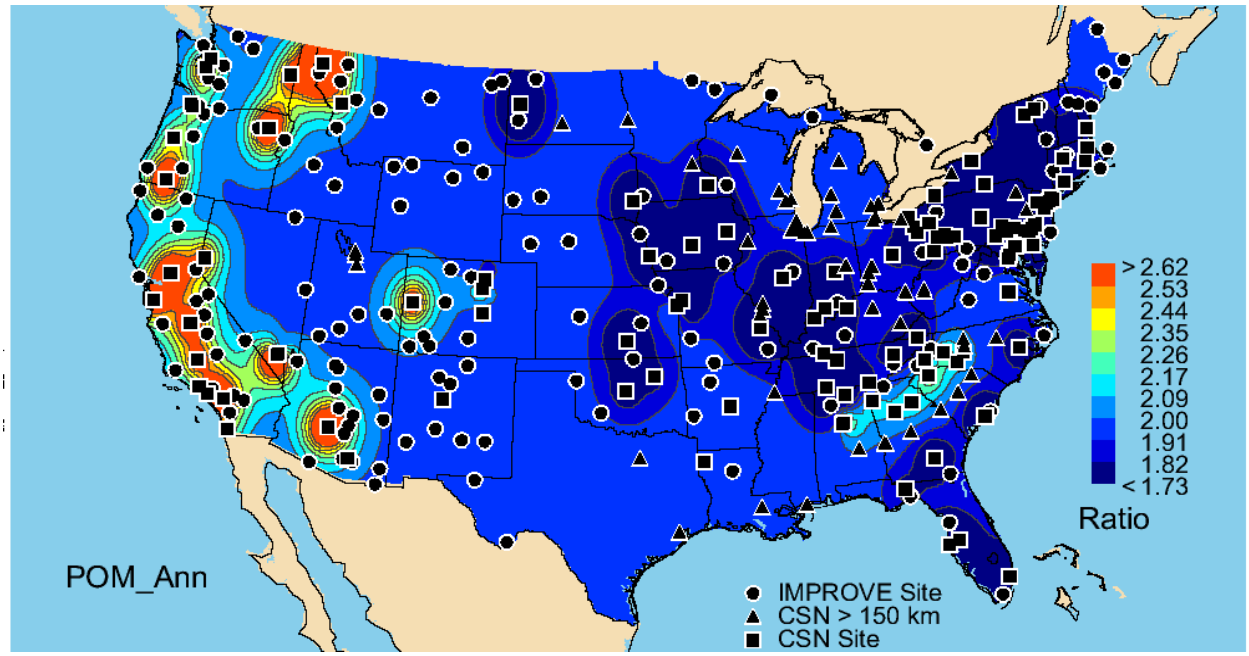

Figure 7.4.3. Interpolated ratios of urban (CSN) to rural (IMPROVE) annual mean particulate organic matter (POM) concentrations for 2005–2008. IMPROVE sites are shown as circles, CSN sites with an IMPROVE monitor within 150 km are depicted as squares, and CSN sites not used in the analyses are shown as triangles.

Similar spatial patterns were associated with urban-rural POM differences (Figure 7.4.4). Higher differences (over 3 μg m^{-3}) corresponded to sites along the western coast and in the northwestern United States. The differences in some western cities, such as Denver, Grand Junction, Phoenix, and Las Vegas were not as pronounced as for the ratio patterns, probably because concentrations were lower in those areas in general (see Figure 7.4.2). Higher differences were associated with the same swath of area in the southeastern United States as was observed in the ratio isopleths, but extended over a larger area. Differences ranged from -0.7 μg m^{-3} (Wilmington) to 9.9 μg m^{-3} (Libby), with an average urban to rural difference in annual mean POM concentration of 1.9 ± 1.6 μg m^{-3}. In general the impacts of urban POM sources were fairly local and contained within the first set of surrounding rural sites.

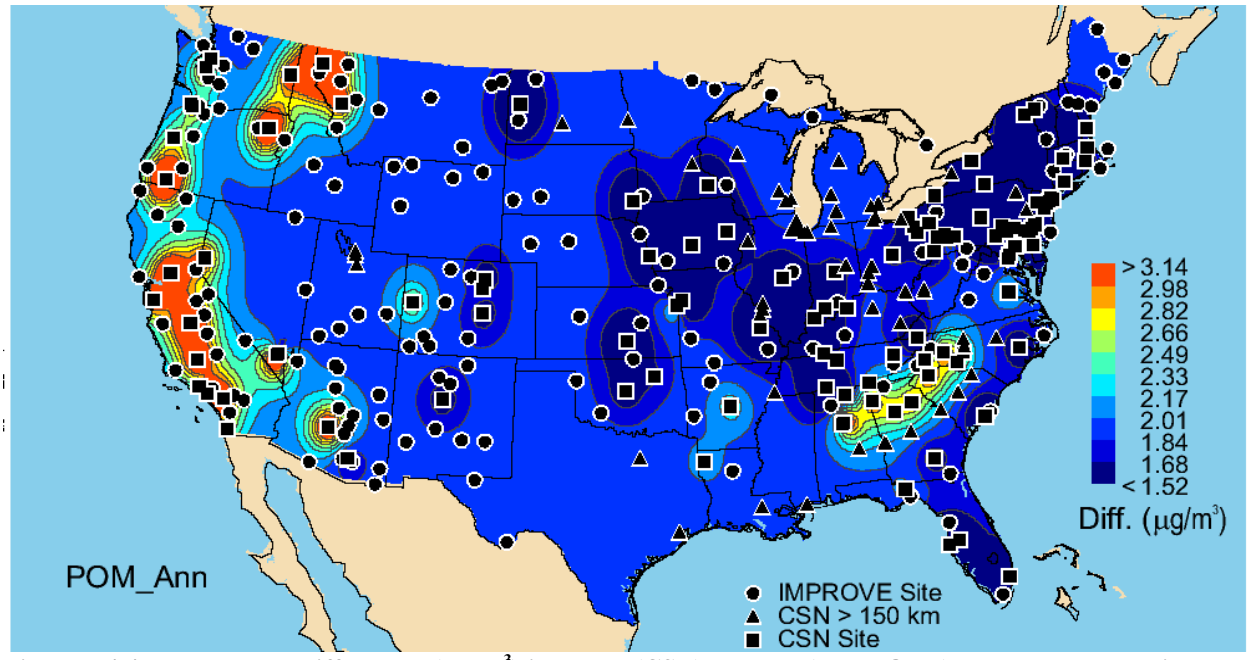

Figure 7.4.4. Interpolated differences (µg m^{-3}) in urban (CSN) to rural (IMPROVE) annual mean particulate organic matter (POM) concentrations for 2005–2008. IMPROVE sites are shown as circles, CSN sites with an IMPROVE monitor within 150 km are depicted as squares, and CSN sites not used in the analyses are shown as triangles.

The NARSTO assessment reported urban to rural ratios of 1.33–1.67 in the eastern United States, corresponding to SEARCH sites in Mississippi, Alabama, Georgia, and Florida, consistent with our findings (Hansen et al., 2003). Studies in California (Kim et al., 2000; Chow et al, 2006) suggested POM sources that were strongly local. An urban to rural ratio of 1.8 was computed at the Saint Louis Supersite during a 3-month study in 2001 (Allen and Turner, 2008). Rao et al. (2003) computed urban excess for total carbon, not POM and light absorbing carbon separately. We discuss those estimates at the end of the next section.

7.5 LIGHT ABSORBING CARBON

Spatial patterns in 2005–2008 annual mean rural concentrations of LAC were largely indistinguishable in Figure 7.5.1 when using the same scale as the urban map, suggesting that urban LAC concentrations were much larger than rural values. Urban LAC concentrations generally were localized around individual site locations in the western United States and more regional in extent in the eastern United States, although not to the degree of POM (see Figure 7.5.2). Western U.S. urban sites that corresponded to higher LAC concentrations also corresponded to higher POM concentrations (e.g., Denver, Las Vegas, and Phoenix and sites in California and the northwestern United States).

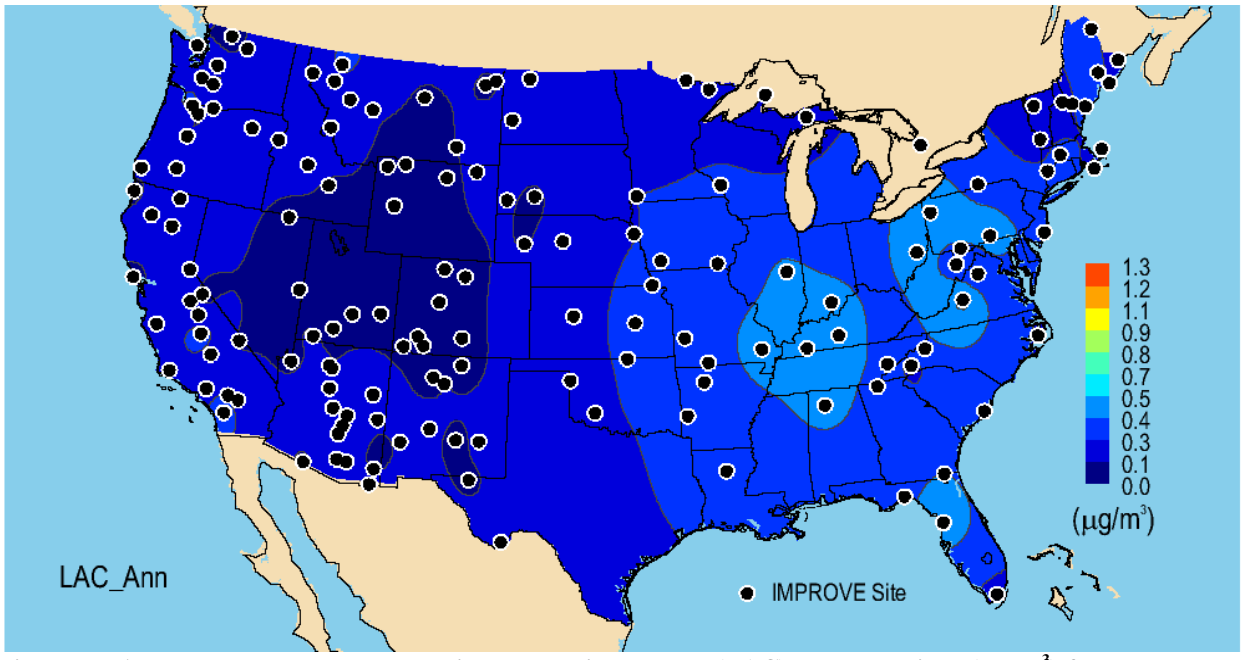

Figure 7.5.1. Interpolated annual mean light absorbing carbon (LAC) concentrations (µg m^{-3}) for the rural IMPROVE network for 2005–2008. IMPROVE site locations are shown as black circles.

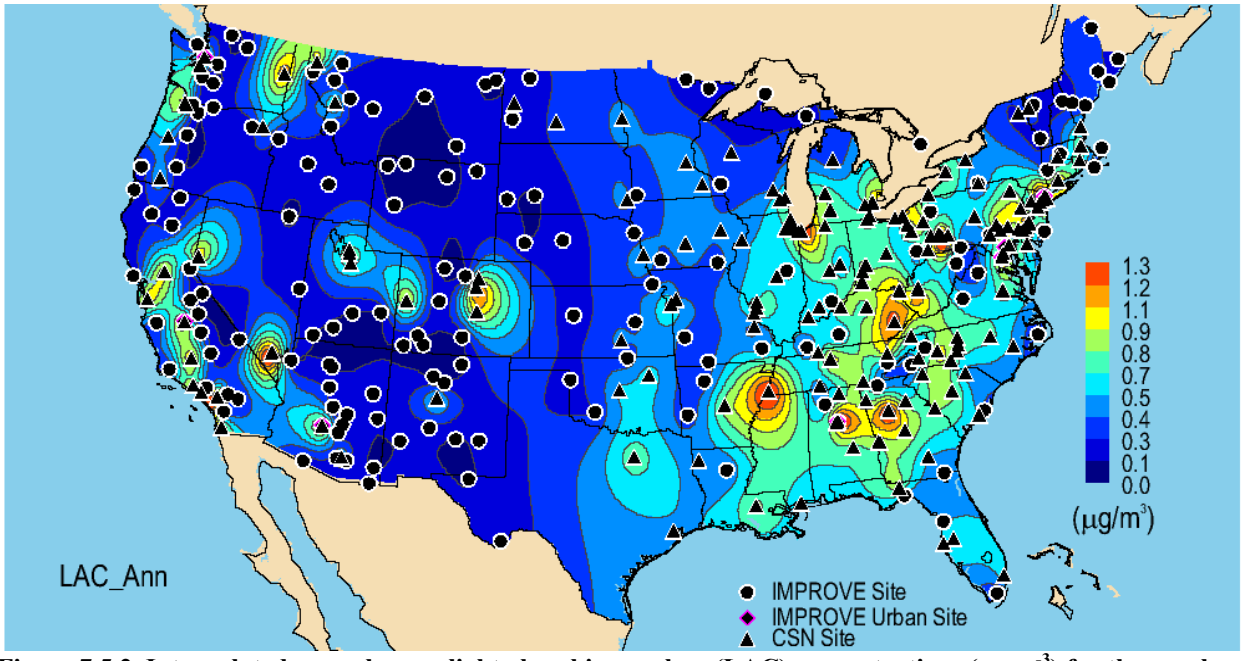

Figure 7.5.2. Interpolated annual mean light absorbing carbon (LAC) concentrations (µg m^{-3}) for the rural IMPROVE and urban CSN networks for 2005–2008. IMPROVE site locations are shown as black circles, CSN sites are shown as black triangles, and urban IMPROVE sites are shown as magenta diamonds.

The ratio of urban to rural LAC concentrations demonstrated the localized impact of LAC on surrounding rural regions. Fewer eastern U.S sites were associated with higher ratios compared to the western United States (Figure 7.5.3). Western U.S. sites in Colorado, Arizona, Nevada, California, Montana, and Washington were associated with high ratios with small spatial extent. In California the LAC excess was more localized compared to the spatial extent of

POM excess. Although the locations associated with high ratios were similar for POM and LAC, LAC ratios were much larger, suggesting urban LAC sources were significantly larger than rural sources and less regional in extent than POM. Ratios ranged from 0.8 in Watford City, North Dakota (#380530002, designated as a "rural" CSN site), to 10.5 in Las Vegas (#320030561). The mean ratio was 3.3 ± 1.9 and was much larger than the mean ratio for AS, AN, or POM.

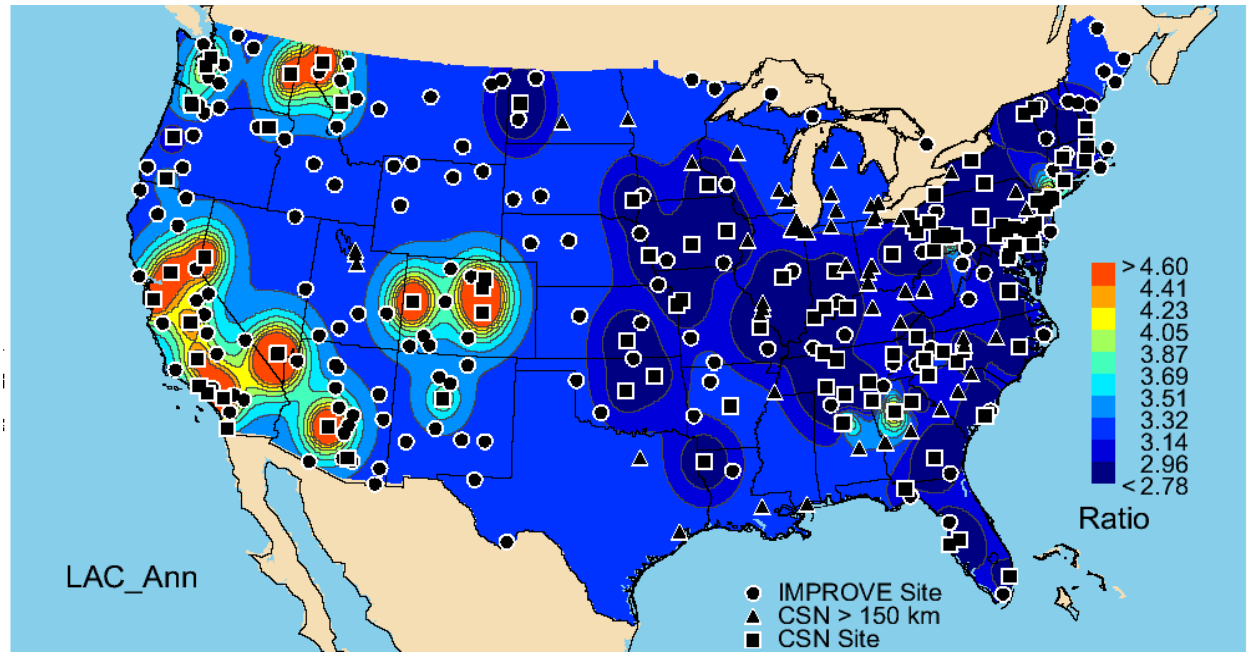

Figure 7.5.3. Interpolated ratios of urban (CSN) to rural (IMPROVE) annual mean light absorbing carbon (LAC) concentrations for 2005–2008. IMPROVE sites are shown as circles, CSN sites with an IMPROVE monitor within 150 km are depicted as squares, and CSN sites not used in the analyses are shown as triangles.

The urban to rural difference in LAC ranged from -0.05 μg m^{-3} in Watford City, North Dakota, to 2.2 μg m^{-3} in Liberty, Pennsylvania (#420030064). The mean difference was 0.6±0.4 μg m^{-3}, the lowest difference of all the species examined, but recall that LAC concentrations were relatively low. Patterns in urban to rural differences were similar to ratios for most western U.S. locations, but several additional locations emerged in the eastern United States (Figure 7.5.4). For most eastern U.S. locations, the differences were associated with tight gradients surrounding individual sampling sites. The spatial pattern in LAC difference was similar to POM differences but differed in the spatial extent, with the impact of urban LAC sources spatially localized.

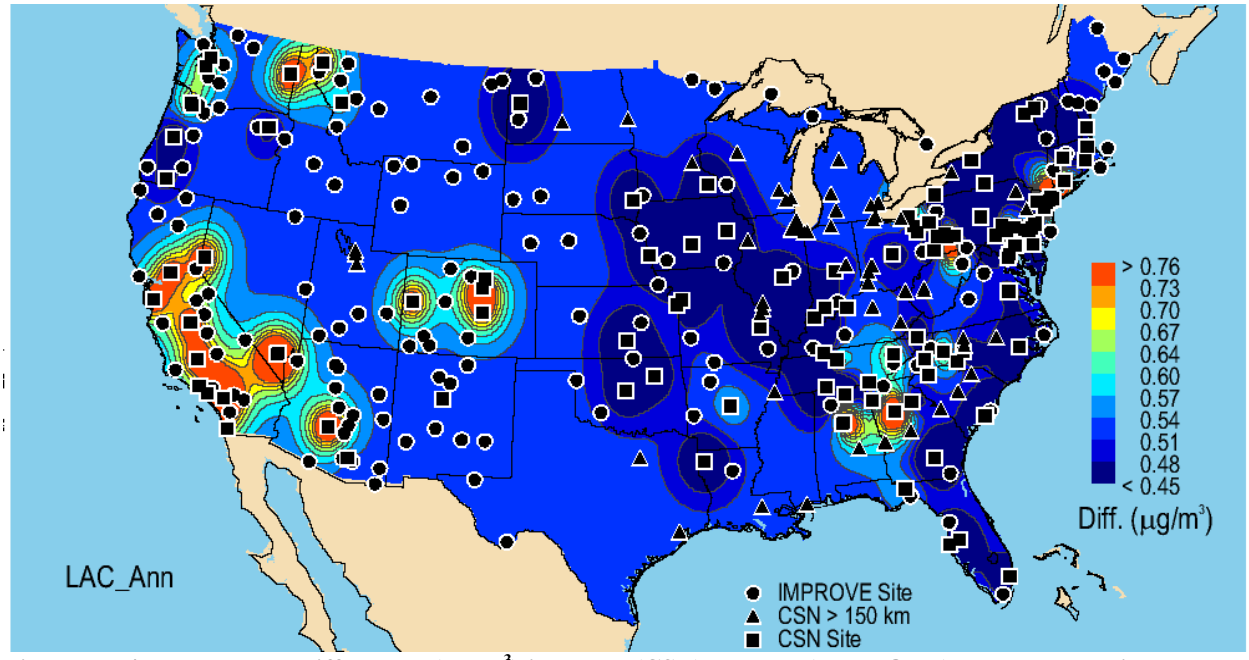

Figure 7.5.4. Interpolated differences (µg m^{-3}) in urban (CSN) to rural (IMPROVE) annual mean light absorbing carbon (LAC) concentrations for 2005–2008. IMPROVE sites are shown as circles, CSN sites with an IMPROVE monitor within 150 km are depicted as squares, and CSN sites not used in the analyses are shown as triangles.

As mentioned in the previous section, Rao et al. (2003) investigated urban excess in total carbon (TC) instead of POM and LAC separately, due to the differences in analytical methods and monitoring equipment between the CSN and IMPROVE networks. They computed TC by assuming an organic multiplier of 1.8 and derived differences in TC that ranged from 2.9 µg m^{-3} to 13.2 µg m^{-3} with a mean of 5.1 µg m^{-3}. Values were higher for cities in the western, northwestern, and southeastern United States. Combining our LAC and POM differences at the same sites resulted in a range of TC differences from 1.9 µg m^{-3} to 6.0 µg m^{-3} with a mean of 3.3±1.3 µg m^{-3}.

7.6 $PM_{2.5}$ GRAVIMETRIC FINE MASS

FM 2005–2008 annual mean concentrations for IMPROVE and CSN are shown in Figures 7.6.1 and 7.6.2, respectively. Plotting isopleths with the same scale reduced peaks in FM for the rural network, resulting in a less resolved pattern of FM concentrations in the eastern United States. In the western United States, urban regions with higher FM were associated with sites in southern California, Montana, Utah, Colorado, Nevada, and Arizona. Discussions from previous sections suggested that these hotspots were most likely associated with AN and POM concentrations. Higher FM concentrations in the eastern United States were associated with sites in the New York City-Philadelphia area and the Ohio River valley and Appalachian Mountains, probably associated with AS, POM, and AN.

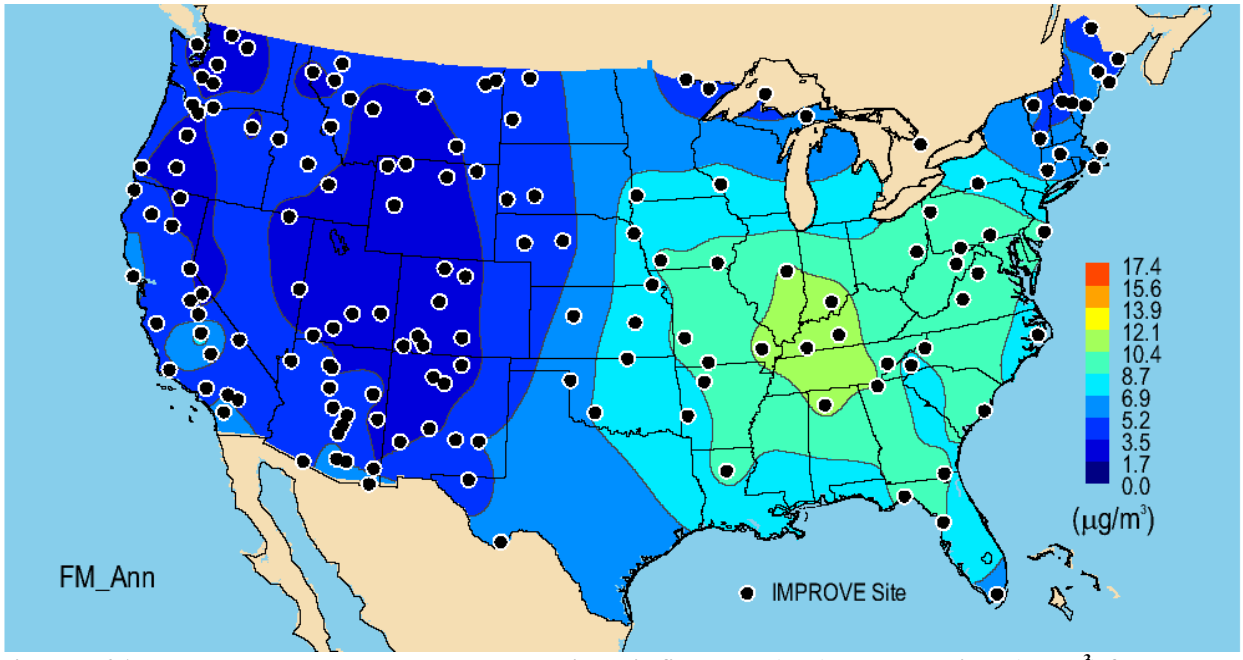

Figure 7.6.1. Interpolated annual mean $PM_{2.5}$ gravimetric fine mass (FM) concentrations (µg m^{-3}) for the rural IMPROVE network for 2005–2008. IMPROVE site locations are shown as black circles.

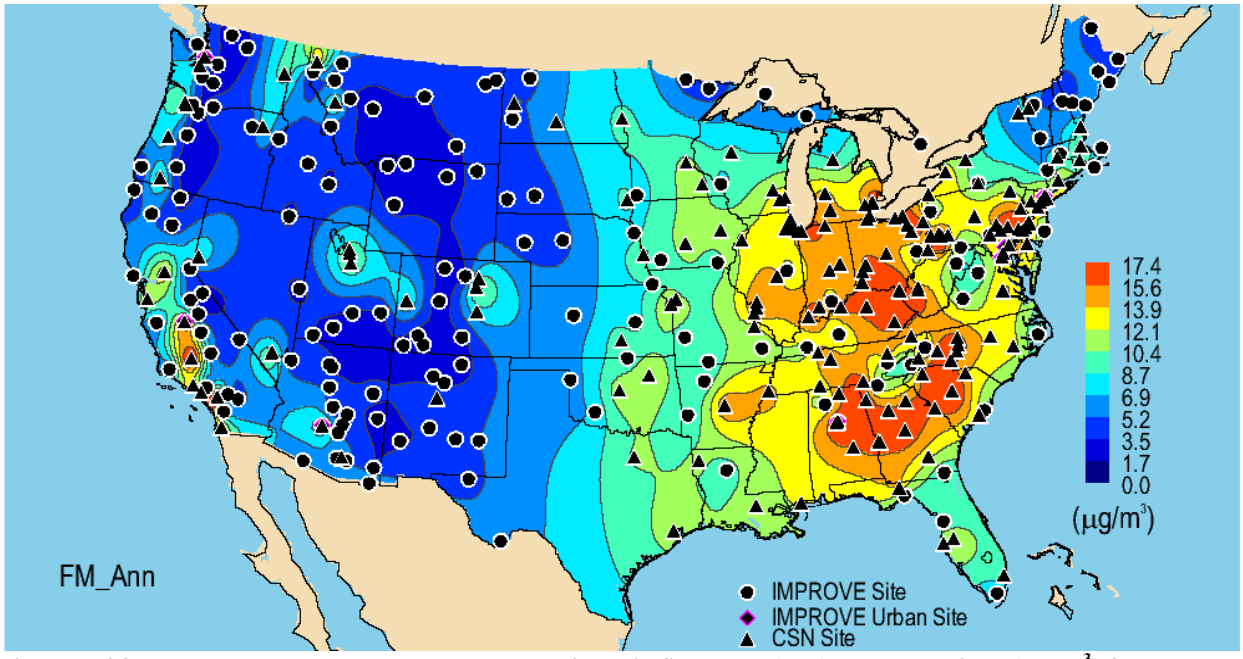

Figure 7.6.2. Interpolated annual mean $PM_{2.5}$ gravimetric fine mass (FM) concentrations (µg m^{-3}) for the rural IMPROVE and urban CSN networks for 2005–2008. IMPROVE site locations are shown as black circles, CSN sites are shown as black triangles, and urban IMPROVE sites are shown as magenta diamonds.

Ratios of urban to rural FM concentrations ranged from 1.0 (Wilmington, New York, #360310003) to 4.3 (Libby, Montana, #300530018), with a mean of 2.0 ± 0.6 and were highest at sites in central and southern California, Montana, Washington, Oregon, and Colorado (Figure 7.6.3). Patterns of high ratios in California were most likely associated with AN (see Figure 7.3.3), whereas patterns of high FM ratios in Washington, Oregon, Montana, Colorado, and Utah

were most likely due to a combination of POM and AN (see Figure 7.4.3). In the eastern United States, the patterns in FM were similar to those of AS (especially southeast of the Appalachian Mountains and the Ohio River Valley, see Figure 7.2.3), and POM (e.g., southeast of the Appalachian Mountains, Figure 7.4.3). Recall the relative bias of 18.4% between CSN and IMPROVE data, with CSN having higher FM concentrations.

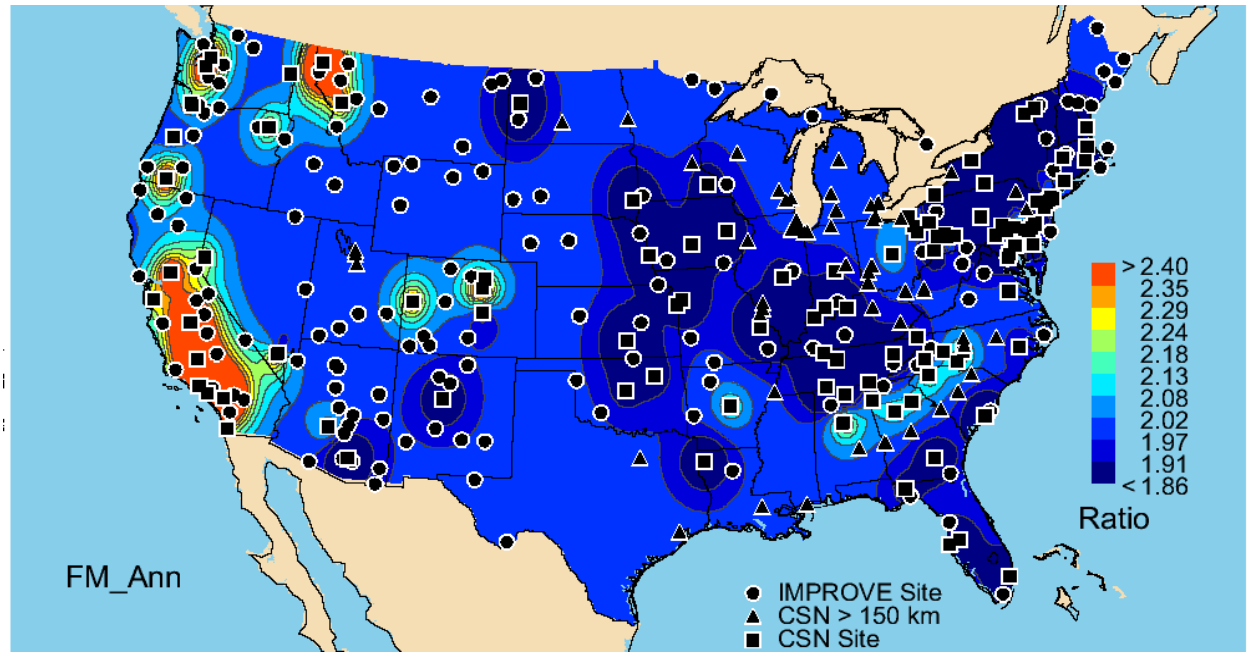

Figure 7.6.3. Interpolated ratios of urban (CSN) to rural (IMPROVE) annual mean $PM_{2.5}$ gravimetric fine mass (FM) concentrations for 2005–2008. IMPROVE sites are shown as circles, CSN sites with an IMPROVE monitor within 150 km are depicted as squares, and CSN sites not used in the analyses are shown as triangles.

Differences in FM concentrations ranged from 0.2 µg m^{-3} in Wilmington, New York, to 15.7 µg m^{-3} in Rubidoux, California (#060658001), with a mean of 7 ± 3 µg m^{-3}. The largest difference in FM corresponded to central and southern California, near Libby, Montana, near the Appalachian Mountains, and the Ohio River valley (see Figure 7.6.4). Excess values greater than 8 µg m^{-3} along the Appalachian Mountains were perhaps due to differences in POM (~3 µg m^{-3}, see Figure 7.4.4) and AS (~2 µg m^{-3}, see Figure 7.2.4).

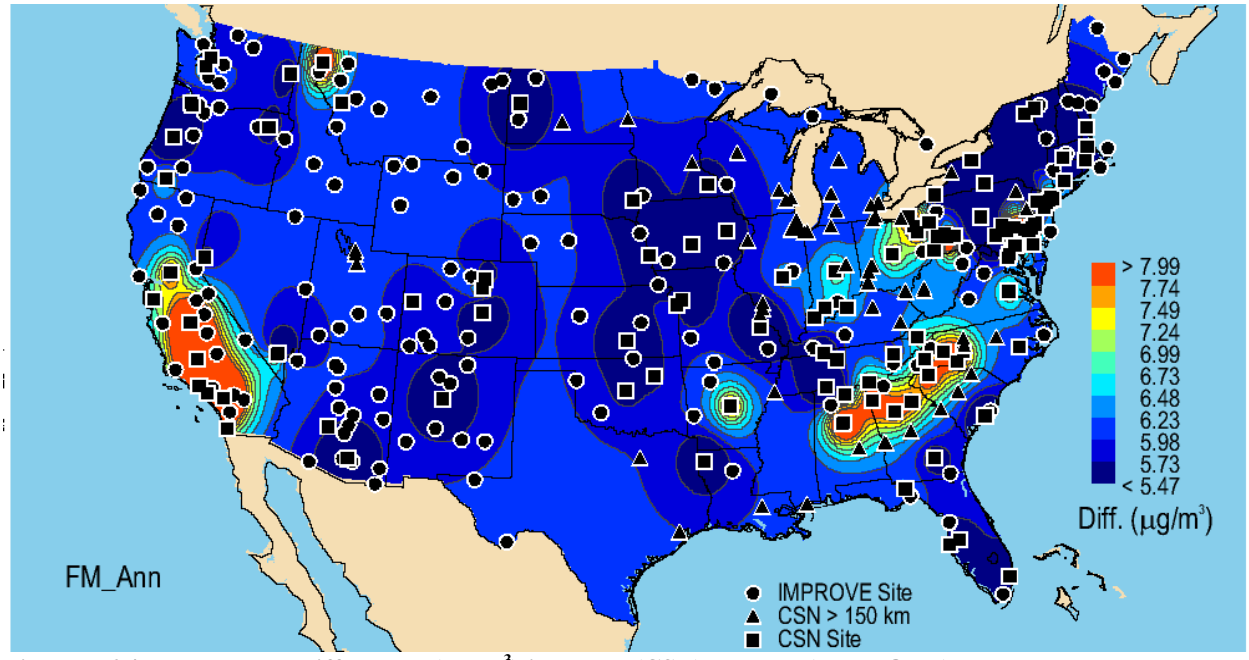

Figure 7.6.4. Interpolated differences (µg m^{-3}) in urban (CSN) to rural (IMPROVE) annual mean $PM_{2.5}$ gravimetric fine mass (FM) concentrations for 2005–2008. IMPROVE sites are shown as circles, CSN sites with an IMPROVE monitor within 150 km are depicted as squares, and CSN sites not used in the analyses are shown as triangles.

Although Rao et al. (2003) included FM in their analyses, they did not report urban excess values for it specifically so we were not able to perform comparisons with those results. However, the graphical display of their data suggested that the FM excess ranged from 4-16 µg m^{-3} (mean of ~8 µg m^{-3}), with higher values corresponded to western sites compared to sites in the East.

7.7 SUMMARY

The spatial patterns and magnitudes of urban excess (defined as either the urban to rural ratio or difference) differed significantly depending on species. This is not unexpected based on the differences in spatial patterns and seasonality of mass concentrations presented here and in Chapter 2 and Chapter 4. Scatter plots of urban and rural concentrations are shown in Figure 7.7.1a and Figure 7.7.1b and correspond only to the sites used in these analyses. The urban concentrations correspond to CSN data, while the rural concentrations correspond to the interpolated IMPROVE data at the CSN site location. Both figures present the same data but with a linear scale (Figure 7.7.1a) and a logarithmic scale (7.7.1b) to enhance the lower magnitude concentrations mainly associated with LAC. The relationship between rural and urban concentrations suggested that the magnitude of rural background concentrations is changing in response to regional influences and perhaps to local sources at nearby urban sites. The mass concentrations corresponding to different species separated according to their relative magnitudes and increased in order from LAC, AN, POM, and AS. These results suggested that the urban excess in AS increased for AS concentrations, as lower AS concentrations were in closer agreement. It was expected that the urban and rural AS concentrations would be similar, given the regional extent of sulfate sources in the area, when in fact the AS urban concentrations were higher than rural concentrations, with an average ratio of 1.4.

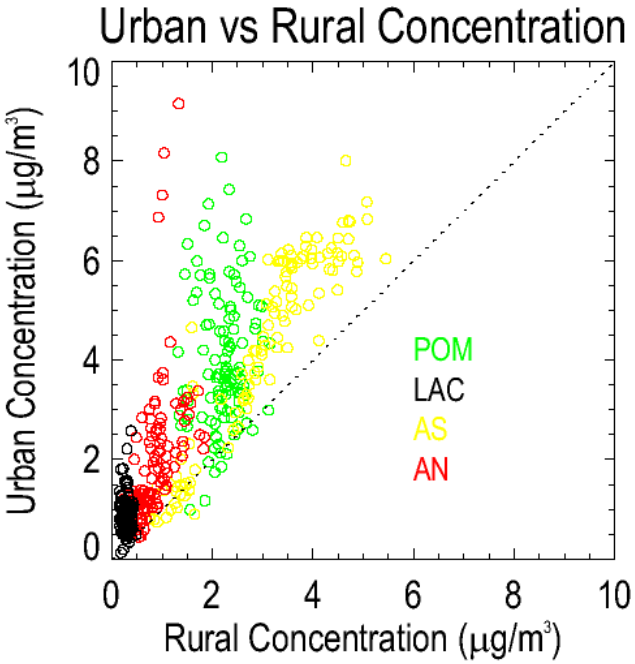

Figure 7.7.1(a). Comparisons of 2005–2008 annual mean IMPROVE rural concentration (interpolated) on the x-axis and CSN urban concentration (data) on the y-axis for ammonium sulfate (AS, yellow), ammonium nitrate (AN, red), particulate organic matter (POM, green), and light absorbing carbon (LAC, black). Concentrations are in µg m^{-3}.

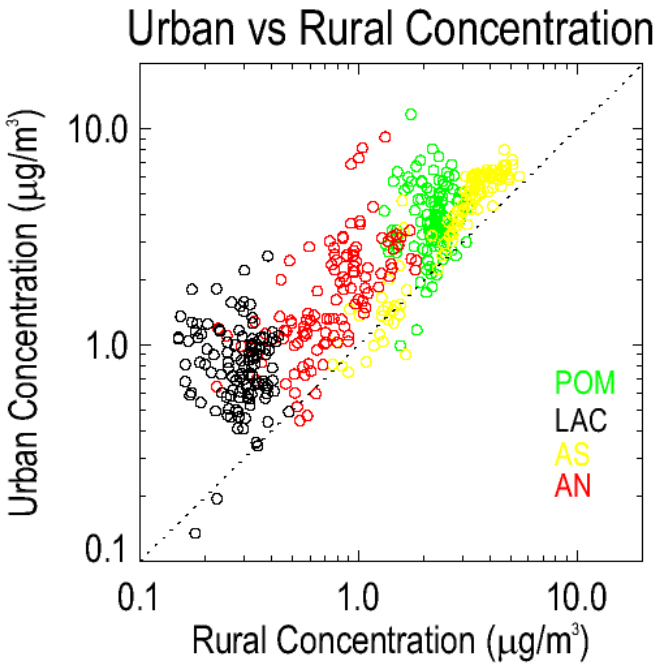

Figure 7.7.1(b). Same as part (a) but with a logarithmic scale.

Although the investigation was constrained to urban sites with rural sites within 150 km, site location (including elevation) and density could bias estimates of urban excess, especially when complicating factors such as wind direction were not accounted for. In addition to the issue

of site coverage, CSN site classification and location could also introduce uncertainties in urban excess estimates. While the CSN designates some sites as "rural", locations vary widely regarding the degree of remoteness of the location. In addition, some rural IMPROVE sites are located near urban sites, with urban influences being inevitable. All CSN sites were assumed to be "urban" and all IMPROVE sites were assumed to be "rural" in this analysis (urban IMPROVE sites were not considered in this analysis), but sites with locations that are not strictly classified into either category could introduce uncertainty into derived estimates. Furthermore, remote sites with elevations above the boundary layer could be sampling very different air masses compared to the urban sites to which they were compared.

These analyses provided urban excess estimates with spatial patterns for the United States. For certain species, such as POM, LAC, and AN, annual mean urban concentrations were considerably higher than rural concentrations. As a summary, the 2005–2008 annual mean AS urban excess mean ratio and difference (and one standard deviation) were 1.4 ± 0.3 and 1.3 ± 0.9 μg m^{-3}, respectively. The AN mean ratio and difference were 2.5 ± 1.3 and 1.2 ± 1.3 μg m^{-3}, respectively. The mean ratio and difference in POM urban to rural concentrations were 1.9 ± 0.9 and 1.9 ± 1.6 μg m^{-3}, respectively, while for LAC they were 3.3 ± 1.9 and 0.6 ± 0.4 μg m^{-3}, respectively. The mean FM ratio and difference were 2.0 ± 0.6 and 7 ± 3 μg m^{-3}, respectively. These estimates varied widely as a function location.

While the isopleths of urban excess were representative of actual concentrations only, they indicate the spatial extent of urban impacts on surrounding rural and remote areas as a function of species. For example, while LAC corresponded to the highest mean urban to rural concentration ratio, its spatial extent was generally the lowest and associated with sharp spatial gradients. In contrast, the spatial patterns in urban excess associated with species such as AS, POM, and FM were more regional in extent, especially in the eastern United States, although impacts from local sources were also apparent.

This type of analysis is simplistic in approach and subject to uncertainty but provides information that improves our understanding of the impact of regional and local urban sources to rural areas and potentially informs more effective regulatory efforts. A more thorough characterization of urban excess requires investigations into seasonal variability as well incorporating source emissions and back trajectory information.

REFERENCES

Allen, D. T. and J. R. Turner (2008), Transport of atmospheric fine particulate matter: Part 1—Findings from recent field programs on the extent of regional transport within North America, *J. Air & Waste Manage. Assoc. 58,* 254-264.

Bench, G., S. Fallon, B. Schichtel, W. Malm, and C. McDade (2007), Relative contributions of fossil and contemporary carbon sources to PM2.5 aerosols at nine Interagency Monitoring of Protected Visual Environments (IMPROVE) network sites, *J. Geophys. Res., 112,* D10205, doi:10.1029/2006JD007708.

Chow, J. C.; L.-W. A. Chen, J. G. Watson, D. H. Lowenthal, K. L Magliano, K. Turkiewicz, D. Lehrman (2006), PM2.5 chemical composition and spatiotemporal variability during the

California Regional PM10/PM2.5Air Quality Study (CRPAQS); *J. Geophys. Res. 111*, D10S04, doi:10.1029/2005JD006457.

Dutkiewicz, V. A., S. Qureshi, A. R. Khana, V. Ferraro, J. Schwab, K. Demerjian, L. Husain (2004), Sources of fine particulate sulfate in New York; *Atmos. Environ.*, *38,* 3179-3189.

Eatough, D. J., R. R. Anderson, D. V. Martello, W. K. Modey, N. F. Mangelson (2006), Apportionment of ambient primary and secondary PM2.5 during a 2001 summer intensive study at the NETL Pittsburgh Site Using PMF2 and EPA UNMIX; *Aerosol Sci. Technol.*, *40,* 925-940.

Hansen, D. A., E. E. Edgerton, B. E. Hartsell, J. J. Jansen, N. Kandasamy, G. M. Hidy, and C. L. Blanchard (2003), The Southeastern Aerosol Research and Characterization Study: Part 1—Overview, *J. Air & Waste Manage. Assoc. 53,* 1460-1471.

Kim, B. M., S. Teffera, and M. D. Zeldin (2000), Characterization of PM2.5 and PM10 in the South Coast Air Basin of Southern California: Part 1—Spatial Variations, *J. Air & Waste Manage. Assoc., 50,* 2034, 2044.

Liu, W. P. K. Hopke, Y. Han, S. Yi, T. M. Holsen, S. Cybart, K. Kozlowski, M. Milligan, (2003), Application of Receptor Modeling to Atmospheric Constituents at Potsdam and Stockton, NY; *Atmos. Environ. 37,* 4997-5007.

Liu, W. Y. Wang, A. Russell, E. S. Edgerton (2005), Atmospheric aerosol over two urban–rural pairs in the southeastern United States: Chemical composition and possible source; *Atmos. Environ. 39,* 4453-4470.

Malm, W. C., B. A. Schichtel, and M. L. Pitchford (2011), Uncertainties in PM2.5 gravimetric and speciation measurements and what we can learn from them, *J. Air Waste Manage,* In press.

McMurry, P. H., M. F. Shepherd, J. S. Vickery, Eds (2004), *Particulate Matter Science for Policy Makers: a NARSTO Assessment*; Cambridge University Press: Cambridge, U.K.

Pekney, N.J., C. I. Davidson, L. Zhou, and P. K. Hopke (2006), Application of PSCF and CPF to PMF-Modeled Sources of PM2.5 in Pittsburgh; *Aerosol Sci. Technol. 40,* 952-961.

Rao, V., N. Frank, A. Rush, and F. Dimmick (2003), Chemical speciation of PM2.5 in urban and rural areas, in Symposium on Air Quality Measurement Methods and Technology—2002 [CD-ROM], Air and Waste Manage. Assoc., Pittsburgh, Pa.

Russell, M. M., D. T. Allen, D. R. Collins, and M. P. Fraser (2004), Daily, seasonal and spatial trends in PM2.5 mass and composition in southeast Texas, *Aerosol Sci. Technol., 38*, 14-26.

Turkiewicz, K., K. Magliano, and T. Najita (2006), Comparison of two winter air quality episodes during the California Regional Particulate Air Quality Study, *J. Air & Waste Manage. Assoc.*, *56,* 467-473.

Turpin, B. J., and H.-J. Lim (2001), Species contributions to $PM_{2.5}$ mass concentrations: Revisiting common assumptions for estimating organic mass, *Aerosol Sci. Technol., 35,* 602-610.

U.S. EPA (1999), Regional Haze Regulations; Final Rule, 40 CFR 51, Federal Register, 64, 35714-35774.

U.S. EPA (2004), The Particle Pollution Report: Current understanding of air quality and emissions through 2003, EPA 454-R-04-002, Contract No. 68-D-02-065, Work Assignment No. 2-01, http://www.epa.gov/airtrends/aqtrnd04/pmreport03/report_2405.pdf.

Chapter 8. Uncertainties in $PM_{2.5}$ Gravimetric and Speciation Measurements

William C. Malm, Bret A. Schichtel, and Marc L. Pitchford

ABSTRACT

The Environmental Protection Agency (EPA) and the federal land management community (National Park Service, United States Fish and Wildlife Service, United States Forest Service, and Bureau of Land Management) operate extensive particle speciation monitoring networks that are similar in design but are operated for different objectives. Compliance (mass only) monitoring is also carried out using federal reference method (FRM) criteria at approximately 1000 sites. The Chemical Speciation Network (CSN) consists of approximately 50 long-term-trend sites, with about another 250 sites that have been or are currently operated by state and local agencies. The sites are located in urban or suburban settings. The Interagency Monitoring of Protected Visual Environments (IMPROVE) monitoring network consists of about 181 sites, approximately 170 of which are in nonurban areas. Each monitoring approach has its own inherent monitoring limitations and biases. Determination of gravimetric mass has both negative and positive artifacts. Ammonium nitrate and other semivolatiles are lost during sampling, while on the other hand, measured mass includes particle-bound water. Furthermore, some species may react with atmospheric gases, further increasing the positive mass artifact. Estimating aerosol species concentrations requires assumptions concerning the chemical form of various molecular compounds, such as nitrates and sulfates, and organic material and soil composition.

Comparing data collected in the various monitoring networks allows for assessing uncertainties and biases associated with both negative and positive artifacts of gravimetric mass determinations, assumptions of chemical composition, and biases between different sampler technologies. All these biases are shown to have systematic seasonal characteristics. Unaccounted-for particle-bound water tends to be higher in the summer, as is nitrate volatilization. The ratio of particle organic mass divided by organic carbon mass (Roc) is higher during summer and lower during the winter seasons in both CSN and IMPROVE networks, and Roc is lower in urban than nonurban environments.

IMPLICATIONS

$PM_{2.5}$ National Ambient Air Quality Standards (NAAQS) are based on gravimetric analysis of particulate matter collected on a Teflon substrate, using federal reference methodologies, while compliance under the Regional Haze Rule (RHR) is based on atmospheric extinction, derived from measurements of individual aerosol species. Gravimetric mass can be over- or underestimated because of volatilization issues and water retention by inorganic species, while species-specific estimates of mass are dependent on assumptions concerning their detailed chemical composition. Over- or underestimation of aerosol species or gravimetric mass could result in violation of standards or failure to meet visibility goals established under the RHR.

8.1 INTRODUCTION

The Environmental Protection Agency (EPA) and the federal land management community (National Park Service, United States Fish and Wildlife Service, United States Forest Service, and Bureau of Land Management) are responsible for the operation of two extensive particle monitoring networks that are similar in their design but serve different objectives. The Chemical Speciation Network (CSN) (http://www.epa.gov/ttn/amtic/speciepg.html) consists of approximately 50 long-term-trend sites, with about another 250 sites that are or have been operated by state and local agencies. The sites are located in urban and suburban settings. The objectives of the CSN are to track progress of emission control programs, develop emission control strategies, and characterize annual and seasonal spatial and temporal trends. The CSN data are also used for validating regional air quality models and source apportionment modeling and for linking health effect endpoints to constituents in particulate matter less than 2.5 microns in size ($PM_{2.5}$). National Aerosol Air Quality Standards (NAAQS) compliance (mass only) monitoring is also carried out using federal reference methods (FRM) at approximately 1000 sites (U.S. EPA, 1998).

The Interagency Monitoring of Protected Visual Environments (IMPROVE) monitoring network consists of about 181 sites, approximately 170 of which are in nonurban areas (Malm et al. 1994). The IMPROVE monitoring program is used primarily to track long-term temporal changes in visibility in protected visual environments, consistent with the needs of the Regional Haze Rule (RHR) (Regional Haze Regulations, 1999). Compliance under the RHR is based on reconstructed aerosol mass and light extinction from aerosol composition. Data collected in IMPROVE is also used to identify chemical species and emission sources responsible for existing man-made visibility impairment in federal Class I areas, for identification of episodes of long-range transport (e.g., smoke, dust, sulfates, nitrates, etc., from distant sources), to serve as a regional backdrop for special studies, for regional modeling validation studies, and to support the development and implementation of $PM_{2.5}$ NAAQS by characterizing nonurban regional background levels (see Sections 169A and 169B of the Clean Air Act (42) U.S.C. §§ 7491, 7492 and implementing regulations at 40 CFR 51.308 and 51.309 containing legally binding requirements).

The $PM_{2.5}$ speciation target analytes for both monitoring networks are similar and consist of an array of ions, carbon species, and trace elements (Malm et al., 1994; Chemical Speciation: Laboratory Standard Operating Procedures, http://www.epa.gov/ttnamti1/specsop.html). Each series of analytes requires sample collection on an appropriate filter medium to allow chemical analysis with methods of adequate sensitivity. The methods used for analyses of these filter media include gravimetry (electro-microbalance) for mass; energy dispersive x-ray fluorescence for trace elements; ion chromatography (IC) for anions and cations; and controlled-combustion thermal optical transmittance and reflectance (TOT/TOR) analysis for carbon.

$PM_{2.5}$ compliance monitoring is based on the gravimetric mass concentrations, while determining progress toward natural visibility conditions under RHR requirements is achieved through estimations of extinction, using speciated mass concentrations and measured relative humidity (RH). Each approach has its own inherent monitoring limitations. $PM_{2.5}$ mass is determined gravimetrically by pre- and post-weighing of Teflon filter media, after equilibrating at 20–23^{o}C and 30–40% RH. Determination of gravimetric mass using this procedure has both

negative and positive artifacts. Ammonium nitrate and other semivolatiles, such as some organic species, are, in part, lost during sampling, while on the other hand, measured mass includes particle-bound water associated with hygroscopic species such as sulfates, nitrates, sea salt, and possibly some organic species (Frank, 2003). Furthermore, some species may react with atmospheric gases, which tend to contribute to a positive artifact. Conditions under which filter substrates are shipped as well as on-site storage practices can also affect retention and evolution of collected aerosol material.

The RHR specifies that measured individual species concentrations be converted to total mass concentrations and extinction. The total mass derived from measured species will be referred to as reconstructed mass. It is assumed that sulfates are fully neutralized as ammonium sulfate, nitrates are in the form of ammonium nitrate, organic carbon mass is estimated from measured organic carbon that has been estimated using TOT/TOR techniques, soil mass is estimated assuming oxide forms of measured soil elements, and sea salt is estimated from chloride measurements (Malm et al., 1994). Each of these estimates may be high or low, depending on actual molecular composition of the aerosol. Semivolatile organic compound (SVOC) species may volatilize, causing organic carbon to be underestimated, while the Roc factor (organic mass/organic carbon) varies as a function of carbon molecular structure.

This paper explores differences in measured organic carbon resulting from using different sampling systems and the implied difference this has on gravimetric mass. Comparison of measured gravimetric mass to reconstructed speciated mass allows for estimating the difference in measured gravimetric and reconstructed mass concentrations as compared to an estimate of true ambient $PM_{2.5}$ concentrations. Identified differences will be explored as a function of season and of urban, suburban, and remote locations. The spatial and seasonal variations in the Roc factor, nitrate volatilizations, and retained water on the Teflon filter at the time of weighing will also be explored.

8.2 SAMPLE COLLECTION SYSTEMS

Chow et al. (2010) provide an overview of sampling procedures and protocols for most particulate samplers that are currently being used, including the IMPROVE samplers and the five samplers that have historically been operated in the CSN. Table 8.1 summarizes these sampler and sampling characteristics, including the number of channels, flow rate, and filter face velocity. The five samplers are referred to as Anderson, Met One, URG, R&P 2300, and R&P 2025.

Table 8.1. Design specifications of the IMPROVE and CSN samplers.

Network	IMPROVE	CSN	CSN	CSN	CSN	CSN
Sampler type	IMPROVE	Andersen RAAS	Met One SASS	URG MASS	R&P 2300	R&P 2025 sequential FRM
Number of sites (2006)	181	18	179	6	14	22
Number of channels	4	4	5	2	4	2
Flow rate	22.7 l/min	7.3 l/min	6.7 l/min	16.7 l/min	10.0 l/min	16.7 l/min
Filter face velocity	107.2 cm/sec	10.3 cm/sec	9.5 cm/sec	23.7 cm/sec	14.2 cm/sec	23.6 cm/sec

Network	IMPROVE	CSN	CSN	CSN	CSN	CSN
Sampling frequency	3rd day	3rd day	3rd day	3rd day	3rd day/6th day	3rd day/6th day
Quartz filter pack configuration	Q for QBQ	QF	QF	QF	QF	QF
Quartz filter type	25 mm Pall	47 mm Whatman	47 mm Whatman	47 mm Whatman	47 mm Whatman	47 mm Whatman

8.2.1 Interagency Monitoring of Protected Visual Environments (IMPROVE)

A full discussion of site locations and monitoring protocols is presented by Malm et al. (1994, 2004) and Hand and Malm (2006). The IMPROVE data are available on line at http://views.cira.colostate.edu/web/DataWizard/.

The IMPROVE sampler consists of four independent modules. Each module incorporates a separate inlet array, filter pack, and pump assembly; however, all modules are controlled by the same singular timing mechanism. It is convenient to consider a particular module, its associated filter, and the parameters measured from the filter as a channel of measurement (e.g., channel A).

Channels A, B, and C are equipped with 2.5 µm cyclones. The channel A Teflon filter is analyzed for fine mass ($PM_{2.5}$) gravimetrically; nearly all elements with atomic mass number >11 (which is Na) and <82 (which is Pb) by x-ray florescence; elemental hydrogen by proton elastic scattering analysis; and for light absorption.

Channel B utilizes a sodium carbonate denuder to remove nitric acid, followed by a single Nylasorb filter as a collection substrate. The material collected from the filter is extracted ultrasonically in an aqueous solution that is subsequently analyzed by IC for the anions sulfate, nitrate, nitrite, and chloride.

Channel C utilizes tandem quartz fiber filters for the collection of fine particles and the estimation of the organic carbon artifact from organic gases collected on the secondary filter. These filters are analyzed by TOR for elemental and organic carbon (Chow et al., 1993). The reported carbon concentrations are corrected for an approximate positive artifact (Dillner et al., 2009). The IMPROVE correction method uses monthly median organic carbon mass measured on backup quartz filters from six nonurban sites, and then this seasonal correction is applied across the entire IMPROVE network (Watson et al., 2009; Chow et al., 2010). This assumes that the adsorbed gaseous material mass is equal throughout the continental United States. The method also assumes that the vapors are adsorbed uniformly throughout the front and back filters (adsorption capacity is attained). Both these assumption may not always be true (Watson et al., 2009).

Channel D, fitted with a PM_{10} inlet, utilizes a Teflon filter, which is gravimetrically analyzed for mass (PM_{10}). Exposed cassettes collected in all channels are placed in sealed plastic bags and shipped for storage under ambient conditions.

8.2.2 The Chemical Speciation Network (CSN)

The CSN data are available on line at http://www.epa.gov/ttn/airs/airsaqs/detaildata/downloadaqsdata.htm.

Substrates and analytic procedures used in the CSN are similar to IMPROVE. However, there are important differences between the networks. In the CSN, the sample collected on the Nylasorb filter is analyzed for both anions and cations, and PM_{10} samples are not collected. In addition, the quartz filters are analyzed using thermal optical transmittance (TOT) and a method similar to the National Institute for Occupational Safety and Health (NIOSH) 5040 protocol. The carbon concentrations are not corrected for a positive organic carbon artifact (Chow et al., 1993, 2001, 2004, 2005; Chow and Watson, 1999). Last, samples are shipped cold from the field to the laboratories for analysis. A general discussion of the handling of laboratory and field blanks can be found in Chow and Watson (1999).

Although the networks have these differences, comparison of collocated data shows that the $PM_{2.5}$ mass concentrations, anions, and a number of the elemental components are in general agreement between the networks. However, there are significant differences in the carbon concentrations.

8.2.3 Exploration of the Differences in the IMPROVE and CSN Carbon Measurements

Collection of $PM_{2.5}$ samples on quartz fiber filters, followed by thermal optical analysis for OC and EC content, is subject to a number of artifacts. This includes sampling artifacts due to adsorption of VOC gases by the quartz fiber filter, leading to positive additive artifacts (Kukreja and Bove, 1976; Watson et al., 2009), and evaporation of particles, leading to negative artifacts proportional to the semivolatile organic compounds (Galasyn et al., 1984). In addition, filter handling procedures and thermal optical analysis protocols can cause artifacts and differences in the OC and EC concentrations (Currie et al., 2002; Dillner et al., 2009). The following explores the differences between the IMROVE and CSN carbon concentrations at collocated sites and develops relationships to reconcile these differences. Other have also explored the carbon artifacts in the IMPROVE, CSN, and other networks. Most recently, White (2008), Watson et al. (2009), and Chow et al. (2010) performed a number of analyses, including the examination of field blanks, backup quartz fiber filters, and collocated carbon data, to assess the sampling artifacts and their causes. The following is based on work by White (2008). The analysis is similar to some of those by Chow et al. (2010), but we develop a different physical model, use different sets of data, and estimate monthly artifacts as opposed to seasonal and annual artifacts.

As shown in Figure 8.1, collocated IMPROVE and CSN samplers were operated at twelve urban sites for different time periods and with different CSN samplers. For this comparative analysis, only data from 2005 through 2006 are used, because in 2005 the carbon analyzers used by IMPROVE were upgraded, the precision of the CSN carbon concentrations improved after 2005, and after 2006 the EPA began changing the samplers and analytical methods used by the CSN for carbonaceous PM to be nearly identical to those used by IMPROVE, so the differences described here will not be applicable to more recent data.

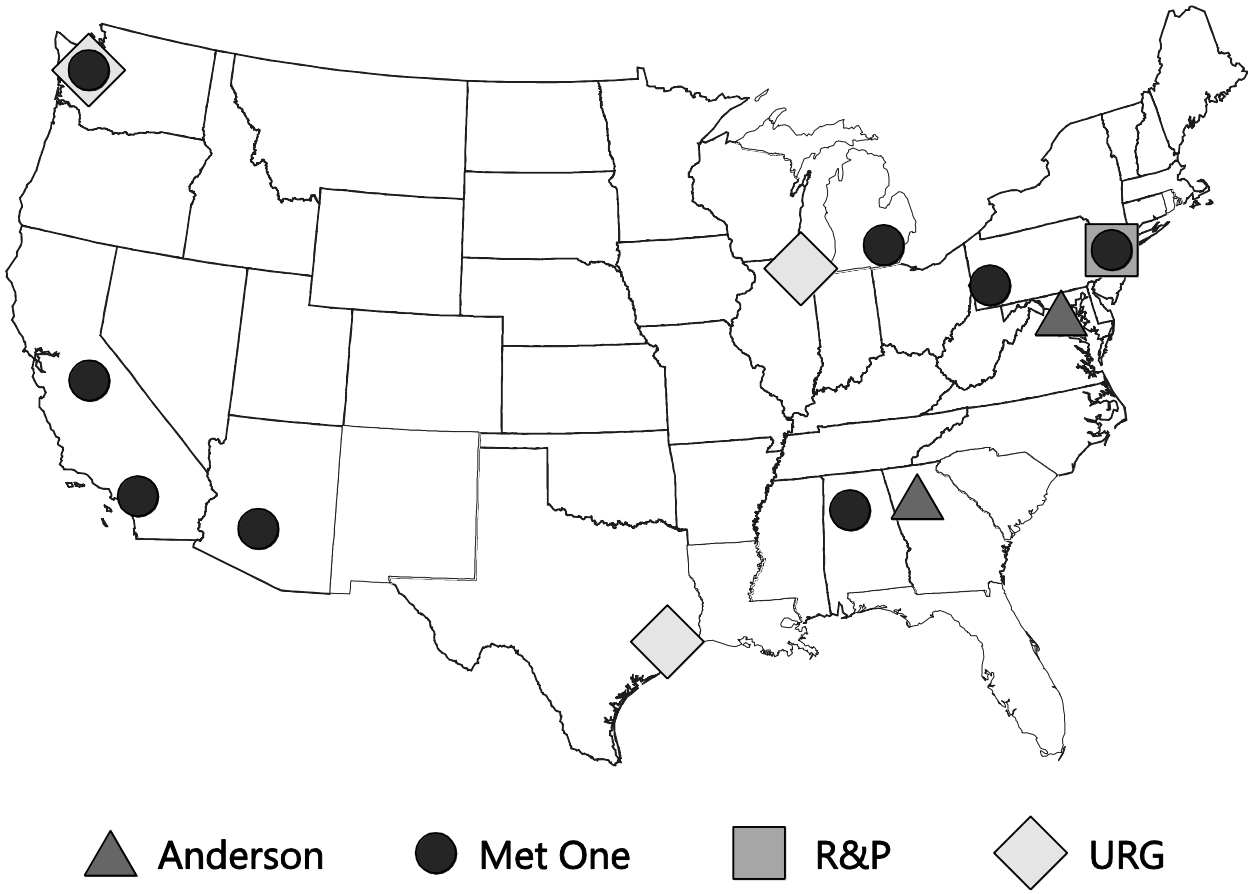

Figure 8.1. Location of the twelve urban sites with collocated IMPROVE and CSN carbon measurements and the time period the samplers were operating.

The comparison of the total carbon (TC) concentrations from all collocated samplers is presented in Figure 8.2. As shown, CSN TC concentrations are generally higher than IMPROVE TC, with the magnitude of the difference dependent on the CSN sampler but independent of the monitoring site. This difference, or bias, has two components. One is additive, as evident by the positive intercept as the IMPROVE TC concentrations approach 0; the second is concentration dependent, or multiplicative, as evident by the increasing difference with concentration. The additive bias varies by CSN sampler type and, though not shown in Figure 8.2, there is also a seasonal dependence, with a generally higher difference in the summer months compared to winter. The IMPROVE data have been corrected for an additive positive carbon artifact, while the CSN data have not. The additive bias in the CSN data is viewed as the positive organic carbon artifact associated with quartz filters (Watson et al, 2009; Chow et al., 2010).

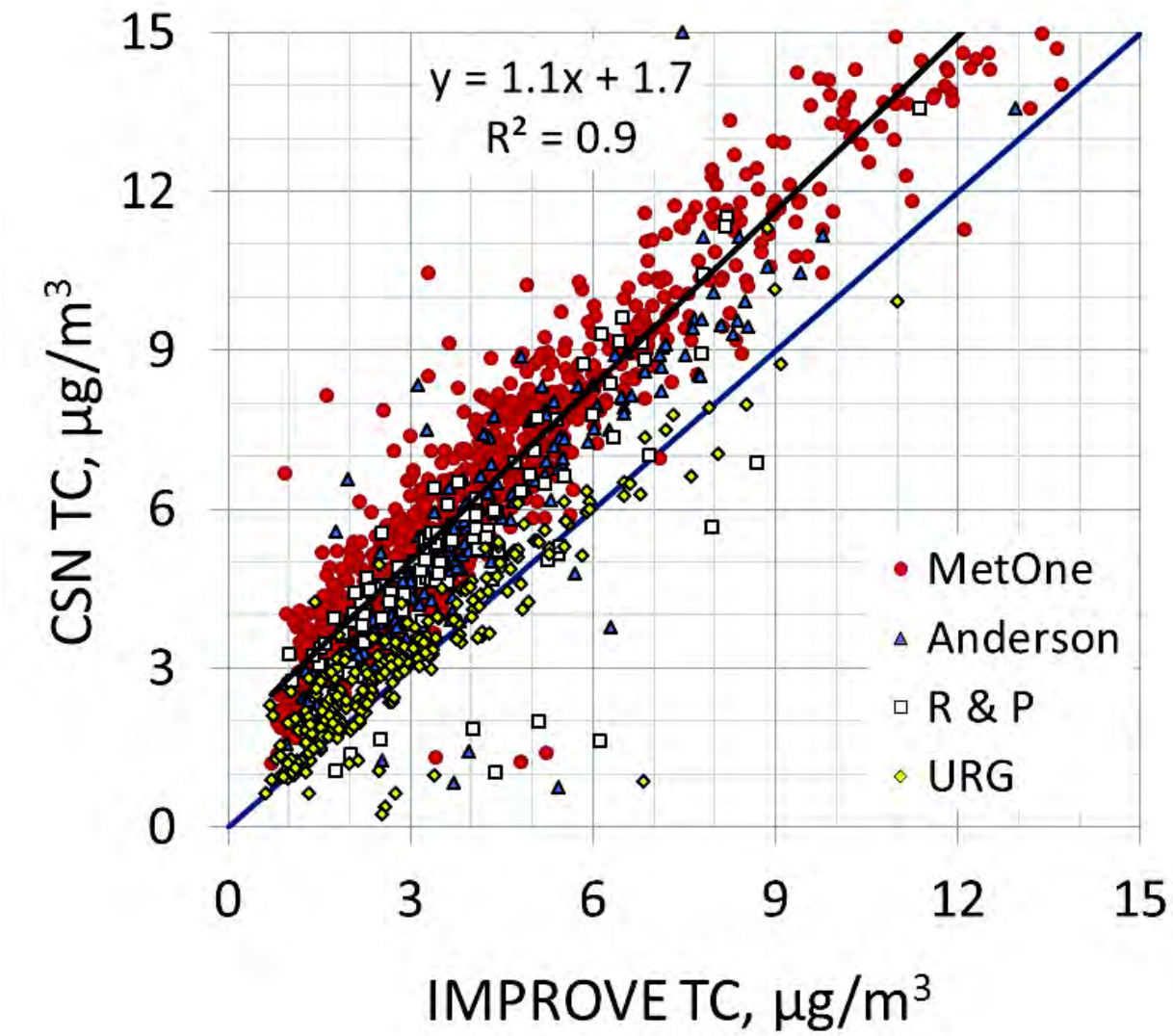

Figure 8.2. Comparison of CSN TC and IMPROVE TC concentrations from collocated monitors for 2005–2006 data. The data are color coded based on the CSN sampler. The regression line is for the Met One data.

The difference also appears to be sampler dependent, with the lowest differences for the URG sampler and highest for the Met One sampler, though the difference was not found to vary by season. One potential cause for these differences is that these samples are subject to a negative organic carbon artifact associated with the loss of SVOC, due to pressure differences across the filters. The IMPROVE sampler has the highest face velocity, thus the highest pressure drop, while the face velocity of the Met One sampler is an order of magnitude lower than IMPROVE, and URG's is between IMPROVE and Met One (Table 8.1). Other possible causes include different concentrations of SVOCs at the location of the monitoring site and different filter handling procedures. For example, CSN ships the filters cold while IMPROVE does not. Dillner et al. (2009) found that filters lost 10% of TC when maintained at temperatures at 40°C for 96 hr. However, the lack of seasonal dependence in the multiplicative bias suggests that these are not the principal causes of the bias.

Figure 8.3 presents the comparison of the IMPROVE and CSN elemental carbon (EC) concentrations for collocated monitors. As shown, the IMPROVE EC concentrations are generally higher than the CSN EC. This difference is near 0 at low EC concentrations and increases with EC concentrations, indicating a multiplicative bias. The difference between CSN and IMPROVE EC dependencies is not dependent on the CSN sampler, suggesting that it is an analytical bias. Laboratory studies (Currie et al., 2002) have shown that the NIOSH TOT method used for carbon measurements in the CSN results in lower EC and higher OC concentrations compared to the IMPROVE TOR method. The lack of an additive bias is supported by little to no EC measured on IMPROVE backup filters that are used to estimate the positive carbon artifact (Watson et al., 2009).

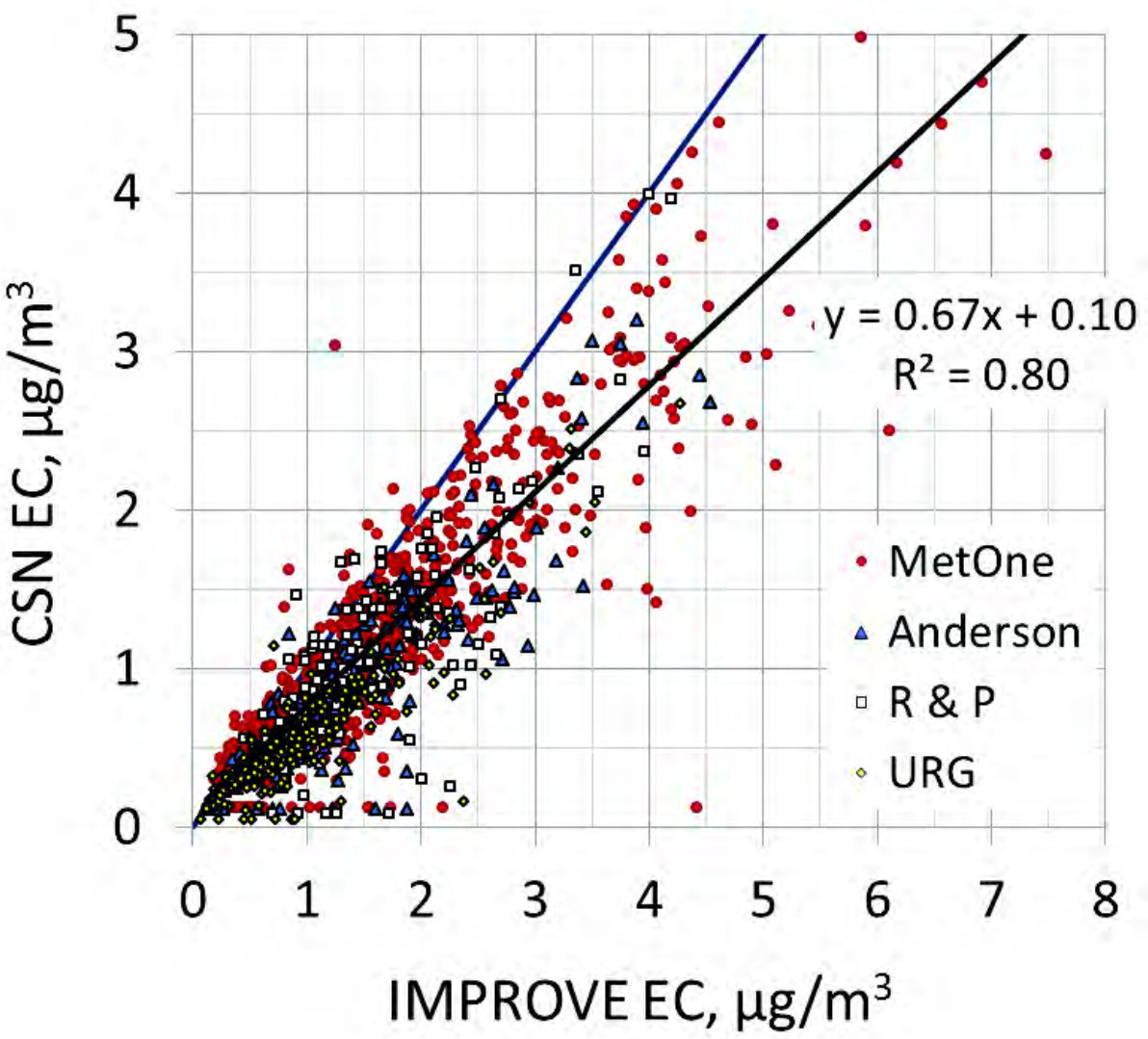

Figure 8.3. Comparison of CSN EC and IMPROVE EC concentrations from collocated monitors for 2005–2006 data. The data are color coded based on the CSN sampler. The regression line is for the Met One data.

8.2.4 Relating CSN to IMPROVE Carbon Concentrations

The TOR and TOT analytical analyses used in IMPROVE and the CSN have equivalent estimates of TC but different OC and EC subfractions (Currie et al., 2002). However, as discussed above, TC concentrations, reported from data collected using collocated samplers, differ. These differences apparently are due to the use of different sampling hardware and how known sampling artifacts are incorporated into reported data. In order to contrast and compare carbon concentrations derived from the IMPROVE and CSN monitoring networks, the CSN data are normalized or adjusted to account for the relative biases between sampling systems. This is done using data collected from collocated IMPROVE and CSN samplers. Each CSN sampler will necessarily have unique adjustment factors; however, only the Met One sampler has sufficient data for a statistical comparative analysis.

In this analysis, it is assumed that the TC concentrations measured from the filter samples differ from those in the atmosphere, due only to an additive positive organic carbon artifact resulting from filter adsorption of SVOC gases, and a multiplicative negative organic carbon artifact associated with volatilization of collected organic carbon mass such that

$$[TC]^F = [TC] - B[OC] + A \quad 8.1$$

where

[TC] and [OC] are the actual ambient total and organic carbon concentrations, respectively

$[TC]^F$ is the TC concentration on the filter

B is the negative multiplicative sampling artifact

A is positive additive artifact on the filter, represented as a concentration

Because IMPROVE data-handling protocol calls for a correction for the positive artifact, it is assumed that $A^{IMP} = 0$, and undoubtedly there is some volatilization of OC from both the CSN and IMPROVE samplers. However, because the existing routine monitoring datasets do not allow for the determination of B^{CSN}, the strategy taken here is to normalize IMPROVE to CSN. Therefore B^{CSN} is set to zero and B^{IMP} is estimated relative to the CSN Met One sampler.

Under these assumptions, equation 8.1 for the reported IMPROVE and CSN TC concentrations becomes

$$[TC]^{IMP} = [TC] - B^{IMP}[OC] \quad 8.2$$

$$[TC]^{CSN} = [TC] + A^{CSN} \quad 8.3$$

If it is further assumed that it is $[OC]^{IMP}$ and not $[EC]^{IMP}$ that is volatilized and that the volatilization is proportional to organic mass concentration, then

$$[OC] = (1 + B^{IMP})\,[OC]^{IMP} \quad 8.4$$

Combining equations 2–4, it can be shown that

$$[TC]^{CSN} = [EC]^{IMP} + (1 + B^{IMP} + (B^{IMP})^2)[OC]^{IMP} + A^{CSN} \quad 8.5$$

Equation 8.5 relates the CSN TC concentrations to the IMPROVE EC and OC concentrations, with IMPROVE OC corrected for a negative artifact and the CSN TC corrected for the positive artifact.

The form of equation 8.5 lends itself to a statistical regression model of the form

$$[TC]^{CSN} = [EC]^{IMP} + (1 + b_{OC})[OC]^{IMP} + a_i + e \qquad 8.6$$

where

$b_{OC} = (B^{IMP} + (B^{IMP})^2)$

a_i is the positive artifact, $[A^{CSN}]$, for each month, i, of the year

The OLS regression resulted in a significant $b_{OC} = 0.22 \pm 0.03$. A $b_{OC} = 0.22$ is equivalent to an IMPROVE multiplicative artifact $B^{IMP} = 0.19$. This suggests that ~20% of the organic carbon collected by IMPROVE is lost due to the negative artifact. The OLS-derived CSN monthly positive organic artifacts for the Met One sampler are presented in Table 8.2. As shown, these artifacts are seasonal, with about a 1 $\mu g/m^3$ artifact during the winter and 2 $\mu g/m^3$ during the summer.

Table 8.2. The multiplicative artifact (1 + bOC) and the monthly positive organic artifact (a) used to relate the CSN and IMPROVE carbon concentrations. The units for the positive artifacts are μg/m3 and 1 + bOC is unitless.

	Met One
$1+b_{OC}$	1.2
a_{Jan}	1.1
a_{Feb}	1.3
a_{Mar}	1.2
a_{Apr}	1.4
a_{May}	1.6
a_{Jun}	1.7
a_{Jul}	1.8
a_{Aug}	1.9
a_{Sep}	1.5
a_{Oct}	1.2
a_{Nov}	1.0
a_{Dec}	1.1

8.2.4.1 Converting CSN to IMPROVE Carbon Concentrations.

As shown in Figure 8.3, the differences between the IMPROVE and CSN EC are approximately multiplicative. Therefore,

$$[EC]^{IMP} = m[EC]^{CSN} \qquad 8.7$$

where

m is the multiplicative factor relating the two EC measurements

Solution of equation 8.7, using OLS, results in m = 1.3±0.2. Therefore, the reported IMPROVE EC concentrations can be approximated by the CSN Met One data via

$$[EC]^{IMP} \sim 1.3*[EC]^{CSN} \quad 8.8$$

To approximate IMPROVE OC using CSN concentrations, equations 6 and 8 can be combined such that

$$[OC]^{IMP} \sim [OC]^{CSN\ adj} = ([TC]^{CSN} - [EC]^{CSN\ adj} - a_i)/(1 + b_{OC}) \quad 8.9$$

Incorporating equation 8.8 into equation 8.9 and rearranging gives

$$[OC]^{IMP} \sim [OC]^{CSN\ adj} = ([OC]^{CSN} - 0.3[EC]^{CSN} - a_i)/(1 + b_{OC}) \quad 8.10$$

The adjusted CSN TC is then simply the sum of OC^{CSN_adj} and EC^{CSN_adj}:

$$[TC]^{IMP} \sim [TC]^{CSN\ adj} = ([OC]^{CSN\ adj} + [EC]^{CSN\ adj}) \quad 8.11$$

Figure 8.4 compares the CSN Met One carbon concentration to the reported IMPROVE concentrations for both the reported and adjusted CSN data. As shown, the adjustments of the CSN data significantly improve the comparison to the IMPROVE data. The positive intercepts for the reported TC and OC data are now near 0 for the adjusted data, and the slopes of the regression lines are near 1. The slope of the regression line for the EC data has also significantly improved from 0.68 to 0.89. In all cases the correlation between the data is high, with $r^2 \geq 0.8$.

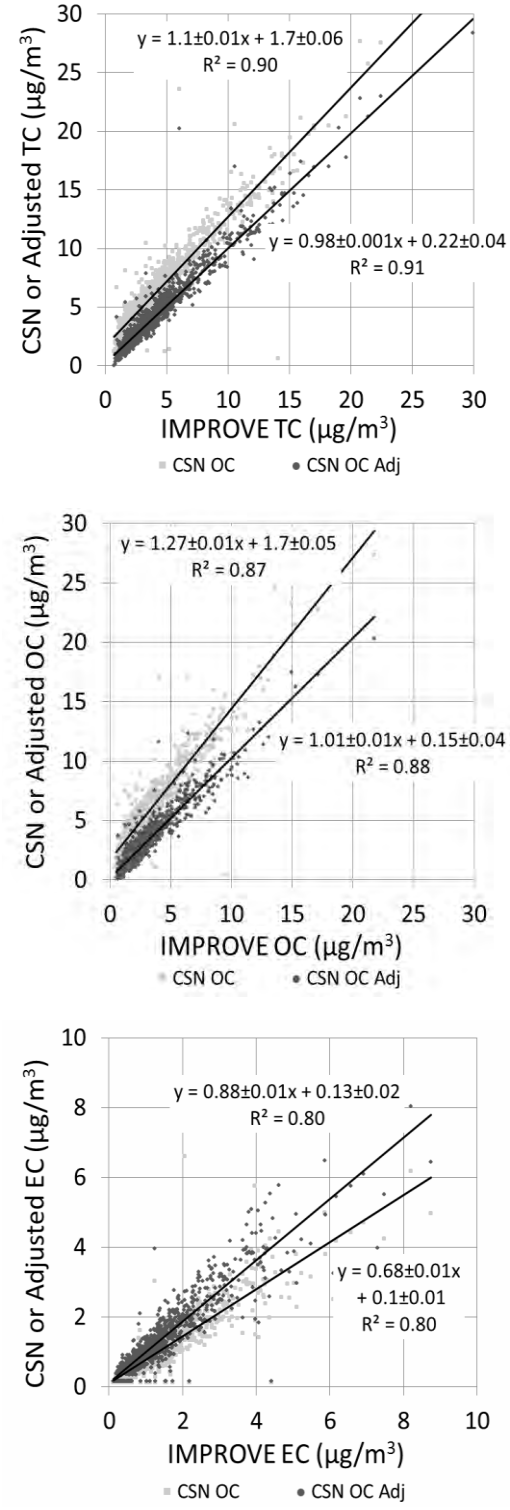

Figure 8.4. The CSN and IMPROVE TC, OC, and EC concentrations for all collocated IMPROVE and CSN Met One samplers that collected data in 2005 and 2006. The lighter data points are for the reported CSN carbon concentrations and the darker data points are for the adjusted CSN carbon concentrations.

As evident by the remaining scatter between the IMPROVE and adjusted CSN data in Figure 8.4, the adjustments do not account for all variability between the CSN and IMPROVE

carbon concentrations. In addition, the artifacts were derived using data from only five urban sites and may not be applicable to other sites and years. An alternative method for estimating the positive artifact is to regress the OC against $\Delta PM_{2.5}$, where $\Delta PM_{2.5} = PM_{2.5}$ – inorganic compounds (Watson et al., 2009). The $PM_{2.5}$ mass on the Teflon filter would not have a positive OC artifact, so the regression intercept would be an estimate of the positive OC artifact. This was done using all CSN Met One data from 2000 to 2006 for each season, with winter comprising the months December–February. The resulting intercepts were approximately 1 $\mu g/m^3$ for the winter, 2 $\mu g/m^3$ for the summer, and 1.35 $\mu g/m^3$ for the spring and fall, which are similar to those in Table 8.2. Although the average values are similar, there is some spatial variability in the intercept, with generally higher intercepts in California than the eastern United States. These results indicate that the derived artifacts in Table 8.2 are applicable to other years and sites but are most appropriate for examining aggregated data across multiple sites and time periods.

8.2.5 Comparison of Reconstructed to Measured Mass

In the CSN, five different samplers have been employed; however, about 75% were Met One samplers (Table 8.1). To minimize the influence of the different samplers, only samples collected using the Met One spiral aerosol speciation sampler (SASS) are used in the comparative analysis of reconstructed and gravimetric $PM_{2.5}$. Data collected between 2000 and 2008 are used in the CSN analysis, while data collected between 1988 and 2008 are used for the IMPROVE analysis. Where appropriate, CSN data is adjusted or calibrated to IMPROVE using equations 8 and 10.

$PM_{2.5}$ and $PM_{2.5}$ species are often used in a closure-type calculation where assumed forms of aerosol mass species are added together and compared to gravimetrically measured $PM_{2.5}$. Even though ammonium concentrations are measured in the CSN, they will not be used in the following analysis. First, because ammonium is not routinely measured in the IMPROVE system, and second, unless volatilized ammonium is accounted for, which it is not in the CSN, the reported concentrations of ammonium can be significantly underestimated (Yu et al., 2006).

The governing equation, assuming NH_4 concentrations are not measured, is

$$RPM_{2.5} = \left[xSO_4 + 1.29NO_3\right] f'_{salts}\,(RH_{lab}) + R_{oc}OC\,(composition) + EC + Soil + SSf'_{salts}(RH_{lab}) \qquad 8.12$$

where

$RPM_{2.5}$ = reconstructed $PM_{2.5}$ mass

SO_4 = sulfate ion concentration

NO_3 = nitrate ion concentration

Roc = POM/OC

POM = organic mass concentration

OC = organic carbon concentration

EC = elemental carbon

Soil = oxides of crustal elements

SS = sea salt

$$f'_{salts}(RH_{lab}) = \left[\frac{\rho_{mix,species}}{\rho_{species}}\right]^3 \left(\frac{D}{D_o}(RH_{lab})\right)^3$$

D/Do = wet over dry particle diameter

RH = relative humidity

x = ammoniated sulfate to sulfate ion ratio

which varies from a minimum of 1.02 for sulfuric acid to a maximum of 1.375 for fully neutralized ammonium sulfate, a difference of about 30%. $PM_{2.5}$ can be biased low because of volatilization of SVOCs and other volatile species such as ammonium nitrate or high because of retained water associated with inorganic salts and some water-soluble organic species. Typically, $PM_{2.5}$ concentrations are reported and used without correcting for these potential biases. In IMPROVE, SO_4 is usually assumed to be in the form of ammonium sulfate, which is an upper bound of mass associated with inorganic sulfate, the nitrate ion is assumed to be in the form of ammonium nitrate, and f'_{salts} is usually assumed to be 1, when in reality it is more likely to be between 1.15 and 1.3, assuming a laboratory RH between 30% and 40% and typical D/Do factors at these RHs (Tang, 1976; Tang and Munkelwitz, 1994), Roc is usually assumed to be a constant between about 1.2 and 2.0, and the algorithms used to estimate soil and sea salt from elemental measured concentrations are assumed to be constant in both space and time (Malm et al., 1994).

Some of these assumptions may have a seasonal dependence, such as sulfate ammoniation (Gebhart et al., 1994; Liu et al., 1996; Day et al., 1997; Lowenthal et al., 2000; Lefer and Talbot, 2001; Quinn et al., 2002; Chu, 2004; Hogrefe et al., 2004; Schwab et al., 2004; Tanner et al., 2004; Zhang et al., 2005). Furthermore, it has been well documented that ammonium nitrate volatilization from a Teflon substrate is greater during the warmer summer season as opposed to cooler winter conditions (Zhang and McMurry, 1992; Mozurkewich, 1993; Chang et al., 2000; Ashbaugh and 2004; Chow et al., 2005). Nitrate volatilization as high as 90% in the summer and as low as 10% in the winter has been reported. However, even though more nitrate is retained on a fractional basis in the winter months, on an absolute basis the nitrate loss during the winter may be greater than summer.

Many authors have reported average Roc values that range from as low as 1.2 to values greater than 2.0 (Turpin and Lim, 2001; Kiss et al., 2002; Russell, 2003; El-Zanan et al., 2005, 2009; Yu et al., 2005; Gilardoni et al., 2007; Reff et al., 2007; Aiken et al., 2008; Liu et al., 2009; Russell et al., 2009; Sun et al., 2009; Chan et al., 2010). Turpin and Lim (2001) concluded that a factor of about 1.6 would be appropriate for an urban organic aerosol, while a factor of 2.1 may be more appropriate for an aged, nonurban aerosol.

A few authors have reported some seasonal dependence of Roc (Bae et al., 2006a, 2006b; Chen and Yu, 2007; Polidori et al., 2008; El-Zanan et al., 2009; Lowenthal et al., 2009). Polidori et al. (2008), using extraction/fractionation techniques, reported somewhat higher Roc values of 1.9–2.1 in the summer/winter for the Pittsburgh aerosol, probably because of a greater contribution of oxidized species.

Summing assumed forms of all species other than OC, subtracting this value from gravimetric $PM_{2.5}$, and assuming this value represents particulate organic matter (POM), Roc is estimated as POM/OC (El-Zanan et al., 2005, 2009). This method of estimating Roc will be referred to as the mass difference technique (MDT). Chen and Yu (2007), using a modified MDT for a Hong Kong dataset, did not find any seasonal variability in Roc but did find the Roc was dependent on whether the air mass was "continental" or "marine". Bae et al. (2006a), using an MDT for rural and urban New York datasets, reported a slight seasonal dependence for a nonurban site, with the warm season having a ratio of 2.1, while the urban site did not have a seasonal dependence but did have lower Roc factors of 1.3–1.6. Bae et al. (2006b) used the MDT approach for a dataset collected in St. Louis to estimate a Roc factor of 1.95 ± 0.17 in the summer and 1.77 ± 0.13 in winter. El-Zanan et al. (2009) reported on Roc factors derived from an Atlanta dataset. They concluded that there was a slight seasonal difference in Roc, with a value of 1.77 in December and 2.39 in July. Lowenthal et al., (2009), using a Great Smoky Mountain National Park summer dataset, reported Roc factors of 2.4 and 1.9 for water-soluble and dichloromethane extracts, respectively.

Figure 8.5 shows summary plots of gravimetric fine mass, sulfate as ammonium sulfate, nitrate as ammonium nitrate, soil as oxides of the soil elements, sea salt as 1.8*Cl, POM as 1.8*OC, and EC for IMPROVE and CSN urban and nonurban sites. CSN urban and nonurban sites were identified based on their classification in the EPA CSN database (http://www.epa.gov/ttn/airs/airsaqs/detaildata/downloadaqsdata.htm).

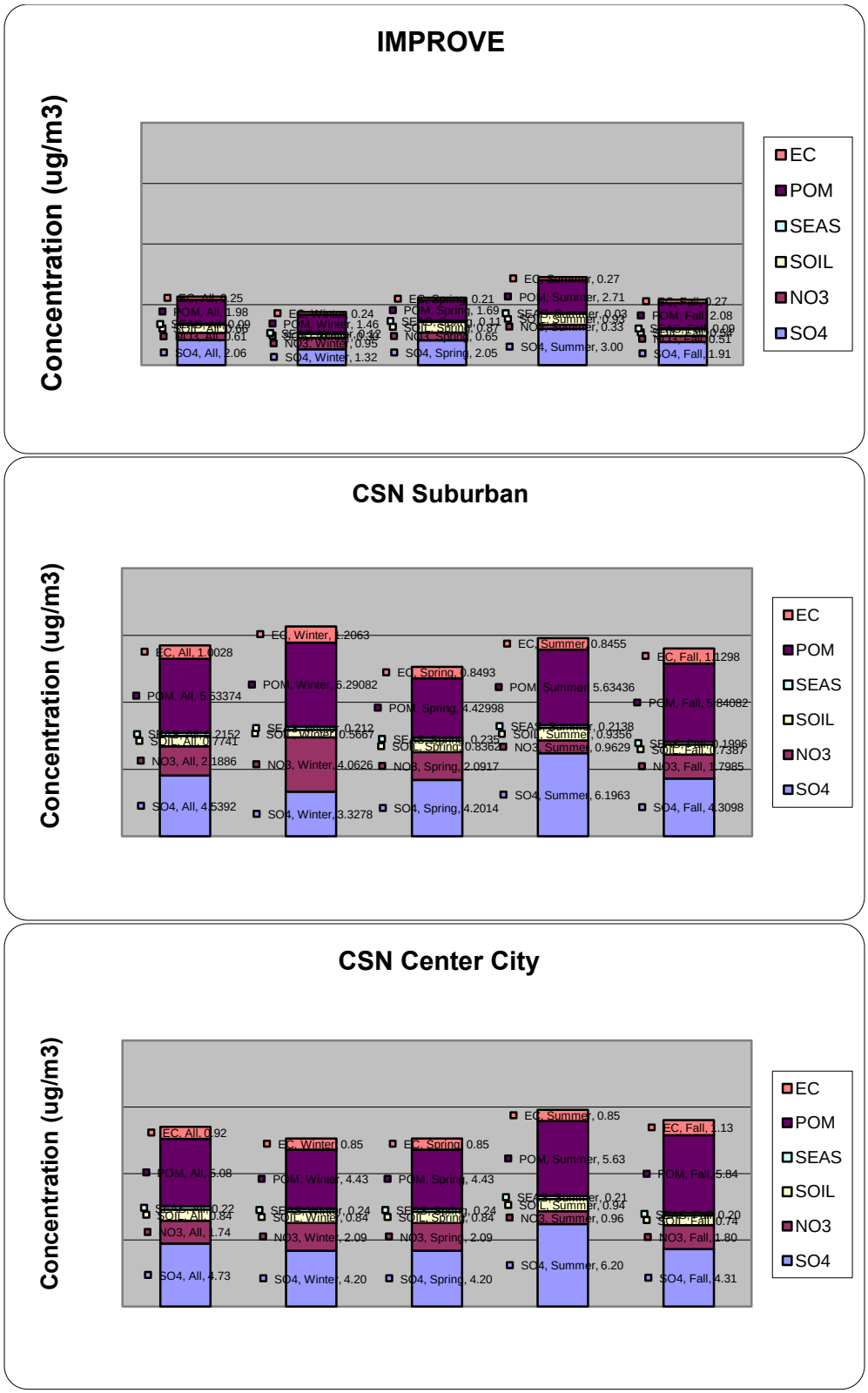

Figure 8.5. Stacked bar charts showing average concentrations of each species for all and each season for IMPROVE, CSN suburban, and CSN center city.

Notice that CSN total fine mass concentrations are about a factor of 3 times greater than in the IMPROVE network. This difference is undoubtedly in part due to the difference in urban/suburban and remote concentrations but also because most of the CSN sites are in the East, where regional sulfate concentrations are high, whereas IMPROVE sites are spread more uniformly across the country. There is also more seasonal variability in the IMPROVE dataset, with concentrations being lowest in winter and highest during the summer months. Data for the suburban locations actually show the highest total concentrations during winter, primarily because of POM and nitrates. In the urban dataset, winter and spring $RPM_{2.5}$ is about the same and lower than either summer or fall. Possibly, during winter months, during more stable and stagnant meteorological conditions, aerosols are more constrained to concentrate around the source areas, with less transport into the more remote locations where most IMPROVE monitors are located. Furthermore, nitrate and POM are a larger fraction of $RPM_{2.5}$ in urban locations, while in the IMPROVE network, soil, on a fractional basis, is elevated relative to CSN sites.

To see if there are systematic spatial and seasonal differences between reconstructed and gravimetric mass in the CSN and IMPROVE datasets, timelines of the percent difference between gravimetric and reconstructed $PM_{2.5}$, $\% \Delta PM_{2.5} = ((PM_{2.5} - RPM_{2.5})/PM_{2.5})*100$, were plotted for each of the approximately 300 CSN and 170 IMPROVE sites. For these plots, it is assumed that x = 1.375 (fully neutralized ammonium sulfate), $NH_4NO_3 = 1.29*NO_3$, f'(RH) = 1, Roc = 1.8, sea salt = 1.8*Cl-, and Soil = 2.2[Al] + 2.49[Si] + 1.94[Ti] + 1.63[Ca] + 2.42[Fe]. An example plot of $\% \Delta PM_{2.5}$ is shown in Figure 8.6 in green for Brigantine National Wildlife Refuge (NWR).

Also presented in Figure 8.6 in blue is a temporal plot of $PM_{2.5} - PM_{2.5avg}$, where $PM_{2.5avg}$ is the average $PM_{2.5}$ over the entire time period. Notice that there is a systematic seasonal bias in $\% \Delta PM_{2.5}$ with summer being biased high and winter low by as much as ±15%. Also notice that this bias tends to follow increases and decreases in $PM_{2.5}$ concentrations. Gravimetric mass, $PM_{2.5}$, is greater than $RPM_{2.5}$ during summer time periods, when $PM_{2.5}$ is high, and is lower than $RPM_{2.5}$ during winter months, when $PM_{2.5}$ is lower. It is also of interest to point out that the seasonal temporal trends in both $PM_{2.5}$ and $\% \Delta PM_{2.5}$ are more systematic after about 1999, possibly indicating a higher degree of precision in the post-1999 dataset. The difference between pre- and post-1999 data is evident throughout the IMPROVE dataset.

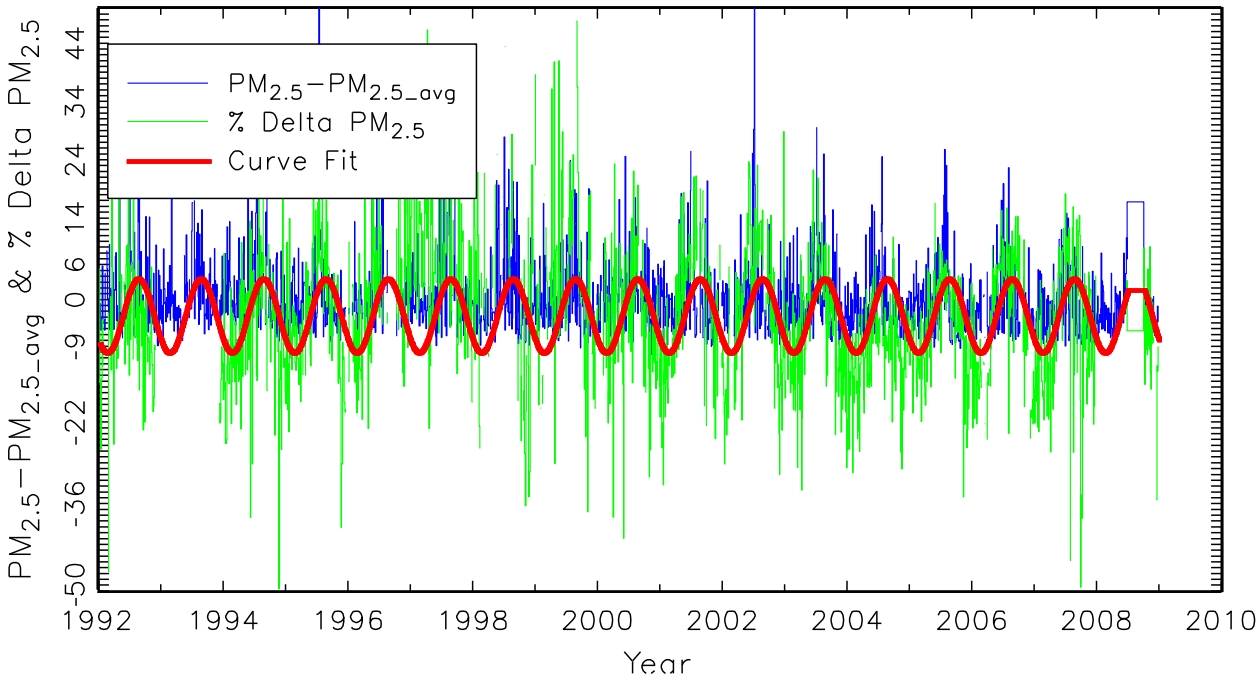

Figure 8.6. Temporal plot of $PM_{2.5} - PM_{2.5avg}$ and the percent difference between reconstructed and gravimetric mass for Brigantine National Wildlife Refuge. The red line is a sinusoidal curve fit to the percent difference between reconstructed and gravimetric mass.

The seasonal variability exhibited in Figure 8.6 was modeled using a simple time-dependent cosine function relationship:

$$\% \Delta PM_{2.5} = [(PM_{2.5} - RPM_{2.5})/PM_{2.5}]*100 = b_1 + b_2(\cos(f(T)) \quad 8.13$$

where

f(T) was adjusted to yield a maximum and minimum during the summer and winter seasons, respectively

b_1 and b_2 are regression coefficients that have a physical interpretation of b_1 being equal to the average positive or negative percent bias, while b_2 is the average percent variability between summer and winter

The red line in Figure 8.6 is the curve fit of equation 8.13 for the data shown. $b_1 = -4.3$ and $b_2 = 16.4$, implying that on the average $PM_{2.5}$ is 4.3% lower than $RPM_{2.5}$ and there is an average difference between summer and winter of 16.4%. The t statistic for this site was 15.1, indicating a high level of significance.

This analysis was carried out for each site in both the IMPROVE and CSN networks. Only coefficients with t values greater than 1.7 are reported. Figure 8.7 shows the percent variability, b_2, between the summer and winter seasons and the average bias, b_1, for the IMPROVE and CSN networks.

The number of observations varies significantly from site to site, especially in the CSN, where site start dates vary considerably. Of the 168 sites with t values greater than 1.7, about 30% have 100–300 observations, while another 40% of the sites have 300–500 data points. A

few sites have as many as 900 observations. In the IMPROVE network, 80% of the monitoring sites have over 800 observations. Therefore the statistical significance of the bias estimations presented Figure 8.7 varies from site to site and should be viewed as being semiquantitative. All sites were included in the analysis to elucidate possible spatial and seasonal trends across the spatial and temporal scales that these networks represent.

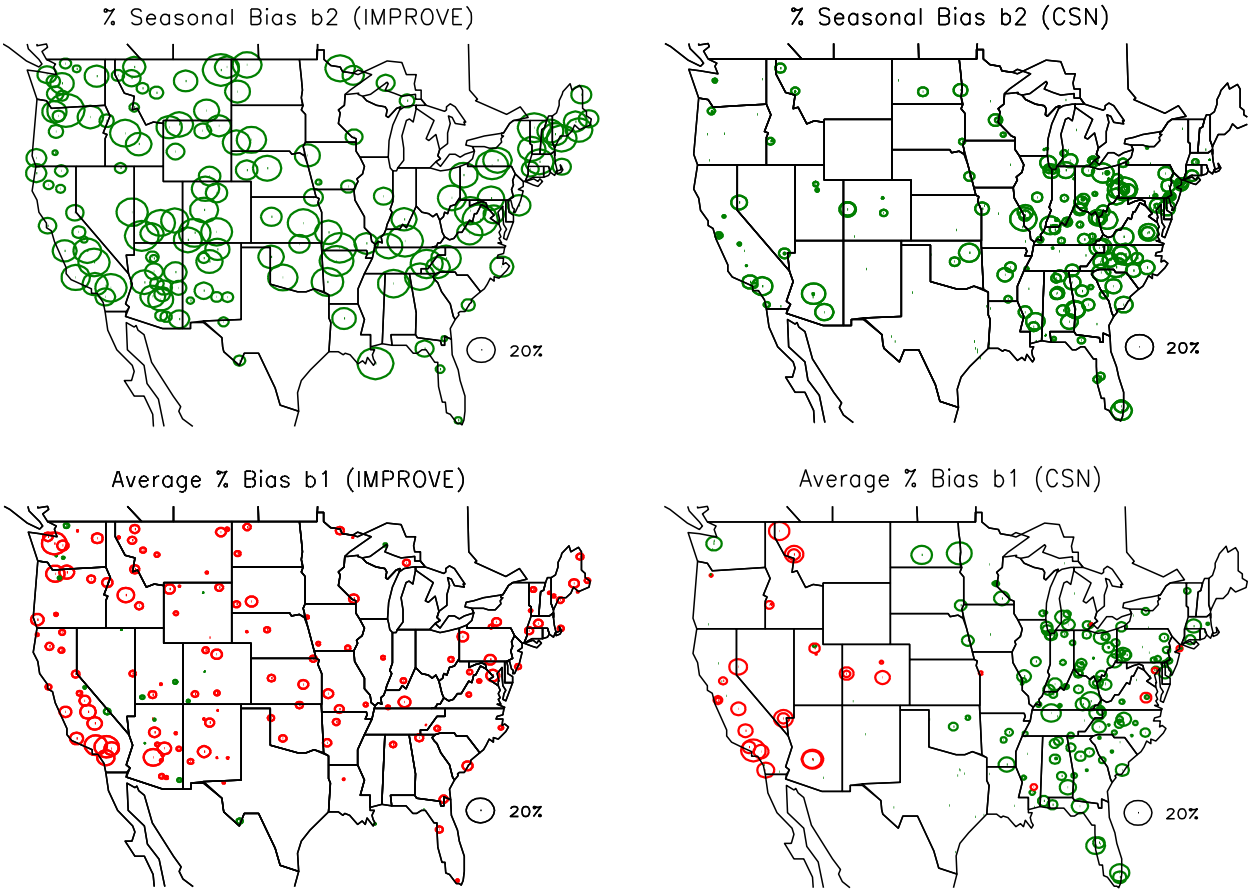

Figure 8.7. Average percent seasonal variability (b_2) and percent difference (b_1), as represented by equation 8.13, between reconstructed and gravimetric mass for the IMPROVE and CSN monitoring networks. Green represents a positive value while red represents a negative bias.

A statistical summary of seasonal variability and average bias is presented in Table 8.3 for all IMPROVE and CSN sites. Referring to Table 8.3 and Figure 8.7, notice that the seasonal variability in the IMPROVE network is on the average about twice as high as in the CSN, with average values of 14.9% and 7.6%, respectively. The maximum value of seasonal variability is also higher for the CSN.

Table 8.3. Summary of the percent seasonal variability and average difference of reconstructed versus gravimetric mass.

Variable	Mean	Std dev	Minimum	Maximum	N
Seasonal variability (IMPROVE)	14.9	6.14	0.0	26.7	158
% Seasonal variability (CSN)	7.6	4.51	0.0	19.0	168
Avg difference (IMPROVE)	-3.9	4.44	-17.9	9.4	158
Avg difference (CSN)	3.4	7.00	-17.7	22.7	168

Interestingly, almost all sites exhibit some seasonal dependence of % $\Delta PM_{2.5}$. There are some qualitatively consistent spatial patterns that emerge from both networks. The high plateau (Mogollon Rim) region of northern Arizona and New Mexico and a region extending down into Texas (Big Bend National Park) have lower seasonal variability, as do areas of the northern California Sierra Nevada mountains. Generally, the upper Midwest and parts of Florida also have low seasonal variability. The Columbia River Gorge and Snake River valley have high variability, with lower values to the immediate north and south.

Figure 8.7 also shows the overall average percent bias, b_1, for the IMPROVE and CSN networks. Red symbols indicate that the average bias is negative ($PM_{2.5} < RPM_{2.5}$), while green symbols represent a positive bias ($PM_{2.5} > RPM_{2.5}$). Referring to the map for IMPROVE, notice that except for a few sites in the West, in the IMPROVE network reconstructed mass is greater than gravimetric mass. This is especially true in the warm Southwest and southern California, where nitrate mass concentrations are high relative to other species, suggesting nitrate volatilization from the Teflon filter on which gravimetric analysis is performed. Referring to the map for the CSN, one can see that $RPM_{2.5} > PM_{2.5}$ in almost every urban/suburban area in the West, while $RPM_{2.5} < PM_{2.5}$ in almost every urban/suburban site in the East. Notice the very interesting dichotomy between the rural/remote and urban/suburban sites in the East. On the average, $RPM_{2.5}$ is an underestimate of $PM_{2.5}$ by about 4% and an overestimate of about 3% in the IMPROVE and CSN networks, respectively.

The average biases and seasonal variability in % $\Delta PM_{2.5}$ could have significant ramifications. In the RHR guidance, it is recommended that reconstructing extinction, the parameter used to determine whether progress is being made toward improvement of visibility in Class I areas, is based on the assumption that days with high $PM_{2.5}$ concentrations have average mass size distributions that are more conducive to efficient scattering of light. The high concentration days tend to occur during summer months, and possibly all or part of this observed relationship between increased scattering on higher concentration days is a result of assuming an Roc, the level of sulfate ammoniation, or an assumed molecular form of other species is constant, when in fact one or more may have significant seasonal variability.

Furthermore, interpreting $PM_{2.5}$ as it relates to health endpoints may be problematic. The bias associated with gravimetric mass determinations varies from one region of the country to the other. For instance, in the Midwest where nitrate makes up a significant fraction of $PM_{2.5}$, if 70% of the nitrate is volatilized and nitrate contributed 80% of the $PM_{2.5}$, then $PM_{2.5}$ would be underestimated by 56%. Likewise, if SO_4 were 80% of $PM_{2.5}$, more than 20% of reported mass would be due to water on the hygroscopic species.

8.3 INVESTIGATING BIAS ASSOCIATED WITH EACH SPECIES

Differences between gravimetric and reconstructed mass are a function of the difference between the gravimetric and assumed mass of each species. The differences between species-by-species $PM_{2.5}$ and $RPM_{2.5}$ are given by

$$PM_{2.5} - RPM_{2.5} = \sum_i (FM_i - RFM_i) = (PM_{2.5SO4} - 1.375*SO_4) + \quad 8.14$$

$$(PM_{2.5NO3} - 1.29*NO_3) + (PM_{2.5POM} - 1.8*OC) + (PM_{2.5other} - Other)$$

where

Other is the sum of elemental carbon (EC), sea salt, and soil dust

$PM_{2.5i}$ refers to the various species on the Teflon filter from which gravimetric mass is determined, while the remaining variables are defined in equation 8.12. Each of the terms in the parentheses contributes to either a positive or negative bias between $PM_{2.5}$ and $RPM_{2.5}$.

The relationship between $PM_{2.5}$ and aerosol species concentrations can be explored with a regression model of the form

$$PM_{2.5} = a_1*1.375*SO_4 + a_{2*}1.29*NO_3 + a_3OC + a_4*Other \quad 8.15$$

where

Other = Soil + EC+ Sea salt

a_i = the regression coefficients

The regressions were carried out for all data (across all sites) collected in the IMPROVE monitoring network and for the dataset subdivided into seasons. The same analysis was carried out using CSN data after it had been subdivided into urban and suburban categories. Results of these analyses are presented in Tables 8.4a–8.4c.

Table 8.4a. Results of OLS regression analysis using equation 8.15 for the IMPROVE monitoring data.

Variable	Estimate	Std error	t-value	Prob>|t|
All				
$R^2 = 0.95$				
ASO_4	1.12	0.00	1328.90	0.00
ANO_3	0.75	0.00	410.67	0.00
POM	1.60	0.00	822.62	0.00
Other	1.06	0.00	597.08	0.00
Winter				
$R^2 = 0.96$				
SO_4	1.02	0.00	391.99	0.00
NO_3	0.92	0.00	403.37	0.00
POM	1.42	0.00	301.41	0.00
Other	1.05	0.00	234.18	0.00
Spring				
$R^2 = 0.93$				
SO_4	1.10	0.00	560.18	0.00
NO_3	0.70	0.00	200.96	0.00
POM	1.52	0.00	344.45	0.00
Other	1.09	0.00	402.66	0.00
Summer				
$R^2 = 0.96$				

Variable	Estimate	Std error	t-value	Prob>|t|
SO_4	1.15	0.00	793.24	0.00
NO_3	0.51	0.01	47.14	0.00
POM	1.70	0.00	465.24	0.00
Other	1.08	0.00	295.10	0.00
Fall				
$R^2 = 0.96$				
SO_4	1.09	0.00	696.73	0.00
NO_3	0.75	0.00	206.21	0.00
POM	1.59	0.00	467.48	0.00
Other	1.06	0.00	273.71	0.00

Table 8.4b. Results of OLS regression analysis using equation 8.15 for the CSN/suburban monitoring data.

Variable	Estimate	Std error	t-value	Prob>|t|
All				
$R^2 = 0.96$				
SO_4	1.23	0.00	412.51	0.00
NO_3	0.94	0.00	237.83	0.00
OC	1.52	0.01	230.17	0.00
SS_Soil_	1.16	0.01	111.73	0.00
Winter				
$R^2 = 0.92$				
SO_4	1.22	0.01	109.01	0.00
NO_3	1.04	0.01	151.13	0.00
OC	1.41	0.01	110.58	0.00
SS_Soil_	1.10	0.03	42.38	0.00
Spring				
$R^2 = 0.89$				
SO_4	1.20	0.01	155.65	0.00
NO_3	0.90	0.01	118.87	0.00
OC	1.53	0.01	107.78	0.00
SS_Soil_	1.31	0.02	70.84	0.00
Summer				
$R^2 = 0.93$				
SO_4	1.19	0.01	230.61	0.00
NO_3	0.77	0.02	47.88	0.00
OC	1.77	0.01	125.08	0.00
SS_Soil_	1.23	0.02	58.29	0.00
Fall				
$R^2 = 0.94$				
SO_4	1.20	0.01	216.18	0.00
NO_3	0.96	0.01	126.32	0.00
OC	1.43	0.01	114.22	0.00
SS_Soil_	1.14	0.02	62.40	0.00

Table 8.4c. Results of OLS regression analysis using equation 8.15 for the CSN/urban monitoring data.

Variable	Estimate	Std_error	t-value	prob>|t|
All				
$R^2 = 0.90$				
SO_4	1.25	0.00	370.11	0.00
NO_3	0.97	0.00	197.57	0.00
OC	1.44	0.01	233.14	0.00
SS_Soil_	1.07	0.01	102.34	0.00
Winter				
$R^2 = 0.94$				
SO_4	1.25	0.01	100.28	0.00
NO_3	1.06	0.01	128.23	0.00
OC	1.33	0.01	96.02	0.00
SS_SOIL_	1.04	0.03	38.43	0.00
Spring				
$R^2 = 0.880$				
SO_4	1.24	0.01	139.37	0.00
NO_3	0.93	0.01	87.96	0.00
OC	1.34	0.02	86.97	0.00
SS_Soil_	1.22	0.02	62.96	0.00
Summer				
$R^2 = 0.93$				
SO_4	1.23	0.01	217.79	0.00
NO_3	0.71	0.03	20.50	0.00
OC	1.61	0.01	155.65	0.00
SS_Soil_	1.23	0.02	62.47	0.00
Fall				
$R^2 = 0.91$				
SO_4	1.24	0.01	197.59	0.00
NO_3	0.98	0.01	101.19	0.00
OC	1.39	0.01	112.29	0.00
SS_Soil_	1.00	0.02	50.08	0.00

The coefficients in the regression model represented by equation 8.15 have physical interpretations. a_1*1.375*SO_4 is $PM_{2.5SO4}$, or the sulfate plus water mass on the Teflon substrate used to determine gravimetric mass. Therefore, for fully neutralized sulfate one would expect a_1 to be greater than 1 and $1 - a_1$ to be the fraction of sulfate mass that is particle-bound water. However, a_1 is an upper bound because sulfate may not be fully neutralized, and the regression coefficient a_1 will necessarily be decreased to reflect the difference between the assumed fully neutralized sulfate and sulfate mass actually contributing to gravimetric mass.

a_2*1.29*NO_3 is interpreted as the nitrate mass plus water as measured on the Teflon filter used for gravimetric analysis ($PM_{2.5NO3}$). This value includes the nitrate not volatilized from the Teflon filter as well as bound water on the nitrate aerosol. Assuming that $1 - a_1$ is also a representation of the mass fraction of water associated with nitrate aerosol, then $1 - a_2/a_1$ is an approximation of the fraction of nitrate volatilized from the Teflon filter, assuming that sulfate was fully neutralized.

a_3*1.8 is the Roc factor, assuming that POM collected on the Teflon and quartz substrates is the same. The OC^{CSN} data were adjusted according to equation 8.9 to account for the differences between TOT and TOR but were not adjusted for the volatilization loss associated with the IMPROVE sampling system. The Roc factors associated with the Met One and IMPROVE samplers could be different for the same ambient POM aerosol because of preferential volatilization of some POM species.

The annual and seasonal estimates for the fractional increase in sulfate mass due to water retention, fraction of nitrate lost from the Teflon filter, and Roc factor for IMPROVE and CSN urban and suburban sites are summarized in Figures 8.8–8.10. Referring to Figure 8.8, notice that water retention is on the order of 1.2–1.25 for center city/suburban sites. This range of fractional retention of water is consistent with measured and theoretical values of D/Do ratios of about 1.05–1.1 or an increase of mass of about 15–30% at 30–40% RH. It is greatest at center city sites and decreases as one moves to suburban and rural/remote areas. There is very little seasonal dependence for the center city/suburban sites but a very pronounced seasonal dependence for the rural/remote IMPROVE sites. There is little predicted water retention during the winter months, while during the summer season the water retention factor is 1.15. The difference between times when sulfates retain water at the low RH found in the laboratory may be due to sulfate neutralization and the mixing characteristics of urban aerosols. Sulfates during winter months tend to be more neutralized than during the summer and may not have deliquesced and therefore retain little water. Furthermore, measurements in the eastern areas of the United States, where most CSN monitors are located, show f(RH), and D/Do functions that have continuous growth curves showing neither deliquescence or crystallization characteristics (Malm et al., 2000a, 2000b; Day and Malm, 2001).

Estimated seasonal variability of nitrate volatilization from a Teflon filter is consistent with reported values. In Figure 8.9, winter fractional loss of nitrate is about 10%, while during the summer the average loss is estimated to be 40–50%, with spring and fall loss being intermediate compared to summer/winter. There is very little difference of nitrate volatilization between urban and suburban sites.

Figure 8.10 shows that there is a rather dramatic seasonal difference in Roc factors, with winter and summer being at about 1.3–1.4 and 1.6–1.8, respectively. Spring and fall have intermediate values as compared to winter/summer. Because of less photochemistry during winter months, one might expect POM to be less oxygenated and have lower Roc factors than summer months. Also, because urban areas are likely sources of OC, it might be expected that a "young" urban organic aerosol would have a lower Roc factor than a more aged rural or remote aerosol. Figure 8.10 shows that these differences, if they exist, are not large. The center city Roc factors are systematically lower than either suburban or rural sites but only by about 5–15%. Interestingly, suburban and rural Roc factors are about the same. Because the Roc factors between IMPROVE and CSN Met One monitoring systems are nearly the same, in spite of a 20% loss of OC using the IMPROVE system, it seems reasonable to hypothesize that the Roc factor of the volatilized SVOC is about the same as the OC that is retained.

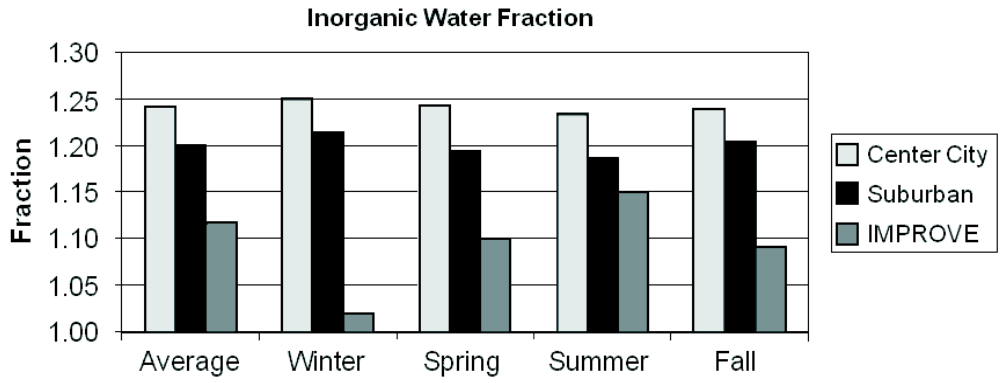

Figure 8.8. Average fractional increase in sulfate and nitrate mass, a_1, due to retained water for the IMPROVE and CSN monitoring networks.

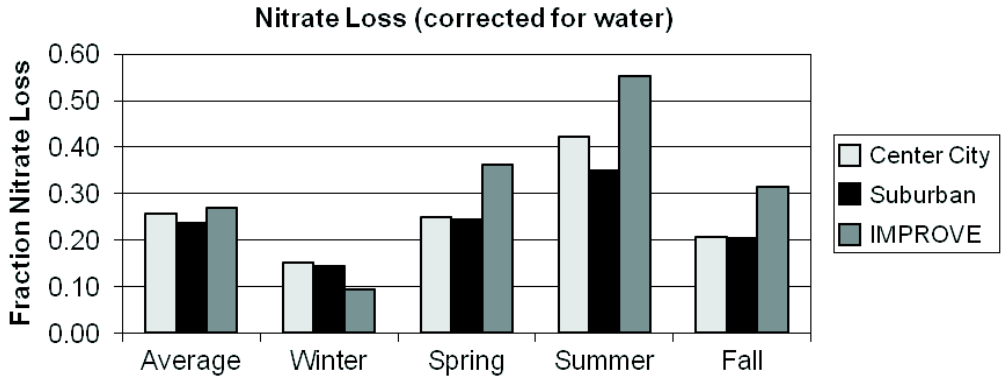

Figure 8.9. Average fraction of nitrate volatilized from a Teflon filter, $(1 - a_2/a_1)$, for the IMPROVE and CSN monitoring networks.

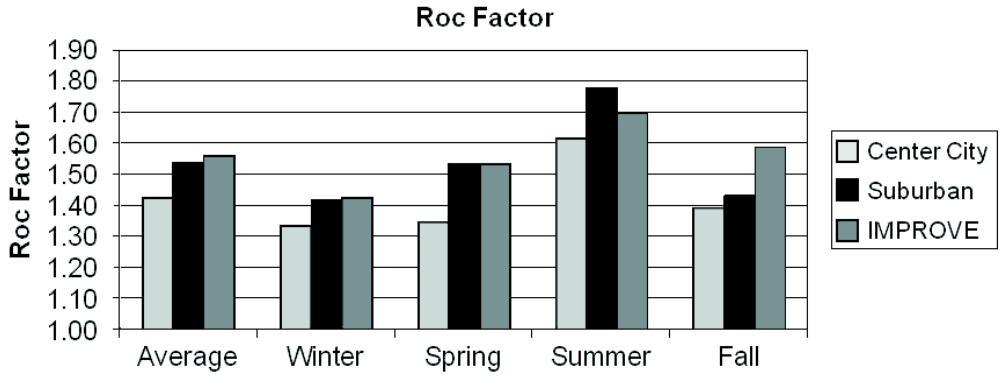

Figure 8.10. Average Roc factor, a_3, for the IMPROVE and CSN monitoring networks.

Using the regression results summarized in Tables 8.4a–8.4c, it is possible to assess the average difference between $PM_{2.5}$ and $RPM_{2.5}$ as a function of species as represented by equation 8.14 and shown for one location in Figure 8.6. Typically, $PM_{2.5} - RPM_{2.5}$ cycles between having its highest and lowest values during the summer and winter, respectively. Figures 8.11–8.13 show the combined difference ($PM_{2.5} - RPM_{2.5}$) and the difference associated with each species for the IMPROVE network and for the CSN, subdivided into center city and suburban, as a function of season.

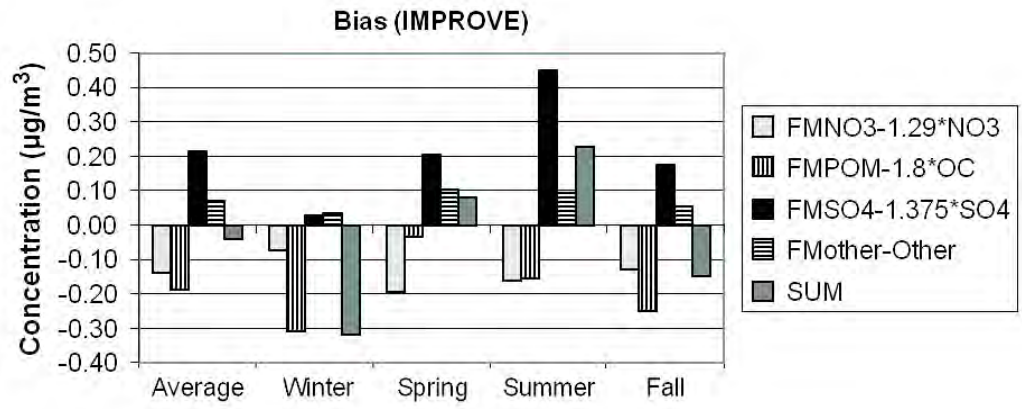

Figure 8.11. The estimated average difference between gravimetric and assumed forms of the various aerosol species contributing to $PM_{2.5}$ for IMPROVE. The differences are estimated as $1.375*SO_4(a_1 - 1)$, $1.29*NO_3(a_2 - 1)$, $OC*(a_3 - 1.8)$, and $Other*(a_4 - 1)$ for sulfates, nitrates, organics, and Other, respectively.

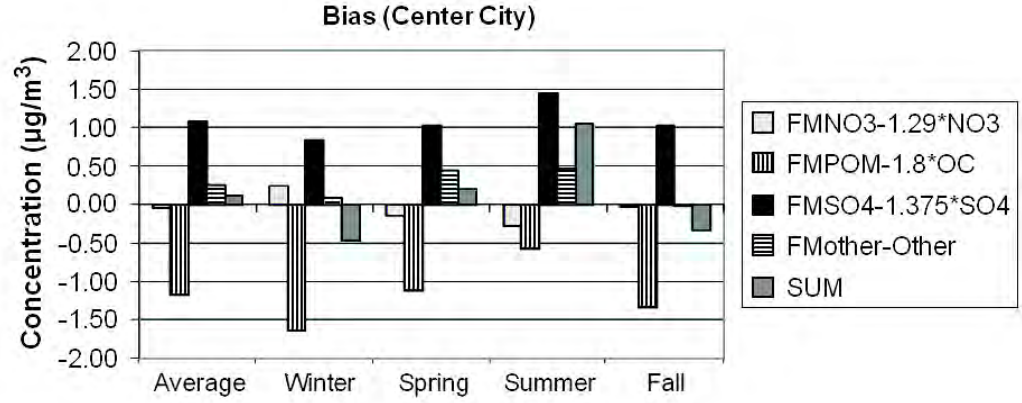

Figure 8.12. The estimated average difference between gravimetric and assumed forms of the various aerosol species contributing to $PM_{2.5}$ for CSN center city. The differences are estimated as $1.375*SO_4(a_1 - 1)$, $1.29*NO_3(a_2 - 1)$, $OC*(a_3 - 1.8)$, and $Other*(a_4 - 1)$ for sulfates, nitrates, organics, and Other, respectively.

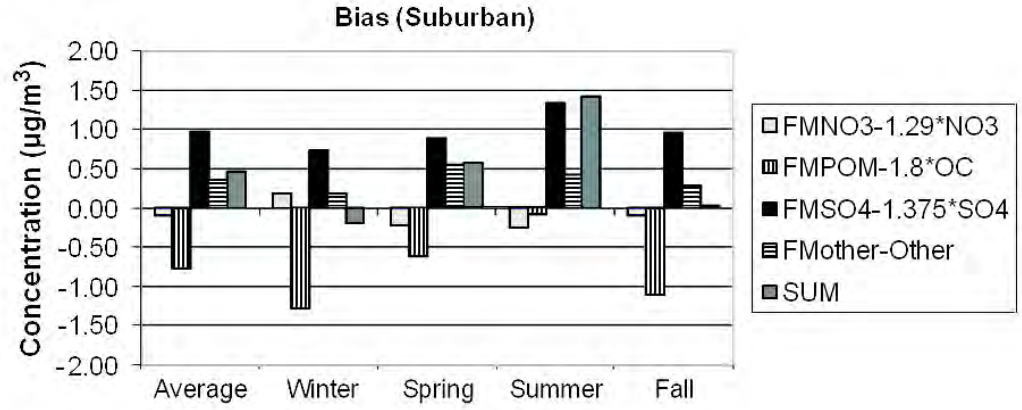

Figure 8.13. The estimated average difference between gravimetric and assumed forms of the various aerosol species contributing to $PM_{2.5}$ for CSN suburban. The differences are estimated as $1.375*SO_4(a_1 - 1)$, $1.29*NO_3(a_2 - 1)$, $OC*(a_3 - 1.8)$, and $Other*(a_4 - 1)$ for sulfates, nitrates, organics, and Other, respectively.

First, notice that the scale of the ordinate axis on the IMPROVE and CSN graphs are different in that the range of values for IMPROVE is -0.4 to +0.5 $\mu g/m^3$, while for the CSN graphs it is -2.0 to +2.0 $\mu g/m^3$, reflecting the higher aerosol concentrations in urban/suburban areas. On the average the difference between $PM_{2.5}$ and $RPM_{2.5}$ is only a few percent, at 1.5% and 4% for urban and suburban, respectively, and 3% for IMPROVE. These overall average low differences between $PM_{2.5}$ and $RPM_{2.5}$ suggest a false sense of certainty as to the chemical characteristics of individual species, as well as the confidence in gravimetric mass levels. It is evident from Figures 8.11–8.13 that there are compensating uncertainties or errors both in the species differences and in temporal or seasonal difference characteristics.

The two largest average differences are in sulfate and POM mass. The temporal trend of the difference for both species is the same in that the difference is lowest in winter and highest during the summer months. However, the sulfate difference is always positive, while the POM difference is always negative. In the IMPROVE network, the water/sulfate difference is near 0 during the winter months and approaches 0.5 $\mu g/m^3$ during the summer, which is about 6% of the gravimetric mass and about 16% of the sulfate mass. Both center city and suburban water/sulfate differences vary from near 0.5 to 1.5 $\mu g/m^3$ during winter and summer, respectively. On a percentage basis, this is about 3–10% of gravimetric mass and 15–25% of ammonium sulfate mass.

In the IMPROVE network, POM difference varies from -0.35 $\mu g/m^3$ (-20%) to -0.15 $\mu g/m^3$ (-5%) during the winter and summer months, respectively. The POM winter difference for center city is about -1.5 $\mu g/m^3$ (-40%) for the winter, while the summer difference is -0.5 $\mu g/m^3$ (-16%). The average POM suburban difference is about the same as center city for the winter months but is only -0.08 $\mu g/m^3$ (-3%) for summer months. The implication here is that an Roc factor of 1.8 may be, on the average, a bit high for the higher-POM-concentration summer months but substantially high for the lower-concentration time periods, which correspond to the winter season.

Nitrate difference has the opposite seasonal trend in that the difference is lowest in winter months and highest during summer, when ambient temperatures are higher and therefore conducive to more ammonium nitrate volatilization. The average difference across the IMPROVE network during the winter is -0.08 $\mu g/m^3$ (9%), while during the summer it is -0.17 $\mu g/m^3$ (56%). There is little variation in nitrate difference between center city and suburban. In both the center city and suburban datasets, the wintertime nitrate difference is on the order of 0.25 $\mu g/m^3$ (4–6%), while during the summer it is about -0.25 $\mu g/m^3$ (-25%). Even though nitrate is volatilized from the PM Teflon filter during the winter season, the nitrate plus bound water on the Teflon filter is greater than nitrate alone on the nylon filter. During the summer there is enough nitrate volatilized from the Teflon filter such that the nitrate plus particle-bound nitrate water is substantially less than the nitrate collected on the nylon substrate.

Other (sea salt + EC+ soil) also has systematic seasonal differences, although they are harder to interpret. It is assumed that sea salt is represented by 1.8*Cl. This could be an over- or underestimate, depending on the aging and reactions that a sea salt aerosol has undergone and the assumed form of oxides of the elements that make up the "soil" fraction. For instance, the elemental composition, internationally transported dust is different from that found in the desert Southwest and, for that matter, anywhere in the continental United States. The "correction" or

regression factors were on the order of 1.04–1.08 for IMPROVE and a bit higher for CSN data, at about 1.2, indicating that Other has been underestimated by about 10–20%.

8.3.1 Bias in Gravimetric Mass

Having an approximate understanding of the difference between measured and reconstructed mass concentrations, it is possible, with some assumptions, to develop over- or underestimates of the policy-relevant variables as they relate to $PM_{2.5}$ NAAQS and the RHR. First, it must be pointed out that the above analysis does not establish the bias associated with volatilization of SVOCs from various filter media as a function of sampler design and physical characteristics. However, it was shown that OC collected using the IMPROVE sampling system is systematically about 20% lower than OC collected using the MET One sampler and that the difference may be in part due to filter face velocity. This suggests that all samplers have some inherent loss of semivolatile species, although the amount cannot be quantified with the datasets that are currently routinely collected.

The average difference between $PM_{2.5}$ gravimetric mass and true ambient mass ($TPM_{2.5}$) concentration is estimated by assuming that POM, crustal material, and sea salt gravimetric mass are measured without bias and that the positive difference due to retained water on the nitrate and sulfate aerosol at the time of filter weighing and nitrate loss due to volatilization can be estimated using regression coefficients a_1 and a_2:

$$PM_{2.5} - TPM_{2.5} = (a_1 - 1)*1.375*SO_4 + (a_2 - 1)*1.29*NO_3. \quad 8.16$$

These results are summarized in Figure 8.14 for the IMPROVE and the center city and suburban CSN datasets. The difference associated with nitrate volatilization from the Teflon filter is compensated for by retained water on the hygroscopic inorganic species. The only time when nitrate volatilization is greater than retained water mass is during the winter season in the IMPROVE network, when the average $PM_{2.5}$ mass is underestimated by less than 0.1 $\mu g/m^3$. The average difference for the IMPROVE dataset is 0.07 $\mu g/m^3$ or about 1%. The maximum difference occurs during the summer season and is about 0.3 $\mu g/m^3$ or 4%. The difference associated with the CSN dataset is nearly the same for all seasons and always positive at about 0.8 – 1.2 $\mu g/m^3$, which is about 6%. These values are well within measurement uncertainty.

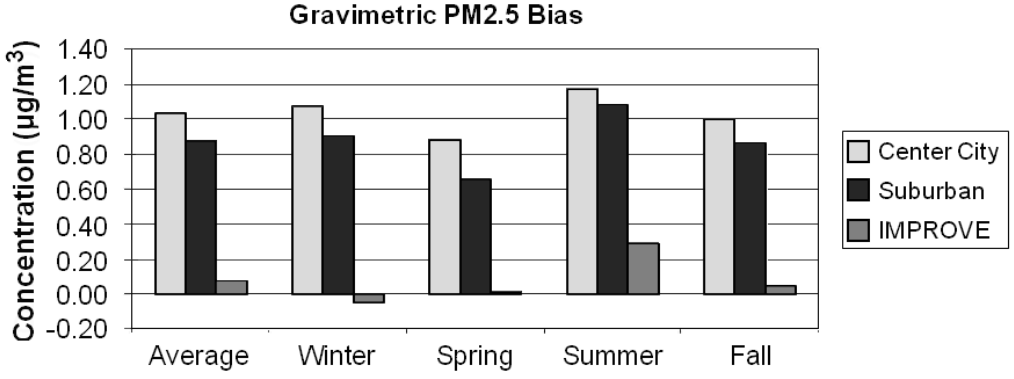

Figure 8.14. Average difference between gravimetric and estimated true $PM_{2.5}$ mass concentration for the IMPROVE and CSN datasets (see equation 8.16).

8.3.2 Bias in Reconstructed Mass

The sum of biases shown in Figure 8.15 associated with OC and Other can be used to estimate the average difference of reconstructed $PM_{2.5}$ relative to $TPM_{2.5}$ concentrations:

$$RPM_{2.5} - TPM_{2.5} = (1 - a_3)*1.8*OC + (1 - a_4)*1.29*NO_3 \quad 8.17$$

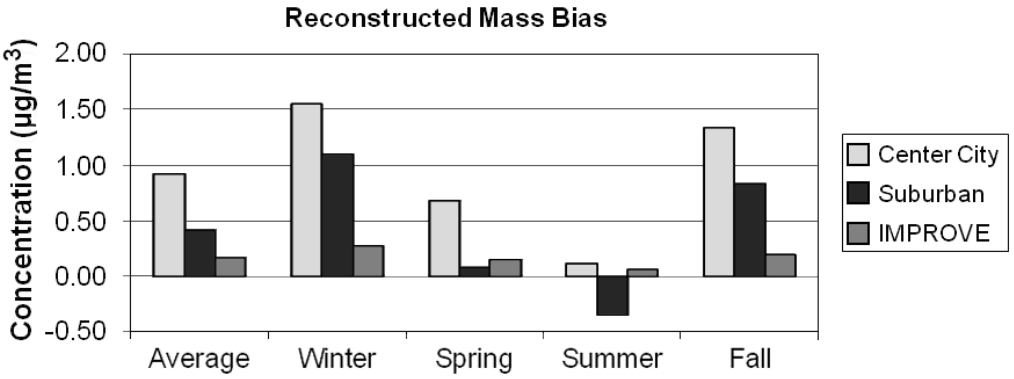

Figure 8.15. Average difference between reconstructed and estimated true $PM_{2.5}$ concentrations for the IMPROVE and CSN datasets (see equation 8.17).

The bias of assuming sulfates are fully neutralized is not addressed, nor are differences associated with assuming all nitrates are in the form of ammonium nitrate. Furthermore, equation 8.17 implicitly assumes that, after correction for positive artifacts associated with the quartz substrate that is used in the OC TOT/TOR analysis, the volatilization (negative artifact) of SVOCs from the Teflon substrate used in the gravimetric analysis and quartz filter used in OC determination is the same.

Figure 8.15 shows the estimated overall average and seasonal differences between reconstructed and $TPM_{2.5}$. The average overall difference for the IMPROVE dataset is 0.2 $\mu g/m^3$, or about 3.5%. The average differences for the center city and suburban sites are 0.9 and 0.4 $\mu g/m^3$, respectively. These values correspond to 7% and 3% of measured fine mass. The greatest difference occurs during the winter season, primarily because POM is overestimated (see Figures 8.11–8.13). The winter difference for IMPROVE is 0.3 $\mu g/m^3$, while for center city and suburban sites it is 1.6 $\mu g/m^3$ and 1.1 $\mu g/m^3$, respectively. These values correspond to about a 7% difference for IMPROVE and suburban sites and about a 10% difference for center city data. The least difference occurs during the summer months, when it is on the order of only 1% or 2%. Differences for the spring and fall seasons are intermediate to winter and summer.

8.4 SPATIAL AND SEASONAL VARIABILITY IN $PM_{2.5}$ AND $RPM_{2.5}$ BIASES

The approximate seasonal and spatial variability in CSN and IMPROVE fine gravimetric and reconstructed fine mass biases can be explored by applying the regression coefficients a_1, a_2, a_3, and a_4 derived from the CSN and IMPROVE seasonal datasets for all sites to the site-specific sulfate, nitrate, POM, and Other concentration averages. Alternatively, regressions could be carried out using site-specific data; however, because of an insufficient number of data points, the regression coefficients can be highly variable with large standard errors. It is recognized that the regressions using the site-combined datasets may not be entirely representative of physical

and chemical processes that might occur on a site-specific basis. However, they will capture the implications of seasonal variability in aerosol mix that occurs on a site by site basis.

Figure 8.16 shows the spatial distribution in the estimated difference between gravimetric and true mass concentration ($PM_{2.5} - TPM_{2.5}$) for the combined urban/suburban datasets as a function of season, while Figure 8.17 shows the same information for the IMPROVE dataset. The circles are color coded so that green and red correspond to gravimetric mass being greater or less than true mass. First of all, notice that for both datasets the differences associated with the West, except for southern California, are lower than for the eastern United States. Furthermore, the central-eastern United States has the highest difference at about 1.5–2.0 $\mu g/m^3$ for the CSN and for the summer months in the IMPROVE network. The positive difference is associated with retained water on an aerosol primarily made up of sulfate. This sulfate-driven positive difference in the eastern United States should be compared to southern California, where during the summer there is a greater than 1.5 $\mu g/m^3$ negative difference in both networks. In the IMPROVE network there is a negative difference in gravimetric mass at nearly all monitoring sites during the winter and spring months, when sulfate concentrations are lowest and nitrate concentrations the highest. The negative difference corresponds to volatilization of a nitrate-dominated ambient aerosol.

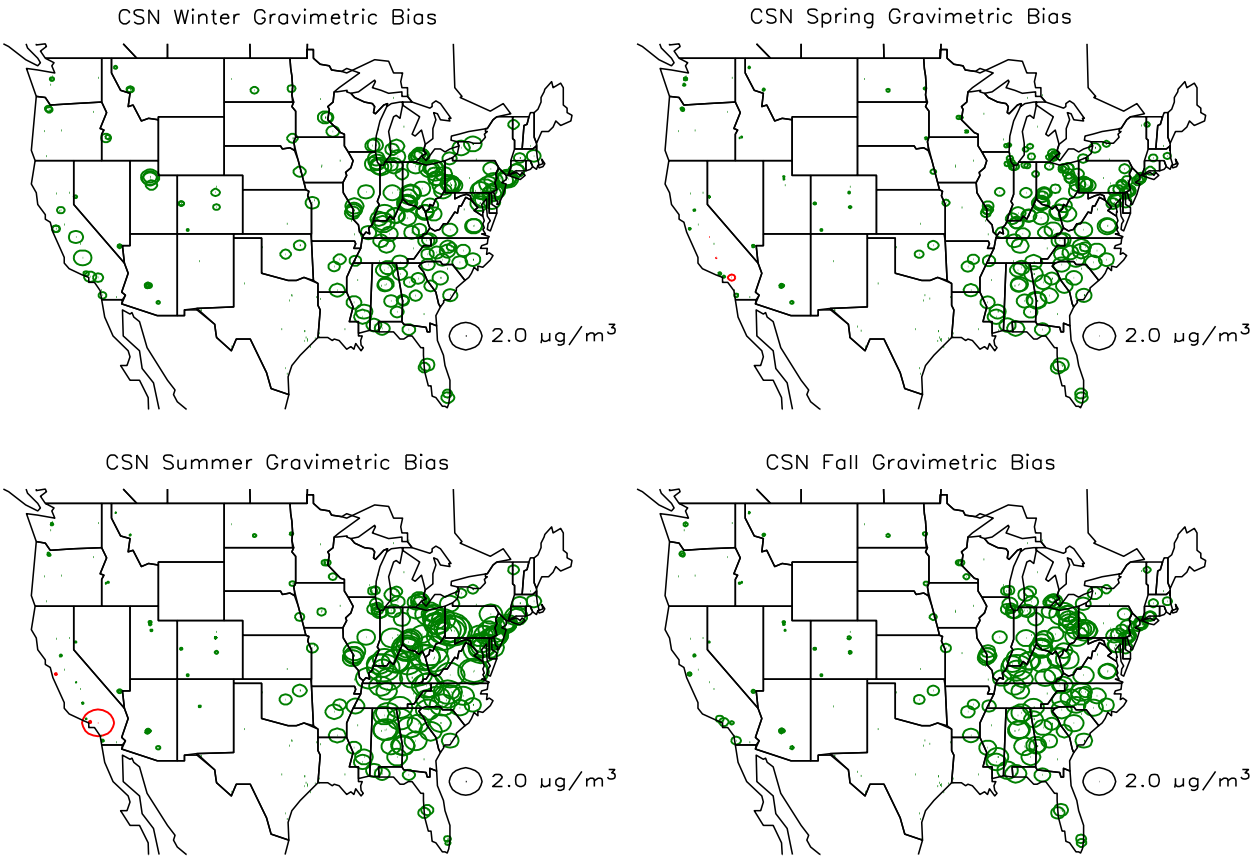

Figure 8.16. Seasonal and spatial variability in difference between gravimetric and true mass concentration ($PM_{2.5} - TPM_{2.5}$) for the CSN monitoring network. Green color refers to positive and red to negative numbers.

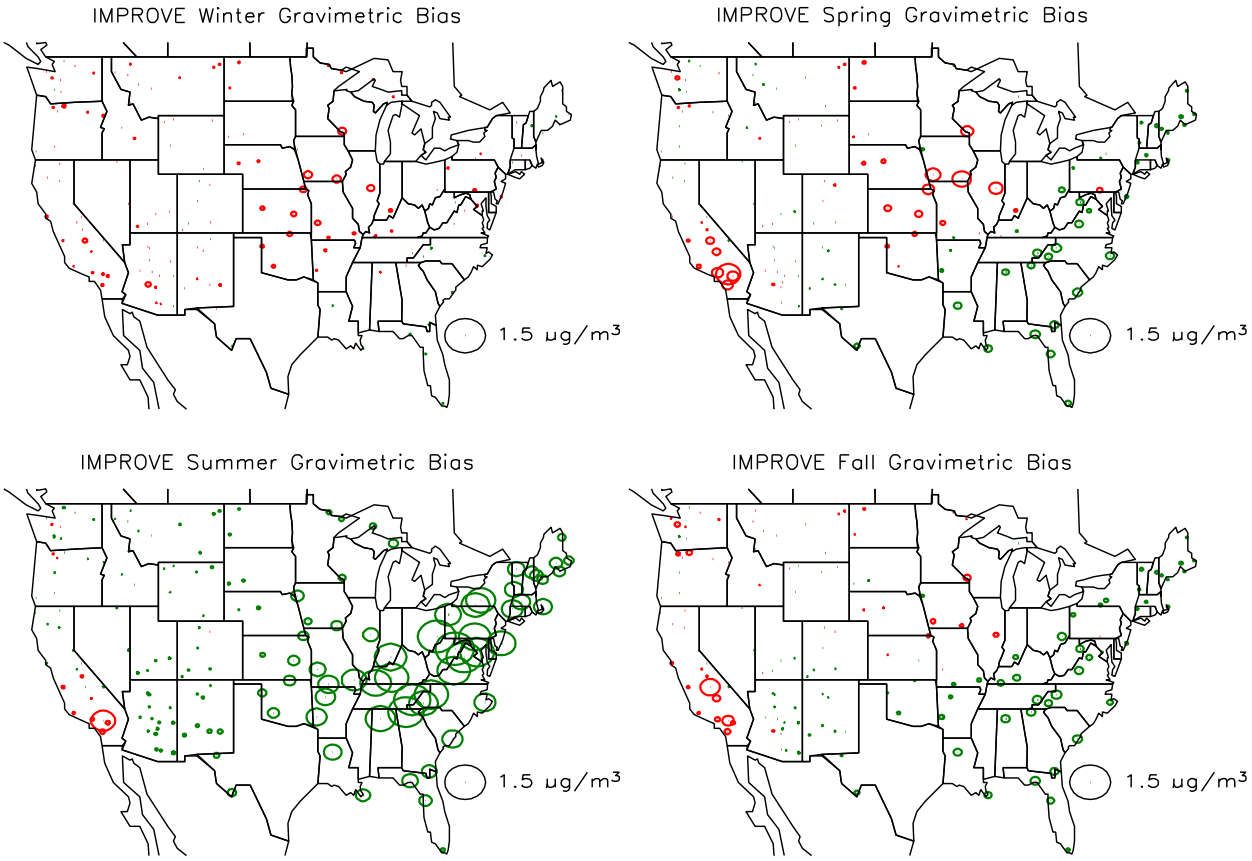

Figure 8.17. Seasonal and spatial variability in difference between gravimetric and true mass concentration ($PM_{2.5} - TPM_{2.5}$) for the IMPROVE monitoring network. Green color refers to positive and red to negative numbers.

Figure 8.18 shows the spatial and seasonal distribution in the variability between true and reconstructed mass concentration ($TPM_{2.5} - RPM_{2.5}$) for the CSN combined urban/suburban datasets, while Figure 8.19 shows the same information for the IMPROVE dataset. Circles coded red correspond to reconstructed mass being greater than ambient mass concentration. In both datasets the negative difference is greatest in the winter and lowest in the summer months. This difference is primarily associated with an assumed Roc factor used to estimate POM from measured OC that is too high during winter months and about right during summer. As shown in Figure 8.10, the Roc factor was shown to vary from about 1.4 during the winter months to near 1.8 in the summer, and the Roc factor used in estimating reconstructed mass concentrations for all months was 1.8. It should also be noted that during the winter there are negative-difference "hot spots" around western urban areas. These hot spots correspond to elevated concentration levels of OC in urban areas such as Phoenix, Arizona, Spokane, Washington, the California San Joaquin valley, and the south coast air basin in California that are located in valleys and basins where wintertime emissions are trapped by shallow mixing heights.

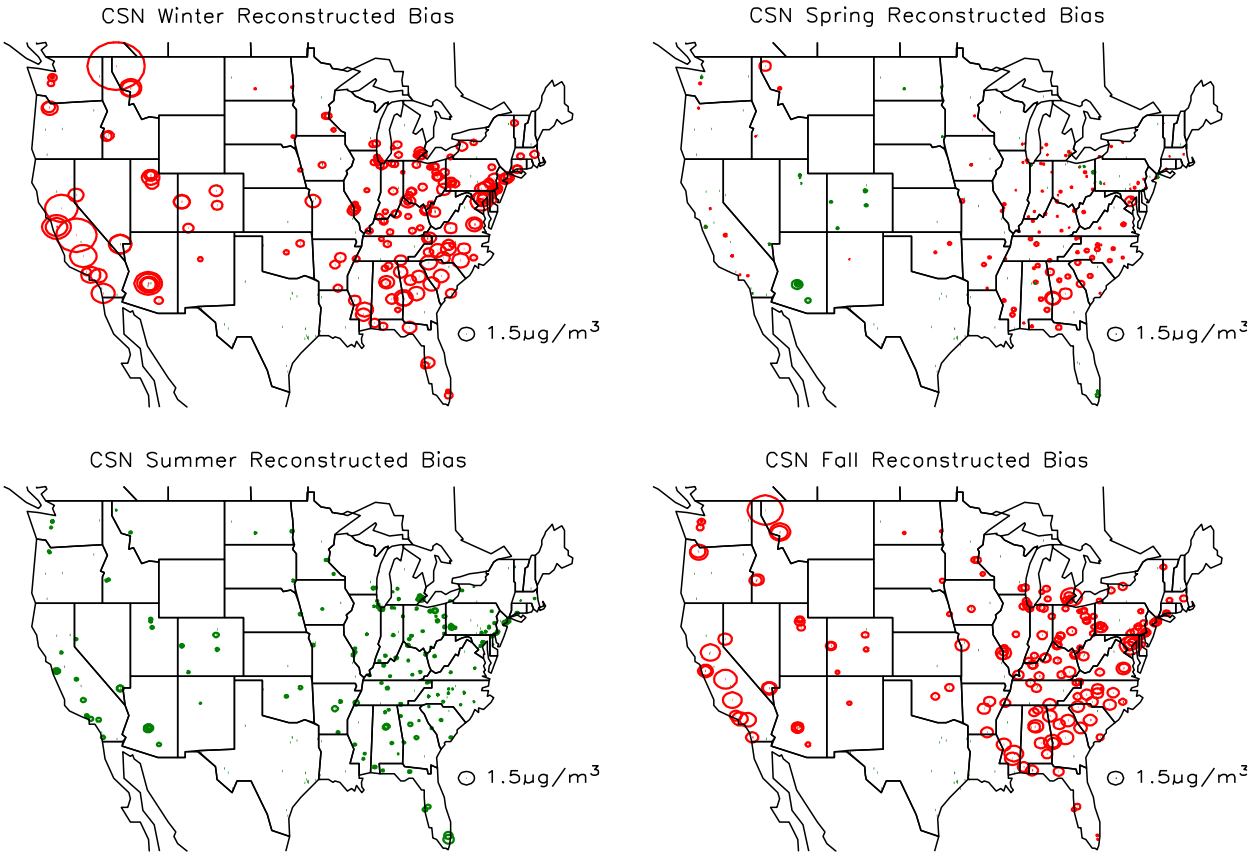

Figure 8.18. Seasonal and spatial variability in difference between true and reconstructed mass concentration ($TPM_{2.5} - RPM_{2.5}$) for the CSN monitoring network. Green color refers to positive and red to negative numbers.

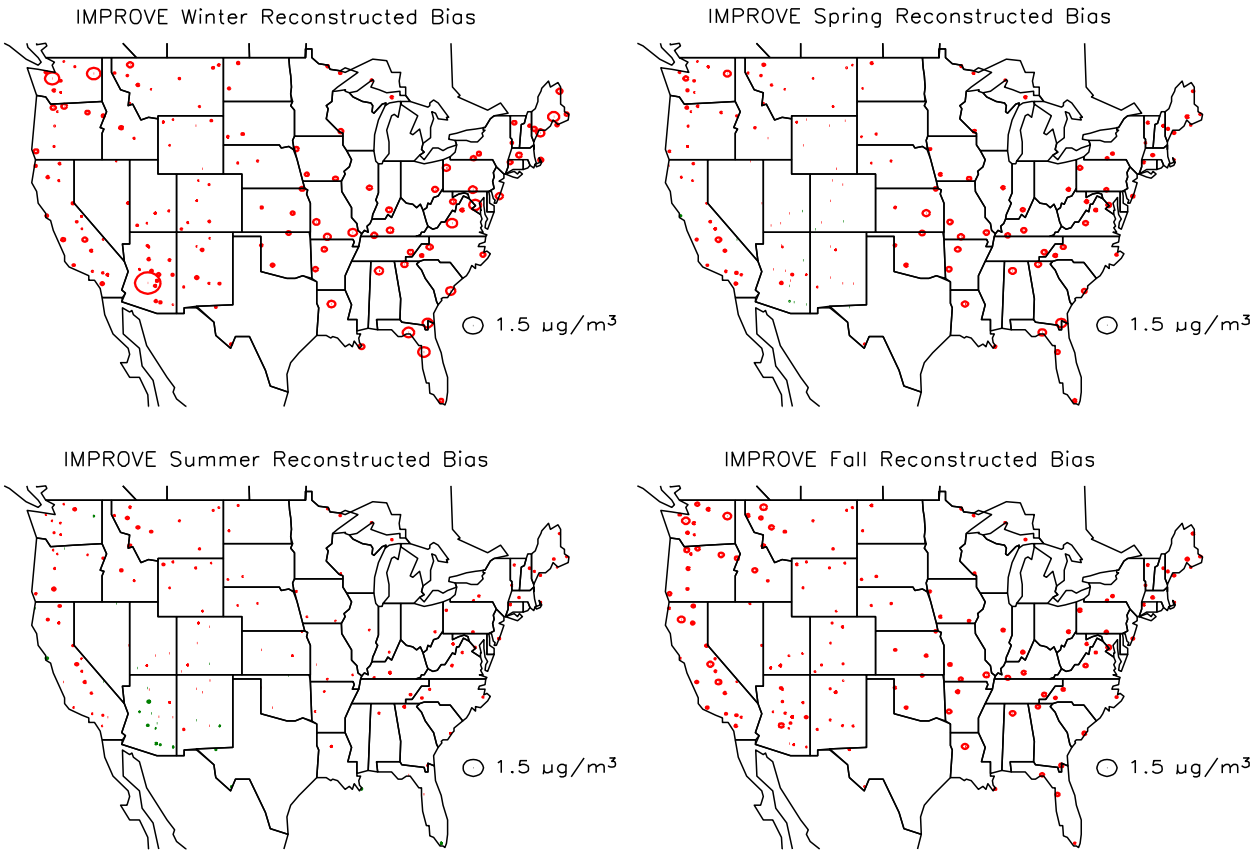

Figure 8.19. Seasonal and spatial variability in difference between true and reconstructed mass concentration ($TPM_{2.5} - RPM_{2.5}$) for the IMPROVE monitoring network. Green color refers to positive and red to negative numbers.

8.5 SUMMARY

The NAAQS guideline for $PM_{2.5}$ is based on a gravimetric analysis of particulate matter collected on a Teflon substrate using federal reference methodologies. To help understand which of the many aerosol species contribute to elevated levels of PM, the EPA and the states also operate the CSN at approximately 200 sites. Filter substrates collected in the CSN are analyzed for gravimetric mass, inorganic ions, carbon, and elements. The IMPROVE monitoring program is operated to meet the needs of the Regional Haze Program, which is mandated to track long-term temporal changes in visibility in certain protected visual environments such as national parks and wilderness areas. The IMPROVE monitoring program is similar to the CSN, with exceptions being the sampling system hardware used to collect the aerosols, some filter handling protocols, and some quality assurance procedures. Only one type of sampling system is used throughout the IMPROVE monitoring network, while five systems have been used in the CSN, all of which are different from the IMPROVE system. Compliance under the RHR is based on reconstructed aerosol mass and light extinction from aerosol composition. Anions, OC, and elements are measured, and aerosol species concentrations are estimated assuming molecular forms of sulfates, nitrates, POM, sea salt, and soil dust.

Both measured and reconstructed mass have inherent biases. Compliance monitoring for $PM_{2.5}$ mass concentrations relies on a gravimetric analysis of aerosols that have been collected

on a Teflon filter, while reconstructed mass is estimated from the sum of aerosol species that contribute to PM, assuming an average molecular form of those species. Collection of aerosols on a Teflon substrate results in volatilization of semivolatile species such as ammonium nitrate and some organic species, which corresponds to an overall loss of mass or negative artifact. These losses are to some degree compensated for when the filters are weighed in environments where the RH is between 30–40%. Hygroscopic species can retain significant amounts of water at these RHs. For instance, sulfate and nitrate mass may be increased by as much as 30% due to retained water.

On the other hand, the aerosol species used in reconstructed mass are derived from assumed forms of sulfates, nitrates, OC, and soil dust. Typically, sulfates and nitrates are assumed to be fully neutralized by ammonium, a POM to OC ratio is assumed, and a form of oxides of soil-related elements is assumed. Furthermore, it is assumed that EC as derived from TOR/TOT is elemental and does not have other carbon compounds associated with it. It is known that all these assumptions can be violated at times.

A regression analysis between $PM_{2.5}$ and the assumed mass concentrations of derived aerosol species allows for an estimation of how each of the major aerosol species contributes to differences between $PM_{2.5}$ and $RPM_{2.5}$, and with certain assumptions, the bias from true mass in gravimetric and reconstructed mass concentration estimates.

First of all, it was demonstrated that there is on the order of a 20% difference in OC mass, depending on which sampling system was used. It is suggested that this loss may be associated with volatilization of SVOCs and may be dependent on filter face velocity. This implies that there may be some loss of SVOCs from all sampling systems; however, the specific loss as a function of sampler characteristics cannot be addressed with data that is routinely collected in the IMPROVE and CSN monitoring programs.

Assuming that the gravimetric mass of POM, crustal material, and sea salt is measured without bias and that the positive bias due to retained water at the time of filter weighing and nitrate loss due to volatilization can be estimated from the regression analysis, the overall difference between gravimetrically determined and true ambient fine mass was estimated. On the average, the difference is about the same for the urban and suburban datasets at about 1 $\mu g/m^3$ or 6%. The average difference for the IMPROVE dataset is 0.1 $\mu g/m^3$ or 4%. The biggest difference for the IMPROVE dataset occurs during the summer at 0.3 $\mu g/m^3$, while for the CSN datasets, both summer and winter have the greatest bias at 1.0 $\mu g/m^3$, with spring and fall having somewhat intermediate differences at 0.6–0.8 $\mu g/m^3$.

Differences between reconstructed and true ambient mass concentrations associated with assumed molecular forms of species used in the RHR guidelines were estimated by assuming that sulfates and nitrates are accurately speciated and that the gravimetrically determined mass of POM, EC, sea salt, and soil dust accurately reflects these species' true mass. It was further assumed that, after correction for positive artifacts associated with the quartz substrate that is used in the OC TOT/TOR analysis, the volatilization (negative artifact) of SVOCs from the Teflon substrate used in the gravimetric analysis and the quartz filter used for OC determination is the same. Under these assumptions, the average overall difference between reconstructed and true mass for the IMPROVE dataset is 0.2 $\mu g/m^3$, or about 3.5%. The average differences for the

center city and suburban sites are 0.9 μg/m^3 and 0.4 μg/m^3, respectively. These values correspond to 7% and 3% of measured fine mass. The greatest difference occurs during the winter season, primarily because of POM overestimation. The winter difference for IMPROVE is 0.3 μg/m^3, while for center city and suburban sites it is 1.6 μg/m^3 and 1.1 μg/m^3, respectively. These values correspond to about a 7% difference for IMPROVE and suburban sites and about a 10% difference for center city data. The least difference occurs during the summer months, when the difference is on the order of only 1% or 2%. Differences for the spring and fall seasons are intermediate to winter and summer.

Fine gravimetric mass concentration bias in the western United States, except for southern California, is lower than the eastern United States, and the central-eastern United States has the highest bias at about 1.5–2.0 μg/m^3 for both networks. The positive bias is associated with retained water on an aerosol primarily made up of sulfate. This sulfate-driven positive bias in the eastern United States should be compared to southern California, where during the summer there is a greater than 1.5 μg/m^3 negative bias in both networks, primarily associated with a region of the country where ambient nitrate concentrations are high and nitrate volatilization becomes the biggest contributor to gravimetric mass concentration bias. In the IMPROVE network, there is a negative bias in gravimetric mass at nearly all monitoring sites during the winter and spring months.

Negative differences in reconstructed and estimated true mass concentrations in both the CSN and IMPROVE datasets are greatest in the winter and lowest in the summer months. These differences are primarily associated with an assumed Roc factor that is too high during winter months and about right during summer. The derived Roc factor is about 1.4 during the winter months to near 1.8 in the summer. Furthermore, there are negative-bias "hot spots" linked to western urban areas. These hot spots correspond to elevated concentration levels of OC in western urban areas that are located in valleys and basins, where wintertime emissions tend to be trapped by shallow mixing heights.

REFERENCES

Aiken, A. C., P. F. Decarlo, J. H. Kroll, D. R. Worsnop, J. A. Huffman, K. S. Docherty, I. M. Ulbrich, C. Mohr, J. R. Kimmel, D. Sueper, Y. Sun, Q. Zhang, A. Trimborn, M. Northway, P. J. Ziemann, M. R. Canagaratna, T. B. Onasch, M. R. Alfarra, A. S. H. Prevot, J. Dommen, J. Duplissy, A. Metzger, U. Baltensperger, and J. L. Jimenez (2008), O/C and OM/OC ratios of primary, secondary, and ambient organic aerosols with high-resolution time-of-flight aerosol mass spectrometry, *Env. Sci. Technol.*, *42*, 4478-4485.

Ashbaugh, L. L. and R. A. Eldred (2004), Loss of particle nitrate from Teflon sampling filters: Effects on measured gravimetric mass in California and in the IMPROVE network, *J. Air Waste Manage. Assoc.*, *54*, 93-104.

Bae, M. S., J. J. Schauer, and J. R. Turner (2006), Estimation of the monthly average ratios of organic mass to organic carbon for fine particulate matter at an urban site, *Aerosol Sci. Technol.*, *40*, 1123-1139.

Bae, M. S., K. l. Demerjian, and J. J. Schwab (2006), Seasonal estimation of organic mass to organic carbon in PM2.5 at rural and urban locations in New York State, *Atmos. Environ.*, *40*, 7467-7479.

Chan, T. W., L. Huang, W. R. Leaitch, S. Sharma, J. R. Brook, J. G. Slowik, J. P. D. Abbatt, P. C. Brickell, J. Liggio, S. M. Li, and H. Moosmuller (2010), Observations of OM/OC and specific attenuation coefficients (SAC) in ambient fine PM at a rural site in central Ontario, Canada, *Atmos. Chem. Phys.*, *10*, 2393-2411.

Chang, M. C., C. Sioutas, S. Kim, H. Gong, and W. S. Linn (2000), Reduction of nitrate losses from filter and impactor samplers by means of concentration enrichment, *Atmos. Environ.*, *34*, 85-98.

Chen, X. and J. Z. Yu (2007), Measurement of organic mass to organic carbon ratio in ambient aerosol samples using a gravimetric technique in combination with chemical analysis, *Atmos. Environ.*, *41*, 8857-8864.

Chow, J. C., J. G. Watson, L. C. Pritchett, W. R. Pierson, C. A. Frazier, and R. G. Purcell (1993), The DRI thermal/optical reflectance carbon analysis system: description, evaluation, and applications in U.S. air quality studies, *Atmos. Environ.*, *27A*, 1185-1201.

Chow, J.C., J.G. Watson, (1999), In *Elemental Analysis of Airborne Particles*; Landberger, S., Creatchman, M., Eds., Gordon and Breach Science, Amsterdam, Vol. 1, pp. 97-137.

Chow, J. C., J. G. Watson, D. Crow, D. H. Lowenthal, and T. Merrifield (2001), Comparison of IMPROVE and NIOSH carbon measurements, *Aerosol Sci. Technol.*, *34*, 23-34.

Chow, J. C., J. G. Watson, L. W. A. Chen, W. P. Arnott, and H. Moosmuller (2004), Equivalence of elemental carbon by thermal/optical reflectance and transmittance with different temperature protocols, *Env. Sci. Technol.*, *38*, 4414-4422.

Chow, J. C., J. G. Watson, L. W. A. Chen, G. Paredes-Miranda, M. C. O. Chang, D. Trimble, K. K. Fung, H. Zhang, and J. Z. Yu (2005), Refining temperature measures in thermal/optical carbon analysis, *Atmos. Chem. Phys.*, *5*, 2961-2972.

Chow, J. C., J. G. Watson, D. H. Lowenthal, and K. L. Magliano (2005), Loss of $PM_{2.5}$ nitrate from filter samples in central California, *J. Air Waste Manage. Assoc.*, *55*, 1158-1168.

Chow, J. C., J. G. Watson, L. W. A. Chen, J. Rice, and N. H. Frank (2010), Quantification of $PM_{2.5}$ organic carbon sampling artifacts in U.S. networks, *Atmos. Chem. Phys.*, *10*, 5223-5239.

Chu, S. H. (2004), $PM_{2.5}$ episodes as observed in the speciation trends network, *Atmos. Environ.*, *38*, 5237-5246.

Currie, L. A., B. A. Benner, J. D. Kessler, D. B. Klinedinst, G. A. Klouda, J. V. Marolf, J. F. Slater, and S. A. Wise (2002), A critical evaluation of interlaboratory data on total,

elemental and isotopic carbon in the carbonaceous particle reference material, NIST SRM 1649a, *Journal of Research of the National Bureau of Standards*, *107*, 279-298.

Day, D. E., W. C. Malm, and S. M. Kreidenweis (1997), Seasonal variations in aerosol composition and acidity at Shenandoah & Great Smoky Mountains national parks, *J. Air Waste Manage. Assoc.*, *47*, 411-418.

Day, D. E. and W. C. Malm (2001), Aerosol light scattering measurements as a function of relative humidity: A comparison between measurements made at three different sites, *Atmos. Environ.*, *35*, 5169-5176.

Dillner, A. M., C. H. Phuah, and J. R. Turner (2009), Effects of post-sampling conditions on ambient carbon aerosol filter measurements, *Atmos. Environ.*, *43*, 5937-5943.

El-Zanan, H. S., D. H. Lowenthal, B. Zielinska, J. C. Chow, and N. Kumar (2005), Determination of the organic aerosol mass to organic carbon ratio in IMPROVE samples, *Chemosphere*, *60*, 485-496.

El-Zanan, H. S., B. Zielinska, L. R. Mazzoleni, and D. A. Hansen (2009), Analytical determination of the aerosol organic mass-to-organic carbon ratio, *J. Air Waste Manage. Assoc.*, *59*, 58-69.

Frank, N. H. (2006), Retained nitrate, hydrated sulfates, and carbonaceous mass in Federal Reference method fine particulate matter for six eastern U.S. cities, *J. Air Waste Manage. Assoc.*, *56*, 500-511.

Galasyn, J. F., J. F. Hornig, and R. H. Soderberg (1984), The Loss of Pah from quartz fiber high volume filters, *J. Air Poll. Control Assoc.*, *34*, 57-59.

Gebhart, K. A., W. C. Malm, and D. Day (1994), Examination of the effects of sulfate acidity and relative humidity on light scattering at Shenandoah National Park, *Atmos. Environ.*, *28*, 841-849.

Gilardoni, S., L. M. Russell, A. Sorooshian, R. C. Flagan, J. H. Seinfeld, T. S. Bates, P. K. Quinn, J. D. Allan, B. Williams, A. H. Goldstein, T. B. Onasch, and D. R. Worsnop (2007), Regional variation of organic functional groups in aerosol particles on four U.S. east coast platforms during the International Consortium for Atmospheric Research on Transport and Transformation 2004 campaign, *J. Geophys. Res.-Atmospheres*, *112*,

Hand, J.L.; Malm, W.C. *Review of the IMPROVE Equation for Estimating Ambient Light Extinction Coefficients;* Cooperative Institute for Research in the Atmosphere (CIRA), ISSN 0737-5352-71: Colorado State University, Fort Collins, Colorado, March 2006; http://vista.cira.colostate.edu/improve/Publications/GrayLit/016_IMPROVEeqReview/IMPROVEeqReview.htm.

Hogrefe, O., J. J. Schwab, F. Drewnick, G. G. Lala, S. Peters, K. l. Demerjian, K. Rhoads, H. D. Felton, O. V. Rattigan, L. Husain, and V. A. Dutkiewicz (2004), Semicontinuous PM2.5

sulfate and nitrate measurements at an urban and a rural location in New York: PMTACS-NY summer 2001 and 2002 campaigns, *J. Air Waste Manage. Assoc.*, *54*, 1040-1060.

Kiss, G., B. Varga, I. Galambos, and I. Ganszky (2002), Characterization of water-soluble organic matter isolated from atmospheric fine aerosol, *J. Geophys. Res.-Atmospheres*, *107*,

Kukreja, V. P. and J. L. Bove (1976), Determination of Free Carbon Collected on High-Volume Glass-Fiber Filter, *Env. Sci. Technol.*, *10*, 187-189.

Lefer, B. L. and R. W. Talbot (2001), Summertime measurements of aerosol nitrate and ammonium at a northeastern U.S. site, *J. Geophys. Res.-Atmospheres*, *106*, 20365-20378.

Liu, L. J. S., R. Burton, W. E. Wilson, and P. Koutrakis (1996), Comparison of aerosol acidity in urban and semirural environments, *Atmos. Environ.*, *30*, 1237-1245.

Liu, S., S. Takahama, L. M. Russell, S. Gilardoni, and D. Baumgardner (2009), Oxygenated organic functional groups and their sources in single and submicron organic particles in MILAGRO 2006 campaign, *Atmos. Chem. Phys.*, *9*, 6849-6863.

Lowenthal, D., B. Zielinska, B. Mason, S. Samy, V. Samburova, D. Collins, C. Spencer, N. Taylor, J. Allen, and N. Kumar (2009), Aerosol characterization studies at Great Smoky Mountains National Park, summer 2006, *J. Geophys. Res.-Atmospheres*, *114*,

Lowenthal, D. H., J. G. Watson, and P. Saxena (2000), Contributions to light extinction during project MOHAVE, *Atmos. Environ.*, *34*, 2351-2359.

Malm, W. C., J. F. Sisler, D. Huffman, R. A. Eldred, and T. A. Cahill (1994), Spatial and seasonal trends in particle concentration and optical extinction in the United States, *J. Geophys. Res.*, *99*, 1347-1370.

Malm, W. C., D. E. Day, and S. M. Kreidenweis (2000), Light scattering characteristics of aerosols at ambient and as a function of relative humidity: Part II - A comparison of measured scattering and aerosol concentrations using statistical models, *J. Air Waste Manage. Assoc.*, *50*, 701-709.

Malm, W. C., D. E. Day, and S. M. Kreidenweis (2000), Light scattering characteristics of aerosols as a function of relative humidity: Part I: A comparison of measured scattering and aerosol concentrations using the theoretical models, *J. Air Waste Manage. Assoc.*, *50*, 686-700.

Malm, W. C., B. A. Schichtel, M. L. Pitchford, L. L. Ashbaugh, and R. A. Eldred (2004), Spatial and monthly trends in speciated fine particle concentration in the United States, *J. Geophys. Res.*, *109*, doi:10.1029/2003JD003739.

Mozurkewich, M. (1993), The dissociation constant of ammonium nitrate and its dependence on temperature, relative humidity and particle size, *Atmos. Environ.*, *27A*, 261-270.

Polidori, A., B. J. Turpin, C. I. Davidson, L. A. Rodenburg, and F. Maimone (2008), Organic $PM_{2.5}$: Fractionation by polarity, FTIR spectroscopy, and OM/OC ratio for the Pittsburgh aerosol, *Aerosol Sci. Technol.*, *42*, 233-246.

Quinn, P. K., T. L. Miller, T. S. Bates, J. A. Ogren, E. Andrews, and G. E. Shaw (2002), A 3-year record of simultaneously measured aerosol chemical and optical properties at Barrow, Alaska, *J. Geophys. Res.-Atmospheres*, *107*,

Reff, A., B. J. Turpin, J. H. Offenberg, C. P. Weisel, J. Zhang, M. Morandi, T. Stock, S. Colome, and A. Winer (2007), A functional group characterization of organic $PM_{2.5}$ exposure: Results from the RIOPA study, *Atmos. Environ.*, *41*, 4585-4598.

Regional Haze Regulations (1999), *Code of Federal Regulations*, Part 51, Title 40, *Fed. Regist.*, *64* (126), 35714-35774.

Russell, L. M. (2003), Aerosol organic-mass-to-organic-carbon ratio measurements, *Env. Sci. Technol.*, *37*, 2982-2987.

Russell, L. M., S. Takahama, S. Liu, L. N. Hawkins, D. S. Covert, P. K. Quinn, and T. S. Bates (2009), Oxygenated fraction and mass of organic aerosol from direct emission and atmospheric processing measured on the R/V Ronald Brown during TEXAQS/GoMACCS 2006, *J. Geophys. Res.-Atmospheres*, *114*,

Schwab, J. J., H. D. Felton, and K. l. Demerjian (2004), Aerosol chemical composition in New York State from integrated filter samples: Urban/rural and seasonal contrasts, *J. Geophys. Res.-Atmospheres*, *109*,

Sun, Y., Q. Zhang, A. M. MacDonald, K. Hayden, S. M. Li, J. Liggio, P. S. K. Liu, K. G. Anlauf, W. R. Leaitch, A. Steffen, M. Cubison, D. R. Worsnop, A. van Donkelaar, and R. V. Martin (2009), Size-resolved aerosol chemistry on Whistler Mountain, Canada, with a high-resolution aerosol mass spectrometer during INTEX-B, *Atmos. Chem. Phys.*, *9*, 3095-3111.

Tang, I. N. (1976), Phase transformation and growth of aerosol particles composed of mixed salts, *J. Aerosol Sci.*, *7*, 361-371.

Tang, I. N. and H. R. Munkelwitz (1994), Water activities, densities, and refractive indices of aqueous sulfates and sodium nitrate droplets of atmospheric importance, *J. Geophys. Res.*, *99*, 18,801-18,808.

Tanner, R. L., W. J. Parkhurst, M. L. Valente, and W. D. Phillips (2004), Regional composition of $PM_{2.5}$ aerosols measured at urban, rural and "background" sites in the Tennessee valley, *Atmos. Environ.*, *38*, 3143-3153.

Turpin, B. J. and H. J. Lim (2001), Species contributions to $PM_{2.5}$ mass concentrations: Revisiting common assumptions for estimating organic mass, *Aerosol Sci. Technol.*, *35*, 602-610.

U.S. EPA (1998), *SLAMS/NAMS/PAMS: Network Review Guidance*; EPA-454/R-98-003; Office of Air Quality, Planning and Standards, Research Triangle Park, NC.

Watson, J. G., J. C. Chow, L. W. A. Chen, and N. H. Frank (2009), Methods to assess carbonaceous aerosol sampling artifacts for IMPROVE and other long-term networks, *J. Air Waste Manage. Assoc.*, *59*, 898-911.

White, W.H. (2008), *Interim approach for relating the two datasets: Discussion and action plan development*; presented at the IMPROVE – CSN PM Monitoring Workshop, Davis, CA, January; http://vista.cira.colostate.edu/improve/Publications/Workshops/Carbon_Jan2008/IMP-CSN_White.ppt.

Yu, X. Y., T. Lee, B. Ayres, S. M. Kreidenweis, J. L. Collett Jr., and W. C. Malm (2005), Particulate nitrate measurement using nylon filters, *J. Air Waste Manage. Assoc.*, *55*, 1100-1110.

Yu, X. Y., T. Lee, B. Ayres, S. M. Kreidenweis, W. C. Malm, and J. L. Collett (2006), Loss of fine particle ammonium from denuded nylon filters, *Atmos. Environ.*, *40*, 4797-4807.

Zhang, Q., M. R. Canagaratna, J. T. Jayne, D. R. Worsnop, and J. L. Jimenez (2005), Time- and size-resolved chemical composition of submicron particles in Pittsburgh: Implications for aerosol sources and processes, *J. Geophys. Res.-Atmospheres*, *110*,

Zhang, X. and P. H. McMurry (1992), Evaporative losses of fine particulate nitrates during sampling, *Atmos. Environ.*, *26A*, 3305-3312.

Chapter 9. Regional Haze Rule Progress Tracking Metrics

Charles T. (Tom) Moore, Jr., and Scott Copeland

9.1 INTRODUCTION

The U.S. Environmental Protection Agency (EPA) established the Regional Haze Rule (RHR, U.S. EPA, 1999) to achieve the national visibility goal established by the Clean Air Act, which called for the virtual elimination of anthropogenic visibility impairment in 156 areas designated as Class I federal areas (CIAs), (i.e., principally large national parks and wilderness areas). The RHR requires periodic state implementation plans (SIPs) from each state to demonstrate "reasonable progress" toward achieving RHR-defined natural visibility conditions by a nominal target date of 2064. The initial baseline SIPs must include a long-term strategy for emissions reductions and Best Available Retrofit Technology (BART) on certain existing sources and set "reasonable progress goals" for the conditions with the most impaired visibility (worst visibility days) and least impaired visibility (best visibility days) at each CIA, to be achieved in the first planning period. Toward that end, the RHR requires a comprehensive assessment of current conditions and causes of visibility impairment that includes analyses of IMPROVE particulate data and use of comprehensive air quality modeling for source apportionment assessment to support the development of individual SIPs. These technical assessments were conducted by five Regional Planning Organizations (http://www.epa.gov/visibility/regional.html), composed of state, federal, and tribal air quality representatives, and included stakeholder participation and funding support by the EPA. For further reading, the EPA and others have provided additional documentation and evaluations related to the RHR (U.S. EPA, 2005, 2006, 2007; Moore and Brewer, 2007; Brewer and Moore, 2009).

The RHR also mandates periodic 5-year assessments of progress in meeting the SIP visibility progress goals. This chapter includes information that is pertinent to the first required progress assessment. Specifically, it contains an analysis of the changes in visibility conditions and major species contributions to light extinction within the 5-year baseline period (i.e., 2000–2004) and the first 5-year progress period (i.e., 2005–2009) for the IMPROVE monitoring sites identified as representing the CIA. As such, this information should be useful input to the states responsible for preparing mid-SIP progress assessments. However, this report does not contain everything that might be required, such as emissions trends analysis, assessment of the relative role of emission changes and variations in meteorological factors, to explain visibility changes at each site. It also does not include additional assessments that could be helpful, such as characterizing the role of highly variable natural sources (wildfire and windblown dust) and international contributions to worst haze levels. These labor-intensive and sophisticated assessments are outside the scope of this report. The last section in this chapter presents case studies of five locations and briefly illustrates some of the analyses that should be included in the mid-SIP progress assessments.

9.2 REGIONAL HAZE RULE ASSESSMENT

The following is a brief overview of the RHR assessment of visibility progress trends analysis. For a more complete description, see discussions provided by the EPA (U.S. EPA, 2003a,b). The first RHR baseline SIPs to determine and control emissions that lead to regional haze were due in December 2007, with a progress report due in 2013. The RHR calls for improvements in the average of the 20% haziest ("worst") days from the 2000–2004 baseline period to ultimately reach the goal of worst haze level caused solely by natural sources by the 2064 target year for each CIA. The RHR also calls for no degradation of visibility for the average of least hazy ("best") 20% days for each CIA. To mitigate the impacts of interannual variability in determining progress towards these goals, the RHR mandates the use of non-overlapping, 5-year-averaged values of both the annual mean 20% best and 20% worst days determined for each site. The baseline period is defined as 2000 through 2004 and the first trend period as being 2005 through 2009. The visibility index used is based on the deciview (dv) scale, a logarithmic transformation of light extinction, which for the RHR is derived from IMPROVE aerosol composition data (as described below). There are 110 IMPROVE monitoring sites, referred to here as the regional haze tracking sites (RHTSs), that were selected to represent 155 visibility-protected regions.

9.2.1 Uniform Rate of Progress

The EPA published default natural-conditions targets to be achieved at each CIA by 2064. The presumption of the RHR was that anthropogenic emissions could be reduced in a gradually declining fashion to reach natural conditions for the worst haze conditions over the nominal 60-year duration of the RHR. Each of the 50 states is required to submit a complete baseline regional haze SIP addressing the various requirements of the RHR. The analyses in this chapter focus on the

- IMPROVE data for the 2000–2004 RHR baseline period at the IMPROVE RHTS monitoring sites;
- IMPROVE data for the first progress period (period 1) of 2005–2009 under the RHR; and
- the nominal default 2018 uniform rate of progress (URP) value for each CIA as defined in the RHR and supporting guidance documents.

Central to setting the individual CIA 2018 "reasonable progress" planning goals by each state under the RHR is the concept of the URP. The URP is the yearly rate of change required to achieve natural dv conditions by 2064 in a linear fashion beginning in 2004. The URP provides a reference to evaluate progress made in the context of the long-term emissions reductions and associated improvement in visibility required to reach natural conditions in 60 years. The conceptual glide path example of URP provided by the EPA in the 1999 RHR is shown as the solid black line in Figure 9.2.1. Baseline and period 1 dv values are based on the mean of five yearly values of the 20% best and 20% worst visibility days at each site. Natural conditions are marked with the dashed line. For each CIA, if the state-selected 2018 reasonable progress target value for the 20% worst visibility days in dv units is not on or below the glide path, the state

must explain why the 2018 URP goal cannot be reasonably achieved and specify the additional time required to achieve natural conditions beyond 2064. The state must also verify that the 20% best visibility days are not projected to degrade.

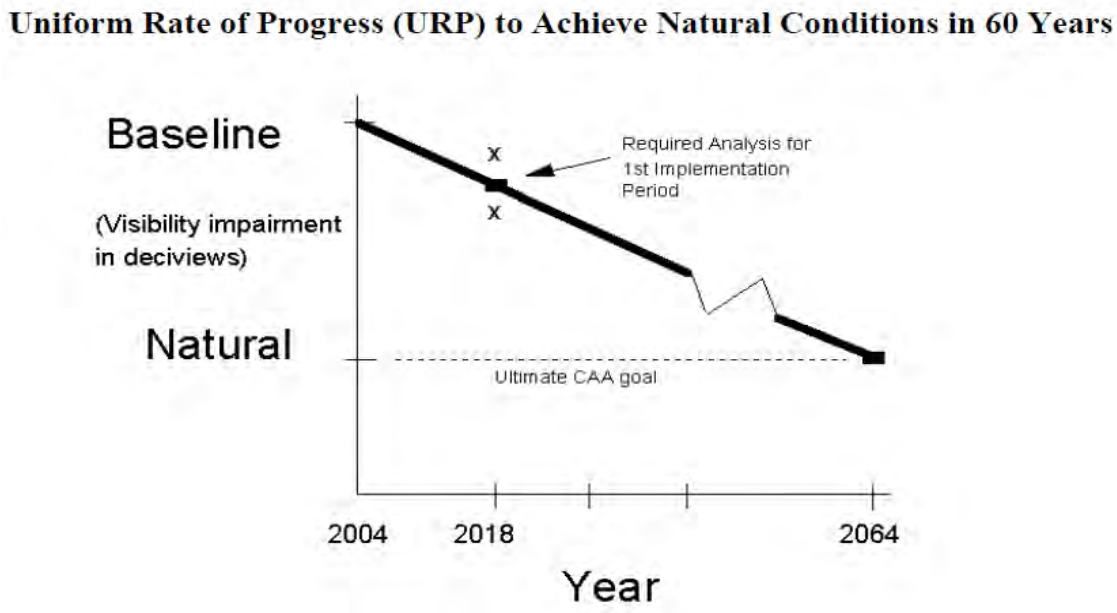

Figure 9.2.1. Depiction of the conceptual uniform rate of progress (URG) glide path (EPA, 1999).

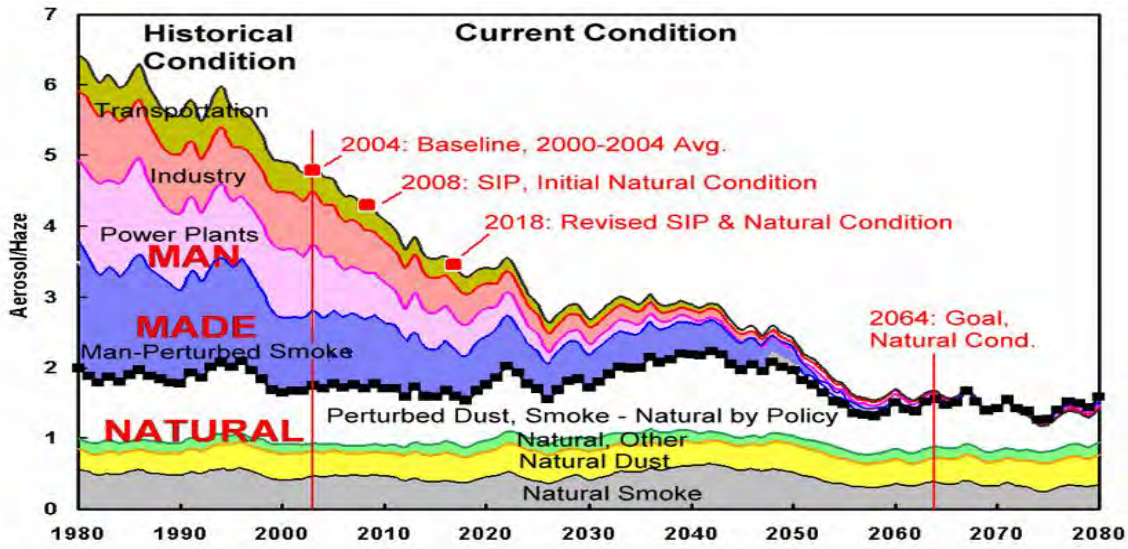

Figure 9.2.2. Depiction of realistic uniform rate of progress (URG) glide path (Husar, 2003).

It should be noted that the nature of emissions control programs plus the intermittent activity of some sources make it likely that actual progress will be somewhat erratic and that failure to achieve the URP at any point in the process should be considered in the context of changes to emissions inventories. A more realistic depiction of the variability in haze due to different sources is shown in Figure 9.2.2. The magnitude of haze in this schematic is displayed on the y-axis, versus time on the x-axis. For RHR planning, states worked with RPOs to define aerosol sources and their historical contributions to regional haze, as well as projected future

emissions, which for many categories were difficult to predict. Biomass smoke and windblown dust sources are significant contributors to haze at many RHTSs, though their contributions to haze are often episodic and vary from one year to another. Unlike the depiction in Figure 9.2.2, the contributions by sources of smoke, dust, and other aerosol components are not known a priori from the IMPROVE measurements, and separating the contributions from anthropogenic versus natural sources of smoke, dust, and other contributors to haze is problematic. Though not explicitly illustrated in Figure 9.2.2, emissions from international sources can be major contributors to haze, due to both anthropogenic (e.g., marine shipping) and natural causes (e.g., fire and North African or Asian dust).

As anthropogenic U.S. emissions sources continue to decline, the effects of emissions reductions for well-characterized sources of sulfur dioxide and oxidized nitrogen are predictable, particularly where those sources dominate visibility impairment. However, there is significant variability in other sources and species that impair visibility in CIAs that need to be understood. Future RHR planning in the most pristine CIAs will be sensitive to the defined classification of the sources (i.e., controllable versus uncontrollable, natural versus anthropogenic). Over the long term, even CIAs that are currently among the most visibility impaired will become increasingly dominated by impacts from natural and/or uncontrollable sources such as wildland fire and geogenic sources, as well as proportionally larger contributions from international sources of both natural and anthropogenic origin.

There are a number of RHR SIP requirements not related directly to IMPROVE monitoring. The RHR SIPs were developed by using regional and state data to define emissions-reduction strategies and controls for anthropogenic sources and consider partially controllable, quasi-natural sources such as fire and dust. The individual states have the authority and responsibility to set their own reasonable progress goals for each CIA for 2018. The 2018 goals chosen must improve visibility on the 20% worst visibility days and not allow the 20% best visibility days to degrade. We do not attempt to evaluate state-selected goals in this report, instead confining our analyses to the 2009 point value on the slope of the nominal URP line in deciviews, as well as selected hypothetical species-specific light extinction coefficients; we also evaluate the progress in visibility conditions from Period 1 compared to the baseline for each CIA.

9.2.2 Regional Haze Rule Metric

Haziness in deciview units is derived from light extinction coefficients (b_{ext}) calculated using the "original" IMPROVE algorithm (designated as RHR1 in the IMPROVE dataset) or the "revised" IMPROVE algorithm (designated as RHR2) (Pitchford et. al., 2007). Since nearly all states used the RHR2 algorithm for SIP development, modeling, and source apportionment, the RHR2 algorithm was applied in this chapter. The daily b_{ext} values were calculated using the following equation:

$$\begin{aligned} b_{ext} = {} & 2.2f_S(RH)[\text{small ammonium sulfate}] + 4.8f_L(RH)[\text{large ammonium sulfate}] + \\ & 2.4f_S(RH)[\text{small ammonium nitrate}] + 5.1f_L(RH)[\text{large ammonium nitrate}] + \\ & 2.8[\text{small particulate organic matter}] + 6.1[\text{large particulate organic matter}] + \\ & 10[\text{light absorbing carbon}] + 1[\text{soil}] + 1.7f_{SS}(RH)[\text{sea salt}] + 0.6\,[\text{coarse mass}] + \\ & \text{site-specific Rayleigh scattering} \end{aligned} \qquad 9.1$$

Note that the first three major particle species (i.e., ammonium sulfate, ammonium nitrate, or particulate organic matter) in equation 9.1 are separated each into "small" and "large" components, which refers to a partitioning of the particles containing those particles into two size distributions within the $PM_{2.5}$ size range (i.e., diameter < 2.5 μm). The small and large mode concentrations of any of the first three components are computed using equations 9.2 and 9.3 for component concentrations less than 20 $\mu g/m^3$:

$$\text{"Large Concentration"} = \frac{\text{Component Concentration}}{20\ \mu g\ m^{-3}} \cdot \text{Component Concentration} \qquad 9.2$$

$$\text{"Small Concentration"} = \text{Component Concentration} - \text{"Large Concentration"} \qquad 9.3$$

When the component concentration exceeds 20 $\mu g/m^3$, all of the component mass concentration is assumed to be in the "large" size distribution. Humidification factors (e.g., $f_S(RH)$ and $f_L(RH)$) are applied for a specific size mode. Units of b_{ext} and Rayleigh scattering are in inverse megameters (Mm^{-1}).

Most component mass concentrations were computed consistent with the previous IMPROVE report (Debell, 2006) but differed for some components in this report (e.g., ammonium sulfate was computed from elemental sulfur concentrations rather than sulfate ion concentrations; see Table 2.1 in Chapter 2). Mass concentrations of aerosol species have units of $\mu g\ m^{-3}$, and mass scattering and absorption efficiencies have units of $m^2\ g^{-1}$. Values of mass scattering efficiencies correspond to the small and large size modes (e.g., 2.2 $m^2\ g^{-1}$ and 4.8 $m^2\ g^{-1}$, respectively, for ammonium sulfate). Recall that in other chapters of this report, b_{ext} was computed using a modified RHR1 IMPROVE equation (see equation 3.4 in Chapter 3) that differs from the RHR2.

Deciview values (dv) were calculated from daily b_{ext} values, using equation 9.4:

$$dv = 10\ln(b_{ext}/10) \qquad 9.4$$

The RHR guidance requires a given site to have at least 3 "complete" years of data out of each 5-year period. Some patching of missing aerosol concentration data under certain specific conditions is allowed. The data presented in this chapter have been processed with a patching algorithm described in the EPA Tracking Progress guidance document (U.S. EPA, 2003a). For the 2000–2009 period at IMPROVE RHTSs, 116,168 valid observations were collected. Of those, 1,464 (~1%) were patched for coarse mass, 421 for ammonium nitrate, 17 for organic carbon and light absorbing carbon, and 6 for fine soil.

Eighteen RHTSs did not meet the completeness criteria for the 2000–2004 baseline period. For these 18 sites, substitutions were performed for missing data by inserting data from a nearby donor site, using a regression analysis technique (Archuleta, et. al., 2007). Seventeen sites with substituted data are presented in this chapter (i.e., BALD1, BOWA1, CAPI1, CHAS1, COHU1, GLAC1, KAIS1, MING1, NOCA1, RAFA1, SAMA1, SEQU1, SHRO1, SWAN1, THRO1, TONT1, and TRIN1). BRET1 is the eighteenth substituted site, and it is not presented because there were insufficient data from 2005 through 2009.

For 2005–2009, three of the 110 IMPROVE RHTSs did not have enough data to be considered in this chapter (Zion National Park (NP), Utah, ZION1; Sierra Ancha Wilderness Area (WA), Arizona, SIAN1; and Breton WA, Louisiana, BRET1). Data for SIAN1 will be substituted for the 2005–2009 period, but the analysis was not completed in time to be included in this chapter. Zion NP was represented by two monitors: ZION1 from 2000 through 2004 and ZICA1 from 2003 through 2009. Evaluating changes across these two sites was beyond the scope of this chapter. Some of the 2009 data have not been fully quality-assured, and minor changes to the concentration values could be made in 2011. While any changes are likely to have little effect on the 2005–2009 haze metrics, the reported values this chapter are not considered final regulatory values but are used for evaluation purposes.

9.3 ASSESSMENT OF CHANGE IN REGIONAL HAZE FROM THE BASELINE (2000–2004) TO PERIOD 1 (2005–2009)

For each RHTS with adequate data (i.e., 107 of the 110), the worst and best haze metrics for the baseline and first 5-year trend period (i.e., period 1), as well as the estimated 2064 natural haze level values, have been determined. These values are displayed in figures and tables in Appendix G. The figures showing the worst haze conditions include the site-specific URP trend lines to facilitate comparisons between the period 1 value and the progress goal for 2009. The tables include these values as well as the individual annual best and worst 20% mean visibility metric values. To gain further insights into the changes between the baseline and period 1, the baseline, period 1, and 2064 natural levels for the major aerosol component's contributions to b_{ext} were also determined and displayed in the tables and figures of Appendix G.

Examples and additional descriptions of the site-specific information from Appendix G are contained in section 9.4 (e.g., Figures 9.4.1 and 9.4.2). The remainder of this section is a national-scale overview description of the results, using maps that show patterns of RHR metrics and the b_{ext} components changes between the baseline and period 1 for some of the components. A complete set of maps is also available towards the end of Appendix G. Note that the natural levels used here were developed to be consistent with the revised IMPROVE algorithm (Copeland et al., 2008) and differ slightly from the natural background as described in the EPA guidance document (2003b).

The change in the 20% worst haze days RHR metric can be examined two ways: as absolute change and as the percent of change compared to the URP goal for each site (i.e., the difference between period 1 and baseline divided by the dv change required to attain the URP for each site). Color dot maps depicting the fractional and absolute worst haze RHR metric changes are shown in Figures 9.3.1 and 9.3.2, respectively. Figure 9.3.3 is a color dot map display of the absolute difference between baseline and period 1 for the 20% best haze RHR conditions.

Broad improvement in the worst 20% visibility levels is apparent across the eastern United States into the Ozark region (see Figure 9.3.1). Increased haze was observed in the Great Lakes region CIAs (Voyageurs NP, VOYA2; Boundary Waters Canoe Area WA, BOWA1; Isle Royale NP, ISLE1; and Seney WA, SENE1). The western United States is characterized by regional improvements in haze especially in the middle and southern Rocky Mountains, Pacific Northwest, and southern California. Western RHTS sites that experienced large changes in dv on the worst 20% visibility days are often influenced by wildfire impacts. Absolute changes in

dv from the baseline to period 1 on the 20% worst visibility days are shown in Figure 9.3.2. The spatial patterns in absolute change in dv are similar to those shown in Figure 9.3.1.

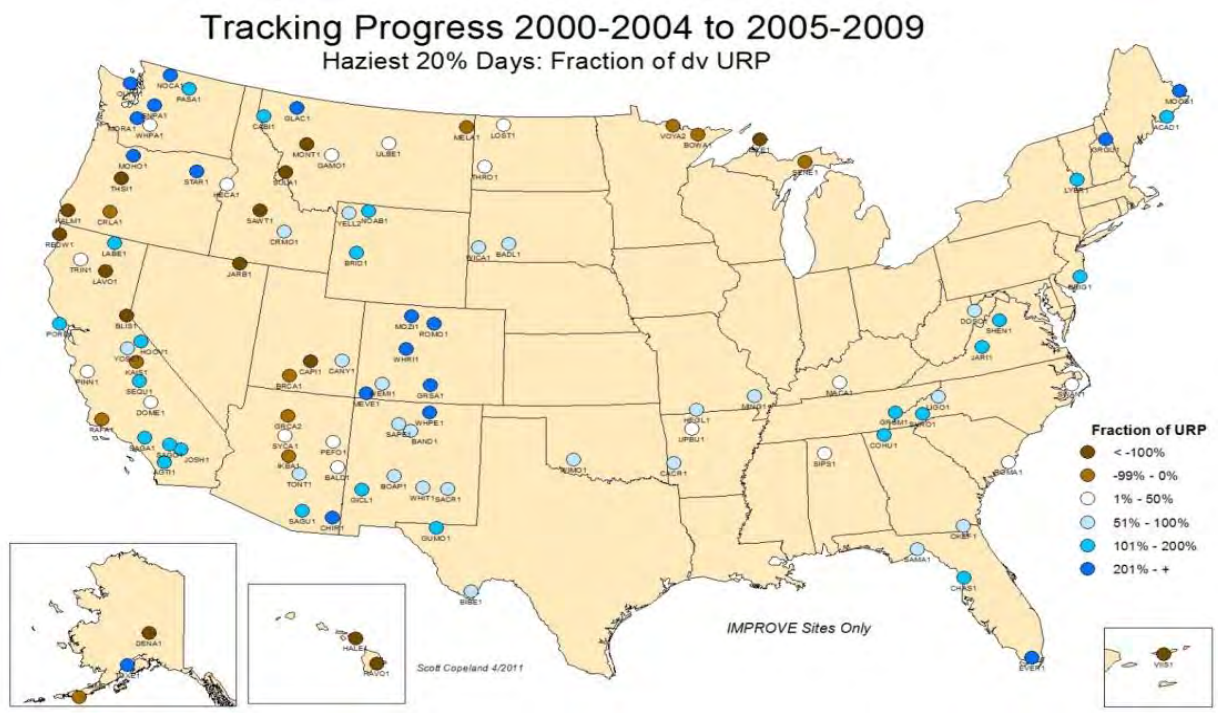

Figure 9.3.1. Fraction of dv uniform rate of progress (URP) from the baseline (2000–2004) to period 1 (2005–2009) for the 20% worst visibility days at 107 of the 110 IMPROVE regional haze tracking sites. Brown circles indicate degradation in the worst 20% visibility days, while blue circles represent improvement in worst 20% visibility days. The two darkest shades of blue indicate progress that is at or better than the 2009 point value on the slope of the nominal URP line.

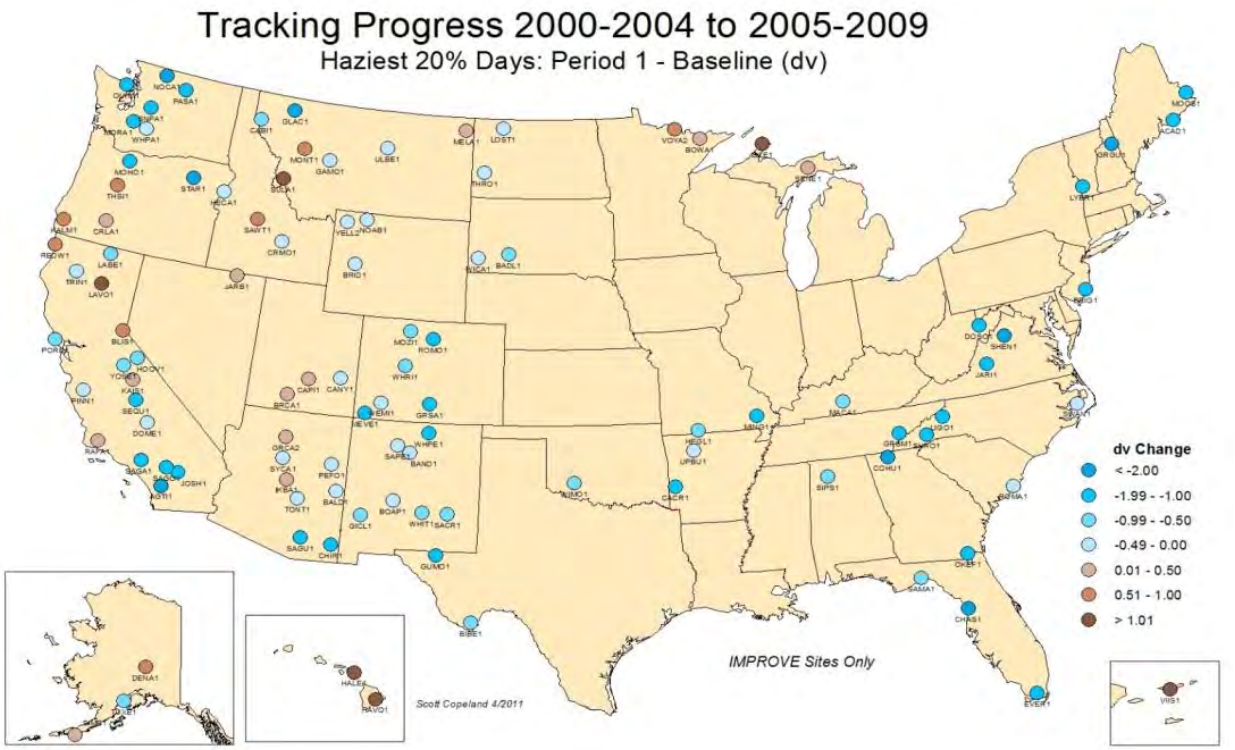

Figure 9.3.2. Absolute change in dv from the baseline (2000–2004) to period 1 (2005–2009) for the 20% worst visibility days at 107 of the 110 IMPROVE regional haze tracking sites. Brown circles indicate degradation in the worst 20% visibility days, while blue circles represent improvement in worst 20% visibility days.

Similarly, Figure 9.3.3 shows the absolute change in dv values on the 20% best visibility days. The goal for these days at all CIAs is no degradation, which was achieved at a substantial majority of sites across the United States. The site at Swanquarter WA (SWAN1) in North Carolina was the only IMPROVE RHTS to experience an increase of over 1 dv on the 20% best visibility days. The increase was mainly driven by roughly equal increases in b_{ext} from ammonium sulfate and sea salt. Because data were incomplete for 2005 and 2008 at SWAN1, and 2008 was a comparatively low year for b_{ext} due to ammonium sulfate at other eastern sites, the period 1 averages for SWAN1 may be skewed by missing data. When considering the annual mean of dv values, all but 12 of the IMPROVE RHTSs showed at least some improvement (see Figure 9.3.4). While the annual mean dv values were still influenced by wildfires, the influence was much less pronounced than in the values for the 20% worst visibility days.

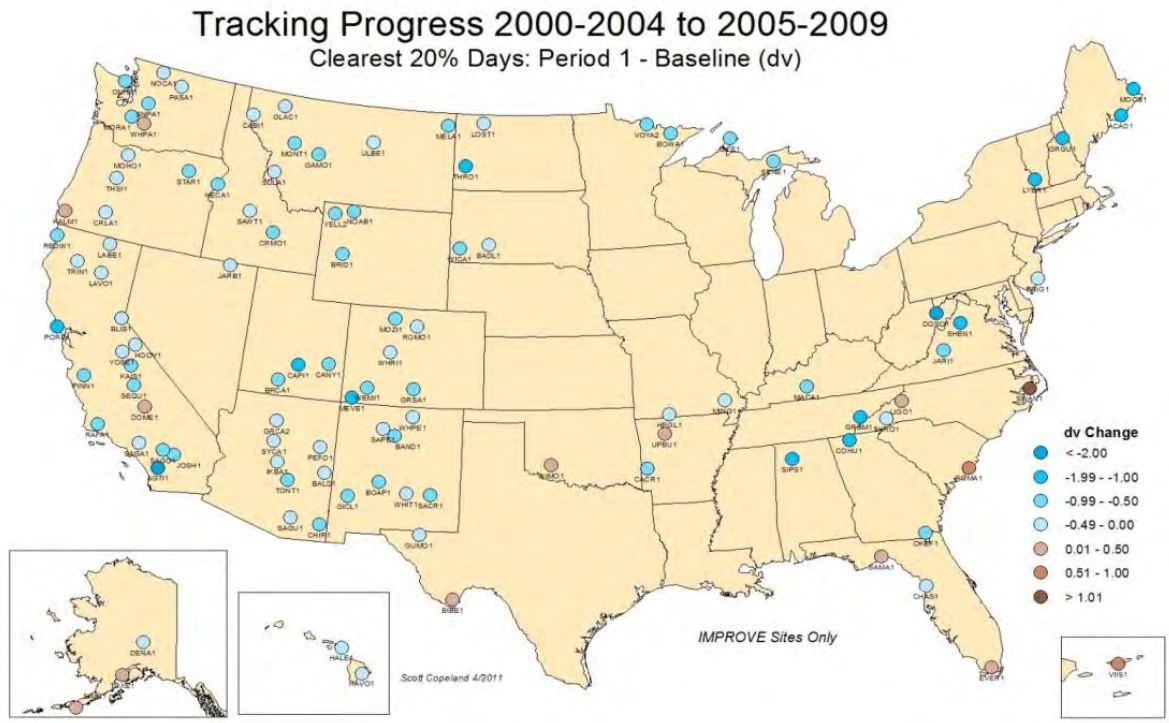

Figure 9.3.3. Absolute change in dv from the baseline (2000–2004) to period 1 (2005–2009) for the 20% best visibility days at 107 of the 110 IMPROVE regional haze tracking sites. Brown circles indicate degradation in the best 20% visibility days, while blue circles represent improvement in best 20% visibility days.

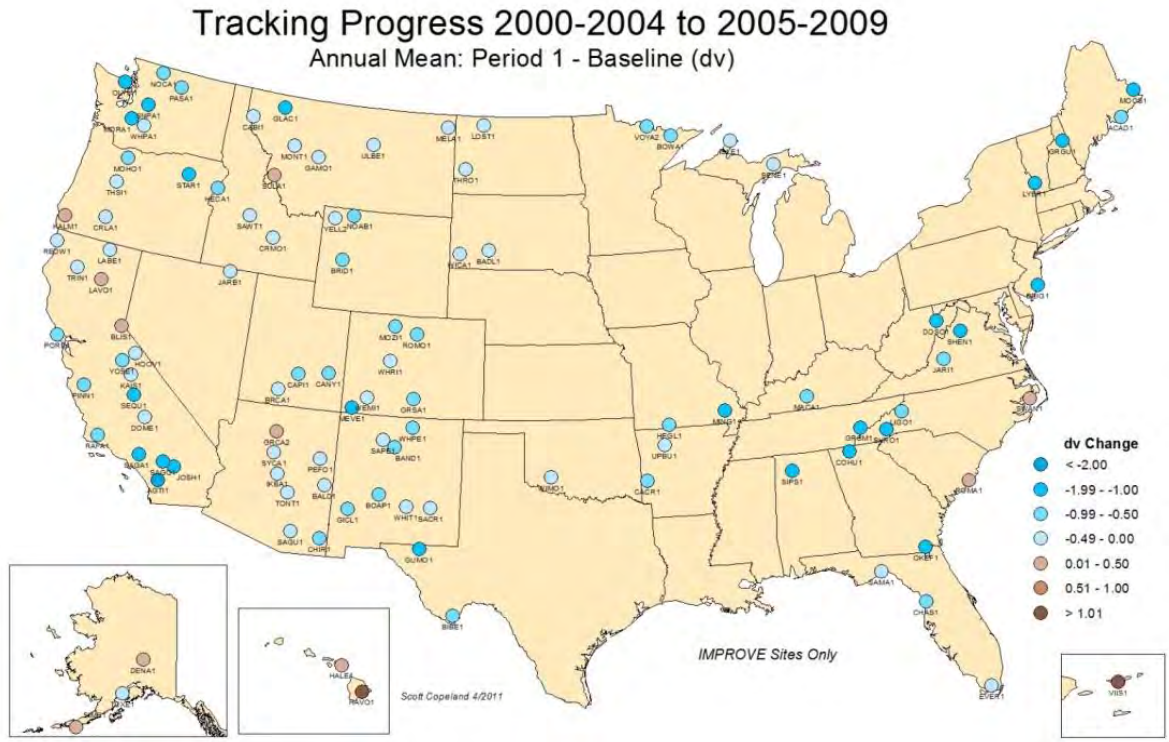

Figure 9.3.4. Absolute change in annual mean dv from the baseline (2000–2004) to period 1 (2005–2009) at 107 of the 110 IMPROVE regional haze tracking sites. Brown circles indicate degradation in annual mean dv, while blue circles represent improvement in annual mean dv.

While there are no official URP values specified in the RHR for any of the major b_{ext} components, hypothetical URP values for 2009 were generated for each site by reducing each component of b_{ext} by the same fraction that would be required in total extinction to evaluate progress toward the conceptual URP in dv. Color dot maps of the fractional change from the hypothetical URP for ammonium sulfate and ammonium nitrate are shown in Figures 9.3.5 and 9.3.6, respectively. In these maps, an asterisk in the place of a site location denotes a site with baseline 20% worst visibility days' b_{ext} below the estimated natural b_{ext} component level. This does not mean that the current conditions at that IMPROVE site are cleaner than natural conditions for any species. It is an artifact caused by selection of sample days for the period 1 worst 20% visibility that have a very different relative composition compared to the worst days in the baseline period. In theory, as anthropogenic contributions decrease over time, the measured values will converge with the estimated natural values. Note there is no figure for the sea salt fraction of URP since sea salt is assumed to be 100% natural; hence, there is no progress to be made. The sea salt concentrations used in equation 9.1 are computed as 1.8 times the chloride ion (see Chapter 2.1.5). Issues related to chloride measurements include possible losses of chloride from aged sea salt aerosols, as well as artifacts due to changing blank corrections (White, 2008). Because of these issues, we do not include sea salt mass concentration trend analyses in Chapter 6; however, we do include trends in b_{ext} due to sea salt in section 9.4 and Appendix G, but any implied sea salt trends should be viewed with caution.

The fraction of hypothetical URP for ammonium sulfate is shown in Figure 9.3.5. Many sites in the Appalachian region, New England, and Florida showed improvements in b_{ext} from ammonium sulfate (b_{ext_AS}). The Great Lakes regional CIAs and many of the sites in the western United States showed significant degradation of b_{ext_AS} with respect to the hypothetical URP. For some of these sites, the b_{ext_AS} for the 20% worst haze days are lower in period 1 than during the baseline period, though not as low as the hypothetical URP. For other of these sites, the values are higher in period 1 than during the baseline period. Trends in the worst 20% haze day RHR metric for a component are not necessarily well correlated to the particle component trends for the 90^{th} percentile as described in Chapter 6. In Chapter 6 the trends for the various percentiles of the components were selected based on the distribution of those component concentrations, while for the 20% worst RHR metric the selection is based on the distribution of visibility conditions. In the eastern United States, where b_{ext_AS} and haze conditions are well correlated, the RHR assessment is generally consistent with the 90^{th} percentile trends analysis. However, in the western United States, any of a number of particulate components may be responsible for the worst haze days (e.g., organic material from wildfire, wind-blown dust, etc.) and the relative numbers of these in any year can vary considerably, resulting in counterintuitive results (e.g., b_{ext_AS} reduced overall and at the 90^{th} percentile but not on RHR worst haze days).

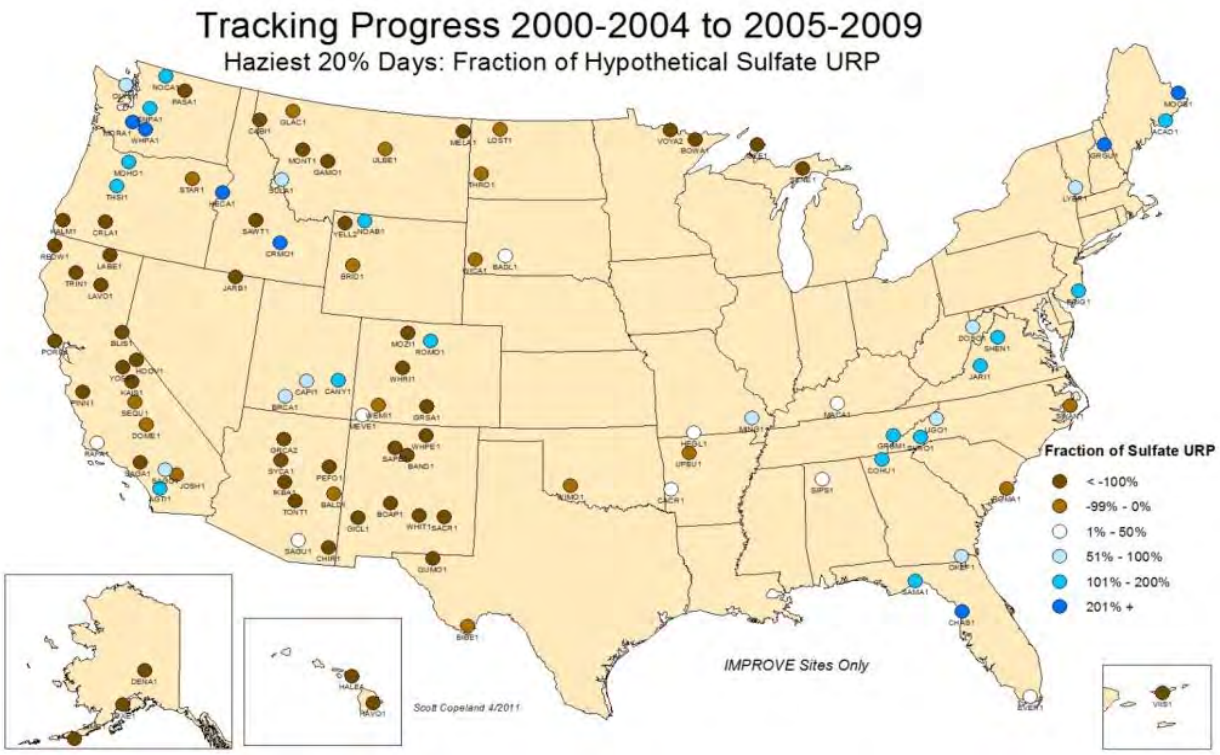

Figure 9.3.5. Fraction of hypothetical ammonium sulfate uniform rate of progress (URP) for the 20% worst visibility days at 107 of the 110 IMPROVE regional haze tracking sites from the baseline (2000–2004) to period 1 (2005–2009). Brown circles indicate degradation in the worst 20% visibility days due to ammonium sulfate extinction, while blue circles represent improvement in worst 20% visibility days due to ammonium sulfate extinction. Only the two darkest blue colored circles indicate progress that is at or better than the hypothetical ammonium sulfate extinction 2009 point value on the slope of the nominal URP line.

Figure 9.3.6 shows a general improvement in 20% worst visibility days corresponding to ammonium nitrate (b_{ext_AN}). Exceptions include three of the Great Lakes region CIAs and the southern Appalachian sites. It can be difficult to discern whether a change in 20% worst visibility days was indicative of decreased emissions or merely an artifact of a shift to the other aerosol components. Therefore it was especially useful to determine overall changes in b_{ext_AS} and b_{ext_AN} by considering the changes in the 5-year annual mean values of b_{ext} from baseline to period 1. Annual mean b_{ext_AN} decreased at all but four of the RHTSs (see Figure 9.3.7), suggesting that the increases in worst 20% visibility days from ammonium nitrate seen in Figure 9.3.6 are likely to have resulted from changes to the distribution of other species' contributions to b_{ext}, not an increase in b_{ext_AN} overall. This change in distribution of worst 20% visibility days will be further illustrated in section 9.4. A similar map for b_{ext_AS} is shown in Figure 9.3.8. Several sites in the western United States corresponded to an increase in b_{ext_AS}, while most sites in the eastern United States were associated with decreases in b_{ext_AS}.

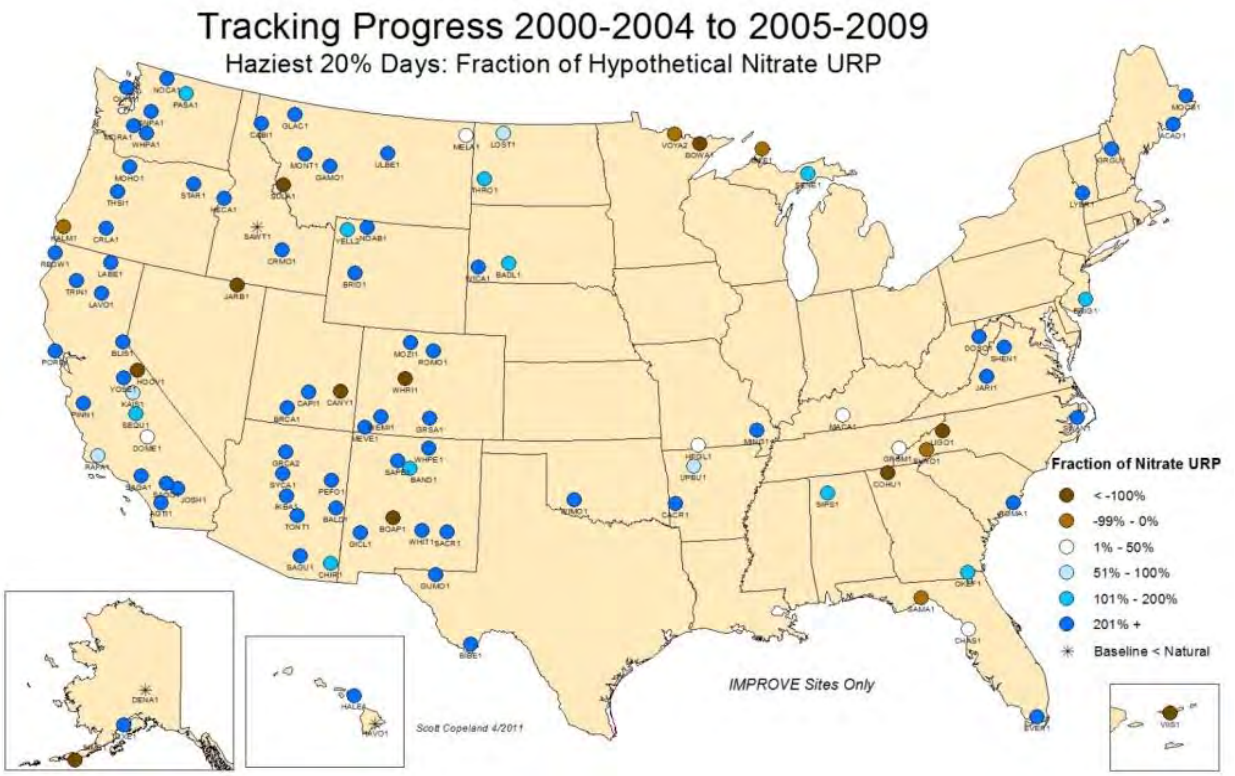

Figure 9.3.6. Fraction of hypothetical ammonium nitrate uniform rate of progress (URP) for the 20% worst visibility days at 107 of the 110 IMPROVE regional haze tracking sites from the baseline (2000–2004) to period 1 (2005–2009). Brown circles indicate degradation in the worst 20% visibility days due to ammonium nitrate extinction, while blue circles represent improvement in worst 20% visibility days due to ammonium nitrate extinction. Only the two darkest blue colored circles indicate progress that is at or better than the hypothetical ammonium sulfate extinction 2009 point value on the slope of the nominal URP line.

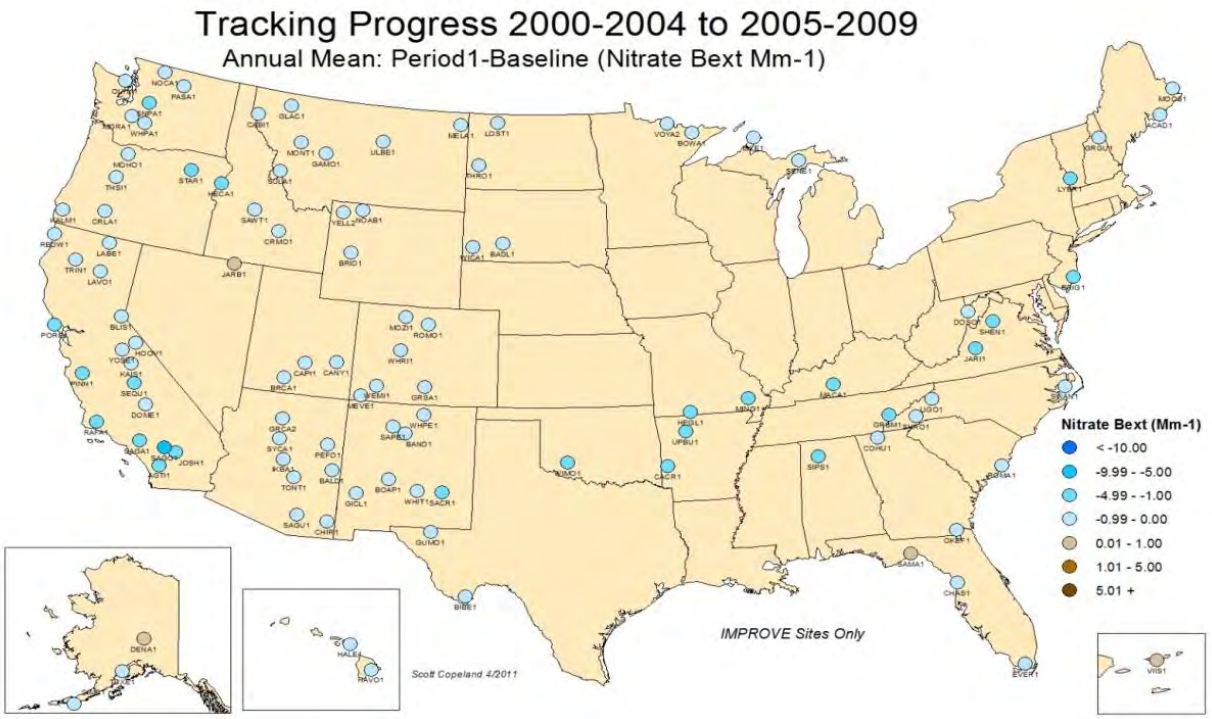

Figure 9.3.7. Change in annual mean ammonium nitrate extinction (b_{ext_AN}, Mm^{-1}) at 107 of the 110 IMPROVE regional haze tracking sites from the baseline (2000-2004) to period 1 (2005-2009). Brown circles indicate an increase of the annual mean b_{ext_AN}, while blue circles represent decreases in annual mean b_{ext_AN}.

Figure 9.3.8. Change in annual mean ammonium sulfate extinction (b_{ext_AS}, Mm^{-1}) at 107 of the 110 IMPROVE regional haze tracking sites from the baseline (2000–2004) to period 1 (2005–2009). Brown circles indicate an increase of the annual mean b_{ext_AS}, while blue circles represent decreases in annual mean b_{ext_AS}.

Additional maps summarizing changes in annual mean, 20% best b_{ext}, and 20% worst b_{ext} for ammonium sulfate, ammonium nitrate, particulate organic matter, light absorbing carbon (or EC), soil, and coarse mass are provided toward the end of Appendix G. In addition, figures for the fractional URP for the 20% worst visibility days for other species are also provided in Appendix G.

9.4 CASE STUDIES OF REGIONAL HAZE RULE PROGRESS

The maps presented in section 9.3 summarized the progress toward achieving the national visibility goal for CIAs at each IMPROVE RHTS across the United States. This section provides a first look at five specific RHTSs that are representative of their regional visibility conditions. For each of the five case studies, the contribution from individual species to the 20% worst and best visibility days for the baseline and period 1 are displayed, as well as daily data for selected years. We include the nominal 2064 default natural conditions visibility targets and in some cases illustrate the projected improvement in visibility by species from the 2018 control strategies included in regional analyses. These five case studies offer a framework for review and assessment of the detailed results for 107 of the 110 RHTSs provided in Appendix G, where the baseline and period 1 averages and the natural conditions targets for tracking progress under the RHR are presented. Detailed composition data for every site can be found on the VIEWS website (http://views.cira.colostate.edu/web/Composition/). More detailed assessments for every RHTS are needed in order to understand whether the emissions control programs cited in the RHR SIPs are yielding the projected changes in visibility conditions, but such analysis are well beyond the scope of this report.

9.4.1 Boundary Waters Canoe Area Wilderness, Minnesota

The Boundary Waters Canoe Area Wilderness (BOWA1) is located on the United States-Canadian border in northern Minnesota. Data from BOWA1 were largely consistent with the other three nearby CIAs (Voyageurs NP, VOYA2; Isle Royale NP, ISLE1; and Seney WA, SENE1). The RHR metric on the worst 20% days increased from 19.6 dv to 20.1 dv between the baseline and period 1. This was principally due to an increase in light extinction by ammonium sulfate (b_{ext_AS}) of about 6 Mm^{-1} (22%) (Figure 9.4.1.1a). There do not seem to be any wildfire influences in this trend, as particulate organic matter (POM, also referred to as OMC) and light absorbing carbon (LAC, also referred to as EC) contributions remained relatively constant (see bottom panel of Figure 9.4.1.1a). Light extinction due to ammonium nitrate (b_{ext_AN}) also increased slightly from the baseline to period 1 for the worst 20% visibility days. In contrast to the worst days, the best 20% b_{ext_AS} and b_{ext_AN} decreased at BOWA1 from the baseline to period 1 (see Figure 9.4.1.1b). Figures 9.4.1.2a and 9.4.1.2b show the daily derived b_{ext} for each aerosol component from 2001 and 2005, respectively. Note the different vertical axis scales. A number of high summer b_{ext_AS} episodes in 2005 could explain the bulk of the increase in the 5-year average worst 20% b_{ext_AS}. The b_{ext} data from 2006 through 2009 were similar to the b_{ext} during the baseline period at BOWA1, ISLE1, and VOYA2. SENE1 also experienced very high b_{ext_AS} episodes in 2007; the cause is unknown. Levels of b_{ext_AS} were relatively high in 2005 across the eastern United States.

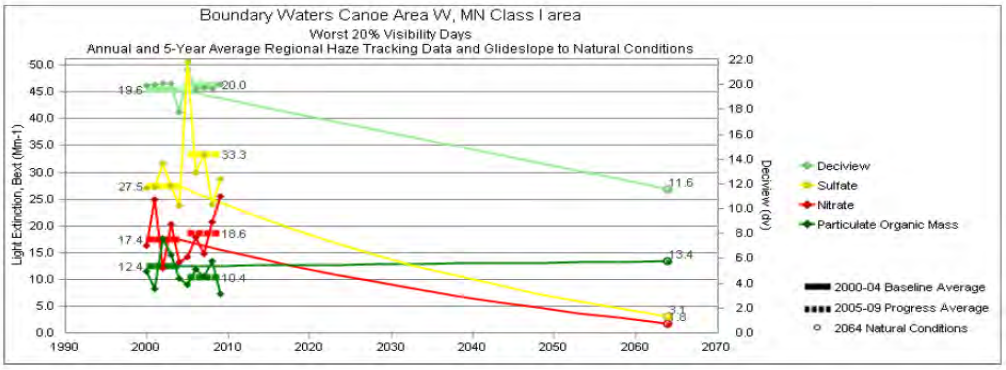

Boundary Waters - Worst 20% Visibility Days – 5-Year Average, Natural Conditions and Annual Data

Parameter	2000-2004	2005-2009	2064 NC	2000	2001	2002	2003	2004	2005	2006	2007	2008	2009
Deciview (dv)	19.6	20.1	11.6	19.9	20.0	20.1	20.1	17.8	21.3	19.6	19.8	19.7	20.0
Sulfate Bext	27.4	33.3	3.1	27.0	27.3	31.7	27.4	23.8	50.4	30.0	33.4	24.1	28.7
Nitrate Bext	17.4	18.6	1.8	16.4	25.0	12.1	20.3	13.3	14.3	17.8	14.8	20.6	25.5
POM Bext	12.4	10.4	13.4	11.5	8.3	17.6	14.6	10.1	8.9	11.9	10.4	13.4	7.4
EC Bext	3.1	2.9	0.4	4.4	3.0	3.3	2.6	2.2	3.5	3.2	3.0	2.7	2.3
Soil Bext	0.5	0.5	0.6	0.8	0.4	0.6	0.4	0.4	0.5	0.4	0.6	0.5	0.5
Coarse Mass Bext	2.6	2.1	3.1	3.7	2.1	2.5	2.2	2.2	2.5	1.9	1.5	1.7	2.8
Sea Salt Bext	0.1	0.2	0.1	0.0	0.0	0.0	0.0	0.2	0.2	0.2	0.2	0.6	0.1

Figure 9.4.1.1a. Deciview and light extinction coefficients (b_{ext}, Mm^{-1}) for ammonium sulfate, ammonium nitrate, and particulate organic mass (POM) for the baseline (2000–2004), period 1 (2005–2009), and 2064 natural conditions estimates for the worst 20% visibility days at Boundary Waters Canoe Area Wilderness, MN. Values of b_{ext} for other species, including elemental carbon (EC), soil, coarse mass and sea salt are listed in the table below the graph (data and graphs obtained at http://vista.cira.colostate.edu/tss/Results/HazePlanning.aspx).

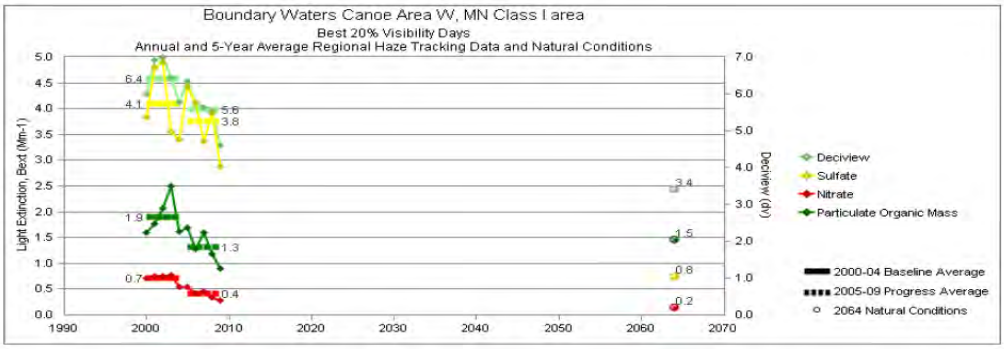

Boundary Waters - Best 20% Visibility Days – 5-Year Average, Natural Conditions and Annual Data

Parameter	2000-2004	2005-2009	2064 NC	2000	2001	2002	2003	2004	2005	2006	2007	2008	2009
Deciview (dv)	6.4	5.6	3.4	6.0	6.9	7.0	6.5	5.8	6.3	5.7	5.6	5.5	4.6
Sulfate Bext	4.1	3.8	0.7	3.8	4.8	4.9	3.6	3.4	4.6	4.1	3.4	3.9	2.9
Nitrate Bext	0.7	0.4	0.2	0.7	0.8	0.7	0.8	0.5	0.6	0.4	0.4	0.3	0.3
POM Bext	1.9	1.3	1.5	1.6	1.8	2.1	2.5	1.6	1.6	1.3	1.6	1.2	0.9
EC Bext	0.6	0.4	0.1	0.6	0.4	0.7	0.7	0.4	0.4	0.5	0.4	0.3	0.3
Soil Bext	0.1	0.1	0.1	0.1	0.1	0.2	0.1	0.1	0.1	0.1	0.1	0.1	0.1
Coarse Mass Bext	0.7	0.5	0.5	0.5	0.7	0.6	0.8	0.7	0.5	0.5	0.5	0.6	0.5
Sea Salt Bext	0.2	0.1	0.1	0.0	0.6	0.0	0.0	0.1	0.1	0.1	0.3	0.1	0.1

Figure 9.4.1.1b. Deciview and light extinction coefficients (b_{ext}, Mm^{-1}) for ammonium sulfate, ammonium nitrate, and particulate organic mass (POM) for the baseline (2000–2004), period 1 (2005–2009), and 2064 natural conditions estimates for the best 20% visibility days at Boundary Waters Canoe Area Wilderness, MN. Values of b_{ext} for other species, including elemental carbon (EC), soil, coarse mass and sea salt are listed in the table below the graph (data and graphs obtained at http://vista.cira.colostate.edu/tss/Results/HazePlanning.aspx).

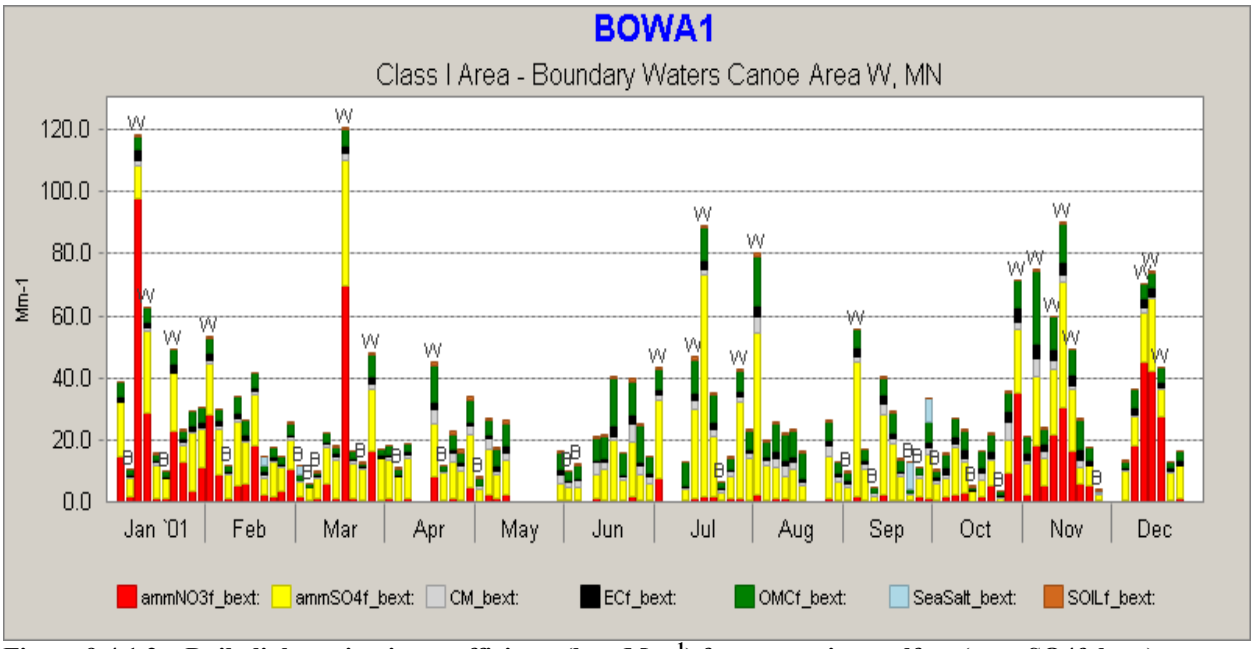

Figure 9.4.1.2a. Daily light extinction coefficients (b_{ext}, Mm^{-1}) for ammonium sulfate (ammSO4f_bext), ammonium nitrate (ammNO3f_bext), particulate organic matter (OMCf_bext), coarse mass (CM_bext), elemental carbon (EC_bext), soil (soil_bext) and sea salt (seasalt_bext) for 2001 Boundary Waters Canoe Area (BOWA1). Worst 20% days are marked with a "W" above the bar for that day, and similarly, best 20% days are marked with a "B" (from http://views.cira.colostate.edu/web/Composition/).

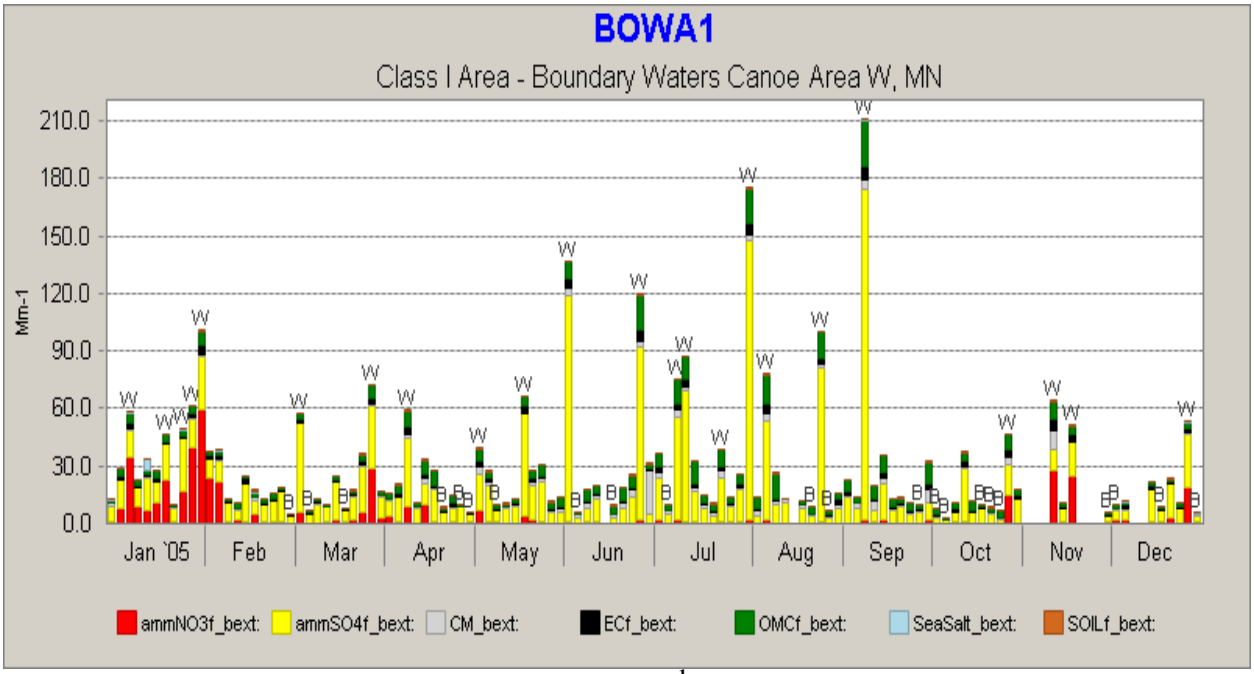

Figure 9.4.1.2b. Daily light extinction coefficients (b_{ext}, Mm^{-1}) for ammonium sulfate (ammSO4f_bext), ammonium nitrate (ammNO3f_bext), particulate organic matter (OMCf_bext), coarse mass (CM_bext), elemental carbon (EC_bext), soil (soil_bext) and sea salt (seasalt_bext) for 2005 Boundary Waters Canoe Area (BOWA1). Worst 20% days are marked with a "W" above the bar for that day, and similarly, best 20% days are marked with a "B" (from http://views.cira.colostate.edu/web/Composition/).

9.4.2 Great Smoky Mountains National Park, Tennessee/North Carolina

Great Smoky Mountains National Park (GRSM1) straddles the border between Tennessee and North Carolina. Data from GRSM1 were similar to data from other Appalachian region sites and most eastern sites with respect to significant reductions in the worst 20% b_{ext_AS}. Data from period 1 show 5-year-average decreases of roughly 28 Mm^{-1} (16%) in the 20% worst b_{ext_AS} (Figure 9.4.2.1a). Extinction coefficients due to other species (e.g., ammonium nitrate, particulate organic matter, elemental carbon, and soil) also decreased or remained steady in period 1, with the exception of coarse mass and sea salt. As with worst days, the best 20% b_{ext_AS} and b_{ext_AN} decreased at GRSM1 (see Figure 9.4.2.1b). Figures 9.4.2.2a and 9.4.2.2b show the daily derived b_{ext} for each aerosol component from 2001 and 2008, respectively. Note the slightly different vertical axis scales. Light extinction coefficients due to ammonium sulfate are generally lower in 2008 compared to 2001. A likely explanation for the decrease in b_{ext_AS} is reduced emissions of sulfur dioxide from coal-fired electric generating units across the United States by 32% from 2000 to 2008 (U.S. EPA, 2011) as a result of emissions controls and the economic slowdown. Specific to GRSM1, emissions reductions under the North Carolina Clean Smokestacks Act (Air Quality/Electric Utilities Bill (SB 1078), which required sulfur dioxide reductions from electric utilities beginning in 2005) and from electric utilities in eastern Tennessee beginning in 2009 may also have contributed to the trends in Figure 9.4.2.1a. Table 9.4.2 is taken from the EPA's proposed partial approval of the Tennessee Regional Haze State Implementation Plan (40 CFR 52 33662) and illustrates the 2018 reasonable progress goals for GRSM and Joyce Kilmer-Slickrock Wilderness are lower (better improvement in visibility) than the 2018 URP. The observed visibility in 2009 (Figure 9.4.2.1a) is lower than the 2018 reasonable progress goal.

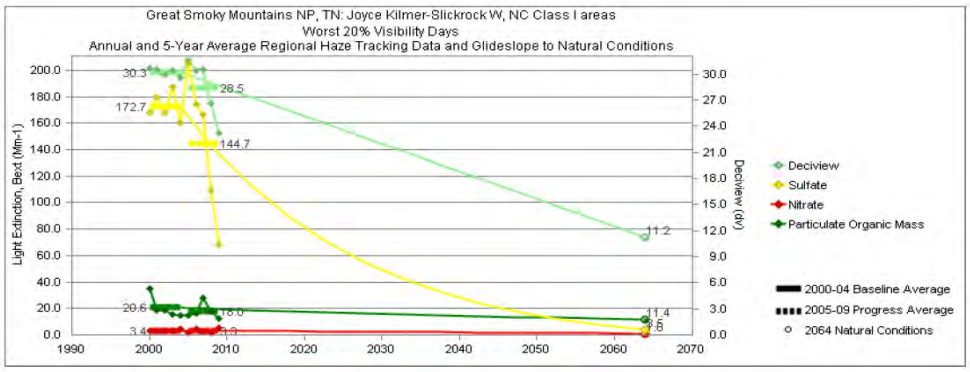

Great Smoky Mountains - Worst 20% Visibility Days – 5-Year Average, Natural Conditions and Annual Data

Parameter	2000-2004	2005-2009	2064 NC	2000	2001	2002	2003	2004	2005	2006	2007	2008	2009
Deciview (dv)	30.3	28.5	11.2	30.7	30.6	29.9	30.5	29.6	31.6	30.5	30.6	26.7	23.2
Sulfate Bext	172.7	144.7	3.5	167.8	179.9	168.3	187.3	160.3	205.1	174.2	166.3	109.6	68.6
Nitrate Bext	3.4	3.3	1.0	3.5	3.0	2.7	3.2	4.6	1.8	5.0	2.7	1.7	5.4
POM Bext	20.6	18.0	11.4	35.1	18.9	18.8	15.7	14.6	14.5	16.3	28.3	18.1	12.6
EC Bext	5.7	5.1	0.3	8.1	5.0	4.8	5.8	4.7	6.1	5.6	5.9	4.2	3.9
Soil Bext	0.8	0.8	0.9	0.6	0.8	1.0	0.7	1.0	0.6	0.9	0.9	0.9	0.6
Coarse Mass Bext	1.9	3.7	2.9	2.6	2.4	2.0	1.5	1.2	4.9	4.6	4.2	2.6	2.1
Sea Salt Bext	0.2	0.3	0.4	0.0	0.5	0.0	0.0	0.3	0.1	0.3	0.3	0.2	0.3

Figure 9.4.2.1a. Deciview and light extinction coefficients (b_{ext}, Mm^{-1}) for ammonium sulfate, ammonium nitrate, and particulate organic mass (POM) for the baseline (2000–2004), period 1 (2005–2009), and 2064 natural conditions estimates for the worst 20% visibility days at Great Smoky Mountains NP, TN and Joyce Kilmer-Slickrock WA, NC. Values of b_{ext} for other species, including elemental carbon (EC), soil, coarse mass and sea salt are listed in the table below the graph (data and graphs obtained at http://vista.cira.colostate.edu/tss/Results/HazePlanning.aspx).

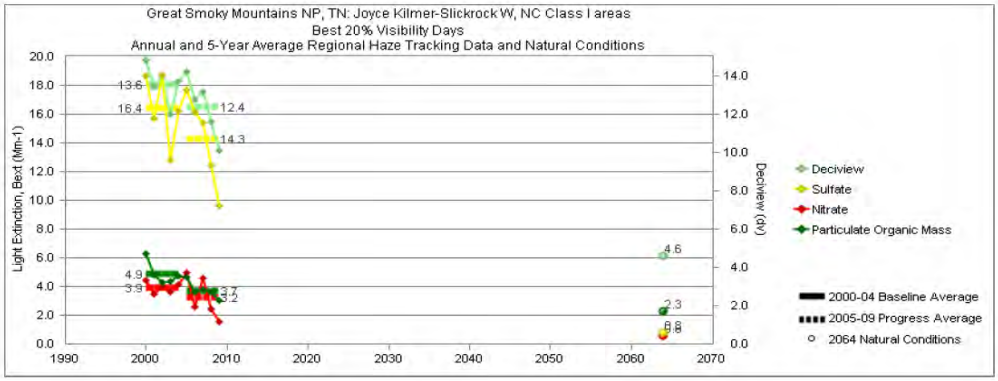

Great Smoky Mountains - Best 20% Visibility Days – 5-Year Average, Natural Conditions and Annual Data

Parameter	2000-2004	2005-2009	2064 NC	2000	2001	2002	2003	2004	2005	2006	2007	2008	2009
Deciview (dv)	13.6	12.4	4.6	14.8	13.4	13.9	12.0	13.7	14.3	12.7	13.2	11.6	10.1
Sulfate Bext	16.4	14.3	0.8	18.7	15.7	18.7	12.8	16.2	17.7	16.2	15.4	12.4	9.6
Nitrate Bext	3.9	3.2	0.6	4.5	3.5	4.0	3.6	4.1	5.0	2.6	4.6	2.5	1.6
POM Bext	4.9	3.7	2.3	6.3	4.8	4.3	4.4	4.7	4.6	3.6	3.8	3.6	3.0
EC Bext	2.2	1.8	0.1	3.0	2.0	2.0	2.0	2.1	2.3	2.0	1.8	1.6	1.2
Soil Bext	0.2	0.2	0.2	0.2	0.2	0.2	0.2	0.2	0.2	0.2	0.2	0.3	0.2
Coarse Mass Bext	1.3	1.4	0.9	1.5	1.5	1.1	1.0	1.5	1.7	1.2	1.1	1.4	1.5
Sea Salt Bext	0.2	0.2	0.1	0.1	0.3	0.2	0.0	0.4	0.2	0.2	0.3	0.2	0.1

Figure 9.4.2.1b. Deciview and light extinction coefficients (b_{ext}, Mm^{-1}) for ammonium sulfate, ammonium nitrate, and particulate organic mass (POM) for the baseline (2000–2004), period 1 (2005–2009), and 2064 natural conditions estimates for the best 20% visibility days at Great Smoky Mountains NP, TN and Joyce Kilmer-Slickrock WA, NC. Values of b_{ext} for other species, including elemental carbon (EC), soil, coarse mass and sea salt are listed in the table below the graph (data and graphs obtained at http://vista.cira.colostate.edu/tss/Results/HazePlanning.aspx).

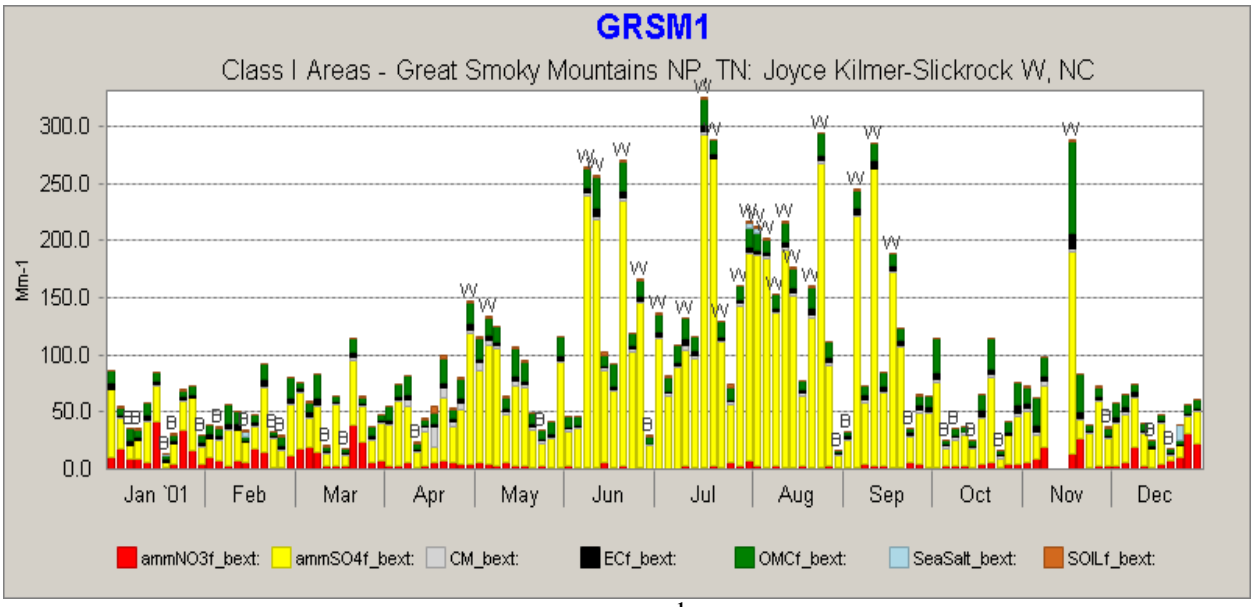

Figure 9.4.2.2a. Daily light extinction coefficients (b_{ext}, Mm^{-1}) for ammonium sulfate (ammSO4f_bext), ammonium nitrate (ammNO3f_bext), particulate organic matter (OMCf_bext), coarse mass (CM_bext), elemental carbon (EC_bext), soil (soil_bext) and sea salt (seasalt_bext) for 2001 Great Smoky Mountains NP, TN (GRSM1) and Joyce Kilmer-Slickrock WA, NC. Worst 20% days are marked with a "W" above the bar for that day, and similarly, best 20% days are marked with a "B" (from http://views.cira.colostate.edu/web/Composition/).

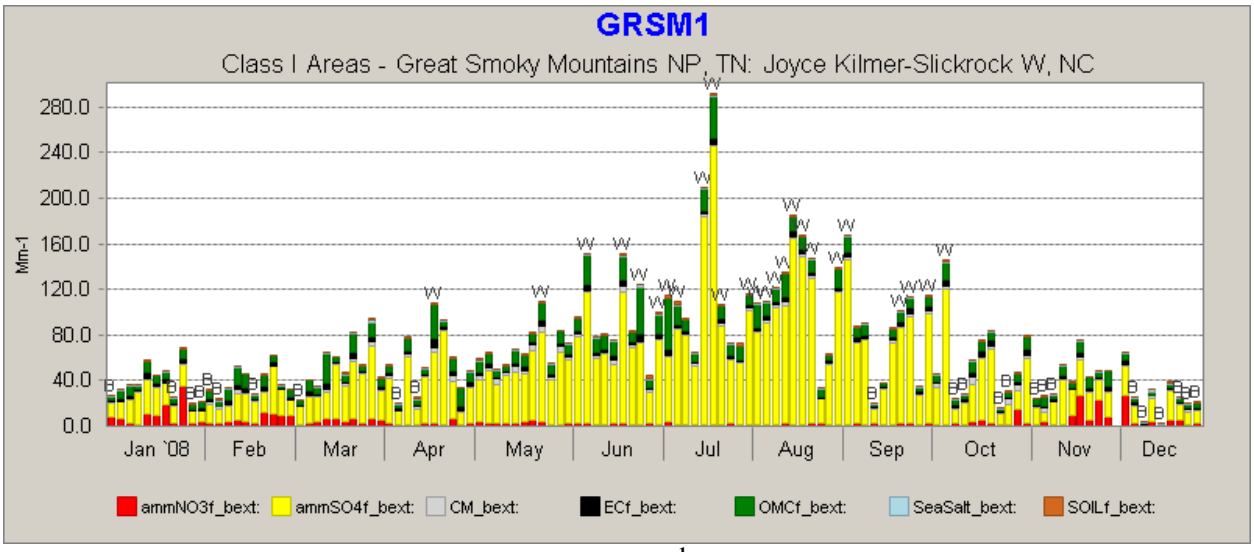

Figure 9.4.2.2b. Daily light extinction coefficients (b_{ext}, Mm^{-1}) for ammonium sulfate (ammSO4f_bext), ammonium nitrate (ammNO3f_bext), particulate organic matter (OMCf_bext), coarse mass (CM_bext), elemental carbon (EC_bext), soil (soil_bext) and sea salt (seasalt_bext) for 2008 at Great Smoky Mountains NP, TN (GRSM1) and Joyce Kilmer-Slickrock WA, NC. Worst 20% days are marked with a "W" above the bar for that day, and similarly, best 20% days are marked with a "B" (from http://views.cira.colostate.edu/web/Composition/).

Table 9.4.2. 2018 Reasonable progress goals compared to baseline visibility and uniform rate of progress, from the Tennessee and North Carolina regional haze state implementation plans.

Class I Area	2000-2004 Baseline Visibility - 20% Worst Days (Mm^{-1})	2018 Uniform Rate of Progress - 20% Worst Days(Mm^{-1})	2018 Reasonable Progress Goal – 20% Worst Days (Mm^{-1}) (Improvement)	2018 Baseline Visibility - 20% Best Days (Mm^{-1})	2018 Reasonable Progress Goal - 20% Best Days (Mm^{-1}) (Improvement)
Great Smoky Mountains National Park	30.28	25.79	23.50 (6.78)	13.58	12.11 (1.47)
Joyce Kilmer-Slickrock Wilderness	30.28	25.79	23.50 (6.78)	13.58	12.11 (1.47)

9.4.3 Mesa Verde National Park, Colorado

For this and the next two sections, we provide additional summary data prepared by the Western Regional Air Partnership (WRAP) regional analyses in support of RHR planning in the western United States. These summaries include IMPROVE monitoring data, estimated 2064 natural conditions, the 2018 URP values discussed in 9.2.1, and projected changes in visibility conditions and emissions by 2018. These data were generated using the WRAP technical support system (TSS) (http://vista.cira.colostate.edu/tss/Results/HazePlanning.aspx).

Mesa Verde National Park (MEVE1) is located in the Four Corners area of southwestern Colorado. Light extinction coefficients for ammonium sulfate, ammonium nitrate, and particulate organic matter for the baseline, period 1, and 2064 are shown for the 20% worst and 20% best visibility days in Figures 9.4.3.1a and 9.4.3.1.b, respectively. The data are summarized in Tables 9.4.3.1 and 9.4.3.2 for the 20% worst and 20% best visibility days, respectively. MEVE1 is illustrative of one category of western RHTS sites, with the baseline period corresponding to relatively high fire activity, followed by a comparatively low fire activity in period 1. As a result, MEVE1 exceeded the URP in dv (see Figure 9.3.1), yet most of this change was related to the decreased fire activity. The low fire activity associated with period 1 did not result in an increase in b_{ext_AS} and b_{ext_AN} contributions to the 20% worst visibility days, as might have been anticipated. An increase was expected because the high fire activity during the baseline period suppressed the contributions to b_{ext} from non-fire-related species. This can in part be attributed to relatively little of the expected seasonality in sulfate and nitrate. Daily values of speciated b_{ext} are shown in Figures 9.4.3.2a and 9.4.3.2b for 2004 and 2008, respectively.

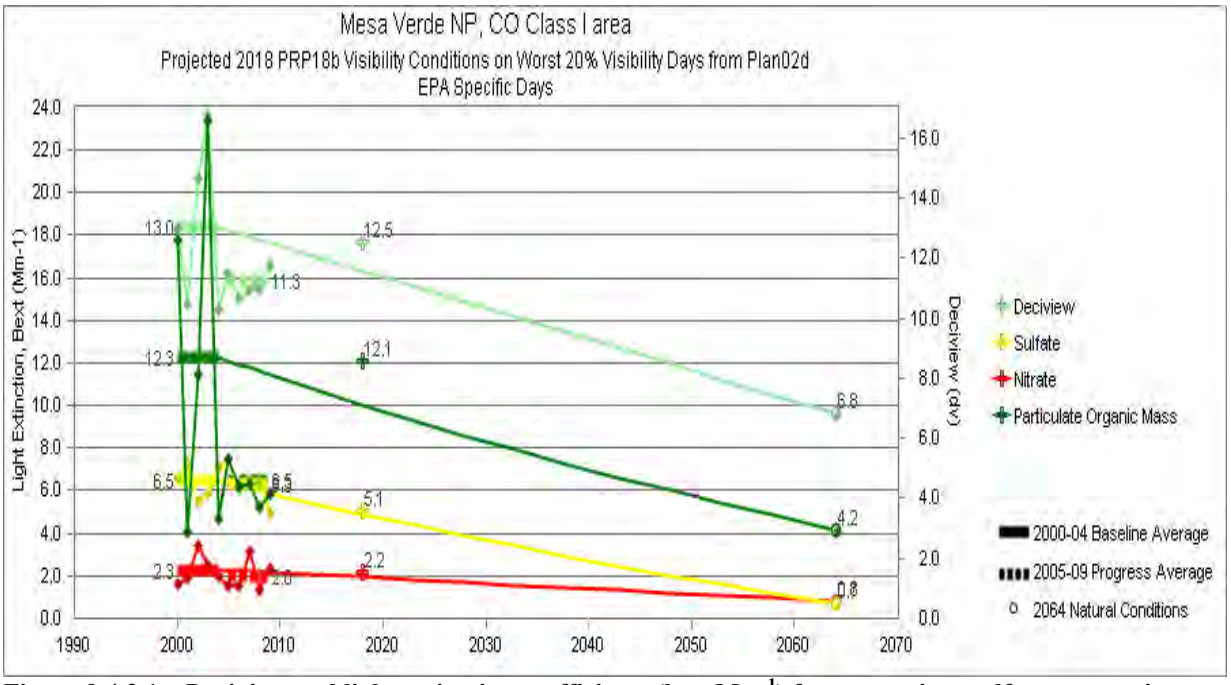

Figure 9.4.3.1a. Deciview and light extinction coefficients (b_{ext}, Mm^{-1}) for ammonium sulfate, ammonium nitrate, and particulate organic mass (POM) for the baseline (2000–2004), period 1 (2005–2009), and 2064 natural conditions estimates for the worst 20% visibility days at Mesa Verde NP, CO. Values of b_{ext} for other species, including elemental carbon (EC), soil, coarse mass, and sea salt are listed in the table below the graph (data and graphs obtained at http://vista.cira.colostate.edu/tss/Results/HazePlanning.aspx).

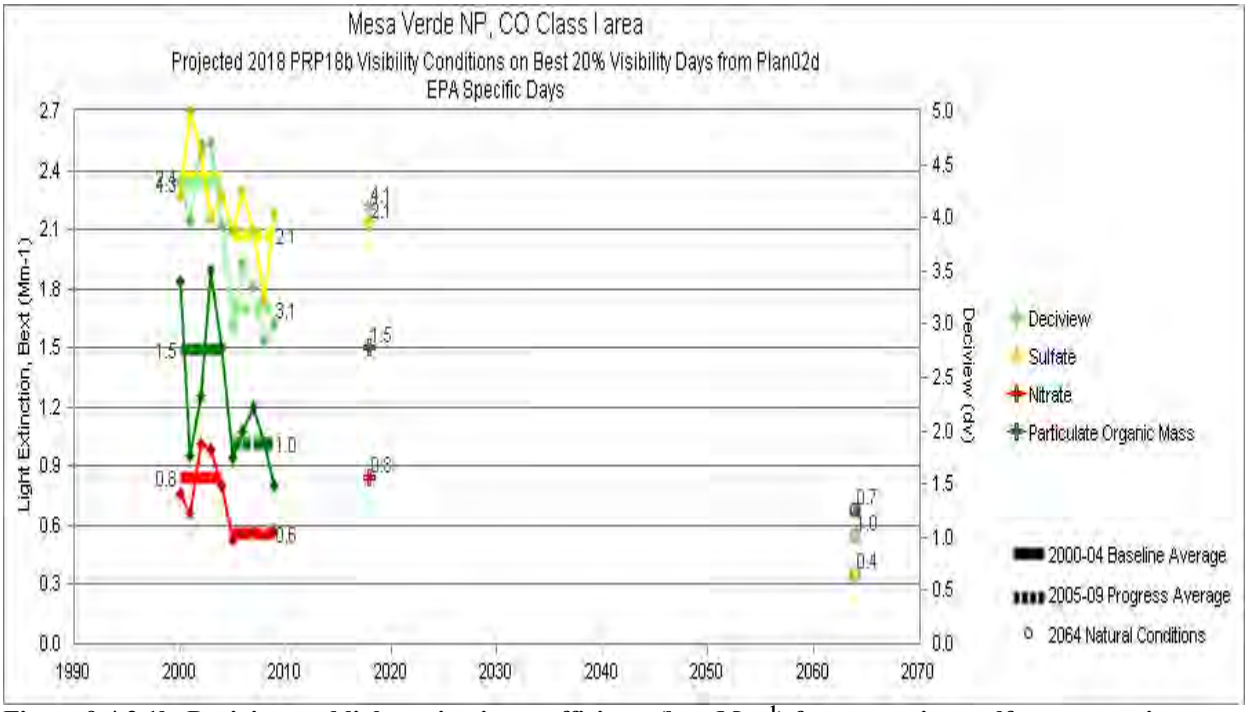

Figure 9.4.3.1b. Deciview and light extinction coefficients (b_{ext}, Mm^{-1}) for ammonium sulfate, ammonium nitrate, and particulate organic mass (POM) for the baseline (2000–2004), period 1 (2005–2009), and 2064 natural conditions estimates for the best 20% visibility days at Mesa Verde NP, CO. Values of b_{ext} for other species, including elemental carbon (EC), soil, coarse mass, and sea salt are listed in the table below the graph. (Data and graphs obtained at http://vista.cira.colostate.edu/tss/Results/HazePlanning.aspx).

Table 9.4.3.1. Monitored, estimated, and projected 2018 visibility conditions and emissions changes for the worst 20% visibility days from WRAP regional analyses for Mesa Verde NP, CO (MEVE1) (from http://vista.cira.colostate.edu/tss/Results/HazePlanning.aspx).

Class I Area Visibility Summary: Mesa Verde NP, CO Class I area **Visibility Conditions:** Worst 20% Days **Model Relative Response Factor Calculation Method:** Specific Days (EPA) **Emissions Scenarios for Projected 2018 Emissions & Visibility Changes:** WRAP 2000-04 Baseline (plan02d) & 2018 PRPb (prp18b)								
	Monitored		**Estimated**		**Projected**			
	2000-04 Baseline Conditions (Mm-1)	2005-09 1st Progress Period Conditions (Mm-1)	2064 Natural Conditions (Mm-1)	2018 Uniform Rate of Progress Target (Mm-1)[1]	2018 Projected Visibility Conditions (Mm-1)	Baseline to 2018 Change in Statewide Emissions (tons / %)	Baseline to 2018 Change in Upwind Weighted Emissions[2] (%)	Baseline to 2018 Change in Anthropogenic Upwind Weighted Emissions[2] (%)
Sulfate	6.46	6.3	0.73	4.90	5.09	-58,907 -51%	-30%	-30%
Nitrate	2.3	2.0	0.83	1.94	2.18	-123,497 -30%	-27%	-28%
Organic Carbon	12.28	6.5	4.19	10.06	12.13	-439 -1%	0%	-1%
Elemental Carbon	2.37	1.6	0.36	1.87	1.84	-2,833 -23%	-20%	-40%
Fine Soil	2.51	2.0	1.16	2.18	2.76	-1,232 -6%	7%	10%
Coarse Material[3]	6.52	4.6	4.3	5.97	Not Applicable	9,024 9%	7%	12%
Sea Salt[3]	0.04	0.1	0.04	0.04		Not Applicable		
Total Light Extinction	41.48	23.0	20.63	35.29	39.57			
Deciview	13.03	11.3	6.81	11.58	12.5			

Table 9.4.3.2. Monitored, estimated, and projected 2018 visibility conditions and emissions changes for the best 20% visibility days from WRAP regional analyses for Mesa Verde NP, CO (MEVE1) (from http://vista.cira.colostate.edu/tss/Results/HazePlanning.aspx).

Class I Area Visibility Summary: Mesa Verde NP, CO Class I area
Visibility Conditions: Best 20% Days
Model Relative Response Factor Calculation Method: Specific Days (EPA)
Emissions Scenarios for Projected 2018 Emissions & Visibility Changes: WRAP 2000-04 Baseline (plan02d) & 2018 PRPb (prp18b)

	Monitored		**Estimated**		**Projected**			
	2000-04 Baseline Conditions (Mm-1)	2005-09 1st Progress Period Conditions (Mm-1)	2064 Natural Conditions (Mm-1)	2018 Uniform Rate of Progress Target (Mm-1)[1]	2018 Projected Visibility Conditions (Mm-1)	Baseline to 2018 Change in Statewide Emissions (tons / %)	Baseline to 2018 Change in Upwind Weighted Emissions[2] (%)	Baseline to 2018 Change in Anthropogenic Upwind Weighted Emissions[2] (%)
Sulfate	2.37	2.1	0.36	Not Applicable	2.13	-58,907 -51%	-30%	-30%
Nitrate	0.84	0.9	0.36	Not Applicable	0.84	-123,497 -30%	-30%	-31%
Organic Carbon	1.49	1.5	0.68	Not Applicable	1.5	-439 -1%	-1%	-3%
Elemental Carbon	0.6	0.4	0.11	Not Applicable	0.44	-2,833 -23%	-19%	-41%
Fine Soil	0.4	0.2	0.17	Not Applicable	0.45	-1,232 -6%	8%	11%
Coarse Material[3]	0.74	0.4	0.4	Not Applicable	Not Applicable	9,024 9%	8%	15%
Sea Salt[3]	0.01	0.0	0	Not Applicable		Not Applicable		
Total Light Extinction	15.46	4.8	11.08	Not Applicable	15.13			
Deciview	4.32	3.1	1.01	Not Applicable	4.1			

1) 2018 Uniform Rate of Progress Target for Best 20% Days is not defined.
2) Results based on Weighted Emissions Potential analysis using the 2000-04 Baseline (plan02d) & 2018 PRPb (prp18b) emissions scenarios.
3) Visibility projections not available due to model performance issues.

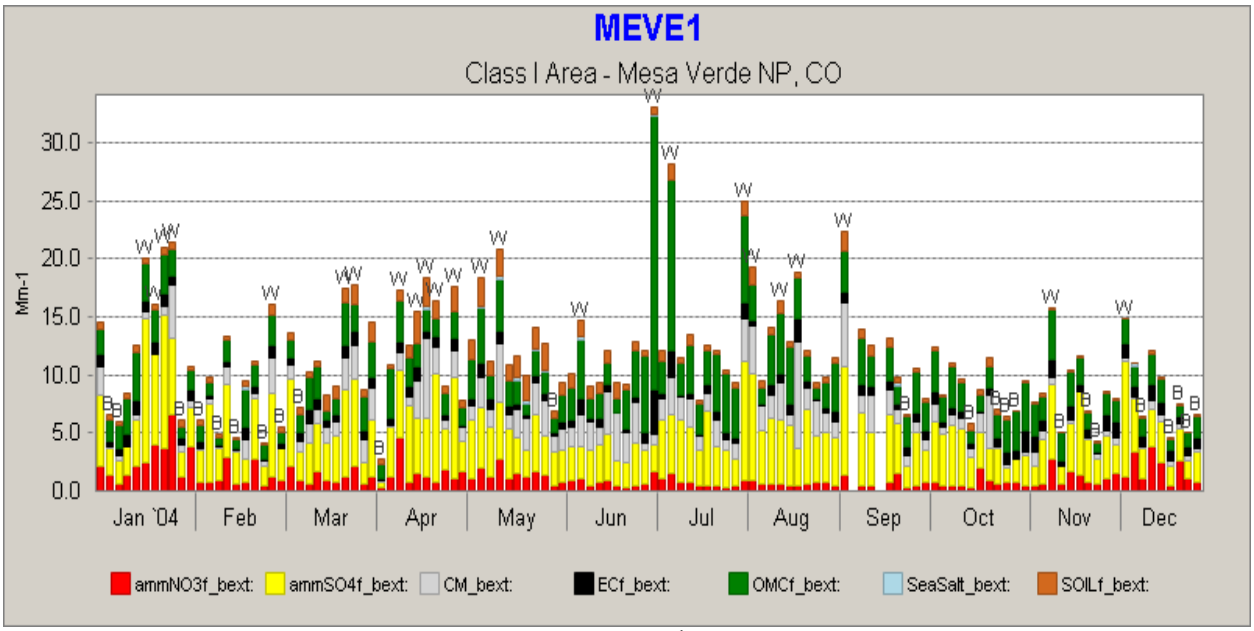

Figure 9.4.3.2a. Daily light extinction coefficients (b_{ext}, Mm^{-1}) for ammonium sulfate (ammSO4f_bext), ammonium nitrate (ammNO3f_bext), particulate organic matter (OMCf_bext), coarse mass (CM_bext), elemental carbon (EC_bext), soil (soil_bext), and sea salt (seasalt_bext) for 2004 Mesa Verde NP, CO. Worst 20% days are marked with a "W" above the bar for that day, and similarly, best 20% days are marked with a "B" (from http://views.cira.colostate.edu/web/Composition/).

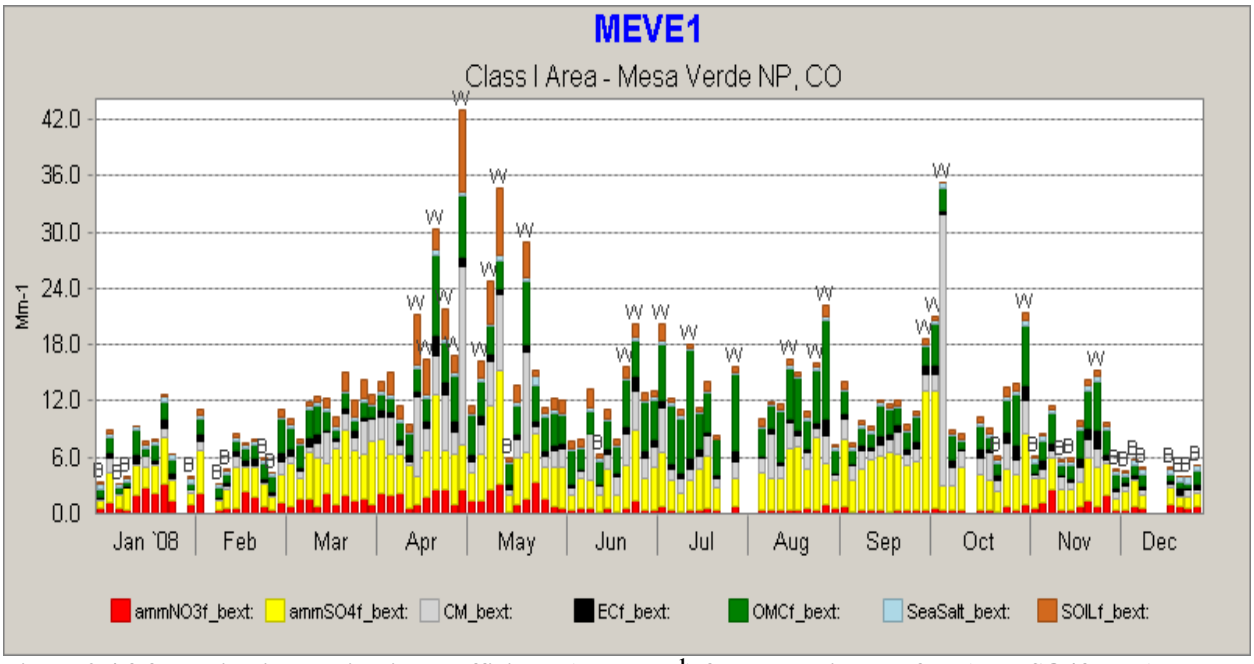

Figure 9.4.3.3b. Daily light extinction coefficients (b_{ext}, Mm^{-1}) for ammonium sulfate (ammSO4f_bext), ammonium nitrate (ammNO3f_bext), particulate organic matter (OMCf_bext), coarse mass (CM_bext), elemental carbon (EC_bext), soil (soil_bext), and sea salt (seasalt_bext) for 2008 Mesa Verde NP, CO. Worst 20% days are marked with a "W" above the bar for that day, and similarly, best 20% days are marked with a "B" (from http://views.cira.colostate.edu/web/Composition/).

9.4.4 Hell's Canyon Wilderness, Oregon/Idaho

Hells Canyon Wilderness (HECA1) straddles the Snake River Canyon along Oregon and Idaho. Conditions at HECA1 were opposite to those at MEVE1 in the context of fire activity. Low fire activity occurred during the baseline period, followed by high fire activity in period 1. Values of b_{ext} at HECA1 exhibited the expected behavior, with b_{ext_AS} and b_{ext_AN} decreasing on the worst 20% visibility days during high fire activity (see Figures 9.4.4.1a and 9.4.4.1b for the 20% worst and 20% best visibility days, respectively). Light extinction due to ammonium sulfate is less important to total b_{ext} at Hells Canyon than at some of the other sites. The seasonality of the worst 20% visibility days in winter/summer/fall in 2004 (Figure 9.4.4.2a) changed to mostly summer in 2006 (Figure 9.4.4.2b). HECA1 also experienced a decrease in annual mean b_{ext_AN}, which can be seen by comparing the first quarter of 2006 to the first quarter of 2004. This reduction in b_{ext_AN}, coupled with a reduction in b_{ext_AS}, actually more than offset the increased fire-related b_{ext} on the 20% worst days, resulting in a net 0.5 dv improvement. This improvement was slightly less than the URP for dv but presumably without the increased fire activity would have been much greater than URP. The reason for the significant reductions in first quarter b_{ext_AN} is unknown. The data for the 20% worst and 20% best visibility days are summarized in Tables 9.4.4.1 and 9.4.4.2, respectively.

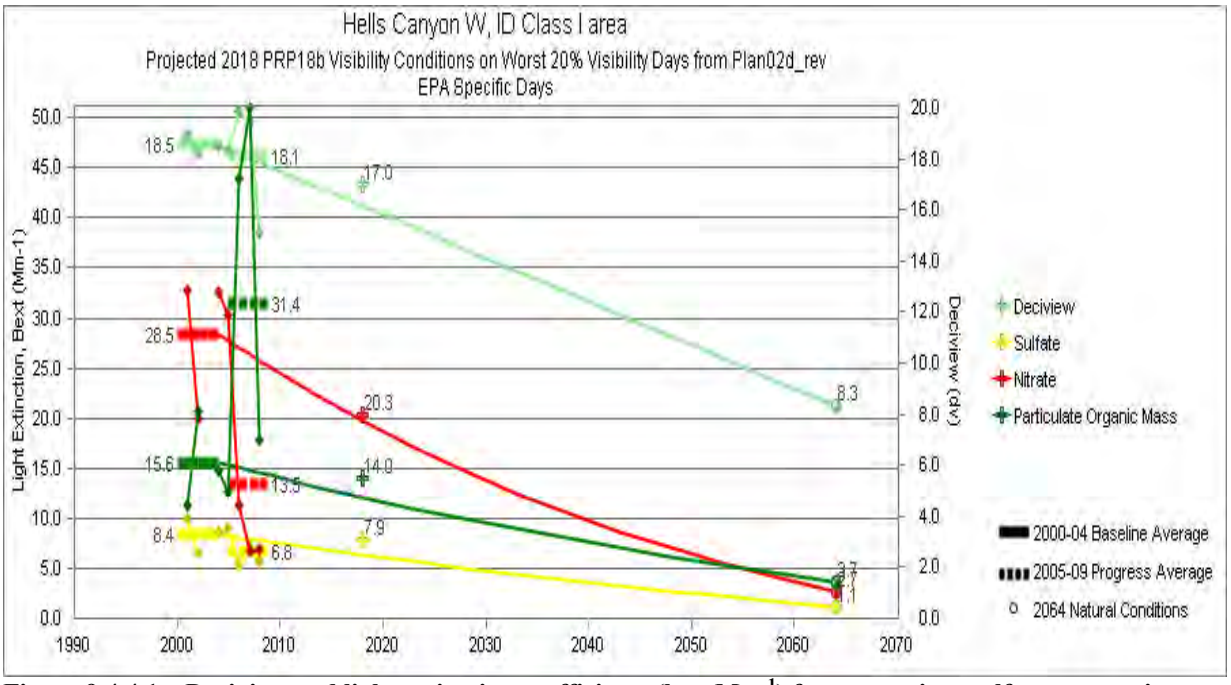

Figure 9.4.4.1a. Deciview and light extinction coefficients (b_{ext}, Mm^{-1}) for ammonium sulfate, ammonium nitrate, and particulate organic mass (POM) for the baseline (2000–2004), period 1 (2005–2009), and 2064 natural conditions estimates for the worst 20% visibility days at Hell's Canyon WA, OR/ID. Values of b_{ext} for other species, including elemental carbon (EC), soil, coarse mass, and sea salt are listed in the table below the graph (data and graphs obtained at http://vista.cira.colostate.edu/tss/Results/HazePlanning.aspx).

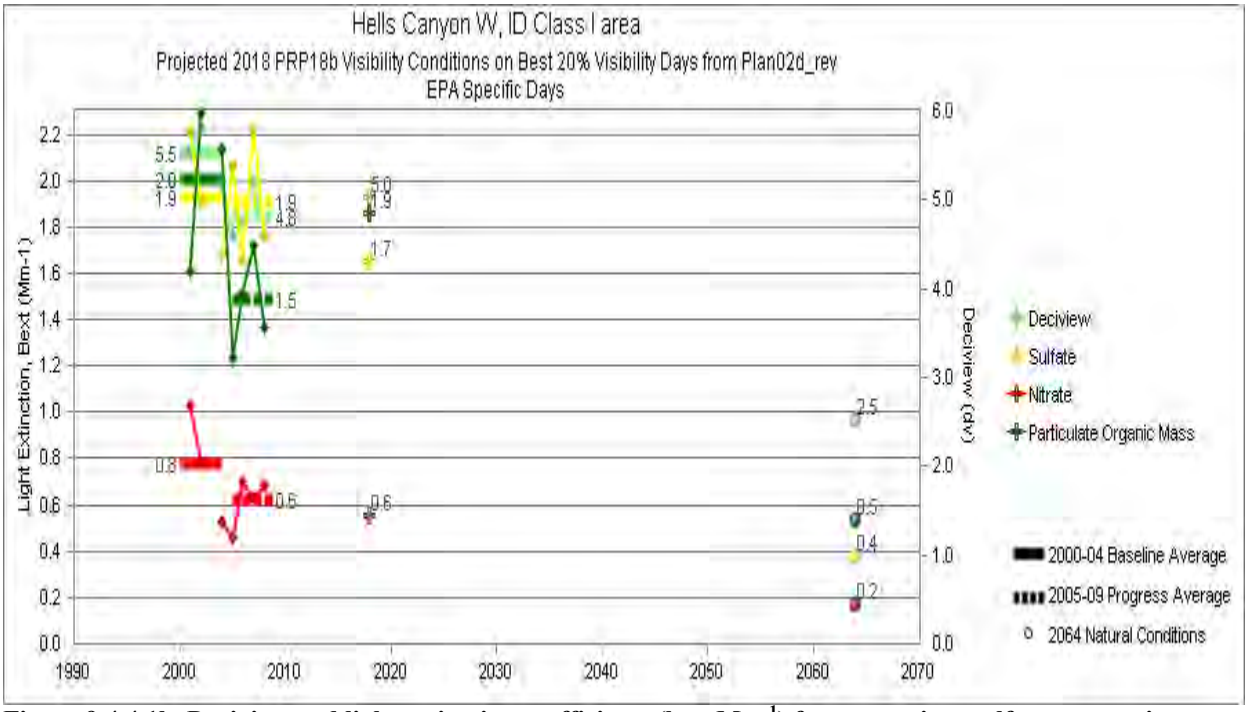

Figure 9.4.4.1b. Deciview and light extinction coefficients (b_{ext}, Mm^{-1}) for ammonium sulfate, ammonium nitrate, and particulate organic mass (POM) for the baseline (2000–2004), period 1 (2005–2009), and 2064 natural conditions estimates for the best 20% visibility days at Hell's Canyon WA, OR/ID. Values of b_{ext} for other species, including elemental carbon (EC), soil, coarse mass, and sea salt are listed in the table below the graph (data and graphs obtained at http://vista.cira.colostate.edu/tss/Results/HazePlanning.aspx).

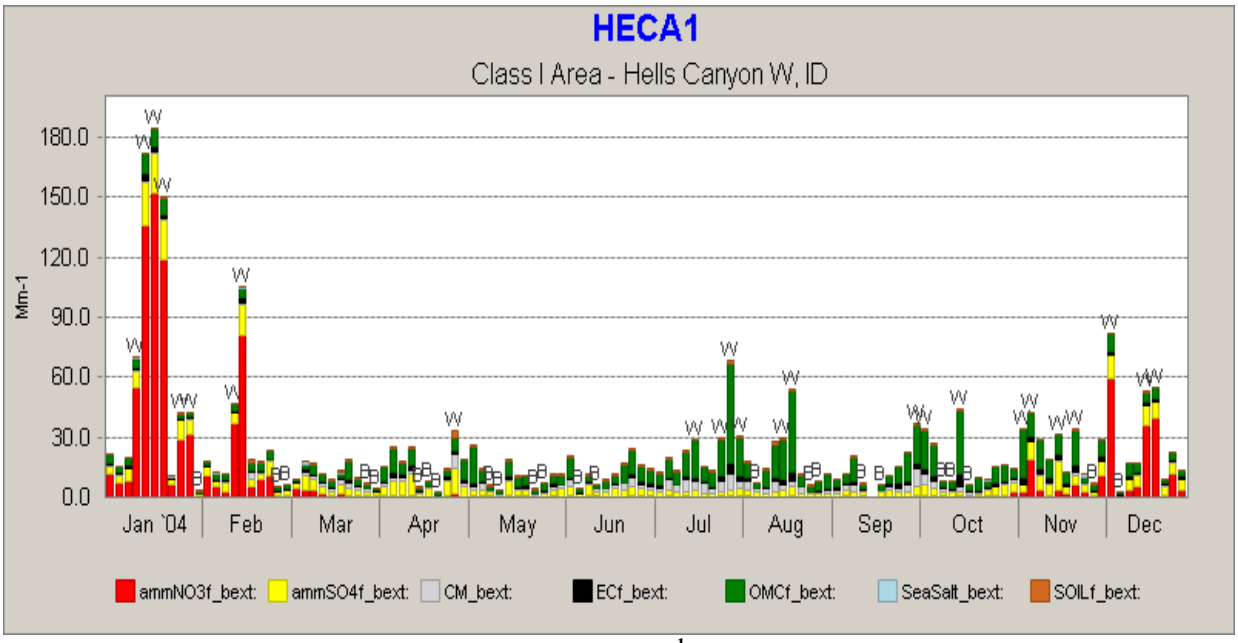

Figure 9.4.4.2a. Daily light extinction coefficients (b_{ext}, Mm^{-1}) for ammonium sulfate (ammSO4f_bext), ammonium nitrate (ammNO3f_bext), particulate organic matter (OMCf_bext), coarse mass (CM_bext), elemental carbon (EC_bext), soil (soil_bext), and sea salt (seasalt_bext) for 2004 Hells Canyon, ID (HECA1). Worst 20% days are marked with a "W" above the bar for that day, and similarly, best 20% days are marked with a "B" (from http://views.cira.colostate.edu/web/Composition/).

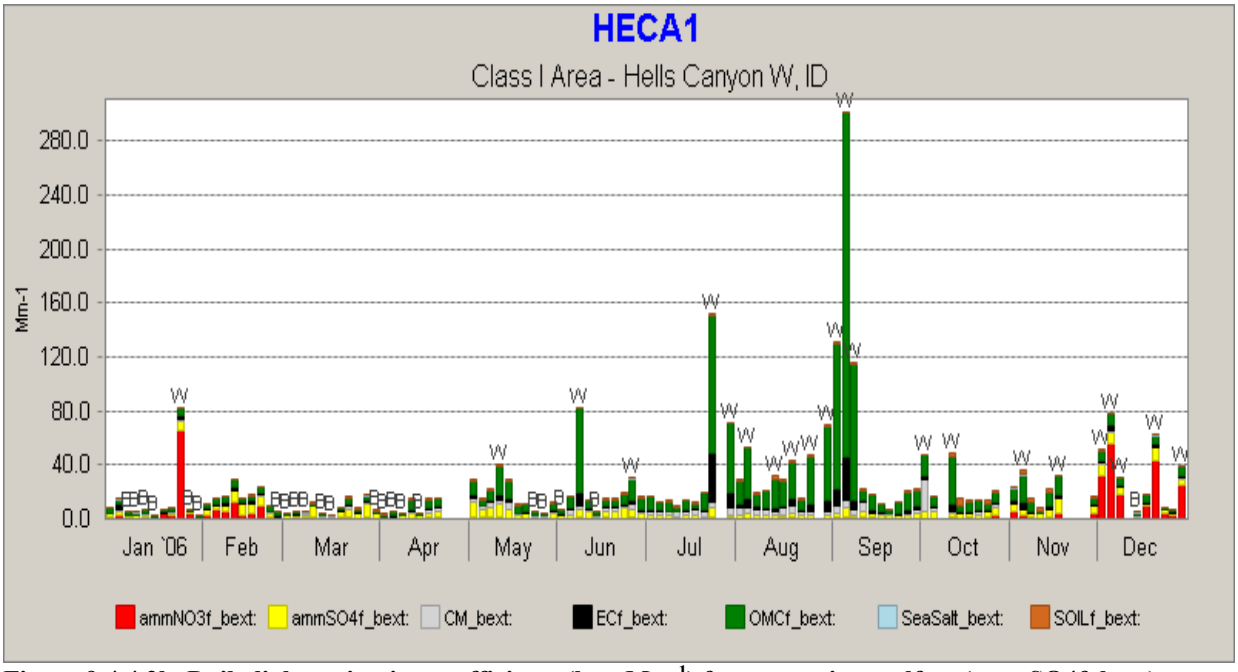

Figure 9.4.4.2b. Daily light extinction coefficients (b_{ext}, Mm^{-1}) for ammonium sulfate (ammSO4f_bext), ammonium nitrate (ammNO3f_bext), particulate organic matter (OMCf_bext), coarse mass (CM_bext), elemental carbon (EC_bext), soil (soil_bext), and sea salt (seasalt_bext) for 2006 Hells Canyon, ID (HECA1). Worst 20% days are marked with a "W" above the bar for that day, and similarly, best 20% days are marked with a "B" (from http://views.cira.colostate.edu/web/Composition/).

Table 9.4.4.1. Monitored, estimated, and projected 2018 visibility conditions and emissions changes for the worst 20% visibility days from WRAP regional analyses for Hell's Canyon Wilderness Area, OR/ID (HECA1) (from http://vista.cira.colostate.edu/tss/Results/HazePlanning.aspx).

Class I Area Visibility Summary: Hells Canyon W, OR/ID Class I area **Visibility Conditions:** Worst 20% Days **Model Relative Response Factor Calculation Method:** Specific Days (EPA) **Emissions Scenarios for Projected 2018 Emissions & Visibility Changes:** WRAP 2000-04 Baseline (plan02d_rev) & 2018 PRPb (prp18b)								
	Monitored		**Estimated**		**Projected**			
	2000-04 Baseline Conditions (Mm-1)	2005-09 1st Progress Period Conditions (Mm-1)	2064 Natural Conditions (Mm-1)	2018 Uniform Rate of Progress Target (Mm-1)[1]	2018 Projected Visibility Conditions (Mm-1)	Baseline to 2018 Change In Statewide Emissions (tons / %)	Baseline to 2018 Change in Upwind Weighted Emissions[2] (%)	Baseline to 2018 Change in Anthropogenic Upwind Weighted Emissions[2] (%)
Sulfate	8.37	6.8	1.14	6.35	7.89	-20,912 -40%	-29%	-38%
Nitrate	28.47	13.5	2.67	19.69	20.34	-96,079 -37%	-22%	-30%
Organic Carbon	15.6	31.4	3.69	12.12	14.01	-3,120 -3%	-12%	-31%
Elemental Carbon	3.06	5.3	0.37	2.37	2.18	-3,043 -11%	-21%	-44%
Fine Soil	0.66	0.8	0.92	0.72	0.73	-909 -3%	10%	15%
Coarse Material[3]	1.93	1.9	3.4	2.26	Not Applicable	31,039 47%	12%	27%
Sea Salt[3]	0.05	0.1	0.05	0.05		Not Applicable		
Total Light Extinction	69.14	60.9	23.24	53.48	58.13			
Deciview	18.55	18.1	8.32	16.17	16.99			

Table 9.4.4.2. Monitored, estimated, and projected 2018 visibility conditions and emissions changes for the best 20% visibility days from WRAP regional analyses for Hell's Canyon Wilderness Area, OR/ID (HECA1) (from http://vista.cira.colostate.edu/tss/Results/HazePlanning.aspx).

Class I Area Visibility Summary: Hells Canyon W, OR/ID Class I area
Visibility Conditions: Best 20% Days
Model Relative Response Factor Calculation Method: Specific Days (EPA)
Emissions Scenarios for Projected 2018 Emissions & Visibility Changes: WRAP 2000-04 Baseline (plan02d_rev) & 2018 PRPb (prp18b)

	Monitored		**Estimated**		**Projected**			
	2000-04 Baseline Conditions (Mm-1)	2005-09 1st Progress Period Conditions (Mm-1)	2064 Natural Conditions (Mm-1)	2018 Uniform Rate of Progress Target (Mm-1)[1]	2018 Projected Visibility Conditions (Mm-1)	Baseline to 2018 Change in Statewide Emissions (tons / %)	Baseline to 2018 Change in Upwind Weighted Emissions[2] (%)	Baseline to 2018 Change in Anthropogenic Upwind Weighted Emissions[2] (%)
Sulfate	1.93	1.9	0.38	Not Applicable	1.65	-20,912 -40%	-36%	-42%
Nitrate	0.78	0.6	0.17	Not Applicable	0.55	-96,079 -37%	-28%	-35%
Organic Carbon	2.01	1.5	0.54	Not Applicable	1.86	-3,120 -3%	-12%	-25%
Elemental Carbon	0.58	0.4	0.08	Not Applicable	0.43	-3,043 -11%	-23%	-41%
Fine Soil	0.25	0.2	0.14	Not Applicable	0.24	-909 -3%	3%	4%
Coarse Material[3]	0.8	0.5	0.48	Not Applicable	Not Applicable	31,039 47%	10%	25%
Sea Salt[3]	0.08	0.1	0.07	Not Applicable		Not Applicable		
Total Light Extinction	17.45	5.3	12.87	Not Applicable	16.62			
Deciview	5.52	4.8	2.52	Not Applicable	5.04			

1) 2018 Uniform Rate of Progress Target for Best 20% Days is not defined.
2) Results based on Weighted Emissions Potential analysis using the 2000-04 Baseline (plan02d_rev) & 2018 PRPb (prp18b) emissions scenarios.
3) Visibility projections not available due to model performance issues.

9.4.5 Agua Tibia Wilderness, California

Agua Tibia Wilderness (AGTI1) is southeast of Los Angeles and is one of seven CIAs in southern California. While visibility is more significantly impaired at AGTI1 compared to many other CIAs in the West (see Appendix G), data from AGTI1 show an apparent success story as virtually all haze components show improvement beyond the URP in period 1 (see Figures 9.4.5.1a and 9.4.5.1b for the 20% worst and 20% best visibility days, respectively). Data from AGTI1 are generally representative of data from the other southern California IMPROVE sites, and do not appear to have been significantly affected by fire-related activity (see daily b_{ext} from 2002 and 2008 in Figures 9.4.5.2a and 9.4.5.2b, respectively). Emissions reductions by the State of California, local air districts, and federal programs to achieve air quality health standards are providing co-benefits for visibility improvement at the Agua Tibia Wilderness. Improvements in b_{ext} for ammonium nitrate are particularly notable. Data are summarized in Table 9.4.5.1 and Table 9.4.5.2 for the 20% worst and 20% best visibility days, respectively.

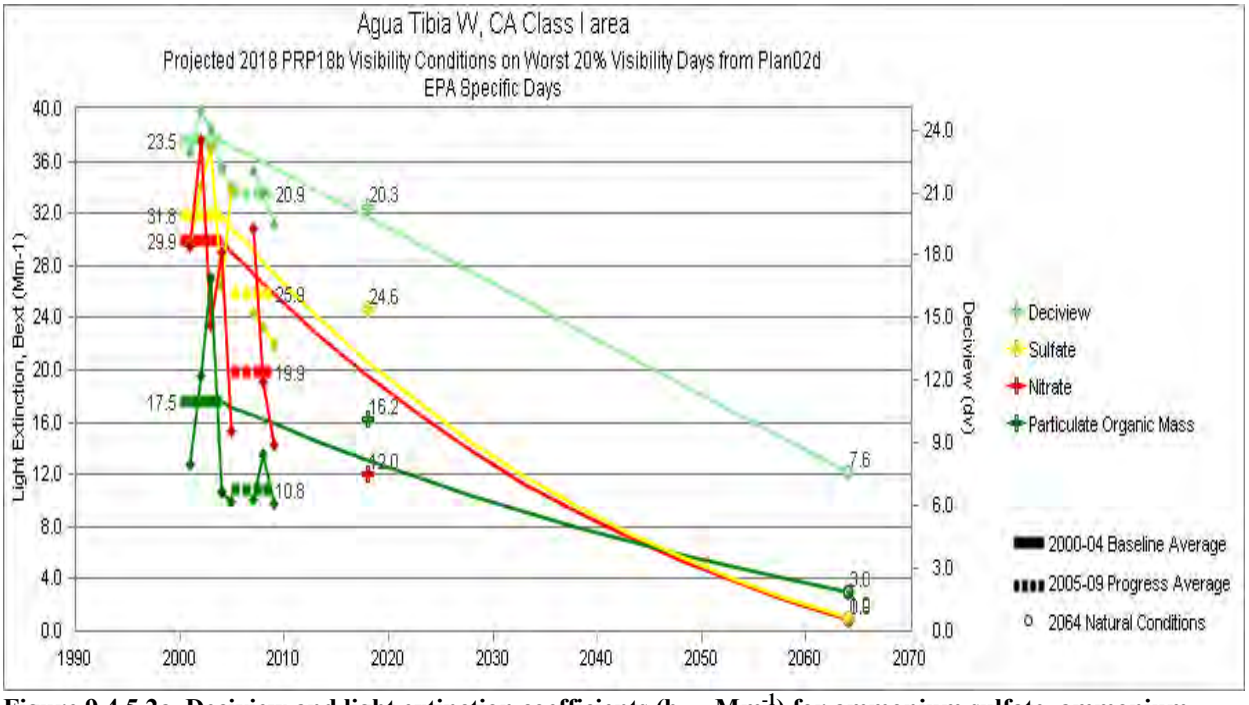

Figure 9.4.5.2a. Deciview and light extinction coefficients (b_{ext}, Mm^{-1}) for ammonium sulfate, ammonium nitrate, and particulate organic mass (POM) for the baseline (2000–2004), period 1 (2005–2009), and 2064 natural conditions estimates for the worst 20% visibility days at Agua Tibia Wilderness, CA. Values of b_{ext} for other species, including elemental carbon (EC), soil, coarse mass, and sea salt are listed in the table below the graph (data and graphs obtained at http://vista.cira.colostate.edu/tss/Results/HazePlanning.aspx).

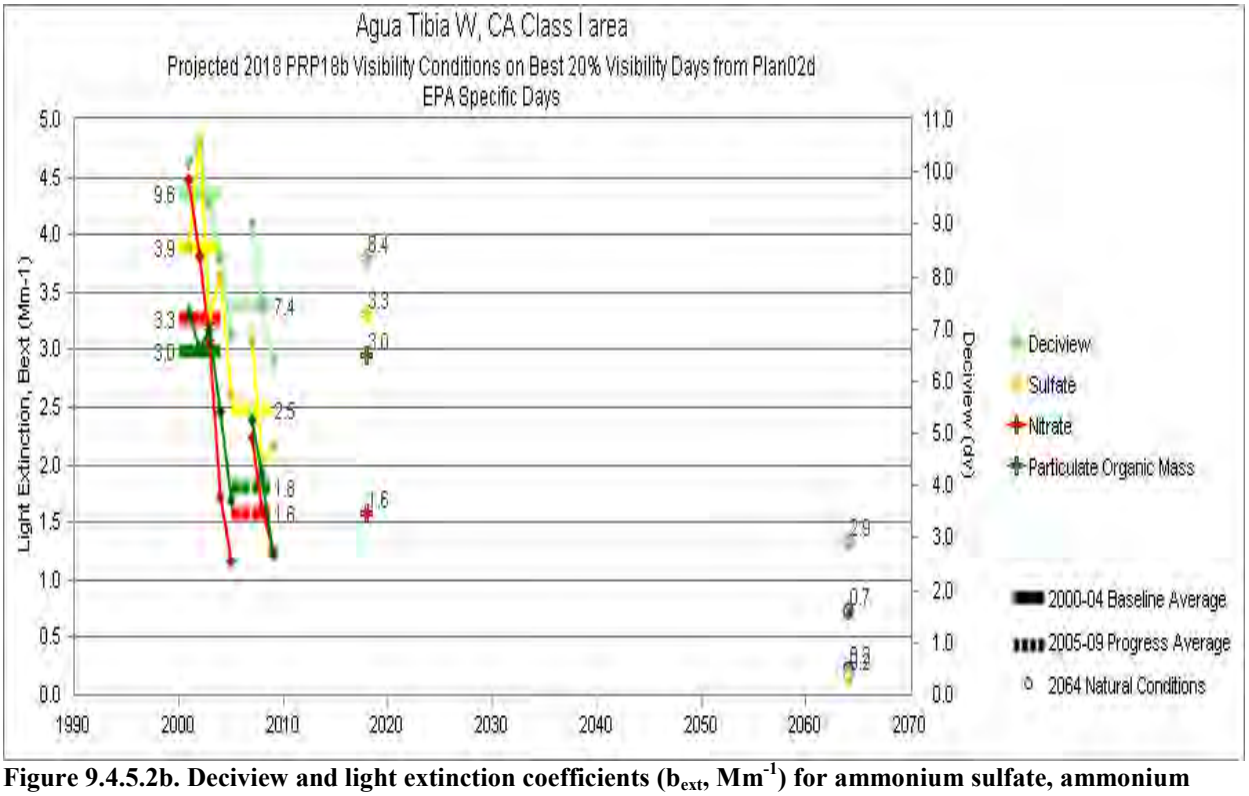

Figure 9.4.5.2b. Deciview and light extinction coefficients (b_{ext}, Mm^{-1}) for ammonium sulfate, ammonium nitrate, and particulate organic mass (POM) for the baseline (2000–2004), period 1 (2005–2009), and 2064 natural conditions estimates for the best 20% visibility days at Agua Tibia Wilderness, CA. Values of b_{ext} for other species, including elemental carbon (EC), soil, coarse mass, and sea salt are listed in the table below the graph (data and graphs obtained at http://vista.cira.colostate.edu/tss/Results/HazePlanning.aspx).

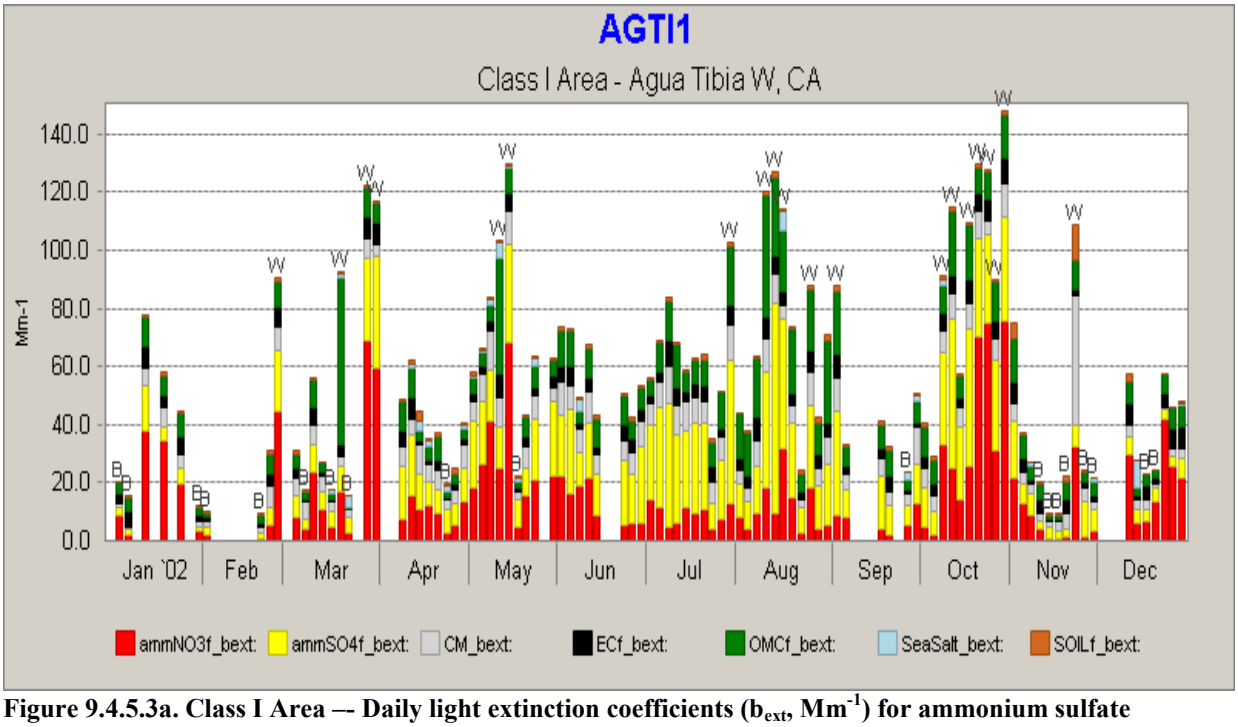

Figure 9.4.5.3a. Class I Area –- Daily light extinction coefficients (b_{ext}, Mm^{-1}) for ammonium sulfate (ammSO4f_bext), ammonium nitrate (ammNO3f_bext), particulate organic matter (OMCf_bext), coarse mass (CM_bext), elemental carbon (EC_bext), soil (soil_bext), and sea salt (seasalt_bext) for 2002 at Agua Tibia Wilderness, CA (AGTI1). Worst 20% days are marked with a "W" above the bar for that day, and similarly, best 20% days are marked with a "B" (from http://views.cira.colostate.edu/web/Composition/).

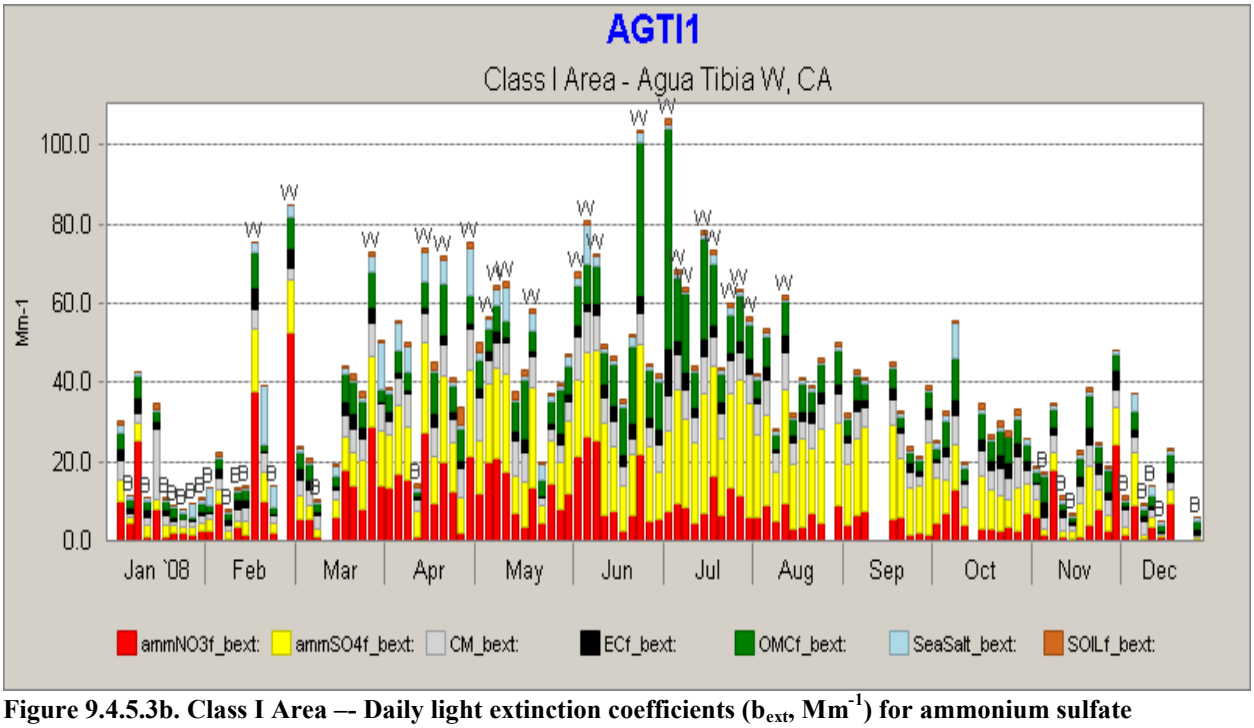

Figure 9.4.5.3b. Class I Area –- Daily light extinction coefficients (b_{ext}, Mm^{-1}) for ammonium sulfate (ammSO4f_bext), ammonium nitrate (ammNO3f_bext), particulate organic matter (OMCf_bext), coarse mass (CM_bext), elemental carbon (EC_bext), soil (soil_bext), and sea salt (seasalt_bext) for 2008 at Agua Tibia Wilderness, CA (AGTI1). Worst 20% days are marked with a "W" above the bar for that day, and similarly, best 20% days are marked with a "B" (from http://views.cira.colostate.edu/web/Composition/).

Table 9.4.5.1. Monitored, estimated, and projected 2018 visibility conditions and emissions changes for the worst 20% visibility days from WRAP regional analyses for Agua Tibia Wilderness, CA (AGTI1) (from http://vista.cira.colostate.edu/tss/Results/HazePlanning.aspx).

Class I Area Visibility Summary: Agua Tibia W, CA Class I area
Visibility Conditions: Worst 20% Days
Model Relative Response Factor Calculation Method: Specific Days (EPA)
Emissions Scenarios for Projected 2018 Emissions & Visibility Changes: WRAP 2000-04 Baseline (plan02d) & 2018 PRPb (prp18b)

	Monitored		**Estimated**		**Projected**			
	2000-04 Baseline Conditions (Mm-1)	2005-09 1st Progress Period Conditions (Mm-1)	2064 Natural Conditions (Mm-1)	2018 Uniform Rate of Progress Target (Mm-1)[1]	2018 Projected Visibility Conditions (Mm-1)	Baseline to 2018 Change in Statewide Emissions (tons / %)	Baseline to 2018 Change in Upwind Weighted Emissions[2] (%)	Baseline to 2018 Change in Anthropogenic Upwind Weighted Emissions[2] (%)
Sulfate	31.82	25.9	0.99	20.62	24.64	-6,243 -8%	-26%	-30%
Nitrate	29.91	19.9	0.94	19.50	11.98	-591,119 -45%	-49%	-51%
Organic Carbon	17.55	10.8	2.98	13.11	16.22	-10,792 -7%	-5%	-14%
Elemental Carbon	6.37	4.6	0.26	4.68	3.57	-12,961 -28%	-28%	-49%
Fine Soil	1.25	0.9	0.83	1.15	1.28	250 0%	3%	3%
Coarse Material[3]	8.64	7.5	2.98	7.13	Not Applicable	29,666 13%	13%	16%
Sea Salt[3]	0.82	1.8	1.68	1.01		Not Applicable		
Total Light Extinction	107.36	71.4	21.66	73.56	78.15			
Deciview	23.5	20.9	7.64	19.80	20.3			

Table 9.4.5.2. Monitored, estimated, and projected 2018 visibility conditions and emissions changes for the best 20% visibility days from WRAP regional analyses for Agua Tibia Wilderness, CA (AGTI1) (from http://vista.cira.colostate.edu/tss/Results/HazePlanning.aspx).

Class I Area Visibility Summary: Agua Tibia W, CA Class I area
Visibility Conditions: Best 20% Days
Model Relative Response Factor Calculation Method: Specific Days (EPA)
Emissions Scenarios for Projected 2018 Emissions & Visibility Changes: WRAP 2000-04 Baseline (plan02d) & 2018 PRPb (prp18b)

	Monitored		**Estimated**		**Projected**			
	2000-04 Baseline Conditions (Mm-1)	2005-09 1st Progress Period Conditions (Mm-1)	2064 Natural Conditions (Mm-1)	2018 Uniform Rate of Progress Target (Mm-1)[1]	2018 Projected Visibility Conditions (Mm-1)	Baseline to 2018 Change in Statewide Emissions (tons / %)	Baseline to 2018 Change in Upwind Weighted Emissions[2] (%)	Baseline to 2018 Change in Anthropogenic Upwind Weighted Emissions[2] (%)
Sulfate	3.9	2.5	0.17	Not Applicable	3.3	-6,243 -8%	-32%	-36%
Nitrate	3.27	1.6	0.22	Not Applicable	1.57	-591,119 -45%	-48%	-50%
Organic Carbon	2.99	1.8	0.74	Not Applicable	2.95	-10,792 -7%	-4%	-12%
Elemental Carbon	1.87	1.2	0.11	Not Applicable	1.01	-12,961 -28%	-27%	-48%
Fine Soil	0.47	0.4	0.26	Not Applicable	0.5	250 0%	4%	5%
Coarse Material[3]	2.41	2.4	0.72	Not Applicable	Not Applicable	29,666 13%	14%	17%
Sea Salt[3]	0.79	0.6	0.2	Not Applicable		Not Applicable		
Total Light Extinction	26.70	10.4	13.42	Not Applicable	23.51			
Deciview	9.58	7.4	2.92	Not Applicable	8.37			

1) 2018 Uniform Rate of Progress Target for Best 20% Days is not defined.
2) Results based on Weighted Emissions Potential analysis using the 2000-04 Baseline (plan02d) & 2018 PRPb (prp18b) emissions scenarios.
3) Visibility projections not available due to model performance issues.

REFERENCES

Archuleta, C., et al. (2007), WRAP IMPROVE Data Substitutions for Regional Haze Planning, http://vista.cira.colostate.edu/docs/wrap/Monitoring/WRAP_Data_Substitution_Methods_April_2007.doc.

Brewer, P., and T. Moore (2009), Source contributions to visibility impairment in the southeastern and western United States, *J. Air Waste Manage. Assoc.,* September.

Copeland, S. A., M. L. Pitchford, and R. B. Ames (2008), Regional haze rule natural level estimates using the revised IMPROVE aerosol reconstructed light extinction algorithm, Air & Waste Management Association Visibility Specialty Conference presentation, Moab, UT, April.

Debell, L. J., K. A. Gebhart, J. L. Hand, W. C. Malm, M. L. Pitchford, B. A. Schichtel, and W. H. White (2006), IMPROVE (Interagency Monitoring of Protected Visual Environments): Spatial and seasonal patterns and temporal variability of haze and its constituents in the United States: Report IV, CIRA Report ISSN: 0737-5352-74, Colo. State Univ., Fort Collins.

Husar, R. (2003), RPO National Technical Workgroup Meeting, St. Louis, MO, http://www.marama.org/visibility/NationalRPO/Presentations/Monitoring/Husar_FASTNET.pdf.

Moore, T., and P. Brewer (2007), Regional haze planning in the western and southeastern United States, *Environmental Manager*, Air & Waste Management Association; September.

U.S. EPA (1999), Regional Haze Regulations; Final Rule, 40 CFR 51, Federal Register, 64, 35714-35774.

U.S. EPA (2003a), Guidance for Tracking Progress under the Regional Haze Rule, EPA-454/B-03-004, http://www.epa.gov/ttn/oarpg/t1/memoranda/rh_tpurhr_gd.pdf)

U.S. EPA (2003b), Guidance for Estimating Natural Visibility Conditions under the Regional Haze Rule, http://www.wrapair.org/forums/aamrf/projects/NCB/EPA_Guidance.pdf.

U.S. EPA (2005), Regional Haze Regulations and Guidelines for Best Available Retrofit Technology (BART) Determinations; Final Rule, http://www.epa.gov/fedrgstr/EPA-AIR/2005/July/Day-06/a12526.pdf.

U.S. EPA (2006), Regional Haze Regulations; Revisions to Provisions Governing Alternative to Source-Specific Best Available Retrofit Technology (BART) Determinations; Final Rule, http://www.epa.gov/fedrgstr/EPA-AIR/2006/October/Day-13/a8630.pdf.

U.S. EPA (2007), Guidance for Setting Reasonable Progress Goals Under the Regional Haze Program, Office of Air Quality Planning and Standards, Air Quality Policy Division, Geographic Strategies Group, http://www.wrapair.org/forums/amc/documents/RPguidance.pdf.

U.S. EPA (2011), Acid Rain Program Emissions, Emission Rates, and Heat Input Changes at National Levels (All Units), http://www.epa.gov/airmarkets/images/ARP1990to2010.pdf.

White, W. H. (2008), Chemical markers for sea salt in IMPROVE aerosol data, *Atmos. Environ.*, *42*, 261-274.

Chapter 10. X-Ray Fluorescence Reference Materials from an Aerosol Generation System

C. E. McDade, H. Indresand, and A. M. Dillner

10.1 INTRODUCTION

A new aerosol generation and mixing-chamber system was developed and designed to deposit samples of known composition on filters, using an IMPROVE sampler. The aerosol generation/mixing system has been used to create reference materials to evaluate the response of the X-ray fluorescence (XRF) system over a wide range of mass concentrations and to assess the calibration of the XRF instrument. Additionally, the new aerosol system has been used to add pure substances to ambient samples to evaluate spectral interferences.

The need for the aerosol generation system emerged from questions regarding the calibration of the XRF system. Ideally, calibration standards mimic ambient samples in mass loadings, deposit pattern, substrate material, and chemical composition. The commercially available standards are prepared on Mylar® or Nuclepore® substrates, not on Teflon® as used in routine IMPROVE sampling. In our system the samples are prepared on Teflon, and they also exhibit the same deposition patterns as field samples since the aerosol chamber is attached to an actual IMPROVE sampler. Commercial standards are typically only available at one or two mass loadings, which are higher than those encountered in the IMPROVE network. The standards are purchased from a single vendor, and there are no alternative sources to provide an independent assessment. Furthermore, XRF calibrations are performed at a reduced instrument current compared to field samples to accommodate the high loadings on the standards. Filter-based reference materials at lower concentrations (representative of IMPROVE field samples) can be prepared using the aerosol generation/mixing system and at a variety of concentrations across the representative range, thereby allowing for multipoint calibration in the range of the samples, which improves the precision of the calibration.

The new system also allows the preparation of samples to evaluate spectral interferences at relevant concentrations. Spectral peaks of sulfur and silicon, for example, lie close to one another in the XRF spectrum, and a large amount of sulfur relative to silicon has been shown to cause interferences to the silicon peak in the IMPROVE network data. By adding ammonium sulfate to ambient filters, it is possible to investigate such interferences under controlled conditions.

10.2 AEROSOL GENERATION SYSTEM

A diagram of the aerosol generation system is shown in Figure 10.1 and a photograph is shown in Figure 10.2. Aerosol deposits are generated from solution with a constant-output atomizer, using compressed air. Aerosols are dried with a diffusion dryer before entering the dilution chamber. Low relative humidity and particle-free dilution air is introduced into the chamber to further dry the aerosol and allow sufficient flow rate for the sampler. The aerosol stream and dilution air are well mixed in the chamber before being pulled through an IMPROVE $PM_{2.5}$ sampler operating at the typical flow rate for IMPROVE samplers. Relative humidity in the chamber is measured continuously to ensure that the particles are completely dry. The

amount of the aerosol deposit is a function of solute, solution concentration, and sampling time. The actual mass deposited on each filter is determined gravimetrically, as described below.

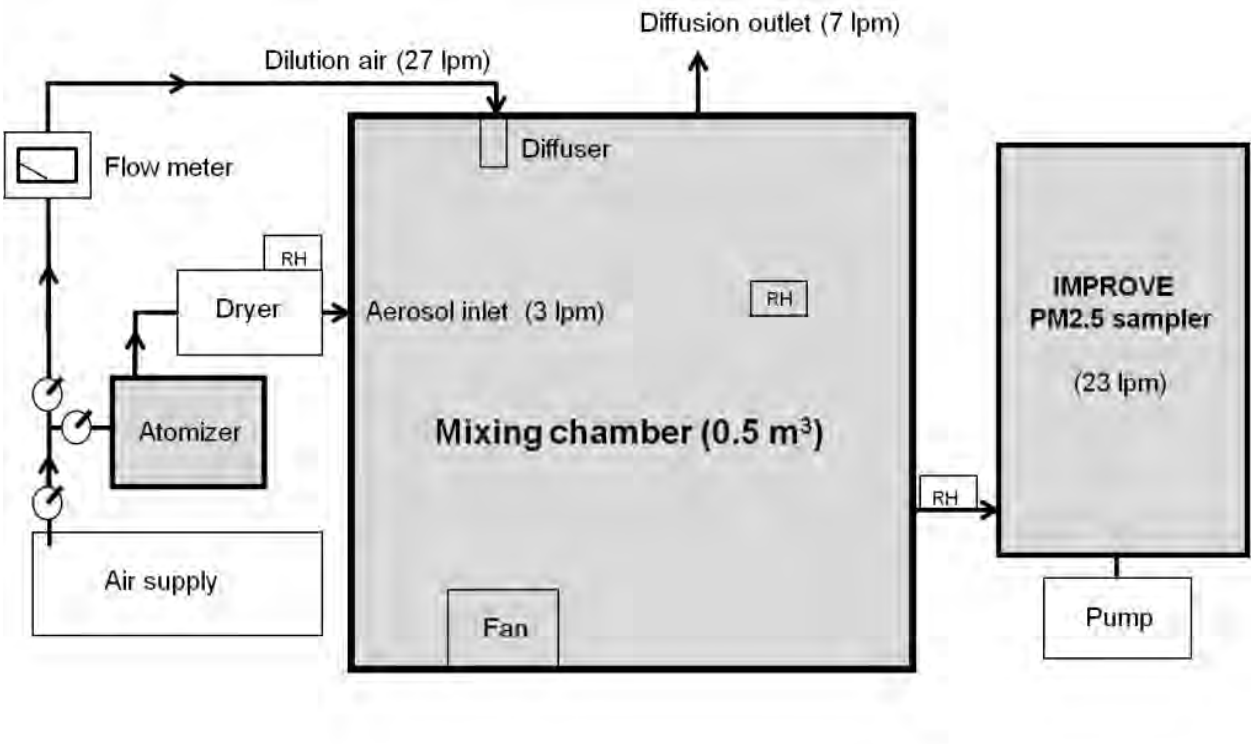

Figure 10.1. Schematic of the particle generation, mixing, and sampling system used to make reference materials. A solution is atomized and the resulting particles are dried and mixed with clean, dry air in the mixing chamber. The suspended particles are drawn through an IMPROVE $PM_{2.5}$ sampler and collected on 25 mm Teflon® filters. Relative humidity (RH) is measured in three locations to ensure that particles are anhydrous.

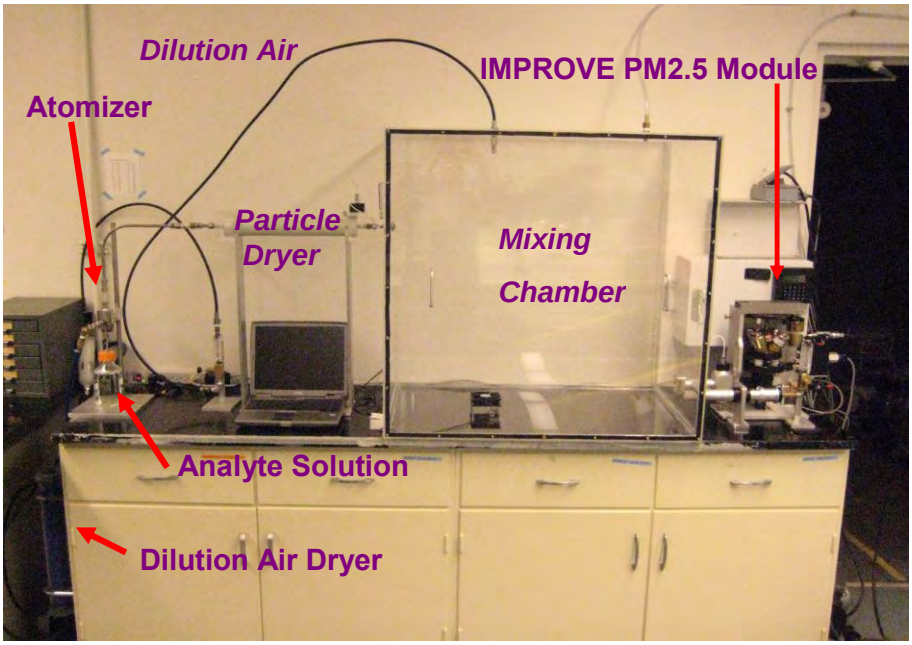

Figure 10.2. Photograph of the aerosol generation system.

10.3 TESTING AND VERIFICATION

Most of the development work thus far has focused on generating sulfate-containing particles. Ammonium sulfate is one of the major components of most ambient aerosols. In addition, sulfate mass loadings on IMPROVE samples are high, allowing for better accuracy in gravimetric measurements. Potassium sulfate was used in some other filter preparations to assess the reliability of the method using a different compound. Solutions were made with 99.999% pure ammonium sulfate or 99.95% pure potassium sulfate in HPLC (high-pressure liquid chromatography) grade, deionized water. Reference materials were made in the mass range representative of field samples and also at higher masses to evaluate XRF instrument performance.

Two types of blanks were generated with each run. Laboratory blanks corresponded to filters that were taken out of the box and analyzed by XRF without ever being installed in the sampler. Chamber blanks were installed in the sampler and collected by running the aerosol generation system with strictly deionized water solutions in the atomizer immediately after a full cleaning of the generation and sampling system. XRF analyses of species in chamber blanks were equivalent to laboratory blanks and showed that elemental contamination was not produced in the generation and sampling systems during filter handling.

As a further test for contamination, transmission FTIR (Fourier transform infrared) spectroscopy was used to scan the prepared reference materials for particle-bound water and organic-compound contamination that, if present, would add unwanted mass. The results showed no detectable amounts of these contaminants.

The fundamental measurement technique of gravimetric analysis was used to determine the mass of sulfur on each ammonium sulfate (or potassium sulfate) filter. The measured mass of ammonium sulfate or potassium sulfate was converted to mass of sulfur, assuming a pure compound was collected (no water or impurities). After the filters were weighed, they were analyzed by XRF, and many were then analyzed by ion chromatography (IC) to provide an independent measure of sulfate concentration. The IC measurement showed that sulfur mass based on ammonium sulfate mass was accurate. IC is a destructive technique (it requires extraction of the filter in solution), so it cannot be performed a priori to determine the concentration before XRF analysis.

Testing using IC has established the reliability of gravimetric mass as a quantitative technique for these sulfur reference materials. Figure 10.3 shows the linear regression of sulfur measured by IC compared to gravimetric analysis as a function of deposit mass. The agreement between gravimetric analysis and IC is within about 2% for ammonium sulfate and within about 3% for potassium sulfate.

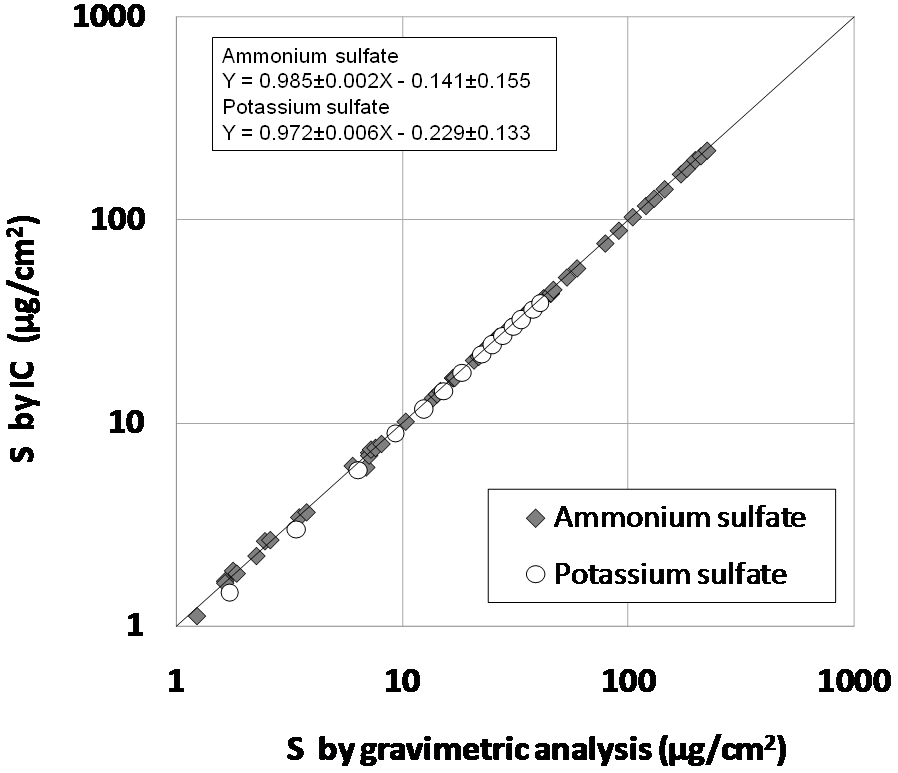

Figure 10.3. Sulfur (S) mass measurements from ion chromatography (IC) compared to gravimetric analysis for ammonium sulfate and potassium sulfate reference materials. The linear regressions (with 95th percentile confidence levels for the slope and intercept) for each reference material are given on the figure and show the good agreement between sulfur from IC and gravimetric analysis.

The sulfur reference materials have been used to evaluate the sulfur response in the UC Davis XRF system and to assess the feasibility of using the new reference materials in routine system calibrations. An additional commercial XRF instrument (PANalytical Epsilon 5) at the Desert Research Institute (DRI) was used in an interlaboratory comparison of the sulfur response of prepared reference materials, two commercial standards, and 28 ambient samples from the IMPROVE network. When each laboratory calibrated its XRF instrument using its own set of commercial standards, the reported sulfur concentrations on the 28 ambient samples differed by over 10% between the two laboratories. When both instruments were calibrated against the new UC-Davis-prepared reference materials, however, sulfur concentration agreement improved to within 1%. Hence, the two laboratories produce the same result when they both calibrate with reference materials that mimic all features of the element and the sample.

Further work has begun to produce deposits on Teflon filters of other elements analyzed in the XRF system. Sodium chloride has been successfully atomized and deposited on filters. Other elements with major importance for the Regional Haze Rule will also be considered for future work. The chamber will also be used to evaluate uncertainty, measurement detection

limits, and spectral interferences. Although the initial development work has focused on the preparation of Teflon filter samples, the aerosol generation system is also applicable to the preparation of samples on quartz and nylon filters. Currently underway is a project that deposits ammonium sulfate on quartz filters to evaluate the impact of particles on pyrolysis of organic carbon.

Chapter 11. Ammonia and Ammonium Measurements from Passive, Modified IMPROVE and CASTNET Samplers.

D. E. Day

11.1 INTRODUCTION

Ammonia, NH_3, is a ubiquitous component of the ambient atmosphere, and although its lifetime in the atmosphere generally ranges from only a few hours to a few days, its impacts can be significant. Ammonia, a strong base, will react quickly with atmospheric acids to form fine particulate matter. Two common reactions, whose products are ammonium salts, are depicted by equations 11.1 and 11.2 below:

$$NH_{3(g)} + H_2SO_{4(g)} \rightarrow NH_4HSO_{4(s)} + NH_{3(g)} \rightarrow (NH_4)_2SO_{4(s)} \quad 11.1$$

$$NH_{3(g)} + HNO_{3(g)} \leftrightarrow NH_4NO_{3(s)} \quad 11.2$$

In the first reaction, NH_3 reacts with sulfuric acid (H_2SO_4) to produce particulate ammonium sulfate ($(NH_4)_2SO_4$). In the second reaction, NH_3 reacts with nitric acid (HNO_3) to produce particulate ammonium nitrate (NH_4NO_3). Note that the second reaction is reversible; hence, an equilibrium exits between the solid and gas phases that is dependent upon temperature, relative humidity (RH), and the concentrations of the precursor gases. These fine aerosol particles efficiently attenuate radiation through the atmosphere, thereby contributing to visibility-reducing haze and climate forcing. The small particles also penetrate deep into lungs, negatively impacting human health by stressing the respiratory, pulmonary, and immune systems, causing increased morbidity and mortality rates.

Ammonia gas deposits directly from the atmosphere onto terrestrial and aquatic ecosystems (dry deposition). Ammonia also dissolves readily into the aqueous phase and will subsequently be washed out of the atmosphere as ammonium ion (NH_4^+) in precipitation (wet deposition). When deposited, either as ammonia or ammonium ion, eventually ammonia causes an over enrichment of nitrogen (N) in the environment. The effects of deposition are numerous and include eutrophication of surface water, with a consequent decrease in biodiversity. In the terrestrial environment, excess NH_3 deposition leads to increased soil acidity, alteration of the soil's chemical balance, and crop damage, and affects ecosystems by favoring species that require higher nitrogen concentrations.

A large fraction of ammonia is emitted from concentrated animal feeding operations (CAFO). Over the past several decades animal husbandry practices have undergone a significant shift from small family farms to much larger factory-type operations. For example, from 1982 through 1997 total livestock production increased by about 10%, while the total number of feeding operations decreased by more than 50%. The remaining CAFO became more geographically concentrated. This combination of larger and more geographically concentrated operations has led to significant regional sources of ammonia emissions. The extensive cultivation of nitrogen-fixing legumes and the use of various types of ammonia-based fertilizer also contribute substantially to reactive forms of nitrogen entering the environment. On a global basis, it is estimated that agriculture practices such as animal husbandry and farming contribute

60–80% of the total ammonia emission budget. Other important sources of ammonia include the oceans, biomass burning, humans and their pets, and natural ecosystems.

Despite the clear importance of the NH_3/NH_4^+ system to atmospheric chemistry and deposition to aquatic and terrestrial ecosystems, there have been relatively few studies performed to understand ammonia emission inventories, atmospheric transport, or ammonia deposition velocities, all of which are needed to model and predict the concentration and effects ammonia might have if concentrations continue to increase. Furthermore, there are no national networks performing routine measurements of ammonia gas to discern the spatial and temporal distribution of ammonia. This study was designed to investigate the feasibility of modifying existing aerosol samplers currently used in various national networks for monitoring the NH_3/NH_4^+ system and evaluating passive samplers for NH_3 measurement.

11.2 INSTRUMENTATION

There are several networks currently operating across the country that monitor various aspects of ambient air quality. Each network utilizes a sampling system designed to monitor the parameters of interest for that particular network. In this study the IMPROVE and Clean Air Status and Trends Network (CASTNET) samplers were modified by adding an acid-impregnated filter for the measurement of ammonia and ammonium ion. The concentration obtained from these samplers is then compared with a denuder-based URG (URG Corporation) sampler and with passive samplers. Each of these sampling systems is described below. In conjunction with the aerosol sampler measurements, meteorological measurements of wind speed and direction, temperature, relative humidity, and solar radiance were also made. The aerosol samplers used in this study were operated on the roof of a trailer located in a somewhat isolated part of the Foothills Campus at Colorado State University. The inlet of the CASTNET sampler, which houses the filter pack, and the IMPROVE, URG, and passive samplers are shown in Figure 11.1 from left to right.

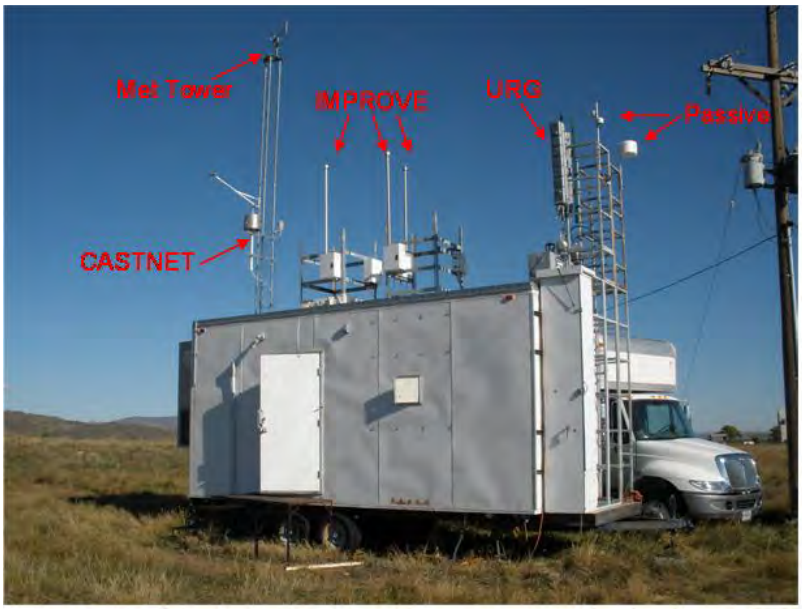

Figure 11.1. Study trailer showing aerosol sampling equipment. The CASTNET, Met tower, IMPROVE, URG, and passive samplers are shown from left to right.

11.2.1 URG Sampler

The URG samplers were configured as follows, in order of sample air flow: a 2.5 µm size-cut, Teflon®-coated cyclone, a sodium carbonate (Na_2CO_3) coated denuder to capture acidic gases (HNO_3 and sulfur dioxide, SO_2), a phosphorous acid (H_3PO_3) coated denuder to capture ammonia, a Nylasorb filter to remove particulate material, and finally a second H_3PO_3-coated denuder to capture any NH_3 from NH_4NO_3 particles that have volatilized from the filter (see Figure 11.2). The samplers operated at a flow rate of 10 LPM; the sample volume was measured using a dry gas meter. This system has been shown to minimize sampling artifacts; therefore, the URG denuder/filter-pack sampler is considered the "field standard" for this study. Two URG samplers operating side by side were used for comparison purposes. One sampler operated on a 24-hour sample collection period. This sampler was used to compare with the 24-hour sampling cycle of the IMPROVE sampler. The other URG sampler operated on a weekly sample collection period to compare with the weekly sampling cycle of the CASTNET sampler. Previous studies have shown the minimum detection limits (MDL) of sulfate, nitrate, and ammonium ion concentrations from the URG are 0.05, 0.07, and 0.03 µg m^{-3}, respectively. The precision (expressed as relative standard deviation, RSD) for these species is 5.2%, 6.7%, and 4.5%, respectively (Yu et al., 2006). Similar results for MDL and RSD are reported by Lee et al. (2004).

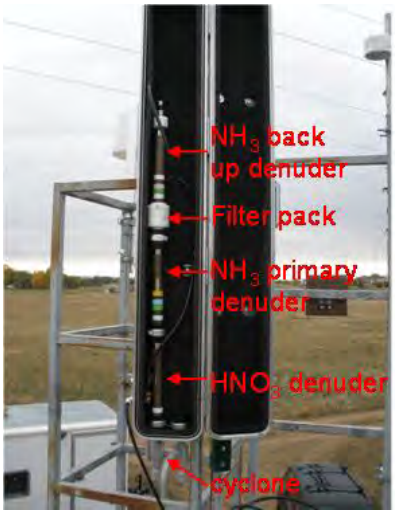

Figure 11.2. URG sampler with the NH_3 backup denuder at top and filter pack, NH_3 primary denuder, HNO_3 denuder, and $PM_{2.5}$ cyclone at bottom. Note the top of the sampler is the outlet and the bottom of the sampler is the inlet.

11.2.2 IMPROVE Sampler

Visibility-impairing particulate matter is monitored within selected national parks and other Class I visibility areas by the IMPROVE network (Malm et al., 1994). This network uses a sampling system which consists of four modules (channels A, B, C, and D). Each module has a separate size selective inlet, filter medium, flow control, and pump, but are connected to a single control unit. Each module utilizes a cassette, which holds four filters allowing the sampler to operate 1–2 weeks unattended. The unmodified Channel B utilizes a Nylasorb filter to collect aerosol samples that are analyzed by ion chromatography (IC) for sulfate and nitrate ion concentrations. However, Channel B was modified for this work by adding a phosphorous-acid-

impregnated cellulose fiber filter to collect NH_3 gas. Figure 11.3 shows the arrangement of the IMPROVE sampler filter cassette. The cellulose fiber filter was placed between the cassette filter holder and the Teflon spacer, while the Nylasorb filter was placed between the Teflon-coated support grid and the top of the cartridge assembly. Figure 11.4 shows the filter cassette in the channel B module ready for sample collection.

Figure 11.3. IMPROVE sampler filter cassette with additional screen and spacer for NH_3 collection. The sampler includes 1) cassette filter holder, 2) Teflon spacer, 3) Teflon-coated support grid, and 4) top of cartridge assembly.

Figure 11.4. IMPROVE sampler channel B with sample cassette installed.

11.2.3 CASTNET Sampler

The CASTNet filter pack uses a Teflon filter to collect the following particulate species: sulfate, nitrate, ammonium, calcium, magnesium, sodium, and potassium. A nylon filter collects nitric acid and some of the SO_2, and dual potassium-carbonate-impregnated cellulose filters collect the remaining SO_2. The CASTNET sampler collects weekly samples at a flow rate of 1.5 LPM in the eastern United States, where aerosol concentrations are higher, and 3 LPM in the western United State, where aerosol concentrations are generally lower. Total aerosol concentrations are collected, as CASTNET does not use a size-selective cyclone. The sampler flow rate is calibrated to standard conditions; thus, volumes were corrected for ambient pressure and temperature before comparing to other samplers. The CASTNET filter packs were prepared at MacTech (MacTech Engineering and Consulting, Inc., Gainesville, Florida) and shipped in

sealed plastic bags as per network protocol. For this study the filter pack was modified to accommodate another filter (citric-acid-impregnated cellulose fiber filter) for the collection of ammonia gas. Figure 11.5 shows a disassembled CASTNET filter pack and a filter pack ready for deployment. Figure 11.6 shows regular and modified CASTNET filter packs in the sampler holder.

Figure 11.5. CASTNET filter pack ready for deployment (left) and a disassembled filter pack (right).

Figure 11.6. Regular (left) and modified (right) CASTNET filter packs in the sample holder.

11.2.4 Passive Samplers

The Radiello (Sigma-Aldrich, St. Louis, Missouri) and the Ogawa (Ogawa & Co. USA Inc., Pompano Beach, Florida) passive samplers were also deployed during this study. These passive samplers work by the simple diffusion of NH_3 through the atmosphere and across a diffusive body surface and, finally, deposition onto a cartridge impregnated with acid. Passive samplers have some advantages over conventional sampling systems: they are self-contained units, relatively inexpensive, and simple to operate, and they have zero power requirements. The Radiello passive sampler was operated in triplicate throughout this study, while two Ogawa

passive samplers were operated side by side. Figure 11.7 shows the passive samplers deployed in the field.

Figure 11.7. Passive samplers deployed in the field. The Ogawa sampler is on the left, and the Radiello sampler is on the right.

11.3 COMPARISONS OF DATA FROM CASTNET, URG, AND IMPROVE SAMPLERS

Although NH_3 was the primary species of interest during this study, other aerosol species such as sulfate and nitrate are also compared. The comparison of other species serves to evaluate the overall quality of analytical procedures, provides estimates of uncertainty, and allows for the evaluation of changes to the samplers caused by the addition of the cellulose fiber filter.

11.3.1 IMPROVE versus URG

The IMPROVE and URG samplers were operated in August–October 2008 for a 24-hour sampling duration starting at 9:00 a.m. Samples were collected each Monday, Tuesday, Thursday, and Friday, while filter blanks were obtained on the non-sampling days. IC analyses were performed at the Atmospheric Chemistry Laboratory at Colorado State University. Figure 11.8 shows a comparison between sulfate ion concentrations from the regular IMPROVE, modified IMPROVE, and URG samplers. The timeline and the scatter plot show some scatter between data points; however, in general, there is good agreement in the concentrations from each sampler. On average there is ~1% difference between concentrations from the two IMPROVE samplers and ~ 5% difference between concentrations from the IMPROVE and the URG samplers. This comparison suggests the addition of the cellulose fiber filter to the IMPROVE Channel B sampler has no adverse effect on the measurement of sulfate ion concentrations and demonstrates good agreement in the data obtained with the URG and IMPROVE samplers.

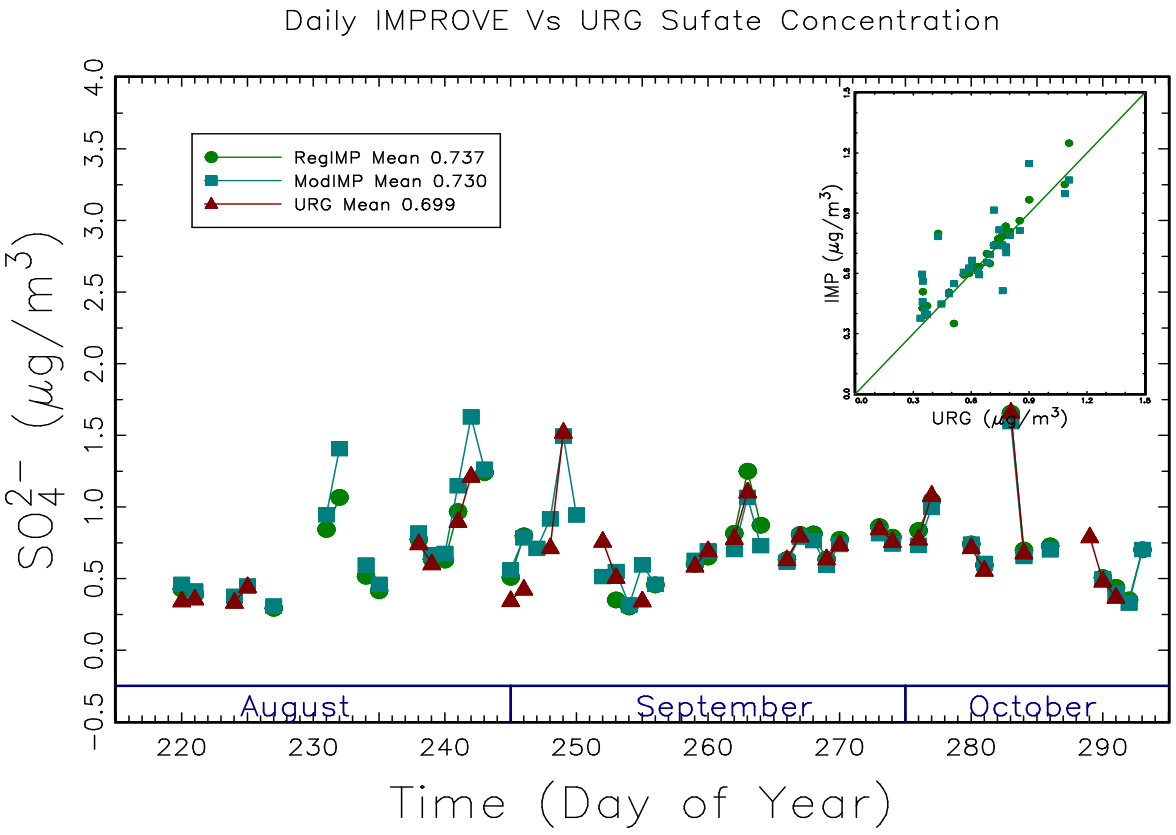

Figure 11.8. Comparisons of sulfate ion (SO_4^{2-}) concentrations from the regular IMPROVE (RegIMP), modified IMPROVE (ModIMP), and URG samplers during fall 2008. Mean sulfate ion concentrations (μg m^{-3}) for each sampler are reported.

A comparison of nitrate ion concentrations between the samplers shows results similar to that of sulfate ion comparisons. Nitrate ion concentrations from the two IMPROVE samplers were nearly identical, and they were both ~5% higher than nitrate ion concentrations obtained from the URG sampler. A timeline and scatter plot of nitrate ion concentrations from the three samplers are shown in Figure 11.9.

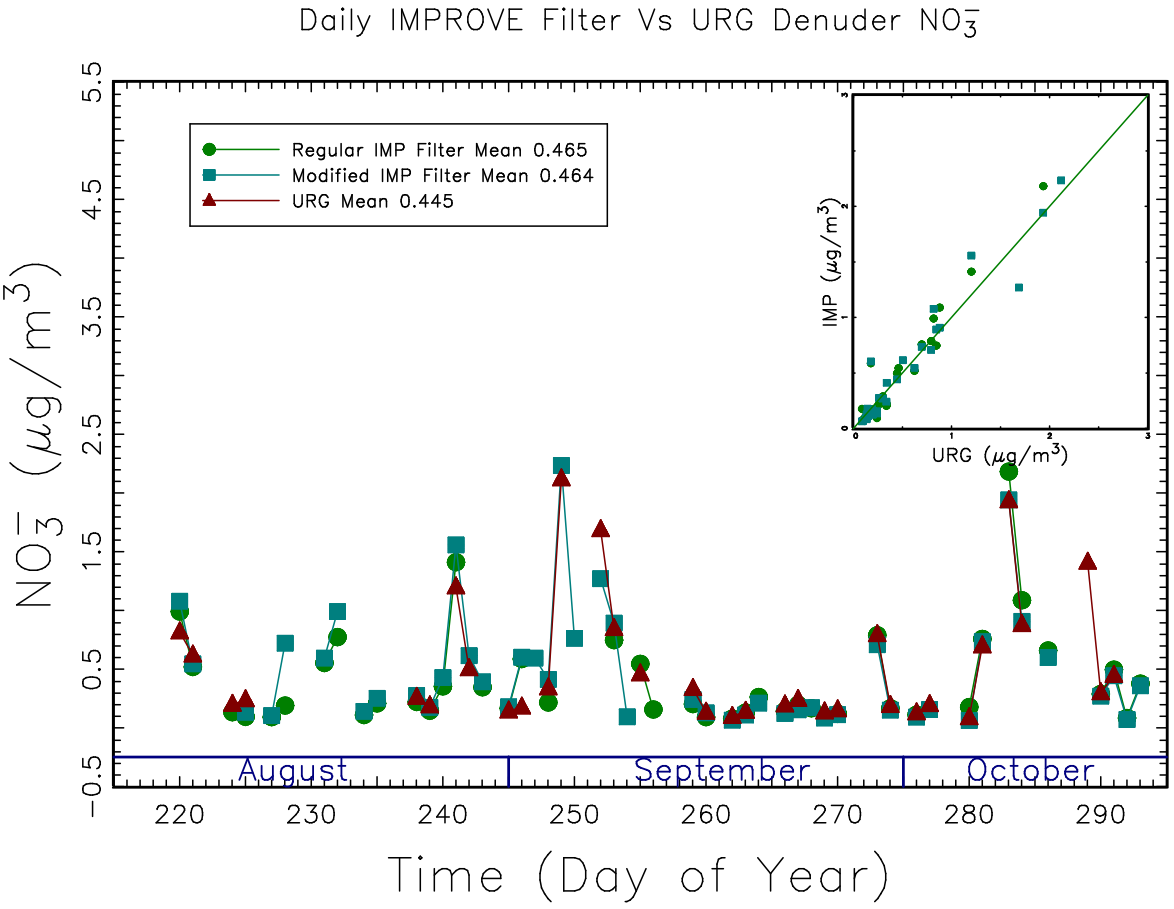

Figure 11.9. Comparisons of nitrate ion (NO_3^-) concentrations from the regular IMPROVE (RegIMP), modified IMPROVE (ModIMP), and URG samplers during fall 2008. Mean nitrate ion concentrations (µg m^{-3}) for each sampler are reported.

Concentrations of ammonium ion are shown below in Figure 11.10. As expected, the concentrations obtained from both of the IMPROVE samplers are lower than those from the URG sampler. Although NH_4NO_3 can be volatilized and NH_3 lost from the Nylasorb filters of both the IMPROVE and the URG samplers, the URG sampler captures the volatilized NH_3 with a backup denuder, thereby mitigating any bias from this dissociation. On average the ammonium ion concentrations were approximately 25–30% less from the IMPROVE sampler compared to the URG sampler. The loss of ammonium ion would of course vary with the concentration of NH_4NO_3, ambient temperature, and RH.

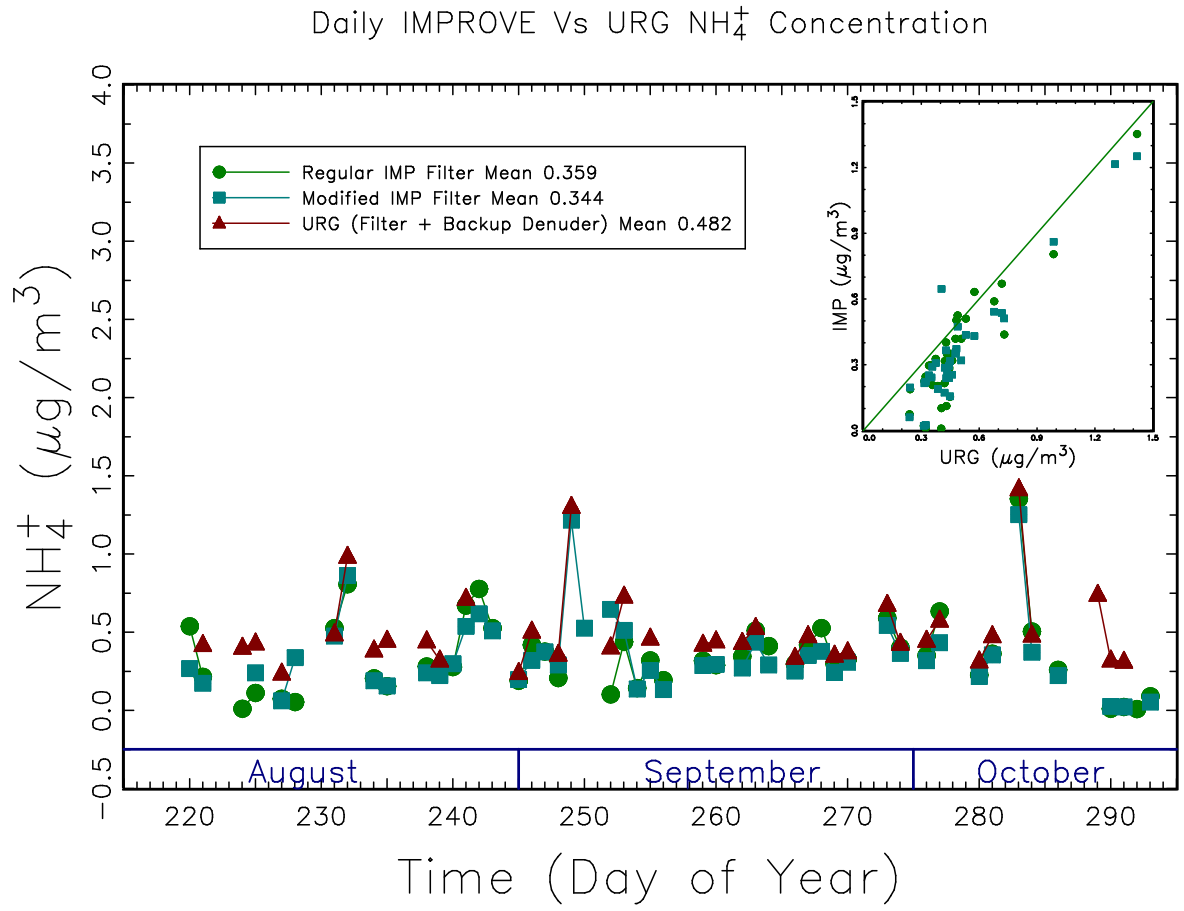

Figure 11.10. Comparisons of ammonium ion (NH_4^+) concentrations from the regular IMPROVE (Regular IMP), modified IMPROVE (Modified IMP), and URG samplers during fall 2008. Mean ammonium ion concentrations (μg m^{-3}) for each sampler are reported.

A comparison of ammonia concentrations from the URG and the modified IMPROVE samplers is shown below in Figure 11.11. The mean ammonia concentration from the IMPROVE sampler was 1.2 times higher than the mean ammonia concentration from the URG sampler. It is expected that concentrations from the IMPROVE sampler would be higher because the acid-impregnated cellulose filter is behind the nylon filter and would therefore collect the ammonia dissociated from ammonium nitrate volatilized from the nylon filter. Clearly, measurements with the IMPROVE sampler will result in some bias in the ammonia and ammonium ion concentrations. The dissociation of ammonium nitrate is the primary reason; however, other acid/base reactions can also occur on the filter to further complicate the interpretation.

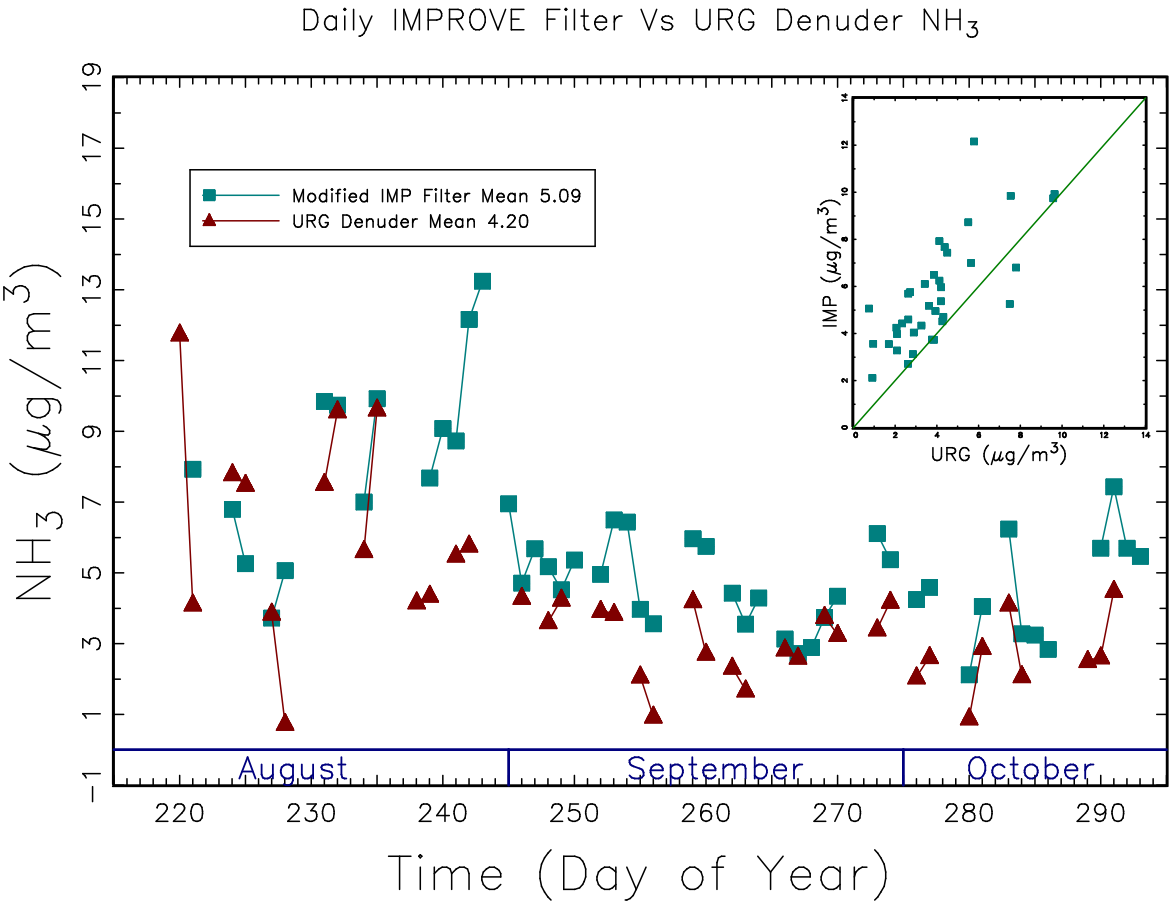

Figure 11.11. Comparisons of ammonia (NH_3) concentrations from the modified IMPROVE (Modified IMP) and URG samplers during fall 2008. Mean ammonia concentrations (µg m^{-3}) for each sampler are reported.

Because of these biases, a comparison of total reduced inorganic nitrogen ($NH_x = NH_3 + NH_4^+$) was also performed. Figure 11.12 shows a comparison of NH_x concentrations from the modified IMPROVE and URG samplers. The mean concentration from the IMPROVE sampler was 1.15 times higher than the mean concentration from the URG sampler. The bias was lower than when comparing NH_3 or NH_4^+ concentrations individually.

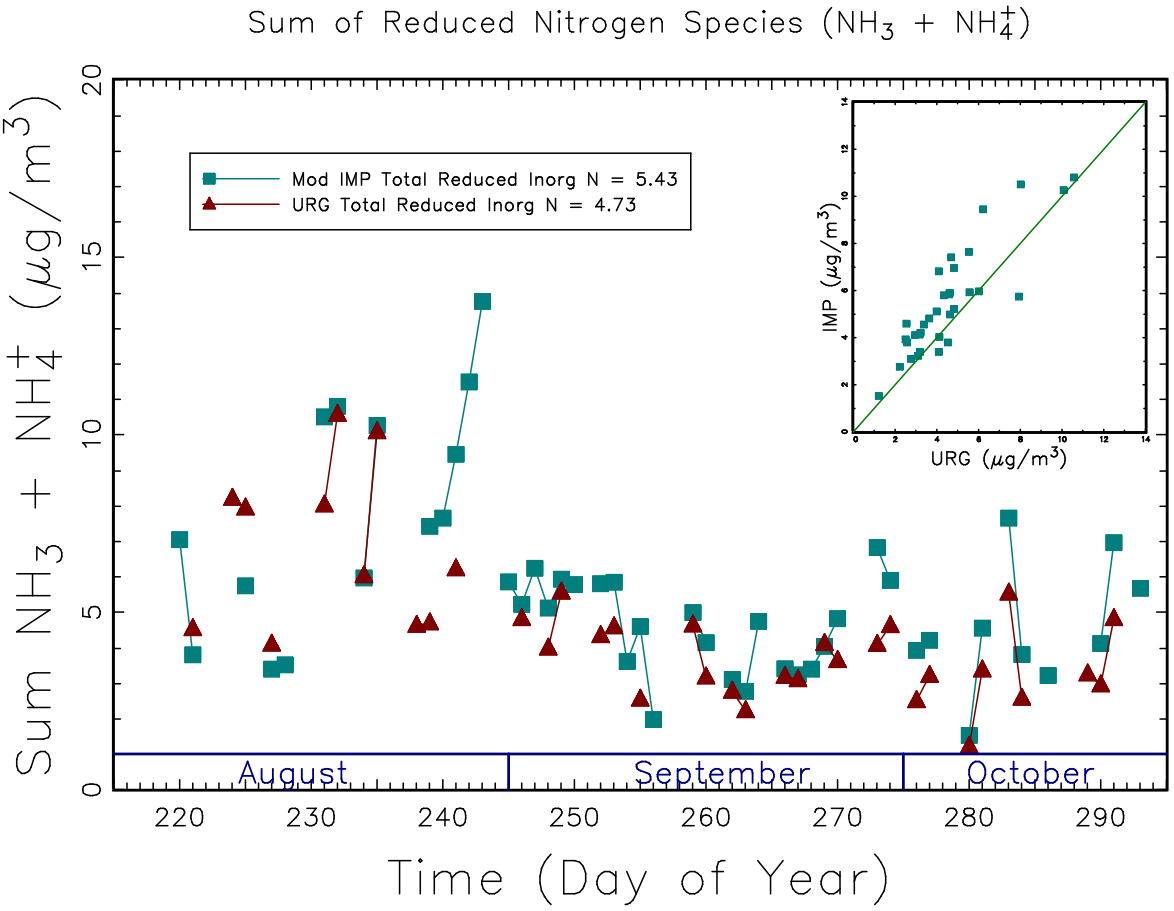

Figure 11.12. Comparisons of NH_x (NH_3 + NH_4^+) concentrations from the modified IMPROVE (Mod IMP) and URG samplers during fall 2008. Mean NH_x concentrations (µg m^{-3}) for each sampler are reported.

Further testing of the IMPROVE NH_x measurements revealed ammonia was coming off the nitric acid denuder. The denuder was removed, the inlet stack was cleaned, and another comparison was performed during spring 2010, using only the acid-impregnated cellulose fiber filter. The results of this comparison are shown in Figure 11.13. The comparison of total NH_x from the modified IMPROVE and URG samplers improved significantly.

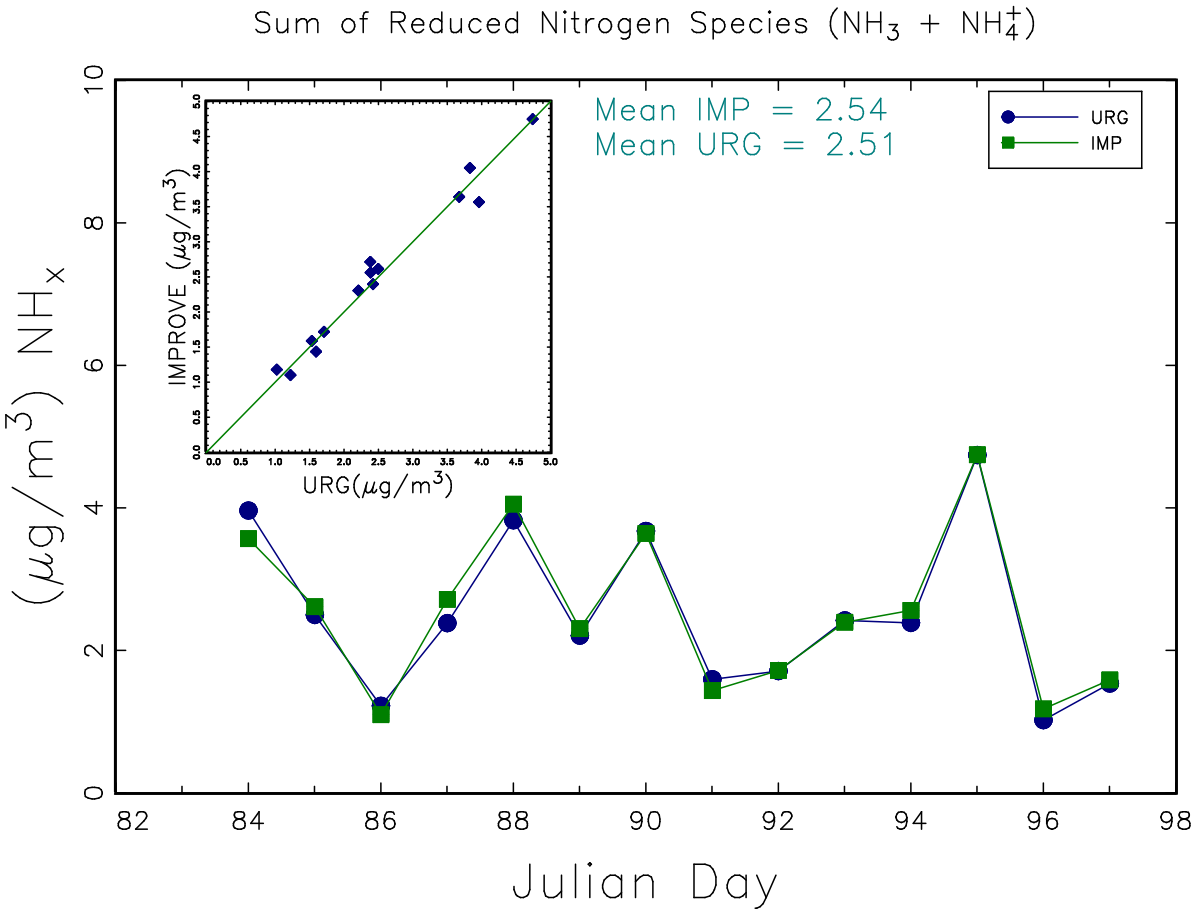

Figure 11.13. Comparisons of NH_x (NH_3 + NH_4^+) concentrations from the modified IMPROVE (IMP) and URG samplers during spring 2010. Mean NH_x concentrations (µg m^{-3}) for each sampler are reported.

11.3.2 CASTNET versus URG

Weekly samples from the URG and CASTNET samplers are compared in this section. Data from the regular and modified CASTNET samplers are compared to investigate if the addition of another filter for NH_3 collection had any impact on the measurements of other species.

Figure 11.14 shows a comparison of sulfate ion concentrations between the regular CASTNET, modified CASTNET, and URG samplers during fall 2008. Concentrations from the regular and modified CASTNET samplers agreed well and were within 3% difference on average. In general, the agreement between data from the URG and CASTNET samplers was within 10% difference on average; however, most of this difference was due to three data points (day of year 232, 239, and 267). Elevated values of Ca, Mg, and NO_3 were also observed for these time periods; thus, it seems possible this discrepancy is due to dust, which would contribute coarse material to the CASTNET sampler but not the URG sampler because of the 2.5 µm size-selective cyclone.

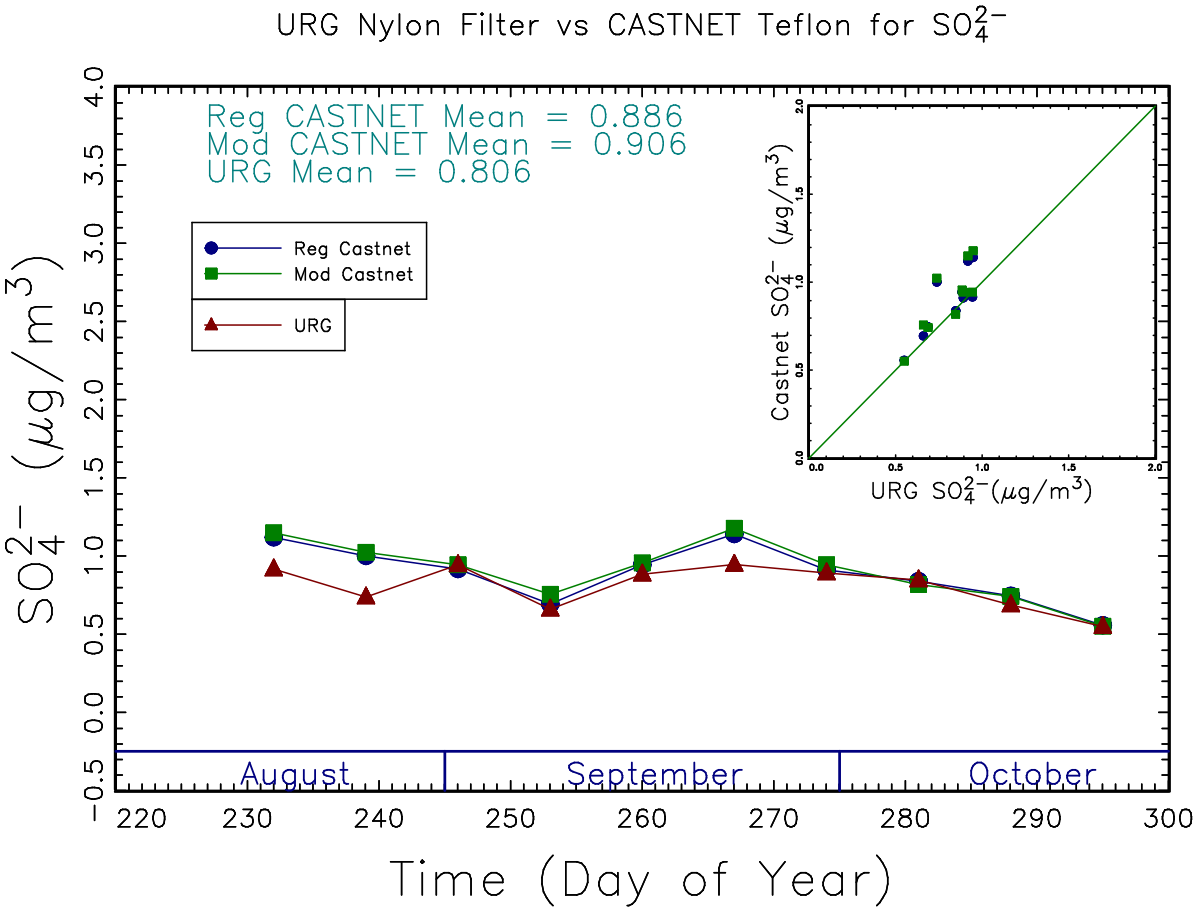

Figure 11.14. Comparisons of sulfate ion (SO_4^{2-}) concentrations from the modified CASTNET (Mod CASTNET), regular CASTNET (Reg CASTNET), and URG samplers during fall 2008. Mean sulfate ion concentrations (µg m^{-3}) for each sampler are reported.

Particulate nitrate ion concentrations are shown in Figure 11.15 for fall 2008 weekly samples. Mean concentrations from the modified and regular CASTNET samplers agreed to within ~2% but were approximately 30% higher than concentrations from the URG sampler. As previously discussed, this could be the result of coarse aerosol particles being sampled by the CASTNET sampler and not the URG sampler (see day of year 232, 239, and 267).

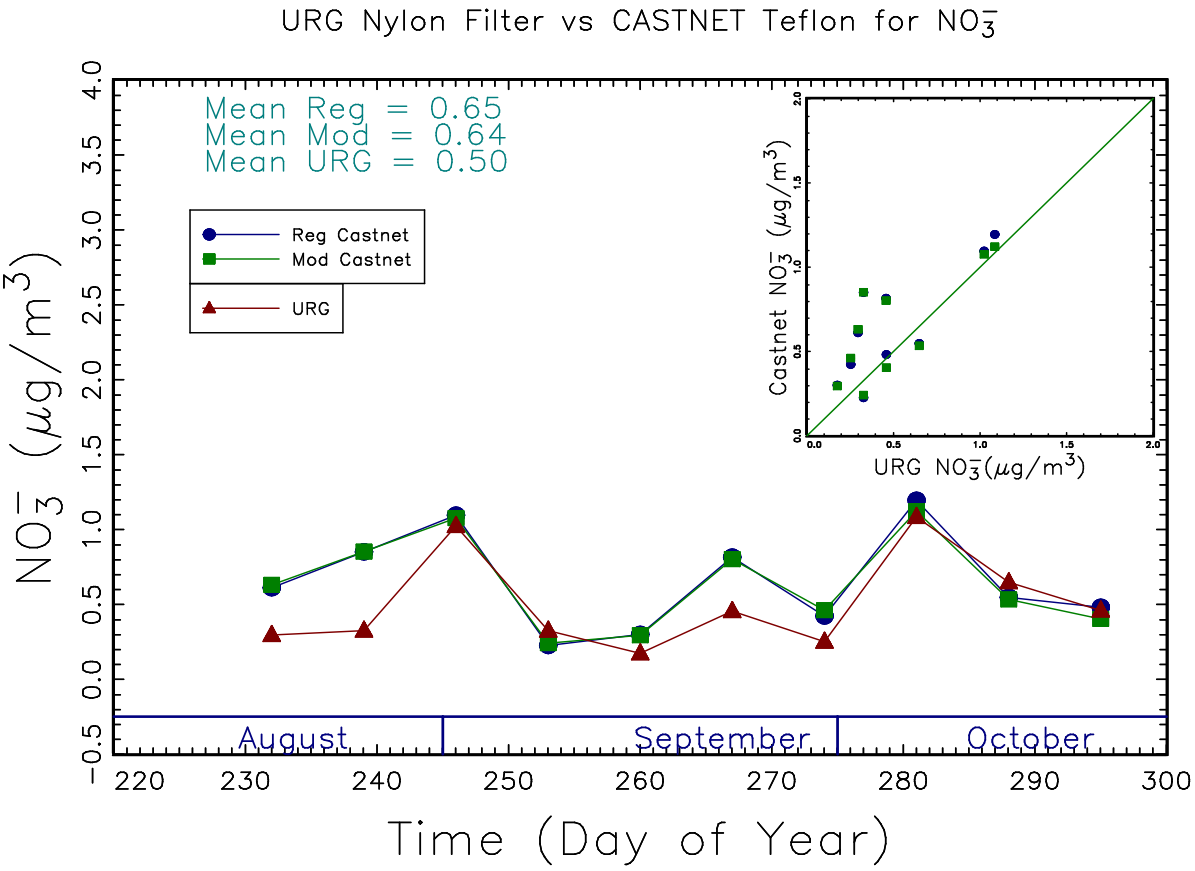

Figure 11.15. Comparisons of nitrate ion (NO_3^-) concentrations from the modified CASTNET (Mod CASTNET), regular CASTNET (Reg CASTNET), and URG samplers during fall 2008. Mean nitrate ion concentrations (µg m^{-3}) for each sampler are reported.

Figures 11.16 and 11.17 show nitric acid (HNO_3) concentrations and total oxidized nitrogen (NO_3^- + HNO_3) concentrations, respectively, from the two CASTNET and the URG samplers. Concentrations of both nitric acid and total oxidized nitrogen from the CASTNET samplers agree to within a few percent; however, they are about 30% higher than concentrations from the URG sampler.

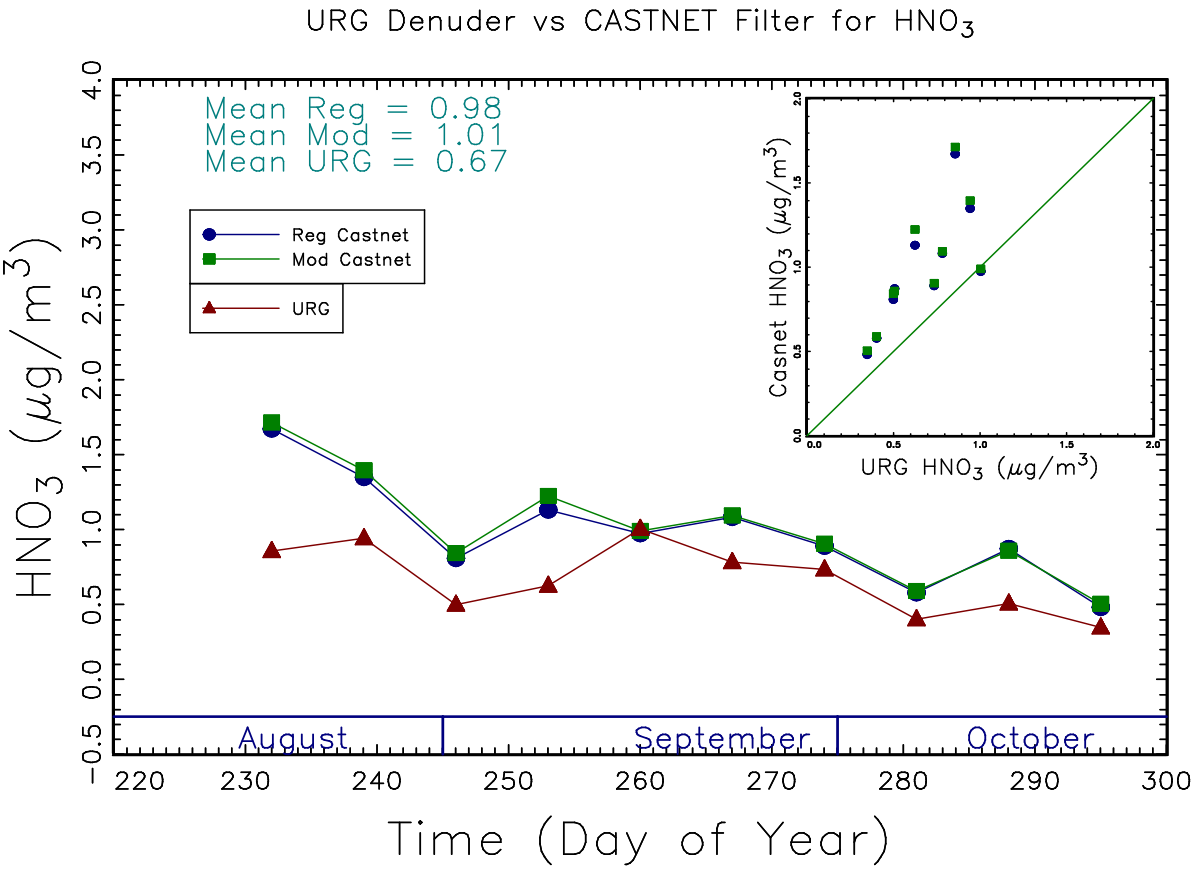

Figure 11.16. Comparisons of nitric acid (HNO_3) concentrations from the modified CASTNET (Mod CASTNET), regular CASTNET (Reg CASTNET), and URG samplers during fall 2008. Mean nitric acid concentrations (µg m^{-3}) for each sampler are reported.

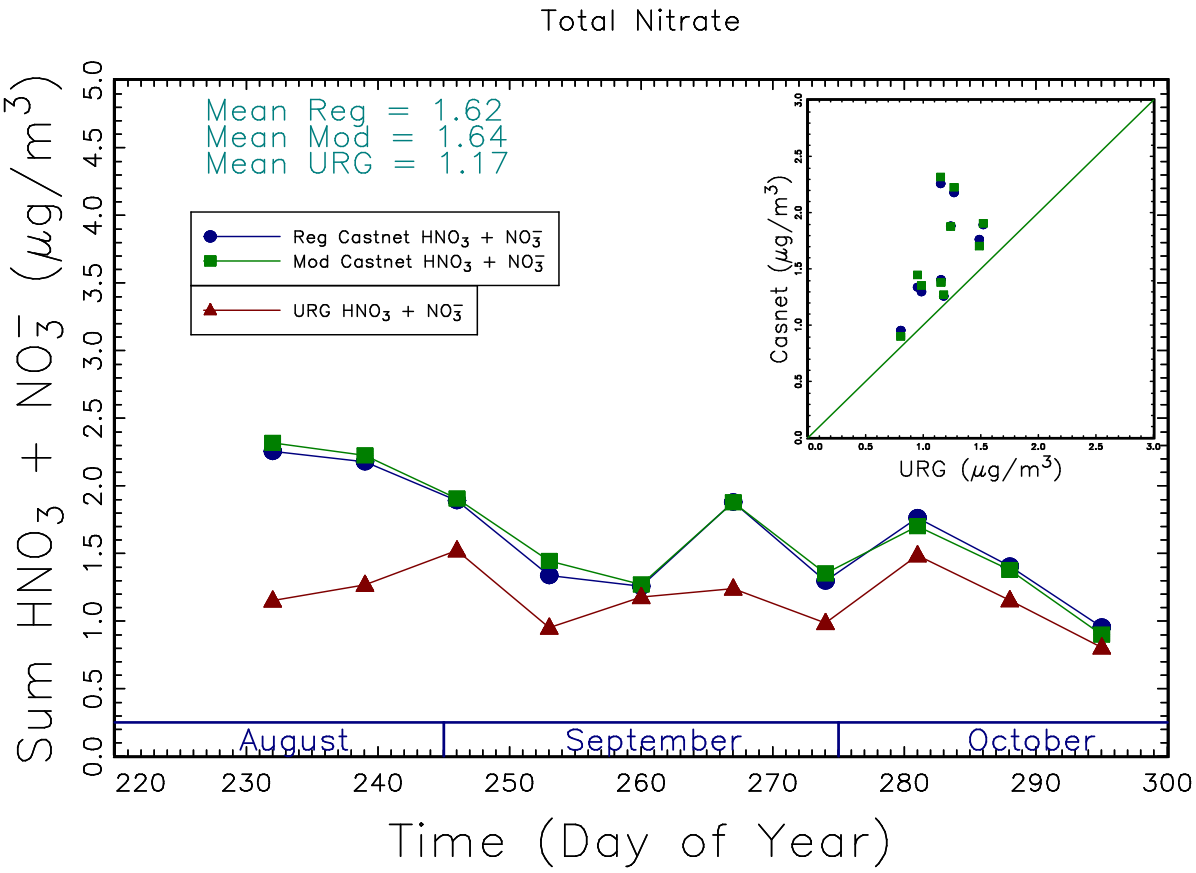

Figure 11.17. Comparisons of total oxidized nitrogen concentrations (NO_3^- + HNO_3) from the modified CASTNET (Mod CASTNET), regular CASTNET (Reg CASTNET), and URG samplers during fall 2008. Total oxidized nitrogen concentrations (µg m^{-3}) for each sampler are reported.

A comparison of particulate ammonium ion concentrations is shown in Figure 11.18 Concentrations from the two CASTNET samplers agreed to within 7% on average. Concentrations from the URG sampler were about 30% higher than the average of the CASTNET samplers. This result is not surprising because there is volatilization of NH_4NO_3 from the filters as equilibrium conditions vary over the week-long sample collection period. The ammonia volatilized from the URG filter is subsequently captured by the backup NH_3 denuder and added back to the concentration of particle NH_4^+; however, the ammonium lost from the CASTNET filter is collected by the backup NH_3 filter and reported as NH_3 gas. The CASTNET sampling system thus shows a negative bias for ammonium ion concentrations.

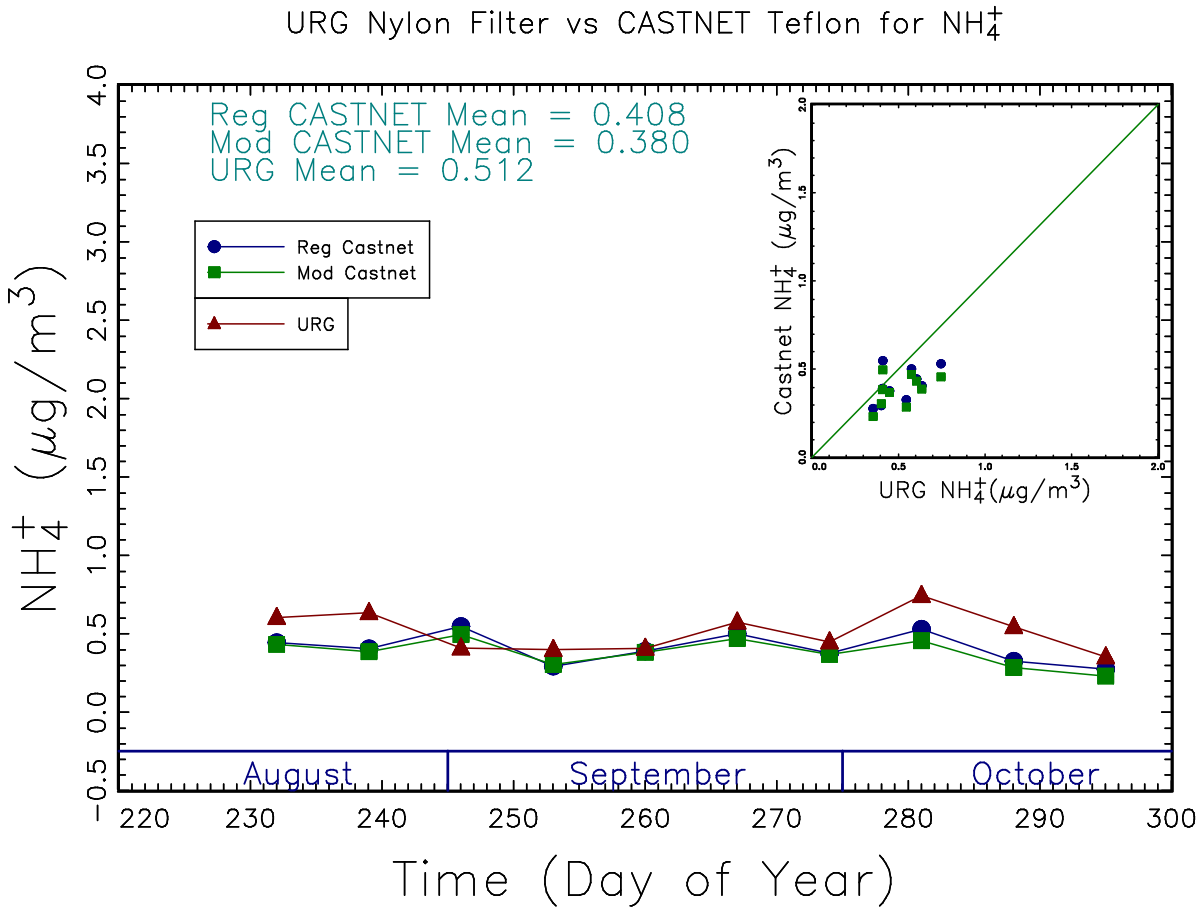

Figure 11.18. Comparisons of ammonium ion (NH_4^+) concentrations from the modified CASTNET (Mod CASTNET), regular CASTNET (Reg CASTNET), and URG samplers during fall 2008. Ammonium concentrations (µg m^{-3}) for each sampler are reported.

Figures 11.19 and 11.20 show ammonia and NH_x concentrations, respectively. As expected, the CASTNET ammonia concentrations are higher (by about 9%) than the URG ammonia concentrations, in part due to the captured NH_3 volatilized from the filter. The NH_x concentrations are expected to be the same, and, indeed, the concentrations from the CASTNET sampler are only about 5–6% higher than the concentrations from the URG sampler. This is well within the estimated uncertainty for these measurements.

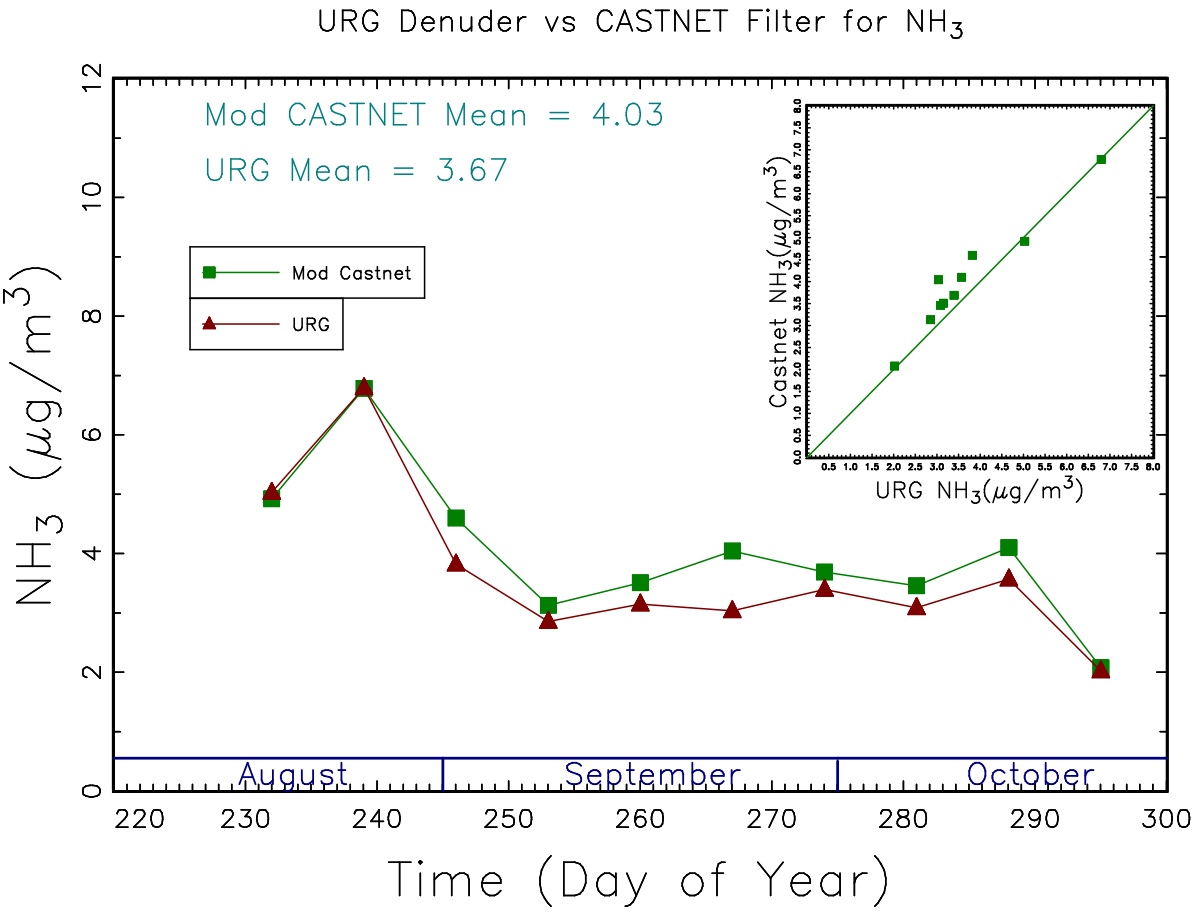

Figure 11.19. Comparisons of ammonia (NH_3) concentrations from the modified CASTNET (Mod CASTNET), and URG samplers during fall 2008. Ammonia concentrations (µg m^{-3}) for each sampler are reported.

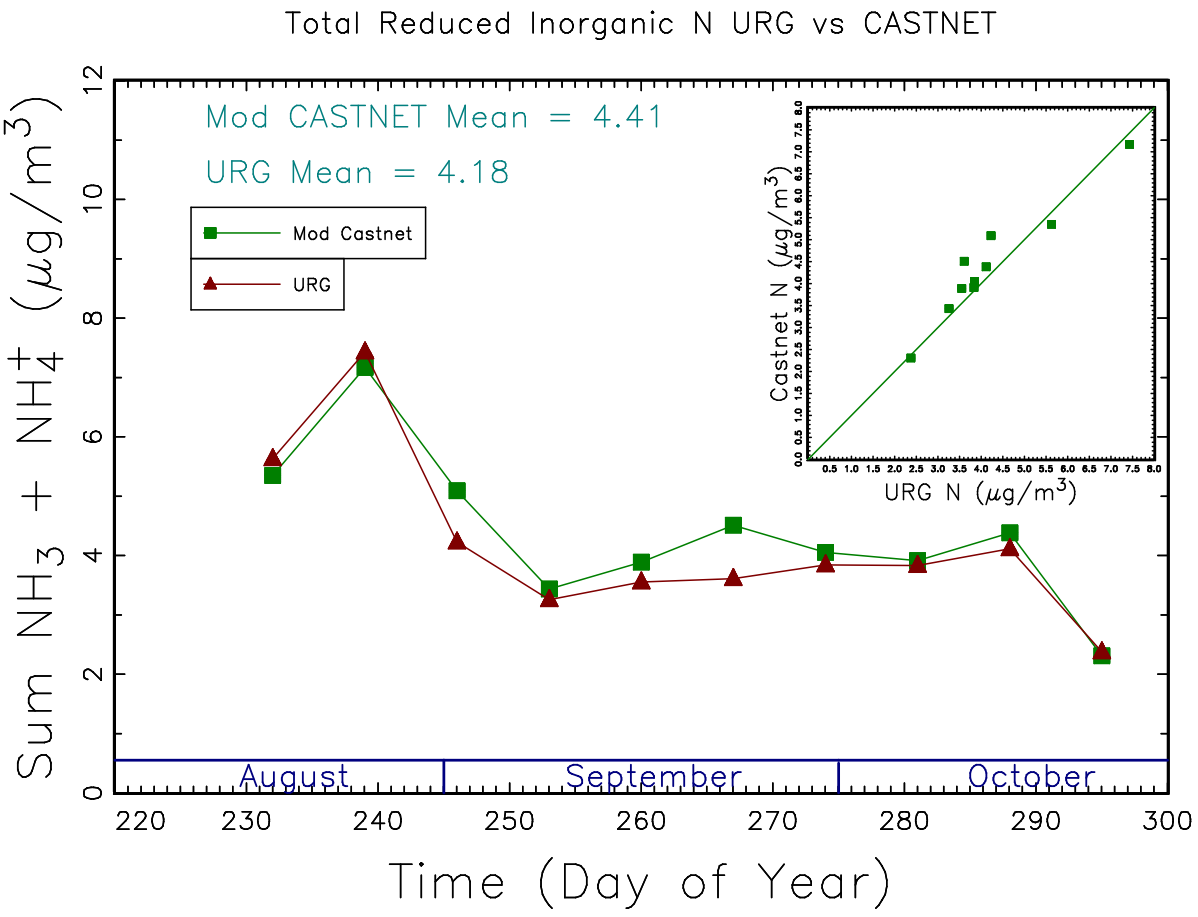

Figure 11.20. Comparisons of total reduced inorganic nitrogen ($NH_x = NH_3 + NH_4^+$) concentrations from the modified CASTNET (Mod CASTNET) and URG samplers for 2008. NH_x (µg m^{-3}) for each sampler are reported.

11.3.3 Ammonia Comparisons from CASTNET, Passive, and URG Samplers

Figure 11.21 shows the comparison of ammonia concentrations from 2-week samples from the Radiello and Ogawa passive samplers during 2008. In addition, weekly samples from the CASTNET and the URG samplers during fall months are also shown. In general, the concentration of NH_3 obtained from all the samplers is in good agreement.

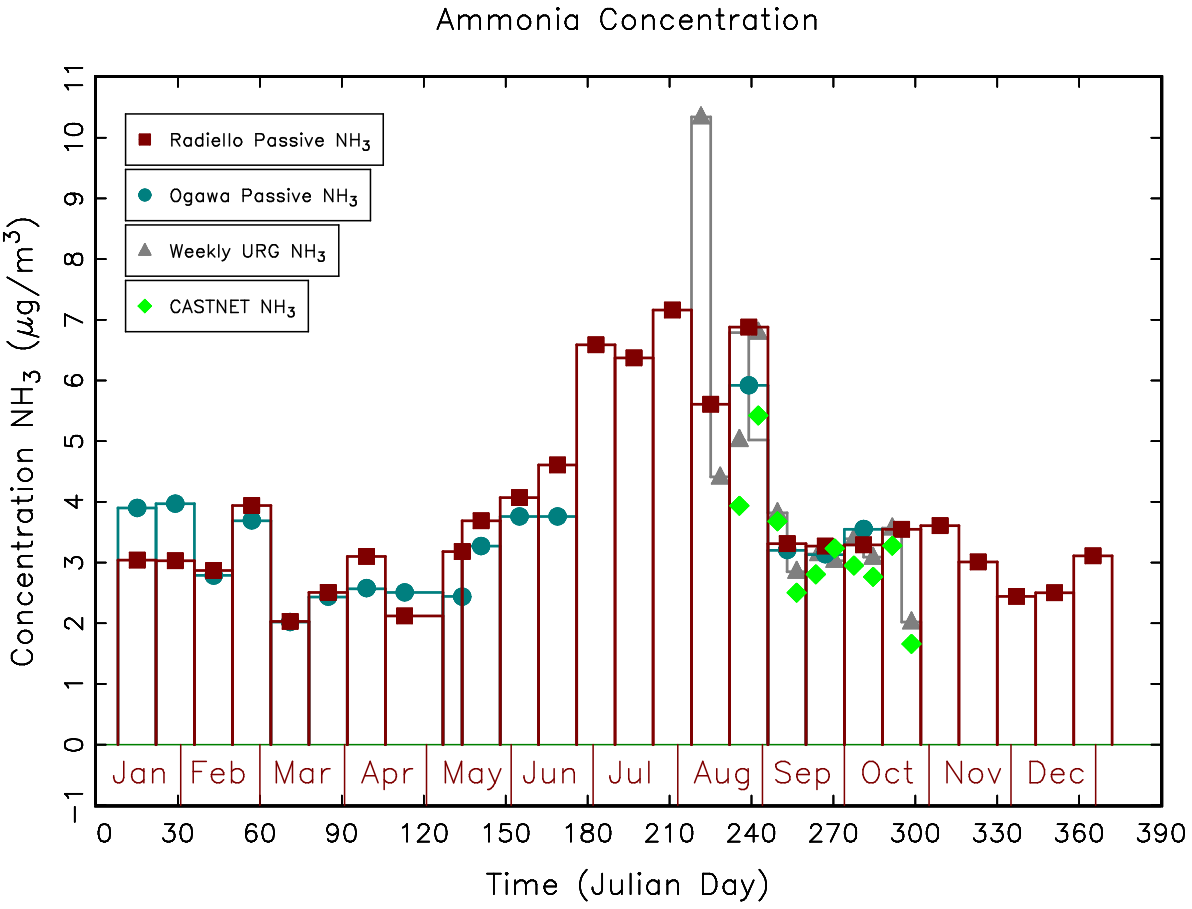

Figure 11.21. Comparison of weekly ammonia (NH_3) concentrations (µg m^{-3}) from URG and CASTNET samplers and 2-week concentrations from the Radiello and Ogawa passive samplers during 2008.

11.4 SUMMARY

The NH_x system plays an important role in atmospheric chemistry, contributing to particle formation and reactive nitrogen deposition. To measure the NH_x system, the IMPROVE and CASTNET samplers have been modified by the addition of an acid-impregnated cellulose fiber filter. Comparisons of concentrations from these modified samplers to data from the URG sampler show agreement within the estimated uncertainty of the samplers, except where known biases are present. These results suggest that modifications to the IMPROVE and CASTNET samplers do not appear to significantly alter the concentration of other species measured by each sampler, which is an important consideration because maintaining consistency with the historical dataset of each sampling network is of critical importance. As observed in this and other

datasets, the sampling of ammonia gas and ammonium ion concentrations using acid-impregnated filters is subject to artifacts. The most significant artifact comes from the dissociation of ammonium nitrate from the Nylasorb filter. This artifact decreases the concentration of ammonium ion and increases the concentration of gaseous ammonia measured.

Because of these biases, we found closer agreement in NH_x concentrations between the URG and IMPROVE or CASTNET samplers. A reasonable approximation of the ammonia and ammonium concentrations could be derived by a simple charge balance calculation. Assuming species concentration in moles and fully neutralized ammonium sulfate and that ammonium ion is the only cation of consequence, the concentrations of NH_3 and NH_4^+ can be approximated from the following equations:

$$2[SO_4^{2-}] + [NO_3^-] = [NH_4^+] \quad 11.3$$

$$[NH_3] = [NH_x] - [NH_4^+] \quad 11.4$$

The concentrations of ammonia measured either with the passive samplers or the CASTNET sampler have been shown to be comparable to the field standard URG sampler. These multiday integrated samples, while acceptable for seasonal and temporal information, are not adequate for source apportionment analyses, which the IMPROVE sampling system, operating for 24 hours every third day, is better suited to address.

ACKNOWLEDGEMENTS

The work of Katie Beam and Misha Schurman from the Atmospheric Chemistry group at Colorado State University is acknowledged and appreciated.

REFERENCES

Lee, T., S. M. Kreidenweis, and J. L. Collett, Jr. (2004), Aerosol ion characteristics during the Big Bend Regional Aerosol and Visibility Observational Study, *J. Air Waste Manage. Assoc., 54*, 585-592, May.

Malm, W. C., J. F. Sisler, D. Huffman, R. A. Eldred, and T. A. Cahill (1994), Spatial and seasonal trends in particle concentration and optical extinction in the United States, *J. Geophys. Res., 99(D1),* 1347-1370.

Yu, X.-Y., T. Lee, B. Ayres, S. M. Kreidenweis, W. C. Malm, J. L. Collett, Jr. (2006), Loss of fine particle ammonium from denuded nylon filters, *Atmos. Environ., 40*, 4797-4807.

Chapter 12. IMPROVE Measurements Bibliography

Compiled by John G. Watson

Ames, R. B., J. L. Hand, S. M. Kreidenweis, D. E. Day, and W. C. Malm (2000), Optical measurements of aerosol size distributions in Great Smoky Mountains National Park: Dry aerosol characterization, *J. Air Waste Manage. Assoc.*, *50*, 665-676.

Ames, R. B. and W. C. Malm (2001), Chemical species' contributions to the upper extremes of aerosol fine mass, *Atmos. Environ.*, *35*, 5193-5204.

Ames, R. B. and W. C. Malm (2001), Comparison of sulfate and nitrate particle mass concentrations measured by IMPROVE and the CDN, *Atmos. Environ.*, *35*, 905-916.

Andrews, E., P. Saxena, S. Musarra, L. M. Hildemann, P. Koutrakis, P. H. McMurry, I. Olmez, and W. H. White (2000), Concentration and composition of atmospheric aerosols from the 1995 SEAVS Experiment and a review of the closure between chemical and gravimetric measurements, *J. Air Waste Manage. Assoc.*, *50*, 648-664.

Andronache, C. (2004), Estimates of sulfate aerosol wet scavenging coefficient for locations in the Eastern United States, *Atmos. Environ.*, *38*, 795-804.

Ashbaugh, L. L., C. E. McDade, W. H. White, P. Wakabayashi, J. L. Collett, Jr., and Y. Xiao-Ying (2004), Efficiency of IMPROVE network denuders for removing nitric acid, in *Proceedings, Regional and Global Perspectives on Haze: Causes, Consequences and Controversies*, Air & Waste Management Association, Pittsburgh, 32-1-32-8.

Ashbaugh, L. L. and R. A. Eldred (2004), Loss of particle nitrate from Teflon sampling filters: Effects on measured gravimetric mass in California and in the IMPROVE Network, *J. Air Waste Manage. Assoc.*, *54*, 93-104.

Bahadur, R., Y. Feng, L. M. Russell, and V. Ramanathan (2011), Impact of California's air pollution laws on black carbon and their implications for direct radiative forcing, *Atmos. Environ.*, *45*, 1162-1167.

Barna, M. G. and E. M. Knipping (2006), Insights from the BRAVO study on nesting global models to specify boundary conditions in regional air quality modeling simulations, *Atmos. Environ.*, *40*, S574-S582.

Barna, M. G., K. A. Gebhart, B. A. Schichtel, and W. C. Malm (2006), Modeling regional sulfate during the BRAVO study: Part 1. Base emissions simulation and performance evaluation, *Atmos. Environ.*, *40*, 2436-2448.

Barna, M. G., B. A. Schichtel, K. A. Gebhart, and W. C. Malm (2006), Modeling regional sulfate during the BRAVO study: Part 2. Emission sensitivity simulations and source apportionment, *Atmos. Environ.*, *40*, 2423-2435.

Begum, B. A., P. K. Hopke, and W. X. Zhao (2005), Source identification of fine particles in Washington, DC, by expanded factor analysis modeling, *Environ. Sci. Technol.*, *39*, 1129-1137.

Bench, G. (2004), Measurement of contemporary and fossil carbon contents of PM2.5 aerosols: Results from Turtleback Dome, Yosemite National Park, *Environ. Sci. Technol.*, *38*, 2424-2427.

Bench, G., S. Fallon, B. Schichtel, W. C. Malm, and C. McDade (2007), Relative contributions of fossil and contemporary carbon sources to PM2.5 aerosols at nine Interagency Monitoring for Protection of Visual Environments (IMPROVE) network sites, *J. Geophys. Res. -Atmospheres*, *112*, (D10).

Brewer, P. F. and J. P. Adloch (2005) Trends in speciated fine particulate matter and visibility across monitoring networks in the southeastern United States, *J. Air & Waste Manage. Assoc., 55,* 1663-1674.

Brewer, P. and T. Moore (2009), Source contributions to visibility impairment in the southeastern and western United States, *J. Air Waste Manage. Assoc.*, *59*, 1070-1081.

Brown, S. G., P. Herckes, L. L. Ashbaugh, M. P. Hannigan, S. M. Kreidenweis, and J. L. Collett, Jr. (2002), Characterization of organic aerosol in Big Bend National Park, Texas, *Atmos. Environ.*, *36*, 5807-5818.

Brown, S. G., A. Frankel, S. M. Raffuse, P. T. Roberts, H. R. Hafner, and D. J. Anderson (2007), Source apportionment of fine particulate matter in Phoenix, AZ, using positive matrix factorization, *J. Air Waste Manage. Assoc.*, *57*, 741-752.

Buzcu-Guven, B., S. G. Brown, A. Frankel, H. R. Hafner, and P. T. Roberts (2007), Analysis and apportionment of organic carbon and fine particulate matter sources at multiple sites in the Midwestern United States, *J. Air Waste Manage. Assoc.*, *57*, 606-619.

Cahill, T. A., R. A. Eldred, N. Motallebi, and W. C. Malm (1989), Indirect measurement of hydrocarbon aerosols across the United States by non-sulfate hydrogen-remaining gravimetric mass correlations, *Aerosol Sci. Technol.*, *10*, 421-429.

Cahill, T. A., P. H. Wakabayashi, and T. A. James (1996), Chemical states of sulfate at Shenandoah National Park during summer, 1991, *Nuclear Instruments and Methods in Physics Research*, *109/110*, 542-547.

Campbell, D. E., S. Copeland, and T. A. Cahill (1995), Measurement of aerosol absorption coefficient from Teflon filters using integrating plate and integrating sphere techniques, *Aerosol Sci. Technol.*, *22*, 287-292.

Carrico, C. M., S. M. Kreidenweis, W. C. Malm, D. E. Day, T. Lee, J. Carrillo, G. R. McMeeking, and J. L. Collett, Jr. (2005), Hygroscopic growth behavior of a carbon-dominated aerosol in Yosemite National Park, *Atmos. Environ.*, *39*, 1393-1404.

Castaneda, C. M., L. L. Ashbaugh, and P. Wakabayashi (2010), Use of proton backscattering to determine the carbon and oxygen content in fine particle samples deposited on PTFE((CF2)(n)) membrane disk filters, *J. Aerosol Sci.*, *41*, 99-107.

Chen, L.-W. A., B. G. Doddridge, J. C. Chow, R. R. Dickerson, W. F. Ryan, and P. K. Mueller (2003), Analysis of summertime $PM_{2.5}$ and haze episode in the mid-Atlantic region, *J. Air Waste Manage. Assoc.*, *53*, 946-956.

Chen, L.-W. A., J. G. Watson, J. C. Chow, D. W. DuBois, and L. Herschberger (2010), Chemical mass balance source apportionment for combined PM2.5 measurements from U.S. non-urban and urban long-term networks, *Atmos. Environ.*, *44*, 4908-4918.

Cheng, M. D. and R. L. Tanner (2002), Characterization of ultrafine and fine particles at a site near the Great Smoky Mountains National Park, *Atmos. Environ.*, *36*, 5795-5806.

Chin, M., T. Diehl, P. Ginoux, and W. C. Malm (2007), Intercontinental transport of pollution and dust aerosols: Implications for regional air quality, *Atmos. Chem. Phys.*, *7*, 5501-5517.

Chow, J. C., J. G. Watson, D. Crow, D. H. Lowenthal, and T. M. Merrifield (2001), Comparison of IMPROVE and NIOSH carbon measurements, *Aerosol Sci. Technol.*, *34*, 23-34.

Chow, J. C., J. D. Bachmann, S. S. G. Wierman, C. V. Mathai, W. C. Malm, W. H. White, P. K. Mueller, N. K. Kumar, and J. G. Watson (2002), 2002 Critical review discussion - Visibility: Science and regulation, *J. Air Waste Manage. Assoc.*, *52*, 973-999.

Chow, J. C. and J. G. Watson (2002), $PM_{2.5}$ carbonate concentrations at regionally representative Interagency Monitoring of Protected Visual Environment sites, *J. Geophys. Res. - Atmospheres*, *107*, ICC 6-1-ICC 6-9.

Chow, J. C., J. G. Watson, L.-W. A. Chen, W. P. Arnott, H. Moosmüller, and K. K. Fung (2004), Equivalence of elemental carbon by Thermal/Optical Reflectance and Transmittance with different temperature protocols, *Environ. Sci. Technol.*, *38*, 4414-4422.

Chow, J. C., J. G. Watson, L.-W. A. Chen, G. Paredes-Miranda, M.-C. O. Chang, D. Trimble, K. K. Fung, H. Zhang, and J. Z. Yu (2005), Refining temperature measures in thermal/optical carbon analysis, *Atmos. Chem. Phys.*, *5*, 2961-2972.

Chow, J. C., J. G. Watson, L.-W. A. Chen, M. C. O. Chang, N. F. Robinson, D. Trimble, and S. D. Kohl (2007), The IMPROVE_A temperature protocol for thermal/optical carbon analysis: Maintaining consistency with a long-term database, *J. Air Waste Manage. Assoc.*, *57*, 1014-1023.

Chow, J. C., J. G. Watson, M. C. Green, and N. H. Frank (2010), Filter light attenuation as a surrogate for elemental carbon, *J. Air Waste Manage. Assoc.*, *60*, 1365-1375.

Chow, J. C., J. G. Watson, L. W. A. Chen, J. Rice, and N. H. Frank (2010), Quantification of PM2.5 organic carbon sampling artifacts in US networks, *Atmos. Chem. Phys.*, *10*, 5223-5239.

Chow, J. C., J. G. Watson, J. Robles, X. L. Wang, L.-W. A. Chen, D. L. Trimble, S. D. Kohl, R. J. Tropp, and K. K. Fung (2011), Quality control and quality assurance for thermal/optical analysis of aerosol samples for organic and elemental carbon, *Analytical and Bioanalytical Chemistry*, submitted.

Christopher, S. A., P. Gupta, U. Nair, T. A. Jones, S. Kondragunta, Y.-L. Wu, J. Hand, and X. Zhang (2009), Satellite remote sensing and mesoscale modeling of the 2007 Georgia/Florida fires, *IEEE J. Selected Topics in Applied Earth Obs. Remote. Sens., 2(3),* doi:10.1109/JSTARS.2009.2026626, 163-175.

Chueinta, W., P. K. Hopke, and P. Paatero (2004), Multilinear model for spatial pattern analysis of the measurement of haze and visual effects project, *Environ. Sci. Technol.*, *38*, 544-554.

Copeland, S. A. (2005), A statistical analysis of visibility-impairing particles in federal Class I areas, *J. Air & Waste Manage. Assoc., 55,* 1621-1635.

Coury, C. and A. M. Dillner (2007), Trends and sources of particulate matter in the Superstition Wilderness using air trajectory and aerosol cluster analysis, *Atmos. Environ.*, *41*, 9309-9323.

Coury, C. and A. M. Dillner (2009), ATR-FTIR characterization of organic functional groups and inorganic ions in ambient aerosols at a rural site, *Atmos. Environ.*, *43*, 940-948.

Davis, R. E. and D. A. Gay (1993), A synoptic climatological analysis of air quality in the Grand Canyon National Park, *Atmos. Environ.*, *27A*, 713-727.

Davis, R. E. and D. A. Gay (1995), Response to "Comments on 'A synoptic climatological analysis of air quality in the Grand Canyon National Park', *Atmos. Environ.*, *29*, 619-625.

Davis, R. E. and D. A. Gay (1995), Response to "Second Response to Comments on 'A synoptic climatological analysis of air quality in the Grand Canyon National Park', *Atmos. Environ.*, *29*, 632-639.

Day, D. E., W. C. Malm, and S. M. Kreidenweis (1997), Seasonal variations in aerosol composition and acidity at Shenandoah and Great Smoky Mountains National Parks, *J. Air Waste Manage. Assoc.*, *47*, 411-418.

Day, D. E., W. C. Malm, and S. M. Kreidenweis (2000), Aerosol light scattering measurements as a function of relative humidity, *J. Air Waste Manage. Assoc.*, *50*, 710-716.

Day, D. E. and W. C. Malm (2001), Aerosol light scattering measurements as a function of relative humidity: A comparison between measurements made at three different sites, *Atmos. Environ.*, *35*, 5169-5176.

Dillner, A. M., C. H. Phuah, and J. R. Turner (2009), Effects of post-sampling conditions on ambient carbon aerosol filter measurements, *Atmos. Environ.*, *43*, 5937-5943.

Dilmaghani, S., I. C. Henry, P. Soonthornnonda, E. R. Christensen, and R. C. Henry (2007), Harmonic analysis of environmental time series with missing data or irregular sample spacing, *Environ. Sci. Technol.*, *41*, 7030-7038.

Draxler, R. R., P. Ginoux, and A. F. Stein (2010), An empirically derived emission algorithm for wind-blown dust, *J. Geophys. Res., 115*, D16212, doi:10.1029/2009JD013167.

Drury, E., D. J. Jacob, R. J. D. Spurr, J. Wang, Y. Shinozuka, B. E. Anderson, A. D. Clarke, J. Dibb, C. McNaughton, and R. Weber (2010), Synthesis of satellite (MODIS), aircraft (ICARTT), and surface (IMPROVE, EPA-AQS, AERONET) aerosol observations over eastern North America to improve MODIS aerosol retrievals and constrain surface aerosol concentrations and sources, *J. Geophys. Res, 115*, D14204, doi:10.1029/2009JD012629.

Eatough, D. J., L. J. Lewis, M. Eatough, and E. A. Lewis (1995), Sampling artifacts in the determination of particulate sulfate and SO2(g) in the desert southwest using filter pack samplers, *Environ. Sci. Technol.*, *29*, 787-791.

Eatough, D. J., M. C. Green, W. Moran, and R. Farber (2001), Potential particulate impacts at the Grand Canyon from northwestern Mexico, *Sci. Total Environ.*, *276*, 69-82.

Eatough, D. J., W. X. Cui, J. Hull, and R. J. Farber (2006), Fine particulate chemical composition and light extinction at Meadview, AZ, *J. Air Waste Manage. Assoc.*, *56*, 1694-1706.

El Zanan, H. S., D. H. Lowenthal, B. Zielinska, J. C. Chow, and N. K. Kumar (2005), Determination of the organic aerosol mass to organic carbon ratio in IMPROVE samples, *Chemosphere*, *60*, 485-496.

Eldred, R. A., T. A. Cahill, M. L. Pitchford, and W. C. Malm (1988), IMPROVE - A new remote area particulate monitoring system for visibility studies, in *Proceedings, 81st Annual Meeting of the Air Pollution Control Association*, Air & Waste Management Association, Pittsburgh.

Eldred, R. A., T. A. Cahill, L. K. Wilkinson, P. J. Feeney, J. C. Chow, and W. C. Malm (1990), Measurement of fine particles and their chemical components in the NPS/IMPROVE Networks, in *Transactions, Visibility and Fine Particles*, Mathai, C. V., editor, Air & Waste Management Association, Pittsburgh, 187-196.

Eldred, R. A. and T. A. Cahill (1994), Trends in elemental concentrations of fine particulates at remote sites in the United States of America, *Atmos. Environ.*, *28*, 1009-1019.

Eldred, R. A. (1997), Comparison of selenium and sulfur at remote sites throughout the United States, *J. Air Waste Manage. Assoc.*, *47*, 204-211.

Eldred, R. A., T. A. Cahill, and R. G. Flocchini (1997), Composition of PM(2.5) and PM(10) aerosols in the IMPROVE network, *J. Air Waste Manage. Assoc.*, *47*, 194-203.

Eldred, R. A. and T. A. Cahill (1997), Sulfate sampling artifact from SO_2 and alkaline soil, *Environ. Sci. Technol.*, *31*, 1320-1324.

Eldred, R. A., P. J. Feeney, P. K. Wakabayashi, J. C. Chow, and E. Hardison (1998), Methodology for chemical speciation measurements in the IMPROVE network, in *Proceedings, $PM_{2.5}$: A Fine Particle Standard*, J. C. Chow and Koutrakis, P., editors, Air & Waste Management Association, Pittsburgh, 352-364.

Eldred, R. A., P. J. Feeney, and P. K. Wakabayashi (1998), The major components of $PM_{2.5}$ at remote sites across the United States, in *Proceedings, $PM_{2.5}$: A Fine Particle Standard*, J. C. Chow and Koutrakis, P., editors, Air & Waste Management Association, Pittsburgh,13-27.

Engling, G., P. Herckes, S. M. Kreidenweis, W. C. Malm, and J. L. Collett (2006), Composition of the fine organic aerosol in Yosemite National Park during the 2002 Yosemite Aerosol Characterization Study, *Atmos. Environ.*, *40*, 2959-2972.

Fancy, S. G., J. E. Gross, and S. L. Carter (2009), Monitoring the condition of natural resources in US national parks, *Environ. Mon. Assess.*, *151*, 161-174.

Farber, R. J., L. C. Murray, and W. A. Moran (2000), Exploring spatial patterns of particulate sulfur and OMH from the Project MOHAVE Summer Intensive Regional Network using analyses of variance techniques and meteorological parameters as sort determinants, *J. Air Waste Manage. Assoc.*, *50*, 724-732.

Farina, S. C., P. J. Adams, and S. N. Pandis (2010), Modeling global secondary organic aerosol formation and processing with the volatility basis set: Implications for anthropogenic secondary organic aerosol, *J. Geophys. Res. -Atmospheres*, *115*,

Fu, T. M., D. J. Jacob, and C. L. Heald (2009), Aqueous-phase reactive uptake of dicarbonyls as a source of organic aerosol over eastern North America, *Atmos. Environ.*, *43*, 1814-1822.

Fung, K. K., J. C. Chow, and J. G. Watson (11/2002), Evaluation of OC/EC speciation by thermal manganese dioxide oxidation and the IMPROVE method, *J. Air Waste Manage. Assoc.*, *52*, 1333-1341.

Ganguly, D., P. Ginoux, V. Ramaswamy, O. Dubovik, J. Welton, E. A. Reid, and B. N. Holben (2009), Inferring the composition and concentration of aerosols by combining AERONET and MPLNET data: Comparison with other measurements and utilization to evaluate GCM output, *J. Geophys. Res. -Atmospheres*, *114*.

Gao, N., A. E. Gildemeister, K. Krumhansl, K. Lafferty, P. K. Hopke, E. Kim, and R. L. Poirot (2006), Sources of fine particulate species in ambient air over Lake Champlain Basin, VT, *J. Air Waste Manage. Assoc.*, *56*, 1607-1620.

Gebhart, K. A., D. A. Latimer, and J. F. Sisler (1990), Empirical orthogonal function analysis of the particulate sulfate concentrations measured during WHITEX, in *Transactions, Visibility,*

and Fine Particles, Mathai, C. V., editor, Air & Waste Management Association, Pittsburgh, 860-871.

Gebhart, K. A., W. C. Malm, and D. Day (1994), Examination of the effects of sulfate acidity and relative humidity and light scattering at Shenandoah National Park, *Atmos. Environ.*, *28*, 841-850.

Gebhart, K. A. and W. C. Malm (1997), Spatial and temporal patterns in particle data measured during the MOHAVE study, *J. Air Waste Manage. Assoc.*, *47*, 119-135.

Gebhart, K. A., W. C. Malm, and M. Flores (2000), A preliminary look at source-receptor relationships in the Texas-Mexico border area, *J. Air Waste Manage. Assoc.*, *50*, 858-868.

Gebhart, K. A., S. M. Kreidenweis, and W. C. Malm (2001), Back-trajectory analyses of fine particulate matter measured at Big Bend National Park in the historical database and the 1996 scoping study, *Sci. Total Environ.*, *276*, 185-204.

Gebhart, K. A., S. Copeland, and W. C. Malm (2001), Diurnal and seasonal patterns in light scattering, extinction, and relative humidity, *Atmos. Environ.*, *35*, 5177-5191.

Gebhart, K. A., W. C. Malm, and L. L. Ashbaugh (2005), Spatial, temporal, and inter-species patterns in fine particulate matter in Texas, *J. Air Waste Manage. Assoc.*, *55*, 1636-1648.

Gebhart, K. A., B. A. Schichtel, M. G. Barna, and W. C. Malm (2006), Quantitative back-trajectory apportionment of sources of particulate sulfate at Big Bend National Park, TX, *Atmos. Environ.*, *40*, 2823-2834.

Gebhart, K. A., B. A. Schichtel, W. C. Malm, M. G. Barna, M. A. Rodriguez, and J. L. Collett (2011), Back-trajectory-based source apportionment of airborne sulfur and nitrogen concentrations at Rocky Mountain National Park, Colorado, USA, *Atmos. Environ.*, *45*, 621-633.

Gego, E. L., P. S. Porter, J. S. Irwin, C. Hogrefe, and S. T. Rao (2005), Assessing the comparability of ammonium, nitrate and sulfate concentrations measured by three air quality monitoring networks, *Pure and Applied Geophysics*, *162*, 1919-1939.

Geiser, L. H., A. R. Ingersoll, A. Bytnerowicz, and S. A. Copeland (2008), Evidence of enhanced atmospheric ammoniacal nitrogen in Hells Canyon national recreation area: Implications for natural and cultural resources, *J. Air Waste Manage. Assoc.*, *58*, 1223-1234.

Geiser, L. H., S. E. Jovan, D. A. Glavich, and M. K. Porter (2010), Lichen-based critical loads for atmospheric nitrogen deposition in Western Oregon and Washington Forests, USA, *Environ. Poll.*, *158*, 2412-2421.

Green, M. C., M. L. Pitchford, and L. L. Ashbaugh (1996), Identification of candidate clean air corridors for the Colorado Plateau, *J. Air Waste Manage. Assoc.*, *46*, 441-449.

Green, M. C. and K. A. Gebhart (1997), Clean air corridors: A geographic and meteorologic characterization, *J. Air Waste Manage. Assoc.*, *47*, 403-410.

Green, M. C. (1999), The project MOHAVE tracer study: Study design, data quality, and overview of results, *Atmos. Environ.*, *33*, 1955-1968.

Green, M. C. and I. H. Tombach (2000), Use of Project MOHAVE perfluorocarbon tracer data to evaluate source and receptor models, *J. Air Waste Manage. Assoc.*, *50*, 717-723.

Green, M. C., H. D. Kuhns, M. L. Pitchford, R. Dietz, L. L. Ashbaugh, and T. Watson (2003), Application of the tracer-aerosol gradient interpretive technique to sulfur attribution for the Big Bend Regional Aerosol and Visibility Observational Study, *J. Air Waste Manage. Assoc.*, *53*, 586-595.

Green, M. C., R. Farber, N. Lien, K. A. Gebhart, J. V. Molenar, H. Iyer, and D. J. Eatough (2005), The effects of scrubber installation at the Navajo Generating Station on particulate sulfur and visibility levels in the Grand Canyon, *J. Air Waste Manage. Assoc.*, *55*, 1675-1682.

Green, M. C. and J. Xu (2007), Causes of haze in the Columbia River Gorge, *J. Air Waste Manage. Assoc.*, *57*, 947-958.

Green, M. C., J. Xu, and N. Adhikari (2008), Transport of atmospheric aerosol by gap winds in the Columbia River Gorge, *Journal of Applied Meteorology and Climatology*, *47*, 15-26.

Green, M. C., S. Kondragunta, P. Ciren, and C. Y. Xu (2009), Comparison of GOES and MODIS Aerosol Optical Depth (AOD) to Aerosol Robotic Network (AERONET) AOD and IMPROVE PM2.5 mass at Bondville, Illinois, *J. Air Waste Manage. Assoc.*, *59*, 1082-1091.

Gutknecht, W., J. Flanagan, A. McWilliams, R. K. M. Jayanty, R. Kellogg, J. Rice, P. Duda, and R. H. Sarver (2010), Harmonization of uncertainties of x-ray fluorescence data for PM2.5 air filter analysis, *J. Air Waste Manage. Assoc.*, *60*, 184-194.

Hand, J. L., R. B. Ames, S. M. Kreidenweis, D. E. Day, and W. C. Malm (2000), Estimates of particle hygroscopicity during the Southeastern Aerosol and Visibility Study, *J. Air & Waste Manage. Assoc., 50,* 677-685.

Hand, J. L. and S. M. Kreidenweis (2002), A new method for retrieving particle refractive index and effective density from aerosol size distribution data, *Aerosol. Sci. Techol., 36,* 1012-1026.

Hand, J. L., S. M. Kreidenweis, D. E. Sherman, J. L. Collett, Jr., S. V. Hering, D. E. Day, and W. C. Malm (2002), Aerosol size distributions and visibility estimates during the Big Bend Regional Aerosol and Visibility Observational (BRAVO) Study, *Atmos. Environ.*, *36*, 5043-5055.

Hand, J. L., S. M. Kreidenweis, N. Kreisberg, S. Hering, M. Stolzenburg, W. Dick, P. H. McMurry (2002), Comparisons of aerosol properties measured by impactors and light

scattering from individual particles: refractive index, number and volume concentrations and size distributions, *Atmos. Environ, 36,* 1853-1861.

Hand, J. L., S. M. Kreidenweis, J. Slusser, and G. Scott (2004), Comparisons of aerosol optical properties derived from Sun photometry to estimates inferred from surface measurements in Big Bend National Park, Texas, *Atmos. Environ., 38,* 6813-6821.

Hand, J. L., N. M. Mahowald, Y. Chen, R. L. Siefert, C. Luo, A. Subramaniam, and I. Fung (2004), Estimates of atmospheric-processed soluble iron from observations and a global mineral aerosol model: Biogeochemical implications, *J. Geophys. Res., 109,* D17205, doi:10.1029/2004JD004574.

Hand, J. L., W. C. Malm, A. Laskin, D. Day, T. Lee, C. Wang, C. Carrico, J. Carrillo, J. P. Cowin, J. Collett, Jr., and M. J. Iedema (2005), Optical, physical, and chemical properties of tar balls observed during the Yosemite Aerosol Characterization Study, *J. Geophys. Res., 110,* D21210, doi:10.1029/2004JD005728.

Hand, J. L. and W. C. Malm (2007), Review of aerosol mass scattering efficiencies from ground-based measurements since 1990, *J. Geophys. Res. -Atmospheres*, *112*, (D18).

Heald, C. L., D. J. Jacob, R. J. Park, B. Alexander, T. D. Fairlie, R. M. Yantosca, and D. A. Chu (2006), Transpacific transport of Asian anthropogenic aerosols and its impact on surface air quality in the United States, *J. Geophys. Res. -Atmospheres*, *111*, (D14).

Henry, R. C. (1997), Receptor model applied to patterns in space (RMAPS) Part I - Model description, *J. Air Waste Manage. Assoc.*, *47*, 216-219.

Henry, R. C. (1997), Receptor model applied to patterns in space (RMAPS) Part II - Apportionment of airborne particulate sulfur from Project MOHAVE, *J. Air Waste Manage. Assoc.*, *47*, 220-225.

Henze, D. K., J. H. Seinfeld, and D. T. Shindell (2009), Inverse modeling and mapping US air quality influences of inorganic PM2.5 precursor emissions using the adjoint of GEOS-Chem, *Atmos. Chem. Phys.* , *9*, 5877-5903.

Herckes, P., G. Engling, S. M. Kreidenweis, and J. L. Collett (2006), Particle size distributions of organic aerosol constituents during the 2002 Yosemite Aerosol Characterization Study, *Environ. Sci. Technol.*, *40*, 4554-4562.

Hering, S. V., M. R. Stolzenburg, J. L. Hand, S. M. Kreidenweis, T. Lee, J. L. Collett, Jr., D. Dietrich, and M. Tigges (3/2003), Hourly concentrations and light scattering cross sections for fine particle sulfate at Big Bend National Park., *Atmos. Environ.*, *37*, 1175-1183.

Hess, A., H. Iyer, and W. C. Malm (2001), Linear trend analysis: A comparison of methods, *Atmos. Environ.*, *35*, 5211-5222.

Hess, A., H. Iyer, and W. C. Malm (2002), Author's reply to linear trend analysis: A comparison of methods [Atmos. Environ. 36 (2002): 3055-3056], *Atmos. Environ.*, *36*, 3719-3720.

Hopke, P. K., L. M. Zhou, and R. L. Poirot (2005), Reconciling trajectory ensemble receptor model results with emissions, *Environ. Sci. Technol.*, *39*, 7980-7983.

Horvath, H. (1997), Comparison of the light absorption coefficient and carbon measures for remote aerosols - An independent analysis of data from the IMPROVE Network I and II: Discussion, *Atmos. Environ.*, *31*, 2885-2887.

Hu, Y. T., S. L. Napelenok, M. T. Odman, and A. G. Russell (2009), Sensitivity of inverse estimation of 2004 elemental carbon emissions inventory in the United States to the choice of observational networks, *Geophys. Res. Lett.*, *36*.

Huffman, D. (1996), Comparison of light absorption coefficient and carbon measures for remote aerosols: An independent analysis of data from the IMPROVE network-I, *Atmos. Environ.*, *30*, 73-83.

Huffman, H. D. (1996), Comparison of the light absorption coefficient and carbon measures for remote aerosols: An independent analysis of data from the IMPROVE NETWORK - I, *Atmos. Environ.*, *30*, 73-83.

Huffman, H. D. (1996), The reconstruction of aerosol light absorption by particle measurements at remote sites: An independent analysis of data from the IMPROVE NETWORK - II, *Atmos. Environ.*, *30*, 85-99.

Hwang, I. and P. K. Hopke (2007), Estimation of source apportionment and potential source locations of PM2.5 at a west coastal IMPROVE site, *Atmos. Environ.*, *41*, 506-518.

Hyslop, N. P. and W. H. White (2008), An empirical approach to estimating detection limits using collocated data, *Environ. Sci. Technol.*, *42*, 5235-5240.

Hyslop, N. P. and W. H. White (2008), An evaluation of Interagency Monitoring of PROtected Visual Environments (IMPROVE) collocated precision and uncertainty estimates, *Atmos. Environ.*, *42*, 2691-2705.

Hyslop, N. P. and W. H. White (2009), Estimating precision using duplicate measurements, *J. Air Waste Manage. Assoc.*, *59*, 1032-1039.

IMPROVE (2010), Network operation status, *IMPROVE Newsletter*, *19*, 3.

In, H. J., D. W. Byun, R. J. Park, N. K. Moon, S. Kim, and S. Zhong (2007), Impact of transboundary transport of carbonaceous aerosols on the regional air quality in the United States: A case study of the South American wildland fire of May 1998, *J. Geophys. Res. - Atmospheres*, *112*.

Ito, K., W. F. Christensen, D. J. Eatough, R. C. Henry, E. Kim, F. Laden, R. Lall, T. V. Larson, L. Neas, P. K. Hopke, and G. D. Thurston (2005), PM source apportionment and health effects: 2. An investigation of intermethod variability in associations between source-apportioned fine particle mass and daily mortality in Washington, DC, *J. Expo. Anal. Environ. Epidemiol.*

Iyer, H., P. Patterson, and W. C. Malm (2000), Sampling duration calculations, *J. Air Waste Manage. Assoc.*, *50*(5), 888-893.

Iyer, H., P. Patterson, and W. C. Malm (2000), Trends in the extremes of sulfur concentration distributions, *J. Air Waste Manage. Assoc.*, *50*, 802-808.

Jaffe, D., I. McKendry, T. Anderson, and H. Price (2003), Six „new" episodes of trans-Pacific transport of air pollutants, *Atmos. Environ., 37,* 391-404.

Jaffe, D., S. Tamura, and J. Harris (2005), Seasonal cycle and composition of background fine particles along the west coast of the US, *Atmos. Environ.*, *39*, 297-306.

Jaffe, D., D. Chand, W. Hafner, A. Westerling, and D. Spracklen (2008), Influence of fires on O3 concentrations in the western US, *Environ. Sci. Technol.*, *42*, 5885-5891.

Jaffe, D., W. Hafner, D. Chand, A. Westerling, and D. Spracklen (2008), Interannual variations in PM2.5 due to wildfires in the western United States, *Environ. Sci. Technol.*, *42*, 2812-2818.

Jaffe, D. A. and D. R. Reidmiller (2009), Now you see it, now you don't: Impact of temporary closures of a coal-fired power plant on air quality in the Columbia River Gorge National Scenic Area, *Atmos. Chem. Phys.*, *9*, 7997-8005.

Joseph, D. B., J. C. Metsa, W. C. Malm, and M. L. Pitchford (1987), Plans for IMPROVE: A federal program to monitor visibility in Class I areas, 113-125.

Karydis, V. A., A. P. Tsimpidi, and S. N. Pandis (2007), Evaluation of a three-dimensional chemical transport model (PMCAMx) in the eastern United States for all four seasons, *J. Geophys. Res. -Atmospheres*, *112*, (D14).

Kavouras, I. G., V. Etyemezian, J. Xu, D. W. DuBois, M. C. Green, and M. L. Pitchford (2007), Assessment of the local windblown component of dust in the western United States, *J. Geophys. Res. -Atmospheres*, *112*, (D8).

Kavouras, I. G., V. Etyemezian, and D. W. DuBois (2009), Development of a geospatial screening tool to identify source areas of windblown dust, *Environ. Modelling & Software*, *24*, 1003-1011.

Kavouras, I. G., V. Etyemezian, D. W. DuBois, J. Xu, and M. L. Pitchford (2009), Source reconciliation of atmospheric dust causing visibility impairment in Class I areas of the western United States, *J. Geophys. Res. -Atmospheres*, *114*.

Kim, E. and P. K. Hopke (2004), Comparison between conditional probability function and nonparametric regression for fine particle source directions, *Atmos. Environ.*, *38*, 4667-4673.

Kim, E., P. K. Hopke, T. V. Larson, N. N. Maykut, and J. Lewtas (2004), Factor analysis of Seattle fine particles, *Aerosol Sci. Technol.*, *38*, 724-738.

Kim, E. and P. K. Hopke (2004), Improving source identification of fine particles in a rural northeastern US area utilizing temperature-resolved carbon fractions, *J. Geophys. Res. - Atmospheres*, *109*, 1-13.

Kim, E. and P. K. Hopke (2004), Source apportionment of fine particles at Washington, DC, utilizing temperature-resolved carbon fractions, *J. Air Waste Manage. Assoc.*, *54*, 773-785.

Kim, E. and P. K. Hopke (2005), Improving source apportionment of fine particles in the eastern United States utilizing temperature-resolved carbon fractions, *J. Air Waste Manage. Assoc.*, *55*, 1456-1463.

Kim, E., P. K. Hopke, D. M. Kenski, and M. Koerber (2005), Sources of fine particles in a rural Midwestern US area, *Environ. Sci. Technol.*, *39*, 4953-4960.

Kim, E. and P. K. Hopke (2006), Characterization of fine particle sources in the Great Smoky Mountains area, *Sci. Total Environ.*, *368*, 781-794.

Kim, E. and P. K. Hopke (2008), Characterization of ambient fine particles in the northwestern area and Anchorage, Alaska, *J. Air Waste Manage. Assoc.*, *58*, 1328-1340.

Knipping, E. M., N. Kumar, B. K. Pun, C. Seigneur, S. Y. Wu, and B. A. Schichtel (2006), Modeling regional haze during the BRAVO study using CMAQ-MADRID: 2. Source region attribution of particulate sulfate compounds, *J. Geophys. Res. -Atmospheres*, *111*, (D6).

Kreidenweis, S. M., L. A. Remer, R. Bruintjes, and O. Dubovik (2001), Smoke aerosol from biomass burning in Mexico: Hygroscopic smoke optical model, *J. Geophys. Res.*, *106*, 4831-4844.

Kuhns, H. D., M. C. Green, M. L. Pitchford, L. Vasconcelos, W. H. White, and V. Mirabella (1999), Attribution of particulate sulfur in the Grand Canyon to specific point sources using Tracer-Aerosol Gradient Interpretive Technique (TAGIT), *J. Air Waste Manage. Assoc.*, *49*, 906-915.

Laidlaw, M. A. S. and G. M. Filippelli (2008), Resuspension of urban soils as a persistent source of lead poisoning in children: A review and new directions, *Applied Geochemistry*, *23*, 2021-2039.

Landreman, A. P., M. M. Shafer, J. C. Hemming, M. P. Hannigan, and J. J. Schauer (2008), A macrophage-based method for the assessment of the reactive oxygen species (ROS) activity of atmospheric particulate matter (PM) and application to routine (daily-24 h) aerosol monitoring studies, *Aerosol Sci. Technol.*, *42*, 946-957.

Lane, T. E., N. M. Donahue, and S. N. Pandis (2008), Simulating secondary organic aerosol formation using the volatility basis-set approach in a chemical transport model, *Atmos. Environ.*, *42*, 7439-7451.

Latimer, D. A., H. K. Iyer, and W. C. Malm (1990), Application of a differential mass balance model to attribute sulfate haze in the Southwest, in *Transactions, Visibility and Fine Particles*, Mathai, C. V., editor, Air & Waste Management Association, Pittsburgh, 819-830.

Lavery, T. F., C. M. Rogers, R. Baumgardner, and K. P. Mishoe (2009), Intercomparison of Clean Air Status and Trends Network nitrate and nitric acid measurements with data from other monitoring programs, *J. Air Waste Manage. Assoc.*, *59*, 214-226.

Lee, J. H., Y. Yoshida, B. J. Turpin, P. K. Hopke, R. L. Poirot, P. J. Lioy, and J. C. Oxley (2002), Identification of sources contributing to mid-Atlantic regional aerosol, *J. Air Waste Manage. Assoc.*, *52*, 1186-1205.

Lee, S. and L. L. Ashbaugh (2007), Comparison of multi-receptor and single-receptor trajectory source apportionment (TSA) methods using artificial sources, *Atmos. Environ.*, *41*, 1119-1127.

Lee, T., X. Y. Yu, B. Ayres, S. M. Kreidenweis, W. C. Malm, and J. L. Collett (2008), Observations of fine and coarse particle nitrate at several rural locations in the United States, *Atmos. Environ.*, *42*, 2720-2732.

Lee, T., X. Y. Yu, S. M. Kreidenweis, W. C. Malm, and J. L. Collett (2008), Semi-continuous measurement of PM2.5 ionic composition at several rural locations in the United States, *Atmos. Environ.*, *42*, 6655-6669.

Levin, E. J. T., S. M. Kreidenweis, G. R. McMeeking, C. M. Carrico, J. L. Collett, and W. C. Malm (2009), Aerosol physical, chemical and optical properties during the Rocky Mountain Airborne Nitrogen and Sulfur study, *Atmos. Environ.*, *43*, 1932-1939.

Liao, H., D. K. Henze, J. H. Seinfeld, S. L. Wu, and L. J. Mickley (2007), Biogenic secondary organic aerosol over the United States: Comparison of climatological simulations with observations, *J. Geophys. Res. -Atmospheres*, *112*, (D6).

Liu, W., P. K. Hopke, and R. A. VanCuren (2003), Origins of fine aerosol mass in the western United States using positive matrix factorization, *J. Geophys. Res. -Atmospheres*, *108*, (D23).

Liu, J., D. L. Mauzerall, and L. W. Horowitz (2008), Source-receptor relationships between East Asian sulfur dioxide emissions and Northern Hemisphere sulfate concentrations, *Atmos. Chem. Phys., 8,* 3721-3733.

Lowenthal, D. H., J. G. Watson, and P. Saxena (2000), Contributions to light extinction during project MOHAVE, *Atmos. Environ.*, *34*, 2351-2359.

Lowenthal, D. H. and N. K. Kumar (2003), $PM_{2.5}$ mass and light extinction reconstruction in IMPROVE, *J. Air Waste Manage. Assoc.*, *53*, 1109-1120.

Lowenthal, D. H. and N. K. Kumar (2004), Variation of mass scattering efficiencies in IMPROVE, *J. Air Waste Manage. Assoc.*, *54*, 926-934.

Lowenthal, D. H. and N. K. Kumar (2006), Light scattering from sea-salt aerosols at Interagency Monitoring of Protected Visual Environments (IMPROVE) Sites, *J. Air Waste Manage. Assoc.*, *56*, 636-642.

Lowenthal, D. H., B. Zielinska, B. Mason, S. Samy, V. Samburova, D. Collins, C. Spencer, N. Taylor, J. Allen, and N. K. Kumar (2009), Aerosol characterization studies at Great Smoky Mountains National Park, summer 2006, *J. Geophys. Res. -Atmospheres*, *114*.

Lowenthal, D. H., J. G. Watson, D. Koracin, L.-W. A. Chen, D. DuBois, R. Vellore, N. Kumar, E. M. Knipping, N. Wheeler, K. Craig, and S. Reid (2010), Evaluation of regional scale receptor modeling, *J. Air Waste Manage. Assoc.*, *60*, 26-42.

Malm, W. C., H. K. Iyer, and K. A. Gebhart (1990), Application of tracer mass balance regression to WHITEX data, n *Transactions, Visibility and Fine Particles*, Mathai, C. V., editor, Air & Waste Management Association, Pittsburgh,806-818.

Malm, W. C., M. L. Pitchford, and H. K. Iyer (1990), Design and implementation of the Winter Haze Intensive Tracer Experiment - WHITEX, in *Transactions, Receptor Models in Air Resources Management*, Watson, J. G., editor, Air & Waste Management Association, Pittsburgh, 432-458.

Malm, W. C. (1992), Characteristics and origins of haze in the continental United States, *Earth Sci. Rev.*, *33*, 1-36.

Malm, W. C., K. A. Gebhart, H. Iyer, J. G. Watson, D. Latimer, and R. Pielke (1993), Response to "The WHITEX Study and the role of the scientific community: A critique" by Gregory R. Markowski, *J. Air Waste Manage. Assoc.*, *43*, 1128-1136.

Malm, W. C., K. A. Gebhart, J. V. Molenar, T. A. Cahill, R. A. Eldred, and D. Huffman (1994), Examining the relationship between atmospheric aerosols and light extinction at Mount Rainier and North Cascades National Parks, *Atmos. Environ.*, *28*, 347-360.

Malm, W. C., J. F. Sisler, D. Huffman, R. A. Eldred, and T. A. Cahill (1994), Spatial and seasonal trends in particle concentration and optical extinction in the United States, *J. Geophys. Res.*, *99*, 1347-1370.

Malm, W. C., J. V. Molenar, R. A. Eldred, and J. F. Sisler (1996), Examining the relationship among atmospheric aerosols and light scattering and extinction in the Grand Canyon area, *J. Geophys. Res.*, *101*, 19251-19266.

Malm, W. C. and K. A. Gebhart (1996), Source apportionment of organic and light-absorbing carbon using receptor modeling techniques, *Atmos. Environ.*, *30*, 843-855.

Malm, W. C. and M. L. Pitchford (1997), Comparison of calculated sulfate scattering efficiencies as estimated from size-resolved particle measurements at three national locations, *Atmos. Environ.*, *31*, 1315-1325.

Malm, W. C. and K. A. Gebhart (1997), Source apportionment of sulfur and light extinction using receptor modeling techniques, *J. Air Waste Manage. Assoc.*, *47*, 250-268.

Malm, W. C., D. E. Day, and S. M. Kreidenweis (2000), Light scattering characteristics of aerosols as a function of relative humidity - Part I: A comparison of measured scattering and aerosol concentrations using theoretical models, *J. Air Waste Manage. Assoc.*, *50*, 686-700.

Malm, W. C., D. E. Day, and S. M. Kreidenweis (2000), Light scattering characteristics of aerosols as a function of relative humidity - Part II: A comparison of measured scattering and aerosol concentrations using statistical models, *J. Air Waste Manage. Assoc.*, *50*, 701-709.

Malm, W. C. and D. E. Day (2000), Optical properties of aerosols at Grand Canyon National Park, *Atmos. Environ.*, *34*, 3373-3391.

Malm, W. C., B. A. Schichtel, R. B. Ames, and K. A. Gebhart (2002), A ten-year spatial and temporal trend of sulfate across the United States, *J. Geophys. Res. -Atmospheres*, *107*, ACH 11-1-ACH 11-20.

Malm, W. C., D. E. Day, S. M. Kreidenweis, J. L. Collett, Jr., and T. Lee (2003), Humidity-dependent optical properties of fine particles during the Big Bend Regional Aerosol and Visibility Observational Study (BRAVO), *J. Geophys. Res. -Atmospheres*, *108*, ACH 13-1-ACH 13-16.

Malm, W. C., B. A. Schichtel, M. L. Pitchford, L. L. Ashbaugh, and R. A. Eldred (2004), Spatial and monthly trends in speciated fine particle concentration in the United States, *J. Geophys. Res.*, *109*, (D03306).

Malm, W. C., D. E. Day, S. M. Kreidenweis, J. L. Collett, Jr., C.M. Carrico, G.R. McMeeking, and T. Lee (2005), Hygroscopic properties of an organic-laden aerosol, *Atmos. Environ.*, *39*(27), 4969-4982.

Malm, W. C., D. E. Day, C. Carrico, S. M. Kreidenweis, J. L. Collett, Jr., G. R. McMeeking, T. Lee, J. Carrillo, and B. Schichtel (2005), Intercomparison and closure calculations using measurements of aerosol species and optical properties during the Yosemite Aerosol Characterization Study, *J. Geophys. Res. -Atmospheres*, *110*, (D14).

Malm, W. C. and J. L. Hand (2007), An examination of the physical and optical properties of aerosols collected in the IMPROVE program, *Atmos. Environ.*, *41*, 3407-3427.

Malm, W. C., M. L. Pitchford, C. McDade, and L. L. Ashbaugh (2007), Coarse particle speciation at selected locations in the rural continental United States, *Atmos. Environ.*, *41*, 2225-2239.

Malm, W. C., G. R. McMeeking, S. M. Kreidenweis, E. Levin, C. M. Carrico, D. E. Day, J. L. Collett, T. Lee, A. P. Sullivan, and S. Raja (2009), Using high time resolution aerosol and number size distribution measurements to estimate atmospheric extinction, *J. Air Waste Manage. Assoc.*, *59*, 1049-1060.

Markowski, G. R. (1992), The WHITEX Study and the role of the scientific community: A critique, *J. Air Waste Manage. Assoc.*, *42*, 1453-1460.

Markowski, G. R. (1993), Reply to Malm, et al.'s Discussion of the WHITEX Critique, *J. Air Waste Manage. Assoc.*, *43*, 1137-1142.

Mathai, C. V. (1995), The Grand Canyon Visibility Transport Commission and visibility protection in Class I areas, *EM*, *1*, 20-31.

Mathai, C. V., S. B. Kendall, E Trexler, A. J. Carlson, M. L. Teague, and D. S. Steele (1996), Integrated assessment and recommendations of the Grand Canyon Visibility Transport Commission, *EM*, *2*, 16-24.

Maykut, N. N., J. Lewtas, E. Kim, and T. V. Larson (2003), Source apportionment of PM2.5 at an urban IMPROVE site in Seattle, Washington, *Environ. Sci. Technol.*, *37*, 5135-5142.

McDade, C. E., A. M. Dillner, and H. Indresand (2009), Particulate matter sample deposit geometry and effective filter face velocities, *J. Air Waste Manage. Assoc.*, *59*, 1045-1048.

McMeeking, G. R., S. M. Kreidenweis, C. M. Carrico, T. Lee, J. L. Collett Jr., and W. C. Malm (2005), Observations of smoke-influenced aerosol during the Yosemite Aerosol Characterization Study: Size distributions and chemical composition, *J. Geophys. Res., 110,* D09206, doi:10.1029/2004JD005389.

McMeeking, G. R., S. M. Kreidenweis, C. M. Carrico, D. E. Day, and W. C. Malm (2005), Observations of smoke-influenced aerosol during the Yosemite Aerosol Characterization Study: 2. Aerosol scattering and absorbing properties, *J. Geophys. Res., 110,* D18209, doi:10.1029/2004JD005624.

McMeeking, G. R., S. M. Kreidenweis, M. Lunden, J. Carrillo, C. M. Carrico, T. Lee, P. Herckes, G. Engling, D. E. Day, J. Hand, N. Brown, W. C. Malm, and J. L. Collett (2006), Smoke-impacted regional haze in California during the summer of 2002, *Agricultural and Forest Meteorology* , *137*, 25-42.

Mebust, M. R., B. K. Eder, F. S. Binkowski, and S. J. Roselle (2003), Models-3 community multiscale air quality (CMAQ) model aerosol component 2. Model evaluation, *J. Geophys. Res.*, *108*, AAC4-1-AAC4-18.

Mirabella, V. A. and R. J. Farber (2000), Relating summer ambient particulate sulfur, sulfur dioxide, and light scattering to gaseous tracer emissions from the MOHAVE Power Project, *J. Air Waste Manage. Assoc.*, *50*, 746-755.

Molders, N., S. E. Porter, C. F. Cahill, and G. A. Grell (2010), Influence of ship emissions on air quality and input of contaminants in southern Alaska National Parks and Wilderness Areas during the 2006 tourist season, *Atmos. Environ.*, *44*, 1400-1413.

Murphy, B. N. and S. N. Pandis (2009), Simulating the formation of semivolatile primary and secondary organic aerosol in a regional chemical transport model, *Environ. Sci. Technol.*, *43*, 4722-4728.

Murphy, D. M., P. K. Hudson, D. J. Cziczo, S. Gallavardin, K. D. Froyd, M. V. Johnston, A. M. Middlebrook, M. S. Reinard, D. S. Thomson, T. Thornberry, and A. S. Wexler (2007), Distribution of lead in single atmospheric particles, *Atmos. Chem. Phys.*, *7*, 3195-3210.

Murphy, D. M., S. L. Capps, J. S. Daniel, G. J. Frost, and W. H. White (2008), Weekly patterns of aerosol in the United States, *Atmos. Chem. Phys.*, *8*, 2729-2739.

Murphy, D. M., J. C. Chow, E. M. Leibensperger, W. C. Malm, M. L. Pitchford, B. A. Schichtel, J. G. Watson, and W. H. White (2011), Decreases in elemental carbon and fine particle mass in the United States, *Atmos. Chem. Phys. Discuss.*, *11*, 2057-2076.

Nejedly, Z., J. L. Campbell, J. R. Brook, R. Vet, and R. Eldred (2003), Evaluation of elemental and black carbon measurements from the GAViM and IMPROVE networks, *Aerosol Sci. Technol.*, *37*, 96-108.

Park, R. J., D. J. Jacob, M. Chin, and R. V. Martin (2003), Sources of carbonaceous aerosols over the United States and implications for natural visibility, *J. Geophys. Res.*, *108*, 4355.

Park, R. J., D. J. Jacob, B. D. Field, and R. M. Yantosca (2004), Natural and transboundary pollution influences on sulfate-nitrate-ammonium aerosols in the United States: Implications for policy, *J. Geophys. Res., 109,* D15204, doi:10.1029/2003JD004473.

Park, R. J., D. J. Jacob, N. Kumar, and R. M. Yantosca (2006), Regional visibility statistics in the United States: Natural and transboundary pollution influences, and implications for the Regional Haze Rule, *Atmos. Environ.*, *40*, 5405-5423.

Park, R. J., D. J. Jacob, and J. A. Logan (2007), Fire and biofuel contributions to annual mean aerosol mass concentrations in the United States, *Atmos. Environ.*, *41*, 7389-7400.

Patterson, P., H. Iyer, J. F. Sisler, and W. C. Malm (2000), An analysis of the yearly changes in sulfur concentrations at various national parks in the United States, 1980-1996, *J. Air Waste Manage. Assoc.*, *50*, 790-801.

Perry, K. D., T. A. Cahill, R. A. Eldred, and D. D. Dutcher (1997), Long-range transport of North African dust to the eastern United States, *J. Geophys. Res.*, *102*, 11225-11238.

Pitchford, M. L. and M. C. Green (1997), Analyses of sulfur aerosol size distributions for a forty day period in summer, 1992 at Meadview, Arizona, *J. Air Waste Manage. Assoc.*, *47*, 136-146.

Pitchford, M. L., B. A. Schichtel, K. A. Gebhart, J. C. Chow, W. C. Malm, I. H. Tombach, and E. M. Knipping (2004), Causes of haze at Big Bend National Park - Results of the BRAVO study and more, in *Proceedings, Regional and Global Perspectives on Haze: Causes, Consequences and Controversies*, Pitchford, M. L. and R. Poirot, editors, Air and Waste Management Association, Pittsburgh, 47-1-47-21.

Pitchford, M. L., B. A. Schichtel, K. A. Gebhart, M. G. Barna, W. C. Malm, I. H. Tombach, and E. M. Knipping (2005), Reconciliation and interpretation of Big Bend National Park's particulate sulfur source apportionment: Results from the BRAVO Study, Part II, *J. Air Waste Manage. Assoc.*, *55*, 1726-1732.

Pitchford, M. L., W. C. Malm, B. A. Schichtel, N. K. Kumar, D. H. Lowenthal, and J. L. Hand (2007), Revised algorithm for estimating light extinction from IMPROVE particle speciation data, *J. Air Waste Manage. Assoc.*, *57*, 1326-1336.

Pitchford, M. L., R. L. Poirot, B. A. Schichtel, and W. C. Malm (2009), Characterization of the winter midwestern particulate nitrate bulge, *J. Air Waste Manage. Assoc.*, *59*, 1061-1069.

Poirot, R. L., P. R. Wishinski, P. K. Hopke, and A. V. Polissar (2001), Comparitive application of multiple receptor methods to identify aerosol sources in northern Vermont, *Environ. Sci. Technol.*, *35*, 4622-4636.

Polissar, A. V., P. K. Hopke, W. C. Malm, and J. F. Sisler (1996), The ratio of aerosol optical absorption coefficients to sulfur concentrations, as an indicator of smoke from forest fires when sampling in polar regions, *Atmos. Environ.*, *30*, 1147-1157.

Polissar, A. V., P. K. Hopke, W. C. Malm, and J. F. Sisler (1998), Atmospheric aerosol over Alaska: 1. Spatial and seasonal variability, *J. Geophys. Res.*, *103*, 19035-19044.

Polissar, A. V., P. K. Hopke, P. Paatero, W. C. Malm, and J. F. Sisler (1998), Atmospheric aerosol over Alaska: 2. Elemental composition and sources, *J. Geophys. Res.*, *103*, 19045-19057.

Polissar, A. V., P. K. Hopke, and R. L. Poirot (2001), Atmospheric aerosol over Vermont: Chemical composition and sources, *Environ. Sci. Technol.*, *35*, 4604-4621.

Pun, B. K., C. Seigneur, K. Vijayaraghavan, S. Y. Wu, S. Y. Chen, E. M. Knipping, and N. Kumar (2006), Modeling regional haze in the BRAVO study using CMAQ-MADRID: 1. Model evaluation, *J. Geophys. Res. -Atmospheres*, *111*, (D6).

Rodriguez, M. A., M. G. Barna, K. A. Gebhart, J. L. Hand, Z. E. Adelman, B. A. Schichtel, J. L. Collett, and W. C. Malm (2011), Modeling the fate of atmospheric reduced nitrogen during the Rocky Mountain Atmospheric Nitrogen and Sulfur Study (RoMANS): Performance evaluation and diagnosis using integrated processes rate analysis, *Atmos. Environ.*, *45*, 223-234.

Roy, B., R. Mathur, A. B. Gilliland, and S. C. Howard (2007), A comparison of CMAQ-based aerosol properties with IMPROVE, MODIS, and AERONET data, *J. Geophys. Res. - Atmospheres*, *112*, (D14).

Ryan, P. A., D. H. Lowenthal, and N. Kumar (2005), Improved light extinction reconstruction in Interagency Monitoring of Protected Visual Environments, *J. Air Waste Manage. Assoc.*, *55*, 1751-1759.

Schichtel, B. A., M. L. Pitchford, K. A. Gebhart, W. C. Malm, M. G. Barna, E. M. Knipping, and I. H. Tombach (2005), Reconciliation and interpretation of Big Bend National Park's particulate sulfur source apportionment: Results from the BRAVO Study, Part 1, *J. Air Waste Manage. Assoc.*, *55*, 1709-1725.

Schichtel, B. A., W. C. Malm, K. A. Gebhart, M. G. Barna, and E. M. Knipping (2006), A hybrid source apportionment model integrating measured data and air quality model results, *J. Geophys. Res. -Atmospheres*, *111*, (D7).

Schichtel, B. A., K. A. Gebhart, M. G. Barna, and W. C. Malm (2006), Association of airmass transport patterns and particulate sulfur concentrations at Big Bend National Park, Texas, *Atmos. Environ.*, *40*, 992-1006.

Schichtel, B. A., W. C. Malm, G. Bench, S. Fallon, C. E. McDade, J. C. Chow, and J. G. Watson (2008), Fossil and contemporary fine particulate carbon fractions at 12 rural and urban sites in the United States, *J. Geophys. Res. -Atmospheres*, *113*, 1-20.

Shannon, J. D., E. C. Trexler, Jr., and R. Sonnenblick (1997), Modeling visibility for assessment, *Atmos. Environ.*, *31*, 3719-3727.

Shaver, C. L., K. A. Tonnessen, and T. G. Maniero (1994), Clearing the air at Great Smoky Mountains national park, *Ecological Applications*, *4*, 690-701.

Shi, Z. B., D. Z. Zhang, H. Z. Ji, S. Hasegawa, and M. Hayashi (2008), Modification of soot by volatile species in an urban atmosphere, *Sci. Total Environ.*, *389*, 195-201.

Sickles, J. E., II and D. S. Shadwick (2008), Comparison of particulate sulfate and nitrate at collocated CASTNET and IMPROVE sites in the eastern US, *Atmos. Environ.*, *42*, 2062-2073.

Simon, H., P. V. Bhave, J. L. Swall, N. H. Frank, and W. C. Malm (2011), Determining the spatial and seasonal variability in OM/OC ratios across the US using multiple regression, *Atmos. Chem. Phys., 11*, 2933-2949.

Sisler, J. F. and W. C. Malm (1993), Assessing the visibility impairment associated with various sulfate reduction scenarios at Shenandoah National Park, 302-318.

Sisler, J. F. and W. C. Malm (1994), The relative importance of soluble aerosols to spatial and seasonal trends of impaired visibility in the United States, *Atmos. Environ.*, *28*, 851-862.

Sisler, J. F. and W. C. Malm (1997), Characteristics of winter and summer aerosol mass and light extinction on the Colorado Plateau, *J. Air Waste Manage. Assoc.*, *47*, 317-330.

Sisler, J. F. and W. C. Malm (2000), Interpretation of trends of $PM_{2.5}$ and reconstructed visibility from the IMPROVE network, *J. Air Waste Manage. Assoc.*, *50*, 775-789.

Snow, J. A., J. B. Dennison, D. A. Jaffe, H. U. Price, J. K. Vaughan, and B. Lamb (2003), Aircraft and surface observations of air quality in Puget Sound and a comparison to a regional model, *Atmos. Environ.*, *37*, 4019-4032.

Song, X. H., A. V. Polissar, and P. K. Hopke (2001), Sources of fine particle composition in the northeastern US, *Atmos. Environ.*, *35*, 5277-5286.

Spak, S. N. and T. Holloway (2009), Seasonality of speciated aerosol transport over the Great Lakes region, *J. Geophys. Res. -Atmospheres*, *114*.

Stocker, R. A. and R. A. Pielke (1990), Source attribution during WHITEX: A modeling study, 831-844.

Tanner, R. L., K. J. Olszyna, E. S. Edgerton, E. Knipping, and S. L. Shaw (2009), Searching for evidence of acid-catalyzed enhancement of secondary organic aerosol formation using ambient aerosol data, *Atmos. Environ.*, *43*, 3440-3444.

Terhorst, J. and M. Berkman (2010), Effect of coal-fired power generation on visibility in a nearby national park, *Atmos. Environ.*, *44*, 2524-2531.

Tombach, I. H., W. H. White, and M. L. Pitchford (1999), Regional-scale modeling of PM2.5: Lessons learned from four recent major projects, in *Proceedings, 92nd Annual Meeting of the Air & Waste Management Association*, Air & Waste Management Association, Pittsburgh, 1-5.

Tombach, I. H. (2001), Comparative evaluation of the performance of two speciated particulate matter samplers for PM and regional haze characterization in the Southeast, in *Proceedings, 94th Annual Meeting of the Air & Waste Management Association*, Air & Waste Management Association, Pittsburgh, 1-5.

Tombach, I. H. and M. L. Pitchford (2007), Eliminating man-made haze in protected areas: A goal of the Regional Haze Rule, *EM*, *12*, 6-11.

Trzepla-Nabaglo, K., P. H. Wakabayashi, and W. H. White (2009), Toward establishing the stability of multi-year monitoring of elements in airborne particles, *J. Air Waste Manage. Assoc.*, *59*, 1040-1044.

Turpin, B. J., P. Saxena, G. A. Allen, P. Koutrakis, P. H. McMurry, and L. M. Hildemann (1997), Characterization of the southwestern desert aerosol, Meadview, AZ, *J. Air Waste Manage. Assoc.*, *47*, 344-356.

U.S. EPA (2006), Modification of carbon procedures in the Speciation Network and FAQs, *PM2. 5 Speciation Trends Network Newsletter*, April, 2-3.

U.S. EPA (2006), Speciation network map, *PM2. 5 Speciation Trends Network Newsletter*, *5*, April, 1.

van Donkelaar, A., R. V. Martin, R. J. Park, C. L. Heald, T. M. Fu, H. Liao, and A. Guenther (2007), Model evidence for a significant source of secondary organic aerosol from isoprene, *Atmos. Environ.*, *41*, 1267-1274.

VanCuren, R. A. and T. A. Cahill (2002), Asian aerosols in North America: Frequency and concentration of fine dust, *J. Geophys. Res.*, *197*, AAC 19-1-AAC 19-16.

VanCuren, R. A. (2003), Asian aerosols in North America: Extracting the chemical composition and mass concentration of the Asian continental aerosol plume from long-term aerosol records in the western United States, *J. Geophys. Res.*, *108*, ACH 1-1-ACH 1-16.

Venkatram, A., P. K. Karamchandani, P. Pai, C. S. Sloane, P. Saxena, and R. Goldstein (1997), The development of a model to examine source-receptor relationships for visibility on the Colorado Plateau, *J. Air Waste Manage. Assoc.*, *47*, 286-301.

Wallace, L. and T. Slonecker (1997), Ambient air concentrations of fine ($PM_{2.5}$) manganese in U.S. national parks and in California and Canadian cities: The possible impact of adding MMT to unleaded gasoline, *J. Air Waste Manage. Assoc.*, *47*, 642-652.

Wang, J., S. A. Christopher, U. S. Nair, J. S. Reid, E. M. Prins, J. Szykman, and J. L. Hand (2006), Mesoscale modeling of Central American smoke transport to the United States: 1. "Top-down" assessment of emission strength and diurnal variation impacts, *J. Geophys. Res., 111,* D05S17, doi:10.1029/2005JD006416.

Watson, J. G. (2002), Visibility: Science and regulation - 2002 Critical Review, *J. Air Waste Manage. Assoc.*, *52*, 628-713.

Watson, J. G., J. C. Chow, D. H. Lowenthal, and K. L. Magliano (2008), Estimating aerosol light scattering at the Fresno Supersite, *Atmos. Environ.*, *42*, 1186-1196.

Watson, J. G., J. C. Chow, L.-W. A. Chen, and N. H. Frank (2009), Methods to assess carbonaceous aerosol sampling artifacts for IMPROVE and other long-term networks, *J. Air Waste Manage. Assoc.*, *59*, 898-911.

Wells, K. C., M. Witek, P. Flatau, S. M. Kreidenweis, and D. L. Westphal (2007), An analysis of seasonal surface dust aerosol concentrations in the western US (2001-2004): Observations and model predictions, *Atmos. Environ.*, *41*, 6585-6597.

White, W. H. (1997), Deteriorating air or improving measurements? On interpreting concatenate time series, *J. Geophys. Res.*, *102*, 6813-6821.

White, W. H., E. S. Macias, L. A. de P.Vasconcelos, R. J. Farber, V. A. Mirabella, M. C. Green, and M. L. Pitchford (1999), Tracking regional background in a haze attribution experiment, *J. Air Waste Manage. Assoc.*, *49*, 599-602.

White, W. H., L. L. Ashbaugh, N. P. Hyslop, and C. E. McDade (2005), Estimating measurement uncertainty in an ambient sulfate trend, *Atmos. Environ.*, *39*, 6857-6867.

White, W. H. (2008), Chemical markers for sea salt in IMPROVE aerosol data, *Atmos. Environ.*, *42*, 261-274.

Xu, J., D. W. DuBois, M. L. Pitchford, M. C. Green, and V. Etyemezian (2006), Attribution of sulfate aerosols in federal Class I areas of the western United States based on trajectory regression analysis, *Atmos. Environ.*, *40*, 3433-3447.

Yu, S. C., R. L. Dennis, P. V. Bhave, and B. K. Eder (2004), Primary and secondary organic aerosols over the United States: Estimates on the basis of observed organic carbon (OC) and elemental carbon (EC), and air quality modeled primary OC/EC ratios, *Atmos. Environ.*, *38*, 5257-5268.

Yu, X. Y., T. Lee, B. Ayres, S. M. Kreidenweis, J. L. Collett, Jr., and W. C. Malm (2005), Particulate nitrate measurement using nylon filters, *J. Air Waste Manage. Assoc.*, *55*, 1100-1110.

Yu, X. Y., T. Lee, B. Ayres, S. M. Kreidenweis, W. C. Malm, and J. L. Collett (2006), Loss of fine particle ammonium from denuded nylon filters, *Atmos. Environ.*, *40*, 4797-4807.

Zeller, K., D. Harrington, A. Riebau, and E. Donev (2000), Annual wet and dry deposition of sulfur and nitrogen in the snowy range, Wyoming, *Atmos. Environ.*, *34*, 1703-1711.

Zeng, T. and Y. H. Wang (2011), Nationwide summer peaks of OC/EC ratios in the contiguous United States, *Atmos. Environ.*, *45*, 578-586.

Zhao, W. X. and P. K. Hopke (2004), Source apportionment for ambient particles in the San Gorgonio wilderness, *Atmos. Environ.*, *38*, 5901-5910.

Zhao, W. X. and P. K. Hopke (2006), Source identification for fine aerosols in Mammoth Cave National Park, *Atmospheric Research*, *80*, 309-322.

Zhao, W. X., P. K. Hopke, and L. M. Zhou (2007), Spatial distribution of source locations for particulate nitrate and sulfate in the upper-Midwestern United States, *Atmos. Environ.*, *41*, 1831-1847.